# Journal of Applied Mechanics

(*Contributions of the ASME Applied Mechanics Division*)


Limit Analysis of Punch Indentation . . . . . *R. T. Shield and D. C. Drucker* 453
Transverse Impact on Beams and Plates . . . . . *A. C. Eringen* 461
Buckling of Reinforced Cylindrical Shells . . . . . *W. A. Nash* 469
Dynamic Load Characteristics in Plastic Bending of Beams . . . . . *P. S. Symonds* 475
Analog Solution for Beams Excited by an Arbitrary Force . . *W. T. Thomson and T. A. Rogers* 482
Thermal Stress in Pipes . . . . . *Henry Parkus* 485
Solutions of Heat-Conduction Problem With the Aid of the Inverse Method . . . *F. S. Weinig* 489
Toroidal-Shell Expansion Joints . . . . . *N. C. Dahl* 497
Flexural Vibrations in Uniform Beams According to the Timoshenko Theory . . *R. A. Anderson* 504
Flexural Wave Solutions of Coupled Equations. . . . . *Julius Miklowitz* 511
Analysis of a Nonlinear Dynamic Vibration Absorber . . . . . *L. A. Pipes* 515
Constant-Strain Waves in Strings . . . . . *J. D. Cole, C. B. Dougherty, and J. H. Huth* 519
Dynamic Stress-Strain Relations for Compression Impact . . . . . *J. E. Johnson, D. S. Wood, and D. S. Clark* 523
The Effect of Strain Hardening in an Annular Slab . . . . . *P. G. Hodge, Jr.* 530
The Rate of Growth of Vapor Bubbles in Superheated Water . . . . . *Paul Dergarabedian* 537
On Reinforced Circular Cutouts . . . . . *E. Levin* 546
Torsional Stiffness Under Tension, Compression, and Bending . *H. L. Engel and J. N. Goodier* 553

Brief Notes
The Complex-Variable Approach to Stress Singularities . . . . . *J. H. Huth* 561
Note on the Maximum Effect of a Moving Force on a Simple Beam . . . . *E. S. Eichmann* 562
A Resistor-Network Solution for the Torsion of Hollow Sections . . . . . *J. H. Weiner* 562
Closed-Form Solutions for Plates of Variable Thickness . . . . . *H. D. Conway* 564
A Note on Mass Flow . . . . . *E. C. Kennedy* 565
Diametral Expansion of Helical Compression Springs During Deflection . . . *A. M. Wahl* 565
Additional Data on the Relaxation Type of Vehicle Suspension . . . . . *Joseph Gallagher and Enrico Volterra* 567
Note on Torsional Oscillation of I-Type Beams . . . . . *J. E. Goldberg* 567
Concentrated Radial Loads on Flat Curved Beams . . . . *J. N. Goodier and J. C. Wilhoit, Jr.* 568

Discussion on previously published papers by *P. F. Chenea; A. W. Cochardt; J. E. Goldberg; G. Horvay; C. W. Hurd, K. P. Chesky, and A. H. Shapiro; R. Jenkins and J. S. Aronofsky; Julius Miklowitz; J. C. New; R. D. Mindlin and H. H. Bleich; H. Poritsky; R. E. Roberson; M. L. Williams; G. A. Zizicas; B. J. Lazan* . . . . . 571
Book Reviews . . . . . 595



## DECEMBER, 1953

VOL. 20, NO. 4

Transactions of The American Society of Mechanical Engineers

# Journal of Applied Mechanics

**Papers Contributed to the Transactions by the ASME Applied Mechanics Division**


EXECUTIVE COMMITTEE OF THE APPLIED MECHANICS DIVISION

DANA YOUNG, *Chairman* — N. M. NEWMARK, *Secretary*

JOHN M. LESSELLS, *Technical Editor*



*Published Quarterly by*

**The American Society of Mechanical Engineers**

**Publication Office, 20th and Northampton Streets, Easton, Pa.**
**Editorial Department at the Headquarters of the Society, 29 West Thirty-Ninth Street, New York 18, N. Y.**



OFFICERS OF THE SOCIETY

FREDERICK S. BLACKALL, JR., *President*

JOSEPH L. KOPF, *Treasurer* — C. E. DAVIES, *Secretary*
E. J. KATES, *Assistant Treasurer*

PUBLICATIONS COMMITTEE

GEORGE R. RICH, *Chairman* — GEORGE A. STETSON, *Editor*
K. W. CLENDENNING, *Mgr. Editor*


By-Law: The Society shall not be responsible for statements or opinions advanced in papers or . . . printed in its publications (B13, Par. 4).


Published quarterly by The American Society of Mechanical Engineers. Publication office at 20th and Northampton Streets, Easton, Pa. The editorial department is located at the headquarters of the Society, 29 West Thirty-Ninth Street, New York 18, N. Y. Cable address, "Dynamic," New York. Price $1.50 a copy, $5.00 a year; to members $2.50 a year; single copy price to members, $1.00. Changes of address must be received at Society headquarters four weeks before they are to be effective on the mailing list. Please send old as well as new address. . . . By-Law: The Society shall not be responsible for statements or opinions advanced in papers or . . . printed in its publications (B13, Par. 4). . . . Entered as second-class matter: March 14, 1955, at the Post Office at Easton, Pa., under the act of August 24, 1912. . . .


Copyrighted, 1955, by The American Society of Mechanical Engineers. Reprints from this publication may be made on condition that full credit be given the JOURNAL OF APPLIED MECHANICS and the author, and that date of publication be stated.

# The Application of Limit Analysis to Punch-Indentation Problems[1]

By R. T. SHIELD[2] AND D. C. DRUCKER,[3] PROVIDENCE, R. I.

**Limit analysis is applied to obtain upper and lower bounds for the punch pressure in the indentation of the plane surface of an elastic-perfectly plastic material by a flat rigid punch. The two-dimensional flat punch and the three-dimensional flat square and rectangular punch problems are considered. The analysis assumes Tresca's yield criterion of constant maximum shearing stress $k$, during plastic deformation. It is shown that the pressure required to produce indentation in the two-dimensional problem lies between $5k$ and $(2 + \pi)k$. The lower bound obtained for any rectangular punch is again $5k$ while the upper bound for a smooth punch lies between $5.71k$ for a square and $(2 + \pi)k$ for a very long rectangle. A value of $5.36k$ is found for a ratio of length to breadth of 3. The limit pressure for a uniformly loaded area, as distinguished from an area loaded by a punch, is bracketed by $5k$ and $(2 + \pi)k$ when the area is convex.**

## Introduction

THE plastic yielding of a semi-infinite body of perfectly plastic material due to indentation by a flat rigid punch under conditions of plane strain was first investigated by Prandtl (1).[4] An alternative solution was suggested by Hill (2). Both of these solutions involve a stress field together with an associated velocity field, and they indicate that there is a uniform pressure $(2 + \pi)k$ over the area of indentation during the incipient plastic flow. The solutions of Prandtl and Hill are incomplete since it remains to be shown that the plastic stress field around the punch can be extended into the rigid region in a satisfactory manner. However, limit-design theorems (3, 4, 5) show that the value $(2 + \pi)k$ is an upper bound for the pressure exerted by the punch because the velocity fields associated with the Prandtl and Hill solutions are kinematically admissible. This bound applies to an elastic-perfectly plastic material (6).

In the first part of the following work the limit-design theorems are applied to obtain the lower bound $5k$ for the pressure on the punch. The lower and upper bounds, $5k$ and $(2 + \pi)k$, respectively, determine the pressure with sufficient accuracy for practical purposes.

Hencky (7) and Ishlinsky (8) have used a hypothesis of Haar and von Kármán (9) to consider the problem of the indentation of a plane surface by a flat circular punch. The authors calculated the indentation pressure by obtaining a plastic stress field around the punch, but it was not shown that the stress fields could be extended throughout the body in a satisfactory manner. Also, it is unlikely that it is possible to associate velocity fields with these stress fields. Any such value obtained for the indentation pressure is therefore not necessarily a lower bound for the pressure nor is it known when it is an upper bound.

In the last part of this work the problems of the indentation of a plane surface by a flat square punch and by a rectangular punch are considered. At the present stage of elastic-plastic analysis the exact solutions of these problems would be difficult if not impossible to obtain. Limit analysis is used in the paper to obtain upper and lower bounds for the indentation force, assuming Tresca's yield condition of constant maximum shearing stress during plastic deformation.

## Limit-Design Theorems

A general method has been developed recently for determining the point at which collapse will occur in assemblages of rigid and of elastic-perfectly plastic bodies (5). The term collapse is used to describe conditions for which plastic flow would occur under constant loads if the accompanying change in the geometry of the body were disregarded. The limit-design theorems in the form required in the following work are outlined briefly here.

The boundary conditions are assumed to be of the stress type. Each of the components $T_x$, $T_y$, $T_z$ of the surface traction is given on the surface of the body except where the corresponding velocity component $v_x$, $v_y$, or $v_z$ or the corresponding relative velocity component at an interface of an assemblage is prescribed to be zero. A stress field is called statically admissible if the stress field satisfies the equations of equilibrium throughout the volume $V$ of the bodies, satisfies the stress boundary conditions, and if the stress field nowhere violates the yield condition. The equations of equilibrium are

$$\frac{\partial \sigma_x}{\partial x} + \frac{\partial \tau_{xy}}{\partial y} + \frac{\partial \tau_{xz}}{\partial z} = 0 \qquad [1]$$

and two similar equations.

Stress fields which have surfaces of discontinuity are permissible and are often useful. On either side of such a surface the stress components must satisfy Equation [1]. Also, if $n_x$, $n_y$, $n_z$ are the components of the unit normal to the surface of discontinuity, then the expression

$$\sigma_x n_x + \tau_{xy} n_y + \tau_{xz} n_z$$

and each of the two similar expressions, must have the same value whether it is evaluated from the stresses on one or the other side of the discontinuity surface.

Strain rates can be derived from any given velocity field. Considering the strain rates as purely plastic strain rates, the internal rate of dissipation of energy can be calculated. A velocity field is said to be kinematically admissible if the velocity components $v_x$, $v_y$, $v_z$ satisfy the incompressibility condition and any imposed velocity boundary condition, and if the rate at which the applied tractions do work on the velocities of their points of

[1] The results presented in this paper were obtained in the course of research sponsored by the Office of Naval Research under Contract N7onr-35801 with Brown University.

[2] Research Associate in Applied Mathematics, Brown University.

[3] Professor of Engineering, Brown University. Mem. ASME.

[4] Numbers in parentheses refer to the Bibliography at the end of the paper.

Presented at the National Conference of the Applied Mechanics Division, Minneapolis, Minn., June 18–20, 1953, of THE AMERICAN SOCIETY OF MECHANICAL ENGINEERS.

Discussion of this paper should be addressed to the Secretary, ASME, 29 West 39th Street, New York, N. Y., and will be accepted until January 11, 1954, for publication at a later date. Discussion received after the closing date will be returned.

NOTE: Statements and opinions advanced in papers are to be understood as individual expressions of their authors and not those of the Society. Manuscript received by ASME Applied Mechanics Division, August 8, 1952. Paper No. 53—APM-21.

application equals or is greater than the internal rate of dissipation of energy.

The following theorems have been formulated for the case of all surface tractions increasing in proportion:

Theorem 1. Collapse will not occur until the largest values of the surface tractions are reached for which it is possible to find a statically admissible stress field.

Theorem 2. Collapse will occur under the smallest values of the surface tractions for which it is possible to find a kinematically admissible velocity field.

These two theorems provide a method for determining lower and upper bounds for the limiting values of the surface tractions.

Tresca's criterion of constant maximum shearing stress is used in the following work. In this case statically admissible stress fields must nowhere involve a shearing stress exceeding the value $k$. The maximum shearing stress is equal to one half the difference between the maximum and minimum principal stresses. It follows that if the principal stresses $\sigma_1$, $\sigma_2$, $\sigma_3$ are used as rectangular Cartesian co-ordinates in a diagram representing states of stress, the states with the maximum shearing stress $k$ are represented by the points on the surface of a right prism which has a regular hexagon for its cross section. The axis of the prism passes through the origin and is equally inclined to the $\sigma_1$, $\sigma_2$, $\sigma_3$ axes. Fig. 1 shows a section through the prism by a plane perpendicular to the $\sigma_3$-axis and at a distance $\sigma_3$ from the origin. It can be verified easily that points on the hexagon $A$-$B$-$C$-$D$-$E$-$F$ represent states of stress with the maximum shearing stress $k$. The center $G$ of the hexagon has the co-ordinates $(\sigma_3, \sigma_3, \sigma_3)$.

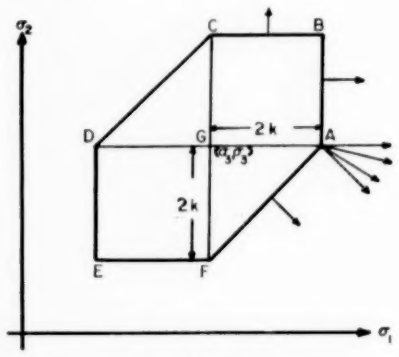


FIG. 1 TRESCA'S YIELD CONDITION

In deriving the limit design theorems in reference (5) it was assumed that the yield surface in the principal stress space had a unique normal at each point. Subsequent work (11) employed Tresca's criterion which gives a surface which has sharp corners. This extension is permissible because the rate of dissipation of energy is uniquely determined by the plastic strain rate.

According to Tresca's criterion, plastic flow can occur under a constant state of stress which is represented by a point on the prism in the $(\sigma_1, \sigma_2, \sigma_3)$ diagram, for example, by a point on the hexagon in Fig. 1. Since the material is isotropic, the principal axes of the plastic strain rate must coincide with the principal axes of stress, and the principal components of the strain rate in the $\sigma_1$, $\sigma_2$, $\sigma_3$ directions will be denoted by $\dot{\epsilon}_1$, $\dot{\epsilon}_2$, $\dot{\epsilon}_3$, respectively. It is convenient to represent the plastic strain rate by a ray with direction cosines proportional to $\dot{\epsilon}_1$, $\dot{\epsilon}_2$, $\dot{\epsilon}_3$ in the $(\sigma_1, \sigma_2, \sigma_3)$ diagram. The projection of this ray onto the plane of Fig. 1 is a ray with direction cosines proportional to $\dot{\epsilon}_1$, $\dot{\epsilon}_2$. The third principal component $\dot{\epsilon}_3$ can be found when $\dot{\epsilon}_1$, $\dot{\epsilon}_2$ are known since the components satisfy the incompressibility condition

$$\dot{\epsilon}_1 + \dot{\epsilon}_2 + \dot{\epsilon}_3 = 0 \quad \ldots\ldots\ldots\ldots\ldots\ldots [2]$$

It follows that the projection of the ray representing the plastic strain rate onto the plane in Fig. 1 determines the plastic strain rate to within an arbitrary scalar factor.

Consider a point on the hexagon in Fig. 1 which does not coincide with a vertex. The concept of perfect plasticity (10) requires that the ray representing the plastic flow which would occur under this state of stress is normal to the side of the hexagonal prism on which the point lies. The projection of the ray is normal to the side of the hexagon, Fig. 1. For a stress point which coincides with a vertex, the ray representing the plastic strain rate is not determined uniquely. However, the ray must lie between the directions of the normals to the two sides of the hexagon which meet at the vertex. For example, at the vertex $A$ the ray must lie in the angular space shown by the arrows in Fig. 1. Although the correspondence between the plastic strain rate and the stress is not one to one, the internal rate of dissipation of energy is uniquely determined by the plastic strain rate. The rate of dissipation of energy is given by

$$D = \sigma_1\dot{\epsilon}_1 + \sigma_2\dot{\epsilon}_2 + \sigma_3\dot{\epsilon}_3 \quad \ldots\ldots\ldots\ldots\ldots\ldots [3]$$

and in the following it will be shown that

$$D = 2k \max |\dot{\epsilon}| \quad \ldots\ldots\ldots\ldots\ldots\ldots [4]$$

where max $|\dot{\epsilon}|$ denotes the absolute value of the numerically largest principal component of the plastic strain rate.

For a point on the side $A$-$B$ of the hexagon, the normal to $A$-$B$ is parallel to the $\sigma_1$-axis so that $\dot{\epsilon}_2 = 0$. Hence $\dot{\epsilon}_3 = -\dot{\epsilon}_1$ from the condition of incompressibility, Equation [2]. Equation [3] then shows that the rate of dissipation of energy is given by

$$D = \sigma_1\dot{\epsilon}_1 + \sigma_3\dot{\epsilon}_3 = 2k\dot{\epsilon}_1$$

since $\sigma_1 = \sigma_3 + 2k$ on $A$-$B$. Now max $|\dot{\epsilon}| = \dot{\epsilon}_1$ in this case so that $2k\dot{\epsilon}_1$ can be written in the form of Equation [4]. If the stress point coincides with the vertex $A$, then $\sigma_1 = \sigma_3 + 2k$, $\sigma_2 = \sigma_3$ and therefore $D = 2k\dot{\epsilon}_1$ on account of the incompressibility condition Equation [2]. Since $\dot{\epsilon}_1$ is the absolutely largest principal component in this case, this again can be written in the form of Equation [4]. In the same way it can be shown that Equation [4] holds at every stress point of the hexagon.

For the particular case of plane strain, $\dot{\epsilon}_2 = -\dot{\epsilon}_1$ and $\dot{\epsilon}_3 = 0$ so that

$$\max |\dot{\epsilon}| = \frac{|\dot{\epsilon}_1 - \dot{\epsilon}_2|}{2} = \frac{\dot{\gamma}_{\max}}{2}$$

where $\dot{\gamma}_{\max}$ is the maximum rate of (engineering) shear strain. Thus for plane strain

$$D = k\dot{\gamma}_{\max} \quad \ldots\ldots\ldots\ldots\ldots\ldots [5]$$

Expression [4] for the rate of dissipation of energy was obtained previously by Hodge and Prager (11) for the special case of plane stress, $\sigma_3 = 0$.

In view of Expression [4] it follows from the definition of a kinematically admissible velocity field that the velocity field $v_x, v_y, v_z$ must satisfy the inequality

$$\int_S (T_x v_x + T_y v_y + T_z v_z)\, dS \geq \int_V 2k \max |\dot{\epsilon}|\, dV \quad \ldots [6]$$

if it is kinematically admissible under the Tresca yield condition. The surface integration extends over the surface $S$ which bounds the body or assemblage of bodies, and max $|\dot{\epsilon}|$ denotes the absolutely largest principal component of the derived plastic strain rate. Rigid bodies in the assemblage contribute nothing to the

right-hand side of Expression [6] since the strain rate is zero for a rigid body. Also, any variation in the value of $k$ from one body to another in the assemblage must be taken into account in the evaluation of the volume integral. A kinematically admissible velocity field may contain discontinuities in the tangential velocity across fixed surfaces. This type of discontinuity is an idealization of a continuous large variation in velocity across a thin transition layer. When surfaces of discontinuity are present, the expression

$$\int_{S_D} k \Delta v \, dS_D \quad \ldots\ldots\ldots\ldots\ldots\ldots\ldots\ldots [7]$$

must be added to the right-hand side of Expression [6]. In this expression $\Delta v$ is the magnitude of the relative change in velocity across the discontinuity surfaces $S_D$, and the expression represents the rate at which energy is dissipated in the thin transition layers as the thicknesses of the layers approach zero.

## Statement of Indentation Problem

The problem under consideration is the indentation of the plane surface of a semi-infinite perfectly plastic material by a normally and centrally loaded flat rigid punch. It is assumed that the force on the punch is increased until penetration occurs as a result of plastic flow in the material. The punch and the semi-infinite body constitute an assemblage of bodies to which the limit-design theorems of the previous section can be applied. Fig. 2 shows a punch on the surface of the plastic material. The force $P$ on the end of the punch not in contact with the material may be a concentrated force or may be distributed in any manner over the end of the punch. In determining statically admissible stress fields in the problems considered below, it will be assumed that the pressure between the punch and the material is normal to the plane surface and is uniformly distributed. These assumptions may be unnecessarily restrictive but they do agree with the requirement that the resultant force over the free end of the punch be a normal force passing through the centroid of the contact area which is the only restriction on the distribution of force on the free end of the punch. It always will be possible to find a stress field in the punch which satisfies the equations of equilibrium and the boundary conditions, viz., uniform normal pressure over the contact area and a certain distribution of traction over the free end. Since the material of the punch is rigid, any equilibrium stress field in the punch will be statically admissible. The force $P$ on the end of the punch is equal to the uniform pressure $p$ between the punch and the material multiplied by the area of contact.

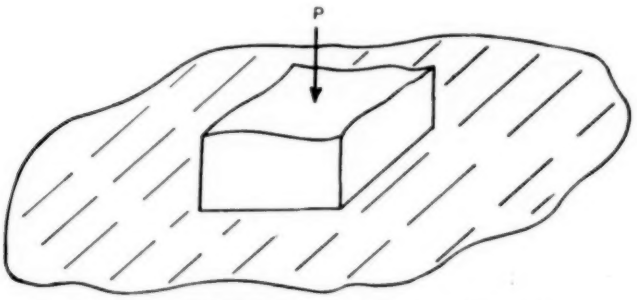


Fig. 2 Rigid Punch on Plane Surface of Material

The omission of shearing stresses over the area of indentation does not in itself require that the punch surface be smooth. If the kinematically admissible velocity fields which are used are such that slip occurs between the punch and the material, then the punch must be smooth. The bounds obtained later for the indentation force in the two-dimensional punch problem apply to either a rough or a smooth punch. In the three-dimensional punch problems, the square and rectangular punches, the upper bounds obtained are applicable only to a smooth punch, although the lower bounds are applicable to either rough or smooth punches.

## Two-Dimensional Flat Punch

As remarked previously, the Prandtl and Hill solutions of this problem provide an upper bound for the indentation force, which is distributed uniformly over the area of indentation in each case. Fig. 3 shows the cross section perpendicular to the plane surface of the material. $A$-$B$ is the flat surface of the punch which is of infinite length in the direction perpendicular to the plane in Fig. 3. The incipient velocity field according to the Hill solution is shown in Fig. 3($a$). Plastic flow is confined to the region above the line of discontinuity $D$-$F$-$G$-$C$-$I$-$K$-$E$. The streamlines are parallel to this line and if the initial downward velocity of the punch is $v$, the velocity has the constant value $\sqrt{2}\,v$ along each streamline. With Tresca's criterion of yielding, which is identical with von Mises' criterion for plane strain, the velocity field is kinematically admissible if the assumed pressure on the punch equals or is greater than $(2 + \pi)k$. It

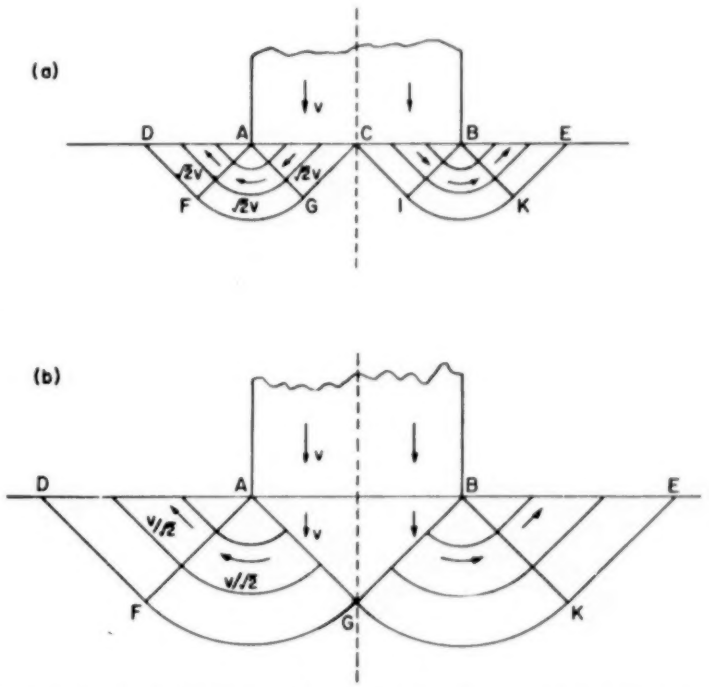


Fig. 3 Velocity Fields for Two-Dimensional Flat Punch According to ($a$) Hill Solution and ($b$) Prandtl Solution

follows from Theorem 2, stated earlier in the paper, that the collapse value of the average pressure is not greater than $(2 + \pi)k$. Since there is slip between the material and the punch, the punch must be frictionless. The Prandtl velocity field is shown in Fig. 3(*b*). The region *A-B-G* moves downward with the punch as a rigid body and the lines *A-G*, *B-G*, and *D-F-G-K-E* are lines of discontinuity in the velocity field. The streamlines in the regions *A-D-F-G*, *B-E-K-G* are parallel to the lines *G-F-D* and *G-K-E*, respectively, and the velocity has the constant value $v/\sqrt{2}$ along each streamline. As in the Hill solution, the velocity field provides the upper bound $(2 + \pi)k$ for the average indentation pressure. In this case there is no slip between the material and the punch, which can be considered rough, and therefore the upper bound is applicable to either a smooth or a rough punch.

To obtain a lower bound for the average indentation pressure we first use a particular case of the discontinuous stress pattern obtained by Winzer and Carrier[5] (12). The pattern is a statically admissible stress field for the loading of a truncated wedge, and Fig. 4(*a*) shows the stress system when the angle of the wedge is taken to be 60 deg. The Mohr's circles for the regions marked I, II, III in Fig. 4(*a*) are shown in Fig. 4(*b*). This stress system at once gives the value $3k$ as a lower bound for the average indentation pressure for the flat-punch problem, if *A-B* is taken to be the surface of the punch indenting the material below the line *G-H*. The region vertically below *D-E* is then in a state of uniaxial compression which does not violate the yield condition.

[5] A more recent discussion of this stress pattern has been given by Prager and Hodge (13).

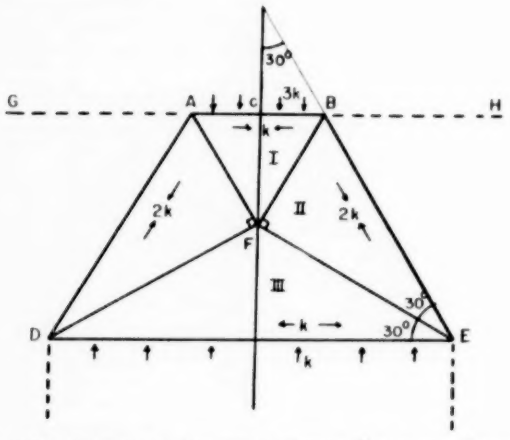


Fig. 4(*a*) Statically Admissible Stress Field for Loaded Wedge

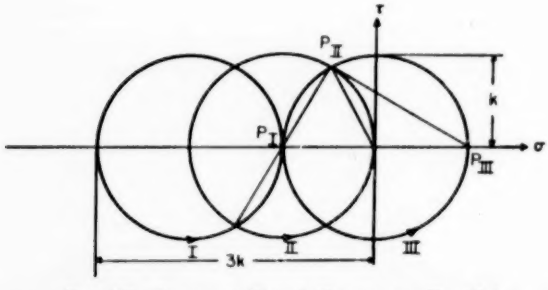


Fig. 4(*b*) System of Mohr's Circles for Fig. 4(*a*)

The points labeled $P_I$, $P_{II}$, $P_{III}$ are the poles of the corresponding Mohr's circles. Line $P_IP_{II}$ is parallel to *F-B* in Fig. 4(*a*) and $P_{II}P_{III}$ is parallel to *F-E*.

More generally when the angle of the wedge is $2\alpha$, the pressure on *A-B* has the value $2k(1 + \sin \alpha)$. To improve the lower bound a vertical compression of amount $Q$ is superimposed in the region vertically below *A-B*, increasing the pressure on *A-B* to $2k(1 + \sin \alpha) + Q$, and a horizontal compression of amount $Q$ is superimposed throughout the material. $Q$ and $\alpha$ must be chosen so that the yield condition is nowhere violated in the resulting stress field. $Q$ must not be greater than $2k$ in order that the yield condition be not violated in the previously unstressed region. The region vertically below *A-B* is subjected to an additional hydrostatic pressure $Q$ which does not affect the yield condition there. Since $Q \leq 2k$, it is found that the critical region which decides which values of $Q$ and $\alpha$ are permissible, is that part of region II which is not vertically below *A-B*. The values which give a maximum value of $5k$ for the pressure on *A-B* are $Q = 2k$ and $\alpha = 30$ deg. The value $5k$ is therefore a lower bound for the average indentation pressure and the corresponding statically admissible stress field is shown in Fig. 5(*a*). In order to show the effect of adding the compressive stress $2k$ in the critical region, the Mohr's circles for region II in Fig. 4(*a*) and for region *d* in Fig. 5(*a*) are shown in Fig. 5(*b*). The stress point *L* gives the stress acting on a horizontal-line element of regions II and *d*, while the stress points *M*, *N* give the stress acting on a vertical line element in regions II and *d*, respectively.

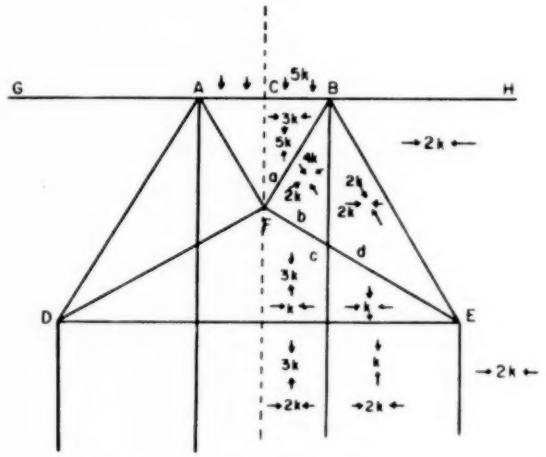


Fig. 5(*a*) Statically Admissible Stress Field for Flat Punch

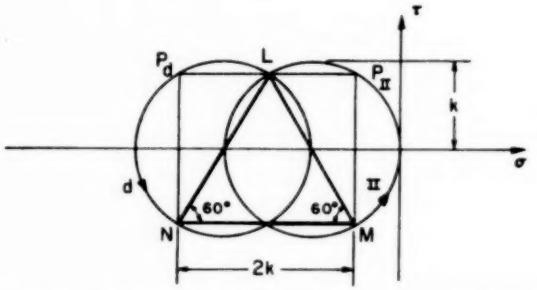


Fig. 5(*b*) Mohr's Circles for Region II in Fig. 4(*a*) and Region *d* in Fig. 5(*a*)

### Three-Dimensional Square and Rectangular Punches

In this section, upper and lower bounds are obtained for the collapse pressures in the indentation of a plane surface by a flat square punch and by a flat rectangular punch, using Tresca's criterion of yielding.

Considering first the lower bound, a modification of the stress field in Fig. 4(*a*) is useful for extension into three dimensions. By drawing two lines through *F* parallel to *A-D* and *B-E* the stress field in Fig. 6 is obtained. The pressure on *A-B* is supported by uniaxial compression of amount $2k$ in the two "legs" of material, *A-F-J-D* and *B-F-K-E*, which extend to infinity, and the rest of the material is stress-free. (The addition of a horizontal compression $2k$ and a vertical compression $2k$ in the region vertically below *A-B* gives an alternative stress field for the lower bound $5k$ of the plane-strain problem.)

The corresponding three-dimensional stress field for the rectangular punch is shown in Fig. 7. *L-M-N-O* is the rectangular area of indentation in the plane surface of the material, *L-O* and *M-N* being the longer sides of the rectangle. The triangular region *A-B-F* in Fig. 6 becomes the volume *L-M-N-O-X-Y*. The line *X-Y* is parallel to the longer sides of the rectangle, and the two triangular faces and the two trapezoidal faces of the volume are all inclined at an angle of 60 deg to the plane of the rectangle. The pressure $3k$ on the rectangular area is supported by uniaxial compression of amount $2k$ in the four prisms, two triangular and two trapezoidal, extending from the inclined faces of the volume *L-M-N-O-X-Y*. For clarity, only two of the prisms are shown in the diagram. The axes of the prisms are inclined at an angle of 60 deg to the plane of the rectangle. Fig. 6 is then the vertical cross section through the mid-points of the longer sides of the rectangle.

By superimposing an all-around horizontal compression $2k$ throughout the material and a vertical compression $2k$ in the region vertically below the rectangle *L-M-N-O*, the pressure on the rectangle is increased to the value $5k$. Also, it can easily be verified that Tresca's criterion is nowhere violated in the resulting stress field so that the field is statically admissible. Hence, by Theorem 1, $5k$ is a lower bound for the collapse value of the average punch pressure.

The lower bound $5k$ for the rectangular punch is obviously applicable to a square punch as a special case. For the square punch, the points *X*, *Y* in Fig. 7 coincide with the point *F*. In fact, the stress field in Fig. 7 can be modified so that it applies to any area of contact which is convex, and the value $5k$ is then a lower bound for any convex area of indentation.

The velocity condition on kinematically admissible velocity fields for this problem is that the area of indentation must move as a plane surface because the punch is a rigid body. When a velocity field which satisfies this condition and the incompressibility condition has been found, the lowest value of the average pressure over the punch which will make the field kinematically admissible is an upper bound for the collapse pressure. A simple discontinuous velocity field for the square punch is shown diagrammatically in Fig. 8. *L-M-N-O* is the square area of indentation on the plane surface of the material, and the initial downward velocity of this area is taken to be $v$. The downward movement of the square area is accommodated by movement of the material as indicated in Fig. 8(*a*). In Fig. 8(*b*) is shown the plan and section in Fig. 8(*a*), and it can be seen that this velocity field is an extension[6] into three dimensions of a simple modification of the two-dimensional velocity field in Fig. 3(*a*). The angles *B-E-K* and *B-C-I*, which are denoted by $\alpha$ and $\beta$, are as yet unspecified. Since the movement is symmetrical about *X-Y*, it is only necessary to consider the movement on the right-hand side of Fig. 8(*a*). The three triangular prisms of material move as rigid bodies in the directions parallel to *C-I*, *I-K*, and *K-E*. The internal dissipation of energy is due to the discontinuity surfaces between the material at rest and the material in motion and the two discontinuity surfaces where the prisms have a common surface. Since the material must remain in contact with the punch, the prism in contact with the punch must move with the velocity $v \cos\epsilon \beta$. The velocity of the prism whose cross section is *B-I-K* is determined by the condition that the relative velocity between this prism and the prism in contact with the punch must have the direction *I-B*. The velocity of the third prism is determined in a similar manner.

It is a simple matter to calculate the areas of the surfaces of discontinuity. The rate of dissipation of energy is then found by multiplying the area of each discontinuity surface by $k$ times

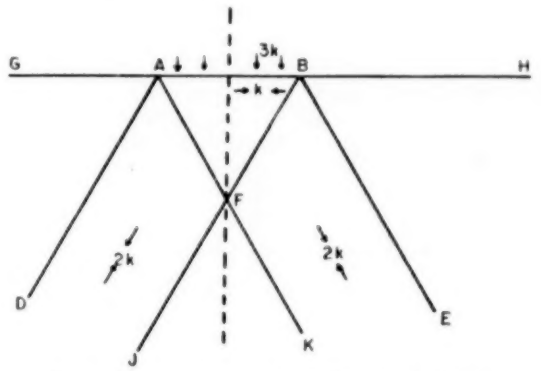


Fig. 6 Modification of Stress Field in Fig. 4(*a*)

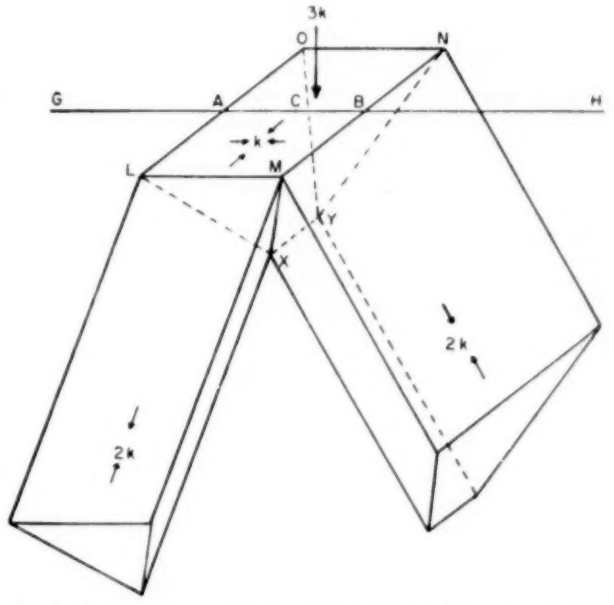


Fig. 7 Stress Field for Three-Dimensional Rectangular Punch

[6] The analogous extension of the Prandtl velocity field in Fig. 3(*b*) into three dimensions gives upper bounds which are higher than those obtained by extending the Hill solution.

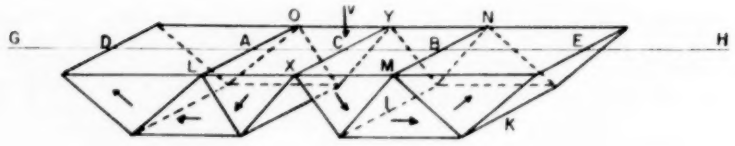


FIG. 8(a) SIMPLE VELOCITY FIELD FOR SQUARE PUNCH

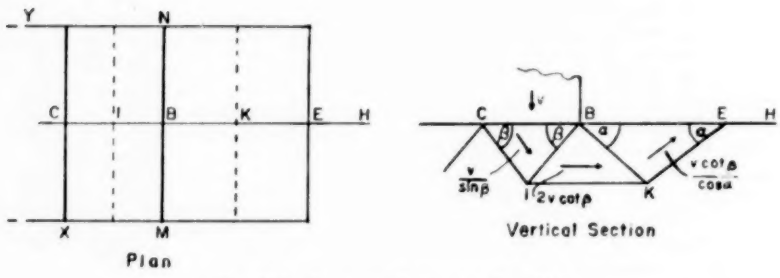


FIG. 8(b) PLAN AND SECTION IN FIG. 8(a)

the discontinuity in velocity across the surface and summing over all the surfaces. It is found, after some simplification, that the rate at which work is done by the applied tractions, i.e., the force on the punch, will not be less than the internal rate of dissipation of energy if the average pressure on the punch is not less than

$$f(\alpha, \beta) = \frac{k}{4}\,[\sec\beta + 8\operatorname{cosec} 2\alpha + 8\operatorname{cosec} 2\beta + 4\cot\alpha + 4\cot\beta + \tan\beta\,(\cot\alpha + \operatorname{cosec}\alpha) + 1]$$

By Theorem 2, $f(\alpha, \beta)$ is an upper bound for the collapse value of the average indentation pressure. The function has a minimum value near the point $\alpha = 57$ deg, $\beta = 48$ deg, where it has the value $6.89k$, so that $6.89k$ is an upper bound for the collapse pressure.

A better upper bound is obtained as follows: In Fig. 9 *L-M-N-O* is the square area of indentation which moves downward with initial velocity $v$. The square is divided into four equal triangles by the diagonals *L-N*, *M-O*. Taking a typical triangle *C-M-N*, the downward movement of the triangle is accommodated by flow in the volume *C-D-E-F-M-N*. *D-C-M-N* and *E-F-M-N* are tetrahedra, the points *D*, *E* being vertically below the line *C-F*. *M-B-D-E* and *N-B-D-E* are two similar sections of right circular cones, the axes of which lie on *M-N*. Fig. 9(*b*) shows the plan and the vertical section through *C-F*. Vertical sections by planes parallel to *C-F* through the volume *C-D-E-F-M-N* are similar in shape to the section shown in Fig. 9(*b*) but are of varying size. The streamlines of the flow are parallel to the line *C-D-E-F* and, if the angle *B-C-D* is denoted by $\beta$, the velocity along each streamline has the constant value $v \operatorname{cosec}\beta$. The downward movement of the other three triangles is accommodated in the same way, the remainder of the material being at rest.

Energy is dissipated in the discontinuity surface between the material at rest and the material moving in the volume *C-D-E-F-M-N*, and also in the conical regions *M-B-D-E* and *N-B-D-E* where the plastic strain rate is nonzero. The rate of dissipation of energy due to the discontinuity surface is equal to the area of the surface multiplied by $kv \operatorname{cosec}\beta$, since the change in velocity across the surface has the constant value $v \operatorname{cosec}\beta$. The flow in the conical regions is a plane-strain motion so that Expression [5] can be used to calculate the rate of dissipation of energy per unit volume. The total rate of dissipation of energy in this region can be found by calculating the rate of dissipation in a vertical cross section parallel to *C-F* and integrating in the direction *M-N*. When these calculations have been carried out, it is found that the velocity field will be kinematically admissible if the average pressure on the square is not less than the value

$$g(\alpha, \beta) = k[\alpha + \beta + \sqrt{1 + \sin^2\beta}\,(\alpha + \beta + \cot\alpha + \cot\beta)]$$

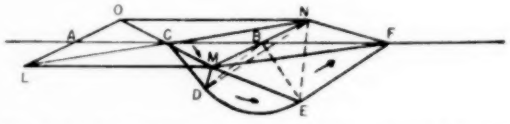


FIG. 9(a) ALTERNATIVE VELOCITY FIELD FOR SQUARE PUNCH

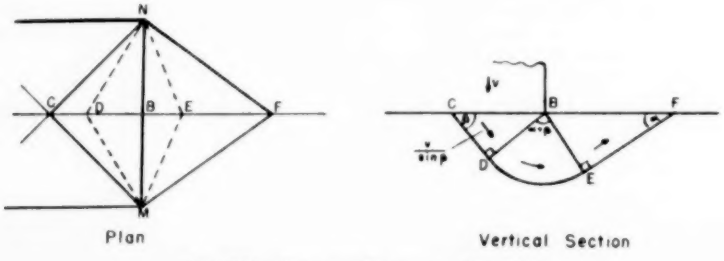


FIG. 9(b) PLAN AND SECTION IN FIG. 9(a)

where $\alpha$ is the angle *B-F-E*. Term $g(\alpha, \beta)$ is therefore an upper bound for the collapse value of the pressure, by Theorem 2. The function has the minimum value $5.80k$ when $\alpha$ and $\beta$ are approximately 47 deg and 34 deg, respectively.

The velocity field which will be discussed now provides an upper bound for the collapse pressure in the rectangular punch problem and also gives a better upper bound for the square punch than those obtained in the foregoing. In Fig. 10 *L-M-N-O* is the rectangular area of indentation on the plane surface of the material. The lengths of *L-O* and *L-M* are denoted by $2a$ and $2b$, respectively, $a$ being greater than or equal to $b$. The velocity field has two planes of symmetry which are the vertical planes through the mid-points of opposite sides of the rectangle, and it is only necessary to consider the part of the velocity field which accommodates the downward velocity $v$ of the area *M-B-C-X*.

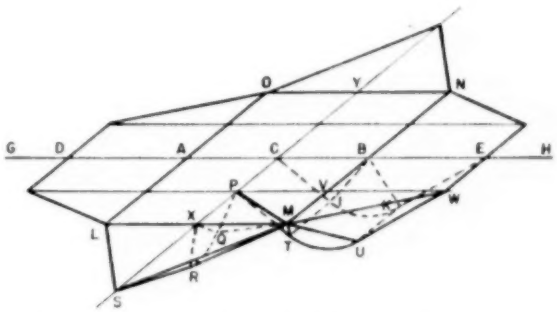


FIG. 10(*a*) VELOCITY FIELD FOR RECTANGULAR PUNCH

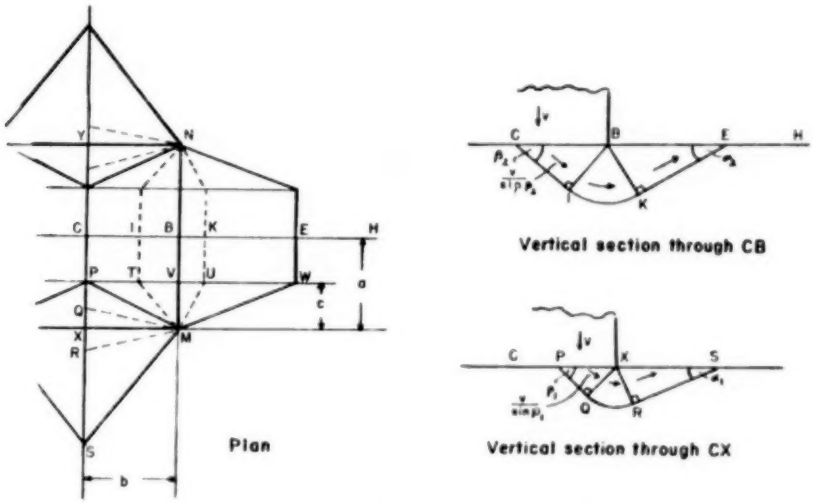


FIG. 10(*b*) PLAN AND TWO SECTIONS IN FIG. 10(*a*)

The plan in Fig. 10(*a*) and the vertical sections through *C-X* and *C-E* are shown in Fig. 10(*b*). The point *P* is chosen on *C-X* at a distance $c$ ($c \leq a$) from the point *X*. For brevity the volumes *M-P-Q-R-S-X* and *M-P-C-B-E-I-K-T-U-W* will be called the volumes 1 and 2, respectively. In volume 1 the streamlines of the flow are parallel to the line *P-Q-R-S* and the velocity on each streamline has the constant value $v \operatorname{cosec} \beta_1$, where $\beta_1$ is the angle *X-P-Q*. In volume 2 the streamlines are parallel to the line *C-I-K-E* and the velocity is $v \operatorname{cosec} \beta_2$, where $\beta_2$ is the angle *B-C-I*. Energy is dissipated in the discontinuity surfaces between the material at rest and the material flowing in the volumes 1 and 2. Energy is also dissipated in the conical region *M-Q-R-X* of volume 1 and in the conical and cylindrical regions *M-T-U-V* and *T-U-V-B-I-K* of volume 2. In these regions the flow is a plane-strain motion and the rate of dissipation of energy can be calculated as in the velocity field in Fig. 9. The total rate of dissipation of energy is obtained by adding the rate of dissipation of energy due to the discontinuity surfaces.

It is found that the velocity field will be kinematically admissible if the average pressure on the rectangle is not less than $k$ times the expression

$$h = 2(\alpha_2 + \beta_2) + \cot \alpha_2 + \cot \beta_2 +$$

$$\frac{1}{2}\frac{c}{a}\left[\alpha_1 + \beta_1 + \left(1 + \frac{c^2}{b^2}\sin^2\beta_1\right)^{1/2}(\alpha_1 + \beta_1 + \cot\alpha_1 + \cot\beta_1) + \left(1 + \frac{b^2}{c^2}\sin^2\beta_2\right)^{1/2}(\alpha_2 + \beta_2 + \cot\alpha_2 + \cot\beta_2) - 3(\alpha_2 + \beta_2) - 2\cot\alpha_2 - 2\cot\beta_2\right] \quad [8]$$

where $\alpha_1$, $\alpha_2$ are the angles, *R-S-X*, *B-E-K*, respectively. By Theorem 2, $k$ times Expression [8] is an upper bound for the collapse value of the average indentation pressure. The substitution of the values $c = b/\sqrt{2}$, $\alpha_1 = 46°17'$, $\beta_1 = 39°$, $\alpha_2 = 47°4'$ $\beta_2 = 34°$ in the expression gives the upper bound

$$k\left(5.24 + 0.17\,\frac{b}{a}\right) \quad [9]$$

Thus for a square, for which $b = a$, Expression [9] gives the value $5.71k$, which is a better upper bound for the square punch than those obtained previously. For rectangles for which $b/a < 0.53$, a better upper bound than Expression [9] is obtained by putting $c = b/\sqrt{2}$, $\alpha_1 = 46°17'$, $\beta_1 = 39°$, $\alpha_2 = \beta_2 = 45°$ in Equation [8] to give

$$k\left(5.14 + 0.66\,\frac{b}{a}\right) \qquad [10]$$

This expression tends to the value $5.14k$ for rectangles whose length is great compared with their breadth, in agreement with the upper bound for the two-dimensional flat punch.

The same value of $(2 + \pi)k$ is an upper bound for any uniformly loaded area as distinguished from an area loaded by a punch. This follows directly from the fact that kinematically admissible velocity fields for this problem are not restricted by the condition that the loaded area move as a plane surface. Therefore the region immediately adjacent to the boundary of the area of contact can escape outward in a manner essentially that of the plane-strain motion as shown in the right half of Fig. 3(*a*). Point *B* is then a point on the boundary; *B-C* lies in the interior; *B-E* is exterior. The value of $(2 + \pi)k$ is obtained by letting *B-C* approach zero.

## BIBLIOGRAPHY

1 "Über die Haerte plastischer Koerper," by L. Prandtl, Nachrichten von der Koeniglichen Gesselschaft der Wissenschaften zu Goettingen, Mathematisch-Physikalische Klasse, 1920, pp. 74–85.

2 "The Plastic Yielding of Notched Bars Under Tension," by R. Hill, *Quarterly Journal of Mechanics and Applied Mathematics*, vol. 2, 1949, pp. 40–52.

3 "Limit Design of Beams and Frames," by H. J. Greenberg and W. Prager, Proceedings of the American Society of Civil Engineers, vol. 77, February, 1951, Separate No. 59.

4 "The Safety Factor of an Elastic-Plastic Body in Plane Strain," by D. C. Drucker, H. J. Greenberg, and W. Prager, JOURNAL OF APPLIED MECHANICS, Trans. ASME, vol. 73, 1951, pp. 371–378.

5 "Extended Limit Design Theorems for Continuous Media," by D. C. Drucker, W. Prager, and H. J. Greenberg, *Quarterly of Applied Mathematics*, vol. 9, 1952, pp. 381–389.

6 "On Plastic-Rigid Solutions and Limit Design Theorems for Elastic-Plastic Bodies," by D. C. Drucker, H. J. Greenberg, E. H. Lee, and W. Prager, Proceedings of the First U. S. National Congress of Applied Mechanics, June, 1951, pp. 533–538.

7 "Über einige statisch bestimmte Faelle des Gleichgewichts in Plastischen Koerpern," by H. Hencky, *Zeitschrift für Angewandte Mathematik und Mechanik*, vol. 3, 1923, pp. 241–251.

8 "The Problem of Plasticity With Axial Symmetry and Brinell's Test," by A. Iu Ishlinsky, *Prikladnaia Matematika i Mekhanika*, vol. 8, 1944, pp. 201–224.

9 "Zur Theorie der Spannungszustaende in plastischen und sandartigen Medien," by A. Haar and Th. von Kármán, Nachrichten von der Koeniglichen Gesellschaft der Wissenschaften zu Goettingen, Mathematisch-physikalische Klasse, 1909, pp. 204–218.

10 "A More Fundamental Approach to Stress-Strain Relations," by D. C. Drucker, Proceedings of the First U. S. National Congress of Applied Mechanics, June, 1951, pp. 487–491.

11 "Limit Design of Reinforcements of Cut-Outs in Slabs," by P. G. Hodge, Jr., and W. Prager, Brown University Report B11-2 to Office of Naval Research, August, 1951.

12 "The Interaction of Discontinuity Surfaces in Plastic Fields of Stress," by A. Winzer and G. F. Carrier, JOURNAL OF APPLIED MECHANICS, Trans. ASME, vol. 70, 1948, p. 261.

13 "Theory of Perfectly Plastic Solids," by W. Prager and P. G. Hodge, Jr., John Wiley & Sons, Inc. New York, N. Y., 1951, pp. 158–163.

# Transverse Impact on Beams and Plates[1]

By A. C. ERINGEN,[2] LAFAYETTE, IND.

**Flexural deflections of several plates and beams under an unknown transverse, concentrated, time-dependent force are solved for various edge conditions. The consideration of displacements and the use of Hertz's law of impact at the point of contact lead to a nonlinear integral equation for the contact force in all cases of transverse impact. Two methods are introduced to treat this equation: (*a*) Generalized Galerkin method; (*b*) collocation method. Method (*a*) is the generalization of the well-known Galerkin method which is suitable for the problems in which part of the boundary is unknown in advance, while certain conditions are given there. The method is applicable to a very large class of differential and integral equations. The collocation method leads to a quick, reasonable, approximate solution. Various auxiliary curves in both cases reduce the solution to a routine. Examples are worked out and plotted for various beams and plates. Deflections are plotted.**

## Introduction

THE problem of central impact of a sphere on a simply supported beam has been formulated and solved, first by Timoshenko (2, 3).[3] He obtained a nonlinear integral equation for the contact force and solved it by stepwise numerical integration procedure. Various other authors (4, 5, 6, 7, 8) have devised approximate methods to solve Timoshenko's integral equation. A criticism of these methods is given by Lee (5) and Hoppmann (7) and the present author (9).

The impact problem involving beams with different types of support conditions and plates with different shapes and noncentral impact problems are as yet untouched, except for the paper by K. Karas (10). He treats the problem of central impact on simply supported rectangular plates using the method given by Lennertz (4) and the step-by-step integration method. Again, the Lennertz method is found to be unsatisfactory.

Application of the energy method devised by Zener and Feshbach (6), and applied by Lee (5) and Hoppmann (7, 8) to beam problems gives very satisfactory results. However, application of this method to plate problems is rather lengthy and leads to a considerable inaccuracy in contact time and force since neither is determined from the integral equation.

In the present paper the problem of noncentral impact on beams and plates having general edge conditions is formulated in such a way as to unify the transverse-impact problems. An integral equation is obtained which is valid for all impact problems. Two general methods are then introduced to solve the integral equation of the impact: (*a*) generalized Galerkin method; (*b*) collocation method.[4]

These methods are applied to various beam and plate problems for the purpose of comparison and for obtaining an idea about reliability of the methods.

A few auxiliary curves are drawn to shorten the computation. Moreover, equations of these curves are given for all plate and beam problems in a standard form. Consequently, to solve plate and beam problems involving new types of boundaries these curves can be drawn once and for all, reducing the problem of impact to a routine. Deflections also are given for the examples worked out in this paper.

## Formulation of the Problem

A beam or a plate is struck transversely by a mass $m$ having a spherical surface at the point of contact, and striking velocity $v_0$, Fig. 1.

The problem is to determine the contact force $F(t)$, deflection $w(x, t)$, and the flexural stresses.

Deflection and the stresses are functionals of the contact force $F(t)$. Consequently, $F(t)$ must be determined first.

The formulation of this problem can be effected only under certain assumptions; namely, (*a*) all assumptions of the classical theory of plates or beams are applicable; (*b*) the Hertz law of impact is valid (11). The last assumption states that

$$\alpha = k F^{2/3}(t) \qquad [1]$$

where $\alpha$ is the relative approach of striking bodies and $k$ is the Hertz constant (12, 13, 14). The relative approach is the difference between displacements of the plate and the striking body measured from the instant of initial contact, Fig. 1. Hence

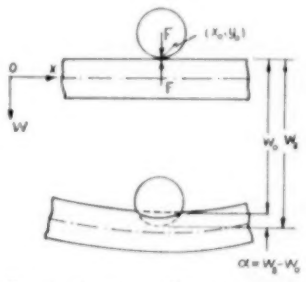


Fig. 1 Sketch of Displacements

$$\alpha = w_s - w_0 \qquad [2]$$

where $w_s$ is the displacement of the sphere under the action of the force $F(t)$ and $w_0$ is the deflection of the plate at the point of contact. Here $w_s$ is given by

$$w_s = v_0 t - \frac{1}{m} \int_0^t (t - \tau) F(\tau)\, d\tau \qquad [3]$$

The deflection of the beam or the plate is in turn obtained by solving the following differential equation

---

[1] The results were obtained in the course of research conducted under Contract N7onr-32909, sponsored by the Office of Naval Research, United States Department of the Navy (1).[3] Presented at The Eighth International Congress on Theoretical and Applied Mechanics, Istanbul University, Istanbul, Turkey, August 20–28, 1952.

[2] Associate Professor of Engineering Mechanics, Purdue University; formerly Research Associate Professor, Illinois Institute of Technology, Chicago, Ill.

[3] Numbers in parentheses refer to Bibliography at end of paper.

Presented at the National Conference of the Applied Mechanics Division, Minneapolis, Minn., June 18–20, 1953, of The American Society of Mechanical Engineers.

Discussion of this paper should be addressed to the Secretary, ASME, 29 West 39th Street, New York, N. Y., and will be accepted until January 11, 1954, for publication at a later date. Discussion received after the closing date will be returned.

Note: Statements and opinions advanced in papers are to be understood as individual expressions of their authors and not those of the Society. Manuscript received by ASME Applied Mechanics Division, October 20, 1952. Paper No. 53—APM-27.

[4] For other methods see reference (9).

$$D\Delta^2 w + \frac{\rho}{g}\frac{\partial^2 w}{\partial t^2} = q(x, y, t) \quad [4]$$

$$D = Eh^3/12(1 - \nu^2), \quad \Delta = \frac{\partial^2}{\partial x^2} + \frac{\partial^2}{\partial y^2} \quad [5]$$

Here $E$ is Young's modulus, $h$ is the thickness, $\rho$ is the weight density per unit area, $g$ is the acceleration due to gravity, $q$ is the load per unit area. Equation [4] reduces to beam equation if one takes $EI$ for $D$ and $y = \partial/\partial y = 0$. In this case, $\rho$ and $q$ must be interpreted as the weight density and the load per unit length. In the following analysis beam and plate problems are interpreted as one. The difference is in the additional dimension $y$ and the interpretation of $D$ and $\rho$ which can be adjusted easily to unify the method of solution. The resulting formulas, however, will be given separately for beams and plates.

The concentrated load $F(t)$ is obtained as a limiting process of a uniformly distributed load $q$ over a small area $\epsilon^2$ having the shape of the plate boundary. In beams, $q$ is distributed uniformly over a range $\epsilon$. Thus, by letting $q \to \infty$ while $\epsilon \to 0$, the contact force $F(t)$ is obtained

$$F(t) = \lim_{\substack{\epsilon \to 0 \\ q \to \infty}} \int_{(A)} q \, dA \quad [6]$$

Hence Equations [4] with $q$ subject to [6] must be solved under appropriate initial and boundary conditions to obtain $w_0$. Once this is done, the force $F(t)$ can then be evaluated by solving the integral equation obtained by combining Equations [1] to [3], namely

$$kF^{3/2}(t) = v_0 t - \frac{1}{m}\int_0^t (t - \tau) F(\tau) \, d\tau - w_0 \quad [7]$$

## Flexural Deflection

Deflection $w$ of a plate or a beam is uniquely determined when Equation [4] is solved under appropriate initial and boundary conditions. Initial conditions are

$$w(x, y, 0) = 0 \quad \dot{w}(x, y, 0) = 0 \quad [8]$$

where the dot represents differentiation with respect to time. Boundary conditions used in practice have great variety. These conditions consist of specifying any two of the following four quantities or their linear combinations on the boundary: Given

$$w, \ \partial w/\partial n, \ M_n, \ V_n \quad [9]$$

Here $n$ represents the external normal to the boundary curve and $M_n$ is the bending moment and $V_n$ is the transverse shear resultant which is represented by the Kirchhoff condition in classical plate theory.

In what follows first a general solution of Equation [4] is found which satisfies initial conditions, Equations [8], and some arbitrary boundary conditions.

Dirac-delta function $\delta(x - x_0)$ is defined by

$$\delta(x - x_0) = \begin{cases} \infty & \text{for } x = x_0 \\ 0 & \text{for } x \neq x_0 \end{cases} \quad \text{and}$$

$$\int_{(A)} \delta(x - x_0)\,\delta(y - y_0)\, dA = 1 \quad [10]$$

where the double integral in Equation [10] is taken over the whole area $A$ of the plate.

Let the time-dependent concentrated load $F(t)$ be applied to the point with co-ordinate $(x_0, y_0)$. Differential Equation [4] can be written in a convenient form by using Equations [6] and [10]

$$D\Delta^2 w + (\rho/g)\ddot{w} = \delta(x - x_0)\,\delta(y - y_0)\,F(t) \quad [11]$$

The solution of this equation is a linear, homogeneous functional of $F(t)$. Thus

$$w(x, y, t) = \int_0^t G(x, y, t - \tau)\,F(\tau)\,d\tau \quad [12]$$

Substitution of Equation [12] into Equations [11] and [8] gives

$$D\Delta^2 G + (\rho/g)\ddot{G} = 0 \quad [13]$$

$$G(x, y, 0) = 0, \ (\rho/g)\dot{G}(x, y, 0) = \delta(x - x_0)\,\delta(y - y_0) \quad [14]$$

The general solution of Equation [13] satisfying the first initial condition given by the first of Equations [14] and all boundary conditions is

$$G = \sum_{m,n} a_{mn}\, g_{mn}(x, y) \sin \alpha_{mn} t \quad (m, n = 1, 2, \ldots) \quad [15]$$

where $a_{mn}$ are arbitrary, and $g_{mn}$ are free of arbitrary constants and satisfy all boundary conditions and the differential equation

$$\Delta^2 g_{mn} - p_{mn}^4 g_{mn} = 0 \quad [16]$$

$$p_{mn}^4 = \rho\,\alpha_{mn}^2/g\,D \quad [17]$$

Functions $g_{mn}$ are the eigenfunctions. Quantities $p_{mn}$ are the eigenvalues and are determined from a frequency equation which will be known when the boundary conditions are given explicitly. Term $a_{mn}$ must now be determined from the second of Equations [14]

$$\sum_{m,n} (\rho/g) a_{mn}\,\alpha_{mn}\, g_{mn}(x, y) = \delta(x - x_0)\,\delta(y - y_0) \quad [18]$$

When eigenfunctions are not orthogonal this represents a difficult problem and there is no universal method of determining $a_{mn}$. In many cases it is possible to use the method used for orthogonal eigenfunctions except that the Series [15] must be employed to sum the resulting series. In many important practical problems the eigenfunctions are orthogonal. Consequently $a_{mn}$ can be determined simply by multiplying Equation [18] by $g_{rs}$ and integrating over the total area of the plate and considering the condition of orthogonality

$$\int_{(A)} g_{mn}\, g_{rs}\, dA = \begin{cases} b_{mn} & r = m, \quad n = s \\ 0 & r \neq m, \quad n \neq s \end{cases} \quad [19]$$

Hence

$$a_{mn} = g_{mn}(x_0, y_0)\, g/\rho\, b_{mn}\, \alpha_{mn} \quad [20]$$

Consequently

$$w(x, y, t) = (g/\rho) \sum_{m,n} (1/b_{mn})\, g_{mn}(x_0, y_0)\, g_{mn}(x, y) \int_0^t (1/\alpha_{mn})\, F(\tau) \sin \alpha_{mn}(t - \tau) d\tau \quad [21]$$

The deflection at the point of contact is therefore found to be

$$w_0 = (2/M) \sum_{m,n} c_{mn} \int_0^t (1/\alpha_{mn})\, F(\tau) \sin \alpha_{mn}(t - \tau)\, d\tau \quad [22]$$

$$c_{mn} = g_{mn}^2(x_0, y_0)\, A/2b_{mn} \quad [23]$$

where $A$ is the total area in case of plates and total length in case of beams, and $M$ is the total mass.

When the free-vibration problems of beams or plates are solved the eigenfunctions $g_{mn}$ and eigenvalues $p_{mn}$ (consequently $\alpha_{mn}$) will be known. Thus the determination of $b_{mn}$ from Equation [19] and $c_{mn}$ from Equation [23] presents no difficulty.

A few practical examples for beams and plates will be given. In all examples eigenfunctions are represented by $g_n$ or $g_{mn}$ and the frequency equation is marked by (FE). Symbols $n$ and $m$ represent positive integers.

(*a*) *Beams.* Eigenfunctions and eigenvalues of the following examples are known (15). Thus $b_n$ and $c_n$ are calculated by using Equations [19] and [23], since in all these cases the eigenfunctions are orthogonal. The origin is at one end of the beam.

*Simply Supported Beams*

$$g_n(x) = \sin n\pi x/L, \quad \alpha_n = n^4\pi^4 g\,EI/\rho\,L^4 \quad \text{(FE)}$$
$$b_n = L/2, \quad c_n = \sin^2 n\pi x_0/L \qquad \ldots [24]$$

*Beams Having Both Ends Clamped*

$$g_n(x) = \frac{\sinh\frac{1}{2}p_nL - \sin\frac{1}{2}p_nL}{\sinh\frac{1}{2}p_nL - \sin\frac{1}{2}p_nL}\left(\sinh\frac{1}{2}p_n(2x-L) - \sin\frac{1}{2}p_n(2x-L)\right)$$
$$\cos p_nL = \operatorname{sech} p_nL \quad \text{(FE)} \qquad \ldots [25]$$
$$b_n = \frac{1}{p_n}\left[\frac{p_nL + \sinh p_nL}{1-\cosh p_nL} + \frac{p_nL + \sin p_nL}{1-\cos p_nL}\right]$$
$$c_n = g_n^2(x_0)L/2\,b_n$$

*Cantilever Beams Clamped at $x = 0$*

$$g_n(x) = \frac{\cosh p_nx - \cos p_nx}{\cosh p_nL + \cos p_nL} - \frac{\sinh p_nx - \sin p_nx}{\sinh p_nL + \sin p_nL}$$
$$\cos p_nL = -\operatorname{sech} p_nL \quad \text{(FE)} \qquad \ldots [26]$$
$$b_n = p_n^{-1}(\cosh p_nL - \cos p_nL)^{-2} \times \left(p_nL - \frac{\cos p_nL - \cosh p_nL}{\sin p_nL + \sinh p_nL}\right)$$
$$c_n = g_n^2(x_0)\,L/2b_n$$

*Beams Pinned at $x = 0$ and Clamped at $x = L$*

$$g_n(x) = \frac{\sinh p_nx}{\sinh p_nL} - \frac{\sin p_nx}{\sin p_nL}$$
$$\tan p_nL = \tanh p_nL \text{ (FE)} \qquad \ldots [27]$$
$$b_n = \frac{L}{2}(\sin^{-2}p_nL - \sinh^{-2}p_nL), \quad c_n = g_n^2(x_0)L/2b_n$$

(*b*) *Circular Plates.* Eigenfunctions and eigenvalues of the following examples are known (15). Equations [19] and [23] give $b_n$ and $c_n$, respectively, since in both of these cases eigenfunctions are orthogonal. The origin is taken at the center of the plate. The outer radius is $a$. Polar co-ordinates $r$ and $\theta$ are used.

*Simply Supported Circular Plate*

$$g_{mn}(r,\theta) = [J_n(p_mr) + BI_n(p_mr)]\sin(n\theta + \gamma_n)$$
$$B = -J_n(p_ma)/I_n(p_ma) \qquad \ldots [28]$$

where $J_n$ and $I_n$ are the Bessel functions of the first kind with real and imaginary arguments

$$\frac{I_{n+1}(p_ma)}{I_n(p_ma)} + \frac{J_{n+1}(p_ma)}{J_n(p_ma)} = \frac{2p_ma}{1-\nu} \quad \text{(FE)} \qquad \ldots [29]$$

Here $\nu$ is the Poisson's ratio.

$$b_{mn} = 2\pi a^2 J_n^2(p_ma)\left[\frac{1+\nu+2n}{\nu-1} - 2\left(\frac{p_ma}{1-\nu}\right)^2 + 2\,\frac{p_ma}{1-\nu}\,\frac{J_{n+1}(p_ma)}{J_n(p_ma)}\right]$$
$$c_{mn} = g_{mn}^2(r_0,\theta_0)\pi a^2/2b_{mn} \qquad \ldots [30]$$

*Circular Plate Clamped at Outer Edge*

$$g_{mn}(r,\theta) = [J_n(p_mr) + BI_n(p_mr)]\sin(n\theta + \gamma_n)$$
$$B = -J_n(p_ma)/I_n(p_ma) \qquad \ldots [31]$$

$$\frac{J_{n+1}(p_ma)}{J_n(p_ma)} + \frac{I_{n+1}(p_ma)}{I_n(p_ma)} = 0 \quad \text{(FE)} \qquad \ldots [32]$$

$$b_{mn} = 2\pi a^2 J_n^2(p_ma), \quad c_{mn} = g_{mn}^2(r_0,\theta_0)/4J_n^2(p_ma) \qquad \ldots [33]$$

(*c*) *Rectangular Plates.* For rectangular plates a quick method similar to the one used for beams can be used to obtain boundary conditions which will produce orthogonal eigenfunctions.

The following is constructed from Equation [16]

$$\int_0^b\int_0^a (g_{rs}\Delta^2 g_{mn} - g_{mn}\Delta^2 g_{rs})\,dx\,dy = (p_{mn}^4 - p_{rs}^4)\int_0^b\int_0^a g_{mn}\,g_{rs}\,dx\,dy \qquad \ldots [34]$$

Integration by part of the left side of this equation leads to

$$(p_{mn}^4 - p_{rs}^4)\int_0^b\int_0^a g_{mn}g_{rs}\,dx\,dy = \int_0^b\left[g_{rs}\frac{\partial^3 g_{mn}}{\partial x^3} - \frac{\partial g_{rs}}{\partial x}\frac{\partial^2 g_{mn}}{\partial x^2} + \frac{\partial^2 g_{rs}}{\partial x^2}\frac{\partial g_{mn}}{\partial x} - \frac{\partial^3 g_{rs}}{\partial x^3}g_{mn} + \frac{\partial^3 g_{rs}}{\partial y^2}\frac{\partial g_{mn}}{\partial x} - \frac{\partial^3 g_{rs}}{\partial y^2\partial x}\right]_{x=0}^{x=a}dy \qquad \ldots [35]$$

and a similar equation for $y = 0$ and $b$ which may be obtained by interchanging $x$ with $y$. The bracket on the right side of Equation [35] is zero for two types of practical boundaries, namely, simple support and clamped edge. Consequently, these two types of support conditions in any order lead to normal modes. Many other conditions can be obtained by making the bracket on the right side of Equation [35] zero, with the proper choice of $g$ and its derivatives. The following two examples are most practical:

*Rectangular Plates Simply Supported at All Edges:* Two perpendicular sides with lengths $a$ and $b$ are taken as the co-ordinate axis, origin being at a corner

$$g_{mn}(x,y) = \sin\frac{m\pi x}{a}\sin\frac{n\pi y}{b}, \quad \alpha_{mn}^2 = \frac{gD}{\rho}\,p_{mn}^4 \quad \text{(FE)}$$
$$p_{mn}^2 = [(m\pi/a)^2 + (n\pi/b)^2], \quad b_{mn} = ab/4$$
$$c_{mn} = 2\left(\sin\frac{m\pi x_0}{a}\sin\frac{n\pi y_0}{b}\right)^2 \qquad \ldots [36]$$

*Rectangular Plate Simply Supported Along $x = 0,\ a$; Clamped Along $y = 0, b$*

$$g_{mn}(x,y) = \cosh\alpha y - \cos\beta y - B\left(\sin\beta y - \frac{\beta}{\alpha}\sinh\alpha y\right)$$
$$B = (\cosh\alpha b - \cos\beta b)\Big/\left(\sin\beta b - \frac{\beta}{\alpha}\sinh\alpha b\right)$$
$$\alpha = [p_{mn}^2 + (m\pi/a)^2]^{1/2}, \quad \beta = [p_{mn}^2 - (m\pi/a)^2]^{1/2} \qquad \ldots [37]$$

$$(\cos \beta b - \cosh \alpha b)^2 + \left(\sin \beta b - \frac{\beta}{\alpha} \sinh \alpha b\right)$$
$$\left(\sin \beta b + \frac{\alpha}{\beta} \sinh \alpha b\right) = 0 \text{ (FE)} \quad \ldots [38]$$

$$b_{mn} = \frac{1}{4} ab\left(1 + \frac{\beta^2}{\alpha^2}\right) + \frac{1}{4} \frac{a}{\alpha}\left(\sin \beta b - \frac{\beta}{\alpha} \sinh \alpha b\right)^{-1}$$
$$\left\{\left[\left(1 - \frac{\beta^2}{\alpha^2}\right) \sinh \alpha b \sin \beta b - 2 \frac{\beta}{\alpha} \cosh \alpha b \cos \beta b\right]\right. \quad [39]$$
$$\left(\cosh \alpha b + \frac{\alpha^2}{\beta^2} \cos \alpha b\right)$$
$$\left. + 2 \frac{\alpha}{\beta}\left(\cosh \alpha b + \frac{\beta^2}{\alpha^2} \cos \beta b\right)\right\}$$
$$c_{mn} = g_{mn}^2(x_0, y_0) ab/2b_{mn}$$

## The Integral Equation

In the previous section it is shown that in all impact problems the flexural deflection at the point of contact is given by Equation [22]. The integral Equation [7] of impact can be written in a common nondimensional form as

$$L(f) \equiv af^{3/2}(x) - x + \int_0^x K(x - y) f(y)\, dy = 0 \quad [40]$$

$$f(x) = T_0 F(T_0 x)/mv_0, \quad K(x) = x$$
$$+ 2\mu \sum_{m,n} \frac{c_{mn}}{\omega_{mn}} \sin \omega_{mn} x, \quad \mu = m/M \quad [41]$$
$$x = t/T_0, \quad a = k\, m^{-1/2} v_0^{-1/2} T_0^{-5/2}, \quad \omega_{mn} = \alpha_{mn} T_0$$

where $T_0$ may be chosen in a suitable manner. Here $c_{mn}$ and $\omega_{mn}$ are given by the solution of the flexure problem.

Another form of Equation [40], which will be used later, is

$$a\phi(x) - x + \int_0^x K(x - y)\, \phi^{3/2}(y)\, dy = 0, \quad \phi(x) = f^{2/3}(x) \quad [42]$$

## Generalized Galerkin Method

In accordance with the fundamental lemma of the calculus of variations (16), in order that the integral $I$

$$I = \int_{x_1}^{x_2} L(f) \psi(x)\, dx \quad \ldots [43]$$

be zero for every permissible variation of an arbitrary function $\psi(x)$, the operator $L$, applied to function $f(x)$, must be zero.

*Theorem:* Let

$$f(x) = f(x, a_1, a_2, \ldots) \quad \ldots [44]$$

where $a_i$ are unknown parameters and $f(x, a_1, a_2, \ldots)$ has a known form. Let also $f_i \equiv \partial f/\partial a_i$ be linearly independent functions and $f_i$ be complete. Let $a_i$ be determined from infinitely many equations

$$\int_{x_1}^{x_2} L\,[f(x, a_1, a_2, \ldots)] f_i\, dx = 0 \quad (i = 1, 2, \ldots) \quad [45]$$

Then it will be proved that $f(x, a_1, a_2, \ldots)$ determined this way is a solution of the equation

$$L(f) = 0 \quad \ldots [46]$$

*Proof:* Multiply Equations [45] by arbitrary constants $b_i$ and sum up with respect to $i$. Hence

$$\int_{x_1}^{x_2} L\,[f(x, a_1, a_2, \ldots)] \sum_i b_i f_i(x, a_1, a_2, \ldots)\, dx = 0 \quad [47]$$

Here $f_i$ are linearly independent and complete. Hence $\sum_i b_i f_i(x, a_1, a_2, \ldots)$ is the expansion of an arbitrary function $\psi(x)$. Equation [47] is thus identical to Equation [43].[5] Thus $f(x, a_1, a_2, \ldots)$ by the fundamental lemma of the calculus of variations, satisfies Equation [46]. This completes the proof.

In practice it is not easy to solve such an infinite system of nonlinear equations represented by Equations [45]. Thus approximation may be made by choosing only a finite number of parameters. Hence, in application of the generalized Galerkin method, Equation [40] is not satisfied exactly but an approximate $f$ is used and chosen so as to make the error $L(f)$ as small as possible in an average sense, over the interval of interest. This average takes the form of certain integrals which are minimized.

The present method contains the well-known Galerkin method. This can be proved by letting $f_i(x, a_1, a_2, \ldots)$ be linear in $a_i$; that is, $f(x) = \sum_i a_i f_i(x)$, which is the known form used in the classical Galerkin method.

## Approximate Solutions of Impact Problem by Generalized Galerkin Method

Let $L(f)$ be given by Equation [40].

Various functions of the following type are suitable to use as $f(x, a_1, a_2, \ldots)$

$$(a)\ f = a_1 \sin a_2 x, \quad (b)\ f = a_1 \sin^{3/2} a_2 x$$
$$(c)\ f = a_1 \sin a_2 x, \quad (d)\ f = \sum_{i=1}^{N-1} a_i \sin i\, a_N x$$

Hence Equations [45] take the form

$$\int_0^{\pi/a_N} L(f)\,(\partial f/\partial a_i)\, dx = 0, \qquad (i = 1, 2, \ldots, N) \quad [48]$$

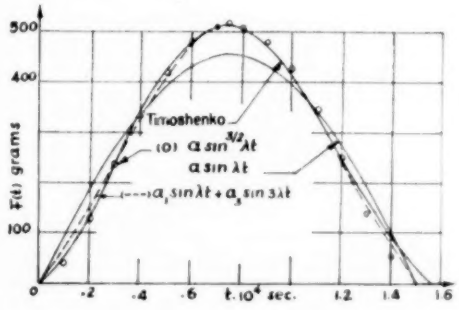


Fig. 2 Generalized Galerkin Method, Beam No. 1

In all examples worked out, very good approximations are obtained. Cases $(b)$ and $(c)$ give better result than case $(a)$ (see

[5] For boundary-value problems, Euler's equation of the calculus of variations leads to additional terms on $\psi$ on the right side of Equation [45]. Either these additional conditions on $\psi$ or the boundary conditions on $f$ must be satisfied at the boundary. Another alternative is to satisfy the conditions on $\psi$, on one part of the boundary, and the conditions on $f$, on the remaining part of the boundary. In the present problem these conditions are $\psi = 0$ or $L(f) = 0$ at either end of the contact interval of which the latter is satisfied everywhere; hence we need not worry about the end conditions.

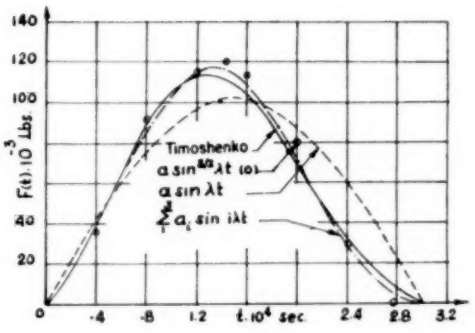


FIG. 3 GENERALIZED GALERKIN METHOD, BEAM NO. 2

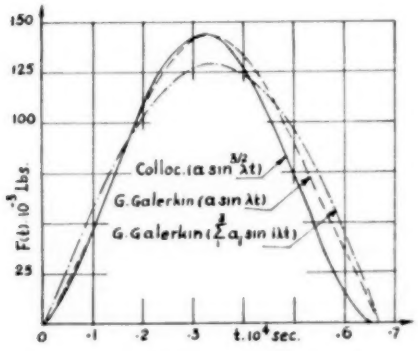


FIG. 4 BOTH METHODS FOR CIRCULAR PLATE

Figs. 2, 3, and 4). In case $(d)$ $a_N$ is chosen as $a_2$ of case $(a)$ since $a_2$ of case $(a)$ is found to be nearly equal to exact value.

Explicit forms of Equations [48] will be given for cases $(a)$, $(b)$, and $(d)$. Computations are carried out for cases $(a)$, $(c)$, and $(d)$.

*Case (a)*

$$\left.\begin{aligned}\left(\frac{1}{2}+2\mu\alpha_1\right)A_1+d\gamma A_1^{3/2}&=1\\ \left(\frac{7}{8}-\frac{1}{4}\mu\delta\right)A_1+\frac{3}{10}d\gamma A_1^{3/2}&=1\end{aligned}\right\}\quad\ldots\ldots[49]$$

Elimination of $A_1$ gives

$$\gamma=\pi^{-1}a_2^{3/2}=\frac{15-10\,\mu(\delta+8\alpha_1)}{d\,28^{3/2}\,[29-\mu(10\delta+24\alpha_1)]^{1/2}}\quad\ldots[49a]$$

*Case (b)*

$$\left.\begin{aligned}\left(\frac{\pi}{6}-\frac{5}{8\pi}+\frac{\mu}{4\pi}\alpha_1'\right)A_1+d'\gamma A_1^{3/2}&=1\\ \left(\frac{\pi}{4}-\frac{9}{32\pi}+\frac{\mu}{4\pi}\delta'\right)A_1+\frac{3}{10}d'\gamma A_1^{3/2}&=1\end{aligned}\right\}\quad\ldots[50]$$

*Case (d)*

$$\sum_{i\neq j}^{N-1}(1+2\mu\beta_{ij})A_i+[1-\tfrac{1}{2}(-)^{j-1}]A_j+2\mu\alpha_j a_j+(-)^{j+1}\gamma\eta_j A_1^{3/2}=1\quad(j=1,2,\ldots)\quad\ldots\ldots[51]$$

where

$$\left.\begin{aligned}&\alpha_i=\beta_{ii}+(-)^i\tfrac{1}{2}\beta_{i},\quad\delta=\beta_1-4\delta_1,\quad A_i=a_i\,a_N\\ &\gamma=a\,a_N^{3/2}/\pi,\quad d=\pi^{1/2}\,\Gamma(4/3)/\Gamma(11/3)\doteq 1.68257\\ &\delta_1=\sum_{m,n}c_{mn}\,[(1-\lambda_{mn}^2)^{-2}\cos\pi\lambda_{mn}+(1-\lambda_{mn}^2)^{-3}\\ &\qquad(1+\lambda_{mn}^2)(\pi\lambda_{mn})^{-1}\sin\pi\lambda_{mn}]\\ &\beta_i=\sum_{m,n}c_{mn}\,[1-(\lambda_{mn}/i)^2]^{-1},\quad\lambda_{mn}=\omega_{mn}/a_N\\ &\beta_{ij}=\sum_{m,n}c_{mn}\,[1-(\lambda_{mn}/i)^2]^{-1}[1-(\lambda_{mn}/j)^2]^{-1}\\ &\qquad(\pi\lambda_{mn})^{-1}\sin\pi\lambda_{mn},\ (i,j=1,2,\ldots)\end{aligned}\right\}\quad\ldots[52]$$

$$\left.\begin{aligned}\alpha_1'&=\sum_{m,n}c_{mn}\left[2(2/\lambda_{mn})^2-\left(1-\frac{1}{4}\lambda_{mn}^2\right)^{-1}-\frac{1}{\pi}\right.\\ &\qquad\left.\left(\frac{1}{2}\lambda_{mn}\right)^{-2}\left(1-\frac{1}{4}\lambda_{mn}^2\right)^{-2}\sin\pi\lambda_{mn}\right]\\ \delta'&=\sum_{m,n}c_{mn}\left[(2/\lambda_{mn})^2+\frac{1}{4}\left(1-\frac{1}{4}\lambda_{mn}^2\right)^{-1}\right.\\ &\qquad-\frac{1}{\pi}(2/\lambda_{mn})^3\left(1-\frac{1}{4}\lambda_{mn}^2\right)^{-2}\\ &\qquad\left.\sin\pi\lambda_{mn}-(2/\lambda_{mn})^3\left(1-\frac{1}{4}\lambda_{mn}^2\right)^{-2}\cos\pi\lambda_{mn}\right]\\ d'&=(14/5\,\pi^{3/2})\,\Gamma(7/6)/\Gamma(5/3)\end{aligned}\right\}\quad\ldots[53]$$

$$A_1^{3/2}\eta_j=\int_0^{\pi}\left(\sum_i A_i\sin i\,u\right)^{3/2}\sin j\,u\,du\quad(i,j=1,2,\ldots,N-1)\quad\ldots\ldots[54]$$

For $N=4$, $\eta_i$ have the explicit forms given in the following, which are obtained by using binomial expansion

$$\left.\begin{aligned}\eta_1&=1.682621+0.101974\,(3A_2/A_1)\\ \eta_2&=1.223724\,(2A_2/A_1)\\ \eta_3&=0.152967+1.265744\,(3A_2/A_1)\end{aligned}\right\}\quad\ldots\ldots[55]$$

$\alpha_i$, $\beta_{ij}$ $(i\neq j)$ and $\delta$ versus $\omega_i/a_2$ are plotted in Fig. 5 for central impact on simply supported beams.

With the help of these curves, Equations [49] or [49a] can be solved for $a_1$ and $a_2$ quickly.

Similar curves may be made for $\alpha_1'$ and $\delta'$ versus $\lambda_{ij}$ which make the computation time very short.

If the contact time $(\pi/a_2)$ is chosen by an approximate method

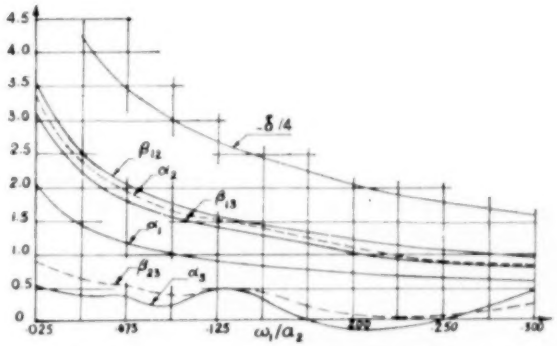


FIG. 5 CURVES FOR GENERALIZED GALERKIN METHOD, BEAM NO. 2

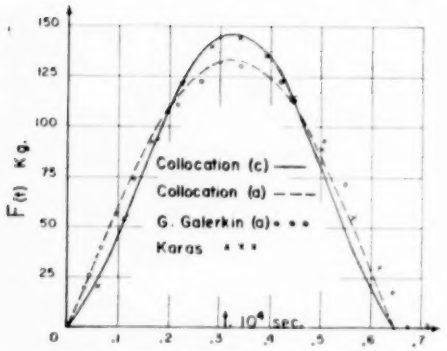


FIG. 6 BOTH METHODS FOR SQUARE PLATE

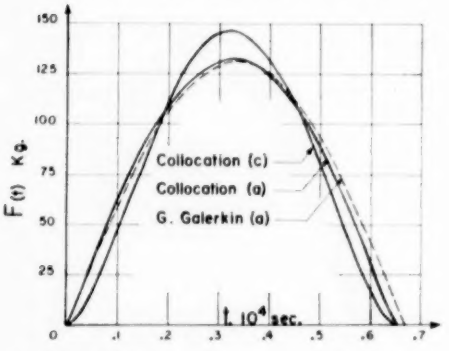


FIG. 7 BOTH METHODS FOR RECTANGULAR PLATE, $a/b = 2$

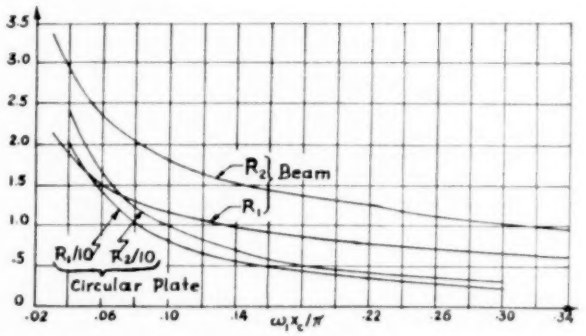


FIG. 8 CURVES FOR COLLOCATION METHOD FOR BEAMS AND CIRCULAR PLATES

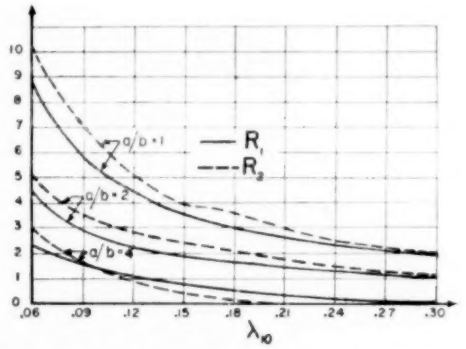


FIG. 9 CURVES FOR COLLOCATION METHOD FOR RECTANGULAR PLATES

as suggested by Zener and Feshbach and E. H. Lee, then only the first of Equations [49] or [50] must be used to determine $a_1$ which cuts down the computation to a few minutes. Determination of $a_2$ is faster if one uses an iteration, namely: take $\mu = 0$ in Equation [49*a*] ... and solve for $a_2^{(0)}$ using the curves for $\omega_1/a_2^{(0)}$ obtain functions $\delta^{(0)}$ and $\alpha_1^{(0)}$, then using [49*a*] obtain $a_2^{(1)}$ and so on.

Two simply supported beams and three simply supported plates under central impact have been worked out (Figs. 2, 3, 4, 6, and 7). Comparison between the present method and the reliable step-by-step method of integration used by S. Timoshenko is excellent. The shape function (*a*) gives almost zero error in contact time while maximum force has an error of 10 to 12 per cent. Shape function (*c*) almost coincides with the exact force curve.

Shape function (*d*) leads to a very reliable result. However, it is tedious and should be used as soon as contact time $\pi/a_2$ is determined by use of one of the other methods, say, case (*a*). It is believed, however, that in most engineering problems it is sufficient to use one of the shapes (*a*), (*b*), (*c*). The results for case (*d*) with $N = 4$ are also plotted in these figures.

## COLLOCATION METHOD

This method consists of satisfying the integral Equation [40] or [42] at various characteristic points. In a contact-force curve the important points are origin, the point of maximum of contact force, the end of contact time. The contact-force curve differs slightly from a symmetric shape. Thus choice of a symmetric curve is reasonable. Let $x_c$ be the unknown nondimensional contact time. Also let

$$\left.\begin{aligned} f(x) &= A^2 X(x), \quad X(0) = X(x_c) = 0, \quad X(x_c/2) = 1 \\ S(x) &= \int_0^x K(x-y)\, X(y)\, dy \end{aligned}\right\} \quad [56]$$

where $A^2$ is the unknown maximum amplitude. Equation [40] must be satisfied at $x = x_c/2$. Also $df/dx$ obtained from Equation [40] must be zero at this point. This leads to two equations to evaluate $A$ and $x_c$, namely

$$\left.\begin{aligned} A^3 &= S_{,x}^{-1}(x_c/2) \\ x_c/2 &= aS_{,x}^{-3/2}(x_c/2) + S(x_c/2)\, S_{,x}^{-1}(x_c/2) \end{aligned}\right\} \quad [57]$$

where

$$S_{,x}(x_c/2) = \left[\frac{d}{dx} S(x)\right]_{x = x_c/2}$$

Equations [57] also are valid if one uses Equation [42] and chooses

$$\left.\begin{aligned} \phi(x) &= A^2 Y(x), \quad Y(0) = Y(x_c) = 0, \quad Y(x_c/2) = 1 \\ S(x) &= \int_0^x K(x-y)\, Y^{3/2}(y)\, dy \end{aligned}\right\} \quad [58]$$

Hence, if shape functions $X(x)$ or $Y(x)$, having the conditions stated in Equations [56] or [58], are chosen, $A$ and $x_c$ can be calculated from Equations [57].

Three practical shape functions are

(*a*) $X(x) = \sin \pi x/x_c$

(*b*) $X(x) = \sin^2 \pi x/x_c$

(*c*) $Y(x) = \sin \pi x/x_c$

The results for $S$ and $S_{,x}$ in these cases may be written

$$\left.\begin{aligned} S(x_c/2) &= (x_c/\pi)^2 (d_1 + 2\mu R_1) \\ S_{,x}(x_c/2) &= (x_c/\pi)(d_2 + 2\mu R_2) \end{aligned}\right\} \quad \ldots\ldots [59]$$

where

*Case (a)*

$$\left.\begin{aligned} d_1 &= \frac{\pi}{2} - 1, \quad R_1 = \sum_{m,n} c_{mn} (1 - \lambda_{mn}^2)^{-1} \\ &\qquad [\lambda_{mn}^{-1} \sin(\pi\lambda_{mn}/2) - 1] \\ d_2 &= 1, \quad R_2 = \sum_{m,n} c_{mn} (1 - \lambda_{mn}^2)^{-1} \cos(\pi\lambda_{mn}/2), \\ &\qquad \lambda_{mn} = \omega_{mn} x_c/\pi \end{aligned}\right\} \quad \ldots [60]$$

*Case (b)*

$$\left.\begin{aligned} d_1 &= \frac{\pi^2 - 4}{16}, \quad R_1 = \frac{1}{8} \sum_{m,n} c_{mn} \left\{ 4\lambda_{mn}^{-2} \right. \\ &\qquad \left. - \left(1 - \frac{1}{4}\lambda_{mn}^2\right)^{-1} \left[1 - \frac{4}{p_{mn}^2} \cos(\pi\lambda_{mn}/2)\right] \right\} \\ d_2 &= \pi/4, \quad R_2 = \sum_{m,n} c_{mn} \lambda_{mn}^{-1} \left(1 - \frac{1}{4}\lambda_{mn}^2\right)^{-1} \\ &\qquad \sin(\pi\lambda_{mn}/2) \end{aligned}\right\} \quad \ldots [61]$$

*Case (c)*

$$\left.\begin{aligned} d_1 &= 0.457906, \quad R_1 = 0.915310\, R_1' - 0.011300\, R_1'' \\ d_2 &= 0.881409, \quad R_2 = 0.915310\, R_2' - 0.033901\, R_2'' \\ R_1' &= \text{Same as } R_1 \text{ of Case } (a); \\ &\qquad R_2' = \text{Same as } R_2 \text{ of Case } (a) \\ R_1'' &= \sum_{m,n} c_{mn} [1 - (\lambda_{mn}/3)^2]^{-1} \\ &\qquad [(3/\lambda_{mn}) \sin(\pi\lambda_{mn}/2) + 1] \\ R_2'' &= \sum_{m,n} c_{mn} [1 - (\lambda_{mn}/3)^2]^{-1} \cos(\pi\lambda_{mn}/2) \end{aligned}\right\} \quad \ldots [62]$$

For central impact on simply supported beams, simply supported circular plates, and rectangular plates $R_1$ and $R_2$ are plotted in Figs. 8 and 9 which make the computation very fast. Examples computed by this method using the shape function $(a)$ and $(c)$ are in excellent agreement with the result of step-by-step integration method (Figs. 4, 6, 7, 10, and 11). The first halves of the contact-force curves of the two theories are indistinguishable. Note that the energy method used by reference (5) gives correct maximum force, but there is a shift in time which makes the contact-force curve considerably inaccurate. No computation is made on the basis of shape function $(b)$. In case of multiple impact the collocation method would not be suitable to determine the contact force. In this case, the contact-force curve has more complicated shape. Double peaked pulse can occur. Hence the shape functions $(a)$, $(b)$, and $(c)$ of this section may not represent the contact force satisfactorily. It is believed, however, that the generalized Galerkin method using shape function $(d)$ would be suitable for this purpose. Otherwise, one must use the stepwise integration method.

Finally, the collocation method may be generalized further based on satisfying the integral equations at various other points (9).

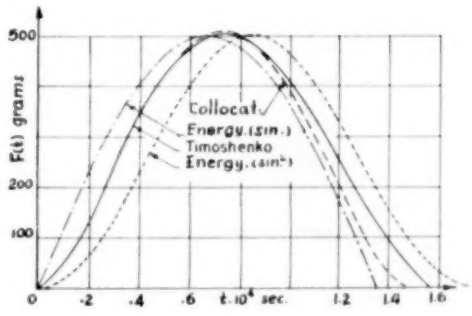


FIG. 10 COLLOCATION METHOD, BEAM NO. 1

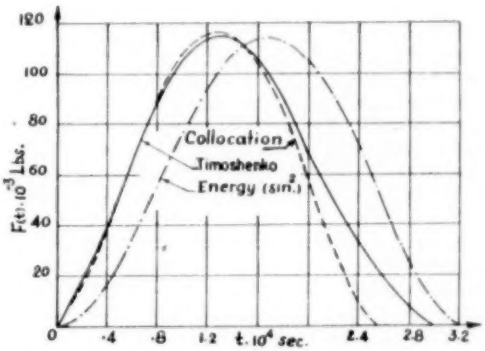


FIG. 11 COLLOCATION METHOD, BEAM NO. 2

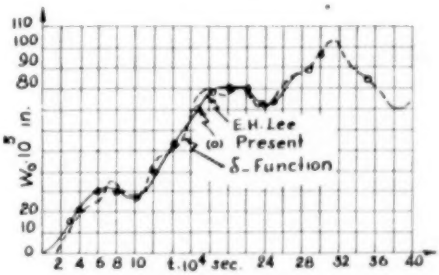


FIG. 12 DEFLECTION, BEAM NO. 2

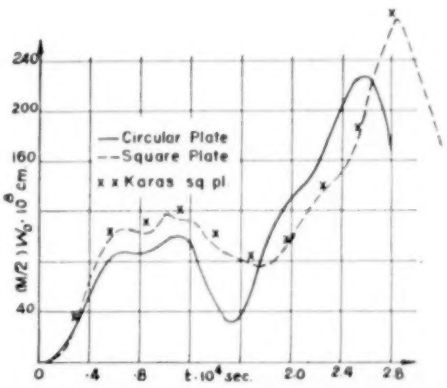


FIG. 13 DEFLECTION FOR CIRCULAR AND SQUARE PLATES

TABLE 1 PROBLEM DATA

| | $mg$ | $Mg$ | $v_0$ | $k$ | $\alpha_n$ rad/sec |
|---|---|---|---|---|---|
| Beam No. 1 | 33.34 gr | 122.2 gr | 1.0 cm/sec | $0.72715 \times 10^{-6}$ cm/gr$^{2/3}$ | $n^2\alpha_1$; $\alpha_1 = 2\pi \times 10^3$ 1/sec |
| Beam No. 2 | 50.0 lb | 298.5 lb | 132 in/sec | $4.4 \times 10^{-6}$ in/lb$^{2/3}$ | $n^2\alpha_1$; $\alpha_1 = 531$ 1/sec |
| Circular plate ($a$ = 10 cm, $h$ = 0.8 cm) | 2.0 kg | 0.03334 kg | 100 cm/sec | $0.727456 \times 10^{-4}$ cm/kg$^{2/3}$ | Roots of Eq. [29] used in Eq. [17]; also see ref. (1) |
| Rectangular plates $a = 20$, $h = 0.8$, $a/b = 1$ | 2.55 kg | 0.03334 kg | 100 cm/sec | $0.727456 \times 10^{-4}$ cm/kg$^{2/3}$ | $\alpha_{mn}$ of Eq. [36] with $\alpha_{10} = 0.622068 \times 10^4$ 1/sec |
| Rectangular plates $a = 20$, $h = 0.8$, $a/b = 2$ | 2.55 kg | 0.03334 kg | 100 cm/sec | $0.727456 \times 10^{-4}$ cm/kg$^{2/3}$ | $\alpha_{mn}$ of Eq. [36] with $\alpha_{10} = 0.622068 \times 10^4$ 1/sec |

where $k$ is calculated from $k = 1.230520\,(E^2/r_0)^{-1/3}$ where $E$ is common moduli of elasticity for both sphere and plates or beams and $r_0$ is radius of sphere.

### Deflection and Flexural Stresses

Deflection $w$ can be calculated from Equation [21] as soon as $F(t)$ is determined by one of the previous methods. Flexural stresses are then obtained by first finding bending moments which contain second derivatives of $w$. Convergence in $w$ is good but in stresses is slow. Plots of $w_0$ are made for the examples of this paper, Figs. 12 and 13. In Fig. 12 is also plotted deflection obtained by using Dirac $\delta$-function, having the same impulse as $F(t)$, for the contact force which is placed at the half of the contact time interval. The result is surprising—the deflection is practically independent of the shape of $F(t)$. Any shape for $F(t)$ with the correct impulse gives almost correct deflection. Hence the deflection must not be used as a criterion of accuracy for the shape $F(t)$. The situation for stresses, of course, is different.

Deflection $w_0$ of a simply supported square plate obtained by Karas with the use of numerical integration method is also in excellent agreement with the present theory, Fig. 13.

Finally, the data for the problems worked out in this paper are given in Table 1. Steel beams, circular plates, and rectangular plates are simply supported at the outer edges. The impact is central.

### Acknowledgment

The author is indebted to Mr. R. J. Bonthron and Mr. T. Taner for their assistance in the computation and in the analytical work.

### BIBLIOGRAPHY

1 "Transverse Impact on Beams and Plates With Arbitrary Edge Conditions," by A. Cemal Eringen, Technical Report No. 2, Office of Naval Research, Department of the Navy, Contract N7onr-32909, 1952.

2 "Zur Frage nach der Wirkung eines Stosses auf einer Balken," by S. Timoshenko, *Zeitschrift für Mathematik und Physik*, vol. 62, 1913, p. 198.

3 "Vibration Problems in Engineering," by S. Timoshenko, D. Van Nostrand Company, Inc., New York, N. Y. second edition, 1937, p. 394.

4 "Beitrag zur Frage nach der Wirkung eines Querstosses auf einen Stab," by J. Lennertz, *Ingenieur-Archiv*, vol. 8, part 1, 1937, pp. 37–46.

5 "The Impact of a Mass Striking a Beam," by E. H. Lee, Journal of Applied Mechanics, Trans. ASME, vol. 62, 1940, p. A-129.

6 "A Method of Calculating Energy Losses During Impact," by C. Zener and H. Feshbach, Journal of Applied Mechanics, Trans. ASME, vol. 61, 1939, p. A-67.

7 "Impact of a Mass on a Damped Elastically Supported Beam," by W. H. Hoppmann, Journal of Applied Mechanics, Trans. ASME, vol. 70, 1948, p. 125.

8 "Impact on a Multispan Beam," by W. H. Hoppmann, Journal of Applied Mechanics, Trans. ASME, vol. 72, 1950, p. 409.

9 "Impact on Elastic Beams," by A. Cemal Eringen, Technical Report No. 1, Office of Naval Research, Department of the Navy, Contract N7onr-32909, 1952.

10 "Plates Under Lateral Impact," by K. Karas, Translation 135, Navy Department, The David W. Taylor Model Basin, Washington, D. C., April, 1951.

11 "On the Production of Vibrations by Forces of Relatively Long Duration, With Applications to the Theory of Collisions," by Lord Rayleigh, *Philosophical Magazine*, Series 6, vol. 11, 1906, p. 283.

12 "Über die Berührung fester Elastischer Körper," by H. Hertz, *Journal für Mathematik*, vol. 92, 1882, p. 156.

13 "Mechanik der Elastischen Körper," *Handbuch der Physik*, vol. 6, 1928, p. 544.

14 "The Mathematical Theory of Elasticity," by A. E. H. Love, Dover Publications, New York, N. Y., 1944, p. 198.

15 "Applied Elasticity," by John Prescott, Dover Publications, New York, N. Y., 1946, pp. 210–213, 597–598.

16 "Lectures on the Calculus of Variations," by G. A. Bliss, University of Chicago Press, Chicago, Ill., p. 10.

17 "Impact Stresses in a Freely Supported Beam," by R. N. Arnold, Proceedings of The Institution of Mechanical Engineers, vol. 137, 1937, p. 217.

# Buckling of Multiple-Bay Ring-Reinforced Cylindrical Shells Subject to Hydrostatic Pressure

By W. A. NASH,[1] WASHINGTON, D. C.

**An analytical solution is presented for the problem of the elastic instability of a multiple-bay ring-reinforced cylindrical shell subject to hydrostatic pressure applied in both the radial and axial directions. The method used is that of minimization of the total potential. Expressions for the elastic strain energy in the shell and also in the rings are written in terms of displacement components of a point in the middle surface of the shell. Expressions for the work done by the external forces acting on the cylinder likewise are written in terms of these displacement components. A displacement configuration for the buckled shell is introduced which is in agreement with experimental evidence, in contrast to the arbitrary patterns assumed by previous investigators. The total potential is expressed in terms of these displacement components and is then minimized. As a result of this minimization a set of linear homogeneous equations is obtained. In order that a nontrivial solution to this system of equations exists, it is necessary that the determinant of the coefficients vanish. This condition determines the critical pressure at which elastic buckling of the cylindrical shell will occur.**

## Introduction

THE first analytical treatment of the problem of the buckling of a cylindrical shell of infinite length subject to external hydrostatic pressure was carried out by Bresse (1)[2] in 1859. In 1888 Bryan (2) published his classical paper deriving the same expression as did Bresse. Bryan's work was based upon the energy criterion for stability. In 1913 Southwell (3) published the first of a series of three papers treating the elastic instability of a geometrically perfect cylindrical shell. In the first of these papers he rederived Bryan's expression for the tube of infinite length in a manner different from that of the original author. In this same paper Southwell discussed the effect of circumferential reinforcing rings upon the hydrostatic buckling pressure of a shell of finite length and derived an expression for the minimum length of tube for which the effect of the rings can be neglected. He used an energy method to obtain the buckling pressure for a shell of finite length, neglecting the effect of the reinforcing rings. This solution considered only radial pressure.

This paper also presented for the first time an analytical treatment of the problem of the number of lobes that would form on a shell subject to external hydrostatic pressure. In 1914 von Mises (4) published his classical analysis of the buckling of a thin elastic shell of finite length subject to uniform radial pressure. However, this study failed to take into account any axial component of pressure. In 1929 von Mises (5) extended his original analysis so as to cover the case of hydrostatic pressure applied to the ends as well as to the curved wall of the shell. In neither of his analyses was there considered the effect of the elastic restraint of the ends (or any reinforcing rings in the case of a ring-reinforced shell) upon the structure.

In 1934 Windenburg (6) presented a simplification of von Mises equation for the buckling pressure of a cylinder subject to hydrostatic pressure. This result is independent of the number of lobes formed upon buckling and differs on the average from the von Mises value by about 1 per cent. Batdorf (7) in 1947 presented a new method of determining the buckling stresses of cylindrical shells under various loading conditions. By this method he obtained a solution to the problem of the collapse of a cylinder of finite length loaded by hydrostatic pressure on all surfaces. His solution is almost identical with that presented by von Mises.

In a recent series of four papers Salerno and Levine (8, 9, 10, 11) treated the elastic instability of a circular cylindrical shell reinforced by evenly spaced circumferential rings having an I-type cross section. The scope of their work is restricted by the assumption that the rings must be thin-walled open sections.

All the foregoing investigations, as well as that presented here, are predicated upon the classical small deformation theory of elastic thin shells as presented by Love (12). This theory assumes:

1 The shell is composed of a material which is elastically homogeneous and isotropic.

2 The material follows Hooke's law.

3 The thickness of the shell at any point is small compared to either of the principal radii of curvature at that point.

4 The normals to the middle surface of the shell before deformation also are normal to the middle surface after deformation.

In addition to these theoretical analyses of the buckling of a cylindrical shell subject to hydrostatic pressure numerous experimental investigations have been conducted within the past hundred years. The principal investigators were Fairbairn (13), Carman (14), Stewart (15), Carman and Carr (16), Southwell (3), Windenburg (17), Sturm (18), and Kirkby (19).

## Analysis

*Fundamental Equations.* The problem of the buckling of a multiple-bay ring-reinforced cylindrical shell subject to hydro-

---

[1] Structural Research Engineer, David Taylor Model Basin, Navy Department. Mem. ASME.

[2] Numbers in parentheses refer to the Bibliography at the end of the paper.

Presented at the National Conference of the Applied Mechanics Division, Minneapolis, Minn., June 18–20, 1953, of The American Society of Mechanical Engineers.

Discussion of this paper should be addressed to the Secretary, ASME, 29 West 39th Street, New York, N. Y., and will be accepted until January 11, 1954, for publication at a later date. Discussion received after the closing date will be returned.

Note: Statements and opinions advanced in papers are to be understood as individual expressions of their authors and not those of the Society. Manuscript received by ASME Applied Mechanics Division, July 2, 1952. Paper No. 53—APM-29.

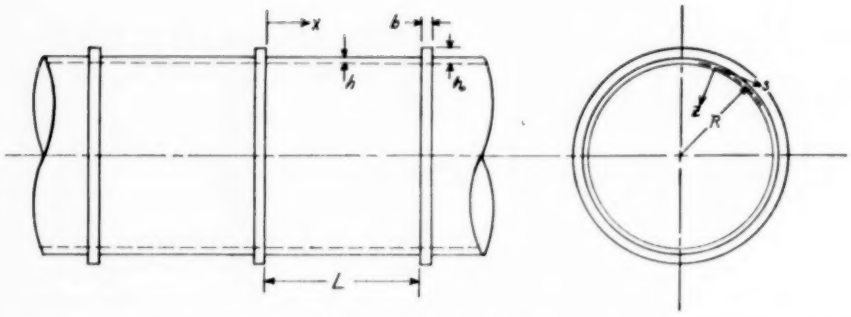


Fig. 1

static pressure may be attacked by the method of minimum potential described by Timoshenko (20). Let us consider a cylinder of mean radius $R$ and thickness $h$ with stiffening rings spaced a distance $L$ apart. Such a shell is shown in Fig. 1. The rings under consideration here are assumed to be spaced equally along the axis of the cylinder and of uniform cross section around the circumference of any ring. Further, it is assumed that all rings are identical. In the first part of the analysis rings of infinite rigidity are discussed and they, of course, may be of arbitrary cross section. In the second part of the analysis, rings of finite rigidity are discussed and their cross sections must be rectangular.

Let $x$, $s$, and $z$ be orthogonal co-ordinates in the axial, tangential, and radial directions, respectively. The positive directions of these co-ordinates are shown in Fig. 1. The shell is subject to a hydrostatic pressure $p$ acting both radially and axially. Let $u_0$, $v_0$, and $w_0$ be the components of displacement (in the $x$, $s$, and $z$-directions) of any point in the middle surface of the shell at an instant before buckling and further let $u$, $v$, and $w$ denote the additional displacements during the buckling process.

For the purpose of this analysis it is sufficient to isolate and study one bay of the shell, i.e., the portion of the structure between the centers of two adjacent rings. In the minimum potential method it is first necessary to obtain values of the additional extensional, bending, and shearing elastic strain energies stored in one bay of the shell during the buckling process. If the axial and tangential strains existing in the shell immediately before buckling are denoted by $\epsilon_{x0}$ and $\epsilon_{s0}$, then, for the case of uniform radial pressure $p$ and axial pressure $P$, these quantities are given by

$$\epsilon_{x0} = \frac{1}{E}\left(-P + \frac{\nu pR}{h}\right) \qquad [1]$$

$$\epsilon_{s0} = \frac{1}{E}\left(-\frac{pR}{h} + \nu P\right) \qquad [2]$$

where $E$ denotes the modulus of elasticity of the material and $\nu$ represents Poisson's ratio. In Equations [1] and [2] the effect of the rings on the strains near the ends of the bay are neglected. The axial and tangential strains existing immediately after buckling are given by

$$\epsilon_x = \frac{[(1 + \epsilon_{x0} + u_x)^2(dx)^2 + w_x^2(dx)^2]^{1/2} - dx}{dx} = \epsilon_{x0} + u_x + \frac{1}{2}w_x^2 \qquad [3]$$

and

$$\epsilon_s = \frac{[(1 + \epsilon_{s0} + v_s - w/R)^2(ds)^2 + (v/R + w_s)^2(ds)^2]^{1/2} - ds}{ds} = \epsilon_{s0} + v_s - \frac{w}{R} + \frac{1}{2}\left(\frac{v}{R} + w_s\right)^2 \qquad [4]$$

The increase in the extensional elastic energy during the buckling process is given by

$$\Delta U_e = \frac{Eh}{2(1-\nu^2)}\int_0^{2\pi R}\int_0^L [(\epsilon_x^2 + 2\nu\epsilon_x\epsilon_s + \epsilon_s^2) - (\epsilon_{x0}^2 + 2\nu\epsilon_{x0}\epsilon_{s0} + \epsilon_{s0}^2)]dx\,ds \qquad [5]$$

With the values of these strains given by Expressions [1] through [4], the increase in extensional energy is found to be

$$\Delta U_e = \frac{Eh}{2(1-\nu^2)}\int_0^{2\pi R}\int_0^L \left[u_x^2 + v_s^2 + \frac{w^2}{R^2} + 2\nu u_x v_s - \frac{2\nu u_x w}{R} - \frac{2v_s w}{R} - \frac{1}{2}\left(\frac{v}{R} + w_s\right)^2\right]dx\,ds + pR\int_0^{2\pi R}\int_0^L \left[\frac{w}{R}\right]dx\,ds - \frac{Ph}{2}\int_0^{2\pi R}\int_0^L w_x^2 dx\,ds - Ph\int_0^{2\pi R}[u_L - u_0]ds \qquad [6]$$

The bending energy immediately before buckling is given by Love (12) and Salerno and Levine (8) to be

$$U_{b0} = \frac{Eh^3}{24R^2(1-\nu^2)}\int_0^{2\pi R}\int_0^L \left[R^2(w_{0xx})^2 + \frac{1}{R^2}(R^2 w_{0ss} + w_0)^2 + 2\nu w_{0xx}(R^2 w_{0ss} + w_0) + 2(1-\nu)\left(Rw_{0xs} + \frac{v_{0x}}{2} - \frac{u_{0s}}{2}\right)^2\right]dx\,ds \qquad [7]$$

The bending energy immediately after buckling is obtained by replacing $u_0$ by $(u_0 + u)$, $v_0$ by $(v_0 + v)$, and $w_0$ by $(w_0 + w)$. Consequently the increase in strain energy of bending during the buckling process is

$$\Delta U_b = \frac{Eh^3}{24(1-\nu^2)}\int_0^{2\pi R}\int_0^L \left[w_{xx}^2 + w_{ss}^2 + 2\nu w_{xx}w_{ss} + 2(1-\nu)(w_{xs})^2 + \frac{w^2}{R^4} + \frac{2}{R^2}w_{ss}w\right]dx\,ds \qquad [8]$$

This expression for the increase in bending energy was obtained by neglecting certain terms differing by $h^2/R^2$, $h^2\dfrac{\partial^2}{\partial x^2}$, or $h^2\dfrac{\partial^2}{\partial s^2}$ from corresponding terms appearing in $\Delta U_e$.

Prior to buckling the cylindrical shell is in a state of uniform compression and the membrane shear stresses are zero. After buckling, the shear energy is given by Love (12) to be

$$U_s = \frac{Eh}{2(1-\nu^2)}\int_A \left(\frac{1-\nu}{2}\right)(\gamma_{x\phi})^2\,dA \qquad [9]$$

where $\phi = \dfrac{s}{R}$

But $$\gamma_{x\phi} = \frac{u_\phi}{R} + v_x \quad \ldots\ldots\ldots\ldots\ldots\ldots [10]$$

Hence $$U_1 = \frac{Eh}{4(1+\nu)} \int_0^{2\pi R} \int_0^L (u_y + v_x)^2 \, dx \, ds \quad \ldots [11]$$

Knowing the elastic strain energy stored in the shell, it is next necessary to calculate the work done by the external forces acting on the shell. The total work done by the external forces acting upon the cylinder may be calculated as the hydrostatic pressure $p$ multiplied by the decrease of volume of the cylinder. This decrease of volume may be considered to consist of a shortening of the radius in any fixed radial plane together with a sliding of the ends of the cylinder along a plate. Any radius is shortened by an amount,

$$w - uw_x - vw_s - \frac{v^2}{2R}$$

(in a fixed radial plane) and hence the decrease in volume between the initial end planes is

$$\int_0^L \pi R^2 dx - \frac{1}{2R} \int_0^{2\pi R} \int_0^L \left[ R - w + uw_x + vw_s + \frac{v^2}{2R} \right]^2 dx \, ds$$

$$= \int_0^{2\pi R} \int_0^L \left[ w - \frac{v^2}{2R} - \frac{w^2}{2R} - uw_x - vw_s \right] dx \, ds \quad \ldots [12]$$

where terms of the third and higher orders have been neglected. The correction to the decrease of volume in the vicinity of the ends of the cylinder is of the form

$$\int_0^{2\pi R} \frac{u}{2} (R - w)^2 \frac{ds}{R} = \int_0^{2\pi R} u \left( \frac{R}{2} - w \right) ds$$

Accordingly, the correction for both ends of the cylinder is

$$\frac{R}{2} \int_0^{2\pi R} (u_L - u_0) \, ds = \int_0^{2\pi R} [(uw)_L - (uw)_0] \, ds$$

The work done by the hydrostatic pressure $p$ is thus given by

$$p \int_0^{2\pi R} \int_0^L \left( w - \frac{v^2}{2R} - \frac{w^2}{2R} - uw_x - vw_s \right) dx \, ds$$

$$- \frac{pR}{2} \int_0^{2\pi R} (u_L - u_0) ds + p \int_0^{2\pi R} [(uw)_L - (uw)_0] \, ds$$

$$\ldots\ldots\ldots [13]$$

For the cylindrical shell, then, the total potential (which is defined to be the algebraic sum of the strain energies and the negative of the work done by the external loads) may be found by use of Equations [6], [8], [11], and [13]. Equation [6] may be simplified by use of the statics relation

$$P = \frac{pR}{2h}$$

Also, Equation [13] may be simplified by using the following result obtained by integration by parts

$$\int_0^L uw_x dx = (uw)_L - (uw)_0 - \int_0^L u_x w \, dx$$

Let us first consider the case of a cylindrical shell reinforced by infinitely rigid reinforcing rings. In this case the rings contain no elastic strain energy and the total potential (i.e., the sum of the strain energies and the potential of the external loads) is

$$U_T = \frac{Eh}{2(1-\nu^2)} \int_0^{2\pi R} \int_0^L \left[ u_x^2 + v_s^2 + \frac{w^2}{R^2} + 2\nu u_x v_s - \frac{2\nu u_x w}{R} - \frac{2v_s w}{R} \right] dx \, ds + \frac{Eh^3}{24(1-\nu^2)} \int_0^{2\pi R} \int_0^L \left[ w_{xx}^2 + w_{ss}^2 + 2\nu w_{xx} w_{ss} + 2(1-\nu)(w_{xs})^2 + \frac{w^2}{R^4} + \frac{2}{R^2} w_{ss} w \right] dx \, ds$$

$$+ \frac{Eh}{4(1+\nu)} \int_0^{2\pi R} \int_0^L (u_s + v_x)^2 \, dx \, ds$$

$$+ pR \int_0^{2\pi R} \int_0^L \left[ -\frac{w_x^2}{2} + \frac{w^2}{2R^2} - \frac{u_x w}{R} - \frac{w_s^2}{4} \right] dx \, ds \quad \ldots [14]$$

*Displacement Pattern.* For the case of infinitely rigid reinforcing rings let us take the additional displacements during buckling to be

$$\left.\begin{aligned} u &= A \cos \frac{ms}{R} \sin 2\delta x \\ v &= B \sin \frac{ms}{R} (1 - \cos 2\delta x) \\ w &= C \cos \frac{ms}{R} (1 - \cos 2\delta x) \end{aligned}\right\} \quad \ldots\ldots\ldots [15]$$

where $A$, $B$, and $C$ are arbitrary constants, $m$ is the number of waves (lobes) in the circumferential direction, $L/n$ represents the period of the function defining the deformed generator in one bay of the shell, and $\delta = n\pi/L$. The elastic strain energies and the potential due to the external loads may now be expressed in terms of the constants $A$, $B$, and $C$ by substituting the displacements, Equations [15], in the energy expressions and integrating. For brevity, let us introduce the following notation

$$\begin{aligned}
k_1 &= \frac{Eh}{2(1-\nu^2)} & k_{12} &= \frac{4(1-\nu)\delta^2 m^2 \pi L}{R} \\
k_2 &= 2\delta^2 \pi R L & k_{13} &= \frac{Eh}{4(1+\nu)} \\
k_3 &= \frac{3m^2 \pi L}{2R} & k_{14} &= \frac{m^2 \pi L}{2R} \\
k_4 &= \frac{3\pi L}{2R} & k_{15} &= 2\delta m \pi L \\
k_5 &= 2\nu\delta m \pi L & k_{16} &= 2\delta^2 \pi R L \\
k_6 &= 2\nu\delta\pi L & k_{17} &= \frac{3\mu m^2 \pi L}{4} \\
k_7 &= \frac{3m\pi L}{R} & k_{18} &= \frac{3\mu\pi L}{4} \\
k_8 &= \frac{Eh^3}{24(1-\nu^2)} & k_{19} &= pR\delta\pi L \\
k_9 &= 8\delta^4 \pi R L & k_{20} &= \frac{p\delta^2 \pi R^2 L}{2} \\
k_{10} &= \frac{3m^4 \pi L}{2R^3} & k_{21} &= \frac{3\pi L}{2R^3} \\
k_{11} &= \frac{4\nu\delta^2 m^2 \pi L}{R} & k_{22} &= \frac{3m^2 \pi L}{R^3}
\end{aligned} \quad \ldots [16]$$

*Minimization of Potential.* The variation of the total potential with respect to each of the constants $A$, $B$, and $C$ must vanish for equilibrium. This means that

$$\frac{\partial U_T}{\partial A} = 0; \quad \frac{\partial U_T}{\partial B} = 0; \quad \frac{\partial U_T}{\partial C} = 0 \quad \ldots\ldots [17]$$

When the differentiations indicated in Equations [17] are carried out they lead to the three linear homogeneous equations

$$k_{24}A + k_{24}B + k_{25}C = 0 \quad \ldots\ldots [18]$$

$$k_{24}A + k_{26}B + k_{27}C = 0 \quad \ldots\ldots [19]$$

$$k_{25}A + k_{27}B + k_{28}C = 0 \quad \ldots\ldots [20]$$

where

$$\left.\begin{aligned} k_{23} &= 2k_1k_2 + 2k_{12}k_{14} \\ k_{24} &= -k_1k_5 - k_{13}k_{15} \\ k_{25} &= k_1k_6 + k_{19} \\ k_{26} &= 2k_3k_5 + 2k_{13}k_{16} \\ k_{27} &= -k_3k_7 \\ k_{28} &= 2k_3k_4 + 2k_5k_9 + 2k_9k_{16} + 2k_9k_{21} \\ &\quad -2k_9k_{22} + 2k_9k_{11} + 2k_9k_{17} - 2k_{17} + 2k_{18} - 2k_{20} \end{aligned}\right\} \quad \ldots [21]$$

The trivial solution $A = B = C = 0$ is of no consequence. For a nontrivial solution to exist, the determinant of the coefficients of the unknowns must vanish. When this is the case, there exist deformed equilibrium configurations in addition to the original one. Such a situation corresponds to neutral equilibrium and the loads under which it exists are the buckling loads. Here, the stability determinant is

$$\begin{vmatrix} k_{23} & k_{24} & k_{25} \\ k_{24} & k_{26} & k_{27} \\ k_{25} & k_{27} & k_{28} \end{vmatrix} = 0 \quad \ldots\ldots [22]$$

The expansion of this determinant leads to a quadratic equation in the unknown buckling pressure $p$. The buckling pressure $p$ predicted by this theory is consequently the minimum positive root of this quadratic equation. It is of interest to note that for the case of an infinitely long cylindrical shell, the buckling pressure obtained by this analysis is

$$p = \frac{Eh^3}{4(1-\nu^2)R^3} \quad \ldots\ldots [23]$$

which agrees with the well-known Bryan-Bresse result (12).

*Other Displacement Patterns.* It might be thought that the somewhat more general displacement pattern

$$\left.\begin{aligned} u &= \left(A \sin \frac{ms}{R} + B \cos \frac{ms}{R}\right) \sin 2\delta x + \frac{Cx}{L} \\ v &= D \sin \frac{ms}{R}(1 - \cos 2\delta x) \\ w &= \left(F \sin \frac{ms}{R} + G \cos \frac{ms}{R}\right)(1 - \cos 2\delta x) \end{aligned}\right\} \quad \ldots [24]$$

would lead to a lower buckling pressure since it contains six constants instead of three as used in Equations [15]. However, by the minimum potential method it may be shown that the same stability determinant, Equations [22], is obtained as in the case of the configuration given by Equations [15].

It is of interest to investigate a slight variation in the configuration given by Equations [15]. Let us assume that the additional displacements during buckling are given by

$$\left.\begin{aligned} u &= A \cos \frac{ms}{R} \sin 4\delta x \\ v &= B \sin \frac{ms}{R}(1 - \cos 2\delta x) \\ w &= C \cos \frac{ms}{R}(1 - \cos 2\delta x) \end{aligned}\right\} \quad \ldots\ldots [25]$$

Using the minimum potential method, three equations analogous to Equations [18], [19], and [20] may be written and a stability determinant formed. However, this configuration will usually indicate a slightly higher buckling pressure than that found by use of the pattern, Equations [15]. This is illustrated in the numerical example given later for one particular geometry. For an infinitely long cylindrical shell the buckling pressure found by use of the Configuration [25] again agrees with the Bryan-Bresse expression.

The displacement configurations discussed thus far are for the case of infinitely rigid reinforcing rings. In all previous analyses investigators have assumed displacement components corresponding to arbitrarily selected boundary conditions without any reference to experimental evidence. As the configuration occurring during buckling of a cylindrical shell reinforced by rings having finite rigidity let us take

$$\left.\begin{aligned} u &= A \sin \frac{ms}{R} \sin 2\delta x + B \sin \frac{ms}{R} \cos \delta x \\ &\quad + C \cos \frac{ms}{R} \sin 2\delta x + D \cos \frac{ms}{R} \cos \delta x + \frac{Fx}{L} \\ v &= \sin \frac{ms}{R}(G + H \sin 2\delta x + J \cos 2\delta x) \\ w &= \left(K \sin \frac{ms}{R} + M \cos \frac{ms}{R}\right)(1 - \cos 2\delta x) + N \end{aligned}\right\} \quad \ldots [26]$$

This configuration permits the ring to (*a*) bend out of its plane, (*b*) undergo a uniform radial compression, (*c*) undergo tangential displacements, and (*d*) translate along the axis of the cylinder. Here, the form of the $w$-component of displacement was obtained from radial-displacement measurements taken shortly before and immediately after the formation of lobes in two ring-stiffened cylinders each subject to hydrostatic pressure. (The reinforcing rings were of rectangular cross section.) These measurements indicated that the ring did not undergo any bending in its plane and further that the profile of the shell along a generator was given very closely by the expression $(1 - \cos 2\delta x)$ with $n = 1$. This experimental evidence has been incorporated into the expressions given in Equations [26] in such a way that all other types of deformation of the ring, namely, (*a*) through (*d*), are possible.

In calculating the total potential of a cylindrical shell reinforced by rings of finite rigidity it is necessary to compute the potential of the rings. This may be done in a manner analogous to that used for the derivation of the potential of the shell and the result, for a ring of rectangular cross section is

$$U_R = \frac{bh_0E}{2} \int_0^{2\pi R_1} \left[\left(v_s \frac{R_1}{R}\right)^2 + \frac{w^2}{R_1^2} - \frac{2v_sw}{R}\right]_{x=0} ds + pbR_1 \int_0^{2\pi R_1} \left[\frac{w^2}{2R_1^2}\right]_{x=0} ds + \frac{EI_{s0}}{2} \int_0^{2\pi R_1} [u_{ss}^2]_{x=0}\, ds \quad \ldots\ldots [27]$$

where $b$ denotes the width of the ring as shown in Fig. 1, $h_0$ denotes the depth of the composite ring-shell section (i.e.,

the ring and the portion of the shell immediately contiguous to it is regarded as monolithic), $R_1$ represents the radius to the centroid of the composite ring-shell section, and $I_{s0}$ denotes the moment of inertia of the ring-shell cross section with respect to an axis through the centroid of the cross section and coinciding with a diameter of the shell.

This potential must be added to the potential of the shell given in Equation [14]. The elastic strain energies and the potential of the external loads may now be expressed in terms of the constants $A, B, C, \ldots N$ by substituting the Displacements [26] in the energy expressions and integrating. Let us introduce the notation

$$
\begin{aligned}
h_1 &= \frac{Eh}{2(1-\nu^2)} & h_{22} &= \frac{3m^2\pi L}{R^2}\\
h_2 &= 2\hat{\delta}^2\pi RL & h_{24} &= \frac{4(1-\nu)\hat{\delta}^2m^2\pi L}{R}\\
h_3 &= \frac{\hat{\delta}^2\pi RL}{2} & h_{25} &= \frac{Eh}{4(1+\nu)}\\
h_4 &= \frac{2\pi R}{L} & h_{26} &= \frac{8m^2L}{3R}\\
h_5 &= \frac{8\hat{\delta}\pi R}{3} & h_{27} &= 2\hat{\delta}^2\pi RL\\
h_6 &= \frac{m^2\pi L}{R} & h_{28} &= 2\hat{\delta}m\pi L\\
h_7 &= \frac{m^2\pi L}{2R} & h_{29} &= \frac{16m\pi}{3}\\
h_8 &= \frac{3\pi L}{2R} & h_{30} &= \frac{3m^2\pi Lp}{4}\\
h_9 &= \frac{2\pi L}{R} & h_{31} &= \frac{3\pi Lp}{4}\\
h_{10} &= 4\nu\pi m & h_{32} &= \pi Lp\\
h_{11} &= 2\hat{\delta}m\pi L\nu & h_{33} &= \hat{\delta}\pi LpR\\
h_{12} &= \frac{4\nu\pi m}{3} & h_{34} &= \frac{8\hat{\delta}pRL}{3}\\
h_{13} &= 2\hat{\delta}\pi\nu L & h_{35} &= 2\pi Rp\\
h_{14} &= \frac{16\nu\pi}{3} & h_{36} &= \frac{\pi R^2L\hat{\delta}^2p}{2}\\
h_{15} &= \frac{2\pi L}{R^3} & h_{37} &= \frac{bh_0E}{2}\\
h_{16} &= \frac{2m\pi L}{R} & h_{38} &= \frac{\pi m^2R_1^3}{R^4}\\
h_{17} &= \frac{m\pi L}{R} & h_{39} &= \frac{2m^2\pi R_1^3}{R^4}\\
h_{18} &= \frac{Eh^3}{24(1-\nu^2)} & h_{40} &= \frac{2\pi}{R_1}\\
h_{19} &= 8\hat{\delta}^4\pi RL & h_{41} &= t\pi p\\
h_{20} &= \frac{3m^4\pi L}{2R^3} & h_{42} &= \frac{EI_{s0}}{2R^3}\\
h_{21} &= \frac{4\nu\hat{\delta}^2m^2\pi L}{R} & h_{43} &= m^4\pi R_1\\
h_{22} &= \frac{3\pi L}{2R^3}
\end{aligned}
\qquad \ldots [28]
$$

Again, the variation of the total potential with respect to each of the constants $A, B, \ldots N$ must vanish for equilibrium. This condition leads to the system of equations

| | $A$ | $B$ | $C$ | $D$ | $F$ | $G$ | $H$ | $J$ | $K$ | $M$ | $N$ | |
|---|---|---|---|---|---|---|---|---|---|---|---|---|
| 1 | $h_{44}$ | $h_{45}$ | | | | | | | $h_{48}$ | | | $= 0$ |
| 2 | $h_{45}$ | $h_{47}$ | | | | | | | $h_{48}$ | | | $= 0$ |
| 3 | | | $h_{44}$ | $h_{45}$ | | | | $h_{49}$ | | $h_{46}$ | | $= 0$ |
| 4 | | | $h_{45}$ | $h_{47}$ | | $h_{51}$ | | $h_{50}$ | | $h_{48}$ | | $= 0$ |
| 5 | | | | | $h_{52}$ | | | | | | $h_{53}$ | $= 0$ |
| 6 | | | | $h_{51}$ | | $h_{53}$ | | $h_{54}$ | | $h_{50}$ | | $= 0$ |
| 7 | | | | | | | $h_{60}$ | | | | | $= 0$ |
| 8 | | | $h_{49}$ | $h_{50}$ | | $h_{54}$ | | $h_{56}$ | | $h_{57}$ | | $= 0$ |
| 9 | $h_{46}$ | $h_{48}$ | | | | | | | $h_{58}$ | | | $= 0$ |
| 10 | | | $h_{46}$ | $h_{48}$ | | $h_{55}$ | | $h_{57}$ | | $h_{58}$ | | $= 0$ |
| 11 | | | | | $h_{59}$ | | | | | | $h_{59}$ | $= 0$ |

$\ldots [29]$

where

$$
\begin{aligned}
h_{44} &= 2h_1h_2 + 2h_{22}h_7\\
h_{45} &= h_1h_8 + h_{23}h_{24}\\
h_{46} &= h_1h_{13} + h_{33}\\
h_{47} &= 2h_1h_3 + 2h_{23}h_7 + 2h_{43}h_{43}\\
h_{48} &= h_1h_{14} + h_{34}\\
h_{49} &= h_1h_{11} + h_{23}h_{28}\\
h_{50} &= h_1h_{12} + h_{23}h_{29}\\
h_{51} &= -h_1h_{10}\\
h_{52} &= 2h_1h_4\\
h_{53} &= 2h_1h_6 + 2h_{32}h_{38}\\
h_{54} &= h_{37}h_{39}\\
h_{55} &= -h_1h_{16}\\
h_{56} &= 2h_1h_7 + 2h_{37}h_{37} + 2h_{37}h_{38}\\
h_{57} &= h_1h_{17}\\
h_{58} &= 2h_1h_5 + 2h_{18}h_{19} + 2h_{18}h_{20} + 2h_{18}h_{21} + 2h_{18}h_{22}\\
&\quad - 2h_{18}h_{25} + 2h_{18}h_{24} - 2h_{30} + 2h_{31} - 2h_{36}\\
h_{59} &= 2h_1h_9 + 2h_{18}h_{18} + 2h_{42} + 2h_{37}h_{40} + 2h_{41}\\
h_{60} &= 2h_1h_7 + 2h_{23}h_{27}
\end{aligned}
\qquad \ldots [30]
$$

These equations show that $H = 0$ for all geometries of ring-reinforced cylindrical shell. Also, the constants $A$, $B$, and $K$ and no others each appear in only three equations and the stability determinant of these three may be solved to obtain a value of $p$. Also, the constants $C$, $D$, $G$, $J$, and $M$ and no others each appear in five equations and the stability determinant of these five may be solved to determine another value of $p$. Lastly, a stability determinant may be formed of the two equations containing $F$ and $N$ and a third value of $p$ determined. (This last corresponds to the case of axial symmetric buckling.) The critical buckling pressure is, of course, the minimum of these three values of $p$. For the particular geometries investigated in this paper the minimum value of $p$ is given by the second of these determinants.

## Numerical Example

Let us consider a multiple-bay ring-reinforced cylinder having the following dimensions:

$$
\begin{aligned}
2R &= 26.753 \text{ in.}\\
h &= 0.065 \text{ in.}\\
L &= 5.08 \text{ in.}\\
b &= 0.1875 \text{ in.}\\
h_0 &= 0.71875 \text{ in.}
\end{aligned}
$$

If the rings are first assumed to be infinitely rigid and the displacement pattern, Equations [15], adopted, the stability determinant, Equations [22], becomes

$$\begin{vmatrix} 3.497362 \times 10^8 + 4.476262 \times 10^6 m^2 & -1.374697 \times 10^7 m & 6.344761 \times 10^6 + 1.320211 \times 10^7 p \\ -1.374697 \times 10^7 m & 3.836798 \times 10^6 m^2 + 1.224077 \times 10^8 & 3.836799 \times 10^6 m \\ 6.344761 \times 10^6 + 1.320211 \times 10^7 p & -3.836799 \times 10^6 m & 4.024995 \times 10^6 + 1.361312 \times 10^6 m^2 + 7.549691 m^4 - 2.395072 \times 10 m^2 p - 1.067641 \times 10^7 p \end{vmatrix} = 0$$

In this form $n$ has been taken equal to unity, as found by the tests of the two ring-reinforced cylinders, but it is necessary to minimize the value of $p$ with respect to the variable $m$. It is found that the minimum value of $p$ occurs with $m = 17$ and is 189 psi. It is of interest to note that if the $p^2$-term of the quadratic equation is neglected (with $m = 17$) the same pressure is obtained.

If the displacement pattern, Equations [25], be adopted it is found that the minimum value of $p$ occurs when $m = 17$ and is 199 psi. If the displacement pattern, Equations [26], is adopted it is found that the fifth-order determinant with $m = 16$ yields a critical buckling pressure of 179 psi, which is a lower value than may be obtained by use of either the second or the third-order determinants that also arose in conjunction with configuration, Equations [26]. Consequently, for a cylinder having the geometry stated it is apparent that the deformations of the ring permitted by the buckling configuration, Equations [26], reduce the buckling pressure 5.3 per cent from that given for a cylindrical shell reinforced by infinitely rigid rings. It is of interest to note that the theory of Reference (10) predicts a buckling pressure of 175 psi for a model having this geometry and reinforced by infinitely rigid rings.

## Conclusions

1 A theoretical analysis is presented for the problem of determining the pressure necessary to cause an elastic instability mode of failure of a geometrically perfect thin cylindrical shell reinforced by equally spaced rings and subject to hydrostatic pressure.

2 The buckling pressures given by this, as well as by all other existing theories, are higher than those found during test. Possible causes of this are initial out-of-roundness or residual welding stresses.

## Acknowledgment

The author expresses his appreciation to Dr. E. H. Kennard of the David Taylor Model Basin for suggesting Equations [6] and [13]. Further, the author would like to express his thanks to Mrs. L. V. Peugh, Mr. R. C. Slankard, and Mr. M. Borg of the David Taylor Model Basin staff, for checking the mathematical analysis and for carrying out the calculations occurring in this paper.

## Bibliography

1 "Cours de Mécanique Applique," by M. Bresse, Paris, France, 1859, pp. 323–338.

2 "Application of the Energy Test to the Collapse of a Long Thin Pipe Under External Pressure," by G. H. Bryan, Proceedings of the Cambridge Philosophical Society, Cambridge, England, vol. 6, 1888, pp. 287–292.

3 "On the Collapse of Tubes by External Pressure," by R. V. Southwell, *Philosophical Magazine*, vol. 25, part 1, May, 1913, pp. 687–698; vol. 26, part 2, September, 1913, pp. 502–511; vol. 29, part 3, January, 1915, pp. 67–77.

4 "Der kritische Aussendruck Zylindrischer Rohre," by R. von Mises, *Zeitschrift des Vereines deutscher Ingenieure*, vol. 58, 1914, pp. 750–755.

5 "Der kritische Aussendruck für allseits belastete zylindrische Rohre," by R. von Mises, Fest. zum 70 Geburstag von Prof. Dr. A. Stodola, Zurich, Switzerland, 1929, pp. 418–430.

6 "Collapse by Instability of Thin Cylindrical Shells Under External Pressure," by D. F. Windenburg and C. Trilling, Trans. ASME, vol. 56, 1934, pp. 819–825.

7 "A Simplified Method of Elastic-Stability Analysis for Thin Cylindrical Shells," by S. B. Batdorf, NACA Report 874, 1947, 25 pages.

8 "Buckling of Circular Cylindrical Shells With Evenly Spaced Equal Strength Circular Ring Frames, Part I," by V. L. Salerno and B. Levine, PIBAL Report No. 167, 1950, 30 pp.

9 "Buckling of Circular Cylindrical Shells With Evenly Spaced, Equal Strength Circular Ring Frames, Part II," by V. L. Salerno and B. Levine, PIBAL Report No. 169, 1950, 21 pp.

10 "Charts for the Determination of the Upper and Lower Limit of Hydrostatic Buckling Pressures for Reinforced Circular Cylindrical Shells," by V. L. Salerno, B. Levine, and J. G. Pulos, PIBAL Report 177, 1950, 25 pp.

11 "The Determination of the Hydrostatic Buckling Pressures for Circular Cylindrical Shells Reinforced With Rings," by V. L. Salerno and B. Levine, PIBAL Report No. 182, 1951, 25 pp.

12 "A Treatise on the Mathematical Theory of Elasticity," by A. E. H. Love, Dover Publications, New York, N. Y., 1944.

13 "On the Resistance of Tubes to Collapse," by W. Fairbairn, Philosophical Transactions, vol. 148, 1858, pp. 389–413.

14 "Resistance of Tubes to Collapse," by A. P. Carman, *Physical Review*, vol. 21, 1905, pp. 381–387.

15 "Collapsing Pressures of Bessemer Steel Lap-Welded Tubes, Three to Ten Inches in Diameter," by R. T. Stewart, Trans. ASME, vol. 27, 1906, pp. 730–822.

16 "Resistance of Tubes to Collapse," by A. P. Carman and M. L. Carr, University of Illinois Engineering Experiment Station Bulletin No. 5, 1906, 23 pp.

17 "Strength of Thin Cylindrical Shells Under External Pressure," by D. F. Windenburg and H. E. Saunders, Journal of Applied Mechanics, Trans. ASME, vol. 53, 1931, pp. A-207–218.

18 "A Study of the Collapsing Pressure of Thin-Walled Cylinders," by R. G. Sturm, University of Illinois Engineering Experiment Station Bulletin No. 329, 1941, 80 pp.

19 "The Collapse of Cylinders Subject to External Pressure," by J. M. Kirkby, Admiralty Mining Establishment Report No. 1032/47, 1947.

20 "Sur la Stabilité des Systemes Élastiques," by S. Timoshenko, *Annales des Ponts et Chaussees*, vol. 13, 1913, pp. 496–566; 73–132; 372–412.

# Dynamic Load Characteristics in Plastic Bending of Beams[1]

By P. S. SYMONDS,[2] PROVIDENCE, R. I.

**This paper continues work previously reported[3] on the analysis of large plastic deformations of beams subjected to transverse dynamic loads. Here we discuss the numerical analysis for central concentrated force pulses of arbitrary shape, using a somewhat different formulation of the equations than in the previous paper.[3] Results are then collected for three types of force pulse: A rectangular pulse, a half-sine wave, and a triangular pulse. These show that the central angle of permanent deformation for all three cases can be computed from the empirical formula $\theta_0 = CI^2P_m^{-2/3}$, where $I$ is the impulse, $P_m$ is the maximum load value, and $C$ depends on the dimensions and properties of the beam, with a numerical factor that varies by about ±15 per cent from the value for the half-sine wave pulse to those for the other two pulse types.**

## Introduction

THE basic hypothesis of a previous paper[3] is adopted. This consists in taking the relation between bending moment and curvature as indicated in Fig. 1(*a*). Specifically, we assume the following:

1 Elastic deformations are negligible compared with plastic deformations; the curvature at any section is assumed constant unless the moment reaches and maintains a definite magnitude $M_0$, termed the "limit moment," or "fully plastic moment."

2 At a section where $M_0$ is maintained the curvature can increase without limit. Thus a discontinuity in slope can occur at such a section, which is termed a "plastic hinge." (In real beams the plastic deformation occurs in a small but finite length, as indicated in Fig. 1(*b*).

3 Relative displacements of parts of the beam are assumed small enough so that shape changes can be neglected.

The determination of $M_0$ from tests or by computation is discussed elsewhere[3,4,5] as are also the limitations and experimental evidence concerning the use of the plastic-hinge concept in the analysis of frame structures under static loads. The validity, in dynamical problems, of neglecting elastic deformations by comparison with plastic ones depends on how much the energy absorbed in plastic deformation exceeds the maximum possible elastic strain energy. This was discussed previously,[3] and a criterion for the validity of the method was put forward involving the ratio of the duration time of the force pulse to the fundamental period of elastic vibration of the bar. However, the more precise evaluation of this criterion will require experimental investigations. It is hoped that the present results will be useful in carrying out and interpreting such investigations.

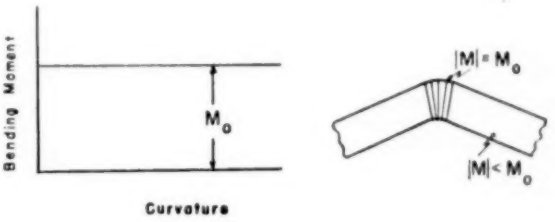


Assumed moment-curvature relation — "Plastic-hinge" behavior

Fig. 1

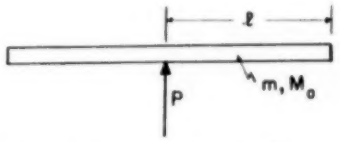


Fig. 2 Nomenclature for Uniform Beam Problem

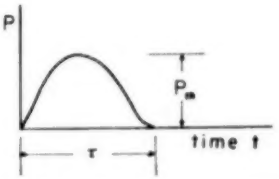


Fig. 3 Type of Dynamic Load Considered in Paper

We consider, as in the earlier paper,[3] the problem of a uniform beam acted on by a force $P$ at the mid-point, Fig. 2. The beam has constant limit moment $M_0$, mass per unit length $m$, and length $2l$. The ends are unconstrained. We are interested in the plastic deformation produced by loads of the sort indicated in Fig. 3, i.e., in force pulses of finite duration, characterized by a maximum load value $P_m$, a duration time $\tau$, and a definite shape. Although the force-time function is taken as one of the basic data of the analysis, in practice the shape of the force pulse usually cannot be predicted or controlled with much accuracy. Hence a main pur-

[1] The results in this paper were obtained in the course of research conducted under Contract N7onr-35810 between the Office of Naval Research and Brown University.

[2] Associate Professor of Engineering, Brown University. Mem. ASME.

[3] "Large Plastic Deformations of Beams Under Transverse Impact," by E. H. Lee and P. S. Symonds, Trans. ASME, vol. 74, 1952, p. 308.

[4] "A Review of Recent Investigations Into the Behavior of Steel Frames in the Plastic Range," by J. F. Baker, *Journal of the Institution of Civil Engineers*, vol. 27, 1949, p. 288.

[5] "Recent Progress in the Plastic Methods of Structural Analysis," by P. S. Symonds and B. G. Neal, *Journal of The Franklin Institute*, vol. 252, 1951, pp. 383–407, 469–492.

Presented at the National Conference of the Applied Mechanics Division, Minneapolis, Minn., June 18–20, 1953, of The American Society of Mechanical Engineers.

Discussion of this paper should be addressed to the Secretary, ASME, 29 West 39th Street, New York, N. Y., and will be accepted until January 11, 1954, for publication at a later date. Discussion received after the closing date will be returned.

Note: Statements and opinions advanced in papers are to be understood as individual expressions of their authors and not those of the Society. Manuscript received by ASME Applied Mechanics Division, October 14, 1952. Paper No. 53—APM-26.

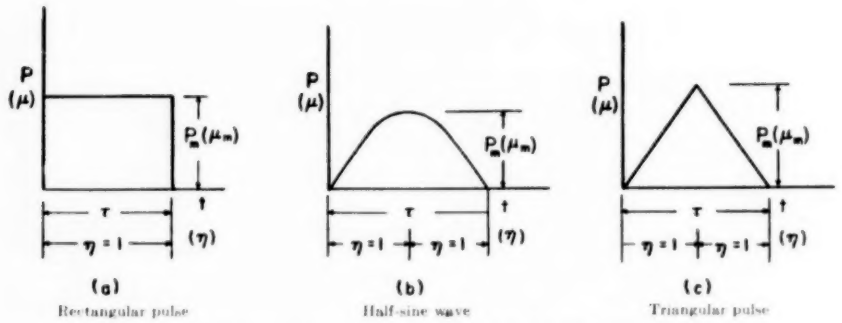


FIG. 4 NOMENCLATURE FOR SPECIFIC FORCE PULSES CONSIDERED
($\eta$ = time $t$/reference time $T$; $\mu = Pl/M_0$.)

pose of this paper is to present results computed for three types of force pulse, which might be considered to cover the range of pulse shapes usually encountered. Therefore we give results for the pulses indicated in Fig. 4, with shape of a rectangle, a half-sine wave, and an isosceles triangle, respectively. The interesting empirical result obtained is that the final plastic deformation depends, over a wide range of maximum load values, primarily on the impulse $I$ of the load, namely

$$I = \int_0^\tau P\,dt$$

It depends less strongly on the maximum load value (for constant $I$) and still less on the precise shape of the force pulse. This means that a simple formula can be given by which the final deformation can be estimated with reasonable accuracy for many shapes of force pulse, provided the impulse and the maximum load value can be reasonably well estimated.

## GENERAL EQUATIONS

As discussed in the earlier paper,[3] three phases of deformation occur, for sufficiently large loads. First, there is a rigid-body translation, during which the bending moment at all sections is less in magnitude than $M_0$. Letting $v$ be the velocity, the acceleration is given by

$$\frac{dv}{dt} = \frac{P}{2ml} \qquad [1]$$

This phase ends when $P$ reaches a value $P_1$ such that the moment at the mid-section is $M_0$. Defining the load parameter $\mu$ as in the previous reference[3]

$$\mu = \frac{Pl}{M_0} \qquad [2]$$

the first phase ends at the value

$$\mu_I = 4 \qquad [3]$$

In the second phase the central moment has the constant magnitude $M_0$, and the two halves of the bar rotate with respect to each other as if hinged at the middle, Fig. 5(*b*). Let $v_0$ denote the transverse velocity of the mid-section, and $\omega_0$ the angular velocity (positive clockwise) of the right-hand half. The equations of motion are

$$\frac{ml^2}{M_0}\frac{dv_0}{dt} = 2\mu - 6 \qquad [4]$$

$$\frac{ml^2}{M_0}\frac{d\omega_0}{dt} = 3\mu - 12 \qquad [5]$$

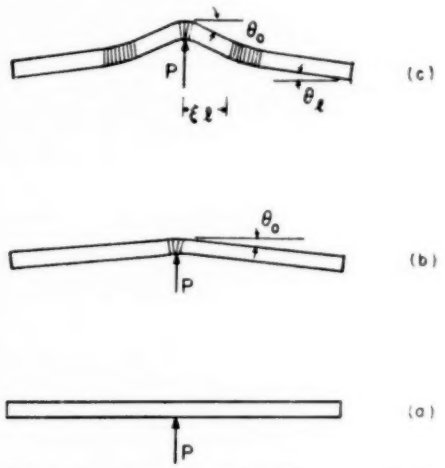


FIG. 5 STAGES IN PLASTIC DEFORMATION OF BEAM

This phase ends when the load parameter reaches the value $\mu_{II}$, where

$$\mu_{II} = 22.89 \qquad [6]$$

At the load corresponding to this value, the bending moment at the cross sections whose distance from the mid-point is $0.404l$, in each half of the beam, reaches the magnitude $M_0$ with sense opposite to that of the bending moment at the mid-point. As the load increases further, these two lateral plastic hinges move inward, leaving behind them regions of permanent deformation as indicated in Fig. 5(*c*).

The analysis of this paper applies to deformations of the types indicated in Fig. 5. In the Appendix it is shown that at sufficiently large loads a different type of deformation may occur under certain conditions. Under the loading conditions considered in this paper this new type of deformation either does not occur or introduces negligible differences in final displacements.

We define symbols and write equations of motion for the right-hand half of the beams as follows: Let $\xi l$ denote the distance of the lateral hinge from the mid-point, Fig. 5(*c*), $v_0$ and $v_t$ the transverse velocities of mid-point and tip, respectively, and $\omega_0$ and $\omega_t$ the angular velocities of the segments to left and to right of the hinge, respectively (positive when clockwise). The four dynamical equations for the two segments of length $\xi l$ and $(1 - \xi)l$ are as follows

$$\frac{ml^2}{M_0}\frac{dv_0}{dt} = \frac{2\mu}{\xi} - \frac{12}{\xi^2} \qquad [7a]$$

$$\frac{ml^2}{M_0}\frac{dv_i}{dt} = \frac{-6}{(1-\xi)^2} \quad [7b]$$

$$\frac{ml^2}{M_0}\frac{d\omega_0}{dt} = \frac{3\mu}{\xi^2} - \frac{24}{\xi^3} \quad [8a]$$

$$\frac{ml^2}{M_0}\frac{d\omega_i}{dt} = \frac{12}{(1-\xi)^3} \quad [8b]$$

An additional equation relating the five unknowns $\xi$, $v_0$, $v_i$, $\omega_0$, $\omega_i$ is required. In the previous paper[3] it was shown that the transverse acceleration varies discontinuously across the moving hinge, and the equation expressing the amount of the jump may be put in the following form

$$\mu\xi + \frac{6\xi^2}{(1-\xi)^2} - 12 = -\frac{ml^3}{M_0}(\omega_0 - \omega_i)\xi^2\frac{d\xi}{dt} \quad [9]$$

Equations [7] to [9] hold as long as $\omega_0 > \omega_i$, so that the kinematic picture in Fig. 5(*c*) is the correct one. Equations [4] and [5] apply in any case when $\omega_0 - \omega_i = 0$ but $\omega_0 > 0$. It is seen that the calculation of the deformation is more difficult when the maximum load is such that Equations [7] to [9] must be used during part of the motion than when only Equations [1], [4], and [5] are involved. In the latter case, which occurs when the maximum value of $\mu$ does not exceed 22.89, the accelerations depend only on the instantaneous load value, and successive quadratures give velocities and displacements directly. When the lateral hinges are present the nature of the additional equation required to determine the unknown $\xi$ makes it impossible to compute accelerations without consideration of velocities, and this makes part of the numerical solution much more laborious, in general.

An alternative equation relating the hinge co-ordinate $\xi$ to the angular velocities can be derived from momentum considerations, and this has certain advantages over Equation [9]. At any instant the linear impulse of the force $P/2$ acting on the right-hand half of the beam is equal to the linear momentum of this half. Let $v_h$ denote the transverse velocity at the hinge section, which at time $t$ is a distance $\xi l$ from the middle. Then the linear momentum equation is

$$\frac{1}{2}\int_0^t P\,dt = m\left[v_h l + \frac{1}{2}\xi^2 l^2\omega_0 - \frac{1}{2}(1-\xi)^2 l^2\omega_i\right] \quad [10]$$

An analogous equation can be written expressing the equality of angular impulse to the moment of momentum of the right-hand half of the beam, about the mid-point of the beam. We note that the external moment acting on this half of the beam has the magnitude $M_0$ at all times after the start of the second phase until the plastic deformation is completed. The transverse velocity of the beam at the close of the first phase is

$$v_1 = \frac{M_0}{2ml^2}\int_0^{t_1}\mu\,dt$$

where $t_1$ is the time corresponding to $\mu_1 = 4$. Hence the moment of momentum about the mid-point at time $t_1$ is readily found to be $\frac{1}{4}M_0\int_0^{t_1}\mu\,dt$. Using this, the equation for the moment of momentum at any time $t$ is

$$\frac{1}{4}M_0\int_0^{t_1}\mu\,dt + M_0(t-t_1) = m\left[\frac{l^2}{2}v_h + \frac{\xi^3 l^3}{6}\omega_0 + \left(\frac{\xi l^3}{2} - \frac{l^3}{3} - \frac{\xi^3 l^3}{6}\right)\omega_i\right] \quad [11]$$

This equation is now combined with Equation [10] so as to eliminate the velocity $v_h$. The result is

$$3\int_{t_1}^{t}\mu\,dt - 12(t-t_1) = \frac{ml^3}{M_0}[(3\xi^2 - 2\xi^3)(\omega_0 - \omega_i) + \omega_i] \quad [12]$$

This holds at all times $t$ until the plastic deformation is completed. It can be regarded as equivalent, in a sense, to the equation for the discontinuity of acceleration, Equation [9]. In fact, the latter can be derived from it by differentiation and use of the acceleration Equations [8].

Our primary interest is in the final plastic deformation. By far the largest deformation is that associated with the central angle $\theta_0$, Figs. 5(*b* and *c*), and this is taken as the main quantity to be computed. As already noted, if $\mu \leq 22.89$, the determination of the final angle of deformation requires only simple quadrature of Equation [5]. Hence the main task is the numerical integration of the equations which apply when lateral hinges are present. It is evident that to find the two angles, $\theta_0$ at the center and $\theta_i$ at the tip, there are only three basic equations to be solved simultaneously, involving the three variables $\xi$, $\omega_0$, $\omega_i$, where $\omega_0 = d\theta_0/dt$, $\omega_i = d\theta_i/dt$. These are the two acceleration Equations [8*a*], [8*b*], and either Equation [9] or Equation [12]. Once the angular velocities $\omega_0$, $\omega_i$ are determined, the corresponding angles $\theta_0$, $\theta_i$ are easily found by direct integration.

It is convenient to rewrite the basic equations in completely nondimensional form. Let $T$ be a time associated with the force pulse, chosen for maximum convenience in numerical integration. For example, in a case of a symmetrical triangular pulse, $T$ most conveniently might be half the duration time of the pulse; for a nonsymmetrical pulse it probably would be the actual duration time. In any event, a dimensionless time $\eta$ can then be defined as

$$\eta = \frac{t}{T} \quad [13]$$

We now can define dimensionless angular velocity and displacement quantities as follows

$$\Omega = \frac{ml^2}{M_0 T}\omega_0, \quad \Psi = \frac{ml^2}{M_0 T}\omega_i \quad [14]$$

$$\Theta = \frac{ml^2}{M_0 T^2}\theta_0, \quad \varphi = \frac{ml^2}{M_0 T^2}\theta_i \quad [15]$$

The basic Equations [8*a*], [8*b*], [9], and [12] now appear as follows in terms of $\xi$, $\Omega$, $\Psi$

$$\frac{d\Omega}{d\eta} = \frac{3\mu}{\xi^2} - \frac{24}{\xi^3} \quad [16a]$$

$$\frac{d\Psi}{d\eta} = \frac{12}{(1-\xi)^3} \quad [16b]$$

$$\mu\xi + \frac{6\xi^2}{(1-\xi)^2} - 12 = -(\Omega - \Psi)\xi^2\frac{d\xi}{d\eta} \quad [17]$$

$$3\int_{\eta_1}^{\eta}\mu d\eta - 12(\eta - \eta_1) = (3\xi^2 - 2\xi^3)(\Omega - \Psi) + \Psi \quad [18]$$

Here $\eta_1$ denotes the nondimensional time at which the central hinge first occurs, corresponding to $\mu_1 = 4$; the load parameter is a known function $\mu(\eta)$. Once $\xi$, $\Omega$, $\Psi$ are determined so as to satisfy Equations [16] to [18] and the initial conditions, the nondimensional angular displacements are found by direct integration from the relations

$$\frac{d\Theta}{d\eta} = \Omega, \quad \frac{d\varphi}{d\eta} = \psi \qquad [19]$$

The actual deformation angles $\theta_0$, $\theta_l$ are then given by Equations [15] in terms of the basic data $m$, $l$, $M_0$, $T$.

### 3 Motion After Conclusion of Force Pulse

In general, the integration of Equations [16] to [18] must be done by a step-by-step or iterative method. Only in the special case of the rectangular pulse, apparently, can the whole solution be obtained in simple analytical form. However, even for general pulse shapes, numerical integration of the equations is required only for the time interval $t \leq \tau$ during which the external load is applied. Let $\eta_\tau = t/\tau$ be the value of $\eta$ at which the force becomes zero. Suppose we know the values $\xi_\tau$, $\Omega_\tau$, $\psi_\tau$, $\Theta_\tau$, $\varphi_\tau$ at this time. Then we can compute the subsequent deformations in terms of these quantities by simple formulas. It seems desirable, since these formulas apply to all types of force pulses, to present them first, and postpone for the moment the discussion of how the required initial values $\xi_\tau$, $\Omega_\tau$, and so on, can be obtained, by numerical integration or otherwise.

For times $\eta \geq \eta_\tau$ we must first solve Equations [16] to [18] with $\mu = 0$. These solutions must agree with the known values $\xi_\tau$, $\Omega_\tau$, $\psi_\tau$, $\varphi_\tau$, at $\eta = \eta_\tau$, and they will be valid until the two angular velocities $\Omega$ and $\psi$ become equal. Let $\eta_s$ be the time at which this occurs. For times $\eta \geq \eta_s$ the lateral hinges are absent, and the two halves of the bar again rotate with respect to each other as hinged rigid bars, as in Fig. 5(*b*). Finally, at a time $\eta_f$, the angular velocities of the two halves are reduced to zero, and plastic deformation ceases.

Considering first the time interval $\eta_\tau \leq \eta \leq \eta_s$, we can show that the basic equations and initial conditions (at $\eta = \eta_\tau$) can all be satisfied by taking

$$\frac{d\xi}{d\eta} = \text{const} = \frac{1}{C} \qquad [20a]$$

where

$$C = \frac{\xi_\tau^2(\Omega_\tau - \psi_\tau)}{12 - \dfrac{6\xi_\tau^2}{(1 - \xi_\tau)^2}} \qquad [20b]$$

This implies, of course

$$\eta = \eta_\tau + C(\xi - \xi_\tau) \qquad [21]$$

To justify the foregoing statements, we note that if Equation [20*a*] is correct, the acceleration Equations [16*a*], [16*b*] can be integrated at once, yielding

$$\Omega = \Omega_\tau - C\left(\frac{12}{\xi_\tau^2} - \frac{12}{\xi^2}\right) \qquad [22a]$$

$$\psi = \psi_\tau + C\left[\frac{6}{(1-\xi)^2} - \frac{6}{(1-\xi_\tau)^2}\right] \qquad [22b]$$

If we now insert these expressions in Equation [17], with $\mu = 0$, we obtain the result

$$C\left[\frac{12}{\xi^2} - \frac{6}{(1-\xi)^2}\right] = \Omega_\tau - \psi_\tau + C\left[\frac{12}{\xi^2} - \frac{6}{(1-\xi)^2}\right] - C\left[\frac{12}{\xi_\tau^2} - \frac{6}{(1-\xi_\tau)^2}\right]$$

This is satisfied at all times when $C$ is given by Equation [20*b*]. Alternatively, as a check, it is not hard to verify that when Equations [22] are substituted in the momentum relation Equation [18], with $\eta$ as given by Equation [21], the constant value of $C$ according to Equation [20*b*] is again obtained.

Equations [22] hold up to time $\eta_s$, when the angular velocities become equalized, and the lateral hinges disappear. The value of the hinge co-ordinate $\xi_s$ at this instant turns out to be the same, irrespective of the previous motion.[6] It is found by setting both $\Omega - \psi$ and $\mu$ equal to zero in Equation [17]. The resulting quadratic equation has the solution

$$\xi_s = 2 - \sqrt{2} \doteq 0.586 \qquad [23]$$

Having this value we can now compute the time $\eta_s$ and the angular velocities and displacements at time $\eta_s$, as follows

$$\eta_s = \eta_\tau + C(0.586 - \xi_\tau) \qquad [24]$$

$$\Omega_s = \Omega_\tau - C\left(\frac{12}{\xi_\tau^2} - 34.97\right) \qquad [25a]$$

$$\psi_s = \Omega_s = \psi_\tau + C\left[34.97 - \frac{6}{(1-\xi_\tau)^2}\right] \qquad [25b]$$

$$\Theta_s = \Theta_\tau + C\left[\Omega_\tau - \frac{12C}{\xi_\tau^2}\right](0.586 - \xi_\tau) + C^2\left(\frac{12}{\xi_\tau} - 20.48\right) \qquad [26a]$$

$$\varphi_s = \varphi_\tau + C\left[\psi_\tau - \frac{6C}{(1-\xi_\tau)^2}\right](0.586 - \xi_\tau) + C^2\left[14.49 - \frac{6}{(1-\xi_\tau)^2}\right] \qquad [26b]$$

An alternative expression for $\Omega_s = \psi_s$ is given directly by the momentum relation, Equation [18], by setting $\eta = \eta_s$, $\Omega = \psi$, as follows

$$\Omega_s = \psi_s = 3\int_{\eta_1}^{\eta_s} \mu d\eta - 12(\eta_s - \eta_1)$$

This is useful as a check.

Finally, we consider the additional deformations in the time interval $\eta_s \leq \eta \leq \eta_f$. Here the kinematic picture in Fig. 5(*b*) is again appropriate, and the equation of motion (from Equation [5]) is

$$\frac{d\Omega}{d\eta} = -12 \qquad [27]$$

Since $\Omega$ is reduced from $\Omega_s$ to zero in the time $\eta_f - \eta_s$, we obtain easily[7]

$$\eta_f = \eta_s + \frac{1}{12}\Omega_s \qquad [28]$$

$$\Theta_f = \Theta_s + \frac{1}{24}\Omega_s^2 \qquad [29]$$

The increment $\Theta_f - \Theta_s$ is often a substantial part of the total plastic deformation.

### Motion During Force Pulse

We return now to the problem of computing the angular velocities and displacements in the time interval $\eta \leq \eta_\tau$, while the external load is acting. We consider first the rectangular pulse,

[6] It is assumed that the lateral hinges still exist at times $\eta > \eta_\tau$.

[7] A useful check on this value of $\eta_f$ is obtained directly from Equation [18] by setting the right-hand side zero and $\eta = \eta_f$, which is the only unknown quantity in the equation.

which is very simple, and then discuss methods of numerical integration for general types of force pulses.

*Rectangular Pulse.* We define symbols specifying the pulse as in Fig. 4(*a*). Thus we have to solve Equations [16] to [18] with $\mu$ given the constant value $\mu_m$ and all velocities and displacements equal to zero at time $\eta = 0$. In particular we want the values $\xi_r$, $\Omega_r$, $\psi_r$, $\Theta_r$, and $\varphi_r$ at the end of the pulse, when $\eta = 1$.

It can easily be verified that Equations [16] to [18] are all satisfied with $\xi$ equal to a constant, say, $\xi_1$, related to $\mu_m$ by the expression

$$\mu_m \xi_1 + \frac{6\xi_1^2}{(1 - \xi_1)^2} - 12 = 0 \quad \ldots\ldots\ldots\ldots [30]$$

Since the accelerations are all constant the angular velocities and displacements are found by integration as

$$\Omega = \left(\frac{3\mu_m}{\xi_1^2} - \frac{24}{\xi_1^3}\right)\eta \quad \ldots\ldots\ldots\ldots [31a]$$

$$\psi = \frac{12\eta}{(1 - \xi_1)^3} \quad \ldots\ldots\ldots\ldots [31b]$$

$$\Theta = \frac{1}{2}\left(\frac{3\mu_m}{\xi_1^2} - \frac{24}{\xi_1^3}\right)\eta^2 \quad \ldots\ldots\ldots\ldots [32a]$$

$$\varphi = \frac{6\eta^2}{(1 - \xi_1)^3} \quad \ldots\ldots\ldots\ldots [32b]$$

As a check, it may be verified that if the expressions for $\Omega$ and $\psi$ given in Equations [31] are substituted in the momentum relation [18] the resulting equation can be reduced to the form of Equation [30]; the latter is obviously the result of setting $d\xi/d\eta = 0$ in Equation [17]. The appropriate form of the momentum relation is found by putting $\eta_1 = 0$, $\mu = \mu_m$ in Equation [18], which becomes

$$3\mu_m\eta - 12\eta = (3\xi^2 - 2\xi^3)(\Omega - \psi) + \psi \quad \ldots\ldots [33]$$

The required values at $\eta = \eta_r = 1$ are obtained by setting $\eta = 1$ in Equations [31] and [32]; $\xi_r$ is obviously $\xi_1$ as determined from Equation [30].

Curve A in Fig. 6 shows the dependence of the final plastic angle $\Theta_f$ on $\mu_m$, for rectangular pulses. These results are discussed further in a later section.

*Arbitrary Pulse Shapes.* No simple analytical solution of Equations [16] to [18] seems to be possible except for the rectangular force pulse. The case of a pulse made up of rectangular steps also may be treated analytically, but the numerical evaluation is still quite laborious, so that this does not appear to be a practicable approach to general pulse shapes.

A reliable method of step-by-step integration, applicable equally well to force pulses of any shape, can be based directly on the momentum relation, Equation [18]. This is basically a method of trial and adjustment to determine a sequence of values $\xi_0, \xi_1, \xi_2, \ldots \xi_r$, corresponding to a chosen sequence of times $\eta_0, \eta_1, \eta_2, \ldots \eta_r$, such that at each of these instants the momentum condition is satisfied with a given degree of accuracy. The starting instant $\eta_0$ corresponds to the appearance of lateral hinges at $\xi_0 = 0.404$, $\mu_0 = \mu_{11} = 22.89$.

To describe the method we show how a typical line of Table I is constructed. This table gives the essential computations for the case of the half-sine wave $\mu = 40 \sin \pi\eta/2$. Intervals of $\eta$ after the first are chosen as 0.100. The first step in the method is to compute values of $\mu$ at the selected instants 0.400, 0.500, . . . 2.000. The function $L(\eta)$ is then computed at these points, where $L$ stands for the left-hand side of Equation [18]; in the present case

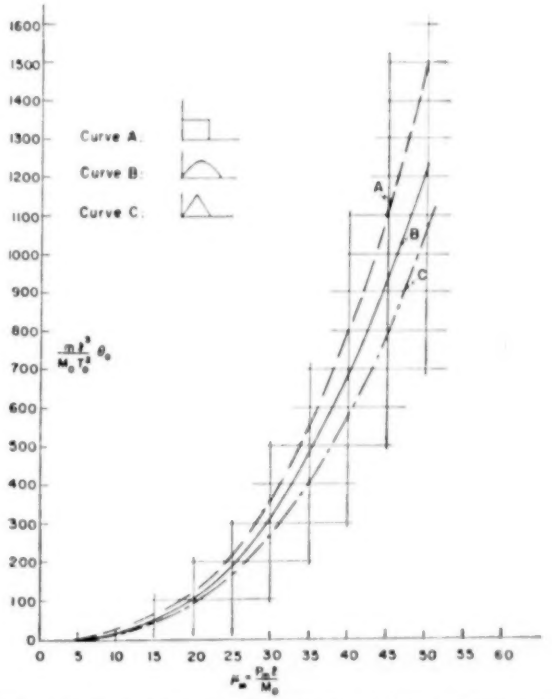


FIG. 6 CURVES SHOWING DEPENDENCE OF FINAL PERMANENT DEFORMATION ON MAXIMUM LOAD, FOR THREE SHAPES OF FORCE PULSE

($T_0$ is defined so that $P_m T_0 = \int_0^\tau P\,dt$; $P_m$ is peak-force value.)

$$L(\eta) = 3\int_{\eta_1}^{\eta} \mu\,d\eta - 12(\eta - \eta_1)$$

$$= 76.39\left(0.9950 - \cos\frac{\pi\eta}{2}\right) - 12(\eta - 0.0637)$$

Supposing all the quantities in the table have been calculated up to and including the instant $\eta = 1.300$, we show how values for $\eta = 1.400$ are found. The slope $d\xi/d\eta$ at $\eta = 1.300$ is found by Equation [17], after the correct values of $\xi$, $\Omega$, and $\psi$ have been computed. A rough value of $\xi$ for the next instant $\eta = 1.400$ is then computed as $0.288 + (0.035)(0.10) = 0.292$. Taking this as the first trial value we compute the following values for $\eta = 1.400$

$$3\xi^2 - 2\xi^3 = 0.2060; \qquad d\Omega/d\eta = 174.6$$

$$d\psi/d\eta = 33.8$$

$$\Omega = 268.4 + \frac{0.1}{3}[370.4 + 4(284.4) + 174.6] = 324.5$$

$$\psi = 40.6 + \frac{0.1}{3}[33.1 + 4(33.2) + 33.8] = 47.3$$

$$\Omega - \psi = 277.2$$

$$(3\xi^2 - 2\xi^3)(\Omega - \psi) + \psi = 104.4$$

The last result is slightly low; it should equal $L(1.400) = 104.9$. Hence for the next trial we take $\xi = 0.293$. With this choice the values listed in the table for $\eta = 1.400$ are computed, and the quantity $(3\xi^2 - 2\xi^3)(\Omega - \psi) + \psi$ is now found to be 104.8. It is evident that the value $\xi = 0.293$ is correct to three significant figures. The values in the table for $\eta = 1.400$ are therefore taken

TABLE 1 NUMERICAL INTEGRATION FOR CASE $\mu = 40 \sin \frac{\pi\eta}{2}$

$$L = 3\int_{\eta_1}^{\eta} \mu\, d\eta - 12(\eta - \eta_{II}) = 76.39\left(0.9950 - \cos\frac{\pi\eta}{2}\right) - 12(\eta - 0.0637)$$

| $\frac{d\xi}{d\eta}$ | $\frac{d^2\xi}{d\eta^2}$ | $\eta$ | $L$ | $\mu$ | $\xi$ | $1-\xi$ | $\frac{d\Omega}{d\eta}$ | $\frac{d\psi}{d\eta}$ | $\Omega$ | $\psi$ | $\Omega - \psi$ | $\frac{N}{3\xi^2 - 2\xi^3}$ | $\frac{L}{[N(\Omega - \psi) + \psi]}$ |
|---|---|---|---|---|---|---|---|---|---|---|---|---|---|
| −0.455 | 2.04 | 0.388 | 9.47 | 22.89 | 0.404 | 0.596 | 56.8 | 56.8 | 9.5 | 9.5 | 0 | | 0 |
| | | 0.400 | 10.17 | 23.51 | 0.399 | 0.601 | 65.3 | 55.3 | 10.20 | 10.14 | 0.06 | 0.3506 | 0.01 |
| | | 0.500 | 16.75 | 28.28 | 0.360 | 0.640 | 140.3 | 45.8 | 20.5 | 15.2 | 5.3 | 0.2955 | 0.0 |
| −0.30 | | 0.600 | 24.7 | 32.36 | 0.342 | 0.658 | 230.0 | 42.1 | 38.8 | 19.4 | 19.4 | 0.2709 | 0.0 |
| −0.13 | | 0.700 | 33.7 | 35.64 | 0.316 | 0.684 | 310.1 | 37.5 | 66.2 | 23.6 | 42.6 | 0.2365 | 0.0 |
| −0.13 | | 0.800 | 43.6 | 38.04 | 0.308 | 0.692 | 381.7 | 36.2 | 100.5 | 27.0 | 73.5 | 0.2262 | 0.0 |
| −0.074 | | 0.900 | 54.0 | 39.51 | 0.295 | 0.705 | 427.0 | 34.2 | 141.7 | 30.8 | 110.9 | 0.2097 | −0.1 |
| −0.047 | | 1.000 | 64.8 | 40.00 | 0.290 | 0.710 | 443.0 | 33.5 | 184.9 | 34.0 | 150.9 | 0.2035 | +0.1 |
| −0.016 | | 1.100 | 75.5 | 39.51 | 0.286 | 0.714 | 423.1 | 33.0 | 229.1 | 37.5 | 191.6 | 0.1986 | −0.1 |
| 0.006 | | 1.200 | 86.0 | 38.04 | 0.287 | 0.713 | 370.4 | 33.1 | 268.4 | 40.6 | 227.8 | 0.1998 | −0.1 |
| 0.035 | | 1.300 | 95.9 | 35.64 | 0.288 | 0.712 | 284.4 | 33.2 | 302.1 | 44.1 | 258.0 | 0.2011 | −0.1 |
| 0.063 | | 1.400 | 104.9 | 32.36 | 0.293 | 0.707 | 176.7 | 34.0 | 324.6 | 47.3 | 277.3 | 0.2072 | +0.1 |
| 0.094 | | 1.500 | 112.8 | 28.28 | 0.300 | 0.700 | 53.9 | 35.0 | 336.9 | 50.9 | 286.0 | 0.2160 | +0.1 |
| 0.125 | | 1.600 | 119.4 | 23.51 | 0.312 | 0.688 | −65.6 | 36.8 | 335.5 | 54.3 | 281.2 | 0.2313 | +0.1 |
| 0.165 | | 1.700 | 124.5 | 18.16 | 0.326 | 0.674 | −180.1 | 39.2 | 323.9 | 58.3 | 265.6 | 0.2495 | −0.1 |
| 0.213 | | 1.800 | 127.9 | 12.36 | 0.346 | 0.654 | −269.7 | 42.9 | 299.9 | 62.2 | 237.7 | 0.2763 | 0.0 |
| 0.275 | | 1.900 | 129.5 | 6.26 | 0.369 | 0.631 | −339.8 | 47.8 | 270.6 | 66.9 | 203.7 | 0.3080 | −0.1 |
| 0.355 | | 2.000 | 129.2 | 0 | 0.402 | 0.598 | −369.4 | 56.1 | 233.3 | 71.9 | 161.4 | 0.3549 | +0.1 |

Summation by Simpson's rule: Interval $\eta$ 0.388 → 0.40: 0.1
Interval $\eta$ 0.40 → 2.0 : 337.1

$\Delta\Theta$: 337.2
$\Theta_{II}$ = 1.1

$\Theta_f$: 338.3

NOTE: Here $\Theta$ is defined as $\frac{ml^2}{M_0T^2}\theta_0$: $T = \frac{1}{2}\tau = \frac{\pi}{4}T_0$

as correct, to this accuracy. The derivative at this instant is computed as 0.063, and the same procedure is repeated to obtain values at the next point, $\eta = 1.500$.

In the neighborhood of the time $\eta_0$ at which the integration is started, the calculation of $d\xi/d\eta$ from Equation [17] involves the quotient of two small numbers, and hence tends to be inaccurate. However, just at the starting time $\eta_0$ the derivatives $d\xi/d\eta$, $d^2\xi/d\eta^2$ and higher derivatives can be computed easily, and it is useful to have these values so that the first few terms of a Taylor's series can be used to obtain trial values of $\xi$ at times close to the starting time. For this purpose we derive the differential equation containing only $\xi$ as dependent variable by differentiating Equation [18] with respect to $\eta$ and making use of Equations [16] and [17] to eliminate $\Omega$, $\psi$, $d\Omega/d\eta$, and $d\psi/d\eta$. The resulting equation is

$$P\xi'' - (\mu'\xi + 2\mu\xi')\xi' = 0 \quad \ldots\ldots\ldots\ldots [34]$$

where

$$P = \mu\xi + \frac{6\xi^2}{(1-\xi)^2} - 12$$

and primes denote differentiation with respect to $\eta$. At the time $\eta_0$, corresponding to $\mu_{II} = 22.89$, $\xi_0 = 0.404$, the expression $P$ is zero, since this is the left-hand side of Equation [17]. Hence we have at once

$$\xi_0' = -\frac{\mu_0'\xi_0}{2\mu_0} \quad \ldots\ldots\ldots\ldots [35]$$

where the subscript means that the function or its derivative is evaluated at the starting time $\eta_0$. To derive a formula for $\xi_0''$, differentiate Equation [34] to obtain

$$P'\xi''' + P''\xi'' - (\mu'\xi + 2\mu\xi')\xi'' = (\mu''\xi + 3\mu'\xi' + 2\mu\xi'')\xi' \ldots [36]$$

Now if values $\xi_0$, $\mu_0$ are inserted, it can be shown that $P_0'$ is zero as well as $P_0$, and hence the right-hand side of Equation [36] also must be zero. It follows that

$$\xi_0'' = -\frac{1}{2\mu_0}(\mu_0''\xi_0 + 3\mu_0'\xi_0') \quad \ldots\ldots\ldots [37]$$

Values of higher derivatives at $\eta_0$ could be determined in a similar manner, but for most purposes the values $\xi_0'$, $\xi_0''$ will suffice.

It may be noted, in passing, that Equation [34] might be expected to be a satisfactory basis for the computation of $\xi$ by one of the standard techniques of step-by-step or iterative numerical integration. However, this is a less satisfactory basis for the numerical integration than Equation [18] because of the fact that in two important regions of the time interval the function $P$ is very small; these regions are the neighborhood of the starting time $\eta_0$, and the region containing the time at which $\xi' = 0$, i.e., when the lateral hinge reverses its direction of motion. In both these regions the computation of $\xi''$ from the equation is inaccurate, unless a large number of significant figures is kept. For this reason the use of the momentum relation Equation [18] has been found preferable.

## Comparison of Results

The computation of the final angle of deformation $\Theta_f = (ml^2/M_0T^2)\theta_{0f}$ has been carried out for force pulses having the shape of a rectangle, half-sine wave, and symmetrical triangle, for values of the maximum load parameter $\mu_m$ up to 50, Figs. 4(*b* and *c*). In making the calculations it was convenient to choose $T$ in various ways. However, in order to compare the resulting deformations with each other, we define a new time $T_0$ such that $P_mT_0$ is the impulse, i.e.

$$P_mT_0 = \int_0^\tau P\,dt = I \quad \ldots\ldots\ldots\ldots [38]$$

Fig. 6 shows plots of the dimensionless quantity $(ml^2/M_0T_0^2)\theta_0$ as a function of $\mu_m$ for each of the three types of force pulse. As would be expected, for the same value of maximum load and time $T_0$ the rectangular pulse produces the greatest plastic deformation, while the triangular pulse produces the least.

It is of interest to try to draw some empirical conclusions from the results shown in Fig. 6:

1 We note that the deformations for the half-sine wave pulse are fairly good averages of the deformations for the rectangular and triangular shapes for the same $\mu_m$ and $T_0$. At $\mu_m = 40$, for example, the value 690 for the half-sine pulse is about 16 per cent below the value for the rectangular pulse and about 16 per cent above that for the triangular pulse. Thus the results for the half-sine wave pulse can be regarded as giving reasonably good

average values for force pulses of most shapes that are likely to occur in practice.

2 If one assumes a rectangular pulse shape for analytical convenience in other problems (for example, in treating a beam of nonuniform mass or strength distribution), the results may be expected to be overestimates of the plastic deformations which the actual force pulse would produce; judging from the present results the amount of the overestimate might be expected to be less than 20 or 30 per cent.

Finally, it is of interest to note that empirical equations for the three curves in Fig. 6 can be written in the form

$$\frac{ml^2}{M_0 T_0^2}\,\theta_0 = A\mu_m^{\,n} \qquad [39]$$

for $\mu_m$ in the range between about 15 and 50, with reasonable engineering accuracy. It turns out that if $n$ is taken as $2^2/_3$ for all three curves, then the number $A$ should have the values 0.043, 0.037, and 0.031 for the rectangular, sinusoidal, and triangular pulses, respectively. Hence as a simple formula by which the angle of plastic deformation can be estimated roughly for any form, we can write

$$\theta_0 = 0.037\,\frac{M_0 T_0^2}{ml^2}\,\mu_m^{\,2^2/_3} \qquad [40]$$

But $\mu_m = P_m l/M_0$ and $P_m T_0$ is the impulse $I$ of the external load by definition. Hence the foregoing can be rewritten as

$$\theta_0 = \frac{0.037}{mM_0^{\,1/3}l^{2/3}}\,I^2 P_m^{\,2/3} \qquad [41]$$

For a flat force pulse the factor 0.037 would be increased somewhat, while for a more pointed pulse form than a sine wave it might be reduced by 10 or 15 per cent.

These conclusions should be tested experimentally. If their limits of accuracy can be established, they should have considerable practical usefulness. A simple formula such as Equation [41], even if the results are fairly rough, would be adequate for certain purposes, and in any case will give useful preliminary information concerning deformation magnitudes.

# Appendix

The present results hold so long as the moment $M$ does not reach the magnitude $M_0$ at any section other than that at the center or at the two traveling hinge sections of Fig. 5(*c*). This requirement can be examined by drawing appropriate diagrams of effective loading resulting from the accelerated motion and the corresponding moment diagrams. For one of the outer segments in Fig. 5(*c*), of length $l(1 - \xi)$, the loading curve is a straight line passing through the middle of the segment, since the acceleration of the mid-point is zero at any instant. This means that in this segment the bending moment decreases steadily from the value $M_0$ at the hinge end to zero at the free end. However, for one of the inner segments in Fig. 5(*c*) of length $\xi l$, the loading curve is a straight line which may have various inclinations and positions depending on the load $P$. Suppose this line cuts the axis so that the effective load $q$ is positive near the end $x = \xi l$ (corresponding to negative accelerations of the right-hand end of the segment). These positive values of $q$ would correspond to positive second derivatives of $M$ and hence to a maximum of $M$ exceeding the value $M_0$. Since this would violate the plasticity condition, it is seen that in order for the present analysis to hold we must have

$$q(\xi) = -ma(\xi) \leq 0$$

where $a(\xi)$ is the acceleration at $\xi$. Using Equations [7*a*] and [8*a*] this becomes

$$\mu\xi - 12 \leq 0 \qquad [42]$$

Thus the present analysis is valid until at some load $\mu\xi = 12$. At higher loads a new type of analysis must be used, since otherwise the foregoing condition would be violated. In the new analysis the length $\xi l$ of the inner rigid segment is governed by the condition $\mu\xi = 12$ and the segment translates and rotates under the action of the known force $P/2$ and moments $-M_0$ and $M_0$ at its ends. There is another rigid segment extending from $x = \zeta l$, where the moment is $M_0$, to the tip. It is easily seen that $\zeta > \xi$, in general, since with $\zeta = \xi$ momentum conditions could not be satisfied; for example, Equation [34] would not be satisfied, in general, with $\mu\xi = 12$. Thus under certain conditions the situation in Fig. 5(*c*) must be replaced by one in which two rigid segments in each half beam are separated by a short segment in which the moment is constant and equal to $M_0$, i.e., by a finite hinge section.

In the case of a rectangular force pulse the condition Equation [42] is always satisfied. This can be seen by inspection of Equation [30] which determines the constant value of $\xi$ during the force pulse. However, with other pulse shapes the load may reach a magnitude such that $\mu\xi = 12$, and then an analysis leading to deformations of the type indicated in the foregoing must be used. Otherwise, the final deformations will be somewhat underestimated.

In the examples of this paper Equation [42] was satisfied in all cases except for the half-sine pulse with $\mu_{max} = 50$. No attempt was made to compute the error in this case, but since the violation of the plasticity condition occurs during only a small fraction of the pulse duration time, and the deformation after the pulse is more than half of the total, the error may be assumed to be negligible at this load.

# Analog Solution for Beams Excited by an Arbitrary Force

By W. T. THOMSON[1] and T. A. ROGERS,[2] LOS ANGELES, CALIF.

WHEN an arbitrary force acts on a beam, its motion within the elastic range can be expressed by the differential equation

$$EI\frac{\partial^4 y(x,t)}{\partial x^4} + m\frac{\partial^2 y(x,t)}{\partial t^2} = p(x,t) \quad [1]$$

where $m$ is the mass of the beam per unit length and $p(x, t)$ is the intensity of loading.

A formal solution of Equation [1] will result in the displacement expressed by an infinite series of orthogonal functions. This fact is made use of in the method of normal functions which assumes both the deflection and the applied force in terms of such series.

It is known that the normal modes of oscillation are orthogonal and the displacement $y$ possesses an orthogonal set of eigen functions $\phi_n(x)$ with eigen values $\beta_n$. These conditions are expressed mathematically by the following equations

$$\frac{d^4\phi_i(x)}{dx^4} = \beta_i{}^4\phi_i(x), \qquad \beta_i{}^4 = \frac{m\omega_i{}^2}{EI} \quad [2]$$

$$\int_0^l \phi_i(x)\phi_j(x)dx = \begin{cases} 0 \text{ for } i \neq j \\ l \text{ for } i = j \end{cases} \quad [3]$$

Expressing the displacement and the arbitrary applied force by the following series of orthogonal functions

$$y(x,t) = \sum_{i=1}^{\infty} Y_i(t)\phi_i(x) \quad [4]$$

$$p(x,t) = \sum_{i=1}^{\infty} P_i(t)\phi_i(x) \quad [5]$$

the coefficients $Y_i(t)$ and $P_i(t)$ are determined from the orthogonality Equation [3] to be

$$Y_i(t) = \frac{1}{l}\int_0^l y(x,t)\phi_i(x)dx \quad [6]$$

$$P_i(t) = \frac{1}{l}\int_0^l p(x,t)\phi_i(x)dx \quad [7]$$

Substituting Equations [4], [5], and [2] into [1], multiplying by $\phi_i(x)dx$ and integrating with limits 0 to $l$, the differential equation for the time domain becomes

$$\frac{d^2Y_i(t)}{dt^2} + \omega_i{}^2Y_i(t) = \frac{1}{ml}\int_0^l p(x,t)\phi_i(x)dx \quad [8]$$

We will assume here that the intensity of loading can be expressed by the following product

$$p(x,t) = \frac{P_0}{l}p(x)f(t) \quad [9]$$

where $p(x)$ and $f(t)$ are the nondimensional space and time distribution of the loading, and $P_0$ is the total load at the time corresponding to the maximum load. Consequently we have

$$\frac{1}{l}\int_0^l p(x)dx = 1 \quad [10]$$

Equation [8] then reduces to

$$\frac{d^2Y_i(t)}{dt^2} + \omega_i{}^2Y_i(t) = \frac{P_0}{ml}K_i f(t) \quad [11]$$

$$K_i = \frac{1}{l}\int_0^l p(x)\phi_i(x)dx \quad [12]$$

The quantity $K_i$ determines the extent to which the various modes contribute to the motion of the beam and hence is appropriately called the participation factor.

The solution of Equation [11] is of the form

$$Y_i(t) = Y_i(0)\cos\omega_i t + \frac{\dot{Y}_i(0)}{\omega_i}\sin\omega_i t + \frac{P_0}{ml}\frac{K_i}{\omega_i}\int_0^t f(\xi)\sin\omega_i(t-\xi)d\xi \quad [13]$$

where $Y_i(0)$ and $\dot{Y}_i(0)$ are the $i$th-mode components of the initial conditions which are generally taken to be zero for such problems. The nondimensional quantity

$$D_i = \omega_i\int_0^t f(\xi)\sin\omega_i(t-\xi)d\xi \quad [14]$$

is generally called the dynamic load factor for the $i$th mode, the significance of the name implying that if the static deflection of the beam is also expanded in terms of $\phi_i(x)$, a comparison between it and the dynamical equation will show that each term of the expansion will differ by $D_i$.

Equation [4] can now be conveniently expressed in terms of the participation factor and the dynamic load factor as follows

$$y(x,t) = \frac{P_0 l^3}{EI}\sum\frac{K_i\phi_i(x)}{(\beta_i l)^4}D_i \quad [15]$$

where all terms within the summation sign are nondimensional. The slope, moment, and shear are obtainable from Equation [15] by successive differentiation.

It is seen from Equation [15] that the calculation of the response of the beam to an arbitrary force is a matter of determining the various nondimensional quantities indicated. The computational task is greatly aided by the work of Young and

[1] Professor of Engineering, University of California. Mem. ASME.

[2] Professor of Engineering, University of California.

Presented at the National Conference of the Applied Mechanics Division, Minneapolis, Minn., June 18–20, 1953, of THE AMERICAN SOCIETY OF MECHANICAL ENGINEERS.

Discussion of this paper should be addressed to the Secretary, ASME, 29 West 39th Street, New York, N. Y., and will be accepted until January 11, 1954, for publication at a later date. Discussion received after the closing date will be returned.

NOTE: Statements and opinions advanced in papers are to be understood as individual expressions of their authors and not those of the Society. Manuscript received by ASME Applied Mechanics Division, October 27, 1952. Paper No. 53—APM-13.

Felgar[3] which presents in tabular form numerical values of $\phi_i(x)$, and $\beta_i l$ for various end conditions, together with other relationships generally encountered in beam calculations. Generally, $K_i$ is easily computed while the determination of the quantity $D_i$ represents a tedious task.[4]

To obviate the difficulties of the numerical task, the $D_i$ is determined by an analog computer which solves the differential equation

$$\ddot{D}_i + \omega_i^2 D_i = \omega_i^2 f(t) \quad \ldots\ldots\ldots\ldots\ldots\ldots [16]$$

## Electronic Analog Equipment

The electronic analog equipment[5] used is well known and needs only brief discussion. As shown in Fig. 1, three amplifiers are used to simulate the homogeneous portion of Equation [16] for each mode. The frequencies of the various modes are set by the potentiometers in each closed loop. The settings need only be relative to each other with the highest mode setting

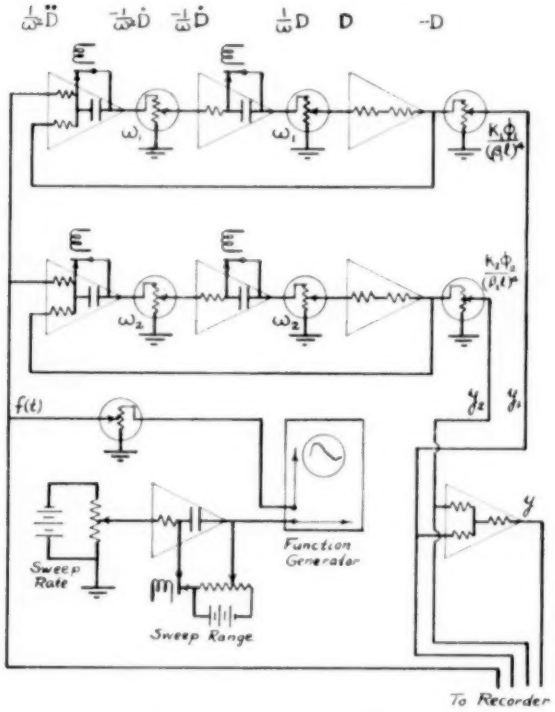


Fig. 1 Electronic Analog Computer

equal to 1.0. The second set of potentiometers establishes the amplitudes $K_i\phi_i/(\beta_i l)^4$ which depend on the load distribution and the position at which the deflection is desired. The various modes are then added together by a summing amplifier. By switching to the terminal before the sign changer, the proper sign for any mode is available.

[3] "Tables of Characteristic Functions Representing Normal Modes of Vibration of a Beam," by D. Young and R. P. Felgar, Engineering Research Series No. 44, University of Texas, Austin, Tex.

[4] "Response of Elastic Beams to Impulsive Loading," by W. T. Thomson and J. Cheney, Weapons Effect Research Report, University of California, Engineering Research, 1951.

[5] "NOTS Analog Computing Facility," by V. R. Briggs, U. S. Naval Ordnance Test Station, Technical Memorandum 4529-23, November 16, 1949.

Auxiliary to the closed loops are the function generator[6] used to simulate the time variation of the driving force and the pen-type recorder. By adjusting the sweep-rate amplifier the time variation of the driving function with respect to the beam periods is established. Simple variations of the foregoing circuit enable one to include the effect of damping.

[6] "Photoelectric Waveform Generator," by D. E. Sunstein, *Electronics*, vol. 22, February, 1949, pp. 100–103.

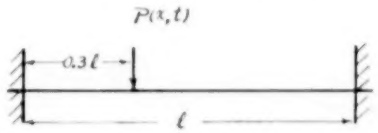


Fig. 2 Force Applied to Beam Clamped at Ends

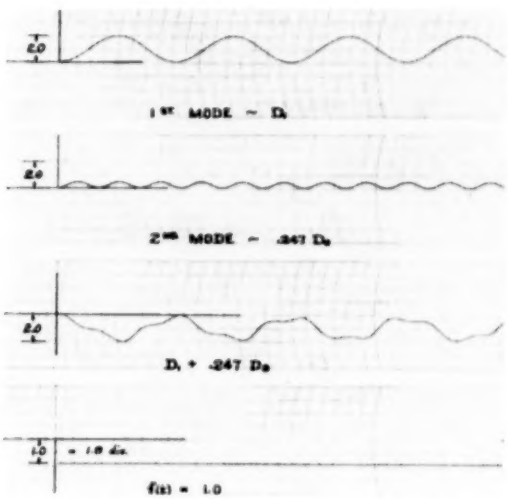


Fig. 3 Amplitudes Due to a Step Function

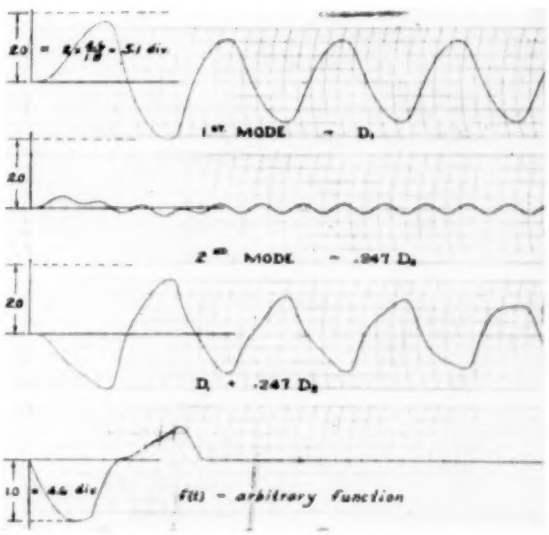


Fig. 4 Response to Arbitrary Time Function

*Example.* The procedure discussed in the paper is illustrated by the following example where an arbitrary time-varying force concentrated at $0.30l$ is applied to a beam with clamped ends as shown in Fig. 2. From the Young and Felgar tables[3] the values in Table 1 are given, where the deflection under the load is desired.

TABLE 1 VALUES FOR USE IN CALCULATING DEFLECTION

| $i$ | $(\beta_i l)^4$ | $\phi_i(0.30)$ | $K_i$ | $\frac{K_i\phi_i(0.30)}{(\beta_i l)^4}$ | Ratio | $\frac{\omega_i}{\omega_3}$ |
|---|---|---|---|---|---|---|
| 1 | 500 | 1.096 | 1.096 | $2.40 \times 10^{-3}$ | 1.0 | 0.362 |
| 2 | 3803 | 1.505 | 1.505 | $0.593 \times 10^{-3}$ | 0.247 | 1.0 |
| 3 | 14617 | 0.868 | 0.868 | $0.0515 \times 10^{-3}$ | 0.021 | ... |

Since the third-mode amplitude is only 2 per cent of the fundamental, it will be neglected. Since only the relative values of the modes are important, we can let

$$\omega_2 = 1.0, \quad \omega_1 = 0.362, \quad \frac{K_1\phi_1(0.30)}{(\beta_1 l)^4} = 1.0$$

and

$$\frac{K_2\phi_2(0.30)}{(\beta_2 l)^4} = 0.247$$

Equation [15] then becomes

$$\frac{yEI}{2.40 \times 10^{-3} Pl^3} = D_1 + 0.247 D_2$$

To establish the scale factor for the computer, the foregoing settings are made on the potentiometers and a step-function input is applied. The amplitude of the step function is adjusted until $D_1$ has a maximum value of 2.0, in which case $D_2$ should have a maximum of $2 \times 0.247$ with a frequency ratio of $\omega_1/\omega_2 = 0.362$, as shown in Fig. 3.

We next apply the desired arbitrary time function shown in Fig. 4. Actually, the maximum value of $f(t)$ should be adjusted to the same height as the step function of Fig. 3. However, since this was not done in this case the scales for the deflection curves must be increased in the ratio shown. The deflection in inches is obtained by multiplying the values on the curves by the factor

$$2.40 \times 10^{-3} \frac{Pl^3}{EI}$$

In the illustration a simple example was chosen and only the deflection under the load was obtained. It should be evident that the same procedure is applicable to a more complex beam such as a continuous beam, provided the normal modes $\phi_i(x)$ are known. Also, other quantities such as the bending moment are obtainable by replacing the settings for

$$\frac{K_i\phi_i}{(\beta_i l)^4} \quad \text{by} \quad K_i \frac{d^2\phi_i}{dx^2}$$

With proper values of $K_i$, any distribution of load may be obtained.

# Thermal Stress in Pipes

By HENRY PARKUS,[1] EAST LANSING, MICH.

**An incompressible, hot liquid in steady-state-flow condition is flowing through a long tube, transferring heat to the surrounding walls. The outer surface of the tube is kept at zero temperature. Temperature distribution and thermal stress in the tube are calculated.**

## Nomenclature

The following nomenclature is used in the paper:

$a$ = inner radius of tube
$b$ = outer radius of tube
$c_f$ = specific heat of liquid
$r$ = co-ordinate in radial direction
$z$ = co-ordinate in axial direction
$F(z)$ = temperature excess of liquid over ambient temperature; average value over cross section at station $z$
$G$ = shear modulus of tube material
$T(r, z)$ = temperature excess of tube over ambient temperature
$V$ = velocity of liquid flow, constant
$\alpha$ = coefficient of linear thermal expansion
$\gamma_f$ = specific weight of liquid
$\lambda$ = coefficient of heat conduction in tube
$\nu$ = Poisson's ratio
$\sigma_r$ = radial-stress component in tube
$\sigma_\varphi$ = circumferential-stress component in tube
$\sigma_z$ = axial-stress component in tube
$\tau_{rz}$ = shearing-stress component in tube
$\omega_n$ = $n$th eigen value
$\theta$ = temperature excess of liquid over ambient temperature at tube entrance $z = 0$, $\theta = F(0)$

## Introduction

An incompressible, hot liquid in steady-state flow enters an infinitely long tube $z \geq 0$ at station $z = 0$ at an initial temperature $\theta$, Fig. 1. The inner radius of the tube is $a$, the outer radius is $b$. Heat is transferred from the flowing fluid to the surrounding tube. The outer surface of the tube is kept at constant temperature $T = 0$.

All thermal and elastic constants are assumed to be independent of temperature within the temperature range considered. The state of stress is assumed to be purely elastic.

## Temperature Distribution

During unit of time (e.g., 1 sec) a short piece of length $dz$ of the tube is passed by a quantity $\gamma_f a^2 \pi V$ (lb per sec) of liquid. On its way from station $z$ to $z + dz$ this quantity cools down from temperature $F(z)$ to $F + (dF/dz)dz$, transferring at the same time the amount of heat

$$dq = \gamma_f a^2 \pi V c_f \frac{dF}{dz} dz$$

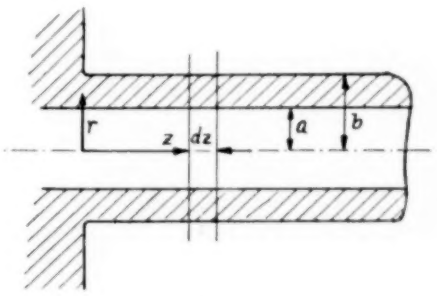


Fig. 1

to the surrounding wall. This amount of heat is conducted from the wall into the tube. We therefore also have

$$dq = \lambda \left( \frac{\partial T}{\partial r} \right)_{r=a} 2a\pi \, dz$$

From the foregoing equations then follows

$$\frac{2\lambda}{a\gamma_f c_f V} \left( \frac{\partial T}{\partial r} \right)_{r=a} = \frac{dF}{dz} \quad [1]$$

Within the tube, $a \leq r \leq b$, the equation of steady-state conduction of heat holds

$$\nabla^2 T = \frac{\partial^2 T}{\partial r^2} + \frac{1}{r} \frac{\partial T}{\partial r} + \frac{\partial^2 T}{\partial z^2} = 0 \quad [2]$$

To simplify the boundary conditions it is assumed that both the inner and the outer surfaces of the tube always have a temperature equal to the temperature of the surrounding medium. Without lack of generalization the ambient temperature may be put equal to zero. Boundary conditions then read

$$T = F(z) \qquad \text{in } r = a \quad [3]$$

$$T = 0 \qquad \text{in } r = b \quad [4]$$

This assumption holds with very large coefficients of heat transfer and it may be expected that owing to the steeper temperature gradients the resulting stress distribution will be a conservative one.

At station $z = 0$, where the tube is joined to the container, let the temperature of the tube be given by

$$T = \theta f(r) \qquad \text{in } z = 0 \quad [5]$$

where $f(r)$ is a given function of $r$, and $f(a) = 1$, $f(b) = 0$.

The solution of the problem can be built up by Bessel functions

$$u(\omega r) e^{-\omega z} \quad [6]$$

with

$$u(\omega r) = \frac{J_0(\omega r)}{J_0(\omega b)} - \frac{Y_0(\omega r)}{Y_0(\omega b)} \quad [7]$$

$J_0$ and $Y_0$ are the Bessel functions of zero order of the first and second kind, respectively.

Function [6] satisfies boundary Condition [4] for all values of

---

[1] Department of Mathematics, Michigan State College.

Presented at the National Conference of the Applied Mechanics Division, Minneapolis, Minn., June 18–20, 1953, of The American Society of Mechanical Engineers.

Discussion of this paper should be addressed to the Secretary, ASME, 29 West 39th Street, New York, N. Y., and will be accepted until January 11, 1954, for publication at a later date. Discussion received after the closing date will be returned.

Note: Statements and opinions advanced in papers are to be understood as individual expressions of their authors and not those of the Society. Manuscript received by ASME Applied Mechanics Division, September 20, 1952. Paper No. 53—APM-19.

$\omega$. Again, for all values of $\omega$, it is a solution of differential Equation [2]. This may easily be verified by using the differential equation of the Bessel functions of zero order

$$u'' + \frac{u'}{\omega r} + u = 0 \quad [8]$$

where

$$u'(x) = \frac{du(x)}{dx}$$

Considering $J_0' = -J_1$, $Y_0' = -Y_1$ we have

$$u'(\omega r) = \frac{1}{\omega}\frac{du(\omega r)}{dr} = \frac{Y_1(\omega r)}{Y_0(\omega b)} - \frac{J_1(\omega r)}{J_0(\omega b)} \quad [9]$$

We now choose $\omega$ as a root of the transcendental equation

$$Hu'(\omega a) + u(\omega a) = 0 \quad [10]$$

with

$$H = \frac{2\lambda}{\gamma_f c_f a V} \quad [11]$$

Function [6] then satisfies differential Condition [1] together with boundary Condition [3].

To satisfy also the last Condition [5], $T(rz)$ is developed into a series of the form

$$T(r, z) = \theta \sum_{n=1}^{\infty} A_n u(\omega_n r) e^{-\omega_n z} \quad [12]$$

$\omega_1, \omega_2 \ldots$ are the positive roots of Equation [10], arranged in ascending order of magnitude. Their calculation is given in the Appendix.

We then have from boundary Condition [5]

$$\sum_{n=1}^{\infty} A_n u(\omega_n r) = f(r) \quad [13]$$

the possibility of the development being supposed. The coefficients $A_n$ of this series are calculated by minimizing the square $E$ of the error, i.e., the deviation of the sum of the series from the prescribed value $f(r)$, (see Appendix). This gives the following system of linear equations for the unknown $A_n$

$$\sum_{m=1}^{\infty} S_{mn} A_m = M_n, \quad (n = 1, 2 \ldots) \quad [14]$$

For $S_{mn}$ and $M_n$ see Appendix.

In practical applications of course a few terms in the series will be considered only.

With coefficients $A_n$ thus determined, the temperature distribution is known from Series [12].

## Thermal Stress

We consider thermal stress only. All other stresses, e.g., those caused by internal pressure, may be superimposed, as long as the resulting state of stress is purely elastic.

The following boundary conditions have then to be satisfied

$$\sigma_r = \tau_{rz} = 0 \qquad \text{in } r = a \text{ and } r = b \quad [15]$$

A particular solution of the thermoelastic equations always may be obtained by introducing the thermoelastic potential[3] $\psi$, satisfying the equation

$$\nabla^2 \psi = \frac{1 + \nu}{1 - \nu} \alpha T \quad [16]$$

In terms of $\psi$ the particular components of displacement, $\bar{u}$ in radial and $\bar{w}$ in the axial direction, are given by

$$\bar{u} = \frac{\partial \psi}{\partial r}, \quad \bar{w} = \frac{\partial \psi}{\partial z}$$

Hence the particular stresses are from Hooke's law

$$\left.\begin{aligned} \bar{\sigma}_r &= 2G\left(\frac{\partial^2 \psi}{\partial r^2} - \nabla^2 \psi\right), \quad \bar{\sigma}_\varphi = 2G\left(\frac{1}{r}\frac{\partial \psi}{\partial r} - \nabla^2 \psi\right) \\ \bar{\sigma}_z &= 2G\left(\frac{\partial^2 \psi}{\partial z^2} - \nabla^2 \psi\right), \quad \bar{\tau}_{rz} = 2G\frac{\partial^2 \psi}{\partial r \partial z} \end{aligned}\right\} \quad [17]$$

In the present case, $\psi$ may be assumed as follows

$$\psi = \theta r \sum_{n=1}^{\infty} C_n u_n'(\omega_n r) e^{-\omega_n z}$$

Considering Equations [8] we then have

$$\nabla^2 \psi = -2\theta \sum_{n=1}^{\infty} C_n \omega_n u(\omega_n r) e^{-\omega_n z}$$

and therefore from Equations [16] and [12]

$$C_n = -\frac{1 + \nu}{1 - \nu} \frac{\alpha}{2} \frac{A_n}{\omega_n} \quad [18]$$

Equations [17] then give the stresses

$$\left.\begin{aligned} \bar{\sigma}_r &= K \sum_{n=1}^{\infty} A_n [\omega_n r u'(\omega_n r) - u(\omega_n r)] e^{-\omega_n z} \\ \bar{\sigma}_\varphi &= -K \sum_{n=1}^{\infty} A_n u(\omega_n r) e^{-\omega_n z} \\ \bar{\sigma}_z &= -K \sum_{n=1}^{\infty} A_n [\omega_n r u'(\omega_n r) + 2u(\omega_n r)] e^{-\omega_n z} \\ \bar{\tau}_{rz} &= -K \sum_{n=1}^{\infty} A_n \omega_n r u(\omega_n r) e^{-\omega_n z} \end{aligned}\right\} \quad [19]$$

with

$$K = \frac{1 + \nu}{1 - \nu} \alpha G \theta \quad [20]$$

As had to be expected, the particular solution $\bar{\sigma}_r \ldots \bar{\tau}_{rz}$ does not fulfill the boundary Conditions [15]. A second state of stress $\sigma_r \ldots \tau_{rz}$ has therefore to be superimposed, pertaining to zero temperature and canceling the boundary stresses of $\bar{\sigma}_r \ldots \bar{\tau}_{rz}$.

This second state of stress may be found by means of Love's displacement function[3] $\Phi$, which is a solution of the bipotential equation

$$\nabla^2 \nabla^2 \Phi = 0$$

The stresses are

[3] "Theory of Elasticity," by S. Timoshenko and J. N. Goodier, second edition, McGraw-Hill Book Company, Inc., New York, N. Y., 1951, p. 433.

[3] Reference 2, p. 343

$$\left.\begin{aligned}\bar{\sigma}_r &= \frac{\partial}{\partial z}\left(\nu\nabla^2\Phi - \frac{\partial^2\Phi}{\partial r^2}\right);\quad \bar{\sigma}_\varphi = \frac{\partial}{\partial z}\left(\nu\nabla^2\Phi - \frac{1}{r}\frac{\partial\Phi}{\partial r}\right)\\ \bar{\sigma}_z &= \frac{\partial}{\partial z}\left[(2-\nu)\nabla^2\Phi - \frac{\partial^2\Phi}{\partial z^2}\right];\\ \bar{\tau}_{rz} &= \frac{\partial}{\partial r}\left[(1-\nu)\nabla^2\Phi - \frac{\partial^2\Phi}{\partial z^2}\right]\end{aligned}\right\} \quad [21]$$

In the present case we assume $\Phi$ in the following form

$$\Phi = \sum_{n=1}^{\infty} [a_n J_0(\omega_n r) + b_n Y_0(\omega_n r) + c_n r J_1(\omega_n r) + d_n r Y_1(\omega_n r)] e^{-\omega_n z}$$

According to Equations [21] we then have the stresses

$$\left.\begin{aligned}\bar{\sigma}_r &= \sum_{n=1}^{\infty} \omega_n^2 \Big\{ [(1-2\nu)c_n - \omega_n a_n] J_0(\omega_n r) \\ &+ [(1-2\nu)d_n - \omega_n b_n] Y_0(\omega_n r) + \left(\frac{a_n}{r} - \omega_n c_n\right) J_1(\omega_n r) \\ &+ \left(\frac{b_n}{r} - \omega_n d_n\right) Y_1(\omega_n r) \Big\} e^{-\omega_n z}\\ \bar{\sigma}_\varphi &= \sum_{n=1}^{\infty} \omega_n^2 \Big[ (1-2\nu)c_n J_0(\omega_n r) + (1-2\nu)d_n Y_0(\omega_n r) \\ &- \frac{a_n}{r} J_1(\omega_n r) - \frac{b_n}{r} Y_1(\omega_n r) \Big] e^{-\omega_n z}\\ \bar{\sigma}_z &= \sum_{n=1}^{\infty} \omega_n^2 \Big\{ -[2(2-\nu)c_n + \omega_n a_n] J_0(\omega_n r) \\ &- [2(2-\nu)d_n + \omega_n b_n] Y_0(\omega_n r) + \omega_n r [c_n J_1(\omega_n r) \\ &+ d_n Y_1(\omega_n r)] \Big\} e^{-\omega_n z}\\ \bar{\tau}_{rz} &= \sum_{n=1}^{\infty} \omega_n^2 \Big\{ -\omega_n r [c_n J_0(\omega_n r) + d_n Y_0(\omega_n r)] \\ &+ [\omega_n a_n - 2(1-\nu)c_n] J_1(\omega_n r) \\ &+ [\omega_n b_n - 2(1-\nu)d_n] Y_1(\omega_n r) \Big\} e^{-\omega_n z}\end{aligned}\right\} \quad [22]$$

If now the boundary Conditions [15] are evaluated for the resulting stress

$$\sigma_r = \bar{\sigma}_r + \sigma_r = 0; \quad \tau_{rz} = \bar{\tau}_{rz} + \tau_{rz} = 0 \quad \text{in } r = a \text{ and } r = b$$

then the following four equations for the four coefficients $a_n \ldots d_n$ are obtained

$$\left.\begin{aligned}&\left[\frac{J_1(\omega_n a)}{a} - \omega_n J_0(\omega_n a)\right] a_n + \left[\frac{Y_1(\omega_n a)}{a} - \omega_n Y_0(\omega_n a)\right] b_n \\ &+ [(1-2\nu)J_0(\omega_n a) - \omega_n a J_1(\omega_n a)] c_n \\ &+ [(1-2\nu)Y_0(\omega_n a) - \omega_n a Y_1(\omega_n a)] d_n \\ &= -K(\omega_n a + H)\frac{u'(\omega_n a)}{\omega_n^2} A_n\\ &\omega_n J_1(\omega_n a) a_n + \omega_n Y_1(\omega_n a) b_n - [2(1-\nu)J_1(\omega_n a) \\ &+ \omega_n a J_0(\omega_n a)] c_n - [(2(1-\nu)Y_1(\omega_n a) \\ &+ \omega_n a Y_0(\omega_n a)] d_n = Ka \frac{u(\omega_n a)}{\omega_n} A_n\\ &\left[\frac{J_1(\omega_n b}{b} - \omega_n J_0(\omega_n b)\right] a_n + \left[\frac{Y_1(\omega_n b)}{b} - \omega_n Y_0(\omega_n b)\right] b_n \\ &+ [(1-2\nu)J_0(\omega_n b) - \omega_n b J_1(\omega_n b)] c_n \\ &+ [(1-2\nu)Y_0(\omega_n b) - \omega_n b Y_1(\omega_n b)] d_n \\ &= -Kb\frac{u'(\omega_n b)}{\omega_n} A_n\\ &\omega_n J_1(\omega_n b) a_n + \omega_n Y_1(\omega_n b)\, b_n - [2(1-\nu)J_1(\omega_n b) \\ &+ \omega_n b J_0(\omega_n b)] c_n - [2(1-\nu)Y_1(\omega_n b) \\ &+ \omega_n b Y_0(\omega_n b)] d_n = 0 \\ &(n = 1, 2, 3 \ldots)\end{aligned}\right\} \quad [23]$$

(continued)

After solving these equations for $n = 1, 2, 3 \ldots$, the resulting state of stress is obtained by superimposing the two stress systems Equations [19] and [22].

For $z \to \infty$, all stress components vanish, corresponding to a free (unloaded) end of the tube. For $z = 0$, a system of stress in equilibrium results, which, in general, will be different from the actual stress distribution there. According to Saint Venant's principle, however, this deviation affects the stress distribution only in the vicinity of $z = 0$ and is of no influence at distant cross sections.

# Appendix

### Calculating Roots of Equation [10]

In calculating the roots of Equation [10]—the eigen values of the problem—the fact may well be used that the nondimensional constant $H$, Equation [11], is in all practical cases very small compared with unity.

The idea therefore suggests itself to develop the eigen values into a power series of $H$; only the first two terms of this series will be retained

$$\left.\begin{aligned}\omega_n a &= \beta_n + H\gamma_n + \ldots\\ \omega_n b &= k\omega_n a = k\beta_n + kH\gamma_n + \ldots\end{aligned}\right\} \quad [24]$$

The constant

$$k = \frac{b}{a} \quad [25]$$

is the diameter ratio.

Introducing Series [24] into Equation [10] and developing into Taylor series gives

$$\begin{aligned}H\{&[J_0'(\beta_n) + H\gamma_n J_0''(\beta_n) + \ldots] [Y_0(k\beta_n) \\ &+ kH\gamma_n Y_0'(k\beta_n) + \ldots] - [Y_0'(\beta_n) + H\gamma_n Y_0''(\beta_n) \\ &+ \ldots] [J_0(k\beta_n) + kH\gamma_n J_0'(k\beta_n) + \ldots]\} \\ &+ [J_0(\beta_n) + H\gamma_n J_0'(\beta_n) + \ldots] [Y_0(k\beta_n) \\ &+ kH\gamma_n Y_0'(k\beta_n) + \ldots] - [Y_0(\beta_n) + H\gamma_n Y_0'(\beta_n) \\ &+ \ldots] [J_0(k\beta_n) + kH\gamma_n J_0'(k\beta_n) + \ldots] = 0\end{aligned}$$

This equation has to be an identity in $H$. By rearranging we obtain a series, progressing in powers of $H$. The coefficients of this series must vanish. This condition gives for the coefficient of $H^0$

$$J_0(\beta_n)Y_0(k\beta_n) - Y_0(\beta_n)J_0(k\beta_n) = 0 \quad \ldots\ldots [26]$$

from which $\beta_n$ has to be determined. The roots of this equation are well known.[4]

From the coefficient of the first power of $H$ one obtains

$$\gamma_n\{J_1(\beta_n)Y_0(k\beta_n) - Y_1(\beta_n)J_0(k\beta_n) + k[J_0(\beta_n)Y_1(k\beta_n) - Y_0(\beta_n)J_1(k\beta_n)]\} + J_1(\beta_n)Y_0(k\beta_n) - Y_1(\beta_n)J_0(k\beta_n) = 0$$

from which $\gamma_n$ has to be determined. This equation may be simplified considerably. We have

$$J_1(\beta_n)Y_0(k\beta_n) - Y_1(\beta_n)J_0(k\beta_n) = \left[\frac{Y_0(k\beta_n)}{J_0(k\beta_n)} - \frac{Y_1(\beta_n)}{J_1(\beta_n)}\right] \times J_0(k\beta_n)J_1(\beta_n) = \left[\frac{Y_0(\beta_n)}{J_0(\beta_n)} - \frac{Y_1(\beta_n)}{J_1(\beta_n)}\right] J_0(k\beta_n)J_{n1}(\beta_n) = \frac{2}{\pi\beta_n}\frac{J_0(k\beta_n)}{J_0(\beta_n)}$$

and

$$J_0(\beta_n)Y_1(k\beta_n) - Y_0(\beta_n)J_1(k\beta_n) = \frac{-2}{k\pi\beta_n}\frac{J_0(\beta_n)}{J_0(k\beta_n)}$$

We therefore get

$$\gamma_n = \frac{1}{\left[\dfrac{J_0(\beta_n)}{J_0(k\beta_n)}\right]^2 - 1} \quad \ldots\ldots [27]$$

With $\beta_n$ from Equation [26] and $\gamma_n$ from Equation [27] the eigen values $\omega_n$ are determined by Equation [24].

By means of asymptotic formulas it can be shown that

$$\gamma_n \backsimeq \frac{1}{k-1} \quad \text{for } k \to 1 \text{ and } n \to \infty$$

[4] "Tables of Higher Functions," by E. Jahnke and F. Emde, Leipzig, Germany, 1952, p. 204.

### Calculating Coefficients $A_n$

As may be seen from the following equations the system of the functions $u(\omega_n r)$—the eigen functions of the problem—is not orthogonal. To calculate the coefficients $A_n$ we therefore start by minimizing the square $E$ of the deviation of the sum of the Series [13] from the prescribed value $f(r)$

$$E = \int_a^b \left[\sum_{n=1}^{h} A_n u(\omega_n r) - f(r)\right]^2 r dr \to \text{Min}$$

for all values of $h = 1, 2 \ldots$

It is necessary for a minimum that $\partial E/\partial A_n = 0$ for all $n$, or

$$\int_a^b \left[\sum_{m=1}^{h} A_m u(\omega_m r) - f(r)\right] u(\omega_n r)\, r dr = 0 \qquad (n = 1, 2 \ldots h)$$

Carrying out the integrations by means of the integrals

$$\int r u(\omega_m r)u(\omega_n r)dr = \frac{r}{\omega_m^2 - \omega_n^2}[\omega_n u(\omega_m r)u'(\omega_n r) - \omega_m u(\omega_n r)u'(\omega_m r)], \quad (m \neq n)$$

$$\int r\,[u(\omega_n r)]^2 dr = \frac{r^2}{2}\{[u(\omega_n r)]^2 + [u'(\omega_n r)]^2\}$$

and taking into account Equation [10] and $u(\omega_n b) = 0$ the following system of linear equations for the $A_n$ is obtained

$$\sum_{m=1}^{h} S_{mn}A_m = M_n \quad \ldots\ldots [28]$$

where

$$\left.\begin{aligned} S_{mn} &= \frac{a u(\omega_m a)u'(\omega_n a)}{\omega_m + \omega_n}, \ (m \neq n) \\ M_n &= \int_a^b r f(r) u(\omega_n r)dr \\ S_{nn} &= \frac{1}{2}\{[bu'(\omega_n b)]^2 - (1 + H^2)\,[au'(\omega_n a)]^2\} \end{aligned}\right\} \quad \ldots [29]$$

It can be shown that Equations [28] converge for $h \to \infty$.

# Solutions of Heat-Conduction Problem With the Aid of the Inverse Method

By F. S. WEINIG,[1] CINCINNATI, OHIO

**Using a known solution of the potential equation for heat conduction it is possible to determine boundaries which fulfill the boundary conditions. This idea was applied to the heat flow with parallel streamlines, from a line source and from a point source. From the parallel flow, fins have been derived on a plane surface having circular arc flanks. From the line source, fins axially and radially on a cylindrical surface and from a point source fins on a sphere are obtained. The improvement of the heat transfer has been found in these examples to depend only on the surface direction at the base of the fins.**

## Nomenclature

The following nomenclature is used in the paper:

- $k$ = thermal conductivity, $k$ cal/m hr deg C or Btu/ft hr deg F
- $h$ = coefficient of heat transfer, $k$ cal/sq m hr deg C or Btu/sq ft hr deg F
- $A$ = surface area, sq m or sq ft
- $B$ = fin-base area, sq m or sq ft
- $r = k/h$ = equivalent convective layer thickness, heat-transfer resistance, m or ft
- $N$ = length along normal to surface, m or ft
- $s$ = length along heat streamline or along thermal gradient, m or ft
- $n$ = length along heat potential line or along isothermal, m or ft
- $-q = \partial t/\partial s$ = temperature gradient, deg C/m or deg F/ft
- $t$ = inside temperature
- $T$ = outside temperature

  (with suitable chosen reference temperature being zero ($\Delta$ deg C or $\Delta$ deg F))
- $\psi$ = heat stream function, $k$ cal/m hr or Btu/ft hr
- $Q$ = ratio of increase of heat transfer by fins (—)
- $\sigma$ = angle between heat streamline direction and normal to boundary (—)
- $\alpha$ = angular direction of heat streamline (—)
- $\beta$ = angular direction of normal to boundary (—)

## The Problem

The differential equation of heat conduction is in the case of constant heat conductivity $k$

$$\Delta t = 0 \qquad [1]$$

where $t$ is the temperature or the heat potential. The boundary condition is

$$t_A + r\left(\frac{\partial t}{\partial N}\right)_A = T_A \qquad [2]$$

where the heat-transfer resistance

$$r = k/h \qquad [3]$$

is the quotient of the heat conductivity $k$, and the heat-transfer coefficient $h$. The latter coefficient is assumed here also to be constant; then with constant heat conductivity $r$ is constant too.

Since the dimension of $k$ is $k$ cal/m hr deg C and of $h$ is $k$ cal/sq m hr deg C, the dimension of $r$ is $m$. Therefore $r$ is a length. It is the equivalent of the thickness of the convective layer expressed by the conductivity and may be called also the equivalent convective layer thickness; $t_A$ is the temperature on the inside of boundary $A$; $T_A$ is the temperature on the outside of the boundary $A$, which is also assumed to be constant here. $N$ means the normal directed to the outside of the boundary $A$, Fig. 1.

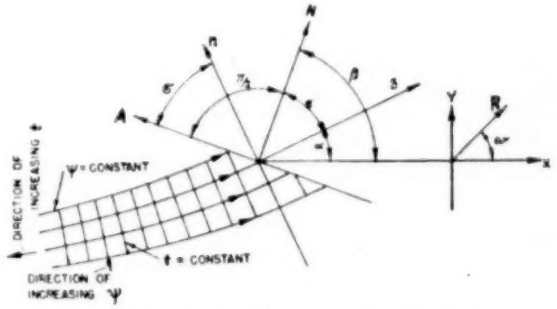


Fig. 1 Illustrative Example of Symbols Used

## Limiting Cases of Solution

Two limiting cases may be distinguished

| I | II |
|---|---|
| $r = 0$ | $r \to \infty$ |
| For $r = 0$, $T_A = t_A$ | For $r \to \infty$, $\dfrac{\partial t}{\partial N} \to 0$ |
| Thus boundary becomes a potential line of heat flow (ideal heat transfer) | In this case boundary becomes a streamline of heat flow (perfect insulation) |

In either of the limiting cases any solution of the potential equation may easily be interpreted as a solution of the heat-conduction problem. In the first case $r = 0$, any potential line may be chosen as a boundary, since $T_A = t_A$ will be the boundary condition. In the other case $r \to \infty$, any streamline may be chosen as a boundary since

$$T_A - t_A = r\frac{\partial t}{\partial N} \quad \text{or} \quad \frac{\partial t}{\partial N} = 0$$

will then be the boundary condition. Nothing can flow across

---

[1] Aerodynamicist, Aircraft Gas Turbine Divisions, General Electric Company.

Presented at the National Conference of the Applied Mechanics Division, Minneapolis, Minn., June 18–20, 1953, of The American Society of Mechanical Engineers.

Discussion of this paper should be addressed to the Secretary, ASME, 29 West 39th Street, New York, N. Y., and will be accepted until January 11, 1954, for publication at a later date. Discussion received after the closing date will be returned.

Note: Statements and opinions advanced in papers are to be understood as individual expressions of their authors and not those of the Society. Manuscript received by ASME Applied Mechanics Division, November 6, 1952. Paper No. 53—APM-25.

this boundary, since the equivalent convective-layer thickness is too large.

### General Solution

Since it is possible to interpret a given solution of the potential equation as a solution of the heat-conduction equation in these limiting cases, the question arises if it is possible to find boundaries; also in a case of finite values of the equivalent convective-layer thickness, $0 < r < \infty$, for a solution of $\Delta t = 0$ such that the boundary condition

$$t_A + r \frac{\partial t}{\partial N} = T_A$$

is fulfilled.[2]

No attempt is made here to solve the direct problem of prescribed boundaries. Instead, the inverse method, by which the field is considered to be given, is applied.

Introducing $s$ as the path length of a heat streamline one may substitute

$$\frac{\partial t}{\partial N} = \frac{\partial t}{\partial s} \frac{ds}{dN} \quad [4]$$

where

$$\frac{ds}{dN} = \cos < s, N > \quad [5]$$

is the cosine of the angle between the direction of the heat streamline or the heat gradient $s$, and of the normal $N$, of the boundary $A$. Then the boundary condition is transformed to

$$t_A + r \frac{\partial t}{\partial s} \cos < s, N > = T_A \quad [6]$$

$-\partial t/\partial s = +q$ is the rate of temperature drop or the temperature gradient.

Hence the angle $< s, N >$ may be determined from

$$\cos < s, N > = \cos \sigma = \frac{t_A - T_A}{r\,q} \quad [7]$$

If the directional angle of $s$ is $\alpha$ and of $N$ is $\beta$ then

$$\beta - \alpha = \sigma = \arccos \frac{t_A - T_A}{r\,q} \quad [8]$$

Primarily any point of the field of the solution of $\Delta t = 0$ may be considered to be a point of a boundary, as long as for given $r$ and $T_A$

$$| \cos < s, N > | = | \cos \sigma | = \left| \frac{t_A - T_A}{r\,q} \right| < 1 \quad [9]$$

If this condition is fulfilled two directions of $N$ satisfy in the two-dimensional case the boundary conditions; in the three-dimensional case this is true for any plane containing the tangent of the heat streamline through the point under consideration.

Since

$$\cos \sigma = \cos -\sigma \quad [10]$$

one finds

$$\left.\begin{aligned} \beta = \beta_1 &= \alpha + \arccos \frac{t_A - T_A}{r\,q} = \alpha + \sigma \\ \beta = \beta_2 &= \alpha - \arccos \frac{t_A - T_A}{r\,q} = \alpha - \sigma \end{aligned}\right\} \quad [11]$$

or if in this plane $Y$ ($X$) means the boundary and if $\alpha$ is measured from the direction of the $X$-axis

$$Y'_{1,2} = \frac{dY_{1,2}}{dX} = \cot \left( \alpha \pm \arccos \frac{t_A - T_A}{r\,q} \right) \quad [12]$$

These differential equations have to be solved in a suitable manner, depending on the problem. The entire solution consists of sections of the one or the other solution which are composed arbitrarily.

In the following, some simple solutions of the potential equation are interpreted as solutions of heat conduction with due regard to the boundary conditions. These examples are the parallel flow, the flow from a line source, and the flow from a point source.

Since the generality of the solutions is not restricted thereby

$$T_A = 0$$

is chosen in the examples.

A comparison of the results is made in Table 2.

### Solutions Which Result From Parallel Flow

The potential

$$t = -x \quad [13]$$

represents a flow parallel to the $x$-axis

$$\alpha = 0 \quad [14a]$$

$$q = 1 \quad [14b]$$

Then the boundary must satisfy at least in sections the condition

$$\cos < s, N > = \cos \sigma = \frac{t_A - T_A}{r\,q} = \frac{x}{r}, \; (T_A = 0) \quad [15]$$

Hence

$$\frac{dY_{1,2}}{dX} = \pm \cot \sigma = \pm \frac{x/r}{\sqrt{1 - (x/r)^2}} \quad [16]$$

and

$$Y_{1,2} = \pm r \sqrt{1 - (x/r)^2} + Y_0 \quad [17]$$

or

$$X^2 + (Y_{1,2} - Y_0)^2 = r^2 \quad [18]$$

This solution exists with $T_A = 0$ only for

$$-1 < \frac{x}{r} < +1$$

In the remaining field, $t = -x$, the boundary condition could not be fulfilled.

The general solution for the possible boundaries consists of the entire family of circles having the radius $r$, the centers of which lie on the $Y$-axis, $X = 0$, and are given by the constants $Y_0$, Fig. 2.[2,3] From these circles any sections may be chosen in succession for a possible boundary.

Fig. 2 shows such a boundary. With the signs chosen, boundaries with $X < 0$ yield emerging heat flow and boundaries with $X > 0$ yield entering heat flow.

In Fig. 3 the event of emerging heat is illustrated for the case of a wall of the thickness $\delta$ on which fins or ribs are arranged on the one side ($o$) but which is smooth on the other side ($i$). The

[2] "Solutions for Conduction of Heat With the Aid of the Inverse Method," by F. Weinig, Wright Field, No. F-TR-2107-ND

[3] "Introduction to the Transfer of Heat and Mass," by E. R. G. Eckert, McGraw-Hill Book Company, Inc., New York, N. Y., 1950, p. 36.

TABLE 1 EFFECTIVENESS COEFFICIENT AND SURFACE RATIO OF FINS HAVING A FLANK RADIUS OF

$$\eta = \frac{1}{\cos\sigma_b\,(A/B)^2}, \quad A/B = \frac{\sigma_b - \sigma_l}{\sin\sigma_b - \sin\sigma_l}$$

| $\cos\sigma_b = \xi_{th}/r_o$ | 1 | 3/4 | 1/2 | 1/3 | 1/4 | 0 | 1 | 3/4 | 1/2 | 1/4 | 0 | 1 | 3/4 | 1/2 | 1/4 | 0 |
|---|---|---|---|---|---|---|---|---|---|---|---|---|---|---|---|---|
| $\xi_{th}/r_o$ | 0.167 | 0.125 | 0.083 | 0.042 | 0 | | 0.333 | 0.25 | 0.167 | 0.083 | 0 | 0.5 | 0.375 | 0.25 | 0.125 | 0 |
| $\cos\sigma_l = \frac{\xi_{th}-\xi}{r_o}$ | 0 | 0.042 | 0.083 | 0.125 | 0.167 | | 0 | | 0.083 | 0.167 | 0.25 | | | | | |
| $\sigma_l$ | 1.403 | 1.403 | 1.403 | 1.403 | 1.403 | | 1.231 | 1.231 | 1.231 | 1.231 | 1.231 | 1.047 | 1.047 | 1.047 | 1.047 | 1.047 |
| $\sigma_l$ | 1.571 | 1.529 | 1.487 | 1.445 | 1.403 | | 1.571 | 1.487 | 1.403 | 1.318 | 1.231 | 1.571 | 1.445 | 1.318 | 1.186 | 1.047 |
| $\sin\sigma_b$ | 0.986 | 0.986 | 0.986 | 0.986 | 0.986 | | 0.943 | 0.943 | 0.943 | 0.943 | 0.943 | 0.866 | 0.866 | 0.866 | 0.866 | 0.866 |
| $\sin\sigma_l$ | 1.000 | 0.999 | 0.997 | 0.992 | 0.986 | | 1.0 | 0.997 | 0.986 | 0.968 | 0.943 | 1.0 | 0.992 | 0.968 | 0.927 | 0.866 |
| $A/B$ | 11.965 | 9.601 | 8.010 | 6.922 | 6.000 | | 5.940 | 4.771 | 3.987 | 3.429 | (3.000) | 3.907 | 3.131 | 2.651 | 2.272 | (2.000) |
| $\eta$ | 0.501 | 0.625 | 0.749 | 0.866 | (1.000) | | 0.505 | 0.629 | 0.752 | 0.875 | (1.000) | 0.512 | 0.583 | 0.755 | 0.879 | (1.000) |
| $\eta \cdot A/B = \frac{1}{\cos\sigma_l}$ | 6 | | | | | | 3 | | | | | 2 | | | | |

| $\cos\sigma_b = \xi_{th}/r_o$ | 1 | 3/4 | 1/2 | 1/4 | 0 | 1 | 3/4 | 1/2 | 1/4 | 0 | 1 | 3/4 | 1/2 | 1/4 | 0 |
|---|---|---|---|---|---|---|---|---|---|---|---|---|---|---|---|
| $\xi_{th}/r_o$ | 0.5 | 0.375 | 0.25 | 0.125 | 0 | 0.667 | 0.5 | 0.333 | 0.167 | 0 | 0.833 | 0.625 | 0.417 | 0.208 | 0 |
| $\cos\sigma_l = \frac{\xi_{th}-\xi}{r_o}$ | 0 | 0.125 | 0.25 | 0.375 | 0.5 | | 0 | 0.167 | 0.333 | 0.5 | | | | | |
| $\sigma_l$ | 1.047 | 1.047 | 1.047 | 1.047 | 1.047 | 0.841 | 0.841 | 0.841 | 0.841 | 0.841 | 0.841 | 0.841 | 0.841 | 0.841 | 0.841 |
| $\sigma_l$ | 1.571 | 1.445 | 1.318 | 1.186 | 1.047 | 1.571 | 1.403 | 1.231 | 1.047 | 0.841 | 1.571 | 1.403 | 1.231 | 1.047 | 0.841 |
| $\sin\sigma_b$ | 0.866 | 0.866 | 0.866 | 0.866 | 0.866 | 0.746 | 0.746 | 0.746 | 0.746 | 0.746 | 0.746 | 0.746 | 0.746 | 0.746 | 0.746 |
| $\sin\sigma_l$ | 1.0 | 0.992 | 0.968 | 0.927 | 0.866 | 1.0 | 0.986 | 0.943 | 0.866 | 0.746 | 1.0 | 0.986 | 0.943 | 0.866 | 0.746 |
| $A/B$ | 2.865 | 2.337 | 1.975 | 1.708 | (1.5) | 2.865 | 2.337 | 1.975 | 1.708 | (1.5) | 2.865 | 2.337 | 1.975 | 1.708 | (1.5) |
| $\eta$ | 0.524 | 0.642 | 0.759 | 0.878 | (1.000) | 0.524 | 0.642 | 0.759 | 0.878 | (1.000) | 0.524 | 0.642 | 0.759 | 0.878 | (1.000) |
| $\eta \cdot A/B = \frac{1}{\cos\sigma_l}$ | 1.5 | | | | | 1.5 | | | | | 1.5 | | | | |

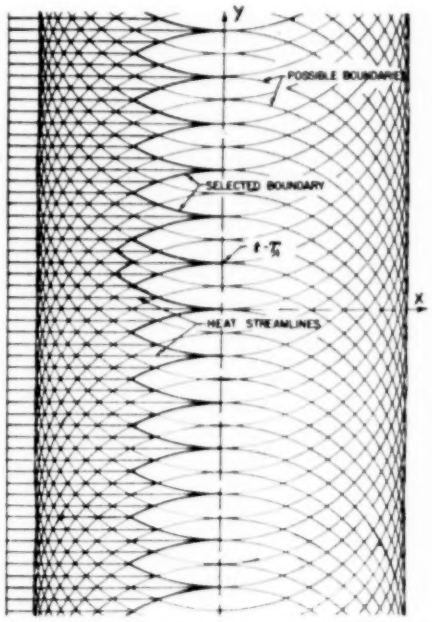


FIG. 2 GENERAL SOLUTION AND SELECTION OF BOUNDARY IN GIVEN PARALLEL FLOW

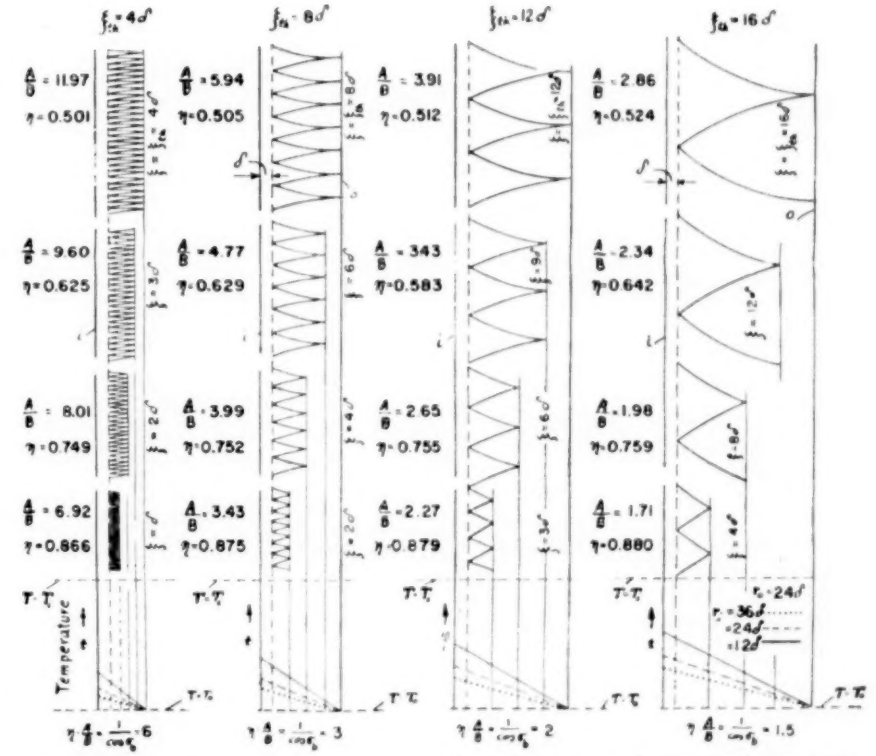


FIG. 3 SEVERAL BOUNDARIES RESULTING FROM PARALLEL FLOW AND COINCIDENT TEMPERATURE COURSES

distribution of the temperature is illustrated for the cases $r = r_a = 24\ \delta$ on the one side and $r = r_b = 36\ \delta$, $24\ \delta$, $12\ \delta$, respectively, on the other side.

First, some extreme lengths of the fins, $\xi_{th}$ (top Fig. 3) have been chosen, which are subsequently shortened to $\xi < \xi_{th}$, without change of the contours at the base of the fins, with resultant change of pitch or spacing, and edge angle of the fins. It may be seen that on the one side ($i$) the temperature decreases with decreasing extremal length $\xi_{th}$ of the fins, that however, it is independent of the ratio $\xi/\xi_{th}$ although, with decreasing $\xi/\xi_{th}$, the structural quantities, i.e., lengths of the fins and wedge angle become more favorable, with at first only a slightly unfavorable decrease of pitch.

When comparison is made under equal length $\xi$, the lower temperatures on the one side ($i$) will be attained with the smaller pitch or spacing; in other words, $\xi/\xi_{th}$ should be as large as possible for a given $\xi$. With actual design, however, it is more important to make the pitch and the edge angles as small as is practically possible. Otherwise Fig. 3 should speak for itself.

In the main, the effect of the fins is to increase the surface available for heat transmission compared to the original surface or base area. Let $A$ be the increased surface area and $B$ the base area. If the conductivity would be very large, then the heat transfer would be increased by the ratio

$$Q_\infty = A/B \qquad [19]$$

since then the temperature would be constant along the surface of the fin and equal to the temperature at the root, which might be considered unchanged. The real heat transfer is less by an effectiveness coefficient, $\eta$

$$Q = Q_\infty \eta \qquad [20]$$

If $t$ and $b$ are used as subscripts for tip and base of the fins one finds

$$Q_\infty = \frac{\sigma_b - \sigma_t}{\sin \sigma_b - \sin \sigma_t} \qquad [21]$$

and

$$\eta = \frac{1}{\cos \sigma_b \, A/B} \qquad [22]$$

where $\cos \sigma_b = \xi_{th}/r_a$ and $\cos \sigma_t = (\xi_{th} - \xi)\, r_a$ have to be substituted for the examples in Fig. 3 (Table 1).

Finally

$$Q = Q_\infty \eta = 1/\cos \sigma_b \qquad [23]$$

Hence $Q$ depends only on the base angle $\sigma_b$.

## Two-Dimensional Plane Solutions Which Result From Line-Source Flow

The potential

$$t = -\log R \qquad [24]$$

represents a flow originating from a line source which is situated in the $z$-axis. $R$ is the distance from this source line.

Let the streamlines be normal to this $z$-axis. Let $\omega$ be the angle between the direction of a streamline and a chosen $x$-axis. Then

$$\alpha = \omega \qquad [25a]$$

Further

$$q = -\frac{\partial t}{\partial R} = +\frac{1}{R} \qquad [25b]$$

The boundary must satisfy at least in sections the condition

$$\cos \langle s, N \rangle = \cos \sigma = \frac{t_A - T_A}{r\, q} = \frac{R \log R}{r}, \quad (T_A = 0) \qquad [26]$$

Hence

$$\cot \sigma = \frac{\dfrac{R \log R}{r}}{\sqrt{1 - \left(\dfrac{R \log R}{r}\right)^2}}$$

Using polar co-ordinates $R$ and $\omega$

$$\frac{R\, d\omega}{dR} = \cot \sigma = \frac{\dfrac{R \log R}{r}}{\sqrt{1 - \left(\dfrac{R \log R}{r}\right)^2}} \qquad [27]$$

and by integration

$$\omega = \pm \int_1^R \frac{\dfrac{\log R}{r}}{\sqrt{1 - \left(\dfrac{R \log R}{r}\right)^2}}\, dR + \omega_0 \qquad [28]$$

Since $T_A = 0$ was assumed and $t = 0$ for $R = 1$, $r$ is measured in the unit of $R$. Hence $r$ is an essential parameter of the problem. In order to obtain all essential solutions, the integration was carried through for a set of values of $r$

$$r = 1.0,\ 0.9,\ 0.8,\ 0.7,\ 0.6,\ 0.5,\ 0.4,\ 0.3,\ 0.2,\ 0.1$$

In the case $r \to 0$ the solution becomes geometrically similar to the solution for the parallel flow, as described before.

For

$$\left|\frac{R \log R}{r}\right| > 1$$

possible boundaries do not exist. The function $R \log R$ is represented in Fig. 4. For $R < 1$ one finds $-R \log R \leq 1/e = 0.368$. Hence for $r = 1/e = 0.368$ the solutions are split in two branches, one for $R > 0.368$ and one for $R < 0.368$.

In Fig. 5 the results of the integration are plotted, however,

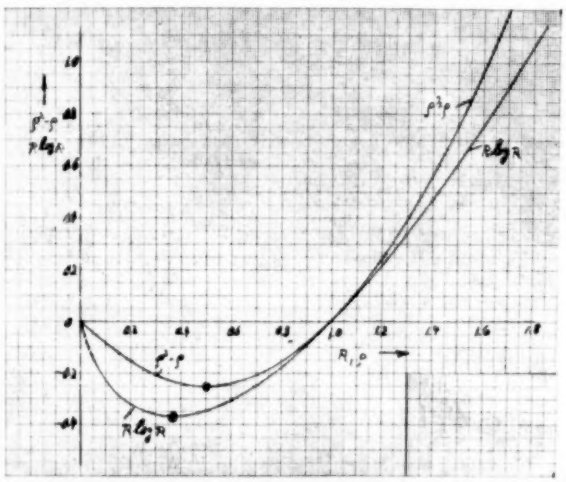

Fig. 4 Functions $R$ Log $R$ and $R^2 - R$

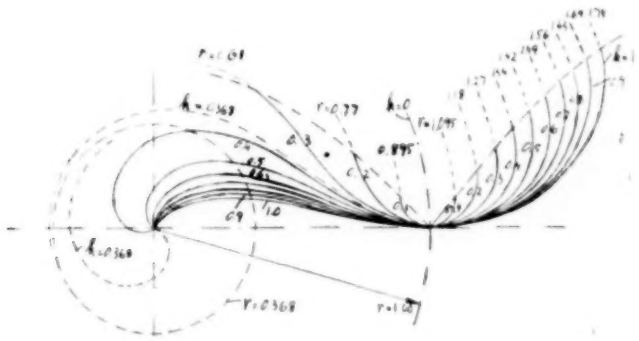

FIG. 5 LONGITUDINAL FINS ON CYLINDER

only for $\omega_o = 0$ and for only one sign of the root. Reflecting these results on the $x$-axis and adding arbitrary constants $\omega_o$ would yield the general solution from which special solutions result in a similar way as was shown for the parallel flow.

In this way fins may be derived which run longitudinally along the cylinder.

## AXISYMMETRIC SOLUTIONS WHICH RESULT FROM LINE-SOURCE FLOW

In the foregoing paragraph the flow of the line source was considered as a two-dimensional plane flow in and parallel to the $X$-$Y$-plane. The solutions obtained represented longitudinal fins.

One may consider this flow also as an axisymmetric one and obtain radial fins. Using cylindrical co-ordinates, $R$, $Z$, the boundary must satisfy again at least in sections the condition

$$\cos < s, N > = \cos \sigma = \frac{t_A - T_A}{r\,q} = \frac{R \log R}{r}, \quad (T_A = 0) \ldots [29]$$

Hence again

$$\cot \sigma = \frac{\dfrac{R \log R}{r}}{\sqrt{1 - \left(\dfrac{R \log R}{r}\right)^2}}$$

Using cylindrical co-ordinates $R$, $Z$

$$\frac{dZ}{dR} = \cot \sigma = \frac{\dfrac{R \log R}{r}}{\sqrt{1 - \left(\dfrac{R \log R}{r}\right)^2}} \ldots [30]$$

and by integration

$$Z_{1,2} = \pm \int_1^R \frac{\dfrac{R \log R}{r}}{\sqrt{1 - \left(\dfrac{R \log R}{r}\right)^2}}\, dR + Z_o \ldots [31]$$

Since $T_A = 0$ is assumed again and $t = 0$ for $R = 1$, $r$ is again measured in the unit of $R$ and is an essential parameter of the problem. The integration was carried through for a set of values of $r$

$$r = 1.0, 0.9, 0.8, 0.7, 0.6, 0.5, 0.4, 0.3, 0.2, 0.1$$

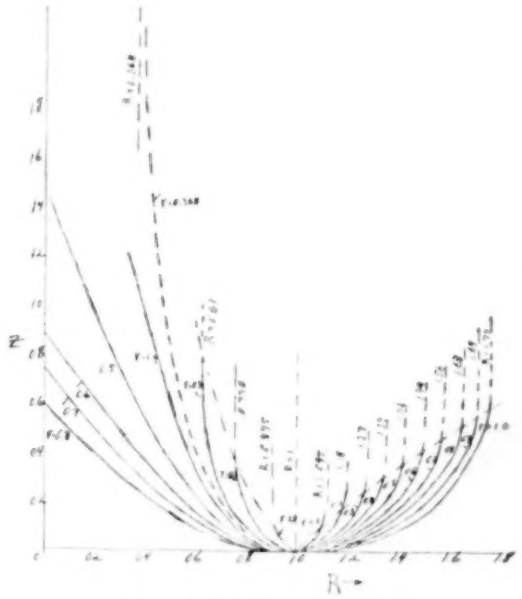

FIG. 6 RADIAL FINS ON CYLINDER

Again, for $r \to 0$ the solution becomes geometrically similar to the solution for the parallel flow. For

$$\frac{R \log R}{r} > 1$$

possible boundaries do not exist. For $R < 1$ again $r = 1/e = 0.368$ splits the solutions into two branches. In Fig. 6 the results of the integration are plotted for $Z_o = 0$ and for only one sign of the root. The general result has to be obtained as described in the foregoing.

The fins obtained in this way run radially.

## AXISYMMETRIC SOLUTIONS WHICH RESULT FROM POINT-SOURCE FLOW

The potential

$$t = \frac{1}{\rho} + 1 \ldots [32]$$

represents a flow originating from a point which is situated at the

origin of the system of cylindrical co-ordinates $Z$, $R$, $\omega$, or of spherical co-ordinates $\rho$, $\varphi$, $\omega$; $\rho$ is the distance from this origin. For

$$\rho = 1, \quad t = 0$$

The streamlines are straight lines originating in the origin of the co-ordinate system. Consider $\omega = 0$ to describe a plane normal to the $z$-axis. Let

$$\alpha = \omega \qquad [33a]$$

For $\omega = 0$

$$R = \rho$$

Further

$$q = -\frac{\partial t}{\partial \rho} = \frac{1}{\rho^2} \qquad [33b]$$

The boundary must satisfy, at least in sections, the condition

$$\cos < s, N > = \cos \sigma = \frac{t_N - T_N}{r\,q} = \frac{\rho^2 - \rho}{r} \qquad [34]$$

Hence

$$\cot \sigma = \frac{\dfrac{\rho^2 - \rho}{r}}{\sqrt{1 - \left(\dfrac{\rho^2 - \rho}{r}\right)^2}}$$

Using spherical co-ordinates $\rho$, $\varphi$, $\omega$

$$\rho \frac{d\omega}{d\rho} = \cot \sigma = \pm \frac{\dfrac{\rho^2 - \rho}{r}}{\sqrt{1 - \left(\dfrac{\rho^2 - \rho}{r}\right)^2}} \qquad [35]$$

and by integration

$$\omega = \pm \int_1^K \frac{\dfrac{\rho - 1}{r}}{\sqrt{1 - \left(\dfrac{\rho^2 - \rho}{r}\right)^2}} \frac{d\rho}{\rho} + \omega_0 \qquad [36]$$

Since $T_A = 0$ was assumed and $t = 0$ for $\rho = 1$, $r$ is again measured in the unit of $\rho$ and $r$ is an essential parameter. The integration was carried through for a set of $r$

$$r = 1.0, 0.9, 0.8, 0.7, 0.6, 0.5, 0.4, 0.3, 0.2, 0.1$$

In the case $r \to 0$ the solution becomes geometrically similar to the solution for the parallel flow.

For $\left|\dfrac{\rho^2 - \rho}{r}\right| > 1$

possible boundaries do not exist. The function $\rho^2 - \rho$ is represented in Fig 4. For $\rho < 1$ one finds $-(\rho^2 - \rho) \leq 1/4 = 0.250$. Hence for $r = 0.25$ the solutions are split in two branches, one for $\rho > 0.500$ and one for $\rho < 0.500$.

In Fig. 7 the results of the integration are plotted, however, only for $\omega_0 = 0$ and for only one sign of the root. The general solution may be found analogously to the previously described cases.

In this way, fins on a sphere may be derived which run with their symmetry axis in planes through the origin of the co-ordinate system or, more generally, in conical surfaces with the apex at the origin of the co-ordinate system.

### Some Generalized Use of the Results

Topologically, the results of the last three examples are related to each other, as a comparison of Figs. 5, 6, and 7 will show.

In the limiting case $k \to 0$ they are all similar to the results which may be derived from the parallel flow. For some easier comparisons the mathematical results are compiled in Table 2.

It is, however, not necessary to confine oneself to the two-dimensional plane and axis-symmetric interpretations given in the foregoing. These interpretations may be extended to three-dimensional conceptions of more general character. To explain these possibilities some models have been sketched as shown in Figs. 8 to 17, inclusive.

Besides simple cooling fins derived from the result of the parallel flow, Fig. 8, there might be a crisscrossing application resulting in cooling pins, Fig. 9, or circular fins obtained by turning, Fig. 10, or radially arranged straight fins, Fig. 11, or some combination of circular and radial fins, Fig. 12.

Besides longitudinal cooling fins along a cylinder, Fig. 13, and radial cooling fins, Fig. 14, there might be a crisscrossing combination, resulting in cooling pins, Fig. 15.

Circular arrangement of cooling fins on a sphere is shown in Fig. 16; Fig. 17 shows a combination of such circular fins near

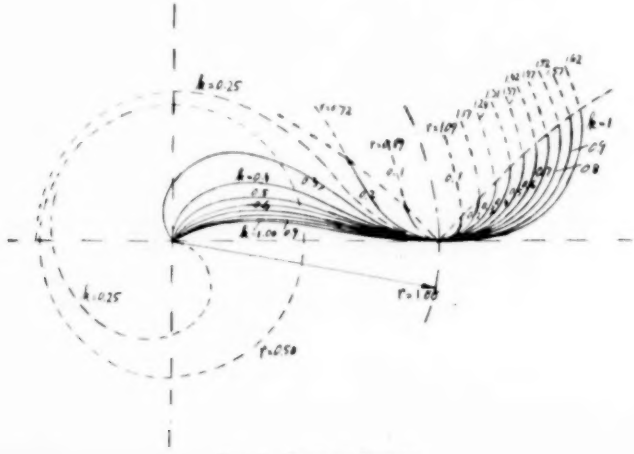

Fig. 7 Fins on Sphere

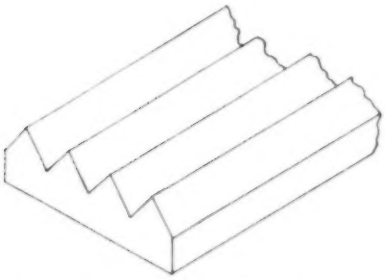

FIG. 8 STRAIGHT FINS ON PLANE SURFACE, SCHEMATICALLY

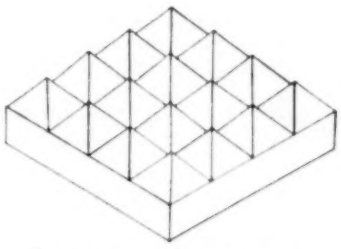

FIG. 9 PINS ON PLANE SURFACE, SCHEMATICALLY

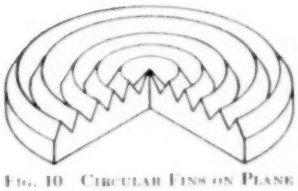

FIG. 10 CIRCULAR FINS ON PLANE SURFACE, SCHEMATICALLY

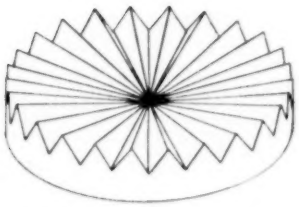

FIG. 11 RADIAL FINS ON PLANE SURFACE, SCHEMATICALLY

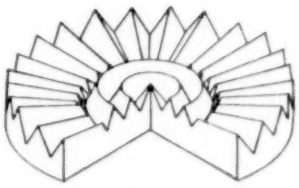

FIG. 12 COMBINATION OF CIRCULAR AND RADIAL FINS ON PLANE SURFACE, SCHEMATICALLY

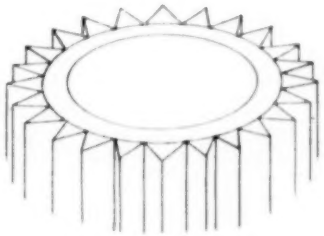

FIG. 13 LONGITUDINAL FINS ON CYLINDER, SCHEMATICALLY

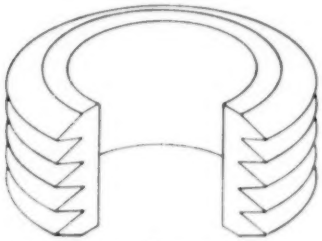

FIG. 14 RADIAL FINS ON CYLINDER, SCHEMATICALLY

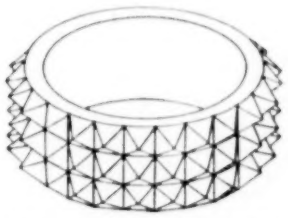

FIG. 15 PINS ON CYLINDER, SCHEMATICALLY

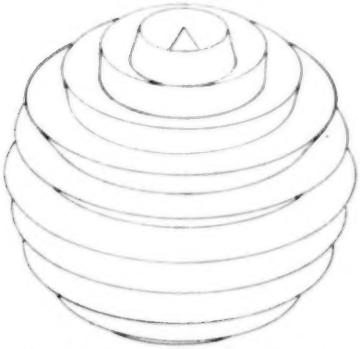

FIG. 16 CIRCULAR FINS ON SPHERE, SCHEMATICALLY

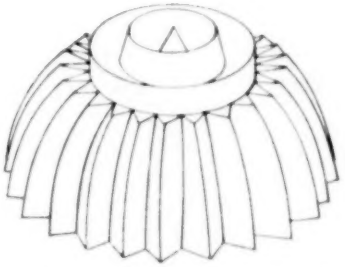

FIG. 17 COMBINATION OF CIRCULAR AND LONGITUDINAL FINS ON HEMISPHERE, SCHEMATICALLY

TABLE 2 COMPARISON OF EXAMPLES

| | Parallel flow | Line source | | Point source |
|---|---|---|---|---|
| | Fins on plane surface | Longitudinal fins on cylinder | Radial fins on cylinder | Fins on spherical surface |
| Co-ordinates | Cartesian $X$, $Y$ | Polar $R$, $\omega$ | Cylindrical $Z$, $R$, $(\omega)$ | Spherical $\rho$, $\omega$, $\varphi$ |
| Potential or temperature | $t = -x$ | $= -\log R$ | $t = -\log R$ | $t = \frac{1}{\rho} - 1$ |
| | $t = 0$ for $x = 0$ | $t = 0$ for $R = 1$ | $t = 0$ for $R = 1$ | $t = 0$ for $\rho = 1$ |
| Temperature gradient | $q = -\frac{dt}{dx} = +1$ | $q = -\frac{dt}{dR} = +\frac{1}{R}$ | $q = -\frac{dt}{dR} = +\frac{1}{R}$ | $q = -\frac{dt}{d\rho} = \frac{1}{\rho^2}$ |
| $\cos\sigma = \cos < s, N >$ for $T_A = 0$ | $\frac{t_A - T_A}{r\,q} = \frac{x}{r}$ | $\frac{t_A - T_A}{r\,q} = \frac{R\log R}{r}$ | $\frac{t_A - T_A}{r\,q} = \frac{R\log R}{r}$ | $\frac{T_A - t_A}{r\,q} = \frac{\rho^2 - \rho}{r}$ |
| $\cot\sigma$ | $\frac{dy}{dx} = \frac{x/r}{\sqrt{1-(x/r)^2}}$ | $\frac{Rd\omega}{dR} = \frac{\frac{R\log R}{r}}{\sqrt{1-\left(\frac{R\log R}{r}\right)^2}}$ | $\frac{dz}{dR} = \frac{\frac{R\log R}{r}}{\sqrt{1-\left(\frac{R\log R}{r}\right)^2}}$ | $\frac{\rho d\omega}{d\rho} = \frac{\frac{\rho^2-\rho}{r}}{\sqrt{1-\left(\frac{\rho^2-\rho}{r}\right)^2}}$ |
| Boundary for $T_A = 0$ | $Y = \pm\sqrt{r^2 - X^2} + Y_o$ | $\omega = \pm\int_1^R \frac{\frac{\log R}{r}}{\sqrt{1-\left(\frac{R\log R}{r}\right)^2}}dR + \omega_o$ | $Z = \pm\int_1^R \frac{\frac{R\log R}{r}}{\sqrt{1-\left(\frac{R\log R}{r}\right)^2}}dR + Z_o$ | $\omega = \pm\int_1^\rho \frac{\frac{\rho-1}{r}}{\sqrt{1-\left(\frac{\rho^2-\rho}{r}\right)^2}}d\rho + \omega_o$ |

the apex with longitudinal fins near the equator of a hemisphere.

These figures may be considered to be self-explanatory. Combinations of such solutions might result, e.g., in a design of cooling fins on a cylinder limited on one side by a hemisphere; with constant wall thickness and constant outside and inside space temperature this would result in constant inside wall temperature.

Finally it might be remarked that in all the examples the heat transfer is given by

$$Q = Q_\infty\,\eta = 1/\cos\sigma_b \qquad [37]$$

where $\cos\sigma_b = \cos < s, N >$ is the value at the base of the fins or pins. $\eta$ and $Q_\infty$ may vary considerably for cases of equal thermal conditions, while the product of both depends on $\sigma_b$ only.

# Toroidal-Shell Expansion Joints

By N. C. DAHL,[1] CAMBRIDGE, MASS.

**The problem considered in this paper is shown in Fig. 1; a thin toroidal shell of center-line radius *a* and torus mid-surface radius *b* is slit at its inner edge and welded to relatively stiff cylindrical pipe sections to form an expansion joint. Stresses and axial deformation under the axial load *P* are desired.**

CLARK,[2] using an analysis, the kernel of which was developed jointly with E. Reissner, has obtained a solution to this problem by asymptotic integration of the differential equations of thin shells of revolution. This solution involves approximations based on the assumption that the following geometric parameter of the shell

$$\mu = \frac{\sqrt{12(1-\nu^2)}\, b^2}{ah} \qquad [1]$$

is sufficiently large. In the present work a solution is obtained using the principle of minimum complementary strain energy. It is found that the results obtained in this way are valid as long as $\mu$ is not too large. The two solutions are plotted to show in what regions of $\mu$ they overlap and both are compared with experimentally determined stresses and deformations.

## Complementary Strain-Energy Solution

It is often usual in approximate solutions to thin-shell problems to seek a solution which consists of the equilibrium membrane solution modified by local bending stresses to take care of edge conditions not satisfied by the membrane stress. This technique is not applicable in the present case because the membrane-stress resultants

$$N_\phi = \frac{P}{2\pi r \sin\phi} \qquad [2]$$

$$N_\theta = \frac{-P}{2\pi a \sin^2\phi} \qquad [3]$$

satisfy the edge conditions but become infinite at $\phi = 0, \pi$, that is, at the top and bottom of the torus. This behavior is typical of any shell of revolution having a point of horizontal tangency and subjected to vertical loads. It is clear that in the problem at hand we must include shearing forces to carry the load in the vicinity of the top and bottom of the torus.

Referring to the element of the torus shown in Fig. 2, the equilibrium equations for the stress resultants can be written in the following form

$$N_\phi b \sin\phi + (rN_\phi) + (rQ_\phi)' = 0 \qquad [4]$$

$$(rN_\phi)' - (rQ_\phi) - N_\theta b \cos\phi = 0 \qquad [5]$$

$$(rM_\phi)' - b(rQ_\phi) - M_\theta b \cos\phi = 0 \qquad [6]$$

where primes represent differentiation with respect to $\phi$. Also, over-all vertical equilibrium of the shell shown in Fig. 1 leads to

$$(rQ_\phi)\cos\phi + (rN_\phi)\sin\phi = aV_0 \qquad [7]$$

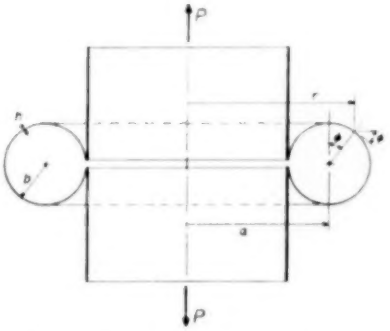


Fig. 1 Geometry of Toroidal Shell

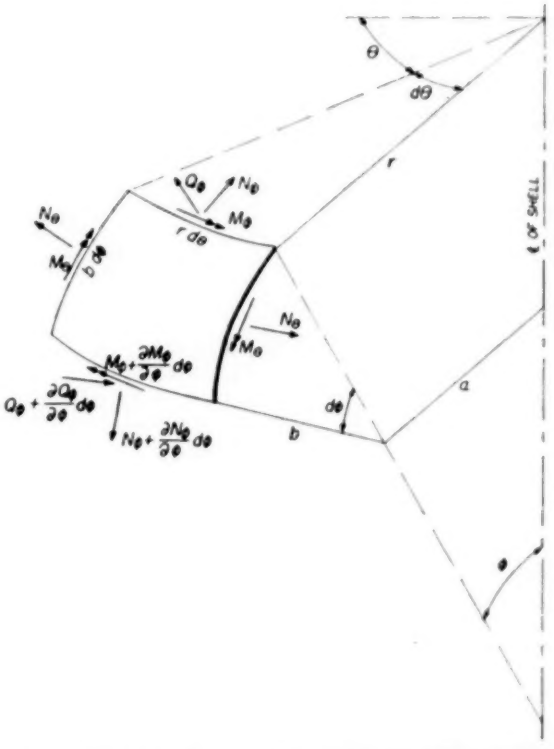


Fig. 2 Element of Toroidal Shell, With Stress Resultants

---

[1] Assistant Professor of Mechanical Engineering, Massachusetts Institute of Technology.

[2] "On the Theory of Thin Elastic Toroidal Shells," by R. A. Clark, *Journal of Mathematics and Physics*, vol. 29, 1950, pp. 146–178.

Presented at the National Conference of the Applied Mechanics Division, Minneapolis, Minn., June 18–20, 1953, of The American Society of Mechanical Engineers.

Discussion of this paper should be addressed to the Secretary, ASME, 29 West 39th Street, New York, N. Y., and will be accepted until January 11, 1954, for publication at a later date. Discussion received after the closing date will be returned.

Note: Statements and opinions advanced in papers are to be understood as individual expressions of their authors and not those of the Society. Manuscript received by ASME Applied Mechanics Division, August 29, 1952. Paper No. 53—APM-30.

where

$$V_0 = \frac{P}{2\pi a} \quad [8]$$

Using the notation

$$\lambda = \frac{b}{a} \quad [9]$$

we can write $r$ as follows

$$r = a(1 + \lambda \sin\phi) \quad [9a]$$

In what follows we shall assume that $\lambda$ is small and that therefore all stresses and deformations are either perfectly symmetric or perfectly antisymmetric about the point $\phi = 0$.

Since $Q_\phi$ exists only to carry the vertical load it is reasonable to assume the boundary condition that $Q_\phi = 0$ at $\phi = \pm\pi/2$. Restricting ourselves to small values of $\lambda$, we assume the following symmetrical form for $Q_\phi$

$$(rQ_\phi) = (aQ_\phi) = aV_0 \cos\phi\,[1 - \sin^2\phi g(\phi)] \quad [10]$$

where the requirements on $g(\phi)$ are that it be even in $\phi$ and that it and its derivatives be finite everywhere. Substitution of Equation [10] into [7] leads to

$$(rN_\phi) = (aN_\phi) = aV_0 \sin\phi\,[\cos^2\phi\, g(\phi) + 1] \quad [11]$$

and Equations [10] and [11] substituted into Equation [5] yield

$$N_\theta = \frac{V_0}{\lambda}\left[\cos 2\phi\, g(\phi) + \frac{\sin 2\phi}{2} g'(\phi)\right] \quad [12]$$

Substitution of Equation [10] into the moment equilibrium Equation [6] gives, assuming $\lambda$ small compared to unity

$$bV_0 \cos\phi\,[1 - \sin^2\phi\, g(\phi)] = M'_\phi + \lambda \cos\phi\, M_\phi - \lambda \cos\phi\, M_\theta \quad [13]$$

It remains to make an assumption about the deflection of the shell. From the theory of thin shells it follows[5] that the moment stress resultants and the deflection of thin shells of revolution can be expressed in terms of a parameter $\beta$ which is the negative of the change, due to deformation, in the tangent angle $\phi$. Using this notation the moment resultants for the toroidal shell can be expressed as

$$M_\phi = \frac{D}{b}\left(\beta' + \nu \frac{r'}{r}\beta\right) \quad [14]$$

$$M_\theta = \frac{D}{b}\left(\frac{r'}{r}\beta + \nu\beta'\right) \quad [15]$$

where

$$D = \frac{Eh^3}{12(1 - \nu^2)}$$

and the vertical deflection $w$ can be given in the form

$$w = b\int(\epsilon_{\phi m}\sin\phi - \beta\cos\phi)d\phi \quad [16]$$

where $\epsilon_{\phi m}\sin\phi$ represents the (small) contribution of the middle surface strain.

Neglecting terms of order $\lambda$ we can write $M_\phi$ and $M_\theta$ as

$$M_\phi = \frac{D}{b}\beta' \quad [17]$$

[5] "Contributions to Applied Mechanics; on the Theory of Thin Elastic Shells," by E. Reissner, Reissner Anniversary Volume, Edwards, Ann Arbor, Mich., 1949, pp. 231–247.

$$M_\theta = \nu\frac{D}{b}\beta' = \nu M_\phi \quad [18]$$

By reason of symmetry we must have $\beta = 0$ at $\phi = +\pi/2$, and because of the presence of the stiff cylindrical shell we also can assume $\beta = 0$ at $\phi = -\pi/2$. Satisfying these boundary conditions we take the following form for $\beta$

$$\beta = -\sum_{\text{odd}} \frac{C_n}{n}\cos n\phi \quad [19]$$

Taking only the first four terms of Equation [19], Equation [13] becomes after expanding and neglecting terms of order $\lambda$

$$bV_0\cos\phi\,[1 - \sin^2\phi g(\phi)] = \frac{D}{b}\cos\phi\,[(C_1 + 3C_3 + 5C_5 + 7C_7) - (12C_3 + 60C_5 + 168C_7)\sin^2\phi + (80C_5 + 560C_7)\sin^4\phi - (448C_7)\sin^6\phi] \quad [20]$$

Thus we obtain for $g(\phi)$

$$g(\phi) = k_0 - k_2\sin^2\phi + k_4\sin^4\phi \quad [21]$$

where

$$k_0 = 12C_3 + 60C_5 + 168C_7$$
$$k_2 = 80C_5 + 560C_7$$
$$k_4 = 448C_7$$

We now have expressions for the stress resultants in terms of the coefficients $C_1$, $C_3$, $C_5$, and $C_7$, which satisfy the equilibrium equations to terms of order $\lambda$.

Neglecting the contribution of $N_\phi$ and $Q_\phi$, and again neglecting terms of order $\lambda$ compared to unity, we can express the complementary strain energy[6] as

$$U^* = \frac{4\pi ab}{Eh}\int_0^{\pi/2}\left[N_\theta^2 + \frac{12}{h^2}(1 - \nu^2)M_\phi^2\right]d\phi \quad [22]$$

Substituting the stress resultants, integrating, and then minimizing the strain energy with respect to variation in the coefficients, we obtain the following results

$$C_n = \frac{b^2P}{2\pi aD}\frac{N_n}{D_0} \quad [23]$$

where

$$\begin{aligned}
D_0 &= 9018\mu^6 + 31{,}745{,}000\mu^4 + 12{,}607{,}000{,}000\mu^2 + 174{,}560{,}000{,}000\\
N_1 &= 105\mu^6 + 1{,}408{,}700\mu^4 + 1{,}697{,}600{,}000\mu^2 + 174{,}560{,}000{,}000\\
N_3 &= 322\mu^6 + 3{,}798{,}500\mu^4 + 3{,}636{,}600{,}000\mu^2\\
N_5 &= 538\mu^6 + 3{,}788{,}200\mu^4\\
N_7 &= 751\mu^6
\end{aligned} \quad [24]$$

and

$$k_m = \frac{N_m}{D_0} \quad [25]$$

where

[6] For systems which obey Hooke's law the minimum complementary strain energy is equal to the strain energy, and the method of minimum complementary strain energy is identical to Castigliano's method of least work. The author prefers the term complementary strain energy as being more explicitly descriptive of a stress system which satisfies equilibrium but not necessarily compatibility, and in the problem at hand we are dealing with such an equilibrium stress system.

$$\begin{aligned} N_1 &= 162{,}310\mu^6 + 272{,}870{,}000\mu^4 + 43{,}640{,}000{,}039\mu^2 \\ N_2 &= 163{,}600\mu^6 + 303{,}050{,}000\mu^4 \\ N_3 &= 336{,}450\mu^6 \end{aligned} \quad [26]$$

Neglecting the small contribution of the direct strain we can express the vertical deflection of the shell as

$$w = -b\int \beta \cos\phi \, d\phi$$

and since $\beta$ is an even function of $\phi$ the over-all vertical deflection of the inner edges of the torus is given by

$$\delta_v = -4b\int_0^{\pi/2} \beta\cos\phi \, d\phi = \pi b C_1 = \frac{bP}{2aD}\frac{N_1}{D} \quad [27]$$

### Correlation With Test Data

Deformations and strains have been measured on a toroidal shell forming the straining section of a commercial expansion joint, details of which are shown in Figs. 3 and 4. The joint was annealed after manufacture and before the tests. Strains were measured on four different cross sections of the torus; the average of these is reported here. The strains were measured with SR-4, A-8, $\frac{1}{8}$ in. wire strain gages; gages were mounted at seven locations on each cross section and on both the inside and outside of the torus at each location.

Fig. 3 Test Shell After Strain Gages Had Been Applied

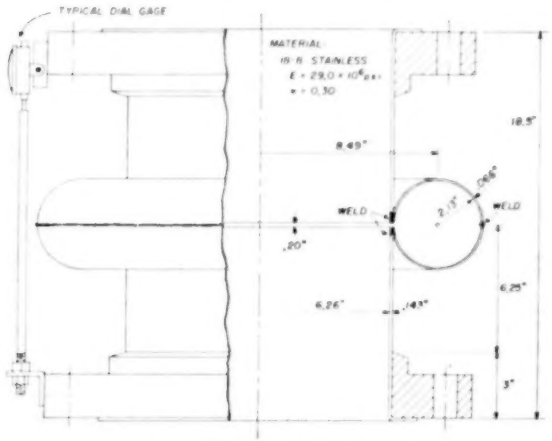


Fig. 4 Details of Test Shell

The results of these tests are shown in Figs. 5 through 9. Also plotted on these graphs are the theoretical stresses predicted by the solution developed in the first section of this paper and those predicted by the asymptotic integration solution of Clark.

The maximum membrane stress will always occur in the tangential direction at the top and bottom of the shell ($\phi = 0, \pi$), as shown in Fig. 6. The maximum bending stress will always be larger than the tangential membrane stress and its location will approach closer to $\phi = 0, \pi$ as the value of $\mu$ increases; in Fig. 9 the maximum occurs at approximately $\phi = \pi/8$.

The value of $\mu$ for the test shell is 27.5 and $\lambda = 0.251$. Except for the tangential bending stress, there is little to choose between the fit of the two solutions. A surprising feature is that the measured stresses are predicted more accurately by both solutions than is the measured deflection; in most approximate solutions one meets with better success in predicting over-all deflections than in predicting local values of stresses.

### Comparison of Asymptotic and Energy Solutions

In this section we will compare the results predicted by the asymptotic and energy solutions for different values of $\mu$. The two solutions should diverge for very small and for very large values of $\mu$ but in an intermediate range of $\mu$ they should coincide. Clark and Reissner[5] have made such a comparison for a closely allied problem, the bending of curved tubes.

Clark's results for the deflection, maximum stresses, and location of maximum bending stress can be expressed as simple explicit functions of $\mu$. The vertical deflection of the torus is given by

[5] "Advances in Applied Mechanics; Bending of Curved Tubes," by R. A. Clark and E. Reissner, Academic Press, New York, N. Y., vol. 2, 1951, pp. 93–112.

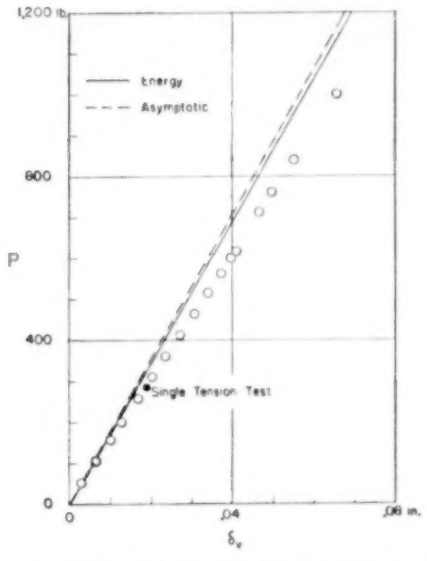


Fig. 5 Load-Deflection Results for Compression of Test Shell

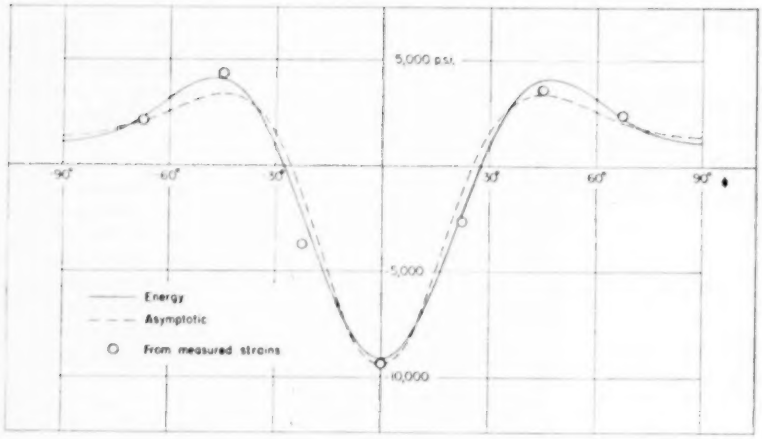


FIG. 6 TANGENTIAL MEMBRANE STRESS FOR 1000-LB COMPRESSIVE LOAD ON TEST SHELL

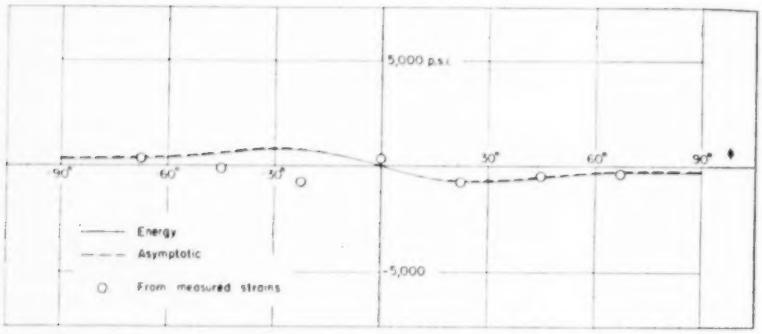


FIG. 7 RADIAL MEMBRANE STRESS FOR 1000-LB COMPRESSIVE LOAD ON TEST SHELL

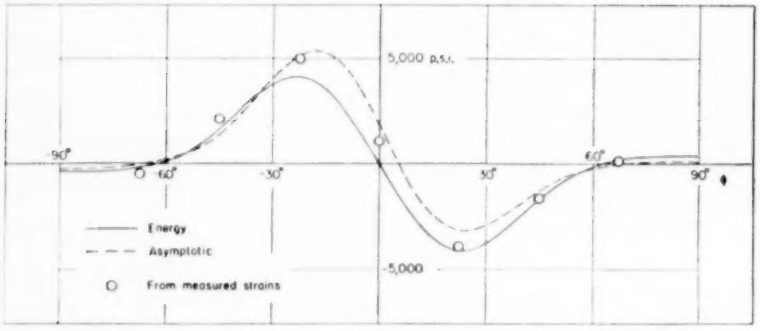


FIG. 8 TANGENTIAL BENDING STRESS FOR 1000-LB COMPRESSIVE LOAD ON TEST SHELL

$$\delta_v = 21.8\,(1 - \nu^2)^{1/2}\,\frac{bP}{2\pi Eh^2} \qquad [28]$$

The maximum tangential membrane stress is

$$\sigma_{\phi B_m} = 2.15(1 - \nu^2)^{1/2}\left(\frac{ab}{h^2}\right)^{1/2}\frac{P}{2\pi ah} \qquad [29]$$

Retaining only the term corresponding to $\beta'$ in Equation [14] for $M_\phi$, the location and magnitude of the maximum bending stress are given by

$$\phi_m = \pm\sin^{-1}\frac{1.225}{\mu^{1/2}} \approx \pm\frac{1.225}{\mu^{1/2}} \qquad [30]$$

$$\sigma_{\phi B_m} = \pm\frac{2.99}{(1 - \nu^2)^{1/2}}\left(\frac{ab}{h^2}\right)^{1/2}\frac{P}{2\pi ah} \qquad [31]$$

Equation [28] can be expressed as follows

$$\delta_v = \frac{2}{\mu}\,\frac{b^2P}{2aD} = \frac{2}{\mu}\,\delta_0 \qquad [32]$$

where $\delta_0$ can be interpreted as the deflection of a straight slit pipe of radius $b$, thickness $h$, and length $2\pi a$, whose slit edges are prevented from rotating when the edges are pulled apart by a force $P$.

The ratio of $\delta_v/\delta_0$ for the two solutions is plotted in Fig. 10. The solutions are seen to overlap closely in the region of $\mu$ between 8 and 30. The single plotted point represents the test result.

The location of the maximum bending stress is shown in Fig. 11. Here the range of overlap is between $\mu = 5$ and $\mu = 40$. It is interesting to note that the point of maximum stress stays at the edge of the torus (which is the location for a straight pipe) until

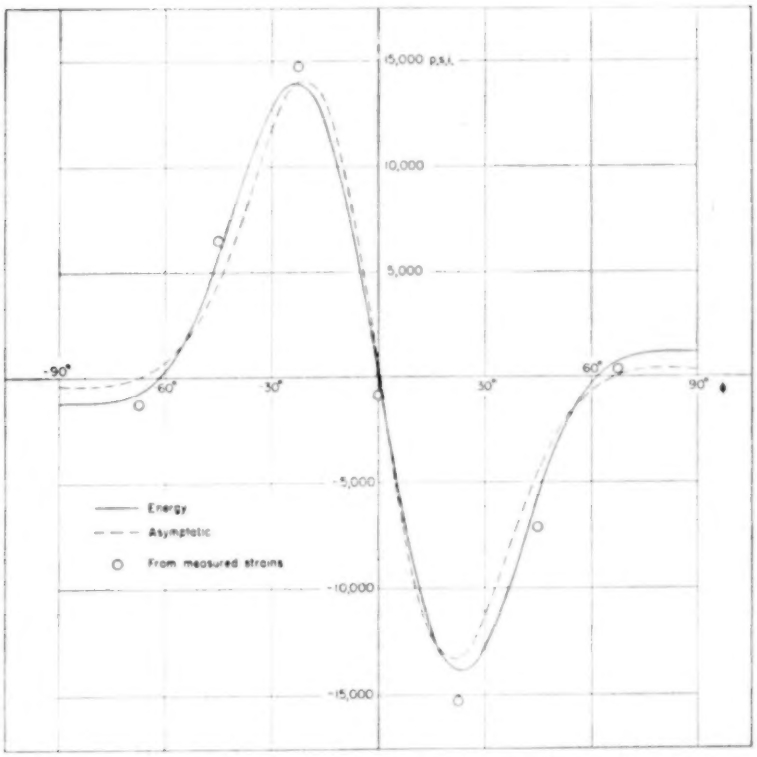


FIG. 9 RADIAL BENDING STRESS FOR 1000-LB COMPRESSIVE LOAD ON TEST SHELL

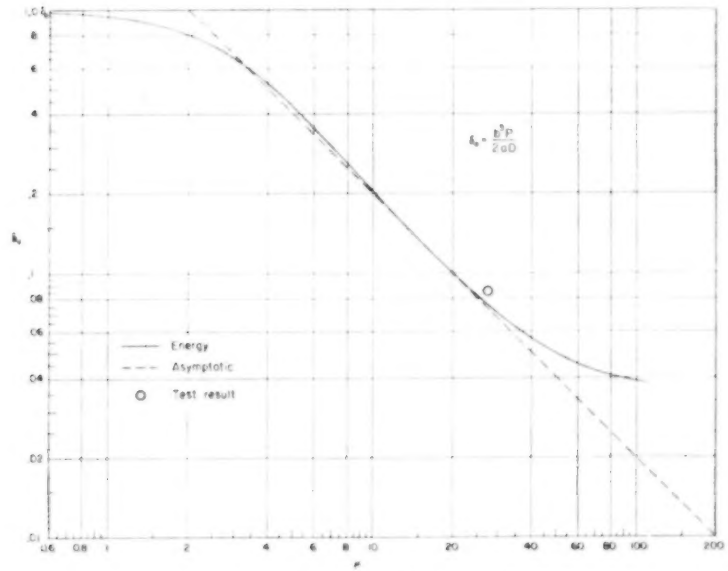


FIG. 10 DEFLECTION OF TOROIDAL SHELL AS A FUNCTION OF $\mu$

($\delta_0$ is deflection of a straight slit pipe of radius $b$, thickness $h$, and length $2\alpha$, whose slit edges are prevented from rotating when the edges are pulled apart by a force $P$. Graph gives effect on deflection of wrapping this straight pipe into a toroidal shell.)

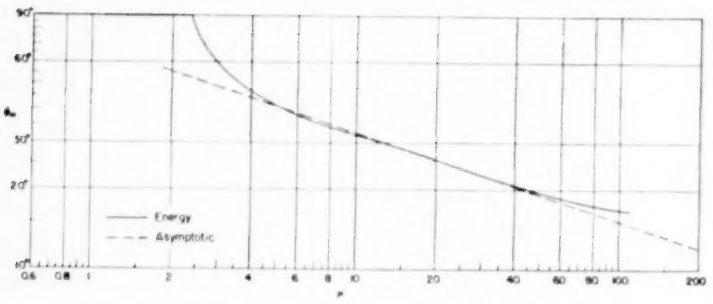


FIG. 11 LOCATION OF MAXIMUM (RADIAL) BENDING STRESS AS A FUNCTION OF $\mu$

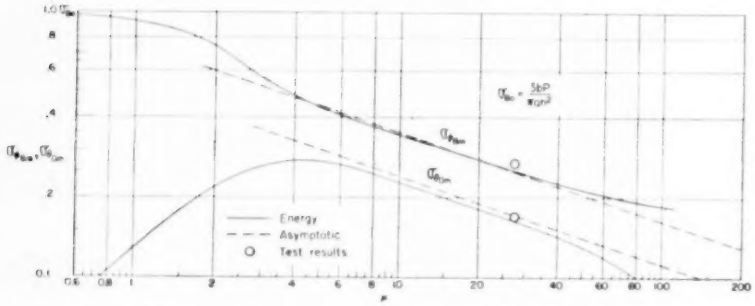


FIG. 12 MAXIMUM BENDING (RADIAL) AND MEMBRANE (TANGENTIAL) STRESSES IN TOROIDAL SHELL AS A FUNCTION OF $\mu$

($\sigma_{B0}$ is maximum bending stress in a straight slit pipe of radius $b$, thickness $h$, and length $2\pi a$, whose slit edges are prevented from rotating when the edges are pulled apart by a force $P$. Graph gives effect on stresses of wrapping this straight pipe into a toroidal shell.)

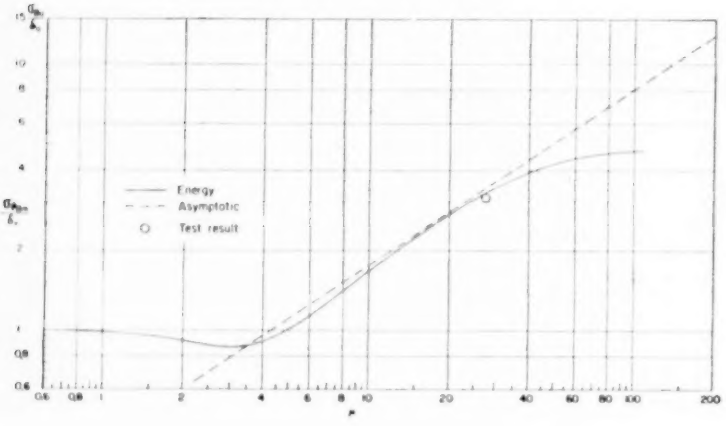


FIG. 13 RATIO OF MAXIMUM BENDING STRESS TO DEFLECTION OF TOROIDAL SHELL AS FUNCTION OF $\mu$, EXPRESSED IN TERMS OF SAME RATIO FOR STRAIGHT SLIT PIPE OF SAME DIMENSIONS

$\mu = 2.3$, at which point a small increase in $\mu$ moves it abruptly toward the center of the torus.

For a value of $\nu = 0.3$, Equations [29] and [31] can be written as

$$\sigma_{\theta Bm} = \frac{0.518}{\mu^{1/3}} \frac{3bP}{\pi ah^2} = \frac{0.518}{\mu^{1/3}} \sigma_{B0} \quad \ldots\ldots [33]$$

$$\sigma_{\phi Bm} = \frac{0.754}{\mu^{1/3}} \frac{3bP}{\pi ah^2} = \frac{0.754}{\mu^{1/3}} \sigma_{B0} \quad \ldots\ldots [34]$$

where $\sigma_{B0}$ can be interpreted as the maximum bending stress in a straight slit pipe of radius $b$, thickness $h$, and length $2\pi a$ whose slit edges are prevented from rotating when the edges are pulled apart by a force $P$.

The maximum stresses for the two solutions are shown in Fig. 12. The bending stresses are in good agreement in the range of $\mu$ between 4 and 40. Agreement between the solutions for tangential membrane stress is not as good, being separated by slightly more than 5 per cent in the interval $\mu = 8$ to $\mu = 40$.

From Figs. 10, 11, and 12 it is evident that the four-term energy solution is not applicable for values of $\mu$ greater than about 30. By taking a larger number of terms in the series this solution could be extended to larger values of $\mu$; however, this is unnecessary in view of the existence of the asymptotic solution.

It is of interest to compare the torus with a comparable straight pipe in terms of the ratio of maximum stress to deflection. This is done in Fig. 13. Surprisingly, for $\mu < 5$ the torus is slightly better in this respect than is the straight pipe.

In the design of a torus for an expansion joint the distance $a$ in most instances will be fixed within small limits by the dimension of the cylindrical pipe to be connected. In Fig. 14 the ratio of maximum bending stress to deflection is given in terms of $E/a$. It is evident from this plot that for a given value of $a$ one should not design for $\mu < 4$. In using this graph for design, the asymp-

totic solution should not be used for $\mu < 10$ and the energy solution should not be used for $\mu > 30$.

### Other Types of Loading

Tests were conducted with a couple $M$, acting in the plane of the cylindrical pipe axes. Strain measurements showed that the maximum stress in the shell can be calculated with good accuracy from the axial-deformation theory by substituting

$$P = \frac{2M}{r_m} \quad [35]$$

where $r_m$ is the radius to the point of maximum bending stress in the axial-deformation theory. The resulting angle $\omega$, between the adjacent cylindrical pipe axes, can be approximated with accuracy by

$$\omega = \frac{\delta_c}{a} \quad [36]$$

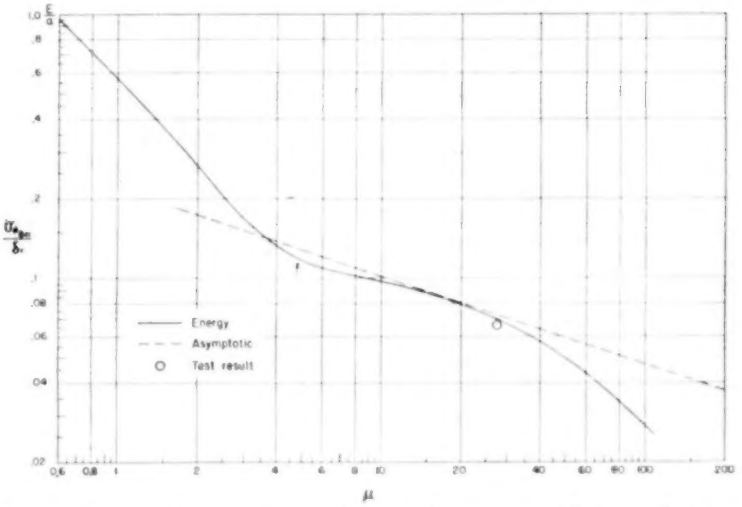


Fig. 14 Ratio of Maximum Bending Stress to Deflection of Toroidal Shell as Function of $\mu$, Expressed in Terms of $E/a$

where $\delta_c$ is calculated using $P = 2M/a$.

A torsion test showed that the shearing stresses and rotation are those predicted by the theory of thin-walled hollow members.[6]

Tests with the shell subjected to internal pressure showed that the membrane stresses are substantially those predicted by the well-known equations from the membrane theory of shells.[7] It was impossibe to detect any systematic bending-stress distribution because of local straining due to small initial noncircularities in the torus cross sections.

### Acknowledgments

The author wishes to thank Prof. J. P. Den Hartog who suggested the problem and arranged for the test equipment. His fruitful counsel during the progress of the work is also greatly appreciated. In addition, the author is indebted to Prof. E. Reissner for many helpful suggestions and to the Standard Oil Development Corporation (ESSO) for the equipment used in the tests.

## Appendix

It may be of interest to indicate a possible alternative development of a set of equilibrium stress resultants, as suggested by E. Reissner.

Let

$$Q_\phi = -H \sin\phi + V \cos\phi \quad [37]$$

where $H$ and $V$ are horizontal and vertical stress resultants. From vertical equilibrium we have

$$V = \frac{P}{2\pi r} = \frac{P}{2\pi a} \quad [38]$$

and $Q_\phi$ becomes

$$Q_\phi = -H \sin\phi + \frac{P}{2\pi a} \cos\phi \quad [39]$$

Horizontal equilibrium gives

$$N_\theta = \frac{a}{b} H' \quad [40]$$

Moment equilibrium gives

$$M'_\phi = bQ_\phi \quad [41]$$

Assuming a trigonometric series for $N_\theta$, with $N_\theta$ even in $\phi$ and $N_\theta(0) = N_\theta(\pi)$

$$N_\theta = \Sigma A_n \cos 2n\phi \quad [42]$$

Then

$$H = \frac{b}{a} \sum \frac{A_n}{2n} \sin 2n\phi \quad [43]$$

and

$$M_\phi = \frac{Pb}{2\pi a} \sin\phi - \frac{b^2}{a} \sum \frac{A_n}{2n} \int \sin\phi \sin 2n\phi \, d\phi$$

$$= \frac{Pb}{2\pi a} \sin\phi - \frac{b^2}{a} \sum \frac{A_n}{4n} \left[ \frac{\sin(2n-1)\phi}{2n-1} - \frac{\sin(2n+1)\phi}{2n+1} \right] \quad [44]$$

$\beta$ and $\delta_c$ are found as follows

$$\beta = \frac{b}{D} \int M_\phi \, d\phi = -\frac{Pb^2}{2\pi aD} \cos\phi + \frac{b^3}{aD} \sum \frac{A_n}{4n} \left[ \frac{\cos(2n-1)\phi}{(2n-1)^2} - \frac{\cos(2n+1)\phi}{(2n+1)^2} \right] \quad [45]$$

$$\delta_c = -4b \int_0^{\pi/2} \beta \cos\phi \, d\phi = \frac{Pb^3}{2aD} - \frac{\pi b^3 A_1}{4aD} \quad [46]$$

The coefficients $A_n$ again may be found by minimizing the complementary strain energy.

[6] "Theory of Elasticity," by S. Timoshenko and J. N. Goodier, McGraw-Hill Book Company, Inc., New York, N. Y., 1951, p. 298.

[7] "Theory of Elasticity," by R. V. Southwell, Oxford University Press, London, England, second edition, 1941, p. 254.

# Flexural Vibrations in Uniform Beams According to the Timoshenko Theory[1]

By R. A. ANDERSON,[2] PASADENA, CALIF.

**The general series solution is given for the flexural vibrations in a uniform beam according to the Timoshenko equations, which include the secondary effects of shear and rotatory inertia. In addition, the series solution is presented for the case of a pin-ended beam. For the special case of a concentrated transient force at the mid-point of a pin-ended beam, the bending-moment and shear-force solutions according to the Timoshenko and elementary equations are compared.**

## Nomenclature

The following nomenclature is used in the paper:

$y$ = total lateral deflection
$y_b$ = lateral bending deflections
$y_s$ = lateral shear deflections
$x$ = index of position along beam axis
$t$ = time
$M$ = elastic bending moment
$V$ = elastic shear force
$w$ = arbitrary distributed transverse force
$F$ = arbitrary concentrated transverse force
$E$ = Young's modulus
$G$ = shear modulus
$k'$ = ratio of average shear stress to maximum shear stress over a cross section
$l$ = length of beam
$r$ = radius of gyration of cross section around principal axis normal to plane of motion
$c_1$ = $\sqrt{E/\rho}$
$I$ = moment of inertia of cross section around principal axis normal to plane of motion
$A$ = cross-section area
$\rho$ = mass density
$m$ = mass of beam

*Elementary equation:*

$\phi_n(x)$ = $n$th mode shape
$q_n(t)$ = $n$th generalized co-ordinate
$M_n$ = $n$th generalized mass
$Q_n(t)$ = $n$th generalized force
$\omega_n$ = $n$th natural frequency
$u_n(t)$ = $n$th dynamic amplification factor

*Timoshenko equation:*

$\phi_n(x)$ = $n$th mode shape in bending deflection
$\psi_n(x)$ = $n$th mode shape in shear deflection

Otherwise, the same definitions as for the elementary equation, except with superscripts 1 and 2 to indicate two sets.

## Introduction

The analytical determination of the transient flexural vibrations of beams generally employs the elementary or Bernoulli-Euler equation. This equation considers only the lateral inertia and the elastic forces caused by bending deflections. However, it is known that secondary effects such as shear deflections and rotatory inertia, not included in the elementary theory may affect the vibrational response profoundly under certain conditions.

The first and best-known equation including the secondary effects of shear deflections and rotatory inertia is that of Timoshenko. The solution of this equation has been found to be difficult. Thus it is advantageous to apply the elementary equation whenever possible. It is important then to evaluate the veracity of the elementary equation under various conditions as compared with the Timoshenko equation and to define its region of usefulness. It is also important to have a general form of the solution to the Timoshenko equation to be applied outside the range of utility of the elementary equation.

The only correct solution to the Timoshenko equation that has been presented to date is that of Dengler and Goland who obtained a Laplace transform solution for the flexural response of a uniform, infinite beam to a transverse impulse (1).[3] Miklowitz also has developed a method for obtaining Laplace transform solutions for the flexural response of semi-infinite and certain finite uniform beams to certain transient loadings (2). While uniquely suited to the study of flexural elastic-wave propagation, the Laplace transform solutions generally are of integral form and are not readily comparable to the usual elementary equation solutions which are of series form. It is believed that a general solution of series form would be most useful for routine calculations since tabulations of a general nature can be made of the elements of the solution such as mode shapes or characteristic functions and natural frequencies.

This paper presents the general solution of mode superposition form for the flexural response of a uniform beam according to the Timoshenko theory. In addition, the general solution for the flexural vibrations in a uniform, pin-ended beam is presented. The special case of the flexural response of a uniform, pin-ended beam to a transient concentrated force at the mid-point is worked out numerically and a comparison is made of the elementary and Timoshenko solutions.

## Equations and BC

Instead of the usual single Timoshenko equation in the total deflection, it is found to be more convenient to use two equations in two variables—the bending deflection and the shear deflection. This results in simplification of the boundary conditions and of the expressions for the elastic bending moment and shear force.

The two equations, in a modified form, are those that were

[1] The results presented in this paper are taken from a thesis in partial fulfillment for the degree of Doctor of Philosophy from the California Institute of Technology.

[2] Mechanical Engineer, U. S. Naval Ordnance Test Station.

Contributed by the Applied Mechanics Division and presented at the Semi-Annual Meeting, Los Angeles, Calif., June 28–July 2, 1953, of The American Society of Mechanical Engineers.

Discussion of this paper should be addressed to the Secretary, ASME, 29 West 39th Street, New York, N. Y., and will be accepted until January 11, 1954, for publication at a later date. Discussion received after the closing date will be returned.

Note: Statements and opinions advanced in papers are to be understood as individual expressions of their authors and not those of the Society. Manuscript received by ASME Applied Mechanics Division, March 3, 1953. Paper No. 53—SA-9.

[3] Numbers in parentheses refer to Bibliography at end of the paper.

combined by Timoshenko to form the usual single equation in the total deflection (3). The modification consists of a transformation of co-ordinates from Timoshenko's total deflection and bending slope to the bending deflection and shear deflection.

$$\psi = \frac{\partial y_b}{\partial x} \quad [1]$$

$$y = y_b + y_s \quad [2]$$

Bending and shear-deflection co-ordinates were used by Meier in developing a beam equation (4). As a result of the transformation the Timoshenko equations are

$$EI\frac{\partial^2 y_b}{\partial x^2} + k'AG\frac{\partial y_s}{\partial x} - I\rho\frac{\partial^3 y_b}{\partial x \partial t^2} = 0 \quad [3]$$

$$\rho A\frac{\partial^2 y_b}{\partial t^2} + \rho A\frac{\partial^2 y_s}{\partial t^2} - k'AG\frac{\partial^2 y_s}{\partial x^2} = w(x, t) \quad [4]$$

The derivation of these equations involves the statement of the equilibrium of the linear and angular, elastic, and inertial forces. The equations require that the slopes be small. It is assumed that cross sections remain plane in bending. The cross sections will warp in shear but the resulting axial inertia is not considered. The equations require that the beam be prismatic and that the force be applied in one of the principal planes.

The equations of motion, Equations [3] and [4], also can be derived from energy considerations utilizing Hamilton's principle and the calculus of variations (5). In the process of this derivation, the end conditions are generated. The necessary and sufficient end conditions for the common beam ends are found to be as follows:

Pinned end

$$y_b + y_s = 0 \quad [5]$$

$$\frac{\partial^2 y_b}{\partial x^2} = 0 \quad [6]$$

Built-in end

$$y_b + y_s = 0 \quad [7]$$

$$\frac{\partial y_b}{\partial x} = 0 \quad [8]$$

Free end

$$\frac{\partial y_s}{\partial x} = 0 \quad [9]$$

$$\frac{\partial^2 y_b}{\partial x^2} = 0 \quad [10]$$

## General Series Solution

The approach to the solution of Equations [3] and [4] is one of synthesis utilizing the usual elements of beam-vibration solution—harmonic functions in time and harmonic and hyperbolic functions in space. This approach leads to solutions of series form having the form of the solution to the elementary or Bernoulli-Euler equation.

Assume the following solutions to the homogeneous part of Equations [3] and [4]

$$y_b = A_b e^{\beta x} e^{i\omega t} \quad [11]$$

$$y_s = A_s e^{\beta x} e^{i\omega t} \quad [12]$$

In order that a solution of the form of Equations [11] and [12] may exist, Equations [3] and [4] require that the following frequency equation exists

$$\omega^2 = -\frac{1}{2}\left[(\beta l)^2\left(\frac{c_1}{l}\right)^2\left(1 + \frac{k'G}{E}\right) - \frac{k'G}{E}\left(\frac{c_1}{l}\right)^2\left(\frac{l}{r}\right)^2\right] \pm \sqrt{\frac{1}{4}\left[(\beta l)^2\left(\frac{c_1}{l}\right)^2\left(1 + \frac{k'G}{E}\right) - \frac{k'G}{E}\left(\frac{c_1}{l}\right)^2\left(\frac{l}{r}\right)^2\right]^2 - \frac{k'G}{E}\left(\frac{c_1}{l}\right)^4(\beta l)^4} \quad [13]$$

At this point it will be assumed that there are two real sets of frequencies. This is necessary for a physically plausible solution since Equations [3] and [4] are fourth order in time. In general, two values of $\beta^2$ correspond to every value of $\omega^2$.

The assumption of two real sets of frequencies points toward a solution of the form

$$y_b(x, t) = \sum_{n=1}^{\infty} \phi_n^{(1)}(x) q_n^{(1)}(t) + \sum_{n=1}^{\infty} \phi_n^{(2)}(x) q_n^{(2)}(t) \quad [14]$$

$$y_s(x, t) = \sum_{n=1}^{\infty} \psi_n^{(1)}(x) q_n^{(1)}(t) + \sum_{n=1}^{\infty} \psi_n^{(2)}(x) q_n^{(2)}(t) \quad [15]$$

The shape functions $\phi_n^{(1)}(x)$, $\phi_n^{(2)}(x)$, $\psi_n^{(1)}(x)$, and $\psi_n^{(2)}(x)$ will be called the first and second sets of mode shapes for the bending and shear deflections. The time functions $q_n^{(1)}(t)$ and $q_n^{(2)}(t)$ will be called the first and second sets of generalized co-ordinates with the first and second sets of natural frequencies. These quantities have the form

$$\phi_n^{(1)}(x) = A_{bn}^{(I)} e^{\beta_n^{(I)} x} + B_{bn}^{(I)} e^{-\beta_n^{(I)} x} + A_{bn}^{(II)} e^{\beta_n^{(II)} x} + B_{bn}^{(II)} e^{-\beta_n^{(II)} x} \quad [16]$$

$$\phi_n^{(2)}(x) = A_{bn}^{(III)} e^{\beta_n^{(III)} x} + B_{bn}^{(III)} e^{-\beta_n^{(III)} x} + A_{bn}^{(IV)} e^{\beta_n^{(IV)} x} + B_{bn}^{(IV)} e^{-\beta_n^{(IV)} x} \quad [17]$$

$$\psi_n^{(1)}(x) = A_{sn}^{(I)} e^{\beta_n^{(I)} x} + B_{sn}^{(I)} e^{-\beta_n^{(I)} x} + A_{sn}^{(II)} e^{\beta_n^{(II)} x} + B_{sn}^{(II)} e^{-\beta_n^{(II)} x} \quad [18]$$

$$\psi_n^{(2)}(x) = A_{sn}^{(III)} e^{\beta_n^{(III)} x} + B_{sn}^{(III)} e^{-\beta_n^{(III)} x} + A_{sn}^{(IV)} e^{\beta_n^{(IV)} x} + B_{sn}^{(IV)} e^{-\beta_n^{(IV)} x} \quad [19]$$

$$q_n^{(1)}(t) = C_n^{(1)} \sin\left[\omega_n^{(1)} t + \epsilon_n^{(1)}\right] \quad [20]$$

$$q_n^{(2)}(t) = C_n^{(2)} \sin\left[\omega_n^{(2)} t + \epsilon_n^{(2)}\right] \quad [21]$$

Only half of the constants of Equations [16] through [21] are independent since $y_b$ and $y_s$ are coupled by Equations [3] and [4]. Equations [3] and [4] require that the following relations exist among the constants

$$A_{sn}^{(I)} = -\frac{E}{k'G}\left(\frac{r}{l}\right)^2\left[(\beta_n^{(I)} l)^2 + \left(\frac{\omega_n^{(1)} l}{c_1}\right)^2\right] A_{bn}^{(I)} \quad [22]$$

$$B_{sn}^{(I)} = -\frac{E}{k'G}\left(\frac{r}{l}\right)^2\left[(\beta_n^{(I)} l)^2 + \left(\frac{\omega_n^{(1)} l}{c_1}\right)^2\right] B_{bn}^{(I)} \quad [23]$$

$$A_{sn}^{(II)} = -\frac{E}{k'G}\left(\frac{r}{l}\right)^2\left[(\beta_n^{(II)} l)^2 + \left(\frac{\omega_n^{(1)} l}{c_1}\right)^2\right] A_{bn}^{(II)} \quad [24]$$

$$B_{sn}^{(\mathrm{II})} = -\frac{E}{k'G}\left(\frac{r}{l}\right)^2\left[(\beta_n^{(\mathrm{II})}l)^2 + \left(\frac{\omega_n^{(1)}l}{c_1}\right)^2\right]B_{bn}^{(\mathrm{II})} \quad [25]$$

$$A_{sn}^{(\mathrm{III})} = -\frac{E}{k'G}\left(\frac{r}{l}\right)^2\left[(\beta_n^{(\mathrm{III})}l)^2 + \left(\frac{\omega_n^{(2)}l}{c_1}\right)^2\right]A_{bn}^{(\mathrm{III})} \quad [26]$$

$$B_{sn}^{(\mathrm{III})} = -\frac{E}{k'G}\left(\frac{r}{l}\right)^2\left[(\beta_n^{(\mathrm{III})}l)^2 + \left(\frac{\omega_n^{(2)}l}{c_1}\right)^2\right]B_{bn}^{(\mathrm{III})} \quad [27]$$

$$A_{sn}^{(\mathrm{IV})} = -\frac{E}{k'G}\left(\frac{r}{l}\right)^2\left[(\beta_n^{(\mathrm{IV})}l)^2 + \left(\frac{\omega_n^{(2)}l}{c_1}\right)^2\right]A_{bn}^{(\mathrm{IV})} \quad [28]$$

$$B_{sn}^{(\mathrm{IV})} = -\frac{E}{k'G}\left(\frac{r}{l}\right)^2\left[(\beta_n^{(\mathrm{IV})}l)^2 + \left(\frac{\omega_n^{(2)}l}{c_1}\right)^2\right]B_{bn}^{(\mathrm{IV})} \quad [29]$$

It is convenient to normalize the mode shapes

$$\int_0^l [\phi_n^{(1)}(x) + \psi_n^{(1)}(x)]^2 dx = l \quad [30]$$

$$\int_0^l [\phi_n^{(2)}(x) + \psi_n^{(2)}(x)]^2 dx = l \quad [31]$$

The normalizing conditions plus the four boundary conditions specify all the constants in the mode shapes and supply an equation in $\omega$ and $\beta$ which, with Equation [13], permits their evaluation. The determination of the four constants in the generalized co-ordinates from the initial conditions requires an orthogonality condition.

The orthogonality condition is given by Equation [31] of reference (6) in terms of the total deflection and the bending slope. With a simple transformation of co-ordinates, Equations [1] and [2], the orthogonality condition is

$$\int_0^l \left[\rho A(y_b + y_s)_m(y_b + y_s)_n + \rho I\left(\frac{\partial y_b}{\partial x}\right)_m\left(\frac{\partial y_b}{\partial x}\right)_n\right]dx = 0, \; m \neq n \quad [32]$$

The subscripts $m$ and $n$ refer to two separate solutions. Equation [32] can be derived from the homogeneous parts of Equations [3] and [4], (5). The orthogonality condition, Equation [32], is not of classical form but it performs the same function in the solution.

In solving the initial value problem, it will be convenient to use for the initial values the total deflection, the total velocity, the bending slope, and the bending-slope velocity. Utilizing the orthogonality condition, it can be shown (5) that the initial values of the two sets of generalized co-ordinates are

$$q_n^{(1)}(0) = \frac{1}{M_n^{(1)}}\int_0^l \left\{y(x, 0)\rho A[\phi_n^{(1)}(x) + \psi_n^{(1)}(x)] + \frac{\partial y_b(x, t)}{\partial x}\bigg|_{t=0}\rho I\frac{d\phi_n^{(1)}(x)}{dx}\right\}dx \quad [33]$$

$$\frac{dq_n^{(1)}(t)}{dt}\bigg|_{t=0} = \frac{1}{M_n^{(1)}}\int_0^l \left\{\frac{\partial y(x, t)}{\partial t}\bigg|_{t=0}\rho A[\phi_n^{(1)}(x) + \psi_n^{(1)}(x)] + \frac{\partial^2 y_b(x, t)}{\partial x \partial t}\bigg|_{t=0}\rho I\frac{d\phi_n^{(1)}(x)}{dx}\right\}dx \quad [34]$$

$$q_n^{(2)}(0) = \frac{1}{M_n^{(2)}}\int_0^l \left\{y(x, 0)\rho A[\phi_n^{(2)}(x) + \psi_n^{(2)}(x)] + \frac{\partial y_b(x, t)}{\partial x}\bigg|_{t=0}\rho I\frac{d\phi_n^{(2)}(x)}{dx}\right\}dx \quad [35]$$

$$\frac{dq_n^{(2)}(t)}{dt}\bigg|_{t=0} = \frac{1}{M_n^{(2)}}\int_0^l \left\{\frac{\partial y(x, t)}{\partial t}\bigg|_{t=0}\rho A[\phi_n^{(2)}(x) + \psi_n^{(2)}(x)] + \frac{\partial^2 y_b(x, t)}{\partial x \partial t}\bigg|_{t=0}\rho I\frac{d\phi_n^{(2)}(x)}{dx}\right\}dx \quad [36]$$

The generalized masses occurring in Equations [33] through [36] are defined by

$$M_n^{(1)} = \int_0^l \left\{\rho A[\phi_n^{(1)}(x) + \psi_n^{(1)}(x)]^2 + \rho I\left[\frac{d\phi_n^{(1)}(x)}{dx}\right]^2\right\}dx \quad [37]$$

$$M_n^{(2)} = \int_0^l \left\{\rho A[\phi_n^{(2)}(x) + \psi_n^{(2)}(x)]^2 + \rho I\left[\frac{d\phi_n^{(2)}(x)}{dx}\right]^2\right\}dx \quad [38]$$

Equations [33] through [36] are sufficient to specify the four sets of constants in the generalized co-ordinates, Equations [20] and [21].

Of more interest is the solution for the case of a general transverse transient force which can be obtained easily from the given solution for the initial value problem. Consider homogeneous initial conditions. Determine first the result of an infinitesimal period of loading. Instantaneously the material of the beam adjacent to the arbitrary force begins in transverse motion in shear. There can be no bending deflections from a transverse force until shear strains build up, resulting in internal elastic forces and moments. The initial conditions after an infinitesimal period of loading $dt$ are

$$y(x, 0) = \frac{\partial y_b(x, t)}{\partial x}\bigg|_{t=0} = \frac{\partial^2 y_b(x, t)}{\partial x \partial t}\bigg|_{t=0} = 0 \quad [39]$$

$$\frac{\partial y(x, t)}{\partial t}\bigg|_{t=0} = \frac{w(x, t)dt}{\rho A} \quad [40]$$

The initial values of the generalized co-ordinates after the infinitesimal loading period $dt$ are, from Equations [33] through [36]

$$q_n^{(1)}(0) = q_n^{(2)}(0) = 0 \quad [41]$$

$$\frac{dq_n^{(1)}(t)}{dt}\bigg|_{t=0} = \frac{dt}{M_n^{(1)}}\int_0^l w(x, t)[\phi_n^{(1)}(x) + \psi_n^{(1)}(x)]dx \quad [42]$$

$$\frac{dq_n^{(2)}(t)}{dt}\bigg|_{t=0} = \frac{dt}{M_n^{(2)}}\int_0^l w(x, t)[\phi_n^{(2)}(x) + \psi_n^{(2)}(x)]dx \quad [43]$$

The motion of the generalized co-ordinates with initial values of Equations [41] through [43] is

$$q_n^{(1)}(t) = \frac{dt \sin \omega_n^{(1)}t}{M_n^{(1)}\omega_n^{(1)}}\int_0^l w(x, t)[\phi_n^{(1)}(x) + \psi_n^{(1)}(x)]dx \quad [44]$$

$$q_n^{(2)}(t) = \frac{dt \sin \omega_n^{(2)}t}{M_n^{(2)}\omega_n^{(2)}}\int_0^l w(x, t)[\phi_n^{(2)}(x) + \psi_n^{(2)}(x)]dx \quad [45]$$

The solutions for the generalized co-ordinates after a finite loading period can be obtained by superposition and are

$$q_n^{(1)}(t) = \frac{Q_n^{(1)}{}_{\max}}{M_n^{(1)}\omega_n^{(1)2}}u_n^{(1)}(t) \quad [46]$$

$$q_n^{(2)}(t) = \frac{Q_n^{(2)}{}_{\max}}{M_n^{(2)}\omega_n^{(2)2}}\, u_n^{(2)}(t) \qquad [47]$$

The generalized forces and dynamic-amplification factors occurring in Equations [46] and [47] are defined by

$$Q_n^{(1)}(t) = \int_0^l w(x,t)[\phi_n^{(1)}(x) + \psi_n^{(1)}(x)]dx \qquad [48]$$

$$Q_n^{(2)}(t) = \int_0^l w(x,t)[\phi_n^{(2)}(x) + \psi_n^{(2)}(x)]dx \qquad [49]$$

$$u_n^{(1)}(t) = \omega_n^{(1)} \int_0^t \frac{Q_n^{(1)}(\tau)}{Q_n^{(1)}{}_{\max}} \sin \omega_n^{(1)}(t-\tau)d\tau \qquad [50]$$

$$u_n^{(2)}(t) = \omega_n^{(2)} \int_0^t \frac{Q_n^{(2)}(\tau)}{Q_n^{(2)}{}_{\max}} \sin \omega_n^{(2)}(t-\tau)d\tau \qquad [51]$$

The form of the solution given by Equations [14], [15], [46], and [47] shows marked similarity with the general solution for the total deflections from the elementary equation given in the Appendix. The definitions of the generalized masses and forces and the dynamic-amplification factors, Equations [37], [38] and [48] through [51], are similar in form to those for the elementary equation given in the Appendix.

The solutions for the bending moment and shear force in the beam are given by

$$M(x,t) = EI \frac{\partial^2 y_0(x,t)}{\partial x^2} \qquad [52]$$

$$V(x,t) = k'AG \frac{\partial y_0(x,t)}{\partial x} \qquad [53]$$

The solution given is sufficient since there are precisely the number of constants in the solution to satisfy all the initial and boundary conditions. The solution is predicated on the existence of two sets of real frequencies. It can be shown that there are two sets for the case of a beam with pinned ends.

### Case of a Pin-Ended Beam

It is evident in this special case that the mode shapes $\phi_n^{(1)}(x)$, $\phi_n^{(2)}(x)$, $\psi_n^{(1)}(x)$, and $\psi_n^{(2)}(x)$ are sinusoidal with nodes at the beam ends. The consequence of this is

$$\beta_n^{(\mathrm{I})}l = \beta_n^{(\mathrm{II})}l = \beta_n^{(\mathrm{III})}l = \beta_n^{(\mathrm{IV})}l = in\pi \qquad [54]$$

Substitution of these values of $\beta$ into the frequency equation, Equation [13], yields two sets of real frequencies

$$\omega_n^{(1)2} = \frac{1}{2}\left[(n\pi)^2\left(\frac{c_1}{l}\right)^2\left(1+\frac{k'G}{E}\right) + \left(\frac{c_1}{l}\right)^2\left(\frac{l}{r}\right)^2\frac{k'G}{E}\right] - \sqrt{\frac{1}{4}\left[(n\pi)^2\left(\frac{c_1}{l}\right)^2\left(1+\frac{k'G}{E}\right) + \left(\frac{c_1}{l}\right)^2\left(\frac{l}{r}\right)^2\frac{k'G}{E}\right]^2 - (n\pi)^4\left(\frac{c_1}{l}\right)^4\frac{k'G}{E}} \qquad [55]$$

$$\omega_n^{(2)2} = \frac{1}{2}\left[(n\pi)^2\left(\frac{c_1}{l}\right)^2\left(1+\frac{k'G}{E}\right) + \left(\frac{c_1}{l}\right)^2\left(\frac{l}{r}\right)^2\frac{k'G}{E}\right] + \sqrt{\frac{1}{4}\left[(n\pi)^2\left(\frac{c_1}{l}\right)^2\left(1+\frac{k'G}{E}\right) + \left(\frac{c_1}{l}\right)^2\left(\frac{l}{r}\right)^2\frac{k'G}{E}\right]^2 - (n\pi)^4\left(\frac{c_1}{l}\right)^4\frac{k'G}{E}} \qquad [56]$$

Utilizing Equations [22] through [31], the normalized mode shapes are

$$\phi_n^{(1)}(x) = \frac{\sqrt{2}\sin\dfrac{n\pi x}{l}}{1+\dfrac{E}{k'G}\left(\dfrac{r}{l}\right)^2\left[(n\pi)^2 - \left(\dfrac{\omega_n^{(1)}l}{c_1}\right)^2\right]} \qquad [57]$$

$$\phi_n^{(2)}(x) = \frac{\sqrt{2}\sin\dfrac{n\pi x}{l}}{1+\dfrac{E}{k'G}\left(\dfrac{r}{l}\right)^2\left[(n\pi)^2 - \left(\dfrac{\omega_n^{(2)}l}{c_1}\right)^2\right]} \qquad [58]$$

$$\psi_n^{(1)}(x) = \frac{\sqrt{2}\,\dfrac{E}{k'G}\left(\dfrac{r}{l}\right)^2\left[(n\pi)^2 - \left(\dfrac{\omega_n^{(1)}l}{c_1}\right)^2\right]\sin\dfrac{n\pi x}{l}}{1+\dfrac{E}{k'G}\left(\dfrac{r}{l}\right)^2\left[(n\pi)^2 - \left(\dfrac{\omega_n^{(1)}l}{c_1}\right)^2\right]} \qquad [59]$$

$$\psi_n^{(2)}(x) = \frac{\sqrt{2}\,\dfrac{E}{k'G}\left(\dfrac{r}{l}\right)^2\left[(n\pi)^2 - \left(\dfrac{\omega_n^{(2)}l}{c_1}\right)^2\right]\sin\dfrac{n\pi x}{l}}{1+\dfrac{E}{k'G}\left(\dfrac{r}{l}\right)^2\left[(n\pi)^2 - \left(\dfrac{\omega_n^{(2)}l}{c_1}\right)^2\right]} \qquad [60]$$

An application of the defining equations, Equations [37] and [38], yields the generalized masses

$$M_n^{(1)} = m\left[1 + \frac{(n\pi)^2\left(\dfrac{r}{l}\right)^2}{\left\{1+\dfrac{E}{k'G}\left(\dfrac{r}{l}\right)^2\left[(n\pi)^2 - \left(\dfrac{\omega_n^{(1)}l}{c_1}\right)^2\right]\right\}^2}\right] \qquad [61]$$

$$M_n^{(2)} = m\left[1 + \frac{(n\pi)^2\left(\dfrac{r}{l}\right)^2}{\left\{1+\dfrac{E}{k'G}\left(\dfrac{r}{l}\right)^2\left[(n\pi)^2 - \left(\dfrac{\omega_n^{(2)}l}{c_1}\right)^2\right]\right\}^2}\right] \qquad [62]$$

The generalized forces for an arbitrary transverse force are, by Equations [48] and [49]

$$Q_n^{(1)}(t) = Q_n^{(2)}(t) = \sqrt{2}\int_0^l w(x,t)\sin\frac{n\pi x}{l}dx \qquad [63]$$

The dynamic-amplification factors can be obtained by Equations [50] and [51].

The quantities in the solution, Equations [55] through [63], are easy to evaluate and tabulate as is the case with the elementary solution. The two sets of frequencies, Equations [55] and [56], are calculated for solid rectangular and solid circular cross sections and are plotted in dimensionless form in Figs. 1 and 2 as functions of the parameter $n(r/l)$. Since it will be seen that the transient response in the first set of frequencies predominates, it is instructive to study the behavior of these frequencies. For small $n(r/l)$ in Fig. 1, corresponding to the lower modes of slender beams, the first set of frequencies approaches asymptotically the frequencies from the elementary equation. For large $n(r/l)$, corresponding to the higher modes of thick beams, the first set of frequencies approaches the frequencies of pure shear vibrations. It appears that the vibrations of the lower modes in slender beams

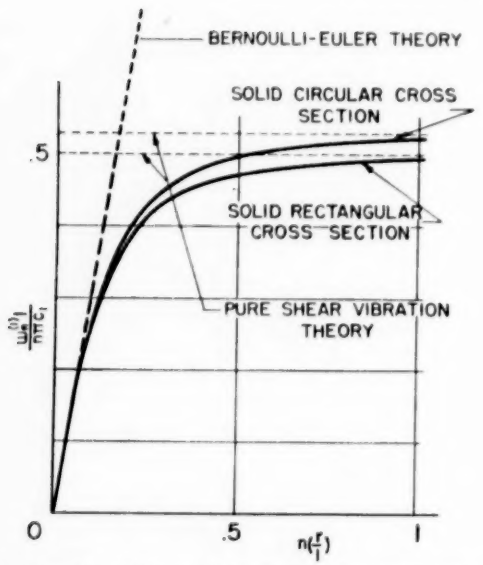


FIG. 1 FIRST SET OF NATURAL FREQUENCIES, TIMOSHENKO THEORY, PIN-ENDED BEAM

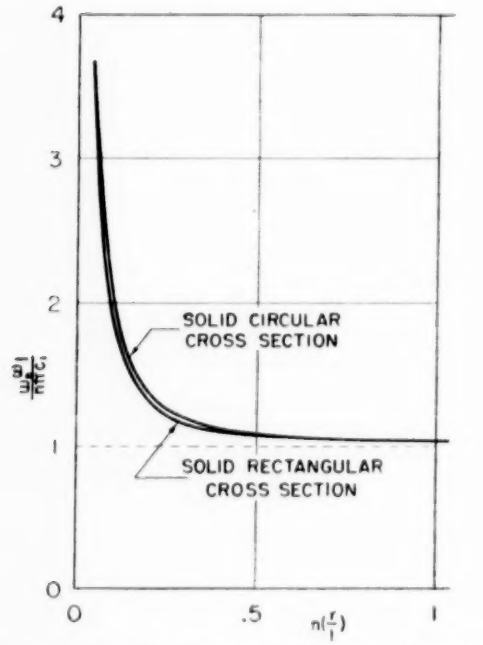


FIG. 2 SECOND SET OF NATURAL FREQUENCIES, TIMOSHENKO THEORY, PIN-ENDED BEAM

are predominantly in bending while those of the higher modes in thick beams are predominantly in shear.

### CASE OF CONCENTRATED TRANSIENT FORCE AT CENTER OF PIN-ENDED BEAM

Since the elastic forces in a beam are generally of more engineering importance than the deflections, only the bending-moment and shear-force responses will be considered here. In this special case it can be shown from Equations [52] and [53] that the bending moment and shear force are

$$\frac{M(x,t)}{lF_{max}} = \sum_{n=1,3,5,\ldots}^{\infty} \sin\frac{n\pi x}{l}\,[A_{mn}u_n^{(1)}(t) + B_{mn}u_n^{(2)}(t)] \quad \ldots [64]$$

$$A_{mn} = \sqrt{2}\left(\frac{r}{l}\right)^2\left[\frac{\phi_n^{(1)}(x)}{\sin\frac{n\pi x}{l}}\right]\left(\frac{m}{M_n^{(1)}}\right)\left(\frac{n\pi c_1}{\omega_n^{(1)}l}\right)^2$$

$$B_{mn} = \sqrt{2}\left(\frac{r}{l}\right)^2\left[\frac{\phi_n^{(2)}(x)}{\sin\frac{n\pi x}{l}}\right]\left(\frac{m}{M_n^{(2)}}\right)\left(\frac{n\pi c_1}{\omega_n^{(2)}l}\right)^2$$

$$\frac{V(x,t)}{F_{max}} = \sum_{n=1,3,5,\ldots}^{\infty} \cos\frac{n\pi x}{l}\,[A_{vn}u_n^{(1)}(t) + B_{vn}u_n^{(2)}(t)] \quad \ldots [65]$$

$$A_{vn} = \sqrt{2}\frac{k'G}{E}\frac{1}{n\pi}\left[\frac{\psi_n^{(1)}(x)}{\sin\frac{n\pi x}{l}}\right]\left(\frac{m}{M_n^{(1)}}\right)\left(\frac{n\pi c_1}{\omega_n^{(1)}l}\right)^2$$

$$B_{vn} = \sqrt{2}\frac{k'G}{E}\frac{1}{n\pi}\left[\frac{\psi_n^{(2)}(x)}{\sin\frac{n\pi x}{l}}\right]\left(\frac{m}{M_n^{(2)}}\right)\left(\frac{n\pi c_1}{\omega_n^{(2)}l}\right)^2$$

Also, for this special case, the bending moment and shear force predicted by the elementary equation are

$$\frac{M(x,t)}{lF_{max}} = \sum_{n=1,3,5,\ldots}^{\infty} \sin\frac{n\pi x}{l}\,C_{mn}\,u_n(t) \quad \ldots [66]$$

$$C_{mn} = \frac{2}{(n\pi)^2}$$

$$\frac{V(x,t)}{F_{max}} = \sum_{n=1,3,5,\ldots}^{\infty} \cos\frac{n\pi x}{l}\,C_{vn}\,u_n(t) \quad \ldots [67]$$

$$C_{vn} = \frac{2}{n\pi}$$

The coefficients $A_{mn}$, $A_{vn}$, $B_{mn}$, and $B_{vn}$ are all functions of the ratio of Young's to shear modulus $E/G$, the shape of the cross section, and the parameter $n(r/l)$. For the purpose of calculations, the ratio of Young's to shear modulus was selected as 8/3 which closely approximates the properties of steel. A solid rectangular cross section was assumed. The slenderness ratio $l/r$ was chosen to be 20 which describes neither a thick nor a slender beam. For these parameter values, the coefficients are evaluated for several mode numbers $n$ and are tabulated in Tables 1 and 2.

A study of Tables 1 and 2 reveals that $B_{mn}$ and $B_{vn}$ are substantially smaller than $A_{mn}$ and $A_{vn}$. It can be seen that $A_{mn} + B_{mn} = C_{mn}$ and $A_{vn} + B_{vn} = C_{vn}$. This fact also can be deduced from Equations [64] through [67]. In the case where the force is applied statically, the Timoshenko and elementary solutions must be equal. Since the dynamic-amplification factors are all unity in this case and, since there can be only one unique expansion for the static bending moment in a sine series or the static shear force in a cosine series, the foregoing equality must be true. In the lower modes $B_{mn}$ is relatively negligible while in the higher modes $B_{mn}$ approaches, as a relative maximum, 1/4 of $A_{mn}$. $B_{vn}$ is relatively unimportant in all the modes.

TABLE 1. MODEWISE BENDING-MOMENT RESPONSE COEFFICIENTS, PIN-ENDED BEAM, TRANSIENT TRANSVERSE FORCE AT MID-POINT

| $n$ | $AM_n$ | $BM_n$ (−) | $CM_n$ |
|---|---|---|---|
| 1 | 100.19 | 0.19 | 100 |
| 3 | 11.68 | 0.57 | 11.11 |
| 5 | 4.509 | 0.509 | 4 |
| 7 | 2.424 | 0.383 | 2.041 |
| 9 | 1.517 | 0.282 | 1.235 |
| 11 | 1.038 | 0.211 | 0.827 |
| 21 | 0.2966 | 0.0699 | 0.2267 |
| 31 | 0.1375 | 0.0334 | 0.1041 |
| 51 | 0.0511 | 0.0126 | 0.0385 |

NOTE: Expressed as per cent of first-mode Bernoulli-Euler response.

TABLE 2. MODEWISE SHEAR-FORCE RESPONSE COEFFICIENTS, PIN-ENDED BEAM, TRANSIENT TRANSVERSE FORCE AT MID-POINT

| $n$ | $AV_n$ | $BV_n$ | $CV_n$ |
|---|---|---|---|
| 1 | 98.39 | 1.61 | 100 |
| 3 | 31.17 | 2.16 | 33.33 |
| 5 | 18.76 | 1.24 | 20 |
| 7 | 13.59 | 0.70 | 14.29 |
| 9 | 10.71 | 0.40 | 11.11 |
| 11 | 8.849 | 0.251 | 9.091 |
| 21 | 4.717 | 0.045 | 4.762 |
| 31 | 3.211 | 0.015 | 3.226 |
| 51 | 1.957 | 0.004 | 1.961 |

NOTE: Expressed as per cent of first-mode Bernoulli-Euler response.

These results show that in the transient bending-moment and shear-force solutions for the Timoshenko equations, the response in the first set of frequencies predominates. It is further apparent that the bending-moment and shear-force solutions for the elementary equation are modewise comparable to those for the Timoshenko equations. These conclusions, however, are dependent also on the magnitude of the dynamic-amplification factors.

In order to consider the additional effects of the dynamic-amplification factors, it will be necessary to study specific force-time transients. Two limiting cases can be discussed here. When the transient force is applied slowly enough to excite statically all the modes, the bending-moment or shear-force solutions for the elementary and Timoshenko equations are modewise identical. This also will be true of all those higher modes that are essentially statically excited even when the lower modes are dynamically excited. If the transient force is applied rapidly enough, some of the modes will be excited impulsively. For these impulsively excited modes, the dynamic-amplification factors vary linearly as the mode frequency. It is apparent from Fig. 1 that the predominant first set of Timoshenko frequencies diverges from the elementary frequencies in the higher modes. This results in a comparative divergence of the dynamic-amplification factors which can be seen in Tables 3 and 4.

## Discussion and Conclusions

The general solution of mode superposition type for the flexural vibrations in uniform beams according to the Timoshenko equations is presented. The form of this solution is similar to that for the elementary equation except that there are two series and two sets of frequencies.

For a pin-ended beam, the first set of frequencies approaches asymptotically the elementary equation frequencies for the lower modes in slender beams and the pure shear vibration frequencies for the higher modes in thick beams. The second set of frequencies has no such physical interpretation.

For the case of a concentrated transient force applied at the mid-point of a pin-ended beam, the bending-moment and shear-force responses in the first set of frequencies predominate. This is true provided the dynamic-amplification factors in the two sets of frequencies are comparable. Also for this special case, the bending-moment and shear-force responses in the first set of frequencies are modewise of the same order of magnitude as those according to the elementary equation.

TABLE 3. MAXIMUM MODEWISE BENDING-MOMENT RESPONSES, PIN-ENDED BEAM, TRANSVERSE IMPULSE AT MID-POINT

| | Timoshenko | | |
|---|---|---|---|
| $n$ | First set of modes | Second set of modes | Bernoulli-Euler |
| 1 | 94.62 | 4.17 | 100 |
| 3 | 74.10 | 16.56 | 100 |
| 5 | 58.86 | 19.79 | 100 |
| 7 | 48.15 | 19.14 | 100 |
| 9 | 40.35 | 17.40 | 100 |
| 11 | 34.52 | 15.37 | 100 |
| 21 | 19.53 | 9.48 | 100 |
| 31 | 13.47 | 6.64 | 100 |
| 51 | 8.27 | 4.12 | 100 |

NOTE: Expressed as per cent of maximum first-mode Bernoulli-Euler response.

TABLE 4. MAXIMUM MODEWISE SHEAR-FORCE RESPONSES, PIN-ENDED BEAM, TRANSVERSE IMPULSE AT MID-POINT

| | Timoshenko | | |
|---|---|---|---|
| $n$ | First set of modes | Second set of modes | Bernoulli-Euler |
| 1 | 92.92 | 43.15 | 100 |
| 3 | 197.78 | 62.09 | 300 |
| 5 | 244.81 | 48.20 | 500 |
| 7 | 270.05 | 34.57 | 700 |
| 9 | 284.84 | 24.97 | 900 |
| 11 | 294.02 | 18.53 | 1100 |
| 21 | 310.66 | 6.04 | 2100 |
| 31 | 314.69 | 2.88 | 3100 |
| 51 | 316.94 | 1.09 | 5100 |

NOTE: Expressed as per cent of maximum first-mode Bernoulli-Euler response.

## Acknowledgments

The author wishes to express his sincere appreciation to Prof. Donald E. Hudson of the California Institute of Technology, who directed this research. The assistance of Prof. George W. Housner, also of the California Institute of Technology, who contributed valuable suggestions, is acknowledged with thanks.

## Bibliography

1 "Transverse Impact of Long Beams, Including Rotatory Inertia and Shear Effects," by M. A. Dengler and M. Goland, Proceedings of the First U. S. National Congress of Applied Mechanics, 1951, published by The American Society of Mechanical Engineers, New York, N. Y., 1952, pp. 179–186.

2 "Flexural Wave Solutions of Coupled Equations Representing the More Exact Theory of Bending," by Julius Miklowitz, published in this issue, pp. 511–514.

3 "Vibration Problems in Engineering," by S. P. Timoshenko, D Van Nostrand Company, Inc., New York, N. Y., second edition, 1947, pp. 337–338.

4 "Impact on Prismatical Bars," by T. Davidson and J. H. Meier, Proceedings of the SESA, vol. 4, 1946, p. 106.

5 "Transient Response of Uniform Beams," by R. A. Anderson, Doctoral thesis submitted to the California Institute of Technology, Pasadena, Calif., 1953.

6 "Normal Modes of Oscillation in Beams," by C. L. Dolph, Report UMM 79, Willow Run Research Center, University of Michigan, Ann Arbor, Mich., 1951.

7 "Dynamic Loads on Airplane Structures During Landing," by M. A. Biot and R. L. Bisplinghoff, NACA Wartime Report W92, 1944.

## Appendix

According to the elementary or Bernoulli-Euler theory, the vibrations in a uniform beam are described by the equation (3)

$$EI\frac{\partial^4 y}{\partial x^4} + \rho A\frac{\partial^2 y}{\partial t^2} = w(x, t) \quad \ldots\ldots\ldots\ldots\ldots\ldots\ldots\ldots\ldots\ldots [68]$$

By way of review, this equation assumes that plane sections remain plane in bending and that bending slopes are small. The equation also requires that the line of centroids be a straight line, that the principal axes of the cross sections form two principal planes, and that the loading be applied in one of these

principal planes. The equation considers only lateral inertia and bending deflections.

The solution of Equation [68] is well known to be of the form (7)

$$y(x, t) = \sum_{n=1}^{\infty} \phi_n(x) q_n(t) \quad [69]$$

Define the generalized masses and forces as

$$M_n = \int_0^l \rho A [\phi_n(x)]^2 dx \quad [70]$$

$$Q_n(t) = \int_0^l \phi_n(x) w(x, t) dx \quad [71]$$

Define the dynamic-amplification factors as

$$u_n(t) = \omega_n \int_0^t \frac{Q_n(\tau)}{Q_{n\max}} \sin \omega_n(t - \tau) d\tau \quad [72]$$

Then, by virtue of the orthogonality condition, the generalized co-ordinates have the form

$$q_n(t) = \frac{Q_{n\max}}{M_n \omega_n^2} u_n(t) \quad [73]$$

From elementary beam theory, the elastic bending moment and shear force are

$$M(x, t) = EI \frac{\partial^2 y(x, t)}{\partial x^2} \quad [74]$$

$$V(x, t) = EI \frac{\partial^3 y(x, t)}{\partial x^3} \quad [75]$$

# Flexural Wave Solutions of Coupled Equations Representing the More Exact Theory of Bending[1]

By JULIUS MIKLOWITZ,[2] PASADENA, CALIF.

**Presented here is a new method for deriving flexural wave solutions for the Timoshenko bending theory. The method is based on a breakdown of the total deflection into its bending and shear components. Instead of treating the full Timoshenko equation (1)[3] an equivalent set of coupled equations, representing the rotational and translatory motions of the beam element, is solved. The advantages of this method stem from (*a*) the simplicity of the associated expressions for the moment and shear force, which are the elementary bending theory relations, and (*b*) the well-defined nature of the related boundary conditions. The latter is particularly important since it is difficult to define the proper boundary conditions associated with the full Timoshenko equation. This is evidenced in the works of Uflyand (2) and Dengler and Goland (3), both of which are concerned with wave solutions for the infinite beam under the action of a concentrated transverse load. The quoted work (3) points out the erroneous boundary conditions used in the Uflyand work (2). The present method is applied to the same case treated in the works (2, 3). Agreement is shown with the Dengler and Goland solution. The Uflyand solution is shown to have meaning when interpreted properly. The derivation of transforms for other beam cases, both finite and infinite, by the present method has also been included in this work.**

## Nomenclature

The following nomenclature is used in the paper:

$A$, $A_j$ = arbitrary functions of $p$

$A_0$ = cross-sectional area of beam, a constant

$B$, $B_j$ = arbitrary functions of $p$

$C = \dfrac{A_0\gamma}{EIg}$, where $E$ = modulus of elasticity; $I$ = moment of inertia of beam cross section with respect to neutral axis of bending; $g$ = acceleration due to gravity; $\gamma$ = specific weight of beam material

$C_j$ = arbitrary functions of $p$

$D_j$ = arbitrary functions of $p$

$M(x, t)$ = moment

$S(x, t)$ = shear force

$c_1$ = a limiting wave velocity, defined by $\sqrt{\dfrac{Eg}{\gamma}}$

$c_2$ = a limiting wave velocity, defined by $\sqrt{\dfrac{k'Gg}{\gamma}}$, where

$k'G$ = effective shear modulus, relating average shear stress acting over a beam cross section to shear deformation at neutral plane in accord with elementary bending

$l$ = length

$m(x, p)$ = Laplace transform of $M(x, t)$

$n$, $n_j$ = roots of characteristic equation

$p$ = transformation parameter

$s(x, p)$ = Laplace transform of $S(x, t)$

$t$ = time

$v(x, p)$, $v_b(x, p)$, $v_s(x, p)$ = Laplace transforms of $y(x, t)$, $y_b(x, t)$, and $y_s(x, t)$

$x$ = co-ordinate along beam

$y(x, t)$ = total lateral deflection of beam element

$y_b(x, t)$ = lateral deflection of beam element due to bending

$y_s(x, t)$ = lateral deflection of beam element due to shear

## Introduction

As a means of studying the propagation of flexural waves in beams, recent work in the literature has been focused on the derivation of wave solutions of the more exact equation of bending due to Timoshenko (1). Uflyand (2) showed that this differential equation, the derivation of which includes considerations of the shear force and rotatory inertia effects, had wave character as against the nonwave character of the elementary bending equation. He was the first to derive wave solutions, treating both the infinite and finite beams subjected to a transverse impact. Later Dengler and Goland (3), focusing on the infinite beam, derived wave solutions of the Timoshenko equation which are related to Uflyand's solution. In this work (3) it is pointed out that the boundary conditions associated with the Uflyand solution (2) are incorrect. With this as an example, Dengler and Goland comment on the difficulty of defining the proper boundary conditions (at a cut) associated with the Timoshenko equation. In their solutions a definite loading is applied at $x = 0$ and no cut is required.

Instead of working with the total deflection equation as was done in the quoted works (2, 3), Anderson (4), concerned with classical solutions (nonwave), used the equivalent set of coupled equations

$$EI\frac{\partial^2 y_b}{\partial x^2} + k'A_0G\frac{\partial y_s}{\partial x} - \frac{I\gamma}{g}\frac{\partial^3 y_b}{\partial x \partial t^2} = 0 \qquad [1a]$$

$$\frac{\gamma A_0}{g}\frac{\partial^2 y_b}{\partial t^2} + \frac{\gamma A_0}{g}\frac{\partial^2 y_s}{\partial t^2} - k'A_0G\frac{\partial^2 y_s}{\partial x^2} = 0 \qquad [1b]$$

[1] The work reported here was supported by the U. S. Naval Ordnance Test Station through the Exploratory and Foundational Research program.

[2] Consultant, Naval Ordnance Test Station.

[3] Numbers in parentheses refer to the Bibliography at the end of the paper.

Contributed by the Applied Mechanics Division and presented at the Semi-Annual Meeting, Los Angeles, Calif., June 28–July 2, 1953, of The American Society of Mechanical Engineers.

Discussion of this paper should be addressed to the Secretary, ASME, 29 West 39th Street, New York, N. Y., and will be accepted until January 11, 1954, for publication at a later date. Discussion received after the closing date will be returned.

Note: Statements and opinions advanced in papers are to be understood as individual expressions of their authors and not those of the Society. Manuscript received by ASME Applied Mechanics Division, February 12, 1953. Paper No. 53—SA-6.

These equations[4] result by employing the transformation

$$\left.\begin{aligned} y &= y_b + y_s \\ \psi &= \frac{\partial y_b}{\partial x} \end{aligned}\right\} \quad \ldots\ldots [2]$$

at the appropriate point in the Timoshenko derivation. Equation [1*a*] is the differential equation for the rotation, and Equation [1*b*] for the translatory motion of the beam element.[5] The advantages in using the coupled equations in deriving solutions for the Timoshenko bending mechanism stem from the simplicity of associated expressions. The moment and shear force are those of the elementary bending theory

$$M(x, t) = EI \frac{\partial^2 y_b}{\partial x^2} \quad \ldots\ldots [3a]$$

$$S(x, t) = -k' A_0 G \frac{\partial y_s}{\partial x} \quad \ldots\ldots [3b]$$

In addition the quoted work (4) points out the well-defined nature of the associated boundary conditions.[6]

This paper presents a method of deriving wave solutions for the Timoshenko theory based on the coupled-equation approach. As might be expected, the simplicity of Equations [3], and particularly the well-defined nature of the boundary conditions associated with Equations [1], in view of the difficulty discussed in the quoted works (2, 3), are definite aids in the wave treatment. The present method is applied to the infinite beam case treated in the literature (2, 3), and agreement is shown with the Dengler and Goland solution (3). The Uflyand solution (2) is shown to have meaning when interpreted properly.

A section of the paper is devoted to a discussion of wave solutions for finite beams.

## The Method

The method presented offers a convenient means of obtaining separate wave solutions for any or all of the basic items of interest in beam action; the deflections $y_b(x, t)$ and $y_s(x, t)$, the moment $M(x, t)$ and the shear force $S(x, t)$. In view of the nature of Equations [1] interest initially focuses on the deflections. With the initial conditions

$$y_b(x, 0) = y_s(x, 0) = \frac{\partial y_b(x, 0)}{\partial t} = \frac{\partial y_s(x, 0)}{\partial t} = 0$$

the Equations [1] transform to

$$\left.\begin{aligned} EI \frac{d^3 v_b}{dx^3} + k' A_0 G \frac{dv_s}{dx} - \frac{I\gamma}{g} p^2 \frac{dv_b}{dx} &= 0 \\ \frac{\gamma}{g} p^2 v_b + \frac{\gamma}{g} p^2 v_s - k' G \frac{d^2 v_s}{dx^2} &= 0 \end{aligned}\right\} \quad \ldots\ldots [4]$$

according to the Laplace transform theory (9).

Equations [4] constitute a system of two homogeneous linear ordinary differential equations. A possible solution of these equations is of the type

$$\left.\begin{aligned} v_b(x, p) &= Ae^{-nx} \\ v_s(x, p) &= Be^{-nx} \end{aligned}\right\} \quad \ldots\ldots [5]$$

The system of Equations [4] is satisfied therefore if

$$\left.\begin{aligned} \left(\frac{I\gamma}{g} p^2 n - EIn^3\right) A - k' A_0 GnB &= 0 \\ \frac{\gamma}{g} p^2 A + \left(\frac{\gamma}{g} p^2 - k' Gn^2\right) B &= 0 \end{aligned}\right\} \quad \ldots\ldots [6]$$

and these equations are compatible if the determinant

$$\begin{vmatrix} \left(\frac{I\gamma}{g} p^2 n - EIn^3\right) & -k' GA_0 n \\ \frac{\gamma}{g} p^2 & \left(\frac{\gamma p^2}{g} - k' Gn^2\right) \end{vmatrix} = 0 \quad \ldots\ldots [7]$$

Equation [7], of fourth degree in $n$, is the characteristic equation of the system of Equations [4]. Introducing the quantities $c_1$, $c_2$, and $C$, Equation [7] may be written as

$$n^4 - p^2 \left(\frac{1}{c_2^2} + \frac{1}{c_1^2}\right) n^2 + p^2 \left(\frac{p^2}{c_1^2 c_2^2} + C\right) = 0 \quad \ldots [7a]$$

Assuming that Equation [7*a*] has four distinct roots $n_1$, $n_2$, $n_3$, and $n_4$, then the general solution of the system of Equations [4] is

$$v_b(x, p) = \sum_{j=1}^{4} A_j e^{-n_j x} \quad \ldots\ldots [8a]$$

$$v_s(x, p) = \sum_{j=1}^{4} B_j e^{-n_j x} \quad \ldots\ldots [8b]$$

where $A_j$, $B_j$, and $n_j$, all functions of $p$, satisfy Equations [6].

Equations [6] must hold for all values of $n_j$, therefore

$$\frac{B_j}{A_j} = \frac{\frac{p^2}{c_1^2} - n_j^2}{c_2^2 C} = -\frac{p^2}{p^2 - c_2^2 n_j^2} \quad \ldots\ldots [9]$$

and eliminating the $B_j$-values we have for Equations [8]

$$v_b(x, p) = \sum_{j=1}^{4} A_j e^{-n_j x} \quad \ldots\ldots [10a]$$

$$v_s(x, p) = \sum_{j=1}^{4} \Phi_j A_j e^{-n_j x} \quad \ldots\ldots [10b]$$

where $$\Phi_j = \frac{\frac{p^2}{c_1^2} - n_j^2}{c_2^2 C}$$

Equations [10] contain the four required arbitrary functions $A_j(p)$ which are determined by the boundary conditions of a particular problem.[7] It may be noted that Equation [7*a*] produces the same biquadratic expression for $n_j$ as in the Uflyand work (2).[8] In terms of his nomenclature then

$$n_j = \pm M \sqrt{p} \sqrt{p \mp N \sqrt{p^2 - a^2}} \quad \ldots\ldots [11]$$

where

$$M = \frac{1}{\sqrt{2}} \sqrt{\frac{1}{c_2^2} + \frac{1}{c_1^2}}, \quad N = \frac{\frac{1}{c_2^2} - \frac{1}{c_1^2}}{\frac{1}{c_2^2} + \frac{1}{c_1^2}}, \quad a = \frac{2\sqrt{C}}{\frac{1}{c_2^2} - \frac{1}{c_1^2}}$$

[4] These equations are also stated in the works of Davidson and Meier (5), and Robinson (6), and suggested in the work of Mindlin (7).

[5] Equations [*c*], [*d*] reference (1), p. 338.

[6] The author learned later of the work of Boley, Heninger, and Zimmoch (8), which contains a variational derivation of the coupled Equations [1] and related boundary conditions similar to that associated with the work (4).

[7] This method of producing Equations [10] is discussed in von Kármán and Biot (10).

[8] See equations [1.6] and [1.7] in reference (2).

Of primary interest in engineering problems are the stresses, hence the importance of the transforms for the moment and shear force. They may be obtained from Equations [10] by making use of Equations [3]

$$m(x, p) = EI \sum_{j=1}^{4} n_j^2 A_j e^{-n_j x} \quad \ldots\ldots [12a]$$

$$s(x, p) = k' A_s G \sum_{j=1}^{4} n_j \phi_j A_j e^{-n_j x} \quad \ldots\ldots [12b]$$

Note that each of the Equations [10*a*], [10*b*], [12*a*], and [12*b*] bears marked resemblance to Ufiyand's transform for the total deflection in a beam (2).[9] Depending on the information desired, the general procedure Ufiyand used in getting his inverse transform could be followed for any or all of the inverse transforms associated with Equations [10*a*], [10*b*], [12*a*], and [12*b*]. The method employs the complex inversion integral and contour integration after the functions $A_j(p)$ are properly defined for the particular problem being solved. The details are given in the quoted work (2).

## Infinite-Beam Solutions

The present method will now be applied to the problem

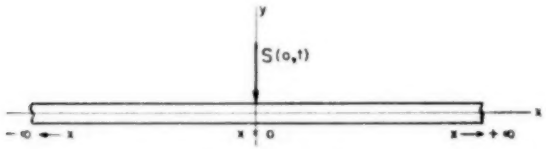


Fig. 1 Infinite-Beam Problem
(Concentrated transverse load at $x = 0$.)

treated in the quoted works (2, 3), that of an infinite beam with a concentrated transverse load applied at the station $x = 0$, Fig. 1. The transform derived agrees with that Dengler and Goland derived (3). Further, the Ufiyand solution (2), previously shown to be in error because of incorrect boundary conditions (3), is given meaning.

The boundary conditions[10] at $x = 0$ are taken as

$$\left.\begin{aligned} \frac{\partial y_s(0, t)}{\partial x} &= -\frac{S(0, t)}{k' A_s G} \\ \frac{\partial y_b(0, t)}{\partial x} &= 0 \end{aligned}\right\} \quad \ldots\ldots [13]$$

and the $x > 0$ portion of the beam is considered. The transformation of these yields

$$\left.\begin{aligned} \frac{dv_s(0, p)}{dx} &= -\frac{s(0, p)}{k' A_s G} \\ \frac{dv_b(0, p)}{dx} &= 0 \end{aligned}\right\} \quad \ldots\ldots [14]$$

Applying these to the Equations [10*a*] and [10*b*] the latter become

$$v_b(x, p) = A_1 e^{-n_1 x} + A_2 e^{-n_2 x} \quad \ldots\ldots [15a]$$

$$v_s(x, p) = \phi_1 A_1 e^{-n_1 x} + \phi_2 A_2 e^{-n_2 x} \quad \ldots\ldots [15b]$$

where

$$A_1(p) = \frac{s(0, p)}{EI n_1 (n_2^2 - n_1^2)}$$

$$A_2(p) = -\frac{s(0, p)}{EI n_2 (n_2^2 - n_1^2)}$$

and

$$n_{1,2} = M \sqrt{p} \sqrt{p \mp N \sqrt{p^2 - a^2}}$$

these two values of $n$ necessarily being chosen to satisfy the Bromwich contour condition of Re $n_1 > 0$, Re $n_2 > 0$. The expression for the moment, and hence bending stress, can be obtained directly from Equation [12*a*]

$$m(x, p) = EI[n_1^2 A_1 e^{-n_1 x} + n_2^2 A_2 e^{-n_2 x}] \quad \ldots\ldots [16]$$

Equation [16] agrees with the transform Dengler and Goland derived for the moment (3).[11] Interesting is the fact that Equation [15*a*] and the transform Ufiyand derived for the total deflection (2)[12] are the same. Hence it is clear that his solution may be used if it is interpreted as just that of the bending deflection.

In concluding this section of the paper the author would like to comment briefly on another basic case he has treated—that

Fig. 2 Semi-Infinite-Beam Problem
(Pure moment at $x = 0$.)

of a pure moment applied to the free end of a semi-infinite beam, Fig. 2. The $x = 0$ boundary conditions for this case are

$$\left.\begin{aligned} \frac{\partial^2 y_b(0, t)}{\partial x^2} &= \frac{M(0, t)}{EI} \\ \frac{\partial y_s(0, t)}{\partial x} &= 0 \end{aligned}\right\} \quad \ldots\ldots [17]$$

Interest in this work was in the bending stresses; hence attention was focused on the moment transform. Equations [17] yield for this case the Equation [16]

where

$$\left.\begin{aligned} A_1 &= \frac{c_2^2 Cm(0, p)\, \phi_2}{EI\,(n_1 - n_2)\left(\frac{p^2}{c_1^2} + n_1 n_2\right) n_1} \\ A_2 &= -\frac{c_2^2 Cm(0, p)\, \phi_1}{EI\,(n_1 - n_2)\left(\frac{p^2}{c_1^2} + n_1 n_2\right) n_2} \end{aligned}\right\} \quad \ldots\ldots [18]$$

and where the same comments on $n$ apply, as in the previous case. The complete solution for this case, with $M(0, t)$ taken as a sharp half-sine input, will be presented in the near future. Curves representing the wave shapes will be included.

## Finite-Beam Solutions

It is of interest engineering-wise to consider wave solutions for the finite-beam cases. The general transformed solutions for the finite beam are contained in Equations [10*a*], [10*b*], [12*a*], and [12*b*]. They can be written in terms of $n_1$ and $n_2$ since $n_3 = -n_1$, and $n_4 = -n_2$ follow from Equation [11]; hence the general transformed solutions for the deflections may be written as

[9] See equation [1.8] in reference (2).

[10] These were considered by the present author to be the proper conditions for this case. They are actually one of four possible sets of associated end conditions generated in the variational derivation mentioned in footnote 6.

[11] See equation [39] of reference (3).

[12] See equations [1.8] and [4.3] of reference (2).

$$v_b(x, p) = C_1 \cosh n_1 x + D_1 \sinh n_1 x + C_2 \cosh n_2 x + D_2 \sinh n_2 x \quad [19a]$$

$$v_s(x, p) = \phi_1[C_1 \cosh n_1 x + D_1 \sinh n_1 x] + \phi_2[C_2 \cosh n_2 x + D_2 \sinh n_2 x] \quad [19b]$$

and for the moment and shear force as

$$m(x, p) = EI[n_1^2(C_1 \cosh n_1 x + D_1 \sinh n_1 x) + n_2^2(C_2 \cosh n_2 x + D_2 \sinh n_2 x)] \quad [20a]$$

$$s(x, p) = -k'A_sG[n_1\phi_1(C_1 \sinh n_1 x + D_1 \cosh n_1 x) + n_2\phi_2(C_2 \sinh n_2 x + D_2 \cosh n_2 x)] \quad [20b]$$

where $C$ and $D$ are functions of $p$, and are determined by the boundary conditions of the problem. The case treated by Uflyand, the simply supported beam with a transverse force at $x = 0$, will now be treated by the present method as an example,

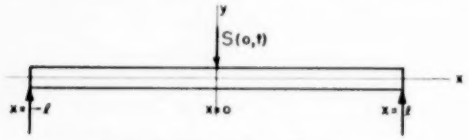


FIG. 3 FINITE-BEAM PROBLEM
(Concentrated transverse load at $x = 0$.)

Fig. 3. For this case, the following conditions at $x = l$ (4) are needed in addition to the conditions at $x = 0$.[13]

$$\left.\begin{aligned} y_b(l, t) + y_s(l, t) &= 0 \\ \frac{\partial^2 y_b(l, t)}{\partial x^2} &= 0 \end{aligned}\right\} \quad [21]$$

These conditions applied to Equations [19a] and [19b] produce the following transform for the bending deflection

$$v_b(x, p) = \frac{s(0, p)}{EI(n_2^2 - n_1^2)}\left[\frac{\sinh n_2(x - l)}{n_2 \cosh n_2 l} - \frac{\sinh n_1(x - l)}{n_1 \cosh n_1 l}\right] \quad [22]$$

and similar expressions for the shear deflection, moment, and shear force. Note here again, as might be expected, that Equation [22] is the same as the transform for the total deflection in the Uflyand work (2).[14] Hence the remainder of his finite-beam solution may be used if the results are interpreted as just the bending deflection. As Uflyand points out, the form of Equation [22] may be interpreted in its wave sense, i.e.

$$\frac{\sinh n(x - l)}{\cosh nl} = -e^{-nx} + e^{-n(2l - x)} + e^{-n(2l + x)} - e^{-n(4l - x)} - e^{-n(4l + x)} + \cdots \quad [23]$$

the terms after the first being related to wave reflections from the beam ends. A transform in this form simplifies the finite-beam case since the complete solution may be written from the infinite-beam solution. The latter is based on the first term on the right-hand side of Equation [23]. Therefore the reflection contributions can be obtained from the infinite-beam solution by substituting $2l - x$, $2l + x$, $4l - x$, and so on, for $x$, according to Equation [23].[15] It should be pointed out that wave solutions of finite-beam problems with boundary conditions involving an odd and an even derivative are much more difficult since the transform cannot be written in the form of Equation [22]. A fixed or free end gives this difficulty, the conditions on the former being

$$\left.\begin{aligned} y_b + y_s &= 0 \\ \frac{\partial y_b}{\partial x} &= 0 \end{aligned}\right\} \quad [24]$$

and on the latter

$$\left.\begin{aligned} \frac{\partial y_s}{\partial x} &= 0 \\ \frac{\partial^2 y_b}{\partial x^2} &= 0 \end{aligned}\right\} \quad [25]$$

The case shown in Fig. 4 would give a convenient solution. The solution for this case would be of interest since it would

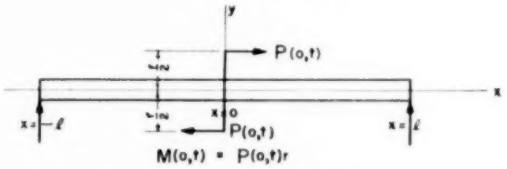


FIG. 4 FINITE-BEAM PROBLEM
(Moment at $x = 0$.)

yield information on the propagation of waves in a finite beam due to a moment source. The boundary conditions at $x = 0$ for this case[16] would be

$$\left.\begin{aligned} \frac{\partial^2 y_b(0, t)}{\partial x^2} &= \frac{M(0, t)}{EI} \\ y_b(0, t) + y_s(0, t) &= 0 \end{aligned}\right\} \quad [26]$$

and the conditions at $x = l$ are again Equations [21].

ACKNOWLEDGMENT

Acknowledgment is made to the U. S. Naval Ordnance Test Station for permission to publish this work.

BIBLIOGRAPHY

1 "Vibration Problems in Engineering," by S. Timoshenko, D. Van Nostrand Company, Inc., New York, N. Y., 1937, p. 338.

2 "The Propagation of Waves in the Transverse Vibration of Bars and Plates," by Ya. S. Uflyand, *Prikladnaia Matematika i Mekhanika*, vol. 12, May–June, 1948, pp. 287–300 (in Russian). See Rev. 33, AMR 3.

3 "Transverse Impact of Long Beams, Including Rotatory Inertia and Shear Effects," by M. A. Dengler and M. Goland, Proceedings of First U. S. National Congress of Applied Mechanics, 1951.

4 "Flexural Vibrations of Uniform Beams According to the Timoshenko Theory," by R. A. Anderson, published in this issue, pp. 504–510.

5 "Impact on Prismatical Bars," by T. Davidson and J. H. Meier, Proceedings of the SESA, vol. 4, 1946, p. 106.

6 "Shock Transmission in Beams," by A. Robinson, Aeronautical Research Council Technical Report No. 2265, Ministry of Supply, London, England, 1950, p. 16.

7 "Influence of Rotatory Inertia and Shear on Flexural Motions of Isotopic, Elastic Plates," by R. D. Mindlin, JOURNAL OF APPLIED MECHANICS, Trans. ASME, vol. 73, 1951, pp. 31–38. Reference is to p. 33.

8 "An Energy Theory of Transverse Impact on Beams," by B. A. Boley, R. E. Heninger, and V. P. Zimnoch, ONR Report, Project NR-064-355, January, 1952.

9 "Modern Operational Mathematics in Engineering," by R. V. Churchill, McGraw-Hill Book Co., Inc., New York, N. Y., 1944.

10 "Mathematical Methods in Engineering," by Th. von Kármán and M. A. Biot, McGraw-Hill Book Co., Inc., New York, N. Y., 1940, p. 41.

[13] See Equations [13].

[14] See equation [7.6] in reference (2). There is a misprint in this equation; $u(x, t)$ should be replaced by $v(x, p)$.

[15] Equations [7.6] to [7.13] in reference (2).

# Analysis of a Nonlinear Dynamic Vibration Absorber

By L. A. PIPES,[1] LOS ANGELES, CALIF.

**This paper presents a mathematical analysis of the action of a dynamic vibration absorber. The system analyzed consists of a main mass attached to a rigid foundation by a linear spring coupled to the absorber mass by a spring of nonlinear characteristics. The forced oscillations of the system produced by a harmonic disturbing force acting on the main mass are studied analytically. It is assumed that the coupling absorber spring has nonlinear force-displacement characteristics of the hyperbolic sine type. Expressions for the amplitudes of the vibrations of the two masses as functions of the frequency of the disturbing force are obtained.**

## Introduction

THE amplitudes of the forced vibrations of systems with one degree of freedom frequently can be reduced by a proper choice of the spring constant involved so that the system will be far away from the condition of resonance, or by proper balancing so that the magnitude of the disturbing force is minimized. When these methods are impractical, the amplitudes of the undesired vibrations are reduced by the use of a device known as a dynamic vibration absorber. An example of such a device is illustrated in Fig. 1. The mass $m_1$ represents, for example, the

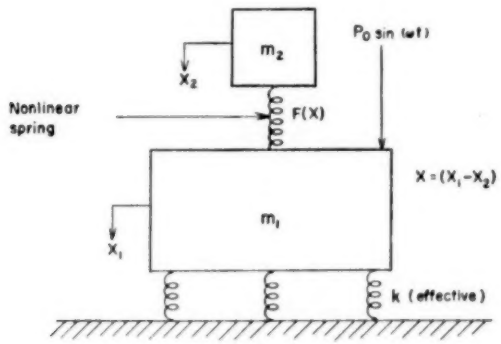


Fig. 1 Vibration Absorber

mass of a machine that is executing vertical oscillations as a result of the influence of a vertical harmonic disturbing force, $P_0 \sin (wt)$, that is acting on it. The machine is suspended above a rigid foundation by means of a linear spring of spring constant, $k$. The dynamic vibration absorber consists of a comparatively small mass $m_2$ attached to the main mass $m_1$ by means of a linear spring. The action of a linear dynamic vibration absorber is well known and has been the subject of considerable investigation (1, 2, 3, 4).[2]

The conventional dynamic vibration absorber is very efficient in inhibiting the vibrations of the main mass. This is accomplished by "tuning" the absorber to the frequency of the harmonic disturbing force. If, however, the frequency of the disturbing force varies over a range in the normal operation of the system, the linear dynamic absorber may become inoperative and might aggravate matters particularly if the system attains a condition of resonance. During recent years attempts have been made to endow the dynamic absorber with greater flexibility in suppressing vibrations throughout a range of frequencies of the disturbing force by introducing springs with nonlinear characteristics into its design. The effectiveness of these devices has been studied by essentially experimental procedures and it appears that in only one recent paper (5) has an analytical investigation been attempted. In that paper, the effect of a nonlinear absorber spring that has cubic characteristics is investigated. In the present paper the effect of a nonlinear absorber spring whose characteristics are those of a hyperbolic sine function is determined by a significantly different procedure.

## Notation and General Equations

Consider the mechanical system in Fig. 1. The following notation will be used in the analysis of this system:

$m_1$ = main mass of system (mass to be stabilized)
$m_2$ = mass of absorber
$k$ = spring constant of spring suspension of main mass
$x_1$ = vertical displacement of main mass from equilibrium
$x_2$ = vertical displacement of absorber mass from equilibrium
$P_0$ = amplitude of harmonic disturbing force
$w$ = angular frequency of the harmonic disturbing force
$t$ = time
$P_0 \sin (wt)$ = harmonic disturbing force
$x = (x_1 - x_2)$ = relative displacement of masses
$F(x)$ = force transmitted by nonlinear absorber spring
$k_0$ = "initial" spring constant of absorber spring
$a$ = positive constant
$F(x) = \frac{k_0}{a} \sinh (ax)$, an analytical expression assumed for nonlinear characteristics of absorber spring
$D = \frac{d}{dt}$ = time-derivative operator
$Z_1(D) = m_1D^2 + k$, an operator
$Z_2(D) = m_2D^2$, an operator
$A$ = amplitude of harmonic relative displacement
$x_a$ = an assumed approximate form for relative displacement
$B = aA$, a constant

[1] Professor of Engineering, University of California.

Contributed by the Applied Mechanics Division and presented at the Semi-Annual Meeting, Los Angeles, Calif., June 28-July 2, 1953, of The American Society of Mechanical Engineers.

Discussion of this paper should be addressed to the Secretary, ASME, 29 West 39th Street, New York, N. Y., and will be accepted until January 11, 1954, for publication at a later date. Discussion received after the closing date will be returned.

Note: Statements and opinions advanced in papers are to be understood as individual expressions of their authors and not those of the Society. Manuscript received by ASME Applied Mechanics Division, April 24, 1953. Paper No. 53-SA-41.

[2] Numbers in parentheses refer to the Bibliography at the end of the paper.

$I_n(B)$ = modified Bessel function of first kind of order $n$ and argument $B$
$w_1 = (k/m_1)^{1/2}$, an angular frequency
$w_2 = (k/m_2)^{1/2}$, an angular frequency
$w_0 = [k/(m_1 + m_2)]^{1/2}$, an angular frequency
$\theta$ = an angle
$\tan(\theta) = w^2/w_1^2 - 1$

## Fundamental Equations of System

As a consequence of Newton's second law, the differential equations of motion of the dynamical system in Fig. 1 are

$$m_1\ddot{x}_1 + kx_1 + F(x) = P_0 \sin(wt) \quad [1]$$

$$m_2\ddot{x}_2 - F(x) = 0 \quad [2]$$

where

$$x = (x_1 - x_2) \quad [3]$$

is the relative displacement of the two masses and $F(x)$ is the force transmitted through the nonlinear absorber spring. It will be assumed that the absorber spring has symmetrical characteristics, so that

$$F(-x) = F(x) \quad [4]$$

## Determination of $F(x)$ to Stabilize the Main Mass

Before proceeding to the general discussion of the problem, it is instructive to determine the required characteristics of $F(x)$ in order for the mass $m_1$ to remain fixed. This may be done by simply placing $x_1$ and its second derivative equal to zero in the foregoing equations. If this is done, the following equations are obtained

$$F(x) = P_0 \sin(wt) \quad [5]$$

$$m_2\ddot{x}_2 = F(x) \quad [6]$$

$$x = -x_2 \quad [7]$$

This leads to

$$m_2\ddot{x}_2 = P_0 \sin(wt) \quad [8]$$

or a steady-state oscillation of $x_2$ of the form

$$m_2x_2 = -P_0 \sin(wt)/w^2 \quad [9]$$

Therefore

$$F(x) = -F(x)_2 = P_0 \sin(wt) = -w^2m_2x_2 = w^2m_2x \quad [10]$$

This leads to the conclusion that the characteristics of the absorber spring, $F(x)$, must be "linear" and of the form

$$F(x) = k_0x \quad [11]$$

and from Equation [10] it is seen that the spring constant $k_0$ must have the precise value

$$k_0 = w^2m_2 \quad [12]$$

This indicates that in order for the dynamic vibration absorber to be completely effective in stopping the motion of the main mass $m_1$, it must have linear characteristics and a spring constant that must satisfy Equation [12]. The resulting Equation [12] is the well-known condition for tuning the absorber given by the conventional linear theory. It indicates that the absorber may be adjusted to be completely effective at only one angular frequency of the disturbing harmonic force.

## Solution of General Equations

In order to solve Equations [1] and [2] it is first necessary to separate the variables. To do this, it is convenient to introduce the following commutative operators

$$Z_1(D) = m_1D^2 + k, \quad D = \frac{d}{dt} \quad [13]$$

$$Z_2(D) = m_2D^2 \quad [14]$$

By the use of these operators, Equations [1] and [2] may be written in the following form

$$Z_1(D)x_1 + F(x) = P_0 \sin(wt) \quad [15]$$

$$Z_2(D)x_2 - F(x) = 0 \quad [16]$$

If the operator $Z_2(D)$ is applied to Equation [15] and the operator, $Z_1(D)$ is applied to Equation [16] the results are

$$Z_1(D)Z_2(D)x_1 + Z_2(D)F(x) = Z_2(D)P_0 \sin(wt) \quad [17]$$

$$Z_1(D)Z_2(D)x_2 - Z_1(D)F(x) = 0 \quad [18]$$

If Equation [18] is now subtracted from Equation [17] the result is

$$Z_1(D)Z_2(D)x + [Z_1(D) + Z_2(D)]F(x) = Z_2(D)P_0 \sin(wt) \quad [19]$$

since $x = (x_1 - x_2)$.

Equation [19] contains only the unknown relative displacement $x$, and the variables are separated. In order to obtain specific results, let it be assumed that the spring of the dynamic absorber has nonlinear characteristics that can be represented by the following analytical expression

$$F(x) = \frac{k_0}{a} \sinh(ax) \quad [20]$$

where $k_0$ and $a$ are positive constants. This analytical expression represents a "hard" spring whose characteristics are given in Fig. 2.

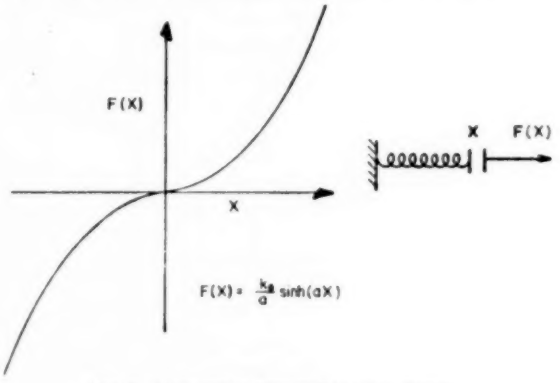


Fig. 2 Nonlinear Spring Characteristic

2. The constant $a$ is a measure of the nonlinearity of this spring. It can be seen that

$$\lim_{a \to 0} F(x) = \lim_{a \to 0} \frac{k_0}{a} \sinh(ax) = k_0x \quad [21]$$

$k_0$ may be called the "initial spring constant." As a consequence of Equations [13] and [14] we have

$$Z_1(D)Z_2(D) = m_1m_2D^4 + km_2D^2 \quad [22]$$

and

$$Z_1(D) + Z_2(D) = (m_1 + m_2)D^2 + k \quad [23]$$

If Equations [20], [22], and [23] are substituted into Equation [19], it takes the following form

$$(m_1m_2D^4 + km_2D^2)x + [(m_1 + m_2)D^2 + k]\frac{k_0}{a}\sinh(ax) = -m_2w^2P_0\sin(wt) \quad [24]$$

This is a nonlinear differential equation of the fourth order to determine the relative displacement of the two masses, $x = (x_1 - x_2)$. If $x$ is determined by solving Equation [24], the displacement of the mass $m_2$ may be determined by solving the differential Equation [2] which may be written in the following form

$$x_2 = \frac{F}{m_2}(x) = k_0\frac{\sinh}{am_2}(ax) \quad [25]$$

Since $x$ is now known as a function of $t$, this equation can be integrated and $x_2$ determined. The displacement of the main mass $x_1$ is now given by

$$x_1 = x + x_2 \quad [26]$$

This outlines the general procedure.

### Determination of Periodic "Steady-State" Solution

It is known that in the case of a linear dynamic absorber for which $a = 0$, after an initial transient period is damped out by small frictional forces that are not considered in the analysis, the masses execute periodic oscillations of the same period as that of the impressed periodic forces of the form

$$\left.\begin{aligned} x_1 &= A_1\sin(wt) \\ x_2 &= A_2\sin(wt) \end{aligned}\right\} \quad [27]$$

where $A_1$ and $A_2$ are amplitudes that are independent of the time but are functions of $w$ and the constants of the system (3, 4). If the spring of the dynamic absorber is only slightly nonlinear, the constant $a$ is small and the masses may be assumed to execute periodic motions similar to those expressed by Equations [27]. This suggests the use of a method similar to that of G. Duffing (6), for the solution of Equation [24]. By the use of Duffing's method, a "one-term" approximation to the periodic steady-state solution of Equation [24] can be obtained that reduces to that based on the linear analysis when the constant $a$ in Equation [20] is put equal to zero. To do this, an approximate solution of Equation [24] of the form

$$x_0 = A\sin(wt) \quad [28]$$

for $x$ is assumed. If Equation [28] is substituted for $x$ in the nonlinear Equation [24] it is necessary to compute the harmonic components of $F(x_0)$. To do this we have

$$F(x_0) = \frac{k_0}{a}\sinh[aA\sin(wt)] = \frac{k_0}{a}\sinh[B\sin(wt)] \quad [29]$$

where

$$B = aA \quad [30]$$

From the theory of Bessel functions (7) we have the result

$$\sinh[B\sin(wt)] = 2[I_1(B)\sin(wt) - I_3(B)\sin(3wt) + I_5(B)\sin(5wt) \ldots] = 2\sum_{n=0}^{\infty}(-1)^nI_{(2n+1)}(B)\sin[(2n+1)wt] \quad [31]$$

where the functions, $I_n(B)$, are the modified Bessel functions of the first kind of order $n$ and argument $B$. These functions have been extensively tabulated (8). The Series [31] is one that converges very rapidly. If Series [31] is substituted into [29] we obtain

$$F(x_0) = \frac{2k_0}{a}[I_1(B)\sin(wt) - I_3(B)\sin(3wt) + I_5(B)\sin(5wt) \ldots] \quad [32]$$

The substitution of Equation [28] into [24] for $x$ results in the following equation

$$(m_1m_2w^4 - km_2w^2)A\sin(wt) + [(m_1 + m_2)D^2 + k]F(x_0) = -m_2w^2P_0\sin(wt) \quad [33]$$

To determine the unknown amplitude $A$, approximately, we follow the procedure of G. Duffing and equate the coefficients of $\sin(wt)$ of both members of Equation [33] to each other. We thus obtain the following equation

$$(m_1m_2w^4 - km_2w^2)A + [k - (m_1 + m_2)w^2]\frac{2k_0}{a}I_1(B) = -m_2w^2P_0 \quad [34]$$

In terms of the original notation, this equation can be written in the convenient form

$$\frac{2k_0}{k}w_2^2\left[\frac{1}{w^2_0} - \frac{1}{w^2}\right]I_1(B) = \frac{aP_0}{k} + \left(\frac{w^2}{w_1^2} - 1\right)B \quad [35]$$

This is a transcendental equation for the determination of $B$. When $B$ is determined, the amplitude $A$ is given by the relation

$$A = \frac{B}{a} \quad [36]$$

Equation [35] will be called the "amplitude equation" in the subsequent analysis.

### Solution of Amplitude Equation

Before discussing a general method for the solution of the amplitude Equation [35], it is instructive to discuss two special cases for which the solution is particularly simple. By inspection, it is seen that matters are considerably simplified if the angular frequency $w$ of the disturbing force assumes the special values $w = w_0$, or $w = w_1$.

*Case $w = w_0$.* If $w = w_0$, the amplitude equation reduces to

$$0 = \frac{aP_0}{k} + (w_0^2/w_1^2 - 1)B \quad [37]$$

after some reductions, it can be seen that this leads to the following values for the amplitude $A$

$$A = \frac{P_0}{k}(m_1 + m_2)/m_2 \quad [38]$$

*Case $w = w_1$*

If $w = w_1$, the amplitude equation reduces to

$$\frac{2k_0}{k}w_2^2[1/w^2_0 - 1/w_1^2]I_1(B) = \frac{aP_0}{k} \quad [39]$$

or

$$I_1(B) = \frac{aP_0}{2k_0} \quad [40]$$

In this case, since the right member of Equation [40] is known, $B$ may be determined from a table of modified Bessel functions such as reference (8), and the amplitude determined by Equation [36].

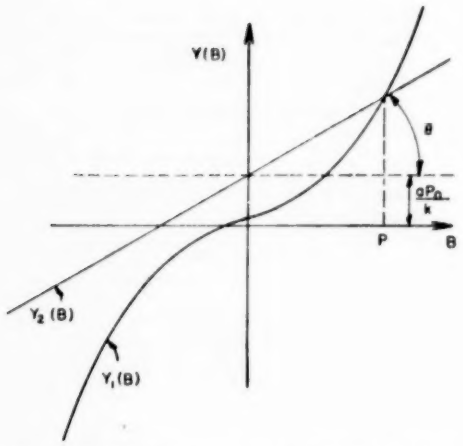


FIG. 3 GRAPHICAL SOLUTION OF AMPLITUDE EQUATION

The general solution of the amplitude equation may be effected by the graphical construction in Fig. 3. If the following notation is introduced

$$y_1(B, w) = \frac{2k_0}{k} w_2^2 (1/w_0^2 - 1/w^2) I_1(B) \quad [41]$$

and

$$y_2(B, w) = \frac{aP_0}{k} + (w^2/w_1^2 - 1)B \quad [42]$$

the amplitude Equation [35] may be expressed in the following form

$$y_1(B, w) = y_2(B, w) \quad [43]$$

It is thus clear that if for a given $w$, the curves $y_1$ and $y_2$ are plotted as functions of $B$, then the abscissa of the point of intersection of these two curves such as $P$, Fig. 3, gives the proper value for $B$ at this frequency. The amplitude at this frequency is then determined by Equation [36]. The curves $y_2(B, w)$ are a family of straight lines one of which is shown in Fig. 3. The angle $\theta$ that these lines make with the horizontal is given by

$$\tan(\theta) = (w^2/w_1^2 - 1) \quad [44]$$

In the range $0 \leq w \leq w_1$, the slope of the line $y_2$ is negative; $y_2$ is horizontal at $w = w_1$ and, as $w$ increases, the slope becomes increasingly positive. If $w$ is large in comparison with $w_0$ so that

$$1/w_0^2 \gg 1/w^2 \quad [45]$$

then $1/w^2$ can be neglected in $y_1$ and it takes the following form

$$y_1(B) = \frac{2k_0}{k} I_1(B)(m_1 + m_2)/m_2 \quad [46]$$

The curve $y_1$ is now proportional to the modified Bessel function, $I_1(B)$. This function has the following power-series expansion (7)

$$I_1(B) = \frac{B}{2}\left(1 + \frac{B^2}{8} + \frac{B^4}{192} + \ldots\right) \quad [47]$$

and it is seen to rise very steeply with $B$. It is thus apparent that for large values of $w$, ($w \gg w_0$), the straight line $y_2$ and the curve $y_1$ intersect at points whose abscissas are small and hence lead to small values of the amplitude $A$.

### POSSIBILITY OF JUMP PHENOMENA

Although it can be seen from Fig. 3 that the abscissas of the points of intersection of $y_1$ and $y_2$ are always small and hence the amplitude of $A$ remains small over a large range in $w$ and no resonance phenomenon is exhibited, there is a possibility of "jump" phenomena arising as the angular frequency $w$ is increased to large values. This can be seen by the following consideration: As the angular frequency $w$ of the disturbing force is increased, the straight line $y_2$ rotates in such a manner that $\theta$ as given by Equation [44] is increased. This eventually gives rise to the possible intersection of $y_1$ and $y_2$ at three points. The abscissa of each one of these points gives a possible value for $B$, and hence for the amplitude $A$. The stability of the possible amplitudes requires a separate investigation.

### DETERMINATION OF MOTION OF MASSES

Having determined the steady-state relative motion of the two masses, $m_1$ and $m_2$ in the form of Equation [28], it now remains to determine the steady-state motion of the individual masses. The displacement $x_2(t)$ of the mass $m_2$ satisfies Equation [25] which now takes the form

$$x_2 = \frac{F}{m_2}(x_0) = \frac{2k_0}{am_2}[I_1(B)\sin(wt) - I_3(B)\sin(3wt) + I_5(B)\sin(5wt) \ldots] \quad [48]$$

as a consequence of Equation [32]. If Equation [48] is integrated, the following steady-state value for $x_2$ is obtained

$$x_2 = \frac{2k_0}{am_2}\left[-I_1(B)\frac{\sin}{w^2}(wt) + I_3(B)\frac{\sin}{9w^2}(3wt) - I_5(B)\frac{\sin}{25w^2}(5wt) + \ldots\right] \quad [49]$$

The motion of the mass $m_2$ is seen to contain odd harmonics of the disturbing force. Since $x_0 = (x_1 - x_2)$, the displacement $x_1(t)$ of the main mass is given by the equation

$$x_1 = x_0 + x_2 = [A - 2k_0 I_1(B)/am_2w^2]\sin(wt) + \frac{2k_0}{am_2}\left[I_3(B)\frac{\sin(3wt)}{9w^2} - I_5(B)\frac{\sin(5wt)}{25w^2} + \ldots\right] \quad [50]$$

The series of harmonic terms in Equations [49] and [50] are rapidly convergent and the fundamental terms are the dominant ones. The effect of the nonlinearity of the spring of the dynamic absorber is to prevent the existence of sharp resonant peaks and to introduce odd harmonic components of relatively small amplitude in the motion of the two masses.

### BIBLIOGRAPHY

1 "Devices for Damping Vibrations of Bodies," by H. Frahm, U. S. Patent 989,958, April, 1911.
2 "The Theory of the Dynamic Vibration Absorber," by J. Ormondroyd and J. P. Den Hartog, Trans. ASME, vol. 50, 1928, p. 9.
3 "Vibration Problems in Engineering," by S. Timoshenko, D. Van Nostrand Company, Inc., New York, N. Y., 1937, pp. 240–244.
4 "Mechanical Vibrations," by J. P. Den Hartog, McGraw-Hill Book Company, Inc., New York, N. Y., 1940, pp. 108–115.
5 "Synthesis of a Nonlinear Dynamic Vibration Absorber," by R. E. Roberson, *Journal of The Franklin Institute*, vol. 254, September, 1952, pp. 205–220.
6 "Nonlinear Vibrations," by J. J. Stoker, Interscience Publishers, Inc., New York, N. Y., 1950, pp. 81–90.
7 "Bessel Functions for Engineers," by N. W. McLachlan, Oxford University Press, London, England, 1941, pp. 50–51.
8 "Tables of Functions," by E. Jahnke and F. Emde, Dover Publications, New York, N. Y., 1943, pp. 232–233.

# Constant-Strain Waves in Strings

By J. D. COLE,[1] C. B. DOUGHERTY,[2] and J. H. HUTH[3]

**A nonlinear theory is developed for constant-strain waves in elastic strings. The speed of longitudinal and transverse waves is related to the strain and tension. The results can be used to calculate tension resulting from impact and thus breaking loads. Some generalizations are suggested.**

## Equations of Motion

IF it is assumed that the tension $T$ in a string is given by

$$T = T_0 + F(\sigma) \quad [1]$$

where

$T_0$ = initial tension = const
$\sigma$ = strain and $F(\sigma) = E\sigma$

then solutions to the equations of motion can be given for the propagation of waves of constant strain and tension. Such solutions are not restricted to small displacements or slopes and hence are of special interest. The waves which propagate consist of straight-line segments which move with constant velocity. The accelerations are thus zero except at points where the velocity jumps. At these points the acceleration is infinite. A convenient way to discuss the speed of propagation is by considering the differential equations of motion. The differential equations can be considered to contain the impulse-momentum laws. Another approach is to apply the impulse-momentum laws directly.

Newton's laws of motion applied to an infinitesimal element of string, are

$$\rho u_{tt} = (T \cos\theta)_x \quad [2]$$

$$\rho v_{tt} = (T \sin\theta)_x \quad [3]$$

where (see Fig. 1)

$u$, $v$ = horizontal and vertical displacements, respectively, of point located at $x$ in unstrained string
$\theta$ = inclination of string
$\rho$ = mass per length = const

No external forces are considered. The horizontal projection of an element originally of length $\Delta x$ is $(1 + u_x)\Delta x$; the vertical projection $v_x\Delta x$; and its length

$$\Delta s = \sqrt{(1 + u_x)^2 + v_x^2}\,\Delta x$$

Therefore

$$\sin\theta = \frac{v_x}{\sqrt{(1 + u_x)^2 + v_x^2}} \quad [4]$$

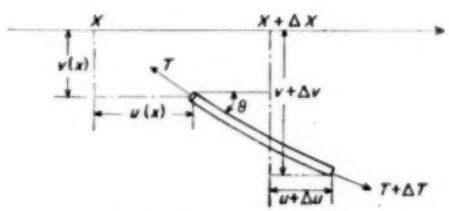


Fig. 1 Element of String

$$\cos\theta = \frac{(1 + u_x)}{\sqrt{(1 + u_x)^2 + v_x^2}} \quad [5]$$

$$\sigma = \frac{\Delta s - \Delta x}{\Delta x} = \sqrt{(1 + u_x)^2 + v_x^2} - 1 \quad [6]$$

The characteristic lines, which represent the locus of possible discontinuities or wave fronts, can be found for the system of Equations [1] to [6]. Two sets of characteristics appear representing different wave velocities. These speeds are

$$C_1 = \sqrt{\frac{1}{\rho}\frac{dF}{d\sigma}} = \sqrt{\frac{E}{\rho}} \quad [7]$$

$$C_2 = \sqrt{\frac{1}{\rho}\frac{T_0 + F(\sigma)}{1 + \sigma}} = \sqrt{\frac{1}{\rho}\frac{T_0 + E\sigma}{1 + \sigma}} \quad [8]$$

where $C_1$ is the speed of longitudinal waves in solid bar of same material; $C_2$, for small strains, becomes speed of transverse waves in a string. For most applications $C_1 > C_2$. It should be noted that one speed of propagation is variable and depends on the strain $\sigma$. The details of the characteristics are not shown here since the same result about propagation speeds is derived by physical considerations early in the paper.

The general solution for constant-strain waves can be written in the form

$$v(x, t) = \text{linear function of } (x, t)$$
$$u(x, t) = \text{linear function of } (x, t)$$

Then since $v_x$, $u_x$, $v_t$, $u_t$ are constants it is easily seen from Equations [1] to [6] that $\theta$, $\sigma$, $T$ are constants and that the differential Equations [2] and [3] are satisfied trivially except where the velocity jumps. The simplest example leading to waves of this type is discussed in the following.

## Radiation Problem—Semi-Infinite String

Consider the string at rest initially with zero displacement

$$u = u_t = v = v_t = 0, \quad t = 0 \quad [9]$$

Also, consider at first an infinite string $-\infty < x < \infty$. Let a constant vertical velocity be imparted at the point where $x = 0$ when $t = 0$. Then by symmetry $u = 0$ at that point for all time and hence $x = 0$ there. The boundary conditions are thus, for $t > 0$

$$v(0, t) = V = \text{const} \quad [10]$$
$$u(0, t) = 0$$

It is now sufficient to consider $x > 0$. The solution of the correct form is

[1] Assistant Professor of Aeronautics, California Institute of Technology, Pasadena, Calif.
[2] Missiles Division, The Rand Corporation, Santa Monica, Calif.
[3] Missiles Division, The Rand Corporation.

Contributed by the Applied Mechanics Division and presented at the Semi-Annual Meeting, Los Angeles, Calif., June 28–July 2, 1953, of The American Society of Mechanical Engineers.
Discussion of this paper should be addressed to the Secretary, ASME, 29 West 39th Street, New York, N. Y., and will be accepted until January 11, 1954, for publication at a later date. Discussion received after the closing date will be returned.
Note: Statements and opinions advanced in papers are to be understood as individual expressions of their authors and not those of the Society. Manuscript received by ASME Applied Mechanics Division, January 21, 1953. Paper No. 53—SA-4.

$$v = \begin{cases} V\left(t - \dfrac{x}{c_v}\right) & t > \dfrac{x}{c_v} \\ 0 & t < \dfrac{x}{c_v} \end{cases} \quad \ldots\ldots\ldots [11]$$

$$u = \begin{cases} \dfrac{Ux}{c_v} & t > \dfrac{x}{c_v} \\ \dfrac{U\left(t - \dfrac{x}{c_u}\right)}{1 - \dfrac{c_v}{c_u}} & \dfrac{x}{c_u} < t < \dfrac{x}{c_v} \\ 0 & t < \dfrac{x}{c_u} \end{cases} \quad \ldots\ldots [12]$$

where

$c_u$ = velocity of $u$ waves, and $c_v$ = velocity of $v$ waves. The various regions in the $(x, t)$ diagram and the shapes of the waves are shown in Fig. 2. The shapes of the waves were determined by the fact that $c_v < c_u$ and that $u = 0$ at $x = 0$ and for $x > c_u t$. It can be shown, and is verified in the following, that the momentum equations cannot be satisfied if $c_v$ is assumed greater than $c_u$. The undetermined constants in Equations [11] and [12] are $U$, $c_v$, $c_u$. These are computed by applying the horizontal impulse-momentum law along $x = c_u t$ and the horizontal and vertical laws along $x = c_v t$.

Before doing this it is convenient to compute the slope and the strains which are constant in the various regions. We have

$$u_{1x} = \frac{U}{c_v}, \quad v_{1x} = -\frac{V}{c_v}$$

$$u_{2x} = \frac{\dfrac{U}{c_u}}{1 - \dfrac{c_v}{c_u}}, \quad v_{2x} = 0$$

$$\sigma_1 = \sqrt{\left(1 + \frac{U}{c_v}\right)^2 + \frac{V^2}{c_v^2}} - 1 \quad \ldots\ldots [13]$$

$$\sin\theta_1 = \frac{-\dfrac{V}{c_v}}{\sqrt{\left(1 + \dfrac{U}{c_v}\right)^2 + \dfrac{V^2}{c_v^2}}}$$

$$\sigma_2 = -\frac{\dfrac{U}{c_u}}{1 - \dfrac{c_v}{c_u}}$$

$$\theta_2 = \theta_3 = \sigma_3 = 0, \quad \cos\theta_1 = \frac{1 + \dfrac{U}{c_v}}{\sqrt{\left(1 + \dfrac{U}{c_v}\right)^2 + \dfrac{V^2}{c_v^2}}}$$

The subscripts denote the regions shown in Fig. 2.

Consider now the vertical motion. Formally, we may write

$$T\sin\theta = T_1 \sin\theta_1 H\left(t - \frac{x}{c_v}\right) \quad \ldots\ldots [14]$$

where

$$H(z) = \text{unit step function} = \begin{matrix} 1 & z > 0 \\ 0 & z < 0 \end{matrix}$$

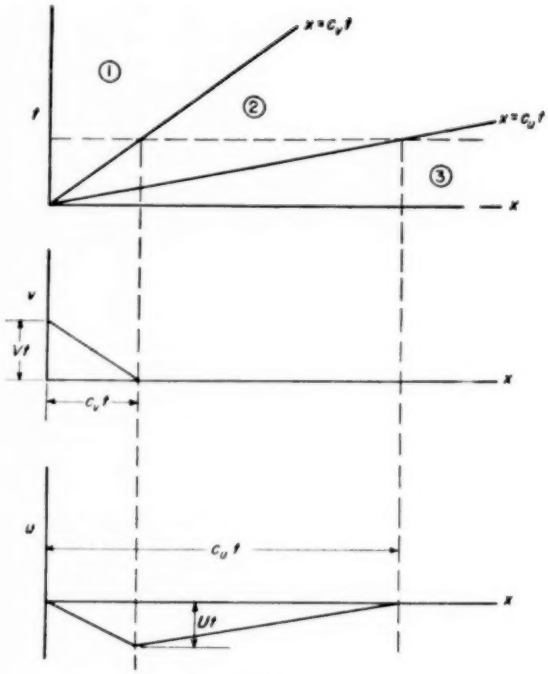


FIG. 2 REGIONS OF DISTURBANCE

Thus Equation [3] becomes

$$\rho v_{tt} = -\frac{1}{c_v} T_1 \sin\theta_1 \delta\left(t - \frac{x}{c_v}\right) \quad \ldots\ldots [15]$$

where $\delta$ = delta function. Integration of Equation [15] with respect to $t$ gives the velocity jump across $x = c_v t$

$$-\frac{1}{c_v} T_1 \sin\theta_1 = \rho v_{1t} \text{ which by Equation [11]} = \rho V \quad [16]$$

Similarly

$$T\cos\theta = T_1 \cos\theta_1 H\left(t - \frac{x}{c_v}\right) + T_2\left[H\left(t - \frac{x}{c_v}\right) - H\left(t - \frac{x}{c_u}\right)\right] + T_3\left[1 - H\left(t - \frac{x}{c_u}\right)\right] \quad [17]$$

and

$$\frac{1}{c_u}(T_3 - T_2) = \rho(u_{2t} - u_{3t})$$

which by Equation [12]

$$= \frac{\rho U}{1 - \dfrac{c_v}{c_u}} \quad \ldots\ldots [18]$$

$$\frac{1}{c_v} T_2 - \frac{1}{c_v} T_1 \cos\theta_1 = \rho(u_{1t} - u_{2t})$$

which by Equation [12]

$$= \frac{-\rho U}{1 - \dfrac{c_v}{c_u}} \quad \ldots\ldots [19]$$

Now, since $\sigma_1$, $\sigma_2$ are known in terms of $(U, c_v, c_u)$, $T_1$ and $T_2$ are

known functions of $U$, $c_s$, $c_u$ and Equations [16], [18], and [19] determine $U$, $c_s$, $c_u$; that is, $T_1$ and $T_2$ can be expressed as

$$\left.\begin{aligned} T_1 = T_0 + E\sigma_1 &= T_0 + E\left[\sqrt{\left(1 + \frac{U}{c_s}\right)^2 + \frac{V^2}{c_s^2}} - 1\right] \\ T_2 = T_0 + E\sigma_2 &= T_0 - E\frac{\dfrac{U}{c_u}}{1 - \dfrac{c_s}{c_u}} \\ T_3 &= T_0 \end{aligned}\right\} \quad [20]$$

Thus Equation [18] becomes

$$\frac{\rho U}{1 - \dfrac{c_s}{c_u}} = \frac{1}{c_u} E \frac{\dfrac{U}{c_u}}{1 - \dfrac{c_s}{c_u}}$$

from which $c_u$ may be found as

$$c_u = \sqrt{\frac{E}{\rho}} = c_1 \quad [21]$$

It follows that Equations [16] and [19] are two equations for $U$ and $c_s$, and these become

$$\left.\begin{aligned} T_1 \sin\theta_1 &= -\rho V c_s \\ T_1 \cos\theta_1 &= T_0 - \rho U c_u \end{aligned}\right\} \quad [22]$$

or

$$\left.\begin{aligned} \tan\theta_1 &= \frac{-\rho V c_s}{T_0 - \rho U c_u} \\ &= \frac{-\dfrac{V}{c_s}}{1 + \dfrac{U}{c_u}} \end{aligned}\right\} \quad [23]$$

which by Equation [13] equals

$$T_1^2 = (\rho V c_s)^2 + (T_0 - \rho U c_u)^2 = (T_0 + E\sigma_1)^2 \quad [24]$$

Equation [23] can be solved for $U$ to yield

$$U = \frac{c^2 - c_s^2}{c_u + c_s} \quad [25]$$

where $c^2 = T_0/\rho$ = speed of $c$-waves in a small-displacement theory. Using Equation [25], [24] is the equation for $c_s$.

Before solving for $c_s$ it is useful to find expressions for the strain. Using Equation [25]

$$\sigma_1 = \sqrt{\left(1 + \frac{U}{c_s}\right)^2 + \frac{V^2}{c_s^2}} - 1 = \frac{1}{c_s}\sqrt{c^2 + c_u c_s^2} + V^2 - 1 \quad [26]$$

also

$$T_0 - \rho U c_u = \rho c_s \left(\frac{c^2 + c_u c_s}{c_u + c_s}\right) \quad [27]$$

Hence Equation [24] becomes

$$T_1^2 = \rho^2 c_s^2 \left[c_s^2 (1 + \sigma_1)^2\right] = (T_0 + E\sigma_1)^2 \quad [28]$$

which can be solved for $\sigma_1$

$$\sigma_1 = \frac{c_s^2 - c^2}{c_u^2 - c_s^2} = \frac{-U}{c_u - c_s}, \text{ or } c_s = C_2 = \sqrt{\frac{c^2 + \sigma_1 c_u^2}{1 + \sigma_1}} \quad [29]$$

A comparison of Equations [20] and [20] yields the interesting result that

$$\sigma_1 = \sigma_2, \text{ and } T_1 = T_2 \quad [30]$$

The strain and tension have the same constant value over the entire disturbed part of the string.

Now, using Equations [27] and [29], Equation [24] yields the following quartic equation for $c_s(V, c_u, c)$

$$(c_u - c_s)^2(c^2 + c_u c_s)^2 + V^2(c_u^2 - c_s^2)^2 = c_s^2(c_u^2 - c^2)^2 \quad [31]$$

When $c_s$ is found from this equation the strain is given by Equation [29]. Two limiting cases are of interest as follows:

1 $V$ is small: Equation [31] shows that as $V^2 \to 0$ a solution exists independent of $V$, namely, $c_s = c$. The strain is zero and this theory goes over to the usual linearized theory.

2 $c^2 \to 0$: waves are sent out in a string whose initial tension is zero. Writing

$$\left.\begin{aligned} V &= \alpha c_u \\ c_s &= \lambda c_u \end{aligned}\right\} \quad [32]$$

Equation [33] becomes

$$\lambda^5(1 + \alpha^2) - 2\lambda^3 - 2\alpha^2\lambda^2 + \alpha^2 = 0 \quad [33]$$

For $\alpha, \lambda \ll 1$ an approximate solution to Equation [33] can be obtained by neglecting the $\lambda^5$ term. Solving the resulting cubic equation yields

$$\lambda = \frac{\alpha^{2/3}}{2^{1/3}} + \theta(\alpha^2) \quad [34]$$

Hence, approximately

$$c_s = \left(\frac{c_u}{2}\right)^{1/3} V^{2/3} \quad [35]$$

The last result clearly shows the nonlinearity dependence of transverse-wave speed on incoming velocity. The corresponding expression for strain is

$$\sigma_1 = \frac{1}{\left(\dfrac{c_u}{V}\right)^{4/3} 2^{2/3} - 1} \doteq \frac{1}{2^{1/3}}\left(\frac{V}{c_u}\right)^{4/3} \quad [36]$$

Now $T_1 = T_2 = E\sigma_1$ so that Equation [36] can be used to compute the velocity of motion which would break a given string.

It can be noted that the stress and strain are independent of the area of string. The inclination of the string is given by

$$\sin\theta_1 = -\frac{1}{2^{1/3}}\left(\frac{V}{c_u}\right)^{5/3}\left[2^{1/3}\left(\frac{c_u}{V}\right)^{4/3} - 1\right] \doteq -2^{1/3}\left(\frac{V}{c_u}\right)^{1/3} \quad [37]$$

and the constant force required to produce the wave is

$$F_1 = -T_1 \sin\theta_1 = \frac{E}{2^{1/3}}\left(\frac{V}{c_u}\right)^{5/3} \quad [38]$$

Some typical numerical values are those for $^3/_{16}$-in. carbon-steel cable where $E = 4.7 \times 10^8$ lb, $c_u = 17{,}050$ fps; if $V = 690$ fps

$$T_1 = 3900 \text{ lb} \quad [39]$$

Reflection problems can be treated in the same way. It can be shown that the reflections of the longitudinal wave at an end travels back with the speed $C_1$ relative to the original co-ordinate $x$. Upon reflection from a fixed end ($u = 0$) the strain, and hence that part of the tension resulting from strain is doubled.

The reflection of the returning longitudinal wave with the oncoming transverse wave also can be worked out in the same way.

## Conclusion

It has been shown how the problem of propagation and reflection of constant-strain waves in an idealized elastic string can be treated. The results are especially interesting since they are not limited to small deflections. Longitudinal and transverse waves occur which travel with different speeds relative to the string. One limiting case shows how a wave propagates because of elasticity in a string with zero initial tension.

The results have a practical application in estimating the suddenly applied constant force which will break a rope. An example of this was presented for zero initial tension which clearly shows the nonlinear dependence of tension on force Equations [38] to [40]. It should be remarked that the results for the idealized string are independent of the cross-section area, so long as the string behaves in a similar manner.

The case of varying velocity applied to a string can be treated by replacing the velocity curve by segments of constant velocity. Then the actual motion can be approximated by various constant-strain waves. Similar problems occur where a load moves as a string.

# Dynamic Stress-Strain Relations for Annealed 2S Aluminum Under Compression Impact

By J. E. JOHNSON,[1] D. S. WOOD,[2] AND D. S. CLARK,[3] PASADENA, CALIF.

**This paper presents the results of an experimental study of the stress-strain relation of annealed 2S aluminum when subjected to compression impact. Two methods of securing a dynamic stress-strain curve are considered, namely, from the measurement of impact stress as a function of maximum plastic strain, and impact stress as a function of the impact velocity. The dynamic stress-strain curves obtained by these methods lie considerably above the static curve. The elevation in stress of the dynamic relations above the static relation increases progressively from zero at the elastic limit to about 20 per cent at a strain of 4.5 per cent. However, the two dynamic relations are not coincident which indicates that the behavior of the material cannot be described by a single stress-strain curve for all impact velocities. A family of stress-strain curves which differ slightly from each other and which depend upon the final strain is postulated in order to correlate both sets of data adequately.**

## Introduction

THE behavior of metals and alloys under dynamic loading conditions has received considerable attention in recent years (1–6).[4] It is found that in the plastic range, the stress for a given strain is increased when the rate of loading is increased. Taylor and Whiffin (7, 8) have found that the strengths of annealed copper and steel under impact conditions are increased above the static values. Habib (9) has shown that in compression impact tests on annealed copper, the stress for a given strain is somewhat greater than the static stress at the same strain. The results of an investigation by Clark and Wood (10) indicate that the ultimate tensile strength of all the materials tested is greater under dynamic conditions than under static conditions.

However, the interpretation of many of the previous investigations in terms of elevated stress-strain relations is questionable as pointed out by Clark and Duwez (6), and Lee and Wolf (11). Furthermore, few tests have been performed in which the complete stress-strain relation followed by a material during high-speed dynamic loading could be determined accurately. Kolsky (12) has performed tests on copper and lead in which the stress-strain relation under very high rates of loading was determined. The results indicate that the stress for a given strain at very high loading rates is equal to about twice the stress under static conditions. However, it is difficult to interpret the results of this investigation since the instantaneous distribution of stress in the specimen may not be simple owing to the shape of the specimen and possible boundary constraints acting upon it.

The present investigation makes use of an experimental technique which is believed to provide a basis for the interpretation of the measurements obtained in terms of the stress-strain relation of a material under impact conditions with considerably greater assurance than has been heretofore possible. The technique used to accomplish this is as follows: A compression stress is suddenly applied to one end of a long cylindrical specimen by longitudinal impact with an elastic anvil bar of the same diameter as the specimen. The stress-time relation at the impact end of the specimen and the plastic-strain distribution in the specimen are measured for various known impact velocities. The theory of plastic-wave propagation in long, thin bars, developed by von Kármán (13, 14), is used to deduce the stress-strain curve of the material from these measurements and to describe the deformation process in the specimen during impact. In the present paper this technique is used to determine dynamic stress-strain relations for annealed 2S aluminum.

## Equipment

The compression-impact tests were made with the vertical impact machine shown in Fig. 1. A stationary tobin-bronze anvil bar of the same diameter as the specimen is held vertically in a central position between the rails of the machine by a guard tube and expendable spacer. An annealed-copper cylinder, positioned between the lower end of the anvil bar and a fixed base, absorbs most of the impact energy in the anvil bar by plastic deformation. Since a slight misalignment between the anvil bar and the specimen may occur, the top end of the anvil bar is provided with a 19-in-radius convex spherical surface to prevent initial impact with the corner of the specimen.

When the specimen impacts the anvil bar, a series of compression strains is propagated through the specimen, and an elastic compression wave is propagated through the anvil bar. Thus any change in stress at the interface between the anvil bar and specimen is transmitted through the anvil bar at the elastic-wave velocity. The length of the specimen is much less than the length of the anvil bar; hence the time required for the first reflecting wave from the lower end of the bar to reach the interface is greater than the time required for complete unloading of the interface by the waves in the specimen. The interface between the anvil bar and specimen is always unloaded by waves reflected from the free end of the specimen; consequently, all complex reflections from the lower end of the anvil bar need not be considered.

The hammer, which slides on the two vertical rails, is provided

---

[1] Research Assistant, California Institute of Technology.

[2] Assistant Professor of Mechanical Engineering, California Institute of Technology. Jun. ASME.

[3] Professor of Mechanical Engineering, California Institute of Technology. Mem. ASME.

[4] Numbers in parentheses refer to the Bibliography at the end of the paper.

Contributed by the Applied Mechanics Division and presented at the Semi-Annual Meeting, Los Angeles, Calif., June 28–July 2, 1953, of THE AMERICAN SOCIETY OF MECHANICAL ENGINEERS.

Discussion of this paper should be addressed to the Secretary, ASME, 29 West 39th Street, New York, N. Y., and will be accepted until January 11, 1954, for publication at a later date. Discussion received after the closing date will be returned.

NOTE: Statements and opinions advanced in papers are to be understood as individual expressions of their authors and not those of the Society. Manuscript received by ASME Applied Mechanics Division, January 28, 1953. Paper No. 53—SA-7.

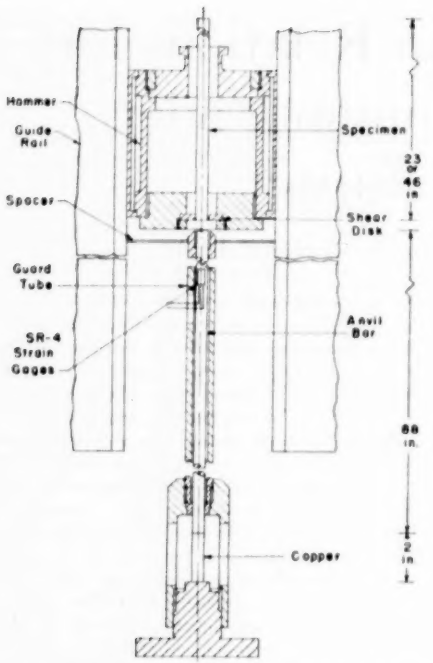


FIG. 1 SECTION THROUGH VERTICAL IMPACT MACHINE

with a central hole through which the guard tube may pass. Twenty rubber bands $^3/_4$ in. thick and 1 in. wide, attached to the hammer and frame of the machine, serve as a means for accelerating the hammer to the desired impact velocity. The specimen is held centrally in the hammer by a lucite shear disk shrunk on the bar and clamped in the hammer. The shear disk strikes the top of the guard tube just prior to the impact of the specimen on the anvil bar. This action is such that the specimen is released from the shear disk and impacts the anvil bar while it is free from any constraints due to the accelerating mechanism. The hammer continues downward, passing around the guard tube, and is decelerated by means of four vertical friction brakes.

The velocity of the hammer, and hence the specimen impact velocity, is determined by measuring the time for the hammer to travel between three fixed points near the position of impact. This is accomplished by electrical contacts made at these three points as the hammer passes them, and the signals are recorded on a cathode-ray oscillograph together with an appropriate time-calibration trace.

Impact velocities less than 19 fps cannot be determined accurately in the vertical impact machine. For this reason, tests at impact velocities lower than 19 fps were performed by supporting the specimen in a horizontal position as a pendulum by six wires attached at two positions along the specimen. The anvil bar was supported in a horizontal position so that the specimen when released from a given height centrally impacted the anvil bar at the minimum point in the swing.

The stress as a function of time at the interface between the anvil bar and specimen is measured during impact by means of SR-4 strain gages cemented to the anvil bar at a position 3 in. from the interface. The strain gages are connected to a suitable recording system employing a single-sweep cathode-ray oscilloscope and recording camera. Means for introducing known resistance changes in the strain-gage circuit are provided to calibrate the stress axis of the records, and appropriate oscillators provide the required time calibrations.

The plastic strain in the specimen after impact is determined with a comparator ruling machine. This machine marks the specimen at various intervals along its length with fine scratches before testing and measures the change in diameter at the positions produced by the impact. The difference between the diameter at any position before and after impact divided by the original diameter is the permanent circumferential plastic strain. The permanent longitudinal plastic strain is equal to twice the circumferential plastic strain, since for the maximum strains reached in these experiments (about 5 per cent), no volume changes are produced. This fact was established by static tests in which both circumferential and longitudinal strains were measured.

The comparator ruling machine consists of a sliding carriage which may be positioned accurately along the entire length of a stationary specimen. A scratching device, a low-power microscope, and a diameter comparator are mounted on the carriage. The scratching device consists of a simple mechanism on which a rigid knife blade is mounted, and this makes reference scratches on the specimen. The low-power microscope is equipped with an eyepiece containing cross hairs which permit the accurate positioning of the carriage relative to any one of the scratches along the specimen. The diameter comparator consists of two knife-edges in conjunction with a dial indicator for measuring the diameter of the specimen.

## TEST PROCEDURE AND EXPERIMENTAL RESULTS

The specimens used in this investigation were $^1/_2$-in-diam extruded 28 aluminum bars. The test specimens were machined to a length of 23 or 46 in. and annealed at 670 F for 2 hr after machining. Static compression and tension tests were performed on specimens machined from the extruded bars, which were annealed in the same manner as the impact specimen.

The velocities of elastic waves in the specimen and in the tobin-bronze anvil bar were determined to compute the relations between the strain waves in the specimen and anvil bar during impact. The elastic-wave velocities were determined by measuring the resonance frequency of the bars in longitudinal vibration. The elastic-wave velocity in the specimen is 195,400 ips, and the velocity in the anvil bar is 139,500 ips.

A series of tests were made to determine the relations between the compression stress, $\sigma_1$, at the impact end of the specimen, the plastic-strain distribution in the specimen after impact, and the particle velocity, $v_1$, imparted to the specimen at the impact end. The particle velocity $v_1$, at the impact end of the specimen, differs from the impact velocity $V_0$, since the acoustic impedance of the anvil bar is finite. The particle velocity $v_1$ is given in terms of measured quantities by

$$v_1 = V_0 - \frac{\sigma_1}{\rho' c_0'} \qquad [1]$$

where

$V_0$ = velocity of impact
$\sigma_1$ = compression stress at interface
$\rho'$ = mass density of anvil bar
$c_0'$ = velocity of propagation of elastic wave in anvil bar

The points representing the particle velocity $v_1$ as a function of the compression stress $\sigma_1$ at the impact end of the specimen are plotted in Fig. 2. The points representing the compression stress $\sigma_1$ as a function of the constant strain $\epsilon_1$ near the impact end of the specimen are plotted in Fig. 3. The strain $\epsilon_1$ consists

of the measured permanent strain at the impact end plus the elastic strain in the material due to the stress $\sigma_1$.

The stress-strain relation exhibited by the material may be deduced rather simply from the experimentally determined $\sigma_1$ versus $v_1$ relation if certain assumptions are made. (*a*) It is assumed that the stress-particle velocity relationship during loading follows this curve continuously up to the point corresponding to the given impact stress. As is discussed later, however, this relation may represent only the locus of the terminal points of a number of distinct stress-particle velocity curves which depend upon the impact stress. (*b*) It is assumed that the kinetic energy and shear stresses associated with the lateral motion of the particles of the specimen can be neglected. The stress-strain relation obtained under these assumptions later will be compared with other experimental results to determine the validity of these assumptions.

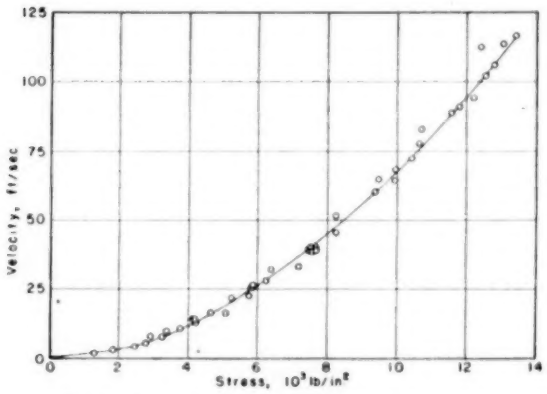


FIG. 2 IMPACT STRESS VERSUS PARTICLE VELOCITY

Under these assumptions the strain corresponding to a given stress may be expressed in terms of a definite integral which depends upon the slope of the stress-particle velocity relation up to the given stress. Thus the strain $\epsilon_1$ at the impact end of the specimen corresponding to a given impact stress $\sigma_1$, may be expressed in terms of the experimental $\sigma_1$ versus $v_1$ relation by

$$\epsilon_1 = \int_0^{\sigma_1} \frac{\rho d\sigma}{\left(\frac{d\sigma}{dv}\right)^2} \quad \ldots\ldots\ldots\ldots\ldots\ldots [2]$$

The slope of the $\sigma_1$ versus $v_1$ curve shown in Fig. 2 is determined at conveniently located points, and the $\sigma_1$ versus $\epsilon_1$ relation is computed numerically using Equation [2]. This stress-strain relation is shown in Fig. 4 by the curve designated as stress-velocity measurements. The static stress-strain curve and the stress-strain relation $\sigma_1$ versus $\epsilon_1$, determined from impact stress and measured plastic strain, are shown for comparison. The latter is designated by the curve, stress-plastic strain measurements.

The stress-strain curve deduced from stress-velocity measurements is somewhat different from the curve determined from stress-measured strain. Thus, for a given stress, the strain deduced from stress-velocity measurements with the theory of plastic-wave propagation is less than the measured strain after impact. However, both of these stress-strain relations lie considerably above the static stress-strain relation. The experimental results indicate that under these impact conditions the excess of the stress at a given strain over the static stress at the same strain increases progressively from zero at the elastic limit to about 20 per cent at a strain of 4.5 per cent. A further series of tests performed at moderate strain rates indicate that for this material the relatively large increase in stress for a given strain under impact conditions is associated with the extremely high loading rates accompanying impact and cannot be produced by moderate loading rates. This is shown by a stress-strain curve of the material at a strain rate of 0.040 per min, which also is given in Fig. 4. The latter curve essentially coincides with the static stress-strain relation.

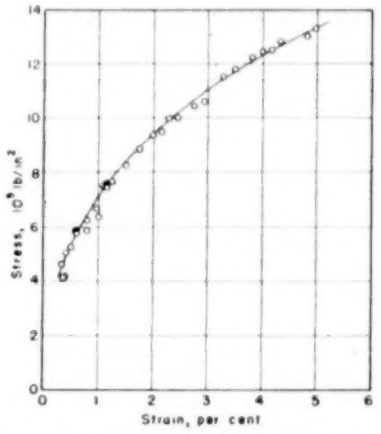


FIG. 3 IMPACT STRESS VERSUS MAXIMUM PLASTIC STRAIN

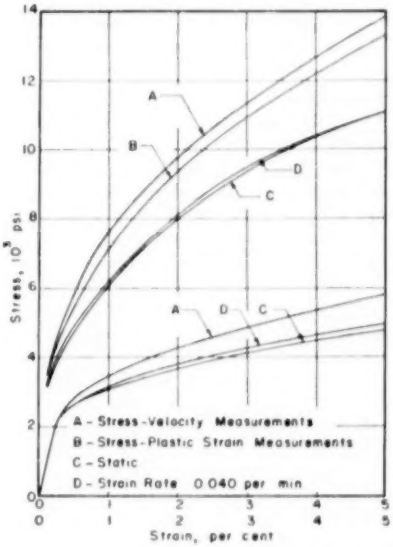


FIG. 4 STATIC AND DYNAMIC STRESS-STRAIN RELATIONS

The process of wave propagation in the specimen can be deduced from a stress-strain relation of the material and represented in a Lagrange or position-time diagram. The stress, strain, and particle velocity are determined as functions of position and time from this diagram. Thus the stress-time and strain-position relations deduced by means of a Lagrange diagram from the stress-strain relation can be compared with the experimentally determined relations. The dynamic stress-strain curve

deduced from maximum stress-impact velocity measurements was used in constructing such a Lagrange diagram. It is assumed that the stress-strain path during loading follows this stress-strain relation and upon unloading follows the normal elastic hysteresis relation. The theory and graphical solutions for strain propagation as developed by von Kármán, Bohnenblust, Hyers, and Charyk (15, 16) were used in constructing the Lagrange diagram shown in Fig. 5.

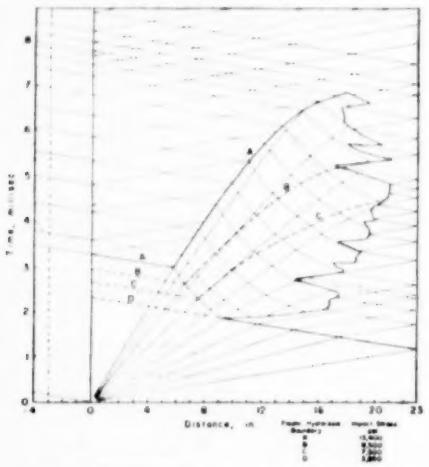

FIG. 5 LAGRANGE POSITION-TIME DIAGRAM

This diagram was constructed for the maximum impact stress, $\sigma_1 = 13{,}400$ psi, employed in the impact tests. The diagram consists of three regions, namely, a plastic region, an elastic-hysteresis region, and the region representing the unloaded state ahead of the initial elastic-wave front. The heavy irregular line represents the boundary between the plastic and hysteresis regions for the maximum velocity of impact. Lighter lines indicate the appropriate characteristics in the Lagrangean plane. The diagram includes the portion of the anvil bar on which the strain gages are mounted so that the stress-time relation at the gages may be determined and compared with the experimental measurements. The line, $x = 0$, represents the interface between the specimen and anvil bar. Similar Lagrange diagrams also were constructed for impact stresses of 9500 psi, 7500 psi, and 3850 psi. The plastic-hysteresis boundary lines for these cases are indicated in Fig. 5 by the heavy dashed lines, together with those portions of the heavy full line which are common to the several diagrams.

A prediction of the stress as a function of time at the interface between the specimen and anvil bar may be determined from the Lagrange diagram. Such a stress-time relation for an impact stress of 13,400 psi is shown in Fig. 6 together with the corresponding experimental relation obtained from stress-time measurements. The plastic-strain distribution determined from the Lagrange diagram for this same impact stress is shown in Fig. 7, together with the measured strain distribution. Similar comparisons between theory and experiment have been made for tests at other values of the impact stress with results of the same general nature as those shown in Figs. 6 and 7.

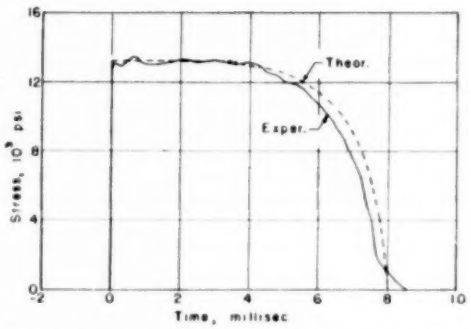


FIG. 6 STRESS VERSUS TIME, IMPACT STRESS 13,400 PSI

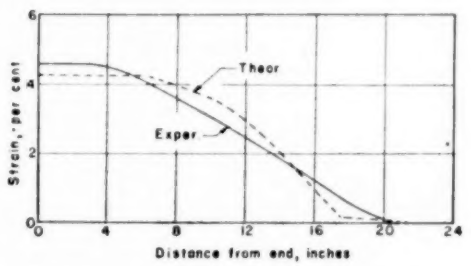


FIG. 7 PERMANENT STRAIN DISTRIBUTION, IMPACT STRESS 13,400 PSI

## DISCUSSION

The experimental results indicate that the stress-strain relation deduced from stress-velocity measurements with the use of the theory of propagation of plastic strains lies above the stress-strain relation determined from stress-plastic strain measurements. Thus, for a given stress, the strain deduced from stress-velocity measurements is less than the strain measured after impact. However, a dynamic stress-strain relation determined from either stress-velocity measurements or stress-plastic strain measurements lies considerably above the static stress-strain relation.

The dynamic stress-strain relation cannot continue to represent the behavior of the material for an indefinite time, and the stress and strain must approach some equilibrium position on the static stress-strain curve if the load is maintained long enough. Thus the plastic strain measured after impact may represent the strain associated with the wave-propagation process and an additional strain due to relaxation which takes place after the initial impact. The stress-strain relation during relaxation cannot be determined from the experimental data, but the over-all magnitude of the maximum strain relaxation compatible with experimental observations can be estimated.

The initiation of any additional plastic strain at the interface between the anvil bar and specimen after initial impact must be accompanied by elastic unloading waves propagating through the specimen and anvil bar. Thus any increase in strain after the initial strain must be accompanied by a decrease in stress at the interface. However, the experimental stress-time records indicate that during impact the stress at the impact end of the specimen remains nearly constant up to the time at which unloading waves originating from the free end of the specimen arrive. This can be seen in Fig. 6. Furthermore, any increase in strain which might take place following the passage of the initial strain waves would be expected to produce a nonuniform distribution of permanent strain in the section of the specimen adjacent to the impact end. That this is not the case is illustrated by the typical experimental permanent strain-distribution relation shown in Fig. 7. For these reasons it may be con-

cluded that no appreciable strain resulting from relaxation effects has taken place in the period of time during which the impact stress is maintained in these experiments (this time may be seen from the Lagrange diagram in Fig. 5 to be from about 0.23 to about 0.33 millisec, depending upon the impact stress). Therefore some other explanation must be sought to explain the differences between the dynamic stress-strain relations as determined from stress-velocity measurements and from stress-permanent strain measurements.

The desired correlation of the experimental data may be obtained by abandoning the assumption that a single dynamic stress-strain relation exists which is capable of describing the behavior of the material for all impact stresses. A family of stress-strain relations, each member of which depends upon the impact stress, may be used to explain the discrepancy between measured strain and strain values deduced from stress-velocity measurements. Each member of this family of stress-strain relations must satisfy several conditions determined by the experimental measurements: (*a*) The end point of the curve must correspond to the measured values of impact stress and permanent strain at the impact end of the bar; that is, the curve must terminate on the stress-plastic strain measurement relation shown in Fig. 4. This condition may be expressed in terms of the wave-velocity function

$$c^*(\epsilon) = \sqrt{\frac{1}{\rho}\frac{d\sigma(\epsilon)}{d\epsilon}} \quad \ldots\ldots\ldots\ldots\ldots\ldots [3]$$

associated with that particular stress-strain curve by means of the relation

$$\sigma_1 = \int_0^{\epsilon_1} \rho[c^*(\epsilon)]^2 d\epsilon \quad \ldots\ldots\ldots\ldots\ldots [4]$$

where $\sigma(\epsilon)$ denotes the desired stress-strain relation. (*b*) The particle velocity due to the impact as given by

$$v_1 = \int_0^{\epsilon_1} c^*(\epsilon) d\epsilon \quad \ldots\ldots\ldots\ldots\ldots [5]$$

must be equal to the particle velocity for that particular impact stress as determined experimentally. (*c*) For strains in the elastic region, the wave velocity must be equal to the normal velocity of elastic waves in long rods, namely

$$c^*(\epsilon) = \sqrt{\frac{E}{\rho}} \quad \text{for} \quad \epsilon \leq \epsilon_0 \quad \ldots\ldots\ldots\ldots [6]$$

where $\epsilon_0$ is the elastic limit strain and $E$ is Young's modulus for the material. Finally, the stress-strain relation must be such that by constructing a suitable Lagrange diagram based upon it, curves of permanent-strain distribution in the specimen may be obtained which agree with the experimental strain-distribution curves. It is not possible to express this last condition in closed mathematical form. Hence it will not be used explicitly, but it will be shown later that the stress-strain relations chosen lead to an improved agreement between predicted and measured strain distributions, particularly in regard to the distance traveled by the maximum strain $\epsilon_1$ during the impact.

Thus all of the explicit conditions to be satisfied by each member of the desired family of stress-strain relations have been expressed in terms of the wave velocity as a function of strain, $c^*(\epsilon)$ as given by Equations [4], [5], and [6]. Once $c^*(\epsilon)$ is determined, the corresponding stress-strain relation may be found by the use of Equation [4] with arbitrary values of $\sigma$ and $\epsilon$ replacing $\sigma_1$ and $\epsilon_1$. Of course these three conditions are insufficient to determine $c^*(\epsilon)$ unambiguously; hence the form of the function must be chosen somewhat arbitrarily. The assumed form of the wave-velocity function is

$$c^*(\epsilon) = c_0 \quad \text{for} \quad \epsilon \leq \epsilon_0$$

$$c^*(\epsilon) = c(\epsilon) + \Delta c(\epsilon) \quad \text{for} \quad \epsilon_1 \geq \epsilon \geq \epsilon_0$$

with

$$\Delta c(\epsilon) = \alpha(\epsilon - \epsilon_0) \quad \ldots\ldots\ldots\ldots [7]$$

where

$c_0 = \sqrt{\frac{E}{\rho}}$ = elastic wave velocity

$c(\epsilon) = \sqrt{\frac{1}{\rho}\frac{d\sigma_1}{d\epsilon_1}}$ = wave velocity corresponding to experimental stress-plastic strain-measurement curve shown in Fig. 4

$\epsilon_0$ = undetermined constant representing elastic limit strain on desired stress-strain curve

$\alpha$ = second undetermined constant

Both $\epsilon_0$ and $\alpha$ depend upon the final strain, $\epsilon_1$, corresponding to each individual member of the family of stress-strain curves to be determined.

Substitution of the assumed form of the wave velocity as given by Equation [7] into Equations [4] and [5] yields two relations in the unknowns $\epsilon_0$ and $\alpha$. A trial-and-error solution was used to determine the values of $\alpha$ and $\epsilon_0$ corresponding to final strains of 2.0, 3.5, and 5.0 per cent. The stress-strain relations then are computed from Equation [4]. These are shown in Fig. 8. The stress-strain relation determined from stress-velocity measurements is shown for comparison.

The family of stress-strain relations deduced in the foregoing manner may be compared with experimental results which are

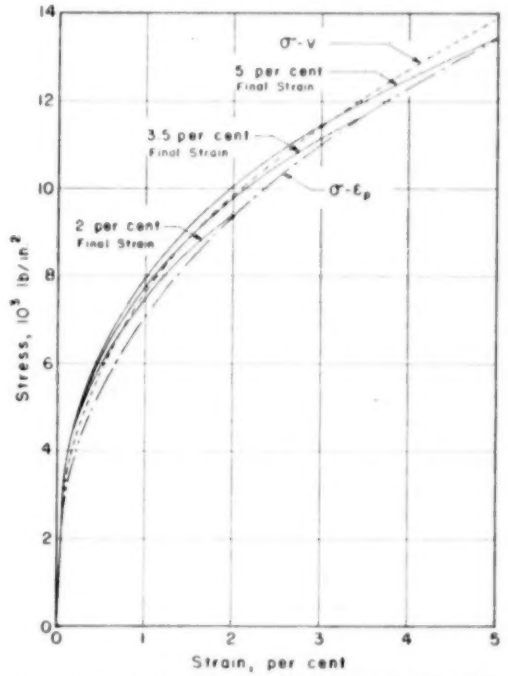


FIG. 8. DERIVED DYNAMIC STRESS-STRAIN CURVES WHICH DEPEND UPON FINAL STRAIN IN RELATION TO CURVES BASED ON $\sigma$-$\epsilon$ AND $\sigma$-$\epsilon_p$ MEASUREMENTS

independent of the data upon which the deduction is based; namely, from any particular member of the family of stress-strain relations, the distance which the maximum strain $\epsilon_1$ should propagate along the specimen may be predicted by constructing a suitable Lagrange diagram based upon that stress-strain relation. This predicted distance of propagation then may be compared with the corresponding experimental value as determined from the measurements of plastic-strain distribution. The required Lagrange diagrams need only be partially constructed to determine the desired propagation distance, and this reduces the labor involved by a large factor. The foregoing procedure has been carried out for the values of the maximum impact strain $\epsilon_1$, equal to 2.0, 3.5, and 5.0 per cent. The results are given in Table 1, together with the corresponding propagation distances predicted from the original Lagrange diagram deduced from stress-velocity measurements and the experimental distances of propagation for the same values of $\epsilon_1$. These results show that the propagation distances, computed from the stress-strain relations which depend upon the final strain, compare more favorably with the measured values than the distances computed from stress-velocity measurements.

The stress-strain relations which depend upon the final strain, shown in Fig. 8, are consistent with the generally accepted idea that stress-strain relations are raised progressively as the rate of loading is increased. In this case the rate of loading increases as the impact velocity (and corresponding impact stress $\sigma_1$, and final strain $\epsilon_1$) is increased. The reason for this is twofold: (*a*) The rise time of the stress at the impact surface decreases as the impact velocity is increased, because the time required for the end surface of the specimen to deform into conformity with the spherical end surface of the anvil bar decreases for increasing impact velocity. (*b*) The impact stress increases with increasing impact velocity. Hence the mean loading rate given by the ratio of the impact stress to the stress-rise time increases with increasing impact velocity.

TABLE 1 PROPAGATION DISTANCES OF MAXIMUM STRAINS

| Maximum strain, per cent | From plastic-strain-distribution measurements, in. | *A*,[a] in. | *B*,[a] in. |
|---|---|---|---|
| 2.0 | 5.0 | 7.0 | 5.9 |
| 3.5 | 4.0 | 6.2 | 5.3 |
| 5.0 | 5.0 | 5.8 | 5.0 |

[a] *A*, From Lagrange diagram deduced from stress-velocity measurements. *B*, From Lagrange diagrams deduced from stress-strain relations which depend upon the final strain $\epsilon_1$.

The behavior of a specimen subjected to a given impact cannot (strictly speaking) be described completely on the basis of the appropriate member of the family of stress-strain relations if it is assumed, as indicated previously, that the differences between the members of this family of curves are due to differences in loading rates. This results from the fact that in such an impact the loading rate varies rather widely with position along the specimen and with time at any given position. In general, the loading rates decrease with increasing distance from the impact surface. Thus, since different stress-strain relations correspond to each loading rate, no single stress-strain relation can be employed, strictly speaking, to describe the behavior of the entire specimen. It may be noted that the family of stress-strain relations determined in the foregoing were deduced from experimental data measured at the impacted end of the specimens. Hence these stress-strain relations correspond to the highest loading rates present in the specimens. The stress-rise times at the impact surface in these experiments are estimated to be in the range of 2 to 20 microsec, with the longer times corresponding to lower impact velocities. Thus the mean loading rates at the impact surface were probably in the range $2 \times 10^6$ to $7 \times 10^6$ psi per sec.

A complete description of the wave-propagation effects under impact loading in a material exhibiting time-dependent mechanical properties must be based upon a complete stress-strain-time relation for that material. One attempt at such a treatment has been given by Malvern (17). Unfortunately, the particular form of the time dependence of the stress-strain properties assumed by Malvern does not seem to be capable of predicting behavior which is consistent with the results of impact experiments. The problem of finding functional relationships between stress, strain, and time which provide for agreement between theory and experiment and are at the same time mathematically feasible to use is probably very difficult.

Fortunately, the complexities and difficulties of theoretical treatment just discussed are concerned with effects of rather minor magnitude in many materials, as judged from experimental investigations. Thus the results of the present experiments indicate that the behavior of annealed 28 aluminum under impact conditions may be predicted with good accuracy, using a single time-independent dynamic stress-strain relation. In this case, for example, a stress-strain relation which was an average between the curve deduced from stress-velocity measurements and the curve deduced from stress-plastic strain measurements could be used to predict plastic wave-propagation phenomena with good accuracy.

Qualitatively similar behavior under impact loading is to be expected for materials which are similar to 28 aluminum in other respects. Thus pure metals and solid-solution alloys which exhibit the face-centered cubic crystal structure may be expected to behave in the same general manner. Examples of such materials are copper and austenitic stainless steel. However, low-carbon steel and probably other body-centered cubic metals behave quite differently under suddenly applied loads (18, 19).

During the preparation of this paper, a report of a similar investigation by J. D. Campbell (20) was published. Campbell's experiments differed from those reported here in that repeated impacts on the same specimen were employed, and the impact velocities used did not cover as wide a range as the present investigation. Nevertheless, Campbell obtains a raised dynamic stress-strain relation for an annealed aluminum alloy for strains up to 0.6 per cent which is similar to the results reported in this paper. Campbell's data and analysis are not sufficient to show that the dynamic stress-strain relation varies slightly with impact stress.

## Summary

The results of this investigation show that the behavior of annealed 28 aluminum under conditions of impact loading into the plastic-strain range can be represented to a good approximation by a single dynamic stress-strain relation. This dynamic stress-strain relation lies above the static stress-strain curve. The excess of dynamic stress over the static values increases progressively with strain, reaching about 20 per cent of the static stress at a strain of 4.5 per cent.

However, the results also show that higher-order effects cannot be correlated with such a single dynamic stress-strain relation. A detailed analysis of the experimental measurements by means of the von Kármán theory of propagation of plastic strains in long rods indicates that the behavior of the material near the impact surface may be described by a family of stress-strain relations. Each member of this family of curves corresponds to a given impact stress, and the curves are arranged consecutively in order of increasing impact stress. All of these curves lie within a narrow region in the stress-strain plane.

ACKNOWLEDGMENT

This investigation was conducted under the sponsorship of the Office of Naval Research. The authors wish to express their appreciation to this agency for the support of the work.

## BIBLIOGRAPHY

1 "High-Velocity Tension Impact Tests," by H. C. Mann, Proceedings of the ASTM, vol. 36, part II, 1936, p. 85.

2 "Stress-Strain Relations Under Tension Impact Loading," by D. S. Clark and G. Datwyler, Proceedings of the ASTM, vol. 38, part II, 1938, p. 98.

3 "High-Speed Tension Tests at Elevated Temperatures," by M. Manjoine and A. Nadai, Proceedings of the ASTM, vol. 40, 1940, p. 822; JOURNAL OF APPLIED MECHANICS, Trans. ASME, vol. 63, 1941, p. A-77.

4 "The Influence of Impact Velocity on the Tensile Characteristics of Some Aircraft Metals and Alloys," by D. S. Clark, National Advisory Committee for Aeronautics, TN No. 868, October, 1942.

5 "An Experimental Study of the Propagation of Plastic Deformation Under Conditions of Longitudinal Impact," by P. E. Duwez and D. S. Clark, Proceedings of the ASTM, vol. 47, 1947, p. 502.

6 "Discussion of the Forces Acting in Tension Impact Tests of Materials," by D. S. Clark and P. E. Duwez, JOURNAL OF APPLIED MECHANICS, Trans. ASME, vol. 70, 1948, p. 243.

7 "The Use of Flat Ended Projectiles for Determining Dynamic Yield Stress. Part I—Theoretical Considerations," by G. I. Taylor, Proceedings of the Royal Society, London, England, vol. 194, series A, 1038, 1948, p. 289.

8 "The Use of Flat Ended Projectiles for Determining Dynamic Yield Stress. Part II—Tests on Various Metallic Materials," by A. C. Whiffin, Proceedings of the Royal Society, London, England, vol. 194, series A, 1038, 1948, p. 300.

9 "A Method of Making High-Speed Compression Tests on Small Copper Cylinders," by E. T. Habib, JOURNAL OF APPLIED MECHANICS, Trans. ASME, vol. 70, 1948, p. 248.

10 "The Tensile Impact Properties of Some Metals and Alloys," by D. S. Clark and D. S. Wood, Trans. ASM, vol. 42, 1950, p. 45.

11 "Plastic-Wave Propagation Effects in High-Speed Testing," by E. H. Lee and H. Wolf, JOURNAL OF APPLIED MECHANICS, Trans. ASME, vol. 73, 1951, p. 379.

12 "An Investigation of the Mechanical Properties of Materials at Very High Rates of Loading," by H. Kolsky, Proceedings of the Physical Society, London, England, vol. 62, 1949, p. 176.

13 "On the Propagation of Plastic Deformation in Solids," by Th. von Kármán, NDRC Report No. A-29 (OSRD No. 365), 1942.

14 "The Propagation of Plastic Deformation in Solids," by Th. von Kármán and P. E. Duwez, *Journal of Applied Physics*, vol. 21, 1950, p. 987.

15 "The Propagation of Plastic Waves in Tension Specimens of Finite Length. Theory and Methods of Integration," by Th. von Kármán, H. F. Bohnenblust, and D. H. Hyers, NDRC Report No. A-103 (OSRD No. 946), 1942.

16 "Graphical Solutions for Problems of Strain Propagation in Tension," by H. F. Bohnenblust, J. V. Charyk, and D. H. Hyers, NDRC Report No. A-131 (OSRD No. 1204), 1942.

17 "The Propagation of Longitudinal Waves of Plastic Deformation in a Bar of Material Exhibiting a Strain-Rate Effect," by L. E. Malvern, JOURNAL OF APPLIED MECHANICS, Trans. ASME, vol. 73, 1951, p. 203.

18 "The Time Delay for the Initiation of Plastic Deformation at Rapidly Applied Constant Stress," by D. S. Clark and D. S. Wood, Proceedings of the ASTM, vol. 49, 1949, p. 717.

19 "Delayed Yielding in Annealed Low-Carbon Steel Under Compression Impact," by J. E. Johnson, D. S. Wood, and D. S. Clark, submitted to American Society for Testing Materials, December, 1952.

20 "An Investigation of the Plastic Behavior of Metal Rods Subjected to Longitudinal Impact," by J. D. Campbell, *Journal of the Mechanics and Physics of Solids*, vol. 1, 1953, p. 113.

# The Effect of Strain Hardening in an Annular Slab[1]

By P. G. HODGE, JR.,[2] LOS ANGELES, CALIF.

**A procedure is outlined for obtaining the stresses and strains in a circular slab with a cutout, subject to uniform biaxial tension. An arbitrary stress-strain curve in tension is approximated by any number of straight-line segments. For biaxial states of stress the material is assumed to satisfy a flow law based on the maximum shear stress, and to be incompressible throughout. The general equations are given and then simplified by assuming that boundary motions may be neglected if the strains are small, and that elastic strain components may be neglected if the strains are large. For the case of linear strain hardening a complete solution is given in closed form. If the rate of strain hardening is small, these results may be simplified further.**

CONSIDER an annular slab of an incompressible material of uniform thickness $H_0$, subjected to a uniform biaxial tension of magnitude $EH_0\lambda$ on the outer edge, Fig. 1.

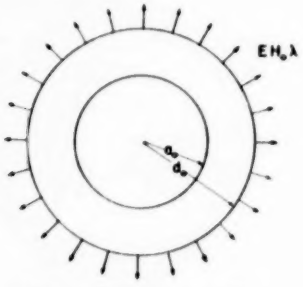


FIG. 1 DIMENSIONS OF SLAB

It is assumed that the slab is in a state of generalized plane stress, even though the thickness may vary as the deformation progresses. Because of symmetry, the mechanical state of the slab may be specified in terms of the following four functions of position and time

$$\left.\begin{aligned} \sigma &= \sigma_r(r, t)/E, \text{ reduced radial stress} \\ s &= \sigma_\theta(r, t)/E, \text{ reduced circumferential stress} \\ u &= u_r(r, t), \text{ radial displacement} \\ h &= h(r, t), \text{ thickness} \end{aligned}\right\} \quad \ldots [1]$$

where $E$ is Young's modulus.

Regardless of the relations between stress and strain, the slab must satisfy the equation of equilibrium

$$\frac{\partial}{\partial r}(rh\sigma) - hs = 0 \quad \ldots [2]$$

and the condition of incompressibility

$$r\frac{\partial h}{\partial t} + \frac{\partial}{\partial r}(rhv) = 0 \quad \ldots [3]$$

Here $v$ is the velocity following the particle

$$v = \frac{\partial u}{\partial r}\frac{\partial r}{\partial t} + \frac{\partial u}{\partial t} = \left(1 + \frac{\partial u}{\partial r}\right)\frac{\partial u}{\partial t}$$

So long as the load is increasing, the material will be assumed to be elastic provided that the maximum shearing stress is less than half the initial yield stress in simple tension. It may be verified a posteriori that the principal stresses satisfy

$$\sigma_\theta \geq \sigma_r \geq \sigma_z = 0 \quad \ldots [4]$$

so that the material is elastic, provided

$$f(\sigma, s) = s - \mu < 0 \quad \ldots [5]$$

where $\mu$ is the reduced initial yield stress in simple tension. If Inequality [5] is valid, then two additional equations are furnished by Hooke's law

$$\left.\begin{aligned} \epsilon_r &= \partial u/\partial r = (2\sigma_r - \sigma_\theta)/2E = \sigma - s/2 \\ \epsilon_\theta &= u/r = (2\sigma_\theta - \sigma_r)/2E = s - \sigma/2 \end{aligned}\right\} \quad \ldots [6]$$

The plastic domain is characterized by the relations

$$s - \mu \geq 0, \dot{s} \geq 0$$

The general form of flow low obtained by Prager and Hodge[3] may be written in terms of the reduced principal stress components

$$\dot{\epsilon}_1'' = F\frac{\partial f}{\partial \sigma_1'}\dot{f}, \dot{\epsilon}_2'' = F\frac{\partial f}{\partial \sigma_2'}\dot{f}, \dot{\epsilon}_3'' = F\frac{\partial f}{\partial \sigma_3'}\dot{f}$$

Here $\dot{\epsilon}_1''$, $\dot{\epsilon}_2''$, $\dot{\epsilon}_3''$ are the plastic strain-rate components, $\sigma_1'$, $\sigma_2'$, $\sigma_3'$ are the reduced-stress components, $f$ is the yield function, and $F$ is a function of stress to be determined from the stress-strain curve. If $f$ is given as in Equation [5], the stress-strain law becomes

$$\dot{\epsilon}_r'' = 0, \dot{\epsilon}_\theta'' = F\dot{s} \quad \ldots [7]$$

Let the given stress-strain curve be approximated by a series of straight-line segments, Fig. 2, and let $\alpha_k$ be the inclination of the $k$th segment in the strain-reduced stress plane. In simple tension, the relation between plastic strain rate and stress rate is then given by

$$E\dot{\epsilon}_z'' = \cot\alpha_k\,\dot{\sigma}_z, \mu_k \leq \sigma_z/E \leq \mu_{k+1}$$

[1] The results presented in this paper were obtained in the course of research conducted as a Consultant under Contract N7onr-35810 between the Office of Naval Research and Brown University.

[2] Department of Mathematics, University of California. Now at Polytechnic Institute of Brooklyn, Brooklyn, N. Y. Mem. ASME.

Contributed by the Applied Mechanics Division, and presented at the Semi-Annual Meeting, Los Angeles, Calif., June 28 July 2, 1953, of THE AMERICAN SOCIETY OF MECHANICAL ENGINEERS.

Discussion of this paper should be addressed to the Secretary, ASME, 29 West 39th Street, New York, N. Y., and will be accepted until January 11, 1954, for publication at a later date. Discussion received after the closing date will be returned.

NOTE: Statements and opinions advanced in papers are to be understood as individual expressions of their authors and not those of the Society. Manuscript received by ASME Applied Mechanics Division, January 16, 1953. Paper No. 53—SA-20.

[3] "A Variational Principle for Plastic Materials With Strain-Hardening," by P. Hodge and W. Prager, *Journal of Mathematics and Physics*, vol. 27, 1948, pp. 1–10.

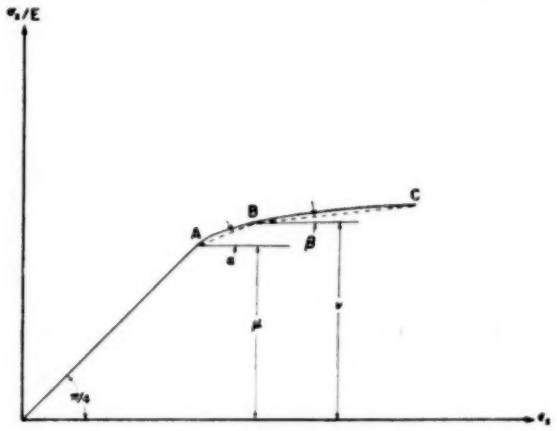


——— Actual – – – – Approximate
FIG. 2 STRESS-STRAIN CURVE

so that Equation [7] becomes

$$\dot{\epsilon}_r^{\,p} = 0,\ \dot{\epsilon}_\theta^{\,p} = \cot \alpha_k\, \dot{s},\ \mu_k \leq s \leq \mu_{k+1}$$

Finally, since the elastic components of strain rate must satisfy the differentiated form of Hooke's law, the plastic stress-strain relations are

$$\left.\begin{aligned} \dot{\epsilon}_r &= \partial u/\partial r = \dot{\sigma} - \dot{s}/2 \\ \dot{\epsilon}_\theta &= u/r = (1 + \cot \alpha_k)\,\dot{s} - \dot{\sigma}/2, \end{aligned}\right\} \quad \mu_k \leq s \leq \mu_{k+1} \ldots [8]$$

Equations [2], [3], and [6] or [8] furnish four equations for the four unknowns $\sigma$, $s$, $h$, and $u$. At the boundaries, the stresses must be in equilibrium with the applied tractions, so that

$$\sigma(a) = 0 \ldots [9a]$$

$$h(d)\,\sigma(d) = H_0\,\lambda \ldots [9b]$$

In addition, all stresses and strains must be continuous throughout the slab, so that if $r = \rho_k$ is the radius which divides one analytic form of solution from another

$$\left.\begin{aligned} &\sigma(\rho_k^-) = \sigma(\rho_k^+),\ s(\rho_k^-) = s(\rho_k^+) \\ &u(\rho_k^-) = u(\rho_k^+),\ \frac{\partial u}{\partial r}(\rho_k^-) = \frac{\partial u}{\partial r}(\rho_k^+) \end{aligned}\right\} \ldots [10]$$

## ELASTIC SOLUTION

Since $h$ and $u$ are both unknown, Equations [2] and [3] are nonlinear, and at present there does not exist a general solution to the boundary-value problem defined in the previous section. However, as long as the strains are small compared to 1, it appears reasonable to neglect motion of the boundaries and changes of the thickness $h$. For a perfectly plastic material[4] it is known that the errors introduced by these approximations are of order $\mu \sim 0.001$.

Regarding $h$ as constant, Equation [3] no longer can be satisfied exactly, and Equations [2] and [6] become linear. The solution for an elastic material is readily found to be

$$\left.\begin{aligned} u &= Br + C/r \\ \left.\begin{matrix}\sigma \\ s\end{matrix}\right\} &= 2(B \mp C/3r^2) \end{aligned}\right\} \ldots [11]$$

[4] "On the Plastic Strains in Slabs With Cutouts," by P. G. Hodge, Jr., JOURNAL OF APPLIED MECHANICS, Trans. ASME, vol. 20, 1953, pp. 183–188.

where $B$ and $C$ are to be determined from the boundary conditions. For $\lambda$ sufficiently small, the slab will be elastic throughout and the Boundary Conditions [9] may both be applied to determine the constants. Since boundary motions are neglected, the initial values of $a$ and $d$ may be used. The resulting solution is

$$\left.\begin{aligned} \left.\begin{matrix}u/r \\ \partial u/\partial r\end{matrix}\right\} &= \frac{\lambda}{2}\,\frac{1 \pm 3\,a_o^2/r^2}{1 - a_o^2/d_o^2} \\ \left.\begin{matrix}\sigma \\ s\end{matrix}\right\} &= \lambda\,\frac{1 \mp a_o^2/r^2}{1 - a_o^2/d_o^2} \end{aligned}\right\} \ldots [12]$$

This solution will be valid so long as Inequality [5] is satisfied throughout the slab. Since $s$ is a maximum at the inner boundary the maximum load for which this is true is found by setting $s(0) = \mu$ and solving for $\lambda$

$$\lambda_1 = \frac{1}{2}\,\mu\,(1 - a_o^2/d_o^2) \ldots [13]$$

For values of $\lambda$ somewhat larger than $\lambda_1$, a plastic ring will form against the inner boundary. If $\rho$ denotes the radius between the elastic and plastic regions, then the slab is still elastic for $\rho \leq r \leq d_o$. In this region, Equations [11] are still valid, but the Boundary Condition [9a] is no longer applicable. In its stead, the condition

$$s(\rho) = 2(B + C/3\rho^2) = \mu$$

must be satisfied. Solving this for $C$ and substituting into Equations [11] one obtains the elastic solution in the form

$$\left.\begin{aligned} \left.\begin{matrix}u/r \\ \partial u/\partial r\end{matrix}\right\} &= B\left(1 \mp 3\,\frac{\rho^2}{r^2}\right) \pm \frac{3}{2}\,\mu\,\frac{\rho^2}{r^2} \\ \left.\begin{matrix}\sigma \\ s\end{matrix}\right\} &= 2B\left(1 \pm \frac{\rho^2}{r^2}\right) \mp \mu\,\frac{\rho^2}{r^2} \end{aligned}\right\} \ldots [14]$$

The boundary condition at $r = d$ will be used to determine a relationship between $\lambda$ and $\rho$, once the constant $B$ has been determined from the plastic solution.

## ELASTIC-PLASTIC SOLUTION—FIRST STAGE

For values of the applied load slightly greater than $\lambda_1$, the plastic portion of the slab will correspond entirely to the first plastic segment $AB$ of the stress-strain curve, Fig. 2. So long as part of the slab is still elastic, the plastic stress-strain laws, Equations [8], may be integrated to yield

$$\left.\begin{aligned} \epsilon_r &= \partial u/\partial r = \sigma - s/2 \\ \epsilon_\theta &= u/r = (1 + \cot \alpha)s - \sigma/2 - \mu \cot \alpha \end{aligned}\right\} \ldots [15]$$

The constants of integration were determined from the fact that when a given particle first enters the plastic domain the strains must be given by Equations [6] and $s$ must equal $\mu$.

If Equations [15] are solved for $s$ and $\sigma$ in terms of $u$, and the results substituted into the equilibrium equation, the resulting linear equation for $u$ is readily solved to yield

$$u/r = Kr^{n-1} + Lr^{-n-1} + \frac{1}{2}\,\mu \ldots [16a]$$

$$\partial u/\partial r = n\,Kr^{n-1} - n\,Lr^{-n-1} + \frac{1}{2}\,\mu \ldots [16b]$$

$$\sigma = \frac{2nK}{2-n}\,r^{n-1} - \frac{2nL}{2+n}\,r^{-n-1} + \mu \ldots [16c]$$

$$s = \frac{2n^2K}{2-n}\,r^{n-1} + \frac{2n^2L}{2+n}\,r^{-n-1} + \mu \ldots [16d]$$

Here $n$ is defined by

$$n = (1 + \cot \alpha)^{-1/n} \quad [17]$$

and functions of $\alpha$ have been replaced by functions of $n$ throughout.

The four functions given in the plastic region by Equations [16] and in the elastic region by Equations [14] must be continuous at the elastic-plastic boundary $r = \rho$. Together with Equation [9a] this provides five equations to determine the three constants $B$, $K$, and $L$. However, in view of the continuity imposed in integrating the plastic stress-strain law, two of these equations are redundant. After some computation it is found that

$$\left.\begin{aligned} B &= \frac{1}{2}(1 - 1/\Delta)\,\mu \\ K &= \frac{2 + n}{2n}\,\frac{\mu}{\Delta}\,\rho^{1+n} \\ L &= \frac{2 - n}{2n}\,\frac{\mu}{\Delta}\,\rho^{1-n} \end{aligned}\right\} \quad [18]$$

where

$$\Delta = (\rho/a_o)^{1+n} + (\rho/a_o)^{1-n} \quad [19]$$

The substitution of Equations [18] into Equations [16] and [14] then yields the following complete solution:

Plastic ($a_o \leq r \leq \rho$)

$$\frac{u}{r} = \frac{1}{2}\mu\left[1 + \frac{2 + n}{n\Delta}\left(\frac{\rho}{r}\right)^{1+n} - \frac{2 - n}{n\Delta}\left(\frac{\rho}{r}\right)^{1-n}\right] \quad [20a]$$

$$\frac{\partial u}{\partial r} = \frac{1}{2}\mu\left[1 - \frac{2 + n}{\Delta}\left(\frac{\rho}{r}\right)^{1+n} - \frac{2 - n}{\Delta}\left(\frac{\rho}{r}\right)^{1-n}\right] \quad [20b]$$

$$\sigma = \mu\left[1 - \frac{1}{\Delta}\left(\frac{\rho}{r}\right)^{1+n} - \frac{1}{\Delta}\left(\frac{\rho}{r}\right)^{1-n}\right] \quad [20c]$$

$$s = \mu\left[1 + \frac{n}{\Delta}\left(\frac{\rho}{r}\right)^{1+n} - \frac{n}{\Delta}\left(\frac{\rho}{r}\right)^{1-n}\right] \quad [20d]$$

Elastic ($\rho \leq r \leq d_o$)

$$\left.\begin{matrix} u/r \\ \partial u/\partial r \end{matrix}\right\} = \frac{1}{2}\mu\left[1 - \frac{1 \mp 3\rho^2/r^2}{\Delta}\right] \quad [20e, f]$$

$$\left.\begin{matrix} \sigma \\ s \end{matrix}\right\} = \mu\left[1 - \frac{1 \pm \rho^2/r^2}{\Delta}\right] \quad [20g, h]$$

Equations [20] give the complete solution in terms of the position of the elastic-plastic boundary. The load necessary to extend the plastic region to a given boundary $\rho$ is obtained from the boundary condition, Equation [9b]

$$\lambda = \sigma(d_o) = \mu\left[1 - \frac{1 + \rho^2/d_o^2}{\Delta}\right] \quad [20i]$$

Since the parameter $n$ occurs as an exponent in Equations [20] the preceding solution is not well adapted to computations. For most real materials $n$ is small compared to 1, so that it appears reasonable to approximate the solution and obtain a more useful formulation. This may be done by expanding the solution as power series in $n$. Since all the quantities are even functions of $n$, the following expressions are correct up to terms $n^4$:

Plastic ($a_o \leq r \leq \rho$)

$$\frac{u}{r} = \frac{1}{2}\mu\left\{1 + \frac{a_o}{r} + 2\,\frac{a_o}{r}\log\frac{\rho}{r} + \frac{a_o}{r}\,\frac{n^2}{6}\left[\left(3 + 2\log\frac{\rho}{r}\right)\left(\log\frac{\rho}{r}\right)^2 - 3\left(1 + 2\log\frac{\rho}{r}\right)\left(\log\frac{\rho}{a_o}\right)^2\right]\right\} \quad [21a]$$

$$\frac{\partial u}{\partial r} = \frac{1}{2}\mu\left\{1 - 2\,\frac{a_o}{r} - n^2\,\frac{a_o}{r}\left[\log\frac{\rho}{r} + \left(\log\frac{\rho}{r}\right)^2 - \left(\log\frac{\rho}{a_o}\right)^2\right]\right\} \quad [21b]$$

$$\sigma = \mu\left\{1 - \frac{a_o}{r} - \frac{1}{2}n^2\,\frac{a_o}{r}\left[\left(\log\frac{\rho}{r}\right)^2 - \left(\log\frac{\rho}{a_o}\right)^2\right]\right\} \quad [21c]$$

$$s = \mu\left\{1 + n^2\,\frac{a_o}{r}\log\frac{\rho}{r}\right\} \quad [21d]$$

Elastic ($\rho \leq r \leq d_o$)

$$\left.\begin{matrix} u/r \\ \partial u/\partial r \end{matrix}\right\} = \frac{1}{2}\mu\left\{1 - \frac{a_o}{2\rho}\left(1 \mp 3\,\frac{\rho^2}{r^2}\right)\left[1 - \frac{n^2}{2}\left(\log\frac{\rho}{a_o}\right)^2\right]\right\} \quad [21e, f]$$

$$\left.\begin{matrix} \sigma \\ s \end{matrix}\right\} = \mu\left\{1 - \frac{a_o}{2\rho}\left(1 \pm \frac{\rho^2}{r^2}\right)\left[1 - \frac{n^2}{2}\left(\log\frac{\rho}{a_o}\right)^2\right]\right\} \quad [21g, h]$$

Load

$$\lambda = \mu\left\{1 - \frac{a_o}{2\rho}\left(1 + \frac{\rho^2}{d_o^2}\right)\left[1 - \frac{n^2}{2}\left(\log\frac{\rho}{a_o}\right)^2\right]\right\} \quad [21i]$$

### Elastic-Plastic Solution — Second Stage

The solution given by Equations [20] (or approximately by Equations [21]) is valid so long as the following two inequalities are both satisfied

$$\rho \leq d_o, \quad s(a) \leq \nu \quad [22]$$

As the load is increased so that one or the other of these inequalities is violated, a variety of behavior may be exhibited depending upon the dimensions of the slab and the parameters in the stress-strain curve.

Consider first the case where these quantities are such that the second Inequality [22] is violated while the first remains valid, and let $\rho_1$ be the value of $\rho$ for which this occurs. To the approximations used in Equation [21d] it follows that $\rho_1$ is given by

$$\mu\,(1 + n^2 \log \rho_1/a_o) = \nu. \quad [23]$$

Since by hypothesis $\rho_1$ is less than $d_o$ the parameters of the problem must satisfy

$$\mu\,(1 + n^2 \log d_o/a_o) > \nu. \quad [24]$$

The approximate load $\lambda_2$ for which this first occurs is obtained by solving Equation [23] for $\rho_1$ and substituting the result into Equation [21i].

For values of $\lambda$ somewhat greater than $\lambda_2$ the solution in the slab will consist of three regions. If $\zeta$ represents the radius where $s = \nu$, then for $a_o \leq r \leq \zeta$ the material is plastic corresponding to the segment $BC$ of the stress-strain curve, Fig. 2; for $\zeta \leq r \leq \rho$ the material is plastic corresponding to $AB$; and for $\rho \leq r \leq d_o$ the material is elastic, corresponding to $OA$. For the latter two regions, the solution is given by Equations [17] and [14], respectively, where the boundary constants must be determined anew.

For the innermost region, the stress-strain law Equation [8] may be integrated again to yield

$$\epsilon_r = \partial u/\partial r = \sigma - s/2$$

$$\epsilon_\theta = u/r = (1 + \cot \beta)s - \sigma/2 - \nu\,(\cot \beta - \cot \alpha) - \mu \cot \alpha. \quad [25]$$

As in the previous section, these relations may be solved for $\sigma$ and $s$ and the results substituted into the equilibrium equation. The resulting equation is solved readily for $u$

$$\frac{u}{r} = Pr^{m-1} + Qr^{-m-1} + \frac{1}{2}(\mu - \nu)\frac{1-n^2}{1-m^2}\frac{m^2}{n^2} + \frac{1}{2}\nu \quad [26]$$

where

$$m = (1 + \cot\beta)^{-1/2} \quad [27]$$

The constants $P$, $Q$, $K$, $L$, and $B$ may now be determined from the continuity conditions (Equations [10]) at $\zeta$ and $\rho$. The Boundary Condition [9$a$] then determines the relation between $\rho$ and $\zeta$, while Equation [9$b$] furnishes the value of the load. The computations and results become quite complicated and are not reproduced here.

Consider now the other possibility characterized by the reverse of Inequality [24]. In this case the slab will become fully plastic for a load $\lambda_2'$ obtained by setting $\rho$ equal to $d_o$ in Equation [20$i$] or [21$i$]. Thus from Equation [21$i$]

$$\lambda_2' = \mu\left[1 - \frac{a_o}{d_o} + \frac{n^2}{2}\frac{a_o}{d_o}\left(\log\frac{d_o}{a_o}\right)^2\right] \quad [28]$$

For values of $\lambda$ slightly greater than $\lambda_2'$, Equations [16] will be valid throughout the slab. The constants $K$ and $L$ may be determined directly in terms of the load $\lambda$ by substituting Equation [16$c$] into Equations [9]. While the results may be obtained accurately, it is somewhat simpler to introduce the approximate power series in $n$ directly. After some computation, the complete solution is found to be

$$\left.\begin{aligned}
\frac{u}{r} &= \frac{1}{n^2}\frac{d_o}{r}\frac{(a_o/d_o)\mu + \lambda - \mu}{\log(d_o/a_o)} \\
\frac{\partial u}{\partial r} &= \frac{d_o/r}{2\log(d_o/a_o)}\left[-\mu\frac{a_o}{d_o}\left(1 + 2\log\frac{d_o}{r}\right)\right. \\
&\qquad \left. + (\lambda - \mu)\left(2\log\frac{r}{a_o} - 1\right)\right] + \frac{1}{2}\mu \\
\sigma &= \frac{d_o/r}{\log(d_o/a_o)}\left[-\mu\frac{a_o}{d_o}\log\frac{d_o}{r}\right. \\
&\qquad \left. + (\lambda - \mu)\log\frac{r}{a_o}\right] + \mu \\
s &= \frac{d_o}{r}\frac{(a_o/d_o)\mu + \lambda - \mu}{\log(d_o/a_o)} + \mu
\end{aligned}\right\} \quad [29]$$

where only the leading terms in $n^2$ have been retained.

Equations [29] will be valid until $s(a) = \nu$, assuming that the strains may still be considered small. On the other hand, assuming for simplicity that the entire stress-strain curve is approximated by the three segments in Fig. 2, the solution obtained from Equations [27], [17], and [14] is valid until $\rho = d_o$. For slightly greater loads in either case, the slab will be plastic throughout, but will be governed by the portion $BC$ of the stress-strain curve for $a_o \leq r \leq \zeta$, and by $AB$ for $\zeta \leq r \leq d_o$. Therefore the solution will consist of Equations [27] for $a_o \leq r \leq \zeta$ and Equations [17] for $\zeta \leq r \leq d_o$, with the four constants $P$, $Q$, $K$, and $L$ to be determined from Equations [9] and [10].

If a more accurate approximation to the stress-strain curve is desired, the solution may be obtained in similar fashion, although the resulting computations would become exceedingly laborious.

## Fully Plastic Solution—Large Strains

The solutions obtained in the preceding sections are valid only so long as $h$ may be considered a constant and the boundary displacements neglected. For an incompressible material these conditions will both be satisfied provided that the strains are small compared to 1 throughout the slab. This generally will be the case so long as any part of the slab is elastic, at least provided $a_o/d_o$ is not too small. However, once the slab is fully plastic, relatively large strains may occur and the previous solutions no longer would be applicable.

Since $h$ no longer can be considered constant, the equations to be solved are nonlinear, and it is necessary to make some other simplifying assumption to obtain a solution. The elastic part of the strain remains proportional to the stress throughout loading and hence can never become large. Therefore, if the total strains are large, it appears reasonable to neglect entirely the elastic component and consider the strains as purely plastic. This is equivalent to assuming that Young's modulus is equal to infinity, so that the elastic portion of the stress-strain curve in Fig. 2 is replaced by a vertical line. For simplicity of exposition it will be assumed that the plastic portion of the stress-strain curve consists of a single linear segment, Fig. 3, although the method can be extended to more general curves as in the previous sections.

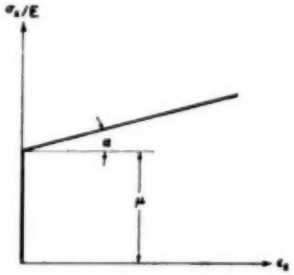


Fig. 3 Stress-Strain Curve for Large Strains

In the case of small deformations, it was not necessary to distinguish between the Lagrangian (original) and Eulerian (current) co-ordinates of a particle. However, for the large strains considered in the present section such a distinction is obligatory. The stress-strain law is a function of the stress and strain of the particular particle in question, and hence must be expressed in terms of the original co-ordinate $r_o$ of a particle now at $r$. Thus, since elastic strain rates are neglected, Equations [8] are replaced by

$$\dot{\epsilon}_r = \partial v/\partial r = 0 \quad [30a]$$

$$\dot{\epsilon}_\theta = v/r = \cot\alpha\,\dot{s} = [(1-n^2)/n^2]\,\dot{s} \quad [30b]$$

The "dot" in Equations [30] customarily refers to time. However, since inertia effects are not considered, time may be replaced by any convenient monotonic function of time. In the present case, the current radius of the inner boundary is such a function.[5] Therefore Equation [30$a$] states that

$$\frac{\partial}{\partial r}\,v\,(r, a) = 0$$

While this equation may be integrated easily to obtain the velocity, it is more convenient first to transform it to the Lagrangian co-ordinate $r_o$. Since the "time" $a$ occurs only as a parameter

$$\frac{\partial v}{\partial r} = \frac{\partial v/\partial r_o}{\partial r/\partial r_o} = 0$$

hence

[5] The validity of this step may be seen by noting that the "rate" at which load is applied will not affect the solution. Thus, in particular, the load may be applied so that the inner boundary moves outward at a uniform rate. Finally, the unit of time may be chosen so that this rate is unity.

$$\frac{\partial v}{\partial r_o} = \frac{\partial}{\partial r_o}\left(\frac{\partial u}{\partial a}\right) = 0$$

where $u(r_o, a)$ is the displacement of the particle. The integral of this equation shows that

$$u(r_o, a) = F(r_o) + G(a)$$

Since elastic strains are neglected, the displacement of all particles is zero at the commencement of plastic flow. Thus

$$u(r_o, a_o) = F(r_o) + G(a_o) \underset{r_o}{\equiv} 0$$

$F(r_o)$ now can be evaluated, the resulting displacement being

$$u(r_o, a) = G(a) - G(a_o)$$

In view of the choice of a time scale, the velocity of the particle initially at the inner boundary (and hence always at the current inner boundary) is unity, so that

$$\left.\frac{\partial u}{\partial a}\right|_{r_o = a_o} = G'(a)\Big|_{r_o = a_o} \underset{a}{\equiv} 1$$

Therefore $G(a) = a$, and hence

$$u(r_o, a) = a - a_o \quad \ldots\ldots\ldots\ldots\ldots\ldots [31a]$$

independently of $r_o$. Further, the current position of the particle initially at $r_o$ is

$$r(r_o, a) = r_o + u(r_o, a) = r_o + a - a_o \quad \ldots\ldots [31b]$$

Finally, the velocity at all points is

$$v = 1 \quad \ldots\ldots\ldots\ldots\ldots\ldots\ldots\ldots [31c]$$

The substitution of Equations [31] into Equation [30b] yields

$$\frac{\partial s}{\partial a} = \frac{n^2}{1 - n^2}\frac{1}{r_o + a - a_o}$$

hence

$$s(r_o, a) = \frac{n^2}{1 - n^2}\log(r_o + a - a_o) + f(r_o) \quad \ldots\ldots [32]$$

The function $f(r_o)$ is to be evaluated from the continuity of $s$ at $a = a_o$. However, since there has been a change of assumption between the small-strain and large-strain solutions, this continuity cannot be exact. The best one can do is to evaluate $s(r_o, a_o)$ so that it is continuous with the solution given by Equation [20d] for $\rho = d_o$. This leads, of course, to a rather awkward expression for $f(r_o)$. However, this expression may be simplified by neglecting terms of order $n^4$. This leads finally to

$$s = \mu + n^2\left(\log\frac{r_o + a - a_o}{r_o} + \mu\frac{a_o}{r_o}\log\frac{d_o}{r_o}\right)$$

a result which could also have been obtained directly from Equation [21d]. Finally, since $\mu$ is very small compared to 1, the second term in the coefficient of $n^2$ may be neglected in comparison with the first, once the deformation has progressed. Thus, to within the approximations considered

$$s = \mu + n^2\log\frac{r}{r_o} \quad \ldots\ldots\ldots\ldots\ldots [33a]$$

where $r$ and $r_o$ are related by Equation [31b]. Equation [31d] predicts that $s = \mu$ throughout the slab at the onset of full plasticity. Thus, physically, the assumptions are equivalent to neglecting the strain hardening which occurs during the elastic-plastic stage of loading. In an example considered later, this approximation appears to be well justified.

In Equation [31c] the functional form of the velocity $v$ is the same referred to either the Lagrangian or Eulerian co-ordinates. Thus the Eulerian form of Equation [3] (incompressibility equation) may be retained

$$\frac{\partial}{\partial a}(rh) + \frac{\partial}{\partial r}(rh) = 0$$

where $h$ is a function of $r$ and $a$. The solution of this equation satisfying the condition $h = H_o$ when $a = a_o$ is

$$h = \left(1 - \frac{a - a_o}{r}\right)H_o = \frac{r_o}{r}H_o \quad \ldots\ldots\ldots [33b]$$

This result also could have been predicted directly as follows: For velocity constant, the thickness $\Delta r$ of a narrow ring will remain constant; hence by incompressibility the volume $2\pi rh\Delta r$ also must remain constant at all times $a$.

The radial stress is then determined by integrating the equilibrium Equation [2] with respect to the Eulerian co-ordinate $r$

$$\left.\begin{aligned}\sigma &= \frac{1}{rh}\int_a^r hs\,dr \\ &= \frac{1}{r_o}\int_a^r\left(\mu\frac{r_o}{r} + n^2\frac{r_o}{r}\log\frac{r_o}{r}\right)dr \\ &= \frac{\mu}{r_o}\left[r - a - (a - a_o)\log\frac{r}{a}\right] \\ &\qquad - \frac{n^2}{r_o}\int_a^r\frac{r_o}{r}\log\frac{r_o}{r}\,dr\end{aligned}\right\} \quad [33c]$$

In the foregoing integrations, $r_o$ is defined as a function of $r$ by Equation [31b]. Finally, the load necessary to enlarge the inner radius from $a_o$ to any value $a$ is obtained from Equation [9b]

$$\begin{aligned}\lambda(a) &= h(d, a)\,\sigma(d, a)/H_o \\ &= \mu\left[1 - \frac{a}{d} - \left(\frac{a - a_o}{d}\right)\log\frac{d}{a}\right] \\ &\qquad - \frac{n^2}{d}\int_a^d\frac{r_o}{r}\log\frac{r_o}{r}\,dr \quad \ldots\ldots [33d]\end{aligned}$$

where the current outer radius $d$ is given by

$$d = d_o + a - a_o \quad \ldots\ldots\ldots\ldots\ldots [33e]$$

For a perfectly plastic material,[4] it was found that the load $\lambda$ decreased as the fully plastic deformation proceeded, so that the maximum load which the slab could support was achieved just as the elastic ring disappeared. For a material with infinite strain hardening, on the other hand, the load could increase indefinitely above the fully plastic value. The question naturally arises as to the rate of strain hardening which separates these two types of behavior. In other words, what is the minimum strain-hardening rate for which the initial fully plastic configuration is stable?

Since $\lambda$ is given as a function of $a$ by Equation [33d] this question is easily answered by differentiating $\lambda$ with respect to $a$, setting $a = a_o$, and observing the sign of the derivative. If it is positive, then an increase in radius must be accompanied by an increase in load. After some computation, it is seen that the derivative at $a$ is positive if and only if

$$n^2 > \mu\frac{1 - a_o/d_o + \log d_o/a_o}{\log d_o/a_o} \quad \ldots\ldots\ldots\ldots [34]$$

Equation [34] states the condition that the fully plastic solution be initially stable. As the deformation progresses, however,

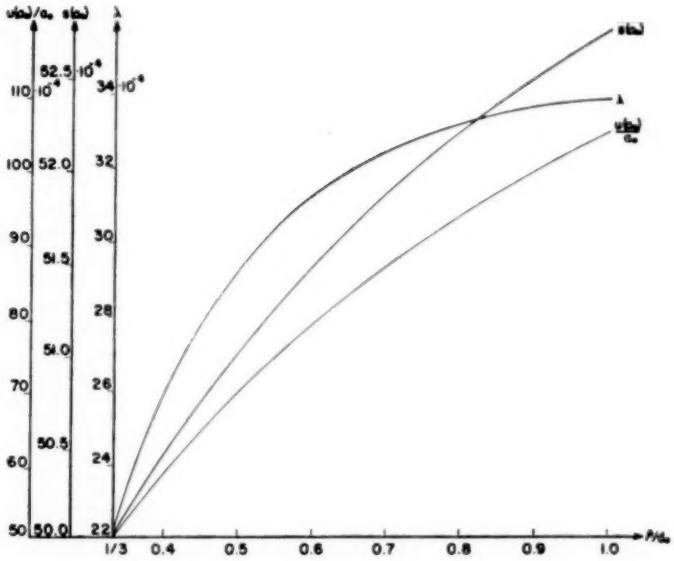


FIG. 4 ELASTIC-PLASTIC LOAD AND CIRCUMFERENTIAL STRESS AND STRAIN AS FUNCTIONS OF RADIUS OF ELASTIC-PLASTIC BOUNDARY ($a_o/d_o = 1/3$)

it follows from Equation [33*b*] that the thickness at the outer edge grows less, so that the same load produces a higher true stress. Therefore, for any finite rate of strain hardening, the actual load which the slab can support will decrease after the deformation has proceeded sufficiently far. The value of $a$ for which this is the case can be found equating $d\lambda/da$ to zero and solving for $a$. Although this cannot be done in closed form, the maximum value of $\lambda$ can be found numerically for any given values of the parameters.

### EXAMPLE—PERFECTLY PLASTIC MATERIAL

A perfectly plastic material is characterized by a zero rate of strain hardening, i.e., by $\alpha = 0$. Therefore the complete solution for a perfectly plastic material would consist of three stages: fully elastic, elastic-plastic, and fully plastic. The elastic solution is still given by Equations [12], while in view of Equation [17] the other two solutions are obtained by setting $n = 0$ in Equations [21], [31], and [33], respectively.

Elastic-plastic solution for $a_o \leq r \leq \rho$

$$u/r = \frac{1}{2}\mu\,[1 + a_o/r + 2(a_o/r)\log(\rho/r)]$$

$$\partial u/\partial r = \frac{1}{2}\mu\,(1 - 2a_o/r)$$

$$\sigma = \mu\,(1 - a_o/r),\ s = \mu$$

Elastic-plastic solution for $\rho \leq r \leq d_o$

$$\left.\begin{matrix} u/r \\ \partial u/\partial r \end{matrix}\right\} = \frac{1}{2}\mu\left(1 - \frac{a_o}{2\rho} \pm 3\,\frac{a_o\rho}{2r^2}\right)$$

$$\left.\begin{matrix} \sigma \\ s \end{matrix}\right\} = \mu\left(1 - \frac{a_o}{2\rho} \mp \frac{a_o\rho}{2r^2}\right)$$

Elastic-plastic load

$$\lambda = \mu\left(1 - \frac{a_o}{2\rho} - \frac{a_o\rho}{2d_o^2}\right)$$

Fully plastic solution

$$u/r = (a - a_o)/r,\ \partial u/\partial r = 0,\ h = [1 - (a - a_o)/r]\,H_o.$$

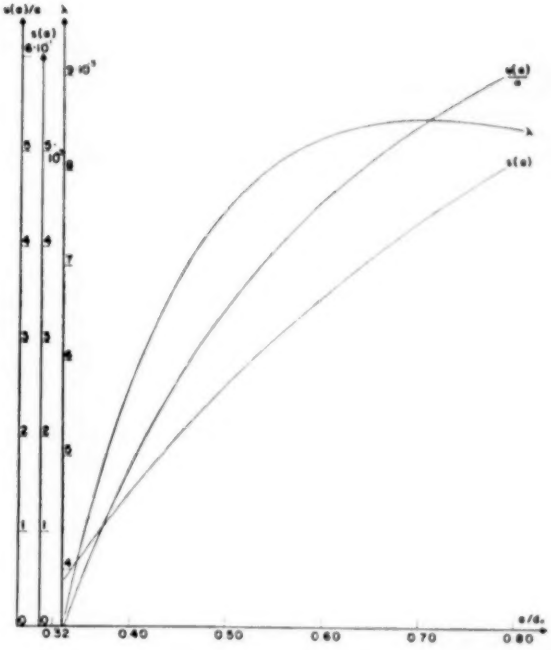


FIG. 5 FULLY PLASTIC LOAD AND CIRCUMFERENTIAL STRESS AND STRAIN AS FUNCTIONS OF INNER RADIUS ($a_o/d_o = 1/3$)

$$\sigma = \mu\,\frac{r - a - (a - a_o)\log(r/a)}{r - a + a_o},\quad s = \mu$$

$$\lambda = \mu\,\frac{1 - a_o/d_o - (a/d_o - a_o/d_o)\log[(d_o + a - a_o)/a]}{1 + a/d_o - a_o/d_o}$$

In a previous paper,[4] the author obtained the complete perfectly plastic solution directly by a perturbation method. It may be verified readily that the first term of each quantity in the

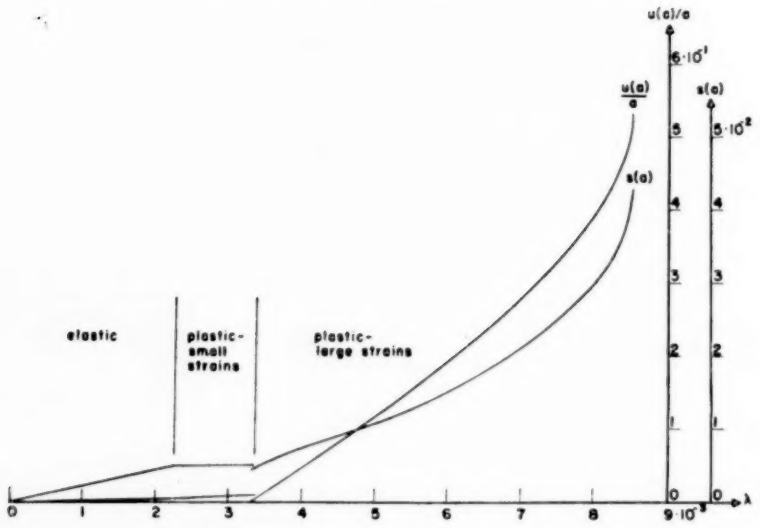


FIG. 6 STRESS AND STRAIN AT INNER BOUNDARY AS FUNCTIONS OF LOAD ($a_o/d_o = 1/3$)

perturbation procedure agrees precisely with Equations [35].[6] In the discussion following the presentation of the previous paper,[4] the question was raised as to whether or not the perfectly plastic solution truly represented a limiting case of a strain-hardening solution; the present example shows that for the problem considered it does indeed.

### EXAMPLE—STRAIN-HARDENING MATERIAL[7]

Some results have been worked out for the following numerical data

$$\mu = 0.005, \quad n^2 = 0.05, \quad a_o/d_o = 1/3$$

The plastic part of the stress-strain curve has been approximated by a single linear segment. Fig. 4 shows the load, circumferential strain $u(a_o)/a_o$ of the inner boundary, and reduced circumferential stress $s(a_o)$ at the inner boundary, all as functions of the radius of the elastic-plastic boundary for the elastic-plastic solution given by Equations [21]. The maximum strain, when the slab first becomes fully plastic, is seen to be greater than one per cent. Since this strain can be shown to increase rapidly with further increase in load, the fully plastic solution for small strains given by Equations [29] does not appear to be applicable for the present example. Therefore, in Fig. 5, the load, maximum stress, and maximum strain are plotted as functions of the radius of the inner boundary according to Equations [31] and [33] for the fully plastic slab. It will be observed that while the slab becomes fully plastic for $\lambda = 0.0034$ it can support a load $\lambda = 0.0085$ with sufficient plastic deformation. This is in marked contrast to the perfectly plastic slab which, in the present example, becomes fully plastic for $\lambda = 0.0033$ and can support no greater load.

Fig. 6 is derived from Figs. 4 and 5, and shows the circumferential stress and strain, respectively, at the inner boundary as functions of the load for the elastic, elastic-plastic, and fully plastic solutions. The discontinuity between the last two sections of the curve in each case is due to the change of assumptions between the two solutions. It is seen to be small in comparison with the other quantities involved.

[6] The elastic-plastic solution is given by Equations [32] of the previous paper,[4] and the fully plastic by Equations [39] through [46]. Note that the dimensionless stresses there were defined by dividing by twice the shear modulus $2G$, rather than Young's modulus $E$, and that $\mu$ was defined by $k/2G$. Since $E = 3G$ for an incompressible material, the results may be converted easily.

[7] The author wishes to thank Mr. R. K. Froyd for his assistance in the computations of this section.

# The Rate of Growth of Vapor Bubbles in Superheated Water[1]

By PAUL DERGARABEDIAN,[2] PASADENA, CALIF.

**Calculations are presented for the dynamic stability of vapor and air bubbles in superheated water. These calculations indicate that the values of the bubble radii for which the equilibrium is unstable are restricted to a finite range of radii whose values are governed by the temperature of the water and the initial air content in the bubble. Two theoretical solutions for the rate of growth of these unstable bubbles are considered: (*a*) Solution of the equation of motion of the bubble radius with the assumption that there is no heat diffusion across the bubble wall; (*b*) solution which includes the effect of heat diffusion. The two solutions differ appreciably. These two solutions are then compared with the experimental data on the growth of the vapor bubbles in superheated water. This comparison shows agreement with the solution with the effect of heat diffusion included.**

## Introduction

ONE of the important problems in the field of hydrodynamics today is the occurrence of cavitation in liquids. Cavitation is defined as the coexistence of a vapor or gas phase with the liquid phase. This vapor or gas phase first becomes evident in the form of bubbles distributed throughout the body of the liquid. Of practical significance is the increase in drag experienced by submerged bodies moving through a liquid when cavitation appears; similarly, pumps and turbines operate less efficiently in cavitating flow. The particular phase of the general field of cavitation presented in this paper is the problem of the dynamic stability and rate of growth of these vapor or gas bubbles.

Since the results in the present study are confined to the macroscopic behavior of the bubbles, it suffices to point out some of the present concepts concerning the initial formation of the bubble. The general view (1)[3] is that bubble formation in cavitating flow, or in boiling, begins from a nucleus within the liquid containing air, or vapor, or both. These gas-phase nuclei are ordinarily submicroscopic in size, and become evident upon the growth of the nuclei through a temperature rise in the liquid or a reduction in the external pressure acting on the liquid.

In dealing with multiple-phase systems the important role of surface phenomena must be considered in the processes involved. Thus in the case of these submicroscopic nuclei the very large forces of surface tension must be overcome to initiate cavitation or boiling. It is well known that degassed pure liquids can withstand very large tensions, or may be superheated considerably, without the formation of bubbles. This effect has been demonstrated by Harvey (2) and subsequently by Pease and Blinks (3). Harvey subjected samples of water saturated with air to pressures of the order of 10,000 psi for several minutes. In this manner the air nuclei are squeezed into solution so that when the solution is brought back to atmospheric pressure, it does not cavitate under the tensions which freely produced cavitation before the pressurization. These same pressure-treated air-water solutions also can be superheated by as much as 80 C without boiling.

For the case of ordinary untreated water the gas-phase nuclei may be stabilized on small solid particles. The presence of a solid, or third phase, is indicated since the surface energy of a bubble bounded by a solid surface and a liquid surface may be very low. Evidence for this condition can be found in the fact that the theoretical boiling point for pure water (4) is much higher than the values obtained by any experiment on superheating of water.

Since the macroscopic behavior of the bubbles formed in a boiling liquid may be considered as entirely analogous to cavitation bubbles, the experiments and calculations in this paper describe the rate of growth of vapor bubbles in superheated water. In the case of boiling liquids by an increase in temperature, the effects upon heat-transfer rates due to the vapor phase are of great interest. The experimental part of this paper is an analysis of high-speed photographs of the growth of vapor bubbles at various degrees of superheat. For the theoretical phase, calculations are presented on the dynamic stability of vapor and air bubbles in order to determine bubble radii for growth. In order to emphasize the important effect of cooling of the bubble wall during the growth, solutions of the equation of motion for the bubble radius are considered both with and without heat conduction across the bubble wall.

## Theoretical Formulation of Problem

Frequent reference is made in the literature on cavitation to Rayleigh's solution for the problem of the collapse of a spherical cavity in a liquid (5). For the present problem of the growth of a bubble the extension of the Rayleigh theory as carried out by Plesset (1) can be used to obtain the equation of motion. The resulting equation is

$$R\ddot{R} + \frac{3}{2}\dot{R}^2 = \frac{p_v - p_\infty + p_a - \dfrac{2\sigma}{R}}{\rho} \qquad [1]$$

where $\rho$ is the density of the fluid, $R$ is the radius of the bubble at any time $t$, $\dot{R} = dR/dt$, $p_v$ is the vapor pressure of the water at the appropriate temperature, $p_a$ is the partial pressure of air which may be in the bubble of radius $R$, $p_\infty$ is the atmospheric pressure, and $\sigma$ is the surface-tension constant for water.

If the assumption is made that the vapor pressure $p_v$ remains

---

[1] This work was supported by the Office of Naval Research under Contract N6onr-24420.

[2] Shell Fellow in Mechanical Engineering at the California Institute of Technology. Present address: U. S. Naval Ordnance Test Station, Pasadena, Calif.

[3] Numbers in parentheses refer to the Bibliography at the end of the paper.

Contributed by the Applied Mechanics Division and presented at the Semi-Annual Meeting, Los Angeles, Calif., June 28–July 2, 1953, of The American Society of Mechanical Engineers.

Discussion of this paper should be addressed to the Secretary, ASME, 29 West 39th Street, New York, N. Y., and will be accepted until January 11, 1954, for publication at a later date. Discussion received after the closing date will be returned.

Note: Statements and opinions advanced in papers are to be understood as individual expressions of their authors and not those of the Society. Manuscript received by ASME Applied Mechanics Division, February 11, 1953. Paper No. 53—SA-10.

constant throughout the growth of the bubble, then the bubble growth is isothermal and

$$p_a = p_{a0}\frac{R_0^3}{R^3} \quad [2]$$

where $p_{a0}$ is the initial pressure of the air in a bubble of radius $R_0$. Equation [2] implies that no air diffuses across the bubble boundary as it grows. Plesset and Epstein (6) have shown that the diffusion process for gas bubbles is so slow compared to the rate of growth of the bubble that it does not affect the air content of the bubble. Thus Equation [2] is a reasonable expression for the air pressure $p_a$ as a function of the bubble radius.

From Equation [1] it can be seen that the bubble is in dynamic equilibrium with the liquid if

$$f(R) = \delta p + p_{a0}\frac{R_0^3}{R^3} - \frac{2\sigma}{R} = 0$$

$$\dot{R} = 0 \quad [3]$$

where

$$\delta p = p_v - p_\infty, \quad R_0 = \frac{2\sigma}{\delta p + p_{a0}}$$

To determine whether the equilibrium of a bubble is dynamically stable or unstable, one may consider $df(R)/dR$ for the given radius. Then the condition $df(R)/dR < 0$ indicates dynamic stability whereas $df(R)/dR \geq 0$ is the condition for dynamic instability. Any bubble which is dynamically stable will dissolve through diffusion of air out of the bubble (6); hence the bubbles that need to be considered are the dynamically unstable ones. It is easily seen that the range of equilibrium radii for which $df(R)/dR \geq 0$ is given by

$$\frac{4\sigma}{3\delta p} \leq R_0 \leq \frac{2\sigma}{\delta p}$$

with

$$\frac{\delta p}{2} \geq p_{a0} \geq 0$$

The solution of Equation [1] is completed as follows: Multiplying by $R^3\dot{R}$ and integrating from $R_0$ to $R$, Equation [1] becomes

$$\dot{R}^3 = \frac{2}{3}\frac{\delta p}{\rho} - \frac{2\sigma}{\rho R} + 2\frac{p_{a0}}{\rho}\frac{R_0^3}{R^3}\log_e R + \frac{R_0^3\dot{R}_0^2 + \frac{2\sigma}{\rho}R_0^2 - \frac{2}{3}\frac{\delta p}{\rho}R_0^3 - 2\frac{p_{a0}}{\rho}R_0^3\log_e R_0}{R^3} \quad [4]$$

Thus

$$\dot{R}^2 \sim \frac{2}{3}\frac{\delta p}{\rho}, \quad R \to \infty$$

This means that the bubble radius approaches a linear increase with respect to time as $R \to \infty$ or

$$R \sim \sqrt{\frac{2}{3}\frac{\delta p}{\rho}}\,t, \quad R \to \infty$$

From Equation [4] it is evident that the terms in $\log_e R/R^3$ and $1/R^3$ become small quite rapidly. Physically, this means that the effect of air in a bubble can be important to initiate the growth of the bubble, but its effect upon the subsequent behavior of the bubble radius is negligible; furthermore, all of the initial conditions such as $R_0$ and $\dot{R}_0$ are involved in the $1/R^3$ term which also vanishes quite rapidly as $R \to \infty$.

The solution of present interest is the case where $p_{a0} = 0$. Thus Equation [1] becomes

$$R\ddot{R} + \frac{3}{2}\dot{R}^2 = \frac{\delta p - \frac{2\sigma}{R}}{\rho} \quad [5]$$

Setting the right-hand side equal to zero, one obtains the equilibrium radius which together with the condition $\dot{R}|_{R=R_0} = 0$ defines the initial equilibrium of the vapor bubble.

It is convenient to express Equation [5] in dimensionless form. This can be done by the substitutions

$$u = \frac{R}{R_0}, \quad \tau = \frac{t}{R_0}\sqrt{\frac{\delta p}{\rho}}, \quad \dot{u} = \frac{du}{d\tau}$$

Equation [5] then becomes

$$u\ddot{u} + \frac{3}{2}\dot{u}^2 = 1 - \frac{1}{u} \quad [6]$$

Multiplying Equation [6] by $u^3\dot{u}$ and integrating from $u_i$ to $u$, where $u_i$ is the dimensionless radius at some initial time of $\tau_i$, one gets

$$\dot{u}^2 = \frac{2}{3} - \frac{1}{u} + \frac{u_i^3\dot{u}_i^2 - \frac{2}{3}u_i^3 + u_i^2}{u^3} \quad [7]$$

where $\dot{u}_i$ is the velocity of the bubble wall for $\tau = \tau_i$. Let $C = u_i^3\dot{u}_i^2 - 2/3\,u_i^3 + u_i^2$, where $C$ is a constant taking on various values depending upon the values chosen for $u_i$ and $\dot{u}_i$. Fig. 1 shows a plot of

$$\dot{u} = \pm\sqrt{\frac{2}{3} - \frac{1}{u} + \frac{C}{u^3}} \quad [8]$$

for various values of $C$. The significance of the graph is as follows: The choice of a point $(u, \dot{u})$ on the graph as an initial value determines the value of $C$ and hence prescribes the subsequent behavior of the bubble radius as governed by Equation [8].

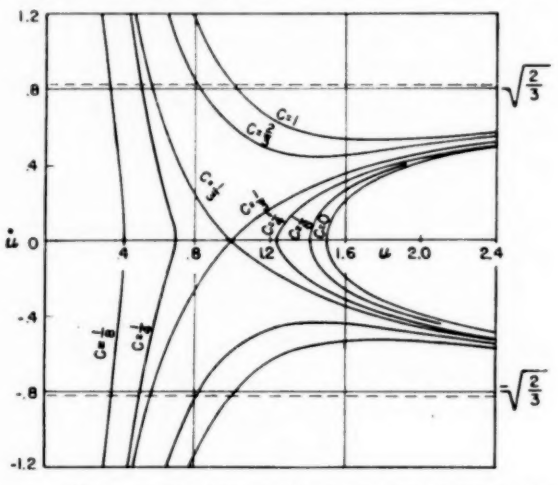


FIG. 1 DIMENSIONLESS VELOCITY $\dot{u}$ FOR VARIOUS VALUES OF $C$ IS SHOWN AS A FUNCTION OF DIMENSIONLESS RADIUS $u$ AS EXPRESSED BY EQUATION [8]

Thus a value of $u_s < 1$ with $u_s = 0$ means that the bubble will collapse, or a value of $u_s > 1$ with $u_s = 0$ means that the bubble will grow. The point $u_s = 1$, $u_s = 0$ is a singular point since a bubble in this state remains in equilibrium, or loosely speaking, it takes an infinite time for the bubble to increase or decrease in size. However, this equilibrium is dynamically unstable. In the actual physical case such an equilibrium would soon be upset by a slight change in temperature. Taking the positive root of Equation [8] and integrating, one gets

$$\tau - \tau_i = \int_{u_i}^{u} \frac{dx}{\sqrt{\frac{2}{3} - \frac{1}{x} + \frac{C}{x^2}}}$$

With the change in variable $y = 1/x$, the integral becomes

$$\tau - \tau_i = \int_{1/u_i}^{1/u} \frac{dy}{y^2\sqrt{\frac{2}{3} - y + Cy^2}} \quad \ldots\ldots [9]$$

The integral in Equation [9] is an elliptic integral except when $C = 1/3$ and 0. For the case $C = 1/3$, Equation [9] can be expressed as

$$\tau - \tau_i = \sqrt{3}\int_{1/u_i}^{1/u} \frac{dy}{y^2(y-1)\sqrt{y+2}} \quad \ldots\ldots [10]$$

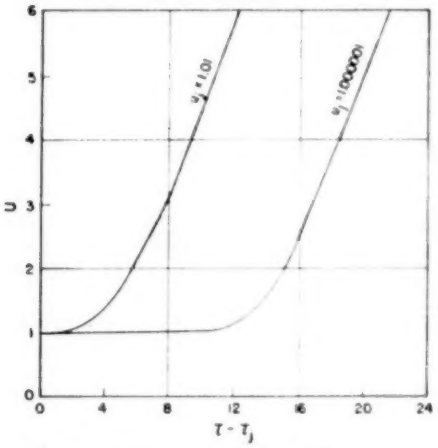


FIG. 2 DIMENSIONLESS BUBBLE RADIUS $u$ IS SHOWN FOR TWO INITIAL VALUES OF BUBBLE RADIUS $u_i$ CORRESPONDING TO TIME $\tau_i$ AS A FUNCTION OF DIMENSIONLESS TIME $\tau - \tau_i$ AS EXPRESSED BY EQUATION [11]

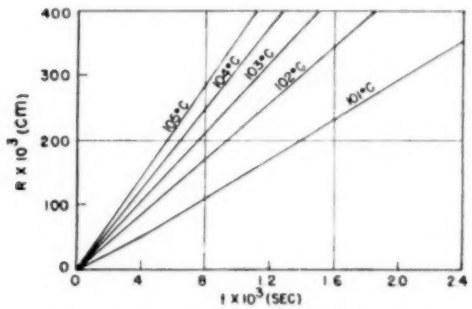


FIG. 3(a) ACTUAL RADIUS $R$ OF BUBBLE IS SHOWN FOR VARIOUS VALUES OF WATER TEMPERATURE $T$ AS A FUNCTION OF THE TIME $t$, AS OBTAINED FROM EQUATION [11]

This corresponds to the case $u_s = 1$, $u_s = 0$, in the expression for $C$. The limit here must be $1/u_i < 1/u_s$ and $\tau_i > \tau_s$, since a limit of $1/u_s = 1$ means that the integral becomes infinite or the bubble does not grow. The choice of a value $u_i > 1$ automatically starts the bubble along the trajectory for $C = 1/3$ at some value $u_i$ and $\dot{u}_i \neq 0$. The closer one picks $u_i$ to 1, the longer it will take the bubble to grow. The integration of Equation [10] is carried out readily by a separation of the integrand into partial fractions resulting in the following relation between $\tau$ and $u$

$$\tau - \tau_i = \frac{u}{2}\sqrt{\frac{3}{u} + 6} - \frac{u_i}{2}\sqrt{\frac{3}{u_i} + 6} + \frac{3}{4}\sqrt{\frac{3}{2}}\log_e\left[\frac{\frac{u}{2}\sqrt{\frac{3}{u} + 6} + \sqrt{\frac{3}{2}\left(u + \frac{1}{4}\right)}}{\frac{u_i}{2}\sqrt{\frac{3}{u_i} + 6} + \sqrt{\frac{3}{2}\left(u_i + \frac{1}{4}\right)}}\right] - \log_e\left\{\left(\frac{u_i - 1}{u - 1}\right)\left[\frac{\frac{u}{2}\sqrt{\frac{3}{u} + 6} + \frac{5}{4}\left(u + \frac{1}{5}\right)}{\frac{u_i}{2}\sqrt{\frac{3}{u_i} + 6} + \frac{5}{4}\left(u_i + \frac{1}{5}\right)}\right]\right\} \quad \ldots [11]$$

Fig. 2 is a plot of $\tau$ as a function of $u$ as expressed by Equation [11] for $u_i = 1.01$ and $u_i = 1.000001$ and shows the effect of taking $u_i$ close to $u_s = 1$. Figs. 3(a) and 3(b) are plots of the actual radius $R$, as a function of the time $t$, for various liquid temperatures using Equation [11].

The assumption has been made that the vapor pressure has a constant value throughout the growth of the bubble. However, evaporation is a process which proceeds at a finite rate and if this rate is not sufficiently high to keep up with the rate of volume

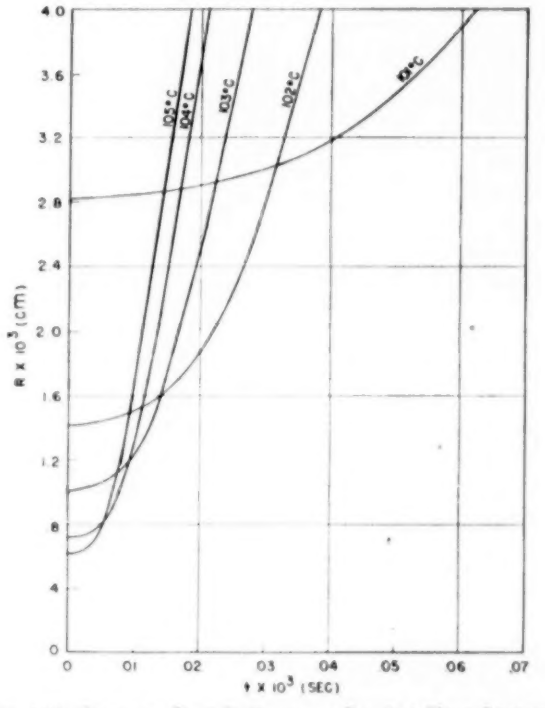


FIG. 3(b) DETAILED PLOT IS SHOWN OF FIG. 3(a) NEAR REGION $R = 0$, $t = 0$

change in the bubble, the vapor in the bubble will behave more like a permanent gas. Plesset tested this assumption for the case of a cavitation bubble (1) with an estimate of evaporation rates based on kinetic theory. Applying a similar analysis here, it turns out that the assumption of $p_v$ constant, as far as evaporation rates are concerned, is a reasonable one.

The problem up to this point has been to assume that the bubble expands isothermally; that is, the vapor pressure has been assumed to remain constant throughout the expansion process, having a value corresponding to the bulk temperature of the water. Now this assumption is nearly correct if one thinks of this in terms of the actual variation in the vapor pressure as compared to the absolute initial value of the vapor pressure. However, in terms of the mechanism of bubble growth the variation in vapor pressure has a marked effect on the rate of growth. Heat must be supplied to the bubble to evaporate water and maintain the vapor pressure during growth. This heat is taken out of a water layer surrounding the bubble. Thus the problem as formulated by Plesset and Zwick (7) is to consider the problem of nonsteady heat diffusion which is encountered in dealing with the dynamics of a vapor bubble in a heated liquid. From this problem one obtains the variation of the temperature at the bubble wall as a function of time.

The diffusion problem is solved assuming that the thermal boundary layer is very thin compared to the bubble radius. For the case of the vapor bubble in a liquid, this assumption is made plausible by the fact that not only is the heat capacity much greater in the liquid state than in the vapor state but the thermal diffusivity is about 1000 times smaller. Thus the zeroth-order approximation for the difference between the temperature at the spherical boundary $T(0, t)$, and the initial temperature of the liquid $T_0$ is given by (7)

$$T(0,t) - T_0 = \frac{D}{K}\eta(t) - \left(\frac{D}{\pi}\right)^{1/2} \times \int_0^t \frac{R^2(x)\left(\frac{\partial T}{\partial r}\right)_{r=R(x)}}{\left[\int_x^t R^4(y)\,dy\right]^{1/2}} dx \quad [12]$$

where $D$ is the thermal diffusivity of the liquid, $K$ is the thermal conductivity of the liquid, and $\eta(t)$ is the heat source per unit volume in the liquid. For the specific case of the vapor bubble, Equation [12] can be written as

$$T(0,t) - T_0 = \frac{D}{K}\eta(t) - \frac{L}{C\sqrt{\pi D}}\frac{\rho'}{\rho}\int_0^t \frac{R^2(x)\dot{R}(x)}{\left[\int_x^t R^4(y)\,dy\right]^{1/2}} dx$$

where $L$ is the latent heat of evaporation of the liquid and $C$ is its specific heat with $\rho'$ being the vapor density, and $\rho$ the liquid density. For the present problem the vapor pressure can be expressed as

$$p_v(T) = p_v(T_0) + A\,[T(0,t) - T_0] + B\,[T(0,t) - T_0]^2$$

Thus the equation of motion becomes

$$R\ddot{R} + \frac{3}{2}\dot{R}^2 = \frac{p_v(t) - p_\infty - \frac{2\sigma}{R}}{\rho}$$

This problem has been solved by Plesset and Zwick (8).

A plot of the radius $R$, as a function of the time $t$, is shown in Fig. 4 for a temperature of 103.05 C for the Plesset-Zwick theory and is compared to the solution obtained with the extended

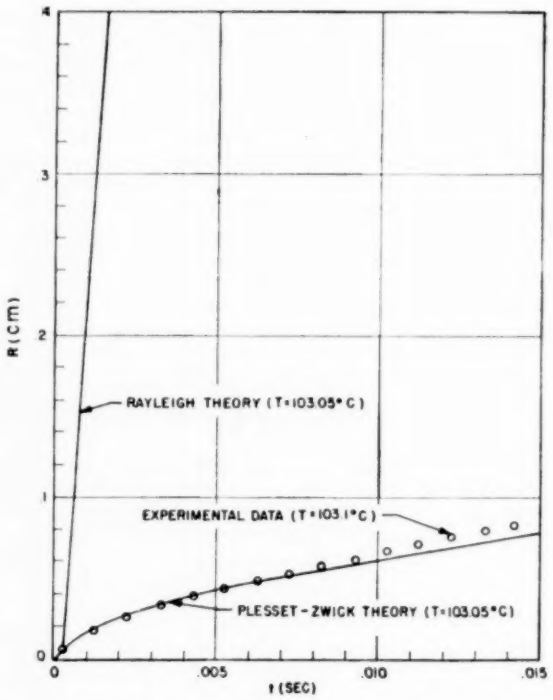


FIG. 4 BUBBLE RADIUS IS SHOWN AS A FUNCTION OF TIME FOR TEMPERATURE OF 103.1 C AS OBTAINED FROM EXPERIMENTAL DATA (BUBBLE NO. 7), THE RAYLEIGH THEORY, AND THE PLESSET-ZWICK THEORY

Rayleigh theory for the same temperature. The marked effect that the cooling of the bubble wall has on reducing the rate of growth is apparent. Thus the Rayleigh theory predicts that the bubble approaches a linear rate of growth as the radius increases, the rate being $\dot{R} = \sqrt{2\delta p/3\rho}$, whereas the Plesset-Zwick theory predicts that as the bubble grows the cooling of the bubble wall due to evaporation of the vapor results in the vapor pressure $p_v$ approaching the value of the atmospheric pressure $p_\infty$, or $\delta p \to 0$ as $R \to \infty$; hence $\dot{R} \to 0$. Consequently a cooling of, say, 2 C may be small compared to 102 C, but in terms of the 2 C of superheat corresponding to the value of $\delta p$, this cooling results in $\delta p \to 0$. Since the driving force for the bubble growth is produced by $\delta p$, its variation has a pronounced effect upon the rate of growth.

## APPARATUS AND PROCEDURE

The requirements for obtaining vapor-bubble formation within the body of the liquid at various degrees of superheat are apparent in theory, but the actual realization of such a condition requires a variation in the usual means for boiling water. The requirements are that the liquid must be heated slowly and uniformly, and the walls of the container of the liquid must not be subjected to temperatures so great that a very large thermal gradient exists within a very narrow boundary adjacent to the walls. In addition, these surfaces must be clean and free of pits or scratches. In the case of such gradients all of the bubbles form either within this layer or actually form on the solid surfaces of the container. Thus in the case of heating a beaker of water with a Bunsen burner most of the bubbles form at the bottom of the beaker and quickly rise out of the thermal layer and intermix with the main

body of the liquid. In this way one has a condition closely approximating the dynamic equilibrium of many large bubbles in the body of the liquid. This condition is realized by the fact that as the bubbles grow they rise into the cooler regions of the liquid above the thermal boundary layer, and their rates of growth are decreased to a point where the bubble can be assumed to be in dynamic equilibrium with the liquid. Since these bubbles are very large, the effects of surface tension are negligible; hence the vapor pressure inside the bubble is very nearly equal to the external pressure on the liquid, which for water heated in a beaker in the laboratory is essentially the atmospheric pressure. Thus the temperature of the boiling water will be very close to that corresponding to the vapor pressure being equal to the atmospheric pressure. For the case of one normal atmosphere of pressure, this temperature will be 100 C.

In order to heat the water uniformly the following procedure was used: A beaker was constructed from pyrex tube stock $2^1/_2$ in. diam. The tube was cut into a 6-in. length and a beaker was formed from the tube with a flat face $1^1/_4$ in. wide and 6 in. high. This was done for photographic purposes. The beaker was annealed carefully to make the inner surface very smooth and free from pits. It was cleaned before each experiment with a detergent to remove any oil films present on the surface. The water used in the tests was doubly distilled, and for some of the tests was contaminated with solid impurities such as powdered chalk or sand to produce various degrees of superheat. The water was first boiled in a large container for about 1 hr to remove most of the air in the water. Water boiled in this way contains about 20 per cent of the initial air content. This was not done in the beaker since too much water would evaporate from the test sample. The container with water thus treated was heated by two 250-watt reflector-type infrared lamps with the beaker located between the lamps.

Fig. 5 shows the arrangement of lamps and beaker. In this way 300 cc of water can be brought to the boiling point in about 10 min. Attempts at obtaining vapor bubbles in the body of the liquid with this technique were completely successful and yielded superheat temperatures up to 107 C.

The reasons for the success of this method can be indicated by considering the nature of the radiation of the infrared lamps and the absorption of this radiation by the beaker and the water. The infrared lamp is rated at 250 watts for a line voltage of 115 volts. Under these conditions the tungsten-filament temperature is 2500 K. Since the lamp radiates nearly as a black body, according to factory specifications, Wien's displacement law can be used to obtain the wave length corresponding to the maximum energy output. Thus for 2500 K, $\lambda_{max} = 1.16\mu$ ($\mu = 10^{-4}$ cm). The distribution corresponding to this temperature shows that approximately 3 per cent of the radiant energy lies between $0.4\mu$ to $0.7\mu$ (visible light region). Since the tungsten filament is enclosed by a pyrex bulb, a certain amount of the radiation is absorbed by the bulb itself. Now pyrex is essentially transparent to radiation from $0.3\mu$ to $3\mu$, but beyond $3\mu$ a sheet of pyrex 2 mm thick absorbs nearly all the radiation. This accounts for about 17 per cent of the total radiated energy originating from the tungsten filament. Thus approximately 80 per cent of the total radiated power is available for heating over a wave band from $0.7\mu$ to $3\mu$. Since the beaker itself is pyrex about 2 mm thick, it will transmit most of the radiation transmitted by the bulb itself. Thus one attains the desired effect of not having the beaker at higher temperatures than the main body of water. The water itself is an excellent absorber of infrared radiation (9) especially from $0.97\mu$ up to $3\mu$ which is 68 per cent of the total radiated energy. For example, a layer of water 1 cm thick absorbs 38 per cent of the radiation of $\lambda = 1\mu$ and 95 per cent of

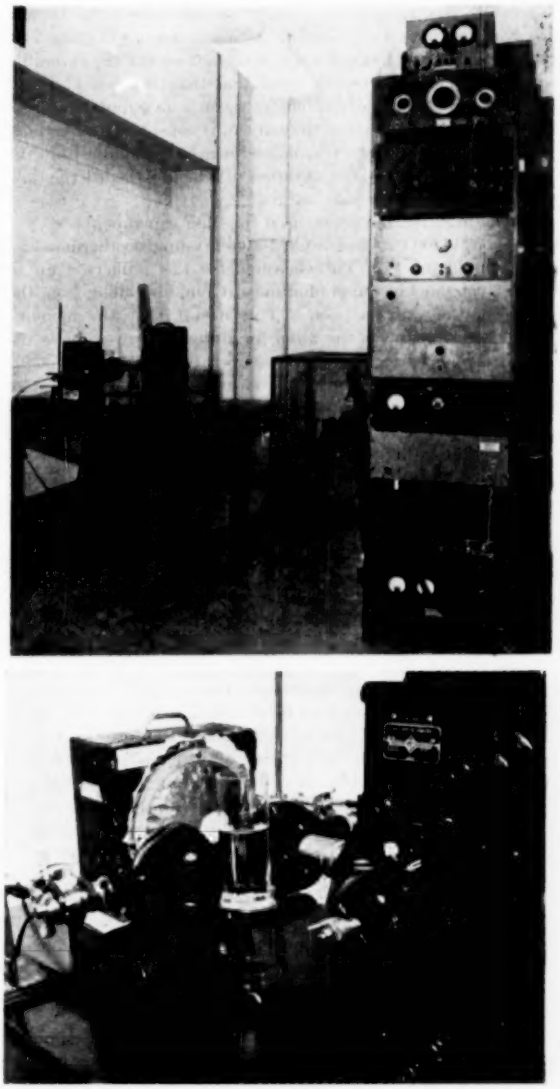

FIG. 5 UPPER FIGURE SHOWS ENTIRE EXPERIMENTAL SETUP OF ELECTRONIC EQUIPMENT, HEAT LAMPS, CAMERA, AND WATER BEAKER; LOWER VIEW IS CLOSEUP OF CAMERA, BEAKER, HEAT LAMPS, AND FLASH LAMP

that at $\lambda = 1.4\mu$ and essentially all the radiation is absorbed in this layer for values of $\lambda > 1.4\mu$. The remaining 12 per cent of the total radiation from $0.7\mu$ to $0.97\mu$ is also absorbed but to a lesser extent. The fact that the water is heated very slowly means that the slight thermal gradients existing in the liquid are removed by heat conduction. Thus the temperature of the liquid is raised essentially in a uniform fashion. This is borne out by temperature measurements throughout the bulk of the liquid.

The selection of the temperature-measuring device was controlled primarily by the necessity for having an instrument which could be placed in the water without having bubbles form from the device, since this would eliminate the possibility of having the bubbles form in the body of the liquid. With this restriction, a

mercury-in-glass thermometer was chosen since the bulbs of most thermometers have a very smooth surface as a result of annealing, and hence provide, in most cases, a surface even more favorable to the prevention of bubble formation than the beaker itself. The thermal lag of the thermometer was not an important factor for these experiments since the only runs considered were those for which the temperature remained nearly constant within 0.1 C during a given test, the duration of which exceeded the time of any thermal lag by a wide margin.

The actual thermometer used in the experiments was a Braun 100 C–200 C nitrogen-filled mercury-in-glass thermometer graduated in 0.1 C. The thermometer was immersed up to a point just short of the graduations to avoid bubbling from the etched portions of the stem. This meant that the mercury column extended out of the water for all temperatures above 100 C, and thus a correction to the temperature reading would be necessary. Using the correction formula from the Bureau of Standards (10) the maximum correction found necessary was approximately 0.005 C. Since this is negligible in terms of 0.1 C accuracy, this correction was neglected.

Another factor affecting the true temperature reading was the fact that the thermometer was not shielded from the effects of radiation. In the discussion on heating water it was shown that the band of infrared radiation from $0.7\mu$ to $0.97\mu$ is the least absorbed by the water, and hence this portion of the radiant energy (12 per cent of the total) is incident upon the thermometer. It should be pointed out that the thermometer was at all times about 2 cm from the walls of the beaker. Thus a layer of 2 cm of water was available for the actual absorption of the radiant energy. The bulb of the thermometer is essentially transparent to the range of radiation from $0.7\mu$ to $0.97\mu$ and the mercury in the bulb is a good reflector of radiation and absorbs very little radiation. Thus it could be said that the water acts as a radiation shield for the thermometer, and the radiation effect on the true temperature reading is negligible in terms of the accuracies in the present measurements. To test this, a shield was made of aluminum tubing for the thermometer. The temperature reading for a thermometer without the shield was compared with the reading of the shielded thermometer and the result was that the two simultaneous readings never varied more than 0.1 C. The temperature variation throughout the bulk of the liquid was checked after the water had reached a state of boiling, and the variations were found to be much smaller than 0.1 C. The accuracy of this type of thermometer is within ±0.1 C. Thus considering the two largest errors, namely, the accuracy of the thermometer and the variation in the temperature during a test, the temperature readings obtained are assumed accurate within 0.2 C.

The photographic equipment used in this study was of the multiflash type. It consisted of a simple camera in which the recording film moves constantly past the focal plane at a high speed. The camera has no shutter; hence the illumination which was provided by a flash lamp also acted as the shutter. This required that the flash duration be so short that neither the image of the object on the film nor the film itself move an appreciable distance while the light was on. For the present experiments pictures were taken at a rate of 1000 exposures per sec. This rate was found fast enough to record the growth of a vapor bubble and still give a normal-sized 35-mm picture. The camera itself was the standard General Radio type of instrument as shown in Fig. 5, fitted with an f 1.5 Kodak Ektar 2-in. lens. The film used was Eastman 35-mm Background X and was run through the camera at an average rate of 100 fps. The flash lamps used were of the type originally developed by Prof. Harold E. Edgerton and his associates at the Massachusetts Institute of Technology.

Since there is no practical way of knowing just where or when a bubble will form, the chances of catching a bubble on a strip of film 50 ft long which runs through the camera in about $^1/_2$ sec is very small and depends on the area of view and the depth of focus. Thus the choice of magnification depends upon the following factors: It is desirable to have great magnifications since the detail in the pictures of small bubbles will be clearer. However, a factor of 2 in the picture size of the radius of the bubble diminishes the area of view by a factor of 4 and reduces the depth of focus. It was found that magnifications from ×0.5 to ×4 were practical in the sense of the amount of film used and the time involved to obtain a bubble history. This difficulty was coupled with the fact, that, if during a run the temperature variation was too great, even a successful bubble history from the photographic viewpoint was useless in terms of usable data for the rate of growth. The over-all efficiency of this method was to obtain a usable bubble history per 150 ft of film.

With a magnification of ×1 the depth of focus was about $^1/_8$ in. The magnification was determined by placing a scale in the water and focusing on a piece of film in the camera. Thus any bubble in focus could be assumed to have the appropriate magnification corresponding to the setting of the camera since the depth of focus was so small. All of the bubble diameters were measured directly from the negative with a microscopic comparator. Each bubble was measured three times and the average value was taken. The actual measurements of the bubble diameters are estimated to be correct within 3 per cent using this technique.

## Analysis of Data and Theory

Since the bubbles rise through the liquid as they grow, they cannot be called spherical bubbles in the strict sense of the word. As the bubbles rise they tend to assume a shape similar to an oblate spheroid. This effect is very slight during the first part of the growth because the translational motion is very slow compared to the rate of growth of the bubble. During the latter part of the growth the translational effect is very great compared to the rate of growth, and essentially determines the shape of the bubble. Thus for the case of a bubble, the net result is that the dimension of the bubble is reduced in the direction of motion and increased at right angles to the motion. However, the bubble dimensions measured from the negatives were restricted to bubbles occurring during the first part of the growth. Thus the diameter measured in the horizontal plane does not exceed the diameter in the vertical plane by more than 3 per cent (the horizontal measurement was used for the data). The effect of translation on the conduction of heat is not known precisely but presumably is not very large in the present situation. The amount of translation in the bubble histories is less than twice the diameter of the first bubble measured. This can be seen from Fig. 6 which shows an actual bubble history.

The effects of the walls of the container and the proximity of other bubbles were neglected since these distances were large compared to the bubble sizes considered and thus their effects on the bubble growth are probably less than the uncertainty of the data.

Since the time between each picture is 0.001 sec, there is an uncertainty in the exact time when the bubble starts to grow from the dynamic equilibrium radius. Thus this time lies between the first visible bubble picture and the frame showing no bubble. Hence one is free to shift the time axis for any bubble history up to the amount of 0.001 sec. This allows one, when comparing bubble histories at a given temperature, to shift the point on the graph ±0.001 sec in time to obtain the best fit. In a sense this uncertainty helps in making the comparisons of

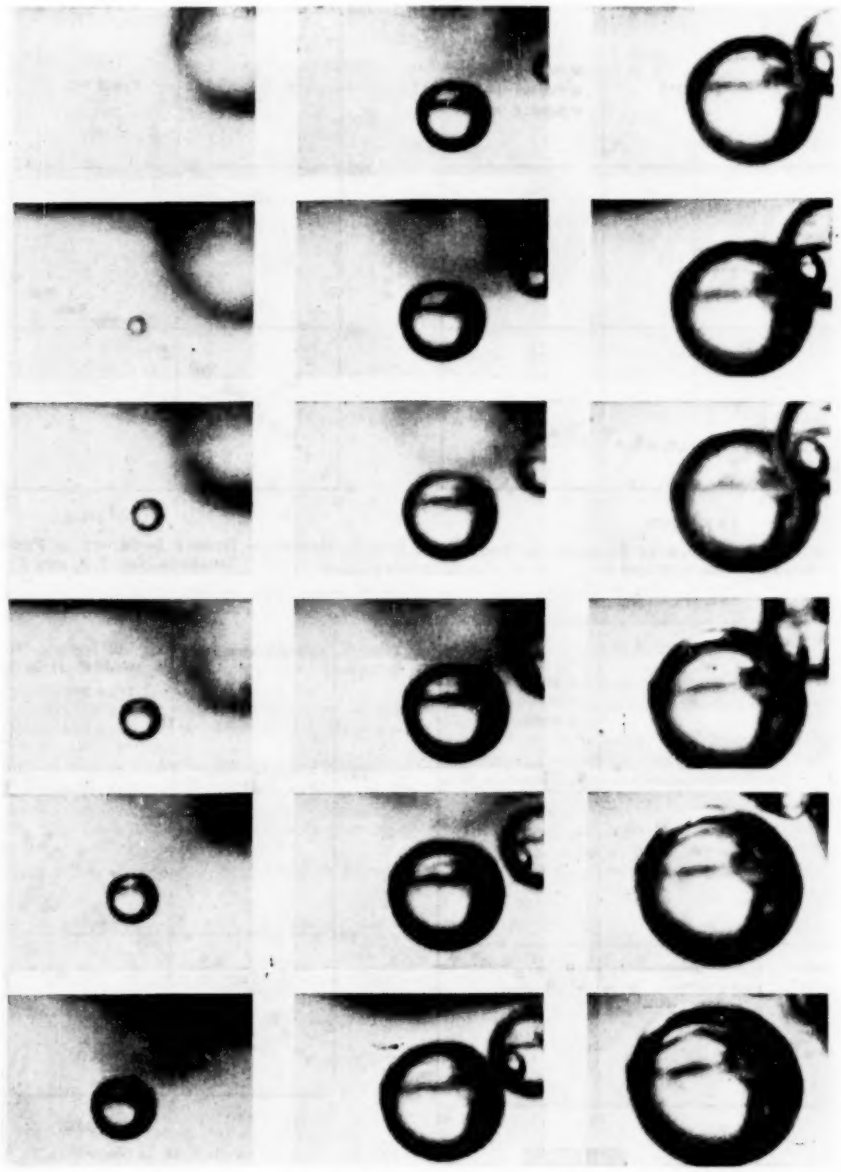

FIG. 6. PHOTOGRAPHIC HISTORY OF RATE OF GROWTH OF BUBBLE NO. 9 ($T$ = 103.1 C).
(Time interval between successive pictures is 0.001 sec.)

several bubble histories seem better than they actually may be. However, this does not alter the actual slopes of the radius-time curves.

Since the temperature measurements are estimated to be accurate within 0.2 C, the corresponding accuracy of the vapor pressure is required. As an example, the thermal rate of variation of the vapor pressure for the temperature range of 100 C to 105 C is approximately $4 \times 10^4$ dynes/cm² C or for 0.2 C this gives an error of $8 \times 10^3$ dynes/cm². Now this error is very small when compared to vapor pressures of the order of $10^6$ dynes/cm² for the temperature range of interest. However, in terms of $\delta p = p_\infty - p_\infty$, which is really the important factor for bubble growth, the order of magnitude is $10^3$ dynes/cm². Therefore the error in $\delta p$ caused by an error of 0.2 C in the thermometer reading is approximately 8 per cent. Since the bubble velocities are roughly proportional to $\sqrt{\delta p/\rho}$, the errors in the general slopes of the radius-time curves obtained from the data should be in error by about 4 per cent from temperature errors alone. This error together with the errors in the negative measurements yields an estimated over-all error in the bubble radii of 10 per cent.

Several bubble histories were obtained for five different temperatures. In some cases all the bubbles for a given temperature were obtained during one run, and for others the histories were

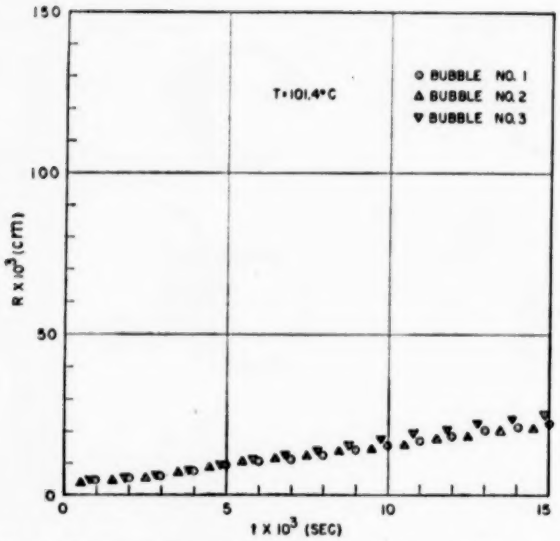


FIG. 7 RADIUS OF BUBBLE IS SHOWN AS FUNCTION OF TIME FOR BUBBLES NOS. 1, 2, AND 3

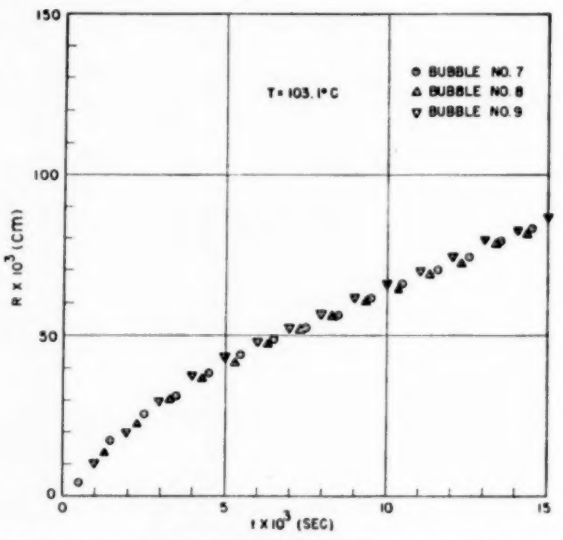


FIG. 9 RADIUS OF BUBBLE IS SHOWN AS FUNCTION OF TIME FOR BUBBLES NOS. 7, 8, AND 9

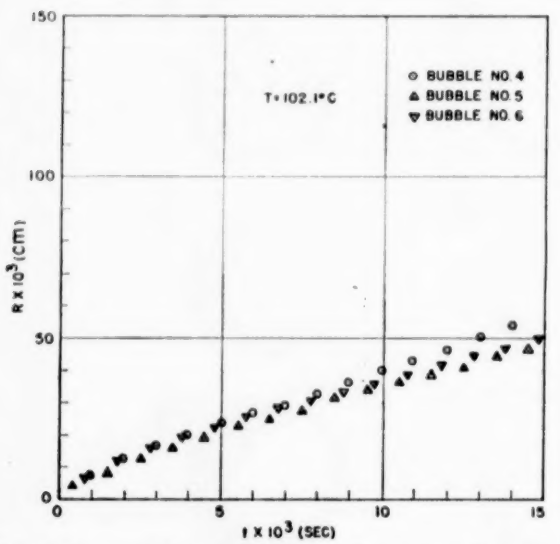


FIG. 8 RADIUS OF BUBBLE IS SHOWN AS FUNCTION OF TIME FOR BUBBLES NOS. 4, 5, AND 6

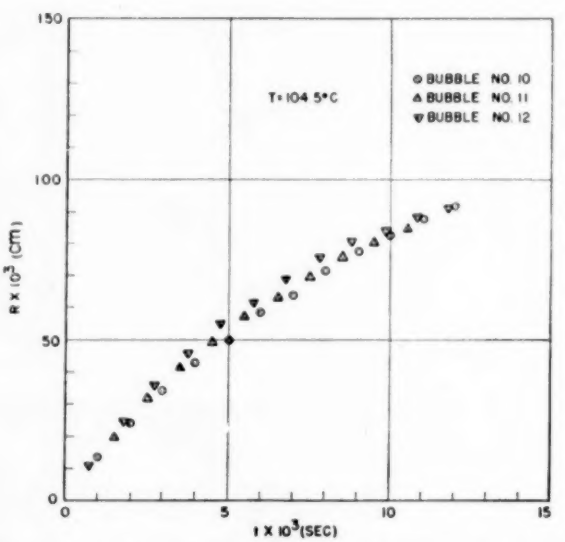


FIG. 10 RADIUS OF BUBBLE IS SHOWN AS FUNCTION OF TIME FOR BUBBLES NOS. 10, 11, AND 12

obtained from independent runs. Thus bubbles Nos. 1 and 3 are from one reel and bubble No. 2 from another reel, Fig. 7. Bubbles Nos. 5 and 6 are from one reel and bubble No. 4 is from another reel, Fig. 8. Bubbles Nos. 7, 8, and 9 are from separate reels, Fig. 9. Bubbles Nos. 11 and 12 are from one reel and bubble No. 10 is from another reel, Fig. 10. Bubbles Nos. 13 and 14 are from the same reel, Fig. 11. For bubble No. 13 two points are missing because the film was blacked out for these two points.

Fig. 4 shows a comparison between the extended Rayleigh theory and the Plesset-Zwick theory with bubble No. 7. From the figure it can be seen that the effect of cooling of the bubble wall has a great effect on the rate of growth. The data follow the Plesset-Zwick theory very closely as compared to the Rayleigh theory. Thus the cooling of the bubble wall affects the dynamics of the bubble growth to a marked extent.

ACKNOWLEDGMENT

The author wishes to thank Prof. Milton S. Plesset for suggesting the investigation of the problem, and Dr. Albert T. Ellis for technical aid in setting up the high-speed photographic system. The support of the Shell Fellowship Committee is gratefully acknowledged.

BIBLIOGRAPHY

1 "The Dynamics of Cavitation Bubbles," by M. S. Plesset, JOURNAL OF APPLIED MECHANICS, Trans. ASME, vol. 71, 1949, p. 277.

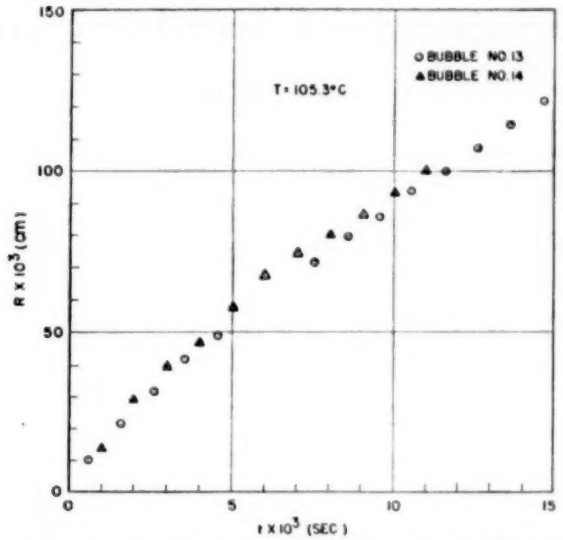


FIG. 11 RADIUS OF BUBBLE IS SHOWN AS FUNCTION OF TIME FOR BUBBLES NOS. 13 AND 14
(The two points missing for bubble No. 13 were the result of faulty negatives.)

2 "On Cavity Formation in Water," by E. Newton Harvey, W. D. McElroy, and A. H. Whitely, *Journal of Applied Physics*, vol. 18, 1947, p. 162.

3 "Cavitation From Solid Surfaces in the Absence of Gas Nuclei," by D. C. Pease and L. R. Blinks, *Journal of Physical and Colloid Chemistry*, vol. 51, 1947, p. 556.

4 "Kinetic Theory of Liquids," by J. Frenkel, Oxford University Press, New York, N. Y., and London, England, 1946, p. 372.

5 "On the Pressure Developed in a Liquid During the Collapse of a Spherical Cavity," by Lord Rayleigh, *Philosophical Magazine*, vol. 34, 1917, pp. 94–98.

6 "On the Stability of Gas Bubbles in Liquid-Gas Solutions," by M. S. Plesset and P. S. Epstein, *Journal of Chemical Physics*, vol. 18, 1950, p. 1505.

7 "A Nonsteady Heat Diffusion Problem With Spherical Symmetry," by M. S. Plesset and S. A. Zwick, *Journal of Applied Physics*, vol. 23, 1952, p. 95.

8 To be published, by M. S. Plesset and S. A. Zwick, California Institute of Technology, Pasadena, Calif.

9 "Properties of Ordinary Water Substances," by N. E. Dorsey, Reinhold Publishing Corporation, New York, N. Y., 1940, table 160, p. 326.

10 "Temperature—Its Measurement and Control in Science and Industry," by Johanna Busse, American Institute of Physics, Reinhold Publishing Corporation, New York, N. Y., 1941, p. 237.

# On Reinforced Circular Cutouts[1]

By E. LEVIN,[2] LOS ANGELES, CALIF.

**A slab with a circular cutout is subjected to stresses in the plane of the slab. The cutout has removed material which would have participated in carrying the load; hence the slab with cutout will fail under the application of stresses which the complete slab could have supported. In order to eliminate at least part of this weakening, the slab with cutout may be reinforced by the addition of material about the cutout. Such a reinforcement may be designed in any shape. The paper is concerned with extending the results of Weiss, Prager, and Hodge (1)[3] for a cylindrical reinforcement to a reinforcement of arbitrary shape. In particular, a method will be described for the determination of a lower bound on the collapse load for a slab with circular cutout and a general reinforcement.**

## 1 Introduction

CONSIDER a uniform plane rectangular slab with a centered circular cutout of radius $a$. The cutout is reinforced by additional material extending to a radius $a + \delta$, and the contour of the reinforcement is prescribed, Fig. 1. The slab is subjected to arbitrary uniform tensions along its outer edges and the inner edge is stress-free.

This paper is concerned with the determination of a lower bound on the maximum safe load. In the next section the physical assumptions made in discussing the problem will be stated, and a precise mathematical problem formulated. In particular, a domain of safe loads will be defined. The third section is concerned with the problem of equal biaxial tensions. The next three sections discuss a reinforcement whose cross section is symmetric about both axes through its center and whose boundary in the first quadrant is monotonically nonincreasing. Some general results are established and it is shown that the cylindrical reinforcement, which was first solved by Weiss, Prager, and Hodge (1), appears as a special case. The general results also are applied to a quasi-toroidal reinforcement. A method for obtaining a lower bound when the reinforcing contour is not symmetric is illustrated in Section 7 with a beveled reinforcement. The table in Section 8 represents a comparison of the reinforcements considered. Limitations and conclusions concerning the results are presented in Section 9.

## 2 Statement of Problem

The analysis will be based on a limit theorem of Drucker, Prager, and Greenberg (2) which is concerned with the determination of a lower bound on the collapse load. The collapse load is defined as the smallest load for which infinitesimal deformations can occur without further increment of load, neglecting geometry changes. In practice, this is essentially the observed load for which a small increment first produces large deformations. A safe load is any load less than the collapse load. The theorem then states that a given system of loads is safe if stresses can be found which (*a*) are in equilibrium with the given loads; and (*b*) do nowhere exceed the limits set by the yield criterion. The slab and the reinforcement are assumed to be of a uniform perfectly plastic material which satisfies Tresca's yield criterion (3).

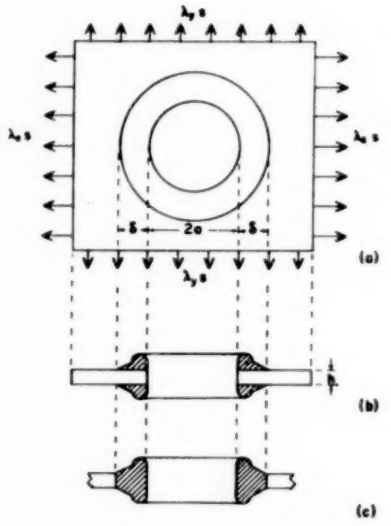


Fig. 1 Plane Slab With Reinforced Cutout
(*a*, Plan view; *b*, Transverse section; *c*, "Hub" and slab.)

Following Weiss, Prager, and Hodge (1), the reinforced slab will be regarded as consisting of a uniform part under conditions of plane stress, and a hub which behaves as a curved beam, Fig. 1(*c*). Let the applied tractions on the outer edge of the slab be $\lambda_x s$ and $\lambda_y s$, where $s$ is the yield strength of the material in simple tension, and it is assumed that the applied loads would be safe if there were no cutout. It follows that in the uniform part of the slab, the homogeneous state of stress $\sigma_x = s\lambda_x$, $\sigma_y = s\lambda_y$, $\tau_{xy} = 0$ satisfies the two conditions of the Drucker, Greenberg, Prager theorem, and transmits total loads of intensities $hs\lambda_x$, $hs\lambda_y$ per unit length to the hub. The problem, then, is to find values of $\lambda_x, \lambda_y$ which lead to a safe stress distribution in the hub.

Previously it has been shown (1, 4) that the safe states of loading for the uniform slab without cutout may be represented by the points on and inside a hexagon, and that any such safe state can be obtained from the stress-free state, the state of uniaxial tension and the state of biaxial tension, by the following operations:

(*a*) If $T_x$, $T_y$ is a safe load, then $-T_x$, $-T_y$ is also a safe load.

(*b*) If $T_x'$, $T_y'$ and $T_x''$, $T_y''$ are safe loads, then $\mu T_x' + (1 - \mu)T_x''$, $\mu T_y' + (1 - \mu)T_y''$ is a safe load for any $0 \leq \mu \leq 1$.

For the reinforced cut slab, the "domain of safe loads" will be

---

[1] The results presented in this paper were obtained in the course of research conducted under Contract N7onr-35810 between the Office of Naval Research and Brown University.

[2] Graduate Student, University of California, Los Angeles.

[3] Numbers in parentheses refer to the Bibliography at the end of the paper.

Contributed by the Applied Mechanics Division and presented at the Semi-Annual Meeting, Los Angeles, Calif., June 28–July 2, 1953, of The American Society of Mechanical Engineers.

Discussion of this paper should be addressed to the Secretary, ASME, 29 West 39th Street, New York, N. Y., and will be accepted until January 11, 1954, for publication at a later date. Discussion received after the closing date will be returned.

Note: Statements and opinions advanced in papers are to be understood as individual expressions of their authors and not those of the Society. Manuscript received by ASME Applied Mechanics Division, January 16, 1953. Paper No. 53—SA-11.

defined as the largest hexagon which may be obtained from the stress-free, uniaxial, and biaxial states by these operations. Hence the problem of determining the domain of safe loads is reduced to the problems of finding lower bounds for $\lambda$ in biaxial tension ($\lambda_x = \lambda_y = \lambda$) and uniaxial tension ($\lambda_x = \lambda$, $\lambda_y = 0$). The case of biaxial tension is fairly simple and may be treated for all reinforcements simultaneously. Uniaxial tension is more difficult and the various types of reinforcements considered will be treated separately.

For a curved beam the state of stress in any section is specified by a bending moment $M$ and an axial force $N$ caused by tensile stresses, and a shear force caused by shear stresses. The effect of the shear force is negligible for solid cross sections and will be disregarded in the subsequent analysis.

## 3 Biaxial Tension

Consider a cutout slab shown in Fig. 1, and let $A$ be the total cross-sectional area of the hub. In biaxial tension the hub is subjected to a uniformly distributed radial force of magnitude $h\lambda s$ per unit length of the circumference of radius $(a + \delta)$. To satisfy the equilibrium requirement, the stress resultants in the hub must be given by

$$N = (a + \delta)h\lambda s, \; M = 0 \qquad [1]$$

at all cross sections. Such resultants are furnished by a uniform tensile stress of magnitude $N/A$. From the yield criterion this stress cannot exceed the yield stress $s$; hence the axial force must satisfy

$$N \leq As \qquad [2]$$

Combining Equations [1] and [2] leads to the inequality

$$\lambda \leq \lambda_1 = A/[h(a + \delta)] \qquad [3]$$

Hence for the case of biaxial tension any value of $\lambda$ satisfying Inequality [3] furnishes a lower bound.

## 4 General Symmetric Reinforcement

The type of reinforcement considered here has the following properties:

1 The hub is symmetric about the $x$ and $z$-axes, where the $x$-axis lies in the plane of the slab and passes through the center of mass of the hub and through the center of the cutout, and the $z$-axis is normal to the slab and also passes through the center of mass of the hub and

2 In the first quadrant, the boundary of the hub, $z = f(x)$, is a continuous, single-valued, monotonically nonincreasing function of $x$, Fig. 2($a$).

To find limiting combinations of bending moment $M$ and axial force $N$ which the beam can support, i.e., which do not violate the yield criterion, consider a fully plastic stress distribution of the type shown in Fig. 2($b$). Part of the section is stressed to the yield limit in tension and the rest in compression. The absolute values of the bending moment and axial force for such a stress distribution are

$$|N| = \left| s\left(2\int_{\zeta}^{\delta/2} f(x)dx - 2\int_{-\delta/2}^{\zeta} f(x)dx\right)\right| = \left|4s\int_0^{\zeta} f(x)\,dx\right| \qquad [4]$$

$$|M| = \left| s\left(2\int_{\zeta}^{\delta/2}\int_0^{f(x)} x\,dx\,dz - 2\int_{-\delta/2}^{\zeta}\int_0^{f(x)} x\,dx\,dz\right)\right| = \left|4s\int_{\zeta}^{\delta/2} x\,f(x)dx\right| \qquad [5]$$

If $N/s$ and $M/s$ are regarded as Cartesian co-ordinates in a stress-resultant space, then Equations [4] and [5] define an interaction curve in the $NM$-plane. It can be shown that this curve will be closed and will bound a convex, symmetric region, which will be defined as the "safe region." Any point within the safe region represents a bending moment and an axial force which do not violate the yield criterion. The boundary of the region is described parametrically in terms of $\zeta$ and represents the limiting admissible combinations of bending moment and axial force.

The exact safe region is defined by Equations [4] and [5] which contain integrals of the arbitrary function $f(x)$ and $xf(x)$. Therefore it is not possible to obtain a direct limiting relation between $N$ and $M$. However, any region which lies wholly within the safe region will itself consist only of safe stress resultants. It will be shown that the domain bounded in each quadrant by a certain parabolic arc is such a safe approximation.

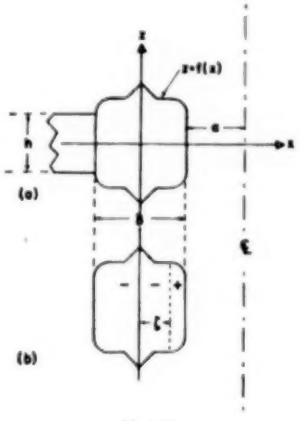


Fig. 2
($a$, General symmetric hub; $b$, Fully plastic stress distribution.)

From symmetry, it is necessary to consider only the first quadrant. Here

$$M/s = 4\int_{\zeta}^{\delta/2} x\,f(x)dx \qquad [6]$$

$$N/s = 4\int_0^{\zeta} f(x)\,dx \qquad [7]$$

Define

$$M_0/s = 4\int_0^{\delta/2} x\,f(x)\,dx \qquad [8]$$

$$N_0/s = 4\int_0^{\delta/2} f(x)dx \qquad [9]$$

where $M_0$ and $N_0$ represent the extreme values in the positive $M$ and $N$-directions, respectively. Thus the end points of the interaction curve in the first quadrant are $(0, M_0/s)$ and $(N_0/s, 0)$ which correspond to $\zeta = 0$ and $\zeta = \delta/2$, respectively. The approximating curve will be taken as the parabola

$$M/M_0 = 1 - (N/N_0)^2 \qquad [10]$$

which passes through the same end points with a horizontal tangent at $N = 0$.

In order to prove that this curve is an admissible approximation it is sufficient to show that for any given value of $\zeta$ between zero and $\delta/2$, the ordinate $M/M_0$ of the approximate curve never exceeds the ordinate $M/M_0$ of the interaction curve. In terms of $\zeta$, the ordinate of the approximate curve is

$$M/M_0 = 1 - (N/N_0)^2 = 1 - \left[\frac{\int_0^\zeta f(x)\,dx}{\int_0^{\delta/2} f(x)\,dx}\right]^2 \quad [11]$$

while the ordinate of the interaction curve is

$$M/M_0 = \frac{\int_\zeta^{\delta/2} xf(x)\,dx}{\int_0^{\delta/2} xf(x)\,dx} \quad [12]$$

Therefore for all $0 \leq \zeta \leq \delta/2$, it must be shown that

$$g(\zeta) \equiv \frac{\int_\zeta^{\delta/2} xf(x)\,dx}{\int_0^{\delta/2} xf(x)\,dx} - 1 + \left[\frac{\int_0^\zeta f(x)\,dx}{\int_0^{\delta/2} f(x)\,dx}\right]^2 \geq 0 \quad [13]$$

It is evident from the definition of the approximate curve that $g(0) = g(\delta/2) = 0$, and $g'(0) = 0$. In the Appendix it is shown that $g'(\delta/2)$ is equal or less than zero, and that the equation $g'(\zeta) = 0$ has not more than two roots in the closed interval $0 \leq \zeta \leq \delta/2$. Since $g(\zeta)$ is continuously differentiable, it follows that in addition to its extremum at $\zeta = 0$, it has only one relative extremum between zero and $\delta/2$. Since the slope is nonpositive at $\zeta = \delta/2$, this extremum must be a maximum. Therefore Inequality [13] is valid, since otherwise $g(\zeta)$ would have a minimum in the interior.

Thus the approximation is safe and the yield condition for the hub may be approximated by

$$|M/M_0| \leq 1 - (N/N_0)^2 \quad [14]$$

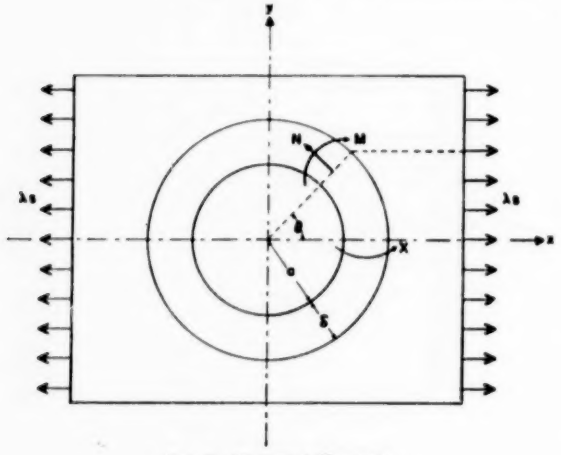


FIG. 3 UNIAXIAL TENSION

Under uniaxial tension, Fig. 3, the stress resultants $M$ and $N$ at any cross section $\theta$ of the hub may be computed from equilibrium considerations to within a redundant bending moment, $X$. This statically indeterminate quantity represents the bending moment at the cross section $\theta = 0$ and from equilibrium is seen to be the only nonvanishing stress resultant there. The stress resultants are found to be

$$N = F \sin\theta = h\lambda s(a + \delta)\sin^2\theta \quad [15]$$

$$M = X + \int_0^{(a+\delta)\sin\theta} h\lambda s\,[(a + \delta/2)\sin\theta - y]\,dy$$

$$= X + \tfrac{1}{2}\,h\,\lambda sa(a + \delta)\sin^2\theta \quad [16]$$

or

$$N/N_0 = d\sin^2\theta \quad [17]$$

$$M/M_0 = Y + c\sin^2\theta \quad [18]$$

where

$$Y = X/M_0, \quad c(\lambda) = h\lambda sa(a + \delta)/2M_0 > 0,$$

$$d(\lambda) = h\lambda s(a + \delta)/N_0 > 0$$

The substitution of Equations [17] and [18] into the yield condition [14] leads to

$$Y + c\sin^2\theta \leq 1 - d^2\sin^4\theta \quad [19a]$$

$$-Y - c\sin^2\theta \leq 1 - d^2\sin^4\theta \quad [19b]$$

These inequalities must be satisfied for all $0 \leq \theta \leq \pi/2$.

Let $w = \sin^2\theta$. Then Equations [19] may be written

$$P(w) = d^2w^2 + cw + Y - 1 \leq 0 \quad [20a]$$

$$Q(w) = d^2w^2 - cw - Y - 1 \leq 0 \quad [20b]$$

Here $P$ and $Q$ represent parabolas concave upward; hence a necessary and sufficient condition that Inequalities [20] hold for all $0 \leq w \leq 1$ is that they hold at both end points. Thus

$$-1 \leq Y \quad [21]$$

$$d^2 - c - 1 \leq Y \quad [22]$$

$$Y \leq 1 \quad [23]$$

$$Y \leq 1 - c - d^2 \quad [24]$$

The actual choice of $Y$ is immaterial, provided only that some $Y$ exists which satisfies all of the foregoing inequalities. A necessary and sufficient condition that this be the case is that each left-hand side be less than each right-hand side. Thus

$$-1 \leq 1 \quad [25]$$

$$-1 \leq 1 - c - d^2 \quad [26]$$

$$d^2 - c - 1 \leq 1 - c - d^2 \quad [27]$$

$$d^2 - c - 1 \leq 1 \quad [28]$$

Since $c$ and $d$ are positive, the foregoing inequalities are equivalent to

$$d^2 + c \leq 2 \quad [29]$$

$$d \leq 1 \quad [30]$$

In view of the definition of $d$, Inequality [30] leads to

$$\lambda \leq 4\int_0^{\delta/2} f(x)\,dx/h(a + \delta) \equiv \lambda_1 \quad [31]$$

where $\lambda_1$ is defined in Equation [3].

With the aid of the definitions of $d$, $c$, and $\lambda_1$, together with $D = 4M_0/N_0$, Inequality [29] may be written

$$F(\lambda) = \lambda^2 + (2a/D)\lambda_1\lambda - 2(\lambda_1)^2 \leq 0 \quad [32]$$

$F(\lambda)$ represents a parabola concave upward; hence Equation [32] will be satisfied for all $\lambda$ between the two roots of $F(\lambda) = 0$. Since the smaller root is negative and $\lambda$ is positive, the restriction on $\lambda$ becomes

$$\lambda \leq \lambda_2 \equiv \lambda_1\left[\sqrt{2 + (a/D)^2} - (a/D)\right] \quad [33]$$

Thus any value of $\lambda$ satisfying both Expressions [31] and [33] furnishes a lower bound for uniaxial loading. It follows from Inequalities [31] and [3] that if $\lambda$ is safe for uniaxial loading it is also safe for biaxial loading. Therefore the domain of safe loads is fully defined by

$$\lambda \leq \min (\lambda_1, \lambda_2) \quad [34]$$

where $\lambda_1$ is given by Inequality [3] and $\lambda_2$ by Inequality [33]. In particular, it may be shown readily that Inequality [34] is equivalent to

$$\left.\begin{array}{ll} \lambda \leq \lambda_1 & \text{if } a/D \leq 1/2 \\ \lambda \leq \lambda_2 & \text{if } a/D \geq 1/2 \end{array}\right\} \quad [35]$$

## 5 Cylindrical Ring Reinforcement

The results of the preceding section are readily applicable to the case of a reinforcement consisting of a hollow cylindrical ring about the cutout, Fig. 4. The hub cross section is now a rectangle and $z = f(x)$ is a constant, $H/2$, where $H$ represents the total height of the reinforcement. Hence

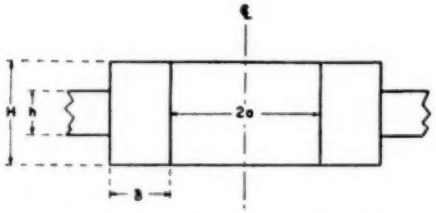


Fig. 4 Cylindrical Reinforcement

$$\lambda_1 = \frac{H\delta}{h(a+\delta)} \quad [36]$$

$$D = \delta \quad [37]$$

$$\lambda \leq \frac{H\delta}{h(a+\delta)} \quad \text{if} \quad a/\delta \leq 1/2 \quad [38]$$

$$\lambda \leq \frac{H}{h}\left(\frac{1}{1+(\delta/a)}\right)\left[\sqrt{1+2(\delta/a)^2}-1\right] \quad [39]$$

$$\text{if } a/\delta \geq 1/2$$

For a "full strength" reinforcement of this type, $\lambda = 1$, and the ring must be so designed that

$$H/h = \frac{1+(\delta/a)}{(\delta/a)} \quad \text{if} \quad a/\delta \leq 1/2 \quad [40]$$

$$H/h = \frac{1+(\delta/a)}{\sqrt{1+2(\delta/a)^2}-1} \quad \text{if} \quad a/\delta \geq 1/2 \quad [41]$$

These results coincide with those obtained directly by Weiss, Prager, and Hodge (1). The exact agreement is accounted for by the fact that for this case only the actual safe region in the stress-resultant plane is bounded by an interaction curve which consists of parabolic arcs. Hence the parabolic approximation used in Section 4 coincides with the true interaction curve.

## 6 Quasi-Toroidal Reinforcement

Consider a reinforcement of the type shown in Fig. 5 where the boundary of the hub cross section is an arc of a circle, $f(x) = \sqrt{r^2 - x^2}$. A lower bound may be obtained readily from Inequalities [31] and [33]. Further, an upper bound may be obtained for the error introduced by approximating the true interaction curve by a parabolic arc.

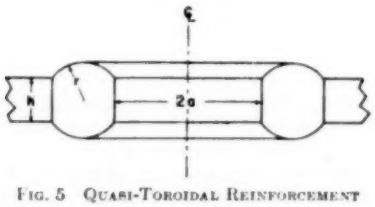


Fig. 5 Quasi-Toroidal Reinforcement

It can be shown that the interaction curve in the first quadrant is given by

$$\frac{1}{2}u = \cos^{-1}(v_1)^{1/2} + (v_1)^{1/2}\sqrt{1-(v_1)^{3/2}} \quad [42]$$

where

$$u = N/sr^2$$

and

$$v_1 = \frac{3}{4}M/sr^2 + \left(\frac{h}{2r}\right)^2$$

The appropriate parabolic approximation is

$$v/v_0 = 1 - (u/u_0)^2 \quad [43]$$

where

$$v = M/sr^2 = \frac{4}{3}\left[v_1 - (h/2r)^2\right]$$

$$v_0 = M_0/sr^2 = \frac{4}{3}\left[1 - (h/2r)^2\right]$$

$$u_0 = N_0/sr^2 = 2\left[\cos^{-1}(h/2r) + (h/2r)\sqrt{1-(h/2r)^2}\right]$$

The curve, Equation [42], may be plotted in a $uv_1$-space. However, the parabolic approximation as well as the actual position of the $u$-axis depends upon the ratio $h/2r$. To obtain an estimate of the error made by using the parabolic Approximation [43], a second parabola is passed through the points ($u = 0$, $v_1 = 1$), ($u = \pi$, $v_1 = 0$). Such a parabola is

$$v_1 = 1 - (u/\pi)^2 \quad [44]$$

It can be shown by methods similar to those employed in Section 4 that the limiting Parabola [44] lies below the approximating Parabola [42] for all values of $h/2r$, so that, independently of the dimensions of the reinforcement, the approximating parabola must lie between the limiting parabola and the interaction curve. As may be seen from Fig. 6 or Table 1, the approximation is a close one. The dotted curve represents a typical approximating parabola for the case $h/2r = 0.5$.

At least for this type of reinforcement (and of course for the cylindrical rings of Section 5), the approximation appears to be satisfactory. In view of the rather drastic physical approximations which were introduced in setting up the problem in Section

TABLE 1 PARABOLA DATA

| $v_1$ | $u$, interaction | $u$, typical parabola | $u$, limiting parabola |
|---|---|---|---|
| 1.00 | 0.0000 | 0.0000 | 0.0000 |
| 0.95 | 0.7287 | 0.7077 | 0.7025 |
| 0.90 | 1.0299 | 1.0009 | 0.9935 |
| 0.85 | 1.2595 | 1.2257 | 1.2167 |
| 0.80 | 1.4521 | 1.4154 | 1.4050 |
| 0.75 | 1.6211 | 1.5824 | 1.5708 |
| 0.70 | 1.7730 | 1.7334 | 1.7207 |
| 0.65 | 1.9118 | 1.8724 | 1.8586 |
| 0.60 | 2.0406 | 2.0016 | 1.9869 |
| 0.55 | 2.1606 | 2.1230 | 2.1074 |
| 0.50 | 2.2735 | 2.2378 | 2.2214 |
| 0.45 | 2.3801 | 2.3471 | 2.3299 |
| 0.40 | 2.4812 | 2.4515 | 2.4335 |
| 0.35 | 2.5775 | 2.5515 | 2.5328 |
| 0.30 | 2.6693 | 2.6480 | 2.6285 |
| 0.25 | 2.7571 | 2.7408 | 2.7207 |
| 0.20 | 2.8411 | 2.8307 | 2.8099 |
| 0.15 | 2.9215 | 2.9178 | 2.8964 |
| 0.10 | 2.9985 | .... | 2.9804 |
| 0.05 | 3.0720 | .... | 3.0621 |
| 0.00 | 3.1416 | .... | 3.1416 |

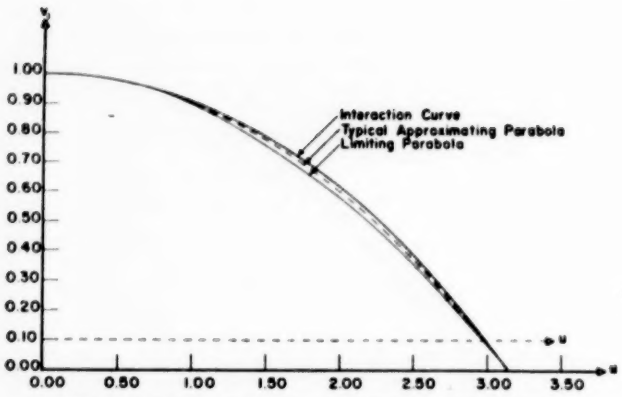


FIG. 6 INTERACTION CURVE AND APPROXIMATING PARABOLAS

2, it appears entirely reasonable to adopt the parabolic approximation to the yield condition.

## 7 BEVELED REINFORCEMENT

Consider a reinforcement of the type shown in Fig. 7. Since the hub cross section is not symmetric, the results of Section 4 do not apply. The analysis, however, will still be based on the Drucker-Greenberg-Prager theorem and the hub is treated as a curved beam.

To find limiting conditions for the bending moment and axial force in terms of the yield stress, four different possibilities must be considered, depending upon whether the neutral axis is located in the beveled or cylindrical part of the hub, and which side of the hub is stressed in tension, Fig. 8. The resultant axial force $N$ and bending moment $M$ about the line 00 separating the beveled and cylindrical parts of the hub will be given by one of the four pairs of equations

$$N(\zeta) = \pm s\left[-2H\zeta + Hb - \frac{1}{2}(H + h)c\right] \quad [45a]$$

$$M(\zeta) = \pm s\left[-H\zeta^2 + \frac{1}{2}Hb^2 + Hc^2/6 + hc^2/3\right] \quad [45b]$$

$$N(\eta) = \pm s\left[(L/c)\eta^2 - 2H\eta - Hb + \frac{1}{2}(H + h)c\right] \quad [45c]$$

$$M(\eta) = \pm s\left[-(2L/3c)\eta^3 + H\eta^2 - \frac{1}{2}Hb^2 - c^2\left(\frac{H}{6} + \frac{h}{3}\right)\right] \quad [45d]$$

Here $\zeta$ or $\eta$ is a parameter which represents the distance from the line 00 to the neutral axis

It is convenient to use dimensionless variables defined by

$$\left.\begin{aligned} u &\equiv (N/s)(L/cH^2) \\ v &\equiv (M/s)(L^2/c^2H^2) \\ A &\equiv (L/cH^2)[Hb - c(2H - L)/2] \\ B &\equiv (L^2/c^2H^2)[(H/2)(b^2 + c^2) - Lc^2/3] \\ \zeta' &\equiv (L/cH)\zeta \\ \eta' &\equiv (L/cH)\eta \end{aligned}\right\} \quad [46]$$

In terms of these variables, Equations [45] become

$$u = \pm[-2\zeta' + A] \quad [47a]$$

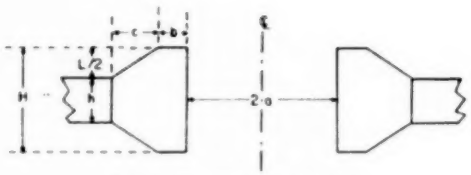


FIG. 7 BEVELED REINFORCEMENT

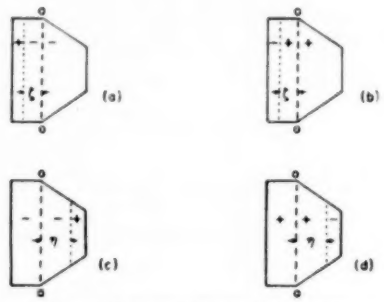


FIG. 8 FULLY PLASTIC STRESS DISTRIBUTIONS

$$v = \pm[-(\zeta')^2 + B] \quad [47b]$$

$$u = \pm[(\eta')^2 - 2\eta' - A] \quad [47c]$$

$$v = \pm[-(2/3)(\eta')^3 + (\eta')^2 - B] \quad [47d]$$

In view of the physical limitations of the constants in Equations [46], (for example, $0 < h < H$), it may be shown that the four curves obtained by plotting Equations [47] in a Cartesian $uv$-space have the general character shown in Fig. 9. Further, since $0 \leq \zeta' \leq Lb/cH$, $0 \leq \eta' \leq L/H < 1$ it follows that only the solid portions of the curves in Fig. 9 have any physical meaning.

The solid curves in Fig. 9 thus represent the interaction curve between the reduced axial force and bending moment at a fully plastic cross section. At a section which is less than fully plastic, i.e., where some of the fibers are stressed with less than the yield stress, the corresponding values must lie between these curves, in the shaded portion of Fig. 9.

A necessary and sufficient condition that this be the case is that for a given value of $u$, the value of $v$ must locate a point above the curve, Equation [47b] and the upper branch of [47c], and below curve, Equation [47a] and the lower branch of [47d]. Thus, if the parameter $\zeta'$ or $\eta'$ is eliminated from Equations [47] and the appropriate sign chosen in accord with Fig. 9, the yield condition may be written as the inequalities

$$v \leq -\left(\frac{A - u}{2}\right)^2 + B \quad [48a]$$

$$v \geq \left(\frac{A + u}{2}\right)^2 - B \quad [48b]$$

$$v \geq -\left(\frac{2}{3} + A + B + u\right) + (2/3)(1 + A + u)^{3/2} \quad [48c]$$

$$v \leq (2/3 + A + B - u) - (2/3)(1 + A - u)^{3/2} \quad [48d]$$

Loads transmitted to the hub may be regarded as safe if stress resultants $u$, $v$ can be found which are in equilibrium with these loads and satisfy the yield Inequalities [48].

As in the symmetric case, it may be shown that if the reinforced slab will support a given load in uniaxial tension, it will

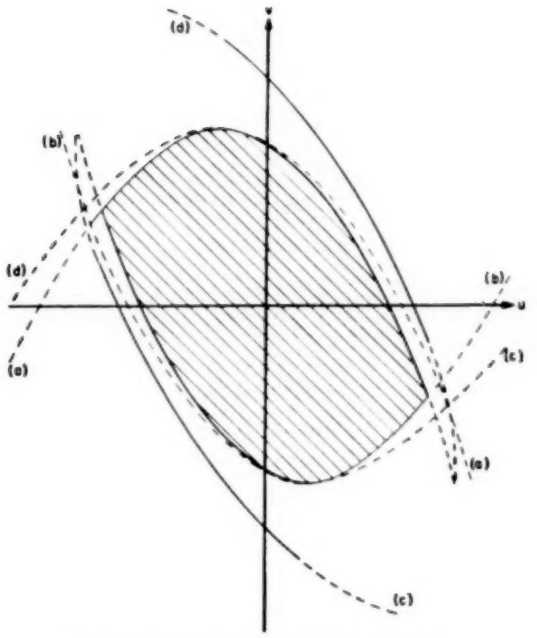


FIG. 9 NONSYMMETRIC INTERACTION CURVE

support the same load in biaxial tension. Under uniaxial tension $\lambda s$, then, the axial force and bending moment are

$$\left.\begin{aligned} N &= h\lambda s(a + b + c)\sin^2\theta \\ M &= X + \frac{1}{2}h\lambda s(a + b + c)(a + b - c)\sin^2\theta \end{aligned}\right\} \quad \ldots [49]$$

where $X$ is the bending moment at $\theta = 0$.

With the quantities defined by Equations [46], together with the dimensionless elements

$$\left.\begin{aligned} Y &\equiv XL^2/sc^2H^3 \\ D &\equiv Lh\lambda(a + b + c)/cH^2 \\ E &\equiv L^2h\lambda(a + b + c)(a + b - c)/2c^2H^3 \end{aligned}\right\} \quad \ldots [50]$$

$$w = \sin^2\theta$$

Equations [49] become

$$\left.\begin{aligned} u &= Dw \\ v &= Y + Ew \end{aligned}\right\} \quad \ldots [51]$$

Equations [51] must now be substituted into Inequalities [48]. Since Equations [51] define $u$ and $v$ for all values of $\theta$, the resulting inequalities must be satisfied for all $0 \leq w \leq 1$. The problem, then, is to determine the redundant reduced moment $Y$, so that $\lambda$ will be a maximum subject to these inequalities. The general method of solution is the same as that used in Section 4. Since some of the inequalities involve cubic functions of $w$, the results cannot, in general, be computed in closed form. However, for any specific values of the parameters, the computations may be carried out numerically.

The techniques used and the details of a typical computation appear elsewhere (5) and will not be entered into here. For a slab with a beveled reinforcement with the dimensions

$$\begin{aligned} H &= 24 \quad a = 24 \\ h &= 10 \quad b = 11 \\ L &= 14 \quad c = 20 \end{aligned}$$

it was found that for the reduced moment

$$Y = -0.153274$$

the load

$$\lambda s = 0.98s$$

could be supported. For no choice of $Y$ could a larger value of $\lambda$ be found which would satisfy the inequalities obtained by substituting Equations [51] into Inequalities [48]. Therefore this beveled reinforcement restores the cutout slab to at least 98 per cent of full strength.

## 8 COMPARISON OF REINFORCEMENTS

It is of some interest to compare this beveled reinforcement with other shaped reinforcements. In each case, the cutout radius $a$, and the slab thickness $h$, have the same value, and the reinforcements are designed so that $\lambda = 0.98$. The following three cases are considered:

(*a*) *Cylindrical Hub of Same Total Width,* $\delta = 31$. In this case Equation [39] shows that the hub thickness must be

$$H \simeq 20.75$$

(*b*) *Cylindrical Hub of Same Maximum Thickness,* $H = 24$. Equation [39] here shows that the total width is

$$\delta \simeq 26.50$$

(*c*) *Quasi-Toroidal Hub.* For a given cutout radius, slab thickness, and desired strength, the radius of the toroid is completely determined and no further choice such as total width is possible. For this case the radius is found to be

$$r \simeq 14.9$$

The salient features of the four reinforcements are compared in Table 2.

TABLE 2 FEATURES OF REINFORCEMENTS

| | Beveled | Cyl. A | Cyl. B | Toroid |
|---|---|---|---|---|
| Cutout radius | 24 | 24 | 24 | 24 |
| Slab thickness | 10 | 10 | 10 | 10 |
| Cutout volume | $18.10 \times 10^3$ | $18.10 \times 10^3$ | $18.10 \times 10^3$ | $18.10 \times 10$ |
| Per cent strength | 98 | 98 | 98 | 98 |
| Maximum hub thickness | 24 | 20.75 | 24 | 29.80 |
| Maximum hub width | 31 | 31 | 26.50 | 28.07 |
| Total hub volume | $14.19 \times 10^3$ | $15.95 \times 10^3$ | $14.90 \times 10^3$ | $14.15 \times 10^3$ |
| Reinforcement volume alone | $6.49 \times 10^3$ | $8.25 \times 10^3$ | $8.68 \times 10^3$ | $7.42 \times 10^3$ |

## 9 CONCLUSIONS AND LIMITATIONS

The results in Section 4 for a symmetric reinforcement and the analysis in Section 7 for a nonsymmetric one provide methods for obtaining an approximate lower bound on the collapse load. The principal approximation made was that of treating the hub as a curved beam with no shear. Although this has proved successful in the elastic range (6) certain limitations must be observed when applying the results. If the maximum thickness of the hub is much larger than that of the slab, the question of the carrying capacity arises. If, on the other hand, the width becomes too large in comparison with the inner radius, the entire concept of a curved beam becomes questionable. Buckling in compression is not considered and must be treated separately.

The foregoing approximations tend to predict an optimistic load capacity. On the other hand, the assumption of perfect plasticity which neglects strain hardening will make the estimate conservative. Also, the slab was regarded as being in a homogeneous state of stress and no stress concentration in the slab was considered.

At present there is insufficient experimental evidence available

to determine the extent to which these various influences tend to cancel.

# Appendix

The differentiation of Equation [13] with respect to $\zeta$ leads to

$$g'(\zeta) = -\frac{\zeta f(\zeta)}{\int_0^{\delta/2} xf(x)\,dx} + 2\left[\frac{\int_0^{\zeta} f(x)\,dx}{\left(\int_0^{\delta/2} f(x)\,dx\right)^2}\right]' f(\zeta) \quad [52]$$

and

$$g'(\delta/2) = \frac{f(\delta/2)32s^2}{M_0N_0}\left[\int_0^{\delta/2} xf(x)dx - \frac{\delta}{4}\int_0^{\delta/2} f(x)\,dx\right] \quad [53]$$

The sign of $g'(\delta/2)$ will be the same as the sign of the bracketed expression since the factor outside the brackets is always positive. By combining the two integrals and performing a change of variable, $t = (x - \delta/4)$, it is found that

$$g'(\delta/2) = \frac{f(\delta/2)32s^2}{M_0N_0}\left\{\int_0^{\delta/4} t[f(\delta/4 + t) - f(\delta/4 - t)]dt\right\} \quad [54]$$

But throughout the range of integration $f(\delta/4 + t) \leq f(\delta/4 - t)$ since $f$ is monotonically nonincreasing. Hence the integrand is nonpositive throughout the range of integration and

$$g'\left(\frac{\delta}{2}\right) \leq 0 \quad [55]$$

In fact, $g'(\delta/2) = 0$ can hold if and only if $f(\delta/4 + t) = f(\delta/4 - t)$ for all $0 \leq t \leq \delta/4$, i.e., $f(\zeta) = c$ and the hub is a rectangle. For this case the interaction curve is itself parabolic and $g(\zeta) \equiv 0$.

Consider the number of solutions of $g'(\zeta) = 0$. Since $f(\zeta) \neq 0$, the problem is to determine the number of solutions of

$$h(\zeta) \equiv K\zeta - \int_0^{\zeta} f(x)\,dx = 0 \quad [56]$$

where

$$K \equiv \left(\int_0^{\delta/2} f(x)\,dx\right)^2 / 2\int_0^{\delta/2} xf(x)\,dx$$

The number of distinct zeroes of $h(\zeta)$ may at most exceed by one the number of sign changes of its derivative

$$h'(\zeta) = K - f(\zeta) \quad [57]$$

Since $f$ is monotonically nonincreasing and $K$ is constant, $h'(\zeta)$ may change sign only once. Therefore $h(\zeta)$ and hence $g'(\zeta)$ have at most two distinct zeroes. But $g'(0) = 0$; thus there is only one extremum in the interval which must represent a maximum since $g'(\delta/2) < 0$ whenever $g(\zeta) \not\equiv 0$.

## BIBLIOGRAPHY

1 "Limit Design of a Full Reinforcement for a Circular Cutout in a Uniform Slab," by H. J. Weiss, W. Prager, and P. G. Hodge, Jr., JOURNAL OF APPLIED MECHANICS, Trans. ASME, vol. 74, 1952, pp. 397–402.

2 "Extended Limit Design Theorems for Continuous Media," by D. C. Drucker, W. Prager, and H. J. Greenberg, *Quarterly of Applied Mathematics*, vol. 9, 1952, pp. 381–389

3 "Mémoire sur l'écoulement des Corps Solides," by H. Tresca, Mémoires presentes par divers Savants, vol. 18, 1868, pp. 733–799.

4 "Upper and Lower Bounds on the Yield Load of a Square Slab With a Centered Circular Cutout," by P. G. Hodge, Jr., Technical Report B11-7, Contract N7onr-35810, Brown University, Providence, R. I., 1952.

5 "The Yield Load of a Uniform Slab With a Cutout Reinforced by a Beveled Ring," by E. Levin and P. G. Hodge, Jr., Technical Report B11-14, Contract N7onr-35810, Brown University, Providence, R. I., 1952.

6 "On Stresses in a Plate With a Circular Hole," by S. Timoshenko, *Journal of The Franklin Institute*, vol. 197, 1924, pp. 505–516.

# Measurements of Torsional Stiffness Changes and Instability Due to Tension, Compression, and Bending[1]

By H. L. ENGEL[2] AND J. N. GOODIER[3]

**The measurements reported verify theoretically predicted effects of tension, compression, and bending, on the torsional stiffness of uniform bars of thin-walled open section. Related modes of buckling and types of nonlinear behavior in torsion are indicated analytically and exhibited in tests, some of these being apparently new.**

## Introduction

IN the ordinary torsion of uniform bars the torque $T$ is given in terms of the twist $\theta$ by

$$T = GC\theta \quad [1]$$

with $G$ for shear modulus, $C$ for the geometrical torsion constant of the section. When the bar carries an initial uniform tensile stress this relation is modified to

$$T = (GC + \sigma I_p)\theta \quad [2]$$

where $I_p$ is the polar moment of inertia about the centroidal axis, which is the axis of the torsional rotations. The formula applies also to compressive initial stress, regarded as negative tensile stress, and indicates a torsional buckling when the bracket in Equation [2] vanishes. When the initial axial stress is due to a bending moment in a principal plane, and given by

$$\sigma = \frac{M}{I}(y - y_0) \quad [3]$$

the torque twist relation becomes

$$T = \left(GC + \frac{\kappa M}{I}\right)\theta \quad [4]$$

and, again, the addition to $GC$ may be positive or negative. The stress $\sigma$ in Equation [3] is tensile when positive. The $x$-$y$-$z$ axes are oriented with $Oz$ (parallel to the generators) along the axis of the torsional rotations, the axes $Ox$, $Oy$ being parallel to the principal centroidal axes of section; the plane of the bending moment $M$ is parallel to the $y$-$z$-plane; $y_0$ is the $y$-co-ordinate of the centroid; $I$ is the appropriate moment of inertia; $\kappa$ is a geometrical constant of the section given by

$$\kappa = \int\int (y - y_0)r^2\,dx\,dy, \quad r^2 = x^2 + y^2 \quad [5]$$

the integral extending over the whole area. This constant vanishes—and with it the effect of bending moment on torsion—in the following cases:

1 The section has two axes of symmetry.

2 The section has "point-symmetry," e.g., the $Z$-section.

3 The section has one axis of symmetry and the bending-moment vector is in the same direction (the axis of symmetry is normal to the plane of bending).

Equations [2] and [4] are special cases of the more general formula

$$T = (GC + \int\int S_{zz}r^2\,dx\,dy)\theta \quad [6]$$

which has been obtained from the theory of elasticity for an axial stress $S_{zz}$ having any distribution over the section, but not varying in the axial direction $z$. It may be residual or thermal stress, as well as the tensile, compressive, or bending stress of Equations [2] and [4]. The derivation is given in reference (1)[4] where mention of earlier theory and tests may be found.

The changes of torsional stiffness indicated by these formulas are significant in many problems of thin-walled open sections (a section with a ratio of wall thickness to over-all dimension of $^1/_{10}$ is thin in this sense). The only measurements available in support of them appear to be those of Wilberforce and Campbell (2), which were obscured by plastic deformation, and measurements of torsional buckling under thrust by Wagner and Pretschner (3), Zahorski (4), and Niles (5). All these measurements relate to the case of uniform tension or thrust, and so to Equation [2]. The buckling measurements involve other effects such as non-uniform torsion and initial imperfection of form.

The first group of measurements reported in this paper was intended to test the validity of Equation [4] as well as Equation [2], and is found to confirm these formulas. The second group exhibits certain related instabilities and nonlinear effects which, in so far as the authors are aware, have not been recognized previously.

## Torsion of a Flat Strip Under Tension

Fig. 1 indicates the tests carried out on a flat strip of 61 S-T aluminum 30 in. long, with cross section 1.489 by 0.030 in. Tension was applied by a tensile-test machine. The ends of the strip were not allowed to rotate, while the mid-section was rotated by torque $2T$ communicated through a torque disk. The twist was measured by means of a mirror attached to the strip a few inches above the torque disk. The ordinary torsional rigidity $GC$ calculated by the approximate formula $^1/_3\,Gbt^3$ is 51.5 psi. The measured value for zero tensile load was 51.4 psi. The torque-rotation curves under three tensile loadings are shown in Fig. 2. They are straight lines in accordance with Equation [2]. Writing the latter as

$$T = GC_e\theta$$

[1] The investigations reported in this paper were supported by the Office of Naval Research, through a contract (N6-ONR-251 T.O. 12) with Stanford University.

[2] Hughes Aircraft Corporation, Research and Development Laboratory, Culver City, Calif.

[3] Professor of Engineering Mechanics, Stanford University, Stanford, Calif. Mem. ASME.

Contributed by the Applied Mechanics Division and presented at the Semi-Annual Meeting, Los Angeles, Calif., June 28–July 2, 1953, of The American Society of Mechanical Engineers.

Discussion of this paper should be addressed to the Secretary, ASME, 29 West 39th Street, New York, N. Y., and will be accepted until January 11, 1954 for publication at a later date. Discussion received after the closing date will be returned.

Note: Statements and opinions advanced in papers are to be understood as individual expressions of their authors and not those of the Society. Manuscript received by ASME Applied Mechanics Division, January 21, 1953. Paper No. 53—SA-5.

[4] Numbers in parentheses refer to the Bibliography at the end of the paper.

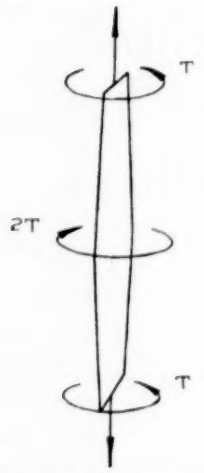


FIG. 1 TORSION IN PRESENCE OF TENSION

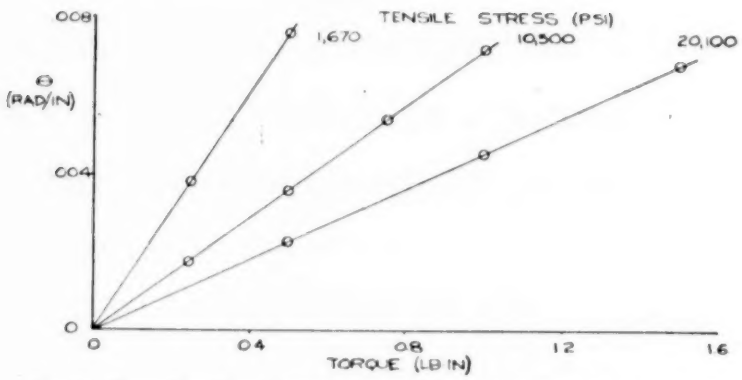


FIG. 2 TWIST PER UNIT LENGTH VERSUS APPLIED TORQUE FOR FLAT STRIP SUBJECTED TO VARIOUS AXIAL TENSILE LOADS

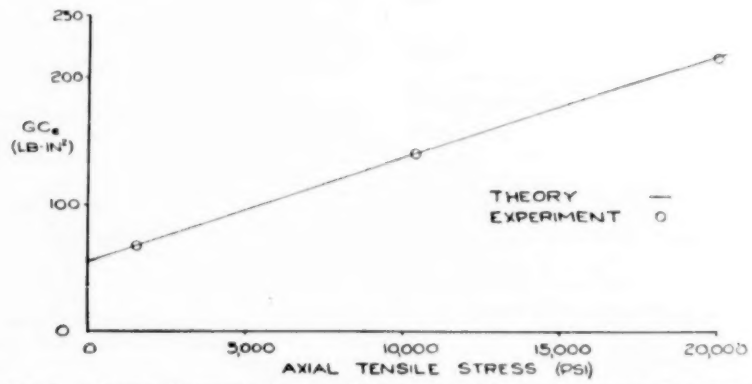


FIG. 3 APPARENT TORSIONAL RIGIDITY VERSUS AXIAL TENSILE STRESS FOR FLAT STRIP; WIDTH 1.489 IN., THICKNESS 0.03 IN.

and calling $GC_a$ the apparent torsional rigidity, Fig. 3, giving the variation of this quantity with the tensile load, shows a very close agreement with the formula, to a tension which increased the torsional stiffness to 4 times its ordinary value.

### TORSION OF A SLIT TUBE UNDER TENSION

The flat strip has negligible torsional warping of cross section, and negligible end effects when this warping is restrained. This is not the case for a slit tube. The material was 61 S-T aluminum, the outside diameter 2.035 in., the wall thickness 0.050 in., and the slit width 0.160 in. By means of the differential equation of nonuniform torsion, calculations were made for both ends fixed against warping, to determine the total length needed to provide a gage length of 10 in. free from end effects (within 1 per cent on the relative rotation of the ends of the gage length). The total length required was about 50 ft. This is an instance of Saint-Venant's principle operating with extreme gradualness.

The actual slit-tube specimen was 12 ft long, but its ends were not prevented from warping. End plates were attached freely by two pins on a diameter, and each end plate was supported pointwise at its center. The slit tube was hung vertically and loaded by weights. Torque was applied through the end plates, and relative rotations measured for the ends of the 10 in. central gage length.

The torque-twist curves (not reproduced) were again straight lines. The variation of apparent torsional rigidity with tensile load is shown in Fig. 4, and again the agreement with Equation [2] is very close. The range of tensile stress here was rather small, the additional torsional rigidity attained being only about 8.5 per cent of the ordinary rigidity. The measured value of the latter was within 3½ per cent of the value calculated from $\frac{1}{3} Gbt^3$, with $b$ as the curved length of the section.

### TORSION OF ANGLE SECTIONS UNDER BENDING

Angle sections were chosen for these tests, as being the simplest section giving stiffness and stability with respect to the bending, and having negligible torsional warping, when sufficiently thin-walled. The material was 61 S-T aluminum, the angle 90 deg, the legs 1 in. long, and the thickness 0.030 in. The angle bar was simply supported at two points and loaded at its ends to produce constant bending moment between supports, the vertical plane of bending containing the axis of symmetry of the section. In this case the constant $\kappa$ given by Equation [5] is $bt^4/6\sqrt{2}$, $t$ being wall thickness and $b$ length of leg. The torque-twist lines for several bending moments are shown in Fig. 5. The largest bending moment, 48.2 lb-in., corresponds to a fiber stress of 6800 psi, and doubles the torsional rigidity. The linearity of the observed torque-twist relations is in accordance with Equation [4].

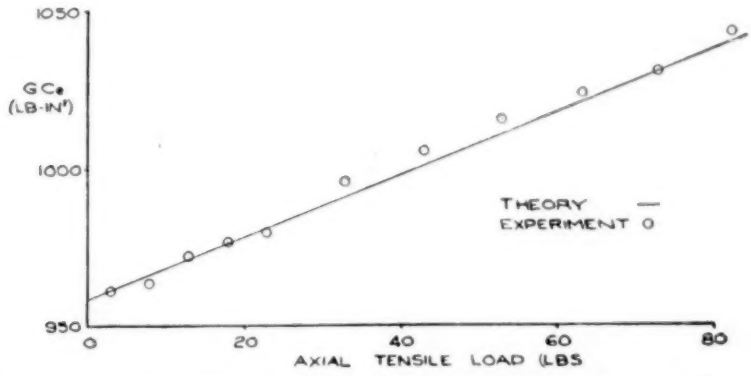


FIG. 4 APPARENT TORSIONAL RIGIDITY VERSUS AXIAL TENSILE LOAD FOR SLIT TU

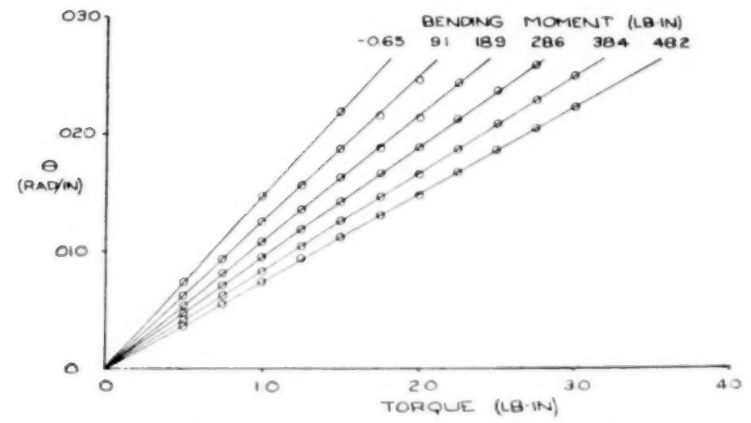


FIG. 5 TWIST PER UNIT LENGTH VERSUS APPLIED TORQUE FOR ANGLE SECTION SUBJECTED TO VARIOUS BENDING MOMENTS

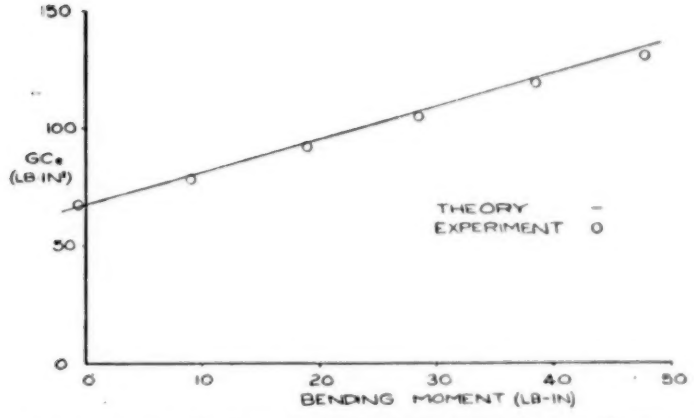


FIG. 6 APPARENT TORSIONAL RIGIDITY VERSUS APPLIED BENDING MOMENT FOR ANGLE SECTION

The dependence of apparent torsional rigidity on the bending moment is shown in Fig. 6 and the agreement with Equation [4] is very close.

The measured value of the ordinary torsional rigidity was 67.5 psi, the value calculated from $^1/_3\ Gbt^3$ being 68.4. A similar test was made on an extruded aluminum angle with legs 1.027 in. × 0.093 in. The predicted increases of torsional rigidity were found with a maximum discrepancy of 6 per cent, on the increase itself.

### Torsion of a Semicircular Section Under Bending

For the semicircular (thin-walled) section, as for the slit tube, the torsional warping and its effects, when the torsion is nonuniform, or when warping is restrained at the ends, are significant. The section tested was cut from a tube of outside diameter 2.032 in., wall thickness 0.050 in., and was short of a semicircle by 0.0374 radians. Again, great length would have been required to provide a gage length substantially free from end effects, and to design end fittings which would permit warping but be strong enough to communicate the bending moment was not found practicable. It was decided to test the effects of the initial bending stress and the end effects in combination, the ends of the specimen being cast into blocks of a low melting-point alloy. Rotation was measured at the center section, where torque was applied. This, in effect, divides the specimen into two halves, with warping prevented at the ends of each.

On account of the end effects the over-all apparent torsional rigidity—torque times length divided by the relative rotation of the ends—is greatly dependent on the length, and so specimens of several lengths were used. The ordinary torsional rigidity was determined on a 10-in-gage length at the middle of a specimen 12 ft long hung vertically.

The equation for the rotation $\beta$ of a section at axial co-ordinate $z$, under torque $T$, in the presence of bending moment $M$, is[5]

$$-E\Gamma \frac{d^3\beta}{dz^3} + \left(GC + \kappa \frac{M}{I}\right)\frac{d\beta}{dz} = T$$

where $\Gamma$ is a geometrical constant of the section, and $E$ Young's modulus. The solution satisfying the conditions at $z = 0$

$$\beta = \frac{d\beta}{dz} = 0$$

at $z = l$

$$\beta = \beta_l, \quad \frac{d\beta}{dz} = 0$$

yields for $\beta_l$ the value

$$\beta_l = \frac{Tl}{\alpha^2 E\Gamma}\left[1 - \frac{2}{\alpha l}\tanh\frac{\alpha l}{2}\right] \quad \ldots\ldots [7]$$

where

$$\alpha^2 = \left(GC + \frac{\kappa M}{I}\right)/E\Gamma \quad \ldots\ldots [8]$$

The apparent torsional rigidity, $Tl/\beta_l$, is therefore

$$GC_e = \frac{GC + \dfrac{\kappa M}{I}}{1 - \dfrac{2}{\alpha l}\tanh\dfrac{\alpha l}{2}} \quad \ldots\ldots [9]$$

and this is a nonlinear function of the bending moment $M$, implicit in $\alpha$.

[5] See, for instance, reference (6). Here of course we replace the ordinary torsional rigidity $GC$ by $GC + \kappa M/I$.

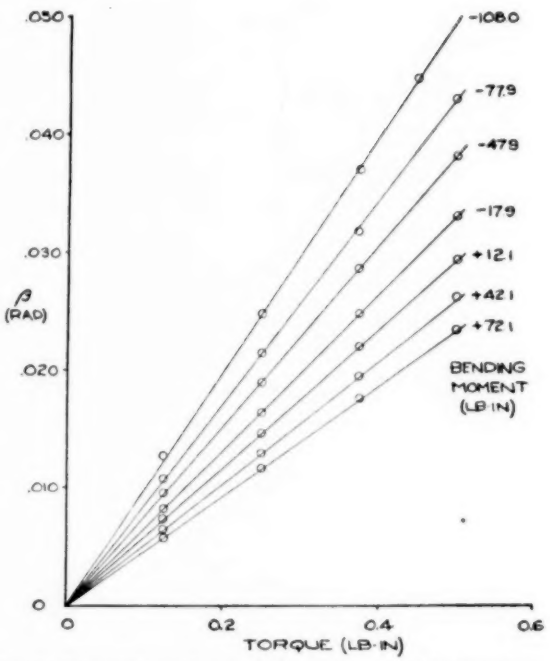


Fig. 7 Twist Versus Applied Torque for a 41.06-In-Long Semicircular Section, End Restrained From Warping, Subjected to Various Bending Moments

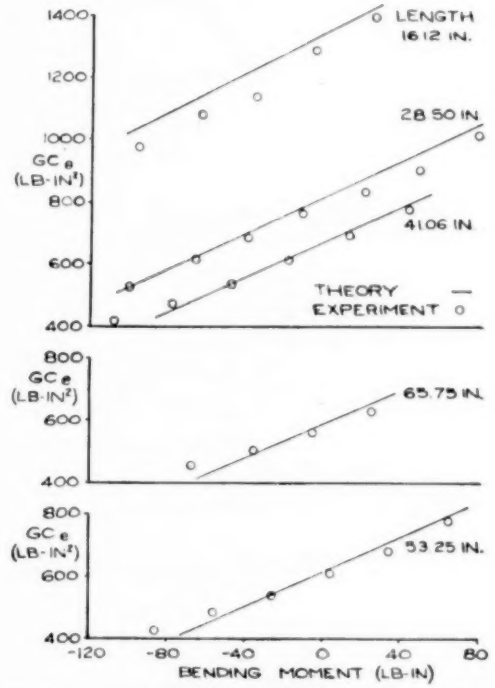


Fig. 8 Apparent Torsional Rigidity Versus Applied Bending Moment for Semicircular Sections of Various Lengths, Ends Restrained From Warping

The theoretical $\beta_t$ — $T$ relation [7] is, however, still a linear one for fixed bending moment. The observed lines are shown, for several bending moments, in Fig. 7. Fig. 8 shows the apparent torsional rigidity curves given by Equation [9] as "theory," and the test points, against bending moment, for the various lengths tested. The nonlinearity is only slight within this range, and the agreement of theory and tests is good. The measured values for the two shortest lengths are lower (by not more than 6 per cent) and this is to be expected, since the end restraint could not be complete. The measured value of the ordinary torsional rigidity $GC$ (from the 12-ft specimen) was used in Equation [9] to obtain the "theoretical" curves. It was 483 psi, the value given by the approximate formula being 504.

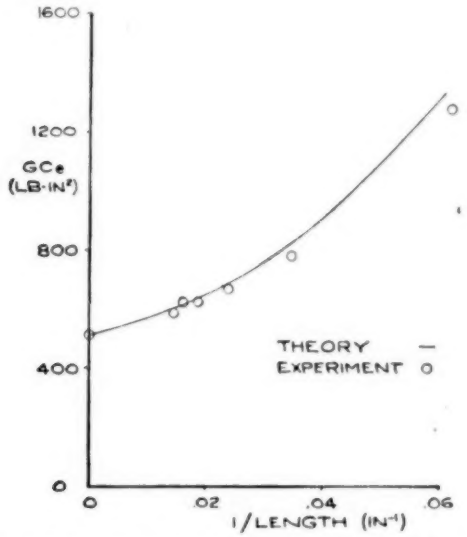


FIG. 9 APPARENT TORSIONAL RIGIDITY VERSUS INVERSE LENGTH FOR SEMICIRCULAR SECTION, ENDS RESTRAINED FROM WARPING

Fig. 9 shows apparent torsional rigidity in the absence of bending moment, as a function of (length)$^{-1}$. This exhibits the effect of end restraint only.[6] The agreement between the curve (theoretical) and the test points is again good. Here again the measured value of the ordinary torsional rigidity $GC$ was used in Equation [9] for the theoretical curve.

### LATERAL AND TORSIONAL BUCKLING UNDER BENDING LOADS

The effects of axial stress on torsional rigidity exhibited in the foregoing tests have been incorporated already into the analysis of modes of buckling which involve torsional deformation, as torsional flexural buckling of columns and lateral buckling of beams. They lead also to the recognition and explanation of certain modes of buckling under bending loads which do not appear to have been considered previously.

The original Prandtl-Michell theory of lateral buckling yields for pure bending in a (vertical) principal plane the critical bending moment

$$M_{cr} = \frac{\pi}{l}\sqrt{EI_1GC}$$

where $GC$ is the ordinary torsional rigidity, and $EI_1$, the flexural rigidity for horizontal bending. For the cantilever it yields the critical (vertical) end load

$$P_{cr} = \frac{4.01}{l^2}\sqrt{EI_1GC}$$

If the section has two axes of symmetry, or point symmetry, no modification in such formulas is required by Equation [4] because the constant $\kappa$ vanishes. However, the Prandtl-Michell theory is limited, as a consequence of its use of first-order approximations for direction cosines and curvatures, to sections which have small ratios of $EI_1$ and $GC$, to the flexural rigidity $EI_2$ of the original bending. This was demonstrated by the more exact investigation of H. Reissner (8) which leads, when the torsional rigidity remains small, to the modified formulas

$$M_{cr} = \frac{\pi}{l}\sqrt{\frac{EI_1GC}{1 - I_1/I_2}} \qquad P_{cr} = \frac{4.01}{l^2}\sqrt{\frac{EI_1GC}{1 - I_1/I_2}}$$

These critical loads increase without limit as $I_1$ approaches $I_2$, as in a set of angle sections with increasing angle, indicating that lateral buckling of the type contemplated becomes impossible. But when account is taken of the torsional effects with which we are concerned, it becomes evident that over-all (primary) buckling remains a practical possibility regardless of the ratio $I_1/I_2$, for sections which have one or no axis of symmetry.

The tests of angle sections under pure bending reported in the section, Torsion of Angle Sections Under Bending, show that the torsional rigidity can be doubled by the bending moment. If the bending moment were reversed, the corresponding torsional rigidity would be zero by Equation [4], and this means instability. The critical moment

$$M = -GCI/\kappa$$

obtained from Equation [4] corresponds to a torsional mode of buckling when transverse displacement of the vertex line of the angle is prevented by a smooth constraint. When there is no such constraint the stability analysis requires general equations (see, for instance, reference 9), which include the geometrical effects characteristic of the Prandtl-Michell-Reissner theory, and a lower critical moment is to be expected.

If the bending moment is not uniform we may expect that the bracket in Equation [4] is an adequate expression of the local torsional rigidity when $M$ is the local bending moment. In a cantilever, Fig. 10, it is evident that as the load $Q$ increases the bending moment at the root can reach the value which reduces the local torsional rigidity to zero (disregarding possible prior failure). This occurs when

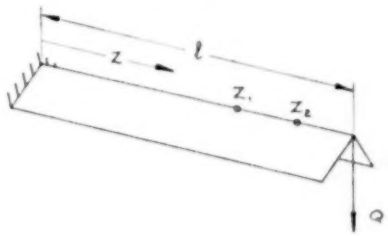


FIG. 10 CANTILEVER OF ANGLE SECTION

$$GC = \frac{\kappa}{l}Ql \qquad [10]$$

The local torsional rigidity is zero, but only for an infinitesimal length. To examine the over-all effect we may consider a cantilever as in Fig. 10, with lateral (horizontal) deflection prevented by a smooth constraint, and twisted by a torque $T$ at the loaded end $z = l$. At any section $z$ the bending moment is $Q(l - z)$, and we have from Equation [4]

[6] Tests of this type, of I-beams, are reported in reference (6).

$$T = \left[ GC - \frac{\kappa}{I} Q(l - z) \right] \frac{d\beta}{dz}$$

with $\beta$ as the torsional rotation at the section $z$. For the particular load $Q$ determined by Equation [10] this reduces to

$$T = \frac{\kappa}{I} Qz \frac{d\beta}{dz}$$

Integration between two sections $z_1$ and $z_2$ yields

$$\beta_2 - \beta_1 = \frac{TI}{\kappa Q} \log \frac{z_2}{z_1}$$

and this relative rotation increases without limit as the section $z_1$ approaches the root ($z_1 \longrightarrow 0$). The over-all torsional rigidity is therefore zero. Evidently the load $Q$ given by Equation [10] provides an upper bound on the buckling load. If the constraint against lateral deflection is removed, the analysis must proceed from general equations for lateral buckling. Energy calculations of this kind are reported in references (10) and (11).

Measurements of vertical and horizontal deflection versus load are shown in Figs. 11 and 12 for six angle sections having included angles 45°, 50°, 62°, 71°, 76°, and 91°. The specimens were made from 61 S-T sheet aluminum 0.032 in. thick, and the leg of each angle was 1 in. The cantilever length was $41^{11}/_{16} \pm {}^{3}/_{16}$ in. The arrangement was as in Fig. 10, no torque being applied. Buckling is indicated by the fairly sharp break which appears in each deflection curve. Critical loads, obtained from

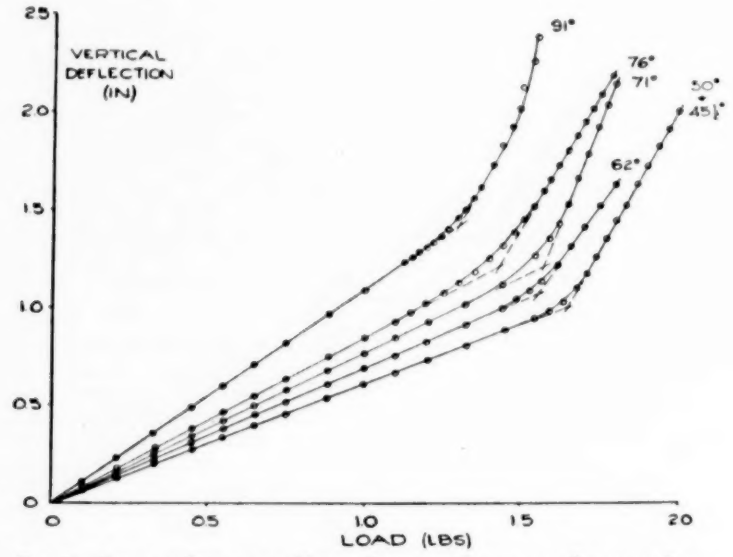


Fig. 11 Vertical Deflection Versus Load for Cantilever Beams as Shown in Fig. 10 for Various Included Angles

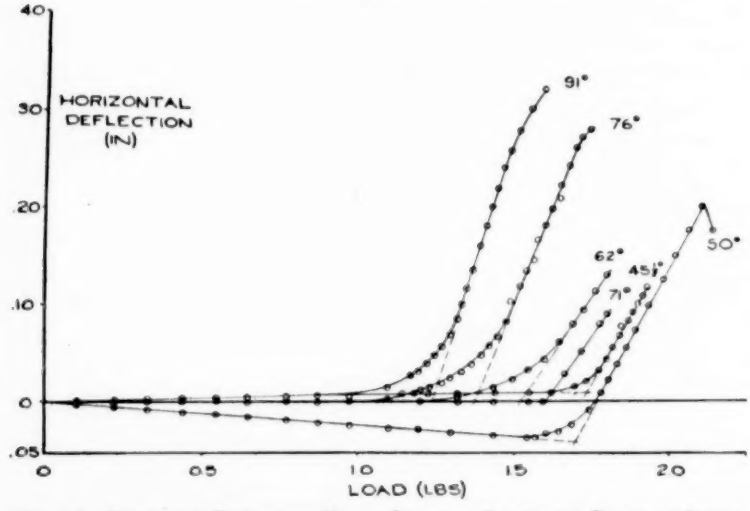


Fig. 12 Horizontal Deflection Versus Load for Cantilever Beams as Shown in Fig. 10 for Various Included Angles

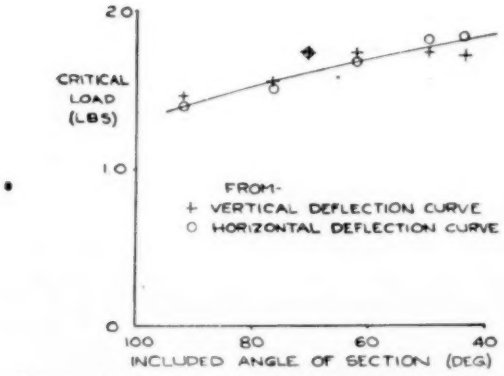


FIG. 13 CRITICAL LOADS OF ANGLE SECTIONS OF CANTILEVERS

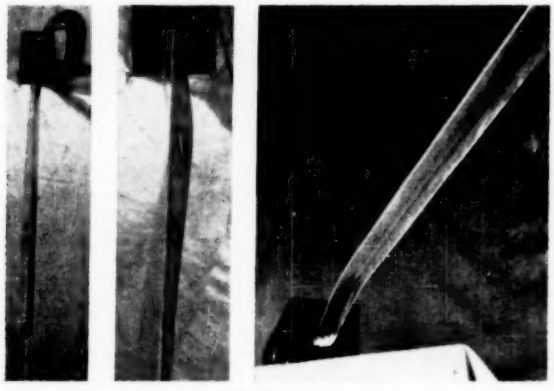

FIG. 14 BUCKLED CANTILEVER

the intersection of the prebreak and postbreak straight parts of the curves, are plotted in Fig. 13 against the section angle. Small corrections for the weight of the bars themselves have been included.

The curve in Fig. 13 represents the load which reduces the torsional rigidity at the root to zero—given by Equation [10]. The agreement with the measured buckling loads is remarkably close—considerably closer than that found for values calculated by general lateral buckling theory (11).

The evanescence of the torsional rigidity at the root section means that excessive local twisting must appear there as the buckling develops. This will bring into significance the nonlinear (at first cubic) terms in $\beta'$ in the expression for the torque. The character of the deformation for typical well-developed buckling (in the 45-deg specimen) is shown in Fig. 14. It appears as a predominantly twisting deformation confined to the neighborhood of the root section—where the specimen is cast into a rectangular block. The twisting has a wavy form. It could be snapped over by hand into very closely similar twisting of the opposite sense, and would remain there, this indicating independence of initial imperfection of form. A prior form of buckling was encountered, under the same load, with twisting rotation in the same sense all along the bar.

A further effect is involved in this kind of buckling. With the bending loads *in* the plane of symmetry of the section, the influence of the bending moment on the torsional rigidity is greatest, and this is the condition of the cantilever in the tests, Fig. 10. On the other hand, when the loads are perpendicular to the plane of symmetry the influence is zero ($Ox$ in Equation [5] is an axis of symmetry and $\kappa = 0$). As a section in Fig. 10 undergoes its twisting rotation, the influence of the bending moment is diminished, since only one component is effective.

This effect is exhibited by itself in torsion tests carried out on a bar of angle section under pure bending, the plane of the bending moment being perpendicular to the plane of symmetry, and the bending-moment vector therefore in the plane of symmetry, Fig. 15($a$). The initial effect of the bending moment on the torsional rigidity is therefore nil. But if a section is rotated by an angle $\beta$, Fig. 15($b$), the bending-moment vector remaining horizontal, the component $M \sin \beta$ is effective, with a constant $\kappa$ calculated from Equation [5], the axes of $x$ and $y$ being as indicated in Fig. 15($b$)—the $y$-axis lies in the plane of the effective bending moment. Thus

$$T = \left(GC - \frac{\kappa}{I} M \sin \beta\right) \frac{d\beta}{dz} \quad \ldots\ldots\ldots\ldots [11]$$

where $I$ now means the moment of inertia relevant to the effective bending moment—that is, about the centroidal axis parallel to $Ox$.

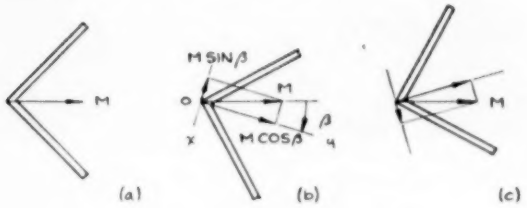


FIG. 15 EFFECT OF SECTION ROTATION

If the rotation is reversed, Fig. 15($c$), the effect of the bending moment also is reversed.

In the torsion test $T$ is a constant, and $\beta$ is zero at $z = 0$. Then Equation [11] integrates to

$$Tl = GC\beta_l - (\kappa M/I)(1 - \cos \beta_l) \quad \ldots\ldots\ldots [12]$$

where $\beta_l$ is the rotation at the end $z = l$.

The bar tested, Fig. 16($a$), was of 90-deg angle section made from 61 S-T aluminum sheet $^1/_{32}$ in. thick. The legs were 1 in. long. The central torque disk divides the bar into two test lengths of 18.4 in. each.

The $T$-$\beta_l$ curves predicted by Equation [12] are shown in Fig. 17($a$) for several bending moments.

The corresponding test results are shown in Fig. 17($b$) but the curves have been displaced vertically for clarity, the zero-torque point being marked on each as 0. The agreement with Fig. 17($a$) is qualitatively good, each set showing decrease of torsional rigidity for twisting one way, increase for twisting the other way. Quantitatively there are considerable differences. These may be attributed at least in part to initial twist of the specimen. In the absence of initial twist the curves in Fig. 17($b$) should all be parallel, at their origins, to the uppermost straight line which corresponds to zero bending moment, since the effect of bending moment is felt only after some rotation has occurred. The curves, however, show tangents parallel to the $M = 0$ line at points further and further to the left as $M$ increases. The horizontal interval between the point of tangency and the origin $O$ of the curve should represent the torsional rotation caused by the bending moment alone in virtue of the initial twist.

Each of the curves in Fig. 17($a$) has a maximum, only that of the lowest being on the diagram. In Fig. 17($b$) the lowest curve appears to be just reaching its maximum at the right. Such a maximum would be, for a sustained load, a point of instability,

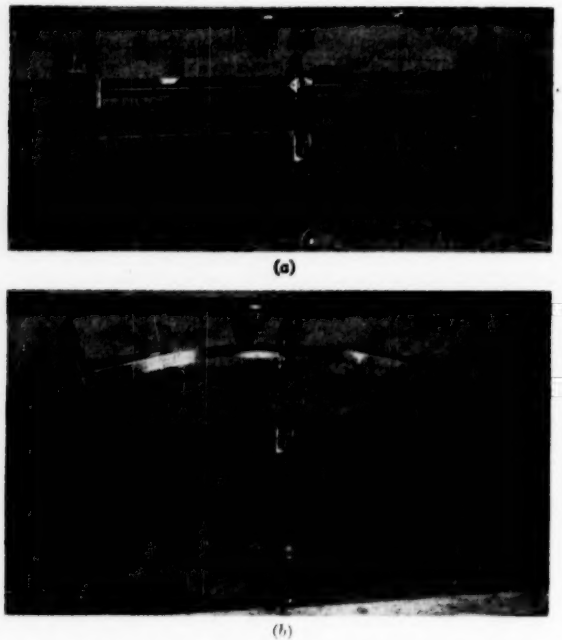


FIG. 16 SNAPOVER TORSIONAL BUCKLING OF ANGLE SECTION UNDER BENDING

since beyond it more torque is available than more rotation requires for equilibrium. Once this point is passed, the curve may descend to intersect the rotation axis (zero torque) and then rise again to intersect it once more, as the cosine in Equation [12] would indicate. In that case the last intersection would represent a stable deformed equilibrium state under zero torque. Fig. 16(*b*) shows such a state. The specimen in Fig. 16(*a*), with the bending moment on it, but no torque, was twisted by hand, and at a certain twist it snapped over to the form in Fig. 16(*b*).

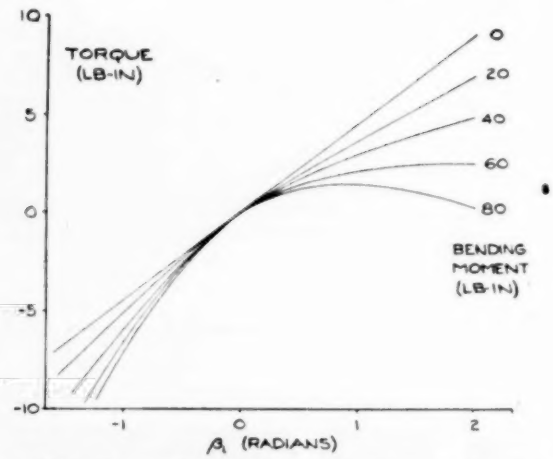


FIG. 17(*a*) TORQUE VERSUS ROTATION PREDICTED BY EQUATION [12] FOR VARIOUS BENDING MOMENTS

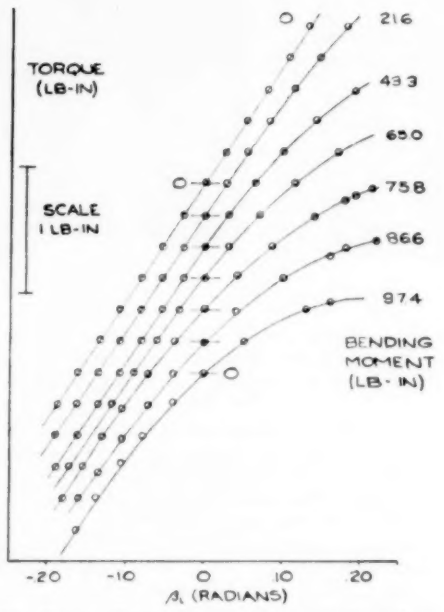


FIG. 17(*b*) TORQUE VERSUS ROTATION PLOTTED FROM EXPERIMENTAL DATA AT VARIOUS BENDING MOMENTS

## BIBLIOGRAPHY

1 "Elastic Torsion in the Presence of Initial Axial Stress," by J. N. Goodier, Trans. ASME, vol. 72, 1950, p. 383.

2 "On Vibration Galvanometers With Unifilar Torsional Control," by A. Campbell, Proceedings of the Physical Society of London, England, vol. 25, 1913, pp. 203–205.

3 "Buckling of Open Sections," by H. Wagner and W. Pretschner, NACA Technical Memo 784, 1936 (Translation).

4 "Torsional Stability of Cylindrical Shells," by A. Zahorski, *Journal of the Aeronautical Sciences*, vol. 5, 1937, p. 62.

5 "Experimental Study of Torsional Column Failure," by A. S. Niles, NACA Technical Note 733, 1939.

6 "The Buckling of Compressed Bars by Torsion and Flexure," by J. N. Goodier, Cornell University Engineering Experiment Station, Bulletin No. 27, 1941.

7 "Structural Beams in Torsion," by Inge Lyse and B. G. Johnston, Proceedings of the ASCE, vol. 61, 1935, p. 469.

8 "Uber die Stabilität der Biegung," by H. Reissner, *Archiv der Mathematik und Physik*, vol. 7, 1904, 4 pp.

9 "Torsional and Flexural Buckling of Bars of Thin-Walled Open Section Under Compressive and Bending Loads," by J. N. Goodier, JOURNAL OF APPLIED MECHANICS, Trans. ASME, vol. 64, 1942, p. A-103.

10 "Lateral Buckling of Beams," by S. E. Kindem, Det Kongelige Norske Videnskabers Selskab, Forhandlinger Bd. XXI, Nr. 1, 1948.

11 "Lateral Buckling of Bars of Monosymmetric Open Cross Section," by H. L. Engel, Technical Report No. 8, Contract N6-ONR-251 T.O. 12, Stanford University, Stanford, Calif., 1950.

# Brief Notes*

**On the recommendations of the Executive Committee of the ASME Applied Mechanics Division, it has been decided to initiate a section devoted to brief notes on technical matters in mechanics. These notes must not be longer than 750 words (about 2½ double-spaced typewritten pages, including figures) and will be subject to the usual review procedure prior to publication. After approval such notes will be published in the next issue of the Journal. The notes should be submitted to the Secretary of the ASME Applied Mechanics Division.**

## The Complex-Variable Approach to Stress Singularities

By J. H. HUTH[1]

RECENTLY some interest has centered on the problem of singularities in sector plates subject to extensions in their plane.[2] This note utilizes an entirely different approach to re-examine earlier results.

Consider an elastic sector of angle $\alpha$ with one face horizontal, and in a state of plane strain. The horizontal face is clamped while the other face is free. To investigate the possibility of non-vanishing stress fields, introduce two analytic functions of the complex variable $z = x + iy$. The conditions along the stress and displacement free faces become, respectively[3]

$$\sigma_\theta - i\tau_{r\theta} = \Phi(z) + \overline{\Phi(z)} + \frac{\bar{z}}{z}\left[z\overline{\Phi'(z)} + \overline{\psi(z)}\right] = 0 \quad [1]$$

$$\frac{\partial u}{\partial r} + i\frac{\partial v}{\partial x} = k\Phi(z) - \overline{\Phi(z)} - z\overline{\Phi'(z)} - \overline{\psi(z)} = 0 \quad [2]$$

Here $\sigma_\theta$ and $\tau_{r\theta}$ are the normal and shearing-stress components, respectively, $u$ and $v$ are Cartesian components of displacement, and $k = 3 - 4\nu$, where $\nu$ represents Poisson's ratio. A primed quantity represents differentiation, while a bar, the complex conjugate.

The function $w = z^{\pi/\alpha}$ maps the sector into the upper half plane. Equations [1] and [2] then become

$$\Phi(w) + \Phi(w) + \frac{\pi}{\alpha} w\,\Phi'(w) + e^{-2i\alpha}\psi(w) = 0 \quad [3]$$

$$k\Phi(w) - \overline{\Phi(w)} - \frac{\pi}{\alpha} w\,\overline{\Phi'(w)} - \overline{\psi(w)} = 0 \quad [4]$$

along the left and right portions, respectively, of the real axis.

Define $\psi$ in terms of $\Phi$ as follows

$$\psi(w) = -\Phi(w) + k\,\overline{\Phi(w)} - \frac{\pi}{\alpha} w\Phi'(w) \quad [5]$$

Equation [4] is then satisfied, and the problem reduces to finding a function analytic in the entire $w$-plane except for a branch cut extending along the real axis from the origin to minus infinity. Substituting Equation [5] into Equation [3] yields the "cut" condition

$$(1 - e^{2i\alpha})\Phi^+ + \overline{\Phi^+} + ke^{2i\alpha}\,\overline{\Phi^-} + \frac{\pi}{\alpha}(1 - e^{2i\alpha})w\Phi^{+\prime} = 0 \quad [6]$$

A superscript + indicates the value of $\Phi$ on the upper side of the cut, while a −, the value on the lower side. Assuming solutions of the form $(a + ib)(-w)^n$ where $a$, $b$, and $n$ are all real, Equation [6] becomes

$$(1 - e^{2i\alpha})(a + ib) + (a - ib) + ke^{2i\alpha}(a - ib)e^{2\pi in} + \frac{\pi}{\alpha} n\,(a + ib)(1 - e^{2i\alpha}) = 0 \quad [7]$$

This yields a pair of simultaneous homogeneous equations for $a$ and $b$. Setting $\theta = (\alpha + \pi n)$, the resulting "eigenequation" for $n$ takes the form

$$\sin^2\theta = \frac{4(1-\nu)^2}{(3-4\nu)} - \left[\frac{\sin^2\alpha}{\alpha^2(3-4\nu)}\right]\theta^2 \quad [8]$$

This equation corresponds to Williams',[2] "clamped-free" case and has a finite number of real roots. Continuity of displacements at the corner requires $\frac{\pi n}{\alpha} > -1$, so that any roots in the range $-1 < \frac{\pi n}{\alpha} < 0$ result in stress singularities. However, only the real root of Equation [8] represents admissable solutions except when $\alpha = \pi$. This contradicts Williams' assumption that all complex roots are admissable.

The particular case of $\alpha = \pi$ is degenerate in that $w = z$, and Equation [6] then only involves $\Phi$. Singularities resulting from the complex roots of the degenerate equation have appeared in the solution of a thermal-stress problem.[4]

General solutions of the form $(a + ib)(-w)^{\gamma + i\beta}$ will result in a set of four simultaneous homogeneous equations for $a$ and $b$. It can be shown that if $\gamma$ and $\beta$ satisfy the following two simultaneous equations, then nontrivial consistent solutions of the original four equations are possible

$$1 - 2\cos 2\alpha - k^2 e^{4\pi\beta}\cos 2(2 + \pi\gamma) + 2\frac{\pi}{\alpha}(1 - \cos 2\alpha)\left(\frac{\pi}{\alpha}\gamma^2 + 2\gamma + \frac{\pi}{\alpha}\beta^2\right) = 0 \quad [9]$$

$$-2ke^{2\pi\beta}\left(1 + \pi\frac{\gamma}{\alpha}\right)[\sin(4\alpha + 2\pi\gamma) - \sin(2\alpha + 2\pi\gamma)] + \frac{2\pi}{\alpha}\beta ke^{2\pi\beta}[\cos(2\alpha + 2\pi\gamma) - \cos(4\alpha + 2\pi\gamma)] + \frac{2\pi}{\alpha}\beta(1 - \cos 2\alpha) - 2\left(1 + \pi\frac{\gamma}{\alpha}\right)\sin 2\alpha = 0 \quad [10]$$

[1] Pacific Palisades, Calif.

[2] "Stress Singularities Resulting From Various Boundary Conditions in Angular Corners of Plates in Extension," by M. L. Williams, JOURNAL OF APPLIED MECHANICS, Trans. ASME, vol. 74, 1952, pp. 526–528.

[3] "Singular Integral Equations," by N. I. Muskhelishvili, Commonwealth of Australia, Department of Supply and Development, Aeronautical Research Laboratories, Fishermen's Bend, Melbourne, Australia, 1949, p. 254.

[4] "Thermal Stresses in a Partially Clamped Elastic Half-Plane," by J. H. Huth, *Journal of Applied Physics*, vol. 23, 1952, pp. 1234–1237.

* Discussion of papers in Brief Notes should be addressed to the Secretary, ASME, 29 West 39th Street, New York, N. Y., and will be accepted January 11, 1954, for publication at a later date. Discussion received after the closing date will be returned.

NOTE: Statements and opinions advanced in papers are to be understood as individual expressions of their authors and not those of the Society. Manuscript received by ASME Applied Mechanics Division, March 17, 1953.

Unfortunately the resulting set of solutions cannot generally be used to satisfy an arbitrary loading on the outer boundary of a finite wedge. In order to handle finite wedges one would probably have to admit such functions as

$$\Phi = \left(\frac{z}{z-1}\right)^{\frac{\ln 2}{2\pi i}} \frac{1}{\sqrt{z(z-1)}} \quad [11]$$

This satisfies Equation [6] for $\alpha = \pi$ and $\nu = 1/4$ but has a branch line along the real axis for $z \geq 1$.

In conclusion, studying an infinite wedge can lead to the order of possible singularities but not, in general, to a set of functions suitable for a complete analysis of the finite sector.

# Note on the Maximum Effect of a Moving Force on a Simple Beam

By E. S. EICHMANN,[1] URBANA, ILL.

THE construction of monorail tracks for high-speed vehicles has revived interest in analysis of the dynamic behavior of a simply supported beam traversed at constant velocity by a concentrated force. In the case in which the force is constant in magnitude, the maximum deflection-amplification factor appears to have been overlooked in the literature. L. E. Goodman[2] has called attention to the fact that the maximum dynamic deflection does not occur at the instant the load leaves the beam, as is implied by Timoshenko,[3] but actually occurs when the load is about three quarters of the way across. Furthermore, the correct maximum amplification factor is appreciably larger than that appearing in the literature and it corresponds to a velocity considerably lower than the so-called "resonance" velocity.

Defining the amplification factor as

$$A = \frac{w_t}{w_{st}} = \frac{\text{Maximum dynamic deflection}}{\text{Maximum static deflection due to concentrated force}}$$

we can obtain an expression, considering only the first mode, which has the form

$$A = \frac{96}{\pi^4} \frac{\sin \pi vt/l - (\pi v/\omega_1 l) \sin \omega_1 t}{1 - (\pi v/\omega_1 l)^2} \quad [1]$$

where $v$ = velocity of the constant force, $l$ = span length, and $\omega_1$ = lowest natural frequency of the beam. The justification for considering only the first mode lies in the rapid convergence of the series solution for the deflection which contains the factor $i^{-4}$, where $i$ denotes the mode order.[3]

We now introduce the dimensionless quantities $\beta = \omega_1 l/v$, a factor which varies inversely with the velocity, and $\kappa = vt/l$, which defines the position of the force on the beam at any time $t$.

Then

$$A = \frac{96}{\pi^4} \frac{\sin \pi\kappa - (\pi/\beta) \sin \beta\kappa}{1 - (\pi/\beta)^2} \quad [2]$$

Differentiating with respect to $\kappa$

$$\frac{dA}{d\kappa} = \frac{96}{\pi^4} \frac{\pi \cos \pi\kappa - \pi \cos \beta\kappa}{1 - (\pi/\beta)^2} \quad [3]$$

So that for a stationary value

$$\pi\kappa = 2n\pi \pm \beta\kappa$$

or

$$\kappa = 2n\pi/(\pi \mp \beta) \quad [4]$$

where the symbol $n$ denotes some integer. From examination of Equation [3] it appears that $n$ must be positive and, therefore, that the positive sign in the denominator of Equation [4] must be used. The most interesting possibilities are $n = 0$ and $n = 1$.

The case $n = 0$ implies $\beta = \pi$. This is the case studied by Timoshenko. It was found by Timoshenko[3] that for $\beta = \pi$ and $\kappa = 1$, i.e., the force just leaving the beam, the amplification factor is 1.547. This value has been used in the literature as the maximum amplification factor. The case $n = 1$, however, actually yields a larger amplification factor. In this case $\kappa = 2\pi/(\pi + \beta)$ and substitution into Equation [2] gives

$$A = \frac{96}{\pi^4} \frac{\sin [2\pi/(1 + \beta/\pi)] - (\pi/\beta) \sin [2\beta/(1 + \beta/\pi)]}{1 - (\pi/\beta)^2} \quad [5]$$

This function has a maximum value of 1.743 for $\beta = 1.64\pi$. Consequently the maximum dynamic deflection is approximately 1.743 times the static deflection which would be caused by the same force if stationary. It occurs when the velocity is such that the time of transit is 0.82 times the fundamental period of the span. The corresponding value of $\kappa$ is 0.757 which means that the force has just passed the third-quarter point of the beam at the instant that the maximum deflection occurs.

The analysis is limited in application by the fact that in practice it is usually a constant mass rather than a constant force which traverses the span. In the former case, structure and load interact in a complex way and the force exerted on the structure is not constant.

Acknowledgment

The author's thanks are due Prof. L. E. Goodman who directed his attention to this deficiency in knowledge of the response of structures to dynamic loads.

[1] Research Assistant in Civil Engineering, University of Illinois.

[2] "Behavior of Structures Under Dynamic Loads"—a course of lectures in the Graduate College of the University of Illinois.

[3] "Vibration Problems in Engineering," by S. Timoshenko, second edition, D. Van Nostrand Company, Inc., New York, N. Y., 1937, pp. 352–356.

Manuscript received by ASME Applied Mechanics Division, July 15, 1953.

# A Resistor-Network Solution for the Torsion of Hollow Sections

By J. H. WEINER,[1] NEW YORK, N. Y.

COLIN and Newmark[2] have presented a numerical solution of the problem of torsion of a cylindrical bar with longitudinal holes. They use finite-difference approximations of the partial differential equation and boundary conditions and solve the resulting set of linear equations by relaxation.

In this note, a method of solution using resistor network is presented. The same finite-difference approximations are made, but the set of linear equations is solved by the network.

[1] Assistant Professor of Civil Engineering; Assistant Technica Director, Heat and Mass Flow Analyzer Laboratory, Columbia University.

[2] "A Numerical Solution for the Torsion of Hollow Sections," by E. C. Colin, Jr. and N. M. Newmark, Journal of Applied Mechanics, Trans. ASME, vol. 69, 1947, pp. A-313 to A-315.

Manuscript received by ASME Applied Mechanics Division, May 7, 1953.

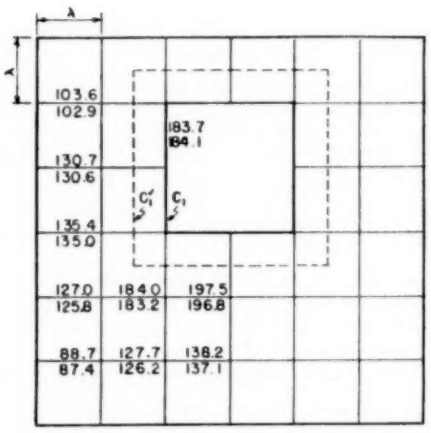


FIG. 1 HOLLOW SECTION STUDIED
(Upper figures, values of $\varphi$ by Colin and Newmark; lower figures from network, $2G\theta\lambda^2 = 100$.)

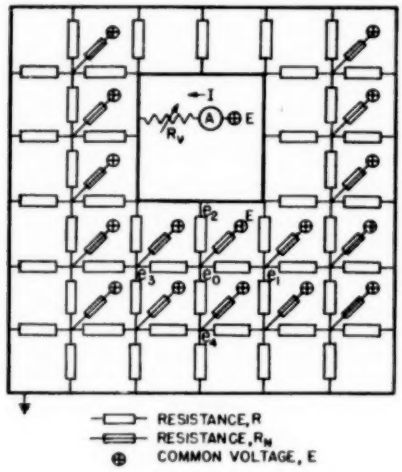


FIG. 2 RESISTOR NETWORK

Consider a cylindrical bar, with $n$ longitudinal holes, subjected to torsion. In the usual notation, the components of shear stress on the cross section are given by

$$\tau_{zx} = \frac{\partial \varphi}{\partial y} \quad \text{and} \quad \tau_{zy} = -\frac{\partial \varphi}{\partial x} \qquad [1]$$

where the stress function $\phi(x, y)$ satisfies the equation

$$\frac{\partial^2 \varphi}{\partial x^2} + \frac{\partial^2 \varphi}{\partial y^2} = -2G\theta \qquad [2]$$

at all interior points of the cross section of the bar, together with the boundary conditions

$$\varphi_{C_i} = k_i, \quad i = 0, 1, 2, \ldots, n \qquad [3]$$

$$\int_{C'_i} \frac{\partial \varphi}{\partial n}\, ds = 2G\theta A_{C'_i}, \quad i = 1, 2, \ldots, n \qquad [4]$$

In Equation [3], $C_0$ is the exterior boundary of the cross section, $C_i$ the internal boundaries. $\varphi_{C_i}$ is the value of $\varphi$ at any point of $C_i$. The $k_i$ are constants. We may set $k_0 = 0$ and the $k_i$, $i = 1, \ldots, n$, must be such that Equations [2] to [4] are satisfied simultaneously. In Equation [4], $C'_i$ is any curve enclosing $C_i$ but no other internal boundary, and $A_{C'_i}$ is the area enclosed by it.

The resistor-network method will be described as applied to the illustrative problem of Colin and Newmark, Fig. 1. Using a square mesh of side $\lambda$, a finite-difference approximation to Equation [2] is

$$\varphi(x, y) = \frac{\varphi(x, y + \lambda) + \varphi(x, y - \lambda) + \varphi(x + \lambda, y) + \varphi(x - \lambda, y) + 2G\theta\lambda^2}{4} \qquad [2a]$$

The finite-difference approximation used for Equation [4] is

$$2G\theta A_{C'_i} = \sum_j \left(\frac{\varphi_{C_1} - \varphi_j}{\lambda}\right)\lambda = \sum_j (\varphi_{C_1} - \varphi_j) \qquad [4a]$$

where $C'_1$ is the dashed curve shown in Fig. 1 and the summation is carried out over all the nodes which are connected directly to the boundary of the hole. $\varphi_j$ is the value of $\varphi(x, y)$ at the $j$th such node.

Consider now the resistor network shown in Fig. 2. (Because of symmetry, only half the network actually was set up.) Applying Kirchhoff's law to the currents flowing into a typical node, the following relation is obtained

$$\frac{e_1 - e_0}{R} + \frac{e_2 - e_0}{R} + \frac{e_3 - e_0}{R} + \frac{e_4 - e_0}{R} + \frac{E - e_0}{R_N} = 0$$

If $E$ is taken very large relative to any nodal value of $e$, the last term is approximately equal to $E/R_N$. Then the foregoing becomes

$$e_0 = \frac{e_1 + e_2 + e_3 + e_4 + RE/R_N}{4} \qquad [2b]$$

Also, the current $I$, indicated in Fig. 2, is given by Equation [4b]

$$I = \sum_j \frac{e_{C_1} - e_j}{R} \qquad [4b]$$

where the summation is carried out over the same nodes as in Equation [4a]. If a scale factor between $e$ and $\varphi$ is established

$$e = K\varphi \qquad [5]$$

then the two sets of equations, Equations [2a] and [4a] and Equations [2b] and [4b], respectively, are identical if

$$RE/KR_N = 2G\theta\lambda^2 \qquad [6]$$

$$I = 2G\theta A_{C'_1} K/R \qquad [7]$$

The solution to Equations [2a] and [4a], therefore, is obtained by means of the resistor network if the resistors and the voltage $E$ are chosen according to Equation [6], and $R_N$ is adjusted until the meter indicates the current calculated from Equation [7]. Equations [3] are satisfied since the nodes on the external and internal boundaries, respectively, are shorted together. The value of $\varphi$ at each node is obtained from the voltage at each node using Equation [5].

The network and numerical solutions, compared in Fig. 1, agree within a maximum discrepancy of 1.5 per cent. A more accurate solution of the original problem would require many more nodes. For a fine mesh, the network approach should be considerably quicker than the numerical one.

A paper by Redshaw[3] recently has come to the author's attention which treats the torsion problem of solid sections by resistor networks and contains a discussion of the treatment of curved exterior boundaries. The foregoing method for rectangular interior boundaries may be modified for curved interior boundaries in a similar manner.

The problem was solved on the resistor-network board of the Heat and Mass Flow Analyzer Laboratory at Columbia University suitable for circuits with up to 576 nodes.

# Closed-Form Solutions for Plates of Variable Thickness

By H. D. CONWAY,[1] ITHACA, N. Y.

THE analysis of the bending of symmetrically loaded circular plates of variable thickness involves the solution of the differential equation (1)[2]

$$D\frac{d}{dr}\left(\frac{d\phi}{dr}+\frac{\phi}{r}\right)+\frac{dD}{dr}\left(\frac{d\phi}{dr}+\frac{\nu\phi}{r}\right)=-\int_0 qrdr \quad [1]$$

where $D$ is the flexural rigidity, $\phi$ is the slope at radius $r$, $\nu$ is Poisson's ratio, and $q$ is the intensity of loading. Having found $\phi$ for a particular problem, the bending moments are given by

$$\left.\begin{aligned} M_r &= D(d\phi/dr+\nu\phi/r)\\ M_\theta &= D(\phi/r+\nu d\phi/dr)\end{aligned}\right\} \quad [2]$$

If the complementary solution of Equation [1] is known for a specific variation in flexural rigidity, the particular solution may be obtained by the method of variation of parameters. The labor involved in obtaining numerical results is likely to be greatly decreased if the complementary solution can be written in closed form, and it is very useful to have a list of flexural rigidity variations for which this is possible.

In so far as the complementary solution is concerned, the differential equation governing the radial deformation of rotating disks of variable thickness is similar to Equation [1], $D$ and $\phi$ being replaced, respectively, by the thickness $h$ and radial displacement $u$. The results of investigations on rotating disks may therefore be applied to plate problems. Timoshenko (2) attributes the discovery of this analogy to L. Föppl.

If a flexural rigidity $D = D_0r^m$ is assumed, where $D_0$ and $m$ are constants, the complementary solution (3) satisfies

$$r^2\frac{d^2\phi}{dr^2}+(m+1)r\frac{d\phi}{dr}-(1-m\nu)\phi=0 \quad [3]$$

This is the well-known Euler equation and the solution is

$$\phi = Ar^{\frac{2\alpha-m}{2}}+Br^{\frac{-2\alpha-m}{2}} \quad [4]$$

where $4\alpha^2 = 4-4m\nu+m^2$.

Assuming now a flexural rigidity $D = D_0(1-kr^m)^n$ where $D_0$, $k$, $m$, and $n$ are constants, substituting in Equation [1], and writing $x = kr^m$, the complementary solution satisfies

$$x(1-x)\frac{d^2\phi}{dx^2}+(1-x-nx)\frac{d\phi}{dx}-\left(\frac{1-x}{m^2x}+\frac{n\nu}{m}\right)\phi=0 \quad [5]$$

This is Riemann's $P$-equation (4), the general solution being in terms of hypergeometric functions. From an investigation by Gran Olsson (5) of rotating disks of variable thickness, and assuming as a special case that $m = n\nu = 1$, the general solution of Equation [5] may be written in the closed form

$$\phi = A\left(\frac{1}{x}+n-1\right)+B\left[\frac{1}{x}(1-x)^{1-n}-\left(\frac{1}{x}-1+n\right)\right] \quad [6]$$

With $n = 3$ and $\nu = 1/3$, this solution has been used to analyze plates having a thickness decreasing linearly toward the rim (6). Other variations of flexural rigidity may be treated by choosing appropriate values of $n$ and $\nu$ such that their product is unity.

Suhara (7) has investigated rotating disks whose thickness varies according to $h = h_0(1-kr^m)^n$ and his results may be applied to plates having a flexural rigidity of the form $D = D_0(1-kr^m)^n$. This investigation shows—after a correction—that for $m = 2/3$, $n = 2$, and $\nu = 1/3$, the solution of Equation [5] is

$$\phi = \frac{Ax^{1/2}}{1-x}+\frac{B}{x^{1/2}(1-x)} \quad [7]$$

For $m = 1/2$, $n = 2$, $\nu = 1/4$, the solution of Equation [5] is

$$\phi = A\frac{x^2}{1-x}+\frac{B}{x^2(1-x)} \quad [8]$$

For the flexural rigidity $D = D_0e^{-kr^m}$, where $D_0$, $k$, and $m$ are constants, the complementary solution of Equation [1] satisfies

$$\frac{d^2\phi}{dr^2}+\left(\frac{1}{r}-mkr^{m-1}\right)\frac{d\phi}{dr}-\left(\frac{1}{r^2}+m\nu kr^{m-2}\right)\phi=0 \quad [9]$$

Substituting $\phi = Ve^{x/2}$ where $x = kr^m$, the equation becomes, for $2\nu = m$

$$\frac{d^2V}{dx^2}+\frac{1}{x}\frac{dV}{dx}-\left(\frac{1}{4}+\frac{1}{m^2x^2}\right)V=0 \quad [10]$$

and it follows that

$$\phi = e^{x/2}\left[AI_{1/m}(x/2)+BK_{1/m}(x/2)\right] \quad [11]$$

where $I$ and $K$ are modified Bessel functions of the first and second kind, respectively. If $(1/m-1/2)$ is an integer, this solution may be written in closed form. For example, if $m = 2/3$ and $\nu = 1/3$, we have after some reduction

$$\phi = x^{-3/2}[Ae^x(2-x)+B(2+x)] \quad [12]$$

Other solutions in closed form are possible for $(m = 2/5, \nu = 1/5)$, $(m = 2/7, \nu = 1/7)$, and so on, but these become progressively more complicated, in addition to which the values of Poisson's ratio become progressively less realistic for metallic plates. An investigation similar to the foregoing has been made by Gran Olsson (8).[3]

## BIBLIOGRAPHY

1 "Theory of Plates and Shells," by S. Timoshenko, McGraw-Hill Book Company, Inc., New York, N. Y., 1940, p. 238.
2 Loc. cit., 1, p. 287.
3 "Note on the Bending of Circular Plates of Variable Thickness," by H. D. Conway, JOURNAL OF APPLIED MECHANICS, Trans. ASME, vol. 71, 1949, pp. 209–210.
4 "Ordinary Differential Equations," by E. L. Ince, Dover Publications, New York, N. Y., 1944, p. 391.

[3] "An Electrical Potential Analyzer," by S. C. Redshaw, Proceedings of The Institution of Mechanical Engineers, vol. 159, 1948, pp. 55–62.

[1] Professor of Mechanics, Cornell University. Jun. ASME.

[2] Numbers in parentheses refer to the Bibliography at the end of the paper.

Manuscript received by ASME Applied Mechanics Division, June 24, 1953.

[3] There appears to be an error in the example given on page 84 of the paper.

5 "Über einige Lösungen des Problems der rotierenden Scheibe," by R. Gran Olsson, *Ingenieur Archiv.*, vol. 8, 1937, pp. 270–275.

6 "Axially Symmetrical Plates With Linearly Varying Thickness," by H. D. Conway, JOURNAL OF APPLIED MECHANICS, Trans. ASME, vol. 73, 1951, pp. 140–142.

7 "On the Stresses in a Rotating Circular Disc Whose Thickness Is Expressed by $z = Ar^k(1 - \lambda r^n)^k$," by T. Suhara, Transactions of the Japanese Society of Mechanical Engineers, vol. 3, February, 1937, pp. 1–6. This rather general expression also yields Riemann's *P*-equation for the complementary solution.

8 "Biegung kreisförmiger Platten von radial veränderlicher Dicke," by R. Gran Olsson, *Ingenieur Archiv.*, vol. 8, 1937, pp. 81–98.

# A Note on Mass Flow

By E. C. KENNEDY,[1] DAINGERFIELD, TEXAS

THE "exact" formula for mass flow of a compressible fluid is rather cumbersome and tedious to use even with a table of logarithms at hand. The object of this paper is to develop a simple and accurate formula for mass flow which will be useful to engineers and scientists interested in that field.

Consider a quantity of gas in a reservoir equipped with a properly designed outlet. It is desired to find the amount of gas discharged from the opening under certain specified conditions. Let $\gamma$ = specific heat ratio of gas; $A$ = area of outlet, in sq in., $P_1$ = pressure, psia at outlet (back pressure); $W$ = weight of gas discharged, lb per sec; $T_0$ = reservoir temperature in deg R; and $P_0$ = reservoir pressure, psia.

Making the usual simplifying assumptions concerning flow (i.e., uniform isentropic flow, and so forth) we write for the mass flow $m$

$$m = \rho V A \quad \ldots\ldots [1]$$

where $V$ is the velocity, $\rho$ the density, and any consistent units of measurement are used.

Using the adiabatic relationship and the compressible-fluid Bernoulli equation, it is easy to obtain the expression

$$m = A\sqrt{\frac{2\gamma}{\gamma - 1}\,P_0\rho_0\left[(P_1/P_0)^{2/\gamma} - (P_1/P_0)^{\frac{\gamma+1}{\gamma}}\right]} \quad \ldots [2]$$

If $\rho_0$ is eliminated in Equation [2] by means of the perfect gas law, $P = \rho RT$, we get for the weight flow of air the well-known formula

$$W = \frac{2.055\,AP_0}{\sqrt{T_0}}\,[(P_1/P_0)^{1.43} - (P_1/P_0)^{1.71}]^{1/2} \quad \ldots [3]$$

where the values $R = 1716.32$ ft$^2$/sec$^2$ deg R, $g = 32.1740$ ft/sec$^2$, and $\gamma = 7/5$ were used in obtaining the constant, 2.055.

Equation [2] is valid for

$$P_1/P_0 \geq \left[\frac{2}{\gamma + 1}\right]^{\frac{\gamma}{\gamma - 1}} = 0.5283$$

For all other values of the pressure ratio (supersonic flow) the formula $W = 0.532\,AP_0/\sqrt{T_0}$ is ordinarily used.

In the former case Equation [3] gives "exact" results, but it is cumbersome and awkward to handle—especially with a slide rule. Fliegner's formula, $W = 1.06\,A\sqrt{P_1(P_0 - P_1)}/\sqrt{T_0}$, is simple and compact but not very accurate in some cases, as will be shown later.

To develop a simple yet accurate formula for weight flow we set $X = 1 - P_1/P_0$ in Equation [3] obtaining

$$W = 2.055\,\frac{AP_0}{\sqrt{T_0}}\,[(1 - X)^{1.43} - (1 - X)^{1.71}]^{1/2}$$

Expanding by the binomial theorem and collecting terms

$$W = 2.055\,\frac{AP_0}{\sqrt{T_0}}\left[\frac{2}{7}X - \frac{15}{49}X^2 + \frac{10}{2401}X^3 \ldots\right]^{1/2}$$

The infinite series in the bracket converges rapidly for $X < 1/2$. Note that the $X^3$ term drops out, a fact that greatly simplifies the formula. Thus to a high degree of accuracy

$$W = 1.0983\,AP_0\left[\frac{X - 1.071\,X^2}{T_0}\right]^{1/2}$$

A small amount of algebraic manipulation leads to the accurate and compact formula for weight flow

$$W = \frac{1.137\,A}{\sqrt{T_0}}\sqrt{(P_0 - P_1)(P_1 - 0.0666P_0)} \quad \ldots [4]$$

Let us compare the foregoing with Fliegner's formula by means of the following examples:

*Example 1.* Given: $P_0 = 40$, $P_1 = 38$, $T_0 = 625$, $A = 1$. We find

$W = 0.3696$ Error = 3.3 per cent (Fliegner)
$W = 0.3823$ Error = 0.01 per cent (Kennedy)

*Example 2.* Given: $P_0 = 40$, $P_1 = 22$, $T_0 = 625$, $A = 1$. Whence

$W = 0.8438$ Error = 0.73 per cent (Fliegner)
$W = 0.8484$ Error = 0.18 per cent (Kennedy)

Note that Fliegner's formula is not so accurate as slide-rule computation whereas the author's exceeds it. Using the same method, a similar formula may be developed for any other gas if $R$ and $\gamma$ are known.

[1] Senior Research Engineer, Consolidated Vultee Aircraft Corporation, Ordnance Aerophysics Laboratory.

Manuscript received by ASME Applied Mechanics Division, February 13, 1953.

# Diametral Expansion of Helical Compression Springs During Deflection

By A. M. WAHL,[1] EAST PITTSBURGH, PA.

**Design formulas are derived for the diametral expansions of helical compression springs assuming (1) ends free to rotate about the helix axis and (2) ends fixed against rotation. The results are of particular interest where helical compression springs are used in cylindrical guides.**

IN many cases where helical compression springs operate inside cylinders or guides, the designer must provide clearance between the spring and the inside surface of the guide. Although the problem of calculating this clearance may be solved theoretically,[2] no simple and yet accurate formula appears to be available for design use. It is the purpose of this note to derive such formulas.

For purposes of this discussion, helical springs may be divided into two cases: (1) Springs with ends free to rotate about the helix axis during deflection and (2) springs with ends fixed against

[1] Advisory Engineer, Research Laboratories, Westinghouse Electric Corporation. Fellow ASME.

[2] "Mechanical Springs," by A. M. Wahl, Penton Publishing Company, Cleveland, Ohio, 1944, Chapter III.

Manuscript received by ASME Applied Mechanics Division, May 28, 1953.

rotation about the helix axis. Case (2) springs will show lower diametral expansions than case (1) springs, while actual springs compressed between parallel plates will usually show a behavior intermediate between these two cases.

*Case (1)—Compression Spring With Ends Free to Rotate About Helix Axis During Deflection.* For this case expressions for the change in curvature $\Delta\kappa$ and the angular twist $\Delta\theta$ per unit length of a rod of helical form (helical spring) when deflection takes place from an initial pitch angle $\alpha_0$ to a final pitch angle $\alpha$ are[3]

$$\Delta\kappa = \frac{\cos^2\alpha}{r} - \frac{\cos^2\alpha_0}{r_0} \quad [1]$$

$$\Delta\theta = \frac{\sin\alpha\cos\alpha}{r} - \frac{\sin\alpha_0\cos\alpha_0}{r_0} \quad [2]$$

In these $r_0$ and $r$ are the initial and final mean coil radii, respectively. If a load $P$ acts along the helix axis then $Pr\sin\alpha = EI(\Delta\kappa)$ and $Pr\cos\alpha = GI_p(\Delta\theta)$, where $EI$ and $GI_p$ are the flexural and torsional rigidities. (We assume round wire springs so that $EI/GI_p = 1.3$ for Poisson's ratio = 0.3.) Using these equations in Equations [1] and [2], and eliminating $P$ we obtain

$$\frac{r}{r_0} = \frac{[EI/GI_p + \tan^2\alpha]\cos^2\alpha}{\sin\alpha_0\cos\alpha_0\tan\alpha + \dfrac{EI}{GI_p}\cos^2\alpha_0} \quad [3]$$

The radial expansion during deflection will be $r - r_0$ and the diametral expansion $\Delta D$ will be

$$\Delta D = 2(r - r_0) = \left(\frac{r}{r_0} - 1\right) D_0 \quad [4]$$

where $D_0 = 2r_0$ = initial mean coil diameter.

Using Equation [3] in Equation [4] and taking $EI/GI_p = 1.3$ we obtain

$$\frac{\Delta D}{D_0} = \left[\frac{(1.3 + \tan^2\alpha)\cos^2\alpha - (1.3 + \tan\alpha\tan\alpha_0)\cos^2\alpha_0}{(\tan\alpha\tan\alpha_0 + 1.3)\cos^2\alpha_0}\right] \quad [5]$$

This equation is not in very convenient form for practical use; hence to simplify the expression further we assume that the spring is compressed from free height (pitch angle $\alpha_0$) to solid height (pitch angle $\alpha$) and calculate the expansion in diameter on this basis.

Taking $p$ initial pitch (or center-to-center distance between coils) at free height and $\epsilon = \Delta D/D_0$, the following relations hold

$$\tan\alpha = \frac{d}{\pi D_0(1+\epsilon)};\quad \tan\alpha_0 = \frac{p}{\pi D_0};\quad \cos^2\alpha_0 = \frac{\pi^2 D_0^2}{\pi^2 D_0^2 + p^2}$$

$$\sin^2\alpha = \frac{d^2}{\pi^2 D_0^2(1+\epsilon)^2 + d^2};\quad \cos^2\alpha = \frac{\pi^2 D_0^2(1+\epsilon)^2}{\pi^2 D_0^2(1+\epsilon)^2 + d^2}$$

In general $\epsilon$ will be a small quantity compared to unity and for a close approximation it may be taken as zero in these formulas. (Furthermore exact calculations indicate that for practical springs the error in $\Delta D/D_0$ obtained by neglecting $\epsilon$ is only a small fraction of 1 per cent.)

Taking $\epsilon = 0$ in the foregoing trigonometric expressions and inserting these into Equation [5], the following expression for $\Delta D/D_0$ results

$$\frac{\Delta D}{D_0} = \frac{1.3p^2 - 0.3d^2 - pd + \dfrac{p^2d^2 - pd^3}{\pi^2 D_0^2}}{1.3\pi^2 D_0^2\left(1 + \dfrac{pd + 1.3\,d^2}{1.3\pi^2 D_0^2}\right)} \quad [6]$$

Further calculations indicate that for practical springs the term $(p^2d^2 - pd^3)/(\pi^2D_0^2)$ in the numerator, and the term $(pd + 1.3d^2)/(1.3\pi^2D_0^2)$ in the denominator of this expression may be neglected without affecting the accuracy more than a fraction of a per cent for the larger indexes where the diametral expansions are greatest. (For the smaller indexes the error may reach 1 or 2 per cent but this is still negligible for practical purposes.)

Thus taking $1.3\pi^2$ as 13 approximately, for design purposes Equation [6] reduces to the relatively simple expression

$$\frac{\Delta D}{D_0} = \frac{1.3p^2 - 0.3d^2 - pd}{13D_0^2} \quad [7]$$

In this, $\Delta D$ is diametral expansion as the springs deflect from free to solid height. Note that this formula also will apply for calculating the diametral "contraction" of a close-coiled tension spring when extended to a deflection $p - d$ per turn, and assuming that the end coils are free to rotate.

Test data[4] on two helical compression springs loaded so that rotation about the helix axis may occur freely, indicate agreement within about 3 per cent with results calculated from Equation [7]. These springs had rather large indexes (12 and 15) and values of $p/D_0$ equal to 0.6 and 0.74.

*Case (2)—Compression Spring With Ends Fixed Against Rotation About Helix Axis.* In this case, since the number of active coils does not change, the coil radius will remain proportional to the cosine of the pitch angle.[2] Hence

$$\frac{r}{r_0} = \frac{\cos\alpha}{\cos\alpha_0} \quad [8]$$

We again assume compression from free to solid height (i.e., from pitch angle $\alpha_0$ to pitch angle $\alpha$). Then if $l$ = total active length of wire or bar and $n$ = number of active coils, the following equation holds

$$\frac{\cos\alpha}{\cos\alpha_0} = \sqrt{\frac{l^2 - n^2d^2}{l^2 - n^2p^2}}$$

Taking $l^2 = \pi^2D_0^2n^2 + n^2p^2$, and using this in Equation [8]

$$\frac{r}{r_0} = \frac{\cos\alpha}{\cos\alpha_0} = \sqrt{1 + \frac{p^2 - d^2}{\pi^2 D_0^2}} \quad [9]$$

Substituting this in Equation [4], the ratio $\Delta D/D_0$ becomes

$$\frac{\Delta D}{D_0} = \sqrt{1 + \frac{p^2 - d^2}{\pi^2 D_0^2}} - 1 \quad [10]$$

In most practical springs the term $(p^2 - d^2)/(\pi^2D_0^2)$ in Equation [10] will be small compared to unity and this equation then reduces to

$$\frac{\Delta D}{D_0} \approx \frac{p^2 - d^2}{2\pi^2 D_0^2} \approx 0.05\,\frac{p^2 - d^2}{D_0^2} \quad [11]$$

Tests made on the compression springs mentioned previously, the ends being fixed against rotation, showed values for $\Delta D/D_0$ around 7 to 20 per cent higher than the values given by Equation [11]. This difference is probably due in part to the imperfect fixity of the end coils in actual compression springs so that results intermediate between the fixed and free-end cases may be expected.

[3] "Mathematical Theory of Elasticity," by A. E. H. Love, fourth edition, Dover Publications, New York, N. Y., 1944, p. 414.

[4] The author is indebted to Messrs. T. R. Weber, B. Sterne, and K. Maier of the SAE Technical Board Spring Committee for test data.

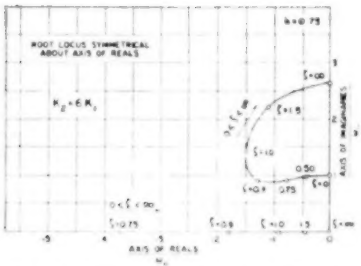

FIG. 1 EFFECT OF DAMPING FACTOR ON ROOT LOCUS

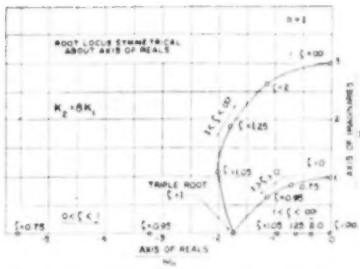

FIG. 2 EFFECT OF DAMPING FACTOR ON ROOT LOCUS

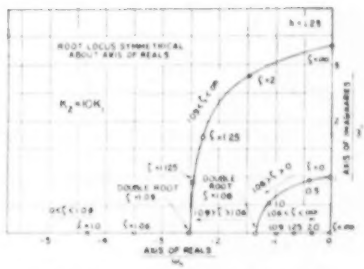

FIG. 3 EFFECT OF DAMPING FACTOR ON ROOT LOCUS

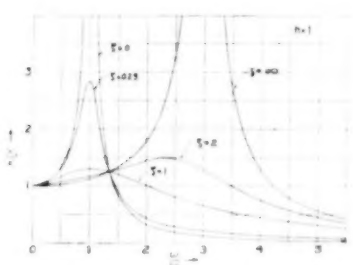

FIG. 4 AMPLITUDE CURVES

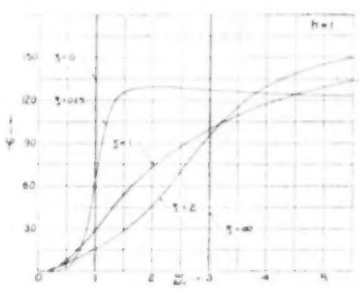

FIG. 5 PHASE-ANGLE CURVES

# Additional Data on the Relaxation Type of Vehicle Suspension

BY JOSEPH GALLAGHER[1] AND ENRICO VOLTERRA[2]

THIS "Brief Note" should be considered as a necessary addition to a previous joint paper,[3,4] in which a mathematical analysis of the relaxation type of vehicle suspension was given.

It is the object of this note to supply further data on the effects of parameter changes on the transient and forced vibrations of such a mechanical system by the presentation and use of root-locus diagrams and amplitudes and phase-angle curves.

Of the five diagrams which are now presented, the first three, Figs. 1 to 3, are root-locus diagrams which show the effect of the damping factor $\zeta$ on the roots of the characteristic equation for three values of the relaxation factor $h = K_2/K_{2c}$, while Figs. 4 and 5 give, respectively, the amplitude and phase-angle curves in the case of critical damping, $h = 1$.

Comparison of the root-locus diagrams for $h = 1$ and $h = 1.25$ indicates that $\zeta = 1$ and $h = 1$ are the minimal values of damping ratio and spring-constant ratio which will just give real roots of the characteristic equation (Equation [15][3]). This determines the boundary between the oscillatory and nonoscillatory solution.

The amplitude and phase-angle curves were calculated from the following equation

$$\frac{X_2}{X_1}(i\omega) = \frac{3\sqrt{3}\,\frac{b}{\zeta} + i\,[1 + 8h]\left(\frac{\omega}{\omega_{11}}\right)}{3\sqrt{3}\,\frac{h}{\zeta}\left[1 - \left(\frac{\omega}{\omega_{11}}\right)^2\right] + i\left[(1 + 8h)\,\frac{\omega}{\omega_{11}} - \left(\frac{\omega}{\omega_{11}}\right)^3\right]}$$

which has been obtained from Equation [27] of the previous paper[3] by replacing $S$ by $i\omega$ in it.

[1] Student, Oak Ridge School of Reactor Technology, Oak Ridge, Tenn. Jun. ASME.

[2] Professor of Mechanics, Rensselaer Polytechnic Institute, Troy, N. Y. Mem. ASME.

[3] "A Mathematical Analysis of the Relaxation Type of Vehicle Suspension," by J. Gallagher and E. Volterra, JOURNAL OF APPLIED MECHANICS, Trans. ASME, vol. 74, 1952, pp. 389–396.

[4] See the discussion on the previous paper,[3] published in the March, 1953, issue of the JOURNAL OF APPLIED MECHANICS, Trans. ASME, vol. 75, pp. 143–146.

Manuscript received by ASME Applied Mechanics Division, April 22, 1953.

# Note on Torsional Oscillation of I-Type Beams

BY J. E. GOLDBERG,[1] LAFAYETTE, IND.

IN dealing with the twisting of I-type beams, it may be assumed[2] that the applied torsional loads are resisted by a combination of shearing stresses distributed according to the Saint Venant theory and superimposed lateral shearing forces in the flanges. These latter, being equal and opposite in the respective flanges, constitute couples about the longitudinal axis of the beam. The internal strain energy of a twisted beam may be assumed, therefore, to consist of the strain energy associated with the Saint Venant torsional stresses plus the strain energy of the flanges in lateral bending.

[1] Associate Professor, School of Civil Engineering and Engineering Mechanics, Purdue University.

[2] "Strength of Materials," by S. Timoshenko, part 2, second edition, D Van Nostrand Company, Inc., New York, N. Y., 1941, p. 282.

Manuscript received by ASME Applied Mechanics Division, January 21, 1953.

The strain energy corresponding to the Saint Venant distribution is

$$U_1 = \frac{C}{2}\int_0^L \left(\frac{\partial\phi}{\partial x}\right)^2 dx$$

where $C$ is the torsional rigidity constant of the cross section and $\phi$ is the angular displacement. It may be noted that, for wide-flange sections, $C$ is approximately equal to $(G/3)(t_w^3 d + 2t_f^3 b)$, in which $G$ is the modulus of rigidity, $d$ is the depth of the section, $b$ is the width of the flanges, and $t_w$ and $t_f$ are the thickness of the web and the flanges, respectively.

If $w$ is the lateral deflection of each flange, the strain energy resulting from lateral bending of the two flanges is

$$U_2 = \frac{2\,EI_f}{2}\int_0^L \left(\frac{\partial^2 w}{\partial x^2}\right)^2 dx$$

Noting that $w = \pm \phi h/2$, where $h$ is the distance between flange centroids, and since the moment of inertia of one flange about its minor axis is only slightly less than one half of $I_{yy}$ of the entire section

$$U_2 = \frac{EI_{yy}}{2}\left(\frac{h}{2}\right)^2\int_0^L \left(\frac{\partial^2\phi}{\partial x^2}\right)^2 dx$$

In the case of a beam which is free to warp but not to twist at the ends, i.e., flanges pinned with respect to lateral bending, the angle of twist may be represented in the form

$$\phi(x, t) = \sum_{n=1}^{\infty} \phi_n \sin\frac{n\pi x}{L}$$

Substituting this series into the strain-energy expression, and performing the indicated integrations, the total strain energy is found to be

$$U = U_1 + U_2 = \frac{CL}{4}\sum_{n=1}^{\infty}\phi_n^2\left(\frac{n\pi}{L}\right)^2 + EI_{yy}\frac{h^2 L}{16}\sum_{n=1}^{\infty}\phi_n^2\left(\frac{n\pi}{L}\right)^4$$

Assuming no appreciable distortion in the cross section, and neglecting displacements out of the plane of the cross section, the kinetic energy is

$$T = \frac{\rho}{2}J\int_0^L \left(\frac{\partial\phi}{\partial t}\right)^2 dx$$

where $\rho$ is the mass density and $J$ is the polar moment of inertia of the cross section. Using the series representation, it is found that

$$T = \frac{\rho}{4}JL\sum_{n=1}^{\infty}\left(\frac{\partial\phi_n}{\partial t}\right)^2$$

The Lagrange equations for free vibration are

$$\frac{d}{dt}\left(\frac{\partial T}{\partial\dot{q}_i}\right) + \frac{\partial U}{\partial q_i} = 0$$

Considering the $\phi_n$ as the generalized co-ordinates, the Lagrange equations become

$$\frac{\rho JL}{2}\frac{\partial^2\phi_n}{\partial t^2} + \left[\frac{CL}{2}\left(\frac{n\pi}{L}\right)^2 + EI_{yy}\frac{h^2 L}{8}\left(\frac{n\pi}{L}\right)^4\right]\phi_n = 0$$

or

$$\frac{\partial^2\phi_n}{\partial t^2} + \left[\frac{C\left(\frac{n\pi}{L}\right)^2 + EI_{yy}\frac{h^2}{4}\left(\frac{n\pi}{L}\right)^4}{\rho J}\right]\phi_n = 0$$

The frequencies are therefore given by

$$f_n = \frac{n}{2L}\sqrt{\frac{C + EI_{yy}\frac{h^2}{4}\left(\frac{n\pi}{L}\right)^2}{\rho(I_{xx} + I_{yy})}}$$

Inasmuch as structural steel framing generally is fabricated with connections which offer very little restraint against warping, the formula derived herewith may be useful in certain problems associated with the design and analysis of elevated machinery platforms and similar structures.

It is interesting to note the magnitude of the error introduced into the frequency calculation by neglecting the term $C$. For the typical case of a 10 × 8-in-wide flange beam weighing 45 lb per ft and 16 ft long, calculation yields the following values for the ratio $f_n'/f_n$, where $f_n'$ is the computed frequency obtained by setting $C$ equal to zero

| $n$ | 1 | 2 | 3 |
|---|---|---|---|
| $f_n'/f_n$ | 0.63 | 0.85 | 0.92 |

# Concentrated Radial Loads on Flat Curved Beams

By J. N. GOODIER[1] and J. C. WILHOIT, JR.,[2] STANFORD, CALIF.

THE problem of concentrated radial loads on a flat curved bar has recently been treated by means of the Fourier Integral.[3] The problem can also be solved by the superposition of a few simple existing solutions for ring plates.

Consider the curved bar with an arbitrary load as shown in Fig. 1. This bar can be thought of as a part of the fully loaded ring shown in Fig. 2, in which each of the loads, that is $(\sigma_r)_{r=a}$, $(\sigma_r)_{r=b}$, $(\tau_{r\theta})_{r=a}'$, $(\tau_{r\theta})_{r=b}$, has been extended in some convenient way over the full ring, observing the requirement of equilibrium. The Fourier-series solution for the problem of a full ring with arbitrary loading is well known, and since the loads can be extended as continuous functions, good convergence can be secured. This solution is given in a particularly complete form in "Photoelasticity" by Coker and Filon.

If a cut is now made at $\theta = \pi$, the stresses across the cut are continuous and, in the general case, will give rise to a resultant normal, a resultant shearing force, and a resultant bending moment on each face of the cut. This is shown in Fig. 3. These resultants may be removed by a combination of the Volterra dislocations shown in Fig. 4, in which the surfaces $r = a$ and $r = b$ are unloaded. These solutions are also given in "Photoelasticity" by Coker and Filon. By a suitable superposition of the solutions of the Volterra dislocations on the solution of Fig. 3, the ring loaded as in Fig. 5 is obtained. The portion of the

[1] Professor of Engineering Mechanics, Stanford University. Mem. ASME.

[2] Graduate Student in Engineering Mechanics, Stanford University.

[3] "The Stresses in a Flat Curved Bar Due to Concentrated Radial Loads," by C. W. Nelson, C. J. Ancker, Jr., and Ning-Gau Wu, JOURNAL OF APPLIED MECHANICS, Trans. ASME, vol. 74, 1952, pp. 529–536.

Manuscript received by ASME Applied Mechanics Division, April 18, 1953.

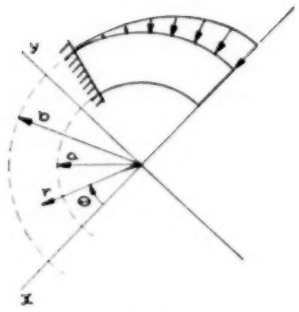


Fig. 1

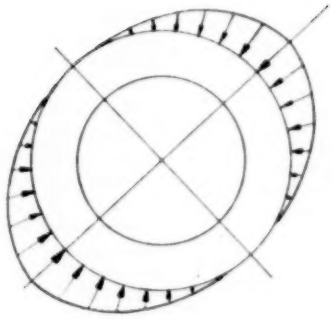

Fig. 2

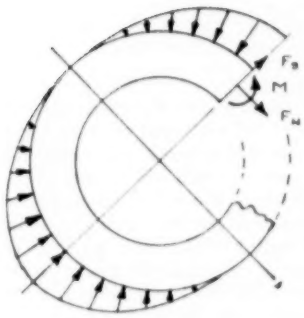


Fig. 3

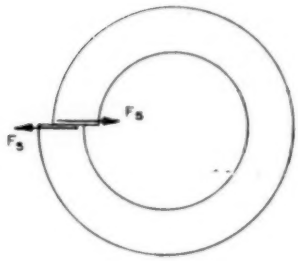


Fig. 4(a)

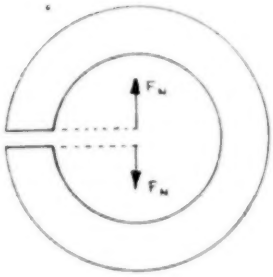


Fig. 4(b)

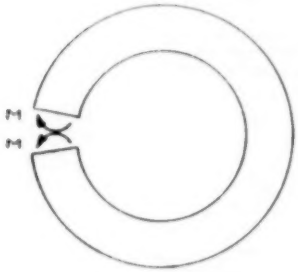


Fig. 4(c)

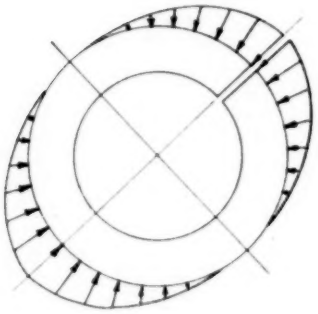

Fig. 5

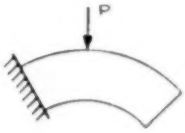


Fig. 6

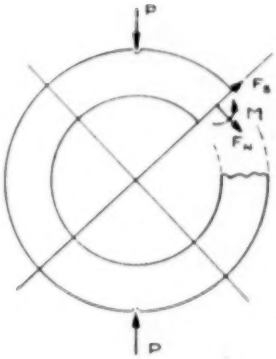


Fig. 9

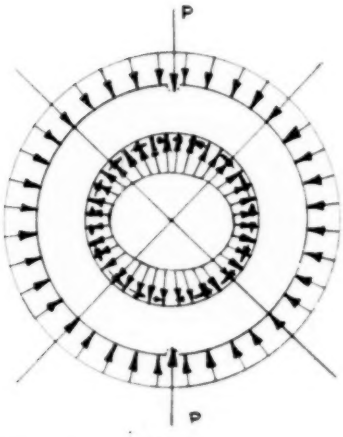


Fig. 7

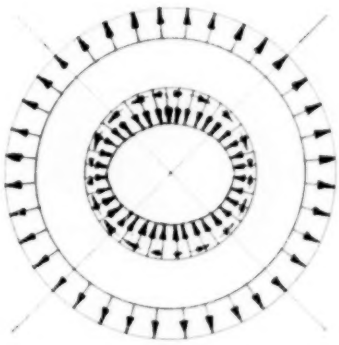

Fig. 8

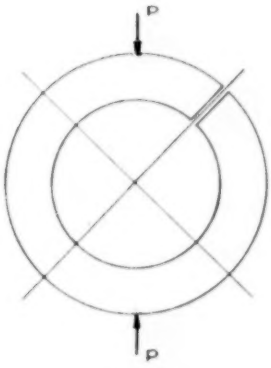


Fig. 10

ring shown in Fig. 1 is removed from Fig. 5 and the desired solution has been obtained.

### Concentrated Radial Load

For the problem of a concentrated radial load, Fig. 6, the solution for the hollow ring shown in Fig. 7 is used. The well-known solution for a concentrated force acting on a semi-infinite boundary yields a certain distribution of stresses on the surfaces $r = a$ and $r = b$. This distribution can be found readily in Fourier series by the complex variable method used by P. S. Symonds.[4]

Two such systems give the two concentrated forces in Fig. 7. Since these form a self-equilibrating system, the boundary distribution will be a self-equilibrating system. Consider now Fig. 8, in which the boundary distribution of Fig. 7 has been reversed in sign. The stresses for this loading are obtained by the Fourier-series solution for an arbitrary loading on a curved ring. If the solutions for Figs. 7 and 8 are superimposed, there results the solution for a ring subjected to two diametrically opposite concentrated forces.[5] A cut is made and the resultant force and moment on this face are removed by the use of the Volterra dislocations given in Fig. 4.

Fig. 9 shows the result of superimposing Figs. 7 and 8 and making a cut, and Fig. 10 shows the resultant force and moment on the cut removed by means of the Volterra dislocations. The desired solution, Fig. 6, can, of course, be considered as a portion of Fig. 10.

In these solutions, the resultant forces and moment at the free end are zero but normal and shear stresses remain. These, by Saint Venant's principle, have only a local effect.

[4] "Concentrated-Force Problems in Plane Strain, Plane Stress, and Transverse Bending of Plates," by P. S. Symonds, Journal of Applied Mechanics, Trans. ASME, vol. 68, 1946, p. A-183.

[5] This problem has been treated in "Stresses in a Ring Compressed by Two Forces Acting Along a Diameter," by S. Timoshenko (in Russian), Polytechnical Institute Bulletin, Kiev, USSR, 1910; also "On the Distribution of Stresses in a Circular Ring Compressed by Two Forces Acting Along a Diameter," by S. Timoshenko, *Philosophical Magazine*, vol. 44, 1922, pp. 1014–1019; and "Critical Stresses in a Circular Ring," by N. Davids and E. A. Ripperger, Trans. ASCE, vol. 112, 1947, pp. 619–628.

# Discussion

## On Application of Impedance Method to Continuous Systems[1]

H. M. Paynter.[2] The use of impedance techniques is well established in all branches of electrical engineering practice, and such methods have been and are being applied successfully in the analysis and synthesis of both lumped (or "discrete") and distributed (or "continuous") networks (or "systems"). The use of impedance and admittance concepts permits the facile determination of behavior under steady-state (statics, free and forced vibrations) as well as transient (unsteady-motion) conditions.

Owing to the generalized nature of all engineering dynamics, at least in the linear case of small amplitudes, it may be inferred from the foregoing statement that such methods can be applied with comparable success in all fields of engineering science. In realization of this fundamental objective, the author has set forth a brief but significant exposition of impedance concepts applied to one-dimensional continuous mechanical systems, with wave-like properties, subjected to free and forced oscillations; particular attention has been given to the problem of determining natural frequencies.

It is the present intent of this writer to show certain connections between these studies and their counterparts in electrical and generalized dynamical concepts. This has value in enabling one directly to transfer established electrical theorems and techniques to corresponding mechanical engineering problems involving elasticity, vibrations, feedback control, and heat flow, for example. In addition, in order to secure fuller realization of the vast storehouse of knowledge to which impedance and admittance concepts are the keys, the writer wishes to supplement the author's treatment by a brief survey of the use and value of impedances in determining the transient and steady-state response of all linear systems subjected to arbitrary input conditions.

In electricity, the impedance concept grew out of the desire to generalize the notion of "resistance" to make certain elementary direct or "constant" current concepts applicable to problems involving periodically and aperiodically "varying" currents. Historically, this need arose in the last few decades of the 19th century, under pressure of the growing electric power and telephone industries. In dynamic analysis, even before 1900, German and British engineering scientists, notable among them Oliver Heaviside, saw the analogous structure of electrodynamics and classical dynamics. For these early writers the natural analog of the electrical impedance, relating voltage to current, was the relation of force to velocity. However, largely due to the historical precedence of static elastic analysis in mechanical problems, the principal variables in mechanical problems were taken to be "force" and "displacement." In this sense, mechanical impedance as a force to displacement ratio may be considered as the attempt to generalize Hooke's law and the notion of a spring constant to problems in dynamics. Perhaps in an intermediate class fall hydrodynamic problems where the notions of pressure and flow are cardinal. In short, the principal justification for differing definitions of impedance between the electrical and mechanical fields is the practical requirement that the steady-state conditions should reduce, at least for small variations, to linear algebraic relations between the principal variables in the respective domains.

In order to compare certain of these significant interrelationships, Table 1 has been drawn up patterned after a comparable table in the text of von Kármán and Biot (1).[3] Of particular interest is the fact that all linear dynamics may be embraced in the practical (but somewhat obscure) matrix operational forms

$$[e] = [z]\,[f] \quad \ldots\ldots [1]$$

$$[f] = p\,[d] \quad \ldots\ldots [2]$$

$$[e] = [pz]\,[d] = [z^d]\,[d] \quad \ldots\ldots [3]$$

where

$d$ = generalized co-ordinate

[1] By P. F. Chenea, published in the June, 1953, issue of the Journal of Applied Mechanics, Trans. ASME, vol. 75, pp. 233–236.

[2] Assistant Professor of Hydraulic Engineering, Massachusetts Institute of Technology, Cambridge, Mass. Mem. ASME.

[3] Numbers in parentheses refer to the Bibliography at the end of this discussion.

TABLE 1

Electrical and Mechanical Impedances

$p = \dfrac{d}{dt}$

| | Electrical systems | | Mechanical systems | | |
|---|---|---|---|---|---|
| | | Impedance | | Impedance | |
| | Element | $[e/i]$ | Element | $[F/V]$ | $[F/d]$ |
| Basic dynamic elements and impedances | Coil | $L_p$ | Mass | $M_p$ | $M_{p^2}$ |
| | Resistor | $R$ | Damper | $B$ | $B_p$ |
| | Condenser | $1/C_p$ | Spring | $K/p$ | $K$ |
| Steady-state impedance | DC networks $z_{ss} = R$ | | Elastic structures $z_{ss} =$ | $K/p$ | $K$ |
| General impedance elements | $z_{ij} = L_{ij}p + R_{ij} + \dfrac{1}{C_{ij}p}$ | | $z_{ij} =$ | $M_{ij}\,p + B_{ij} + \dfrac{K_{ij}}{p}$; $M_{ij}\,p^2 + B_{ij}\,p + K_{ij}$ | |
| Impedance equation | $[e] = [z]\,[i]$ | | | $[F] = [z]\,[V]$ | $[F] = [z^d]\,[d]$ |

Lagrangian Folmulation

$$p\left(\frac{\partial T}{\partial f}\right) - \frac{\partial D}{\partial f} - \frac{\partial V}{\partial d} = 0$$

| Function | Electrical | Mechanical |
|---|---|---|
| Flux energy | $T = \frac{1}{2}\sum\sum L_{ij}\,i_i\,i_j$ | $T = \frac{1}{2}\sum\sum M_{ij}V_iV_j$ |
| Dissipation function | $D = \frac{1}{2}\sum\sum R_{ij}\,i_i\,i_j$ | $D = \frac{1}{2}\sum\sum B_{ij}V_iV_j$ |
| Potential energy | $V = \frac{1}{2}\sum\sum \dfrac{1}{C_{ij}}\,q_i\,q_j$ | $V = \frac{1}{2}\sum\sum K_{ij}d_id_j$ |

$f$ = generalized flux
$e$ = generalized effort
$z$ = flux impedance
$z^A$ = displacement impedance

Table 2 gives the commonly used terminology expressing these generalized variables in certain specific media, as indicated. Included as special cases of these equations are all the linear dynamics in every media, including of course, the continuous mechanical systems of the paper. What is perhaps not generally appreciated in any of the particular media is the fact that it is not always necessary to write the explicit differential equations of a particular system to make use of many of the general impedance concepts. Even more significant is the fact that the impedance operators frequently may be obtained with considerable precision from a few simple experiments (sometimes only one) on the physical system itself. It is this aspect of impedances which should appeal to the engineer.

TABLE 2 VARIABLES IN CERTAIN MEDIA

| Generalized variables | Physical media | | | |
|---|---|---|---|---|
| | Electrical | Mechanical | Fluid | Thermal |
| Displacement<br>$d$ | Charge<br>$q$ | Displacement<br>$d$ | Volume<br>$S$ | Heat<br>$H$ |
| Flux<br>$f$ | Current<br>$i$ | Velocity<br>$V$ | Flow<br>$Q$ | Flow<br>$q$ |
| Effort<br>$e$ | Voltage<br>$e$ | Force<br>$F$ | Pressure<br>$p$ | Temperature<br>$\tau$ |

A particularly useful portion of generalized dynamics is concerned with what are called in electrical language "four-terminal networks" (in acoustics, "transducers"). The generalized counterpart of such systems is depicted in Fig. 1 of this discussion. All the examples of application by the author fall into this category as do most problems in one-dimensional discrete and continuous systems. Instead of considering the input and output efforts and fluxes (or displacements) connected by the matrix operational equation

$$[e] = [z]\,[f] \qquad [4]$$

which, written out, would become

$$e_1 = z_{11}f_1 + z_{12}f_2 \qquad [5]$$

$$e_2 = z_{21}f_1 + z_{22}f_2 \qquad [6]$$

it is found particularly convenient by an inversion to express these relations in a form directly relating input conditions to output conditions, namely

$$e_1 = A_{11}e_2 + A_{12}f_2 \qquad [7]$$

$$f_1 = A_{21}e_2 + A_{22}f_2 \qquad [8]$$

which may be written in operational matrix form

$$[S_1] = [A]\,[S] \qquad [9]$$

where the $s$-variable indicates the state of the system

$$[S_1] = \begin{bmatrix} e_1 \\ f_1 \end{bmatrix}; \quad [S_2] = \begin{bmatrix} e_2 \\ f_2 \end{bmatrix}$$

The advantage of this formulation lies in the ability to "couple together" readily the basic components of a complex structure, as is indicated in the works of Le Corbeiller (2) and Guilleman (3), as well as detailed in all standard works on electric power transmission, such as Woodruff (4). This approach leads simply and directly to a working understanding of the penetrating but olympian tensorial methods of Kron (5, 6, 7).

Thus, if two physical media are connected in tandem or cascade such that

$$[S_1] = [A]\,[S_2] \qquad [10]$$

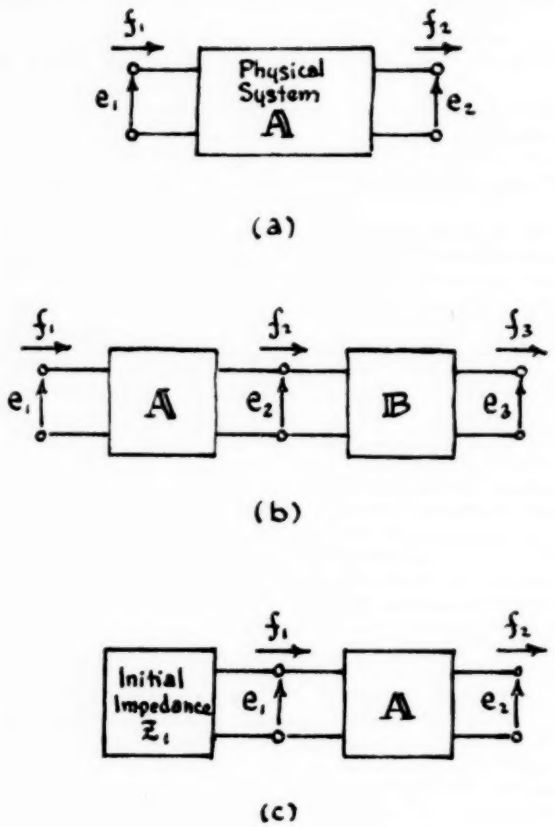


FIG. 1

$$[S_2] = [B]\,[S_3] \qquad [11]$$

then

$$[S_1] = [A]\,[B]\,[S_3] \qquad [12]$$

This technique permits a direct visualization of the coupling process, as indicated in Fig. 1(*b*). Extension to repeated cascade couplings follows intuitively.

Moreover, if the physical medium represented by the matrix operator $[A]$ is spatially uniform (i.e., if $\partial[A]/\partial x = 0$), then the operator has the matrix expansion

$$[A] = \begin{bmatrix} \cosh\gamma & \bar{z}\sinh\gamma \\ \bar{y}\sinh\gamma & \cosh\gamma \end{bmatrix} \qquad [13]$$

where

$\bar{z}$ = characteristic (or specific) impedance
$\bar{y} = 1/\bar{z}$ = characteristic admittance
$\gamma$ = propagation operator

If any input-output medium as described by its four operators $A_{ij}$ is terminated in an initial impedance $z_1$, as indicated in Fig. 1(*c*), such that $e_1 = z_1 f_1$ then the output impedance $z_2$ relating $e_2$ to $f_2$ would be given by

$$z_2 = \frac{A_{22}z_1 - A_{12}}{A_{11} - A_{12}z_1} \qquad [14]$$

For a uniform medium this gives

$$z_2 = \frac{z_1 - \bar{z}\tanh\gamma}{1 - (z_1/\bar{z})\tanh\gamma} \qquad [15]$$

In terms of the author's first example, $\gamma = j(\omega x/c)$, and the foregoing equation reduces to his Equation [9].

If one considers his second example, that of the stepped shaft, this is merely the combination of the cases of Figs. 1(*b*) and (*c*), which would give results identical with his.

There are additional advantages to this *A*-formulation, since one obtains all the operational or behavioral properties of a given medium or element without reference to its neighbors or terminal conditions. Certain dynamical theorems are always appropriate to this form. For example, in any symmetrical structure or system, be it lumped or continuous, $A_{11} = A_{22}$. Moreover, the reciprocity theorem, which is identical with Maxwell's law of reciprocal deflections in elastic structures, and which is valid for all passive linear systems, states that $A_{11}A_{22} - A_{12}A_{21} = 1$. This is equivalent to the statement that $z_{12} = z_{21}$. Finally all the concepts of duality may be applied to all dynamical systems (2).

For nonuniform continuous systems, elementary considerations of series and parallel resistors in d-c circuits or series and parallel springs in elastic statics are sufficient to demonstrate the general nature of the author's Equation [5]. This is demonstrated in Fig. 2(*a* and *b*). From Fig. 2(*c*), it may be seen that

$$Z + dZ = zdx + \frac{1}{ydx + \dfrac{1}{Z}} \qquad [16]$$

which gives the general differential equation for the variable impedance $z$, namely

$$\frac{dZ}{dx} + Z^2 y(x) - z(x) = 0 \qquad [17]$$

which is merely the author's Equation [5] with $y(x) = g(x)$, the generalized shunt admittance per unit length, and $z(x) = -h(x)$, the generalized series impedance per unit length. Substitution in Equation [5] or Equation [17], herewith, of expressions of the form

$$\left.\begin{aligned} y &= y_0(x/L)^{\alpha} \\ z &= z_0(x/L)^{\beta} \end{aligned}\right\} \qquad [18]$$

gives rise to a generalized form of the author's Equation [10] which for certain values of $\alpha$ and $\beta$ also will have solutions expressed in terms of Bessel functions. This knowledge has been used to advantage in the field of hydrodynamics, where it is pertinent to problems in tidal waves (8) and elastic waves (9).

In closing, it is important to note that it was George Green in 1837 (10) who became aware of the fact that if the exponents $\alpha$ and $\beta$ were very close to zero, or more generally, if in the generalized one-dimensional wave equations

$$\left.\begin{aligned} \frac{\partial e}{\partial x} + \phi(x)\frac{\partial f}{\partial t} &= 0 \\ \frac{\partial f}{\partial x} + \psi(x)\frac{\partial e}{\partial t} &= 0 \end{aligned}\right\} \qquad [19]$$

$\phi(x)$ and $\psi(x)$ varied only gradually relative to the significant wave lengths, then the solution of these equations could be expressed approximately in the form

$$e - e_0 = \sqrt{z(x)}\,[E_1(t-\tau) + E_2(t+\tau)] \qquad [20]$$

$$f - f_0 = \sqrt{y(x)}\,[F_1(t-\tau) + F_2(t+\tau)] \qquad [21]$$

This analysis was considerably refined by Evangelisti in the specific context of elastic plane waves (11), but the results are generally applicable to all one-dimensional wave dynamics. In substance, this method of analysis permits the use of uniform media wave relations for nonuniform media by applying appropriate transformations to the variables. Further details on procedure are to be found in the work edited by Tolke (12). Additional information on the mechanism of wave reflections in gradually varying media derives from Rayleigh (13).

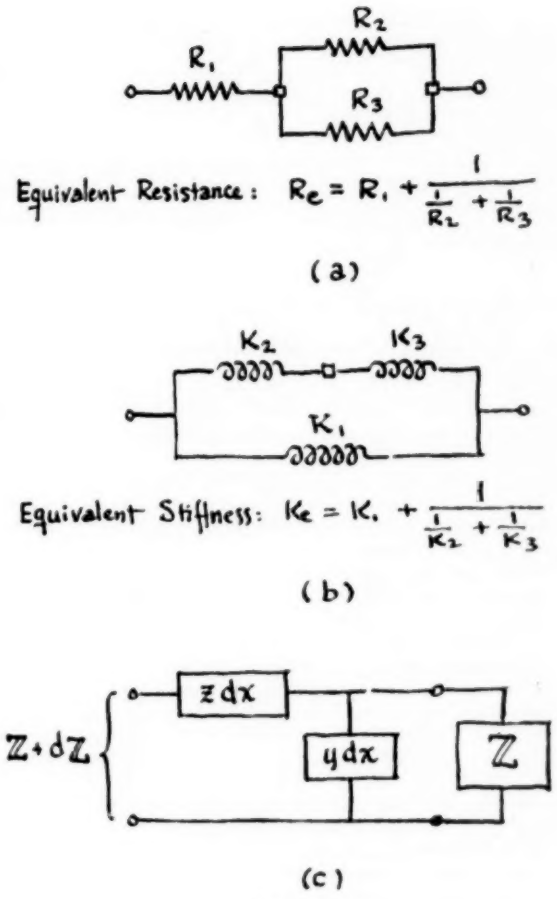


FIG. 2

## BIBLIOGRAPHY


1 "Mathematical Methods in Engineering," by Th. von Kármán and M. Biot, McGraw-Hill Book Company, Inc., New York, N. Y., 1940.

2 "Matrix Analysis of Electric Networks," by P. Le Corbeiller, Harvard-Wiley, Cambridge, 1950.

3 "Communication Networks," by E. A. Guilleman, John Wiley & Sons, Inc., New York, N. Y., vol. 2, 1935.

4 "Principles of Electric Power Transmission," by L. F. Woodruff, John Wiley & Sons, Inc., New York, N. Y., 1938.

5 "The Application of Tensors to the Analysis of Rotating Machinery," by G. Kron, part 16, "The Basic Theory of Networks," *General Electric Review*, vol. 41, 1938, pp. 153–159; part 17, "Non-holonomic Reference Frames," pp. 244–250; part 18, "The Dynamical Equations of Lagrange," pp. 448–454.

6 "Tensor Analysis of Networks," by G. Kron, John Wiley & Sons, Inc., New York, N. Y., 1939.

7 "The Use of Tensors in Mechanical Engineering Problems," by C. Concordia, *General Electric Review*, vol. 39, 1936, pp. 335–341.

8 "Hydrodynamics," by H. Lamb, Dover Publications, New York, N. Y., art. 185, 1945 (American edition).

9 "Caratteristiche di propagazione idrodinamica in tubi elastici di sezione e spessore variabili," by G. Evangelisti, *Atti del 1° Congresso dell'Unione Matematica Italiana*, 1937.

10 "On the Motion of Waves in a Variable Canal of Small Depth and Width," by G. Green, Cambridge Transactions, vol. 6, 1837.

11 "Sul calcolo del colpo d'ariete nelle condotte forzate a caratteristiche Variabili," by G. Evangelisti, *Energia Ellettrica*, vol. 16, December, 1939.

12 "Veröffentlichungen zur Erfurschung der Druckstoss probleme in Wasskraftanlagen und Rohrleitungen," by F. Tolke, Springer Verlag, Berlin, Germany, 1949.

13 "Theory of Sound," by Lord Rayleigh, Dover Publications, New York, N. Y., art. 148, 1945.

# The Origin of Damping in High-Strength Ferromagnetic Alloys[1]

B. J. Lazan.[2] The author has presented an important contribution toward a better understanding of the mechanism of damping in materials at intermediate stress levels. Most of this type of analysis in the past has been concerned with the relatively small damping at very low stress levels and its relationship to physical metallurgical concepts. In the author's work, however, both damping and stress are sufficiently large to have engineering design significance.

However, the writer wishes to present data to indicate that a difference of opinion exists with regard to the relative importance of magnetomechanical and plastic behavior as a cause for damping in materials at engineering stress level. The paper states ". . .in high-strength alloys, . . ., plastic flow occurs noticeably only at stress levels beyond those for which the structure is designed." The author then concludes: "Consequently, only the magnetomechanical effect contributes significantly to the large damping capacity in high-strength alloys; and this effect, of course, is limited to ferromagnetic materials."

The writer differs with the foregoing conclusion. Figs. 1 and 2[3] of this discussion are presented as evidence that extremely high damping (probably caused by plastic flow) occurs at high stresses in the range frequently encountered in engineering applications. These figures indicate the inch-pounds of damping energy absorbed per cubic inch of material per cycle of vibration by several temperature-resistant materials at various stresses near the fatigue limit. In general, each material must be represented by a family of curves to show the effect of stress history since the number of cycles of stress prior to measurement may affect greatly the damping energy in this stress range. If these curves are plotted on a log-log basis rather than on the semilog basis shown in Figs. 1 and 2, it is found that the curves are reasonably straight and, therefore, it is possible to express damping at a given stress history by the equation

$$D = J S^n$$

where $D$ = damping energy in in-lb/cu in/cycle, and $J$ and $n$ are constants, the latter constant being determined from the slope of the log-log plot.

For the materials diagrammed in Figs. 1 and 2 the exponent $n$ has values ranging from 3 to 14 in most cases (in one case being as high as 30 at a high stress level). It is thus apparent that

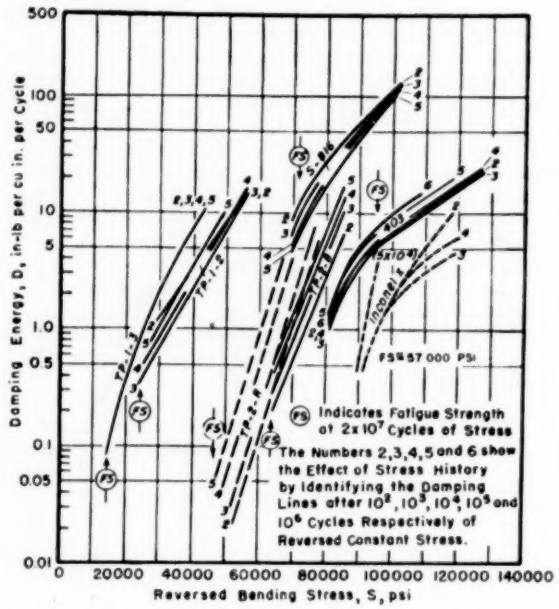
Damping Energy, D, in-lb per cu in. per Cycle
Reversed Bending Stress, S, psi
TP-1-2
TP-1-3
S-816
TP-2-R
TP-2-B
Inconel X
FS=57 000 PSI
FS Indicates Fatigue Strength at 2x10⁷ Cycles of Stress
† The Numbers 2,3,4,5 and 6 show the Effect of Stress History by Identifying the Damping Lines after 10², 10³, 10⁴, 10⁵ and 10⁶ Cycles Respectively of Reversed Constant Stress.

Fig. 1 *D-S-N* Diagrams for Several Temperature-Resistant Materials Comparing Damping Energy at Room Temperature as a Function of Stress History and Stress Magnitude

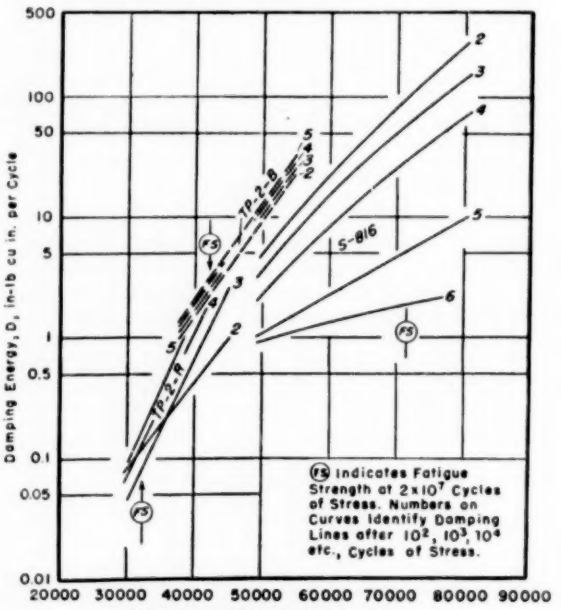
Damping Energy, D, in-lb cu in. per Cycle
Reversed Bending Stress, S, psi
TP-2-B
TP-2-R
S-816
FS Indicates Fatigue Strength at 2x10⁷ Cycles of Stress. Numbers on Curves Identify Damping Lines after 10², 10³, 10⁴ etc., Cycles of Stress.

Fig. 2 *D-S-N* Diagrams for S-816, TP-2-R, and TP-2-B, Comparing Damping Energy at 900 F as a Function of Stress History and Stress Magnitude

damping increases extremely rapidly with increasing stress at high stress levels (near fatigue limit). Furthermore, the fact that damping energy is not constant above a certain critical stress, the variety of damping exponents found, and the fact that

[1] By A. W. Cochardt, published in the June, 1953, issue of the Journal of Applied Mechanics, Trans. ASME, vol. 75, pp. 196–200.

[2] Professor of Materials Engineering and Director of Engineering Experiment Station, University of Minnesota, Institute of Technology, Minneapolis, Minn. Mem. ASME.

[3] These figures are from the paper, "Damping, Elasticity, and Fatigue Properties of Temperature-Resistant Materials," by B. J. Lazan and L. J. Demer, Proceedings of the ASTM, vol. 51, 1951, pp. 611–646.

most of them are well above three would indicate that magnetomechanical effects are not the predominant cause of damping at these stress levels.

A direct comparison between the "12 per cent chrome steel" used by the author and the similar steels diagrammed in Figs. 1 and 2 cannot be made since more details are required on the chemical composition and processing procedure used for the author's steel. However, if the damping of the type 403 stainless steel diagramed in Fig. 1, which contains 12.6 per cent chromium, or that of the other steels in this figure which contain from 12 to 20 per cent chromium, are compared in the same units with the author's steel, it is found that the damping at the fatigue limit is considerably larger than that at the critical stress indicated by the author.

Although considerably more data are required before definite conclusions can be formulated the following tentative statements appear justifiable:

1 Since the high stress damping exponent $n$ averages approximately 7 for the temperature-resistant materials studied to date, magnetomechanical effects probably are not the cause of the damping observed near the fatigue limit.

2 Damping near the fatigue limit (probably caused by plastic-flow effect) appears to be much larger than that caused by magnetomechanical effects at the critical stress (approximately 10 per cent of the fatigue limit for the author's steel) for the materials investigated to date.

3 Thus, although magnetomechanical effects may be the most important cause of damping of ferromagnetic materials near their critical stress, the damping caused by plastic strain appears to predominate near the fatigue limit.

4 The relative importance of low-stress damping, produced, for example, by magnetomechanical effects, and high-stress damping as produced by plastic flow depends on the application and the magnitude of damping exponent $n$. In general, the more concentrated the stress (that is, the smaller the per cent of volume at near peak stress) and the lower the damping exponent, the more important does low-stress damping become as a limiter of near-resonance vibration. In cases, however, where the per cent of material at near peak stress is significant and the damping exponent $n$ is large, the damping at high stress levels becomes the primary consideration. Thus additional work on "stress-distribution function" discussed by the author and the "cross-sectional shape" and "longitudinal stress-distribution" factors[4] is highly desirable to further understanding on this relationship.

It would be appreciated if the author would give more details on the 12 per cent chrome material and type of specimen used in his work so that more direct comparisons may be made with other work.

### Author's Closure

The author is grateful to Professor Lazan for his interesting remarks. Most of the questions raised have been answered in a second paper.[5] The conclusions reached in that paper agree with Professor Lazan's statement 4, but not with statements 1 and 3. The question of whether the high-stress damping (or plastic-flow damping) is more significant than the damping due to magnetomechanical hysteresis depends on the material used and the stress system to which it is subjected. The magnetomechanical damping is of primary importance for ferromagnetic materials when they vibrate similar to cantilever or simple-supported beams. This is explainable since most of the volume of such members is subjected to only a fraction of the peak stress. The high-stress damping therefore does not contribute much to the total damping even if the peak stress is near the fatigue limit and regardless of whether the damping energy increases with the fifth or tenth power of stress at larger stresses.

There are, of course, cases where plastic flow is the primary source of the material damping. This has been explained in detail in the paper mentioned.

The composition of the "12 per cent chrome steel" is Fe—12.5 per cent Cr, 0.5 per cent Ni, and 0.1 per cent C. The alloy was forged at 1950 F and annealed for two hours at 1750 F. Finally, the specimens used were conventional Föppl-Pertz torsion specimens[6] having a diameter of $^1/_2$ inch, an effective length of $6^3/_4$ in., and ends $^5/_8 \times ^5/_8$ in.

[4] See "Effect of Damping Constants and Stress Distribution on the Resonance Response of Members," by B. J. Lazan, JOURNAL OF APPLIED MECHANICS, Trans. ASME, vol. 75, 1953, pp. 201–209.

[5] "A Method for Determining the Internal Damping of Machine Members," by A. W. Cochardt, to be presented at the Annual Meeting of the ASME, Nov. 30–Dec. 4, 1953. Paper No. 53—A-44.

[6] "Föppl-Pertz Damping Machine," *Metals and Alloys*, New Products Section, February, 1931, p. 28.

## Axisymmetric Flexural Temperature Stresses in Circular Plates[1]

H. L. LANGHAAR.[2] The author has obtained a remarkably simple solution of a problem that is becoming increasingly important. The method of "cuts" that he employs provides us with an insight into the nature of the phenomena that accompany temperature gradients in plates. Much of the value of this method is lost, however, if we abandon the classic assumption that normals to the middle surface remain straight and normal. This assumption, which is equivalent to neglecting the shearing stress $\tau_{rz}$, accounts for the simplicity and the generality of the results that have been obtained. Since the shearing stresses may be expected to depend on the dimensionless products $(h/T)\ (dT/dr)$ and $(h^2/T)\ (d^2T/dr^2)$, the conclusions that have been derived are perhaps valid only if the temperature varies gradually in the radial direction.

The case that has been treated belongs to the class of thermal-stress problems in which the temperature distributions are axially symmetrical. This whole class of problems is a fertile field for research. Presumably, some exact solutions can be obtained that represent thermal stresses in plates with special types of axially symmetrical temperature distributions. Such solutions are potentially valuable, not only because they apply for thick disks and for disks with large radial temperature gradients, but also because they supply a check on the assumption, $\tau_{rz} = 0$. However, an exact general solution of the plate problem for all axially symmetrical temperature distributions that vary linearly with the axial co-ordinate $z$ can scarcely be expected.

Possibly approximate solutions for moderately thick plates, and for plates with rather large radial temperature gradients, may be obtained in the form of truncated power series in $z$. This method has been applied to shell problems by P. S. Epstein,[3] though not with consideration of thermal strains.

### Author's Closure

The author is indebted to Professor Langhaar for his interesting and constructive comment. The solution which was presented, since it implied the usual assumptions of classical plate

[1] By J. E. Goldberg, published in the June, 1953, issue of the JOURNAL OF APPLIED MECHANICS, Trans. ASME, vol. 75, pp. 257–260.

[2] Department of Theoretical and Applied Mechanics, University of Illinois, Urbana, Ill. Mem. ASME.

[3] "On the Theory of Elastic Vibrations in Plates and Shells," by P. S. Epstein, *Journal of Mathematics and Physics*, vol. 21, 1942, pp. 198–208.

theory, is valid for thin plates in which the radial temperature gradients are "well-behaved." Indeed, the problem came to the author's attention in connection with the design of certain items of refinery equipment wherein these restrictions were presupposed. However, the solution may give results of sufficient accuracy for engineering purposes in many cases where the restrictions of the parameters mentioned by Professor Langhaar are overlooked and should, at least, serve as a first approximation in such cases.

One notes that the shearing stress $\tau_{rz}$ is identically zero within the "central disks" used in the synthesis of the solution. Also, in the case of unloaded plates, the average value of $\tau_{rz}$ through the thickness at any point must be zero to satisfy statical equilibrium. These facts lend some support to the intuitive feeling that the range of validity of the solution may be stretched a little for engineering purposes.

The present closure affords an opportunity to present a more compact derivation of Equations [8]. In terms of the radial and tangential moments, $M_1$ and $M_2$, respectively, the equilibrium condition for the axisymmetric problem of circular plates is

$$M_1 + r\frac{dM_1}{dr} - M_2 + Vr = 0 \qquad [1]$$

in which $V$ is the unit shear acting on a circumferential arc. The slope-moment-temperature relations are

$$\left.\begin{aligned} M_1 &= D\left(\frac{d\phi}{dr} + \mu\frac{\phi}{r}\right) - \frac{\alpha(1+\mu)DT}{h} \\ M_2 &= D\left(\frac{\phi}{r} + \mu\frac{d\phi}{dr}\right) - \frac{\alpha(1+\mu)DT}{h} \end{aligned}\right\} \qquad [2]$$

where $T$ is the temperature difference between the faces of the plate. Noting that $V = 0$ if the plate is not loaded, and substituting Equation [2] into Equation [1] yields

$$\frac{d^2\phi}{dr^2} + \frac{1}{r}\frac{d\phi}{dr} - \frac{\phi}{r^2} = \frac{\alpha(1+\mu)}{h}\frac{dT}{dr} = k_s\frac{dT}{dr}$$

or

$$\frac{d}{dr}\left[\frac{1}{r}\frac{d}{dr}(r\phi)\right] = k_s\frac{dT}{dr} \qquad [3]$$

Integrating twice, one obtains

$$\rho\phi = k_s\int_0^\rho Tr\,dr + \frac{C_1\rho^2}{2} + C_2$$

Regularity at the origin requires that $C_2 = 0$. Hence

$$\phi = \frac{k_s}{\rho}\int_0^\rho Tr\,dr + C_1\rho \qquad [4]$$

Substituting Equation [4] into Equation [2]

$$\left.\begin{aligned} M_1 &= -\frac{k_m}{\rho^2}\int_0^\rho Tr\,dr + C \\ M_2 &= \frac{k_m}{\rho^2}\int_0^\rho Tr\,dr - k_m T + C \end{aligned}\right\} \qquad [5]$$

Since the integrals in Equation [5] represent the statical moment about the origin of the area under the $T$ curve bounded by the ordinate at $\rho$, they may be replaced by the quantity $A_1 b_1 + T_\rho\frac{\rho^2}{2}$, thus reducing Equation [5] to the form of Equation [8] in the paper.

One may also arrive at Equation [3] by a slightly more physical reasoning. We imagine that while plate is being brought up to its final temperature distribution, it is restrained against displacement by a set of surface loads. If the displacements are zero throughout then, initially, $M_1 = M_2 = -\alpha(1+\mu)DT/h = -k_sDT$. Substitution of these moments into Equation [1] defines, by means of shears, the surface loading necessary to prevent displacements, and it is found that $V = k_sD\left(\frac{dT}{dr}\right)$. To remove these constraints, we merely superimpose a set of equal and opposite surface loads, i.e. a set of loads characterized by $V = -k_sD(dT/dr)$, for which

$$\frac{d^2\phi}{dr^2} + \frac{1}{r}\frac{d\phi}{dr} - \frac{\phi}{r^2} = -\frac{V}{D} = k_s\frac{dT}{dr}$$

This is identical with the predecessor of Equation [3].

# The End Problem of Rectangular Strips[1]

M. Z. v. Krzywoblocki.[2] The author should be congratulated for not following the bad habit of using the doubtful "strain-energy method" and for seeking some new methods of solution of elasticity problems. But since the author mentioned the writer's name and since he mispresented a few facts, it is believed that some remarks are in order to correct the situation.

It should be mentioned that the only rigorous solution of the problem of a minimum of an integral functional like that of minimum of potential or strain energy is connected inseparably with the calculus of variation and with its principal equation, i.e., Euler-Lagrange differential equation. This fact should be known to everybody who attacks any such problem and it is explained thoroughly in such properly written books on elasticity as that of Sokolnikoff.

However, it is also known that the contrary is true and that in this Journal there have appeared in the past many articles whose authors showed a complete lack of knowledge of the facts. Owing to the great difficulty of solving Euler-Lagrange differential equations some approximate solutions must be used. In 1908 a Swiss physicist, Walther Ritz (who died prematurely), proposed a new approximation method of solving the problems of a variational character. One may find its description in the original Ritz's paper, or in many papers on this method written in the last half century.

A few sections from R. Courant's address on this method follow:

"Suppose we seek the minimum $d$ of an integral expression $I(\phi)$. We then start with a minimizing sequence $\phi_1, \phi_2, \ldots, \phi_n \ldots\ldots$, that is, a sequence of functions, admissible in our variational problem, for which $\lim_{n\to\infty} I(\phi_n) = d$, $d$, being the lower bound of the functional $I(\phi)$.

"Ritz's construction proceeds as follows: We start with an arbitrarily chosen system of co-ordinate functions $\omega_1, \omega_2, \ldots, \omega_n, \ldots$, which should satisfy two conditions: ($a$) any linear combination $\phi_n = c_1\omega_1 + c_2\omega_2 + \ldots c_n\omega_n$, of them is admissible in the variational problem; ($b$) they should form a complete system of functions in the sense that any admissible function $\phi$ and its relevant derivatives may be approximated with any degree of accuracy by a linear combination of co-ordinate functions and of their corresponding derivatives, respectively. If we begin with such a system of co-ordinate functions, it is clear that for $n$ sufficiently large and for a suitable choice of the coefficients $c_1, c_2, \ldots, c_n$, we can find admissible functions $\phi_n$ for which $I(\phi_n)$ differs arbitrarily

[1] By G. Horvay, published in the March, 1953, issue of the Journal of Applied Mechanics, Trans. ASME, vol. 75, pp. 87–94.

[2] Professor of Gasdynamics, University of Illinois, Urbana, Ill.

little from $d$. In other words, it is possible to find a minimizing sequence $\phi_n$ as a sequence of linear combinations of co-ordinate functions.

"In order to obtain such a minimizing sequence, we consider any function $\phi_n$ and substitute it in our variational problem. $I(\phi_n)$ then becomes a function $F(c_1, \ldots, c_n)$ of the $n$ parameters $c_i$ which we may now determine from the ordinary minimum problem of the calculus

$$I(\phi_n) = F(c_1, \ldots, c_n) = \min;\ \partial F/\partial c_i = 0 (i = 1, 2, \ldots) \ldots [1]$$

"Often $I(\phi_n)$ is a quadratic or bilinear functional and [1] leads to a system of $n$ linear equations for the parameters, and thus the minimizing sequence is found. But, while the convergence of $I(\phi_n)$ to $d$ is assured, it is by no means generally true that $\phi_n$ tends to $u$, the solution of the original minimum problem, or, even less so, that the derivatives of $\phi_n$ tend to the corresponding derivatives of $u$. From a practical point of view, almost any success depends on the selection of co-ordinate functions. If these functions are chosen without proper regard for the individuality of the problem, the task of computation will become hopeless.

"It is important that the initial function be already a fair approximation, and furthermore, that the function $\phi_n$ should be sufficiently different so that increasing the number of terms will lead to an actual improvement of the approximation. A weak point in the Ritz procedure is that it does not contain a principle for estimating the accuracy of the approximation. The vagueness as to the accuracy of the approximation obtained is only one of the objections to the Ritz method that may be raised. More annoying is that a suitable selection of the co-ordinate functions is often very difficult and that laborious computations are sometimes necessary."

Ritz proved the convergence of the minimizing sequence (but pointed out very clearly that the limit of convergence may be quite different from the sought solution) and applied his method to problems of a plate, vibrating string, that of Dirichlet, etc.

In 1924 Timoshenko published a paper in which he wrote:

"The object of this paper is to outline an approximate method for investigating the two-dimensional problems by using the expression for the potential energy.[1] (Here is the footnote in the paper: "The method was used by the author for calculating the stress distribution in a compressed block. See his 'Treatise on Elasticity,' vol. 1, p. 143, St. Petersburg, 1914, in Russian.")

"We assume that the stress function can be represented by the series $\phi = \phi_0 + \alpha_1\phi_1 + \alpha_2\phi_2 + \ldots$, [3], where $\phi_0$, $\phi_1$, . . ., are functions specified in such a manner as to correspond to the given boundary conditions. If we substitute [3] into the expression for the energy function, we obtain the energy function $V$ as a quadratic function of the coefficients $\alpha_1$, $\alpha_2$, . . . ."

The next condition derived by Timoshenko is $\delta V = 0$ and he continues: "To obtain an approximate solution of any problem, we take a few terms in the series [3], and using the condition $\delta V = 0$, we determine the coefficients $\alpha_1$, $\alpha_2$, . . . . . , from the linear equations $dV/d\alpha_1 = 0$; $dV/d\alpha_2 = 0$, . . . . ., etc."

In the entire paper Timoshenko does not mention the name of Ritz, although he obviously describes Ritz's method. In the list of papers in Timoshenko's 60th Anniversary Volume, the writer did not find any paper of his on this method before 1908.

Let me cite other Timoshenko textbooks. In "Strength of Materials" (p. 326), he wrote:

"§71. Application of Castigliano Theorem. . . . For immovable supports and for the supports whose motion is perpendicular to the direction of the reactions, the partial derivatives of the strain energy with respect to the unknown reactive forces must be equal to zero by the Castigliano theorem. Hence $\partial V/\partial X = 0$, $\partial V/\partial Y = 0$, etc. It can be shown that these equations represent the conditions for a minimum of function $V$, from which it follows that the magnitudes of statistically indeterminate reactive forces are such as to make the strain energy of the system a minimum. This is the principle of least work as applied to the determination of redundant reactions."

It is obvious that the procedure of Castigliano's theorem applied to continuously distributed stresses expressed by means of Equation [3] (as followed by Hoff and his students, for example) is nothing else than again Ritz's method.

Let me cite a few sentences from Timoshenko's "Theory of Elasticity" (p. 150, §43. "Application of the Principle of Least Work—Rectangular Plates"):

". . . the correct expression for the stress function $\phi$ is that satisfying the boundary conditions and making the strain energy a minimum. We take the stress function in the form $\phi = \phi_0 + \alpha_1\phi_1 + \ldots$, such that boundary conditions are satisfied, and the magnitudes of the constants can then be calculated from the minimum conditions $\partial V/\partial\alpha_i = 0$ $(i = 1, \ldots)$, which will be linear equations in $\alpha_1$, $\alpha_2$, . . . . By a suitable choice of the functions $\phi_n$, we can usually get a satisfactory approximate solution by using only a few terms in the series."

This is almost the literal translation of Ritz's paper. Hence it is obvious that the principle of least-work method (identified often with the Castigliano's theorem with partial derivatives equal to zero) is nothing else than the Ritz's method, applied to strain energy. The same procedure was applied by von Kármán (1923), Goodier, Hoff and his students, Conway, and many others. The literature on Ritz's method is enormous. It must be stated beyond any doubt that since all the papers by all the authors were published after 1908, no one other than Ritz can claim the originality for this method.

One has to keep in mind that Ritz was not only the author of the method, but also derived the proof of convergence under certain conditions, discussed the method in all its phases and items, etc., and applied it. Whereas, Timoshenko did only one thing, i.e., he applied, it, without even mentioning the name of Ritz. To avoid any charge of plagiarism, it is a matter of ethics always to cite the names of authors whose method is used.

It is significant that in many papers and books, including all the textbooks of Timoshenko, there are attached to this method either no names or other names, usually that of Timoshenko (for example, Conway, Chow, and Morgan) but not that of Ritz. The living persons, including Timoshenko, do not correct this error, thus doing a great injustice to the late physicist.

In addition, when some time ago I sent a note on the matter to this Journal, with some rigorous derivations and few integrals, the note was returned to me with a remark that it was too mathematical. I am sorry to state that the author is definitely wrong in his statement that Timoshenko was the first to make systematic use of the variational method in problems of stress analysis. In the name of historic facts, I state that it was Ritz who did it first and that his name is omitted as concerning this fact.

Any success of the principle of least-work method, which the writer has shown to be the Ritz method, depends upon the selection of co-ordinate functions. Thus it is obvious that all the attacks on the writer by Conway with a statement by Goodier (maintaining that this procedure always leads to a minimum value of strain energy), or Hay (maintaining that the Fourier series is quite general and must lead to a total elastic energy which is an absolute minimum), etc., prove only a lack of knowledge of the literature.

Depending upon the choice of the minimizing sequence, this procedure may give a very rapid convergence (as shown in some examples by Timoshenko) or may give nonsensical results as shown in the writer's examples in the past. Each particular type of structure possesses its own most proper minimizing sequence which must be known from, say, some experiments.

Hence again, the author's remark regarding the writer's statement on convergence should be corrected in this sense, that it was not the writer but the author of the method, W. Ritz, who almost half a century ago warned about the possibility of obtaining no result at all by his method.

The matter is more odd that Timoshenko, discussing the (total) potential-energy method, cited Ritz's name (Elasticity, p. 252; Timoshenko-Goodier, p. 280) as if there be some difference in Ritz's method in these two cases: strain and potential energy. Finally, it should be mentioned that Pöschl, reviewing writer's paper, called strain-energy method used by the writer the Rayleigh-Ritz procedure, thus also disregarding Timoshenko or anybody's authorship in this case.

REFERENCES

1 "Analysis of Deep Beams," by H. D. Conway, L. Chow, and G. W. Morgan, JOURNAL OF APPLIED MECHANICS, Trans. ASME, vol. 73, 1951, p. 163; also discussion, ibid., p. 422.

2 "Variational Methods for the Solution of Problems of Equilibrium and Vibrations," by R. Courant, Bulletin of the American Mathematical Society, vol. 49, 1943, p. 123.

3 Review of the paper "On the So-Called Principle of Least Work Method," by M. Z. von Krzywoblocki, *Oest. Ing. Archiv.*, vol. 5, 1951, pp. 81–98; by G. E. Hay, *Mathematical Review*, vol. 13, 1952, p. 406.

4 "Über eine Neue Methode zur Lösung Gewisser Variationsprobleme der Mathematischen Physik," by W. Ritz, *Göttinger Nachrichten, Math. Physiks*, vol. KI, 1908, pp. 236–248, or *Journal of Reine und Angewandte Mathematik*, vol. 135, 1909, pp. 1–61. See also: Gesammelte Werke, Gauthier-Villars, Paris, France, 1911.

5 "The Approximate Solution of Two-Dimensional Problems in Elasticity," by S. Timoshenko, *Philosophical Magazine*, vol. 47, series 6, 1924, pp. 1095–1104.

"Strength of Materials," by S. Timoshenko, D. Van Nostrand Company, Inc., New York, N. Y., vol. 1, 1930, p. 326, §71.

"Theory of Elasticity," by S. Timoshenko, McGraw-Hill Book Company, New York, N. Y., 1934, p. 150, §43.

"60th Anniversary Volume," by S. Timoshenko, The Macmillan Company, Inc., New York, N. Y., 1938.

6 "Theory of Elasticity," by S. Timoshenko and J. N. Goodier, McGraw-Hill Book Company, New York, N. Y., 1951.

7 Review of the paper, "On the So-Called Principle of Least Work Method," by M. Z. von Krzywoblocki, *Oest. Ing. Archiv.*, vol. 5, 1951, pp. 81–98; by Th. Pöschl, *Zentralb. Math.*, 42, 421, 1952.

H. PORITSKY.[3] The problem considered in this paper is one of great difficulty and any real contribution to its solution is of interest.

The "energy" or "Rayleigh-Ritz" methods of solving the Airy differential equation

$$\nabla^4 F = 0 \quad \ldots\ldots [1]$$

with proper boundary conditions over the boundary of an area $A$, consist in replacing the satisfaction of Equation [1] by the minimization of the integral

$$I = \int\int (\nabla^2 F)^2 dx\, dy \quad \ldots\ldots [2]$$

among all functions $F$ (possessing proper derivatives) and satisfying the required boundary conditions over the boundary of $A$. A proper solution by the energy method must be capable of rendering $I$ as close to its minimum $I_m$ as desired.

If for the rectangle $x > 0$, $-1 < y < 1$, the expansion

$$F = a_1 f_1(y) g_1(x) + a_2 f_2(y) g_2(x) - \ldots + a_n f_n(y) g_n(y) \ldots [3]$$

where $f_1(y)$, $f_1(y)$, . . . . are the author's orthogonalized polynomials, is applied to the boundary conditions which correspond to the first term $a_1 f_1(y) g_1(x)$ only, then all the coefficients $a_n$, $n > 1$, will vanish. However, the first term does not satisfy Equation [1]. Hence for this example the value yielded by Equation [3] for the integral $I$ is not the true minimum. Only by allowing the first $k$ $g_i$ to vary independently anew with each value $n = k$ of $n$ will the true minimum of $I$ be approached. When this is done there results for $g_i$ combinations of exponentials $e^{\lambda_i x}$ where $\lambda_i$ satisfies an algebraic equation of degree $4n$. The resulting complexity of the determination of $F$ is so great that the direct expansion of $F$ in product solutions of Equation [1] of the form

$$F_k = e^{-\lambda k x} F_k(y) \quad \ldots\ldots [4]$$

is not unfavorable in comparison.

It is of interest to point out that the exact product solutions, Equation [4], of Equation [1] satisfying the boundary conditions

$$F = 0, \quad \partial F/0 = 0 \text{ on } y = \pm 1 \quad \ldots\ldots [5]$$

do possess an orthogonality property, namely, the following one

$$\int_{-1}^{1} (F_n \nabla^2 F_m + \nabla^2 F_n F_m)\, dy = 0, \; n \neq m \quad \ldots\ldots [6]$$

This can be proved by repeated application of Green's theorem to the functions $F_n$, $F_m$. It is not obvious, however, how to utilize this property for the problem in question.

E. STERNBERG.[4] This paper represents an interesting contribution to an important and difficult problem. The difference between the author's approach and that previously adopted by Fadle[5] may be summarized as follows: Fadle's solution satisfies the two-dimensional field equations rigorously and meets the boundary conditions in the mean (in the sense of a minimization of the square error); the present solution satisfies the equilibrium conditions and the boundary conditions rigorously but conforms to the compatibility equations in the mean (in the sense of a strain-energy minimization).

In so far as computational labor is concerned, the lack of orthogonality in the boundary tractions to which Fadle's aggregate of component solutions gives rise is, admittedly, troublesome. On the other hand, a good deal of computational effort is involved in the orthogonalization process employed by the present author. At any rate, it would appear that the question as to which of the two approaches is better suited to this problem cannot be decided on such grounds.

In comparing the two methods, it should be noted that in Fadle's solution the error in the satisfaction of the boundary conditions is known at every stage of the approximating process. No comparably significant error estimate is available in the energy approach. To be sure, the sequence of energy approximations supplies a sequence of upper bounds to the strain energy of the exact solution. Moreover, the "method of the hypercircle"[6] would yield both upper and lower bounds to the exact total strain energy. It is not possible, however, to draw any conclusions as to the error in the local stress values from a knowledge of the error in the strain energy, despite the fact that an independent sequence of upper and lower bounds for the stresses at a fixed point of the medium can be constructed with the aid of the hypercircle method.[7] Finally, although convergence is not the issue here, it may be worth recalling that neither Fadle's nor the present process is assured of convergence.

In conclusion, there is one difficulty inherent in energy methods which is peculiar to problems of the type under consideration.

[3] Consulting Engineer, General Electric Company, Schenectady, N. Y. Mem. ASME.

[4] Professor of Mechanics, Illinois Institute of Technology, Chicago, Ill. Jun. ASME.

[5] Die Selbstspannungs-Eigenwertfunktionen der Quadratischen Scheibe," by J. Fadle, *Ingenieur-Archiv.*, vol. 11, 1941, p. 125.

[6] "Approximations in Elasticity Based on the Concept of Function Space," by W. Prager and J. L. Synge, *Quarterly of Applied Mathematics*, vol. 5, 1947, p. 241.

[7] "Upper and Lower Bounds for the Solution of Problems in Elasticity," by J. L. Synge, Proceedings of the Royal Irish Academy, vol. 53, sect. A, 1950, p. 41.

The kind of averaging process underlying all energy methods is apt to mitigate steep local stress gradients, and to blur local effects in general. Yet it is precisely a local effect which is sought in the problem treated by the author. Perhaps this danger, which is aggravated in case the region extends to infinity, has been dismissed too readily.

## Author's Closure

The author appreciates the interesting comments of Messrs. M. Z. v. Krzywoblocki, H. Poritsky, and E. Sternberg. Four issues appear to be raised:

(*a*) How does one expand the prescribed boundary values of a stress in terms of derivatives of a complete set of nonorthogonal biharmonic eigenfunctions?

(*b*) How does one estimate the error in the stress value that results from the use of approximate eigenfunctions?

(*c*) Will the method prescribed for the improvement of the approximate eigenfunctions guarantee their convergence to the true set?

(*d*) Why doesn't a person quote another author who does not write on the same subject?

To these questions the author wishes to add a question of his own. Does the paper contain any errors of significance, and if so, what?

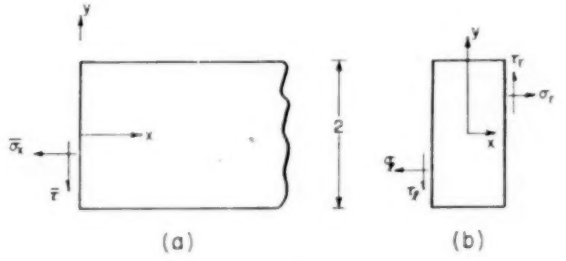


Fig. 1

(*a*) Let the semi-infinite beam in Fig. 1(*a*) of this closure be subject to (self-equilibrating) normal and shear boundary stresses $\bar{\sigma}$, $\bar{\tau}$ on the left edge,[8] and let it be free of tractions along the two horizontal edges. Suppose we have solved the eigenvalue problem

$$\nabla^{16}\Phi(x, y) = 0 \quad \ldots\ldots [1a]$$

$$\Phi_{,x}(x, \pm 1) = \Phi_{,xy}(x, \pm 1) = \Phi_{,yy}(\infty, y) = \Phi_{,xy}(\infty, y) = 0 \quad \ldots\ldots [1b]$$

$$\int_{-1}^{+1} \Phi_{,yy}\, dy = 0, \quad \int_{-1}^{+1} y\, \Phi_{,yy}\, dy = 0, \quad \int_{-1}^{+1} \Phi_{,xy}\, dy = 0 \quad \ldots\ldots [1c]$$

(the three Equations [1*c*] constitute the conditions of self-equilibration) and arrived at Fadle's precise eigenfunctions

$$\left.\begin{aligned} \Phi_{\text{even}} &= e^{-\gamma x}(\cos \boldsymbol{\gamma} y + \lambda y \sin \boldsymbol{\gamma} y) \\ \Phi_{\text{odd}} &= e^{-\gamma x}(\sin \boldsymbol{\gamma} y + \lambda y \cos \boldsymbol{\gamma} y) \end{aligned}\right\} \quad \ldots\ldots [2]$$

(the first of which, $\Phi_2$, has the parameters $\gamma_2 = 2.106196 + 1.125364\,i$, $\lambda_2 = 0.166228 + 0.899240\,i$). What is the remaining task? Clearly, it is to find two expansions

$$\left.\begin{aligned} G(x, y) &= \sum_2^N G_k = \sum_2^N [a_k \Re + A_k \Im]\Phi_k \\ H(x, y) &= = \sum_2^N H_k = \sum_2^N [b_k \Re + B_k \Im]\Phi_k \end{aligned}\right\} \quad \ldots\ldots [3]$$

so that

$$\left.\begin{aligned} G_{,yy} &\to \bar{\sigma}, \quad -H_{,xy} \to \bar{\tau} \\ &\text{as } N \to \infty \\ G_{,xy} &\to 0, \; H_{,yy} \to 0 \end{aligned}\right\} \quad \ldots\ldots [4]$$

The difficulty in obtaining such expansions does not originate with the nonorthogonality of the eigenfunctions $\Re\Phi_k$, $\Im\Phi_k$. This nonorthogonality is a minor matter which may be removed by orthogonalization of the functions by the Gram-Schmidt process. The crux of the difficulty is that Fadle's eigenfunctions violate the "requirement"

$$\bar{G}_{k,xy} = 0, \; H_{k,yy} = 0 \quad \ldots\ldots [5]$$

of "separated boundary values." Requirements of this type do not arise in the case of the Laplace equation, but they do arise in all equations $\nabla^{2n}\Phi = 0$, $n > 1$. Fadle's functions categorically violate the Conditions [5], in the sense that one cannot employ a "finite" aggregate of functions, $\Re\Phi_k$, $\Im\Phi_k$ of the type of [2] and still satisfy [5]—as one can, for instance, employ finite aggregates and satisfy precisely the condition of orthogonality—infinite sets must be used.[9] As a result the expansion coefficients $a_k, \ldots, B_k$ of Equations [3] cannot be determined by conventional methods but must be determined by other means, such as a collocation requirement, or a least-square requirement

$$\int_{-1}^{+1}\left[\left(\sum_2^N G_{k,yy} - \bar{\sigma}\right)^2 + \left(\sum_2^N H_{k,xy} + \bar{\tau}\right)^2\right] dy = \text{minimum} \quad \ldots\ldots [6]$$

and so on. The theoretical and practical difficulties that arise from such determination are discussed by Sommerfeld (2).

In contrast, the self-equilibrating product eigenfunctions proposed by the author, while approximate, do satisfy Conditions [5]. This appears to be an overwhelming advantage in problems where extreme accuracy is not required. True, there is an initial labor involved, that of tabulating these functions, but this has now been completed (3).[11]

(*b*) As always, one can readily bracket the strain energy (4). Using as specific example the strip of Fig. 1(*a*) subject to the normal tractions

$$\bar{\sigma}_y = g_2(0) f_2''(y) = 4N_2(3y^2 - 1), \; N_2 = 1.1093 \quad \ldots\ldots [7]$$

one finds by virtue of the expression

$$\left.\begin{aligned} \boldsymbol{\gamma}_2 &= \boldsymbol{\alpha}_2 + i\boldsymbol{\beta}_2 \\ \alpha_2^2 &= (3/2)(\sqrt{7}/2 + 1) \\ \beta_2^2 &= (3/2)(\sqrt{7}/2 - 1) \end{aligned}\right\} \quad \ldots\ldots [8]$$

[8] Bars denote boundary values at the left edge, $x = 0$. The functions $G_k$, $H_k$ of this discussion are not to be confused with the $G_k$ of the paper. Otherwise we adhere to the original notation.

[9] In contrast, the biharmonic polynomials $\Phi(x, y) = [\Re, \Im, x\Re, x\Im]$ $(z^n)$ may be recombined in finite aggregates so that at the edges $x = \pm a$ of Fig. 1(*b*) they give rise only to $\sigma_x$ stresses (of form $y^k$), $\tau_x, \sigma_l, \tau_l$ being zero, or give rise only to $\tau_x$ stresses, $\sigma_x, \sigma_l, \tau_l$ being zero, etc. This recombination has been carried out in (1)[10] for $k = 0, 1, \ldots, 6$.

[10] Numbers in parentheses refer to the Bibliography at the end of this closure.

[11] It may be mentioned that in a paper on "Thermal Stresses in Rectangular Strips," now being prepared, it is shown that the Airy function of the problem may be developed "precisely" into biharmonic eigenfunctions, without employment of conditions of type [5] or [6]. While the expansion so obtained is exceedingly simple, the labor involved in deriving stresses from the untabulated Functions [2] is formidable, and the present approximate method still appears to be the preferred approach.

of the approximate second eigenvalue, and on the basis of Equation [19b] of the paper, that the strain energy has the upper bound

$$U_{ub} = (32/945E)N_2^2 \int_0^\infty (g_2''^2 + 6g_2'^2 + 63g_2^2/2)dx$$
$$= 0.789N_2^2/E \quad [9]$$

A lower bound is arrived at by starting with deformation functions

$$\left.\begin{aligned} Eu &= 4N_2(3y^2 - 1)g_A(x),\ g_A'(0) = 1 \\ Ev &= 4N_2(3y - 2y^3 + 3y^5/5)g_B(x) \end{aligned}\right\} \quad [10]$$

which were chosen in accordance with the boundary conditions for the normal stresses

$$\left.\begin{aligned} \sigma_x(0,y) &= Eu_{,x}(0,y) = 4N_2(3y^2 - 1) \\ \sigma_y(x, \pm 1) &= Ev_{,y}(x, \pm 1) = 0 \end{aligned}\right\} \quad [11a, b]$$

we have assumed $\mu = 0$; (this is no restriction so long as we are interested in the strain energy only) but ignore the boundary conditions for the shear stresses. On writing the strain-energy expression

$$U = (E/2)\int_{x=0}^{\infty}\int_{y=-1}^{+1} [u_{,x}^2 + v_{,y}^2 + (u_{,y} + v_{,x})^2/2]\,dy\,dx$$
$$= \frac{16}{45E}N_2^2\int_0^\infty \left[g_A'^2 + \frac{15}{2}g_A^2 + \frac{36}{7}g_Ag_B' + \frac{1048}{1155}g_B'^2 + \frac{32}{7}g_B^2\right]dx \quad [12]$$

we find the Euler-Lagrange equation

$$g_j^{IV} - \frac{4815}{917}g_j'' + \frac{4950}{131}g_j = 0 \quad (j = A, B) \quad [13]$$

the eigenvalue

$$\alpha + i\beta = 2.0943 + 1.3270i \quad [14]$$

and the solutions

$$\left.\begin{aligned} g_A &= (A/\alpha)g + h,\ g_B = (B_1/\alpha)g + B_2h \\ g &= e^{-\alpha x}\left(\cos\beta x + \frac{\alpha}{\beta}\sin\beta x\right),\quad h = e^{-\alpha x}\frac{\sin\beta x}{\beta} \end{aligned}\right\} \quad [15]$$

The coefficients

$$A = -1.3794,\ B_1 = -0.9333,\ B_2 = 1.8665 \quad [16]$$

are determined from the requirement that the potential energy

$$\Pi(A, B_1, B_2) = U - \int_{-1}^{+1}(-\bar{\delta})\bar{u}dy \quad [17]$$

be a minimum. (The double minus sign results from our defining positive $\bar{\delta}$ in opposite sense to positive $\bar{u}$.) There results, from Equation [12] or [17], the lower bound estimate

$$U_{lb} = -\Pi = \frac{1}{2}\int_{-1}^{+1}(-\bar{\delta})\bar{u}dy = 0.699N_2^2/E \quad [18]$$

The Upper Bound [9] and Lower Bound [18] are quite close.[12]

Admittedly this does not yet guarantee that our stresses are also fairly close to the true stresses. But it will be recalled that Poritsky has proved (5) that the present approach properly portrays the functional behavior of the various quantities in the $x$-direction and averages out only the behavior in the $y$-direction, the direction of the narrow edge, where the variation of the various quantities is necessarily modest (since the variation of the input stress $\bar{\delta}$ with $y$ is also modest). This suggests that we are on the right track. However, besides presenting such qualitative arguments favoring the expectation of small errors, we may quantitatively estimate the stress error as follows:

Following the suggestion of Prof. E. G. Lee (at the oral discussion of the paper at the meeting) one operates by $\nabla^4$ on the function $g_2(x)f_2(y)$ and obtains

$$\nabla^4 g_2 f_2 = p_2(x,y) \quad [19]$$

The values of the "error" $p_2(x,y)$ are given in Table 1 of this closure and are plotted in Fig. 2. For the correct solution, $\Phi_2$, this error, $\nabla^4\Phi_2$, must be zero.

We provide the correct solution

$$\Phi_2(x,y) = g_2(x)f_2(y) + w_2(x,y) \quad [20]$$

of our problem if we superpose on the approximate, $g_2f_2$, solution, the solution $w_2(x,y)$ of the problem

$$\nabla^4 w_2 = -p_2(x,y) \quad [21a]$$

subject to the boundary conditions

$$\left.\begin{aligned} \bar{\delta} &= \bar{\tau} = 0;\ \text{i.e.,}\ \bar{w}_{,yy} = \bar{w}_{,xyy} = 0 \\ \sigma_y(x, \pm 1) &= \tau(x, \pm 1)\,0;\ \text{i.e.,}\ w_{,yy}(x, \pm 1) = w_{,xyy}(x, \pm 1) = 0 \end{aligned}\right\} \quad [21b]$$

Seemingly, we merely shifted from a homogeneous problem to an inhomogeneous problem. While the difficulties involved still appear to be formidable, our present task is immeasurably simpler than before. (*a*) Since $p_2(x,y)$ is quite small, we may be satisfied with an approximate solution of Equations [21] and yet obtain excellent results, if we are satisfied with engineering accuracy and do not insist on mathematically rigorous results. (*b*) Relaxation-type methods lend themselves more readily to solution of inhomogeneous problems of type [21] than of homogeneous problems of type [1]. (*c*) Since the problem [21] is identical with the problem of finding the curvatures, or the bending moments

[12] It may be mentioned that on assuming in Equation [15] $g_A$ as $(A/\alpha)g + A_2h$, one finds precisely the same results. To the coefficients [16] there is now added $A_2 = 1$.

TABLE 1

| $x/b$ | 0 | 0.2 | 4.0 | 0.6 | 0.8 | 0.9 | 1.0 |
|---|---|---|---|---|---|---|---|
| 0 | 4.13 | 3.83 | 1.51 | −6.97 | −28.58 | −47.21 | −72.99 |
| 0.1 | −0.16 | 0.57 | 1.63 | −0.31 | −10.82 | −21.63 | −37.68 |
| 0.2 | −2.99 | −1.61 | 1.63 | 4.10 | 1.39 | −3.76 | −12.65 |
| 0.4 | −5.64 | −3.74 | 1.44 | 8.31 | 14.25 | 15.75 | 15.56 |
| 0.6 | −5.96 | −4.11 | 1.14 | 8.99 | 17.72 | 21.90 | 25.52 |
| 0.8 | −5.20 | −3.65 | 0.84 | 7.83 | 16.58 | 21.30 | 26.05 |
| 1.0 | −4.09 | −2.91 | 0.58 | 6.19 | 13.60 | 17.85 | 22.38 |
| 1.2 | −3.00 | −2.15 | 0.38 | 4.55 | 10.27 | 13.67 | 17.43 |
| 1.6 | −1.36 | −0.99 | 0.14 | 2.07 | 4.88 | 6.65 | 8.68 |
| 2.0 | −0.49 | −0.36 | 0.04 | 0.75 | 1.87 | 2.60 | 3.48 |
| 2.4 | −0.13 | −0.10 | 0.00 | 0.20 | 0.53 | 0.77 | 1.07 |
| 2.8 | −0.01 | −0.01 | −0.01 | 0.01 | 0.06 | 0.11 | 0.18 |
| 3.2 | 0.02 | 0.01 | −0.00 | −0.03 | −0.05 | −0.06 | −0.06 |
| 3.6 | 0.02 | 0.01 | −0.00 | −0.02 | −0.05 | −0.07 | −0.08 |

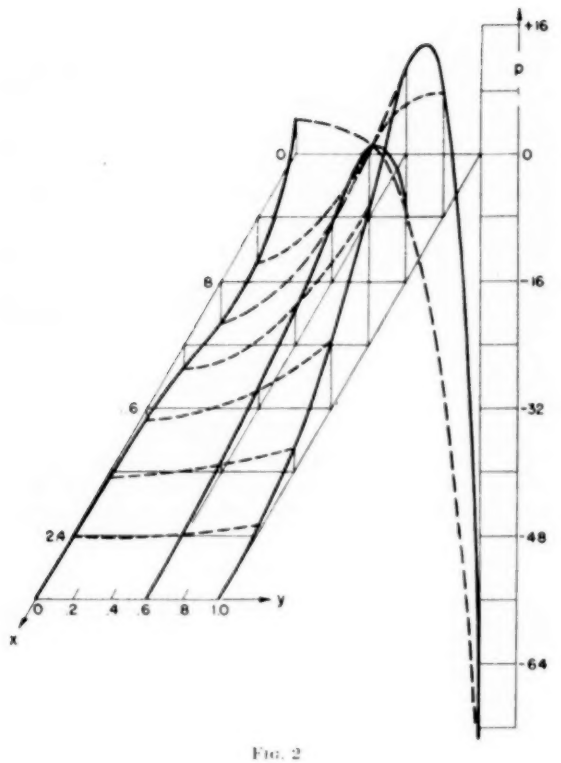


FIG. 2

$$M_x = w_{,xx}, \quad M_y = w_{,yy}, \quad M_{xy} = w_{,xy} \ldots\ldots [22]$$

of a plate, $2 \times \infty$, of unit stiffness $D$, clamped at all edges, and having $\mu = 0$, physical visualization of the deflection shape greatly facilitates locating the critical regions and helps in estimating the stresses, without going into deep analysis.

Indeed, we may conclude at once that the deviation from the original estimate of $\sigma_{y,max}$

$$g_2''(0)f_2(0) = -5.612 \times 1.1093 = -6.24 \ldots\ldots [23]$$

must be in the range

$$-16.6 < w_{,xx}(0,0) < +6 \ldots\ldots [24]$$

as determined from the formula for uniform load (6)

$$w_{,xx}(0,0) = M_x(0,0) = 0.0571 \times 2^2 p \ldots\ldots [25]$$

using for $p$ the lowest value of $p(x,y)$, $-73$, and the highest value, $+26$, respectively. In this manner we may establish definite bounds for the stresses, and it is easy to see that the bounds may be tightened significantly, without too much labor. If, furthermore, we are satisfied with error "estimates" rather than "bounds," then the range can be narrowed down very considerably. From Fig. 2 it is clear that the variation of the load $p$ is very rapid over distances comparable to the strip width, and still the peaks of $p$ are not too high, so that no local effects, as would be associated with concentrated loads, need be considered. Moreover most of $p$ is concentrated along the edges where the plate is particularly rigid; and the effect of $p$ is insignificant beyond $x = 2$. Thus, by regarding the total load

$$P = \int_{x=0}^{\infty}\int_{y=-1}^{+1} p_x dy dx = [\bar{g} f''' + 2g'f' + g'''\bar{f}]_{0,-1}^{\infty,+1} = -11.8 \ldots\ldots [26]$$

as uniformly spread over a $2 \times 2$ built-in plate, we obtain a conservative estimate for the largest $w_{,xx}$ (6)

$$w_{,xx}(0,0) = -0.0513 \times 11.8 = -0.61 \ldots\ldots [27]$$

We conclude that the exact $\sigma_{y,max}$ is lower than the value $-6.24$ given in Equation [23] by less than 10 per cent, probably by 2 to 5 per cent.

A more detailed comparison of approximate and exact stress and deformation distributions in rectangles is carried out in references (7) and (1) and confirms reliability of the present approach.

(*c*) In some problems it will be found that the approximate eigenfunctions $g_k(x)f_k(y)$ are insufficiently accurate. In such cases the present method will lose much of its appeal when awkward but exact eigenfunctions, like Fadle's, are available. It will retain its appeal in problems where exact eigenfunctions are not available, for the method has the distinct advantage, not shared (to the author's knowledge) by other methods, that the improvement of a high mode, $g_n f_n$, does not require the use of all lower modes $g_0 f_0, g_1 f_1, \ldots$ but requires use only of the immediate neighbors $g_{n-1}f_{n-1}$ and $g_{n+1}f_{n+1}$. This can be best illustrated by an example.

Consider the potential problem

$$\nabla^2\Phi = 0, \ \Phi(0,y) = \text{prescribed}, \ \Phi(x, \pm 1) = \Phi(\infty, y) = 0 \ldots [28]$$

in the region of Fig. 1(*a*). This problem leads to the precise eigenvalue

$$\nu_k = (k + 1)\pi/2, \ k = 0, 1, 2, \ldots\ldots [29a]$$

and the precise eigenfunctions

$$\Phi_k = e^{-\nu_k x}\cos \nu_k y \ldots\ldots [29b]$$

By the methods of (8) one finds that the present approach leads to the approximate eigenfunctions $g_k(x)f_k(y)$

$$g_k = e^{-\nu_k x}, \quad \nu_k^2 = c_k = \int_{-1}^{+1} f_k'^2(y)dy \ldots\ldots [30a]$$

$$\left.\begin{aligned}
f_0 &= (15/16)^{1/2}(1 - y^2) \\
f_2 &= (3/4)^{1/2}(1 - 7y^2)f_0 \\
f_4 &= (91/128)^{1/2}(1 - 18y^2 + 33y^4)f_0 \\
f_6 &= (357/512)^{1/2}(1 - 33y^2 + 143y^4 - 143y^6)f_0 \\
f_8 &= (11319/16384)^{1/2}(1 - 52y^2 + 390y^4 \\
&\qquad - 884y^6 + 4199y^8/7)f_0 \\
f_{10} &= (45045/65536)^{1/2}(1 - 75y^2 + 850y^4 - 3230y^6 \\
&\qquad + 4845y^8 - 7429y^{10}/3)f_0 \\
&\ldots\ldots\ldots\ldots\ldots\ldots\ldots\ldots\ldots\ldots
\end{aligned}\right\} [30b]$$

We listed only the functions $f_k$ even in $y$.

The scalar products

$$c_{kl} = \int_{-1}^{+1} f_k' f_l' dy = c_{lk} \ldots\ldots [31]$$

and the $c_k$, for the functions $f_2$ to $f_{10}$, have values as follows

$$\left.\begin{aligned}
c_2 &= 3\cdot 17/2, \ c_4 = 13^2/2, \ c_6 = 17\cdot 23/2, \ c_8 = 7\cdot 107/2, \\
c_{10} &= 3\cdot 5^2\cdot 17/2, \ c_{24} = -(3\cdot 13\cdot 17^2/2^3\cdot 7)^{1/2}, \\
c_{26} &= (17^2/2^3\cdot 7)^{1/2}, \ c_{28} = -(7\cdot 17^2/2^2\cdot 11)^{1/2}, \\
c_{2,10} &= (3\cdot 5^3\cdot 17^2/2^2\cdot 7\cdot 11\cdot 13)^{1/2}, \\
c_{46} &= -(13^3\cdot 17/2^3\cdot 3)^{1/2}, \ c_{48} = (7^2\cdot 13^3/2\cdot 3\cdot 11)^{1/2}, \\
c_{4,10} &= -(5^3\cdot 13^2/2\cdot 11)^{1/2}, \\
c_{68} &= -(7^2\cdot 17\cdot 23^2/2\cdot 11)^{1/2}, \\
c_{6,10} &= (3\cdot 5^3\cdot 17\cdot 23^2/2\cdot 11\cdot 13)^{1/2}, \\
c_{8,10} &= -(3\cdot 5^3\cdot 107/2^3\cdot 13)^{1/2}
\end{aligned}\right\} [32]$$

The first approximation to the 6th eigenvalue

$$\nu_{6I} = c_6^{1/2} = 195.5^{1/2} = 13.982 \quad [33a]$$

differs from the exact eigenvalue

$$\nu_{6E} = 10.996 \quad [33b]$$

by 27.2 per cent. On using the neighboring functions $f_5, f_9$, we obtain from the secular equation

$$\begin{vmatrix} c_5 - \nu^2 & c_{56} & c_{58} \\ c_{56} & c_6 - \nu^2 & c_{69} \\ c_{58} & c_{69} & c_9 - \nu^2 \end{vmatrix} = 0 \quad [34]$$

the second approximation

$$\nu_{6,II} = 11.490 \quad [35a]$$

which differs from $\nu_{6E}$ by 4.5 per cent. The third approximation, utilizing the functions $f_2$ to $f_{10}$, leads to a 5-row determinantal equation and gives

$$\nu_{6,III} = 11.046 \quad [35b]$$

This differs from $\nu_{6E}$ by 0.45 per cent. All these approximations yield upper bounds to the true eigenvalue. However, on replacing in the determinant of the third ($N = III$) approximation all elements $c_{kl}$ with $l - k > 2(N - 2) = 2$ by zero (i.e., on placing $c_{28} = c_{29} = c_{2,10} = c_{48} = c_{4,10} = c_{6,10} = 0$), we obtain a lower bound

$$\nu_6 = 10.682 \quad [36]$$

This remarkable phenomenon was verified also in another example. It also was observed that by replacing the function set $f_k$, which progresses in powers of $y^2$, by a less satisfactory function set $f_k$, which progresses in powers of $y^4$, the upper bound is moved up, the lower bound is moved down. Hence the existence of these bounds is not accidental but is inherent in the method. While at this time no formal proof for the behavior is available, the conclusion is inevitable that there is more in the method than meets the eye.

(*d*) Great men are habitually modest. They do not like to refer to their own work by always pushing their own names ahead. Look at Rayleigh's "Theory of Sound." How often does he refer in it to "Rayleigh's method?" Not a single time. On the other hand, writers, as a rule, will not quote another author's work if they are not aware of its existence, or, if aware, they regard it as nonpertinent to their problem. Admittedly, one meets occasionally people who, because of lack of originality and ability, practice plagiarism in order to achieve fame, but, as a rule, these people are quickly weeded out. It has dismayed and greatly grieved this author to find that there are competent men in the field who do not share his respect and sense of profound indebtedness to one of the most prominent educators and scientists of the century.

Professor Krzywoblocki's other criticism, that this author has failed to mention Ritz's name in the paper is, however, well taken. This author has always used the expressions variational method, and Rayleigh-Ritz method—rightly or wrongly—(and, as a matter of fact, rather wrongly than rightly) interchangeably. On rereading the paper he notes with regret that Rayleigh, Ritz, their predecessor Kirchhoff, and his predecessor (according to reference 2) Ohm, were not mentioned specifically for their contributions. He wishes to make amends for these omissions. He also concurs with Professor Krzywoblocki that the use of the variational method is frequently too uncritical, and that papers are seen here and there, where a Rayleigh-Ritz polynomial and an elasticity problem are thrown into the melting pot, and stresses are pulled out with no regard to convergence difficulties or to possibilities of stress concentrations.

(*e*) (*i*) The deformation expressions, Equations [53] of the original paper, are incorrect. They should read, for any function $g_n f_n$

$$\left.\begin{aligned} Eu &= \bar{g}_n f_n'' - \mu g_n' f_n + J_n(y) \\ Ev &= g_n'' f_n - \mu g_n \bar{f}_n' + K_n(x) \end{aligned}\right\} \quad [37]$$

where the functions $J$ and $K$ are determined from the requirement that the average of

$$E(u_{,y} + v_{,x}) - 2(1 + \mu)\tau \quad [38]$$

over the $x$-range, 0 to $\infty$, and over the $y$-range, $-1$ to $+1$, should vanish. It is to be recalled that $\tau = -g_n' f_n'$. The requirement yields

$$J_n(y) = 0 \quad [39a]$$

$$K_n(x) = \left\{\begin{aligned} &0 \text{ for } n = \text{even} \\ &-\bar{\bar{g}}_n(x) f_n''(1) - g_n''(x) \bar{\bar{f}}_n(1) \text{ for } n = \text{odd} \end{aligned}\right\} \quad [39b]$$

(*ii*) In recent work it has been found convenient to transfer a factor 3 from the expression of $\chi_5$, and a factor 5 from the expression of $\chi_9$ as given in Table 1 of the original paper, to the normalization factor.

## BIBLIOGRAPHY


1 "Solution of Beam Problems by Biharmonic Polynomials Which Separate the Effects of Boundary Shears and Boundary Normal Stresses," by G. Horvay, R. T. Gray, and J. S. Born, to be submitted shortly to a technical journal.

2 "Partial Differential Equations," by A. Sommerfeld, Academic Press, New York, N. Y., 1949, p. 31.

3 "Tables of Self-Equilibrating Eigenfunctions," by G. Horvay and J. S. Born, to be submitted shortly to a technical journal.

4 "The Extremum Principles of the Mathematical Theory of Elasticity and Their Use in Stress Analysis," by W. Prager, University of Washington Engineering Experiment Station Bulletin 119, 1951.

5 "Item (9)" of original Bibliography.

6 "Plates and Shells," by S. Timoshenko, McGraw-Hill Book Company, Inc., New York, N. Y., 1940.

7 "The Use of Self-Equilibrating Eigenfunctions in Solution of Some Beam Problems," by G. Horvay and J. S. Born, to be submitted to the JOURNAL OF APPLIED MECHANICS.

8 "Orthogonal Edge Polynomials in the Solution of Boundary Value Problems," by G. Horvay and F. N. Spiess, *Quarterly of Applied Mathematics*, in press.


# Influence of Viscous Effects on Impact Tubes[1]

DONALD ROSS.[2] The writer recently completed a reanalysis[3] of Nikuradse's[4] smooth-pipe data in which it is shown that Nikuradse actually failed to confirm the existence of the laminar sublayer with his velocity measurements, as originally pointed out by Miller.[5] Although Nikuradse's results are largely attributable to the relatively large diameter of his pitot tube, the viscous effects described by the authors also may be a major cause of similar discrepancies. It can be shown readily that impact

[1] By C. W. Hurd, K. P. Chesky, and A. H. Shapiro, published in the June, 1953, issue of the JOURNAL OF APPLIED MECHANICS, Trans. ASME, vol. 75, pp. 253–256.

[2] Associate Professor of Engineering Research, Ordnance Research Laboratory, The Pennsylvania State College, State College, Pa.

[3] "A New Analysis of Nikuradse's Experiments on Turbulent Flow in Smooth Pipes," by Donald Ross, Proceedings of the Third Midwestern Conference on Fluid Mechanics, March, 1953.

[4] "Gesetzmässigkeiten der turbulenten Strömung in glatten Rohren," by Johann Nikuradse, *Forschungsheft, VDI* 356, 1932.

[5] "The Laminar-Film Hypothesis," by Benjamin Miller, Trans. ASME, vol. 71, 1949, pp. 357–367.

tubes cannot be used to measure accurately the velocities in laminar sublayers.

The Reynolds number of the tube is

$$\text{Rey} = \frac{Va}{\nu} \quad \ldots\ldots [1]$$

which is Equation [2] of the paper. In the laminar sublayer

$$\frac{V}{u_*} \cong \frac{y\,u_*}{\nu} \quad \ldots\ldots [2]$$

where $u_*$ is the friction velocity, $u_* \equiv \sqrt{\tau_w/\rho}$. Substituting for $V$ in Equation [1] yields

$$\text{Rey} = \frac{y}{\delta_s}\,\frac{a}{\delta_s}\left(\frac{\delta_s\,u_*}{\nu}\right)^2 \quad \ldots\ldots [3]$$

where $\delta_s$ is the thickness of the laminar sublayer. The value of $\delta_s\,u_*/\nu$ is of the order of 10; and, to obtain accurate measurements, the diameter of the impact tube should be a small fraction of the laminar sublayer thickness, say less than one fifth. It follows that

$$\text{Rey} < 20 \quad \ldots\ldots [4]$$

The various graphs presented by the authors clearly show that impact tubes operated at such low Reynolds numbers must read high because of viscous effects.

### Authors' Closure

This is an interesting confirmation that impact tubes give false readings in the low-velocity regions of thin boundary layers.

It is of historical interest that the first experimental investigation of how viscous effects enter into impact-tube readings, that of Miss Barker,[6] was motivated by Stanton's suspicion that his measurements of boundary layers close to the wall of a tube were incorrect and that viscosity was at the heart of the matter.

## Unsteady Radial Flow of Gas Through Porous Media[1]

V. Paschkis.[2] This paper presents a most interesting technique and is a worth-while addition to the literature in the field of computing techniques. Several questions come to mind, the answers to which might be of general interest.

1 In the field of analog computers it is customary to work with space increments of equal thickness, rather than with increasing thickness as is done in the paper. One obvious advantage of the increasing thickness as used here is that the resistance elements are the same throughout. Has a study been made indicating if either of the techniques is more accurate?

2 The authors introduce a fictitious thickness, justifying the step by the statement that after a short time span, steady flow occurs in the layers near the well. This statement obviously is meant as an approximation because theoretically steady state does not occur before the field is drained completely of gas. How close is the approximation?

3 The problem dealt with in this paper can be solved on analog computers. Therefore it would be interesting to know what time is required to solve the problem by the technique shown here; obviously the time may be broken down in coding and set-up, operation, and evaluation and plotting. If time records were kept it would be interesting to know the items separately.

### Authors' Closure

The authors appreciate Dr. Paschkis' interest in their work and feel that his comments cover some points of fundamental interest to computing technology. We have the following remarks to make in reply to his questions:

1 The authors do not have any quantitative information on the relative accuracy of space increments of constant versus increasing size. However, the system of exponentially increasing radial increments used by the authors gives a much larger fraction of grid points near the well bore, where pressure gradients are highest. In fact, the pressure gradients decrease continuously with radial position; hence it is desirable to have a grid system whose spacing increases continuously with radius.

2 Calculations were made with a ficticious well radius 8 times the actual well radius that overlapped similar calculations made using the actual well radius; the difference in dimensionless pressure ratio was approximately 2 per cent (relative error). It was found possible to improve this accuracy to less than 0.5 per cent relative error by shifting all the curves the same small distance on the time axis.

3 The authors estimate that 3 to 5 man-days would be required in coding and setup time for this complete problem, with approximately 4 hours of machine operating time for each special case. Time for evaluation and plotting would depend on the manner in which the results are to be presented.

These time estimates are based on use of the IBM type 604 calculator and personnel familiar with its use. Shorter times might be expected with more advanced computing machines.

## Elastic Waves Created During Tensile Fracture[1]

J. D. Campbell.[2] In this most interesting paper the author refers to a "more exact theory" of the propagation of flexural waves in a uniform rod. The writer has not seen that paper,[3] but would like to question the statement, "the fastest flexural wave travels with the speed $c\ [= \sqrt{(Eg/\gamma)}]$."

According to the Timoshenko theory, the maximum phase velocity of flexural waves is 0.5906 $c$, and according to the theory of Pochhammer and Chree it is 0.5764 $c$ (Poisson's ratio being taken as 0.29). These figures are given by Davies,[4] who also shows that the maximum group velocity according to the latter theory is about 0.638 $c$.

It follows from this velocity that the time of arrival of the first flexural disturbance at any point is about 1.57 times that of the

[6] "On the Uses of Very Small Pitot-Tubes for Measuring Wind Velocity," by M. Barker, Proceedings of the Royal Society, London, England, series A, vol. 101, 1922, pp. 435–445.

[1] By R. Jenkins and J. S. Aronofsky, published in the June, 1953, issue of the Journal of Applied Mechanics, Trans. ASME, vol. 75, pp. 210–214.

[2] Technical Director, Heat and Mass Flow Analyzer Laboratory, Department of Mechanical Engineering, Columbia University, New York, N. Y.

[1] By Julius Miklowitz, published in the March, 1953, issue of the Journal of Applied Mechanics, Trans. ASME, vol. 75, pp. 122–130.

[2] Lecturer in Engineering Science, University of Oxford, Oxford, England.

[3] "The Propagation of Waves in the Transverse Vibration of Bars and Plates," by Ya. S. Uflyand, Prikladnaia Matematika i Mekhanika, vol. 12, May-June, 1948, pp. 287–300.

[4] "A Critical Study of the Hopkinson Pressure Bar," by R. M. Davies, Philosophical Transactions of the Royal Society, London, England, series A, vol. 240, 1948, pp. 375–457 (see appendix 3).

first longitudinal wave. Thus at station 2.5, where the first longitudinal wave arrives at $t = 55$ $\mu$sec, the time of arrival of the first flexural wave should be about 86 $\mu$sec; this is considerably greater than the value (67 $\mu$sec) obtained from the analog-computer solution.

It would be interesting to know with what accuracy the time of arrival of the first flexural wave can be obtained from the computer curves.

It seems possible that errors in these curves may be caused by the use of a relatively small number of cells in representing the beam.

E. G. Chilton.[6] The fascinating possibility of studying compression waves in solids without the use of impact has been outlined clearly by the author. It is unfortunate that the method is limited so severely, not only by the use of extremely brittle materials, but also by the limitation of the impact-wave shape. The need for complete definition of the latter has been pointed out by the author, and his future results should be of great interest.

The writer would like to ask if it is not perhaps possible to obtain an experimental verification of $A(t)$ by electrical conductivity measurements of the specimen during the breaking process. Then, if the assumption of a circular front is reasonable, $R(t)$ could be computed readily.

George Gerard.[6] In suggesting an explanation of the phenomenon of double fracture of a tensile specimen, the author states in the Introduction, ". . . this second failure is due to the superposition of the longitudinal strain (from the unloading wave, which through reflections becomes tension) and the resultant flexural strain, which together total more than the original static tensile fracture strain." The flexural strain waves were said to be produced ". . . by the moment that develops as the crack propagates across the bar from its origin at a surface discontinuity."

The statement which is questioned by the writer is contained in the parentheses in the quoted material. Wave-propagation theory clearly indicates that when elastic strain wave strikes a rigid boundary, it is reflected in the same sense as the incoming wave, resulting in a total strain of twice the original magnitude. Thus, for the tensile specimen supported by a grip, which can be considered as a rigid boundary, the unloading wave following fracture is "negative tension" which is reflected as a "compression" from the rigid boundary.

To verify this, refer to Fig. 1 of this discussion which is taken from a paper by Gerard and Becker.[7] Fig. 1 shows a thin aluminum-alloy strip buckled by the unloading wave following fracture which was reflected by the grip. This is a clear indication of the compression character of the wave after reflection from a rigid boundary. The reflection would become tension as stated by the author only after striking a free boundary.

Since the explanation offered by the author apparently must be rejected, it is pertinent to consider a possible mechanism for explaining the phenomenon of double fracture observed in brittle materials. It appears that the theory of impact buckling given in the paper mentioned[7] may apply to this phenomenon.

Accordingly, it is postulated that the tension specimen tends to buckle following reflection of the unloading wave. Since the material is brittle in this case, the fact that a second fracture generally occurs at the fillet of the specimen can be attributed to buckling of the clamped-free column (which is the remainder of the specimen following the first fracture). Because the bar is

[6] Shell Development Company, Emeryville, Calif.

[6] College of Engineering, New York University, New York, N. Y.

[7] "Column Behavior Under Conditions of Impact," by G. Gerard and H. Becker, *Journal of the Aeronautical Sciences*, vol. 19, January, 1952, pp. 58–61.

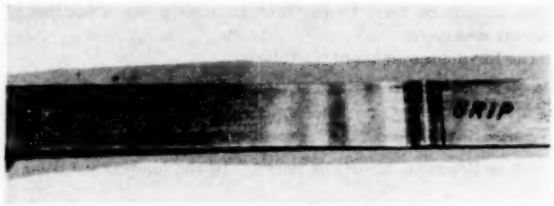


Fig. 1

essentially clamped at the base, the bending moment is a maximum there leading to fracture of the brittle material. If the material were ductile, then buckling would be observed after the test if the conditions were proper to produce permanent wave forms. Tension tests run by the writer on thin round wires have produced severe buckles above the grip.

It is interesting to note that tentative confirmation of the suggested mechanism can be obtained from the test data given in Table 1 of the paper. In fact, the apparently anomolous behavior of the specimens in which single fracture was observed in some cases and double fractures in others can be explained by applying the impact-buckling theory to this case.

In Fig. 2, herewith, the test data are plotted with cantilever length-to-diameter ratio as a function of the initial fracture stress. According to the previous paper the critical slenderness ratio can be given by

$$L_{cr}/\rho = 2\pi(E/\sigma_u)^{1/2} \quad \ldots\ldots [1]$$

For a specimen of circular cross section, $\rho = d/4$, and therefore Equation [1] becomes

$$L_{cr}/d = (\pi/2)(E/\sigma_u)^{1/2} \quad \ldots\ldots [2]$$

Equation [2] is also shown in Fig. 2 for a value of $E = 26 \times 10^6$ psi.

The data shown in Fig. 2 indicate that two regions separated by the theoretical line exist: One in which buckling is not possible

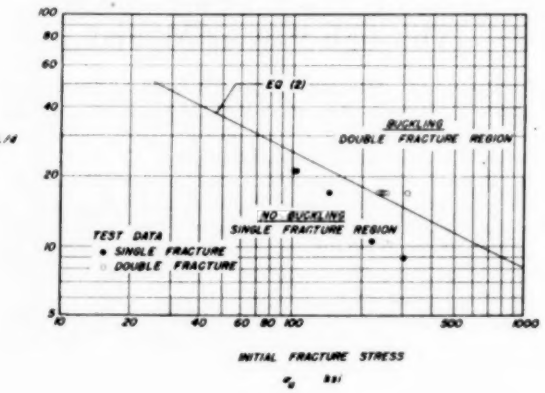


Fig. 2

theoretically, and therefore only single fractures would be observed; and the other where buckling is possible and therefore two fractures are observed. Although the theory of impact buckling does provide a satisfactory check with the test data, additional tests are necessary, particularly for larger length-diameter ratios, to establish confidence in the proposed buckling analysis for the double-fracture phenomenon.

E. B. Shand.[8] This paper points out the importance of elastic waves generated during the fracture process on the failure of brittle bodies. There is no doubt that fracture in brittle bodies may produce elastic waves;[9, 10] in fact, the presence of the parabolic traces on the fracture surfaces (Fig. 2 of paper) are evidences of this effect. It also has been shown that fracture of brittle bodies may be caused by the reflection of intense longitudinal compressive waves.[11, 12] There also are indications that the less violent waves set up by the fracture process can at least produce cracks of limited depth.

While the author's analysis appears to check the phenomena of the primary and secondary fractures, in addition there may be certain discrepancies. The total fracture times of the two fractures are presumably of quite different orders of magnitude, which suggests that the initial breaking stress for the secondary fracture would have to be materially higher than for the primary fracture. This condition is not evidenced in Fig. 7 of the paper. It would be desirable to have further experimental checks made to confirm that the mechanism considered in the paper is that actually causing the second fracture. The measurement of the time interval between the two fractures would be of particular interest.

The author's assumptions regarding the variation of applied stress during fracture are open to serious question, although the effect on the analytical results may not be serious. This matter is complex and cannot be discussed here in detail. However, the stresses during the dynamic phase of fracture will be affected by the load relaxation resulting from the rapid elongation of the specimen at the point of fracture and the inertia of the test equipment. There tends to be a maximum value of local stress which can be attained at the boundary of the crack, as noted by Poncelet,[13] but this again may be modified by the additional energy which may be dissipated in the generation of elastic waves. Probably the assumption of a maximum local stress at the crack boundary will be the most practicable for analytical investigation although this will represent an oversimplification of actual conditions.

An approximation of the stress-concentration factor of the crack, as it extends radially from the origin across the diameter of the specimen, may be represented by Fig. 3 of this discussion. On the basis of the foregoing assumption, the average stress in the part of the section still intact will be proportional to the reciprocals of the stress-concentration factors.

[8] Staff Sales Engineer, Corning Glass Works, Corning, N. Y.

[9] "Über den zeitleichen Ablauf des Bruchvorganges in Glas und Kunstglas," by H. Schardin, D. Elle, and W. Struth, *Zeitschrift der Technische Physik*, vol. 21, 1940, pp. 393–400.

[10] "Derfahren zur Messung und Bruchfortpflanzungs-Geschwindigkeiten an Bruchflächen," by A. Smekal, *Glastechnische Berichte*, vol. 23, 1950, pp. 57–67.

[11] "Glass Cracking Caused by High Explosives," by E. M. Pugh, R. v. Heine-Geldern, S. Foner, and E. C. Mutschler, *Journal of Applied Physics*, vol. 23, 1952, pp. 48–53.

[12] "Fractures Produced in Glass and Plastics by Passage of Stress Waves," by D. G. Christie and H. Kolsky, Trans., Society of Glass Technology, vol. 36, 1952, pp. 65–73.

[13] "A Theory of Static Fatigue for Brittle Solids," by E. F. Poncelet, in a Symposium—"Fracturing of Metals," American Society for Metals, Cleveland, Ohio, 1948, pp. 201–227.

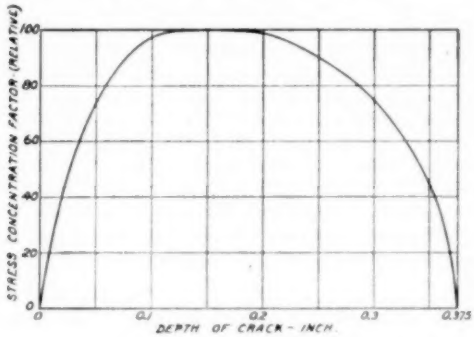


Fig. 3 Stress-Concentration Factor at Boundary of Crack

(Excess over unity, neglecting bending moment.)

### Author's Closure

In considering Dr. Campbell's important comments it should first be stated that the "more exact theory" referred to in the paper is the Timoshenko theory (this terminology is defined in footnote 3 of the paper). It is known that the governing equation of this theory permits two modes of wave transmission for a particular wave length, a low-velocity and high-velocity mode.[14] In the low-velocity mode the velocity approaches 0 for long waves and approaches $c_t$ ($= \sqrt{k'Gg/\gamma}$, the modified shear-wave velocity; in Davies' work this is the 0.5906 $c$ value) for very short waves. In the high-velocity mode the velocity approaches $\infty$ for long waves and approaches $c$ for very short waves. This latter mode is acknowledged in the work of Davies[4] but neglected in accord with the lack of physical significance attached to it by Prescott.[15] A comparison then shows close agreement between the Timoshenko theory and the exact theory (due to Pochhammer and Chree) with regard to the velocity-wave length relation.[4]

The velocities mentioned by Dr. Campbell are the limiting velocities for short waves involved in this comparison. The statement questioned is based on the Uflyand work[3] which presents a method for deriving wave solutions from the governing equation of the Timoshenko theory. Here, the influence of both modes of wave transmission is obviously involved. Actually, it is shown that any particular solution of this equation represents two resultant waves, with $c$ and $c_t$ as respective limiting velocities, i.e., wave-front velocities. A plot of the resultant waves for a particular time $t_0$ would show one of them continuously distributed from the source (say, at $x = 0$) to the limit $x = ct_0$, and the other from the source to $x = c_t t_0$. Hence wave solutions, in accord with the Timoshenko theory, show that there are velocities involved (of component waves) which are greater than $c_t$, but bounded by $c$. The analog solution, in showing its first disturbance at Station 2.5 at $t = 67$ $\mu$sec, gives support to velocities greater than $c_t$. This might have been expected since the analog method used is essentially a finite-difference approximation based on the Timoshenko theory.

Unfortunately, no exact statement can be made on the accuracy of measurement involved in pin-pointing the initial disturbance at a particular station. This point was located by magnifying a diagram and noting, as closely as possible, the first deviation of the moment-time curve from the time axis. Because of the small magnitudes of the initial disturbances, sizable errors were therefore possible. As suggested in footnote 8 of the paper, more accurate determination of the initial point might be accomplished through a focus of attention on the very early times of the analog diagram, employing expanded scales.

It is true, of course, that the number of cells used to represent the beam has a direct bearing on the accuracy of the analog solution. For one thing, the addition of more cells would add to the solution the action of still shorter waves. Such an analog solution might be expected to yield even earlier occurring initial

[14] "Bermerkungen zur Ausbreitung von Beigewellen in Staben und Platten," by L. Cremer, ZAMM, vol. 23, 1943, p. 291.

[15] "Elastic Waves and Vibration of Thin Rods," by J. Prescott, *Philosophical Magazine and Journal of Science*, vol 33, seventh series, 1942, pp. 703–754.

disturbances than the analog solution in the paper, in view of the influence of the velocity $c$ for short waves (limiting velocity of the higher transmission mode, see the foregoing).

With regard to Dr. Chilton's remarks on limitations, some clarifying statements seem in order. Since what is suggested in the paper is a method for studying elastic waves, the author can hardly agree that the use of extremely brittle materials is limiting. Actually, it is in brittle materials, and in normally ductile materials influenced to act in a brittle manner, that elastic waves play their greatest role from a strength-of-materials standpoint. Hence the extremely brittle material becomes the model material for the study. It also should be pointed out that the so-called impact wave is composed of an unloading wave (compression) and a group of flexural waves, and that it is a study of the latter that would be aided the most by additional facts on the associated fracture process. Since the major disturbances of the flexural group travel more slowly than the longitudinal unloading wave, a study of the latter can be isolated from the former. In such a study the unloading-wave rise time (equal to the crack-propagation time) can be measured readily, and the initial amplitude of the wave can be read on the tensile testing machine (fracture-load reading). Further facts on the brittle-fracture process would only influence the shape of the wave front, and this is probably of only secondary importance since the magnitude of the rise time indicates the probability of a well-behaved front.

The author appreciates Dr. Chilton's suggestion for determining the intact area function $A(t)$ experimentally. It seems that the method would be useful but, as Dr. Chilton points out, still requires the assumption of a circular crack front. The brittle-fracture literature supports the occurrence of subsidiary fracture initiations ahead of the main-crack front as discussed in the paper. These initiations are believed to be close to the main-crack front in high-speed fractures which, in view of the indicated radial mode of crack propagation, prompted the author to make the assumption of a regular main-crack front, circular in shape. Obviously, it would be desirable to investigate experimentally the nature of the crack front also. It would seem that high-speed photographs of the initial fracture surfaces during fracture, employing the longitudinal optic system of the plexiglas specimen, could establish this; hence both the $A(t)$ and $R(t)$ functions experimentally.

Unfortunately, Dr. Gerard has misinterpreted the explanation of the double fracture presented by the author. Dr. Gerard has interpreted the work as implying that the second fracture occurs just after the first reflection of the unloading wave. The paper, however, points out that it is not after the first, but the third reflection that the second fracture occurs. Even the very parenthetical expression criticized expresses this in containing the plural of the word reflection. In order to eliminate any further confusion on this point, Fig. 6 of the paper, which clearly describes the reflections involved, is presented again as Fig. 4 of the closure. The upper dashed horizontal line in each of the stages is the initial tension in the specimen. The solid line in stage 1 is the fully developed unloading wave front (i.e., initial fracture just completed). Stage 5 shows the strain state at the second fracture section $x = l/8$ when the first wave reflection arrives there. This stage, which shows the compressive character of the reflection, is in agreement with the well-known facts on wave reflections pointed out by Dr. Gerard. Two subsequent reflections are exhibited in the figure, however. Stage 6 shows one at the initial fracture section (then a free end). The reflected wave is now tension. Stage 7 exhibits the final reflection in the process, which occurs at the fixed end. This of course is also a tension reflection. As the figure and paper point out, the horizontal portions of the curves in each of the stages are actually coincident. They have been separated a little to enable the reader to follow

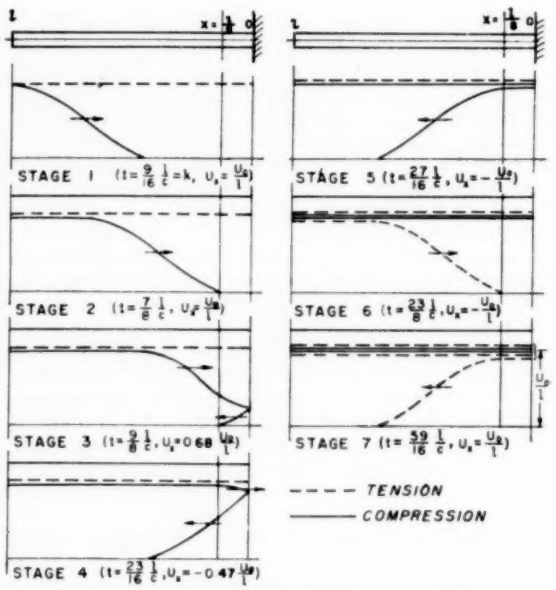


FIG. 4 STAGES IN PROPAGATION OF LONGITUDINAL UNLOADING WAVE INDICATED BY STRAIN DISTRIBUTIONS

the various reflections. Hence in stage 7 the strain at $x = l/8$ is equal to the full value of the unloading wave, $U_0/l$, i.e., the algebraic sum of the five ordinates involved. It is just after stage 7, with the aid of the additional strain due to the flexural waves (see paper for reasons why additional strain is needed), that the second fracture is believed to occur. Fig. 4 was constructed with the aid of Equation [7] of the paper, which gives the strain-wave solution for the unloading-wave problem.

Dr. Gerard's use of the unloading wave in buckling experiments with thin strips is interesting. Aside from what has been written in the foregoing, it is perhaps worthy to consider if buckling plays a role in the author's work, i.e., possibility of fracture after stage 5, but before stage 6. The data in Table 1 of the paper, which are plotted in Fig. 2 of the discussion, can hardly be considered confirming support for the argument. Equation [2] has been plotted in Fig. 2 with $E$ taken as $26 \times 10^6$ psi. This is a rather fictitious steel, to the author's knowledge. $E = 30 \times 10^6$ psi is a more normal value for the average steel. Actually, the modulus for the steel represented in Table 1 (high-speed tool steel, properties given in paper) is closer to $32.5 \times 10^6$ psi.[16] On the basis of this last value the critical line would lie just above the four closely neighboring open circle points (representing double-fractured specimens) instead of just below it, hence putting these double fractured specimens in the single-fracture region. The recent experimental work of Gaumer[17] gives further support for the probability that buckling is not involved in the author's work. Gaumer worked with lucite tensile specimens, similar to the author's plexiglas specimens, but with very short gage lengths. Through conversations with Mr. Gaumer the author learned

[16] "Mechanical Properties of Metals and Alloys," by J. L. Everhart, et al., National Bureau of Standards Circular C447, December, 1943, Table 20, p. 218.

[17] "Study of the Effect of Preloading on the Tensile Strength of Methyl Methacrylate When Strained at a Rate of 890(in./in.)/min," by R. G. Gaumer, thesis for MS in Engineering, UCLA, June, 1953.

that double fractures were produced in roughly 50 per cent of the lucite tests made. Calculations obviously showed that if the results of these tests exhibiting double fractures were plotted in a diagram such as Fig. 2, they would lie far below the critical line; the $L/d$ ratio in most cases was approximately 2.3 and a typical $L_{cr}/d$ value corresponding to one of the cases was 12.8. In connection with the data of Table 1 of the paper, the author did offer a plausible reason for three of the five single-fracture cases. The paper pointed out that the amplitudes of the unloading waves involved in these cases were very low; i.e., the fracture loads were less than one half of some of the fracture loads exhibited by specimens with two fractures (notches employed for instrumentation purposes were evidently the cause of this).

The author appreciates Dr. Shand's interest in this work. In his second paragraph Dr. Shand speaks of the terms "the total fracture times of the two fractures" and "initial breaking stress for the secondary fracture" with relation to Fig. 7 of the paper. These terms, of course, have no meaning in so far as Fig. 7 is concerned. The theory of the paper is involved with only the time up to the onset of the second fracture. Hence "total fracture times of the two fractures" is meaningless. In the event that the region marked "Probable 2nd Fracture Occurrence" in Fig. 7 is involved in Dr. Shand's thoughts on this point, it should be stated that the text of the paper defines this region as being that which probably contains the initiation point of the second fracture, somewhere within its bounds, i.e., corresponding to a short-time region just after stage 7 (see Fig. 4 shown here). Further, Fig. 7 of the paper, as its caption states, is a strain-time plot at the second-fracture section $x = l/8$, in which only the strain due to the unloading wave is plotted. Since the theory points out that the second failure results from the superposition of the unloading-wave strain and the outer-fiber strain due to the flexural waves involved, Fig. 7 obviously would not give the initial breaking stress for the secondary fracture. Superposition of the plots in Figs. 7 and 9 of the paper (outer-fiber strain versus time at $x = l/8$), however, does yield this information. Gaumer's work[17] offers some of the needed experimental verification suggested by Dr. Shand. Fig. 17, and other similar results in that work with short lucite specimens, established that there was a time interval between the two fractures exhibited in the tests. The figure shows eight frames, adjacent to one another, from a Fastax motion-picture-camera study (6000 frames/sec) of one of the tests. The third frame shows no failures, the fourth, one and no sign of another, and the fifth two complete failures. The fifth and last three frames suggest, through the rotation of the center gage section exhibited, that a moment (discussed in the author's work) is involved.

It should be pointed out that the assumptions regarding the variation of applied stress during the initial fracture are not totally those of the author but are based primarily on information available in the brittle-fracture literature (see Analysis in references 3 to 6 of the paper). It is important to mention that the assumption used in the paper of a constant average stress on the intact area during fracture is not void of stress-concentration consideration. Reference to Poncelet[18] (reference 4 of the paper) will show that this assumption is based on the idea that the Inglis factor (stress-concentration factor; ratio of crack-tip stress to average stress on intact area) is a constant throughout most of the fracture process. This idea is supported by the statements Dr. Shand made concerning Poncelet's later work,[12] which also appear in his earlier work.[18]

[18] "Fracture and Comminution of Brittle Solids," by E. F. Poncelet, Metals Technology, AIME, Technical Publication No. 1684, April, 1944 (see particularly footnotes, pp. 16 and 17).

# A Nondestructive Test for Thin Shells[1]

E. Wenk, Jr.[2] The experimental technique described provides an ingenious method for determining the incipient buckling pressures of thin shells subjected to external pressure and should find useful application under certain special conditions. It is believed, however, that the author might amplify the statements regarding both the possible limitations of this procedure and the descriptions of behavior of thin shells under the action of external pressure.

It may be noted that the Equations [1] and [4], as well as [6] and [8] apply to a thin cylindrical shell only if it is of infinite length. Thus all of the subsequent stated relationships which depend upon Equation [1] may not apply to shells of finite length or, as the author has noted, to cylinders reinforced by rings.[3] In lieu of more exact relationships, the following questions arise: Is the short length of model taken into account when determining the effective modulus of the material by these nondestructive tests? Also, is the nonlinearity observed in the relationship between external and differential pressure due to use of non-Hookian materials or to a nonlinear elastic behavior?

Experience with multibay cylinders tested at DTMB indicates that due to inevitable initial imperfections, the pressure at which the first lobe occurs is not usually the maximum. Additional lobes appear with increase of pressure, and the observed maximum, perhaps 20 to 50 per cent above the buckling pressure, is noted when the buckling is so severe that yielding, and finally rupture, at sharply folded lobes occur. Under these circumstances would the pressure-differential relationship demonstrate a marked discontinuity providing the sought-for incipient buckling pressure of the shell or of the shell-stiffener combination?

The observations just cited suggest that the failures with explosive violence do not always occur, and buckling may not even be uniform. The extent of damage is probably a function of the energy available from compression of the pressure fluid and elastic deformations of the pressure tank. Thus a small model in an infinite medium may collapse explosively whereas a model within a tank only slightly greater in size might fail and yet develop only small deformations. In fact, it is possible that if the volume of pressure fluid were sufficiently small, a different technique could be available for a nondestructive test without requiring the use of fluid on the inside of the model. Careful measurements of buckling displacements indicate that a change in volume occurs such that if the available potential energy in the testing system were small, by careful metering of the pressure fluid, deformations in the model could be controlled.

In any case the use of a pressure fluid within the model under test suggests considerable difficulty with instrumentation. In many research investigations, it is desirable to measure the radial displacements or change in circularity as well as elastic strains, and submergence of instruments increases complexities enormously. Also, in tests conducted to check the buckling theory it has been found important to measure the shape of the lobe developed upon buckling for purposes of checking the assumptions in theory. Such measurements do not seem practicable when this technique is employed.

When comparing observed differential curves in Fig. 3 of the

[1] By J. C. New, published in the March, 1953, issue of the Journal of Applied Mechanics, Trans. ASME, vol. 75, pp. 48–52.

[2] Head, Structures Division, Navy Department, David Taylor Model Basin, Washington, D. C.

[3] With short or multibay cylinders, the relationships for $\Delta V/V$ may be obtained from the approximate theory of von Sanden and Gunther or the more exact nonlinear results of Salerno and Pulos (Polytechnic Institute of Brooklyn, PIBAL No. 171A).

paper, with the ideal curves in Fig. 1, questions arise concerning the curvature of graph 3C-a. Up to the yield pressure, it would seem that if the original curvature in graph 3C was attributed entirely to the nonlinear properties of the material the exercising procedure would cause the material to demonstrate linear behavior when loaded a second time. Furthermore, it would be interesting to determine the cause for the curvature of 3C-a to differ from that of 3C after the yield pressure was exceeded.

The stepwise procedure described to obviate need of a high-capacity pressure vessel is quite useful. However, would not the pressure capacity of such a vessel still exceed that needed if no differential-pressure test is employed? This is indicated in Fig. 6 where with the step procedure a tank is required having a capacity of twice that ordinarily provided for a pressure test.

In view of these considerations, would not the nondestructive feature (i.e., no permanent set) possibly be limited to test specimens which fail uniformly by elastic instability where residual stresses and working stresses combined are considerably less than the yield strength of the material?

## Author's Closure

The author is appreciative of Dr. Wenk's thoughtful discussion wherein he raised a number of questions. It is believed that answers to these questions will have more meaning if we first review the essential features of the differential-pressure test.

This test is applicable to any thin shell subjected to external-pressure loading. The experimental technique consists of completely filling the internal volume of the closed shell with a compressible fluid, such as water, and monitoring the internal pressure as the external pressure is increased. The incipient buckling pressure is detected by observing the point at which the difference between the external and internal pressures—the differential pressure—becomes a constant. The extent of shell deformation after buckling is started may be controlled by regulating the external pressure acting on the shell until a state of yield exists. Thus, with proper experimental technique, the test can be performed in a nondestructive manner whenever it is necessary to save the test structure for future service, which is often the case, especially when proof testing is required.

Early in his discussion, Dr. Wenk stated that Equations [1], [4], [6], and [8], in the shell analysis given in the paper under consideration, were applicable only to infinitely long shells. Nevertheless, it is well known that the infinite-length assumption offers no serious restriction when the analysis is applied to many of the thin shells of finite lengths that occur in practice. Although analyses for thin cylindrical shells, which are justifiably claimed to be more exact than the simplified theory, are available in the literature, a review of these analyses shows that their exactness is needed more for the evaluation of stresses than for volume changes. And, in particular, they permit the calculation of higher localized stresses than are unobtainable from the simplified analysis in which a uniform distribution of stress is assumed. Since the differential test, however, integrates the action occurring throughout the shell, the error introduced by the difference between two analyses is usually less than experimental error. For example, if we assume a cylindrical thin-walled steel shell with an $L/t$ ratio of 50 and with rigid end closures, so there is no radial displacement at the ends, the volumetric contraction $\Delta V/V$ is computed to be about two per cent less than the value computed from Equation [1], which is based on the simplified analysis. Under the conditions of the foregoing example and with a value of $C$ determined by test, the effective modulus $E$ computed with the rigorous analysis is found to be less than two per cent smaller than the $E$ calculated from Equation [5], which was derived from the simplified analysis. As the $L/t$ ratio increases, the differences discussed in the foregoing approach zero. In any case, the analysis of the pressure relationships and volumetric changes as they pertain to the differential-pressure test was presented not only to make it available to the profession but also as a concise and convenient illustration of the kind of shell behavior that makes this test functionable. The significant point to remember is that the test leads to valid results that are correct, except for experimental error, irrespective of the analysis that may be chosen for use subsequent to conduct of the test. On the other hand, the accuracy of the calculation of associated parameters, such as the effective modulus, is affected by our choice of formulas, but it can never be better than the accuracy of the experimental results.

The nonlinearity observed in the pressure curves 3C and 3C-a is attributed to (*a*) fabrication imperfections, which permitted nonelastic displacement under loading and (*b*) experimental technique, primarily allowing mechanically entrapped air to remain inside the shell. Also, aluminum alloy and plastic shells have exhibited a certain amount of nonlinear elastic behavior. Many tests have been conducted with more idealized specimens than 3C and with the use of improved experimental methods. The resulting curves have displayed excellent linearity in the first stage of the test. However, the difference in curvature between curves 3C and 3C-a can be attributed to the fact that the initial conditions (volumes and imperfections) for the two trials were not the same owing to yield (as evidenced by the sharp drop near the end of curve 3C) which was allowed to take place during the first trial. Therefore we might reasonably expect a change in curvature during the second trial (3C-a). In addition, the use of non-Hookian materials tends to distort the pressure curve, but this in no way compromises the basic result of the differential-pressure test, i.e., a reliable determination of the incipient buckling pressure.

One salient feature of this test is that it may be used on shells of any geometry or construction—multibay or otherwise. In fact, its usefulness is enhanced in these cases, because, in general, an exact analysis is rarely known, is compromised by manufacturing imperfections, or is unduly cumbersome. This test will detect first buckling, which alters the rate of volume change owing to lobe formation; and, after equilibrium is attained by virtue of the internal pressure, the formation of subsequent lobes will be indicated. Thus an investigator can expect to find both the initial buckling of the shell wall and the later buckling of the shell-stiffener combination, if the latter occurs at 20 to 50 per cent above the former. The limitations that apply in such cases are simply that the wall buckling strength must not be negligibly small and the buckling strength of the shell-stiffener combination must not exceed the capacity of the test vessel. If the shell reaches a state of yield, as Dr. Wenk mentioned, this will be indicated by a drop in the pressure curve, see Fig. 3. Often the operator loses control of the test at this point, because equilibrium can no longer be maintained unless the external pressure is relieved. Under the circumstances described in the foregoing, the precision of the experimental results will be largely controlled by the accuracy and keenness of experimental technique and observation. The detection of an intermediate buckle of small size can be lost if the increment of external pressure is too large. Continuous monitoring, as contrasted to stepwise readings of the differential pressure, is helpful in such instances.

Dr. Wenk's discussion of the role of energy in pressure testing appears to be directed toward the case where there is external pressure only. His deductions expressed in that connection, however, are inapplicable to the differential-pressure test wherein there is internal pressure whose generation is a function of the external pressure. As an explanation of the energy relations in the latter case is rather lengthy, perhaps it will suffice here to say that before and after buckling but prior to yielding of the shell

material the extent of damage is independent of the energy, whether infinite or small, that is available in the pressure fluid and tank as a source for continuance of damage. After yielding, the extent of damage is dependent upon the plastic stress-strain characteristics of the shell material and the compressibility of the fluid inside the shell as well as upon the potential energy in any system that is exterior to the shell.

Before leaving the questions raised by discussing energy, there is one that should be clarified further. It is certain that there is theoretically a nondestructive test which requires no interior fluid in the specimen. Such a test is based on a suitably close matching of the volume changes of the pressure medium and tank with the volume change of the test specimen at incipient buckling. Further thinking along this line indicates how impractical it is to try to set up a test of this kind. We see that to set it up would call for so much pretest data on the displacements of the shell specimen that, after calculating these data, if this could be done without too much inaccuracy for the given shell, there would be no need to conduct the test. Even with careful metering of the pressure fluid, it appears unlikely that a reliable nondestructive pressure test could be established. To maintain the nondestructive feature, the metering response must be induced immediately and continuously by the condition of the shell; and, as quickly as it is required by the shell, the metering system must supply relief from or support of part of the increase of external pressure. These conditions prevail in a water-filled shell, but they have not, as yet, been obtained for an empty shell. Moreover, it seems doubtful that they can be readily obtained in the near future.

In regard to instrumentation, it has been found that radial displacements, elastic strains, and lobe shapes can be measured in the differential-pressure test. It is necessary that the measuring instruments be waterproofed. The writer has successfully measured deflections up to one and two inches with errors below two per cent under pressures up to 1100 psi using linear differential transformers which were enclosed in brass housings to isolate them from water-pressure effects. The leads were brought out of the pressure vessel through copper tubing. Likewise, waterproofing techniques for wire-resistance strain gages are well established. For measuring lobe shapes, it is felt that the differential-pressure test offers a distinct advantage in that not only can the lobe be measured but the progress of its formation can be studied due to slowing its rate by means of the control inherent in the test method. Measurements can be made by the use of a traversing system while the test is being conducted.

In using the stepwise procedure outlined in the writer's paper, one must exercise caution when reducing the internal pressure. If the shell is near the point of buckling, the buckling may occur during the internal-pressure reduction process attended by inadequate control of the test at this point. This can be avoided by slowly reducing the pressure accompanied by the same care in taking readings as that employed when the external pressure is being increased. If we accept the foregoing procedure, the capacity of the pressure vessel need be only slightly greater (of the order of 50 psi) than the capacity of a vessel used in applying external pressure to an empty test shell.

It is hoped that the foregoing discussion will help to clarify questions about the original paper, especially where there may be a tendency to believe that the test is applicable only under certain special conditions. Numerous tests made at the Naval Ordnance Laboratory have successfully demonstrated the general applicability of the method. For the sake of brevity some discussion of this test method has been omitted in this closure and in the original paper, but it may be found in an earlier report, which is available at the Naval Ordnance Laboratory.

The writer is grateful to Dr. Wenk for his stimulating discussion. He would also like to express appreciation to his colleague, Dr. Manford B. Tate, who not only has critically reviewed this discussion but also kindly offered much helpful advice and encouragement with respect to the original work.

## Response of a Cylindrical Shell to a Shock Wave[1]

M. C. Junger.[2] It is believed that certain simplifying assumptions in this analysis may give rise to appreciable errors. The approximation to be discussed here is connected with the differential equations of motion of the shell. In the paper, these equations do not include the coupling effect between flexural and extensional modes for $n > 0$. The importance of this effect increases very rapidly with frequency;[3] this is to be expected, by intuition, since high frequencies excite particularly the high-frequency (i.e., extensional) modes. Since a step-function type of disturbance necessarily has extremely high-frequency components, inevitably it will excite the extensional modes neglected in this analysis. The damping ratios connected with these modes are larger than those connected with the flexural modes.[3] Hence the extensional modes will be damped out at an early stage; the neglect of the coupling effect therefore does not give rise to a significant error in the later stages of the transient response of the shell. However, in the time interval immediately following the incidence of the shock wave, the error may be of the order of 50 per cent for modes $n > 0$. Fortunately, inclusion of the coupling effect introduces only minor complications in the analysis.

### Authors' Closure

The authors agree essentially with Mr. Junger's statement concerning the effect of the extensional modes for $n > 0$, particularly with the conclusion that neglecting them introduces no significant error for the later stages of the response. As a matter of fact, the authors made the approximation for this very reason.

A refined analysis, using the same general approach as the paper but including all extensional effects has been completed recently.[4] While no fundamental difficulty arises, it was found, contrary to the discusser's statement, that the numerical integrations required become much more cumbersome and time-consuming.

## Topics in Gyroscopic Motion[1]

F. B. Jennings.[2] If one wishes to analyze and understand the motion of gyroscopes, the most useful equations are Equations [72] and [74] of the paper. These equations are so im-

[1] By R. D. Mindlin and H. H. Bleich, published in the June, 1953, issue of the Journal of Applied Mechanics, Trans. ASME, vol. 75, pp. 189–195.

[2] Research Fellow in Acoustics, Acoustics Research Laboratory, Harvard University, Cambridge, Mass. Jun. ASME.

[3] "Vibrations of Elastic Shells in a Fluid Medium and the Associated Radiation of Sound," by M. C. Junger, Journal of Applied Mechanics, Trans. ASME, vol. 74, 1952, pp. 439–445.

[4] "A Further Study of the Response of an Elastic Cylindrical Shell to a Transverse Shock Wave," by M. L. Baron, PhD dissertation, Columbia University, New York, N. Y., June, 1953.

[1] By H. Poritsky, published in the March, 1953, issue of the Journal of Applied Mechanics, Trans. ASME, vol. 75, pp. 1–8.

[2] Supervisor of Aircraft Instrument, Development Engineering Unit, General Electric Company, Meter and Instrument Department, West Lynn, Mass.

portant that it will be worth while to investigate their physical significance.

They include the effect of gimbal inertias and apply when the gyroscope's case $R_4$ is stationary. The inner gimbal is assumed to be dynamically balanced, which is not always a valid assumption. Equation [72] gives the total angular momentum of the moving parts

$$\mathbf{M} = \mathbf{i}_2 I\dot{\alpha}_1 + \mathbf{\Phi}\cdot\boldsymbol{\omega}$$

The inner gimbal "effective" inertia dyadic and angular velocity are

$$\mathbf{\Phi} = \mathbf{i}_2\mathbf{i}_2(I + I_2 + K_2) + \mathbf{j}_2\mathbf{j}_2(K + J_2) + \mathbf{k}_2\mathbf{k}_2(\mathrm{K} + \mathrm{K}_2 + \mathrm{K}_3)$$

$$\boldsymbol{\omega} = \boldsymbol{\omega}_2 + \boldsymbol{\omega}_2 = -\mathbf{i}_2\dot{\alpha}_3 \sin\alpha_2 + \mathbf{j}_2\dot{\alpha}_2 + \mathbf{k}_2\dot{\alpha}_3\cos\alpha_2$$

It is interesting to note that the outer gimbal can be considered weightless, if its inertia $K_3$ is added to both the $\mathbf{i}_2$ and $\mathbf{k}_2$ principal inertias of the inner gimbal and locked rotor.

The torques applied to the gyro will be those needed to accelerate and precess the relative spin momentum $\mathbf{i}_2 I\dot{\alpha}_1$ and those needed to move the rigid body whose angular momentum is $\mathbf{\Phi}\cdot\boldsymbol{\omega}$

$$\mathbf{Q} = \dot{\mathbf{M}} = \mathbf{i}_2 I\ddot{\alpha}_1 + \boldsymbol{\omega}\times\mathbf{i}_2 I\dot{\alpha}_1 + \mathbf{\Phi}\cdot\partial\boldsymbol{\omega}/\partial t + \boldsymbol{\omega}\times\mathbf{\Phi}\cdot\boldsymbol{\omega}$$

The partial time derivative gives rate relative to the inner gimbal, $\mathbf{i}_2$, $\mathbf{j}_2$, and $\mathbf{k}_2$ being held constant. It is a useful approximation to ignore the quadratic term $\boldsymbol{\omega}\times\mathbf{\Phi}\cdot\boldsymbol{\omega}$ whenever the spin $\dot{\alpha}_1$ is large compared with $\boldsymbol{\omega}$.

Equations [74] give the torques applied by the rotor-driving motor $Q_{\alpha 1}$, the inner-gimbal torque motor $Q_{\alpha 2}$, and the outer-gimbal torque motor $Q_{\alpha 3}$. Bearing and windage torques are neglected, although they could be included in expressions for the torques. We shall not repeat the author's Equations [74] but instead give the approximate linear equations obtained by ignoring small quadratic terms. An expression for rotor driving torque from a synchronous motor also is included to show that $D\dot{\alpha}_1$ is the main source of damping in a gyro

$$Q_{\alpha 1} = kst - k\alpha_1 - D\dot{\alpha}_1 \cong I\ddot{\alpha}_1 - (I\sin\alpha_2)\ddot{\alpha}_3$$

$$Q_{\alpha 2} = \mathbf{j}_2\cdot\dot{\mathbf{M}} \approx (K + J_2)\ddot{\alpha}_2 + (I\dot{\alpha}_1\cos\alpha_2)\dot{\alpha}_3$$

$$Q_{\alpha 3} = \mathbf{k}_2\cdot\dot{\mathbf{M}} \simeq -(I\sin\alpha_2)\ddot{\alpha}_1 - (I\dot{\alpha}_1\cos\alpha_2)\dot{\alpha}_2 + \{K_3 + (K + K_2)\cos^2\alpha_2 + (I + I_2)\sin^2\alpha_2\}\ddot{\alpha}_3$$

Often the motor stiffness $k$ will be great enough to permit us to set $\dot{\alpha}_1 = s = \text{const}$. The bracketed quantities are considered to be constants in the linear equations. With no applied torques, these equations become the same as Equations [94] used by the author. We have found these linearized equations very useful in analyzing such problems as transient response, stability of servosystems, and effect of rotor acceleration.

### Author's Closure

The author wishes to thank Mr. Jennings for his interesting comments regarding the usefulness of the Equations [72] and [74] of the paper.

## On an Iterative Method for Nonlinear Vibrations[1]

K. Klotter.[2] In the writer's opinion, the significance of the paper, which discusses a previous one by J. E. Brock, rests on the following points:

1 The author frees Brock's procedure from some incidental accessories (e.g., the use of a particular method for numerical integration) and he appraises the role of that procedure from an analytical point of view.

2 The author shows that the same treatment may be applied to systems of more than one degree of freedom.

3 He shows, furthermore, that dissipative systems need not be excluded from the treatment.

The method, however, is reviewed exclusively for its own merits, and no comparison is attempted to assess its advantages or disadvantages in regard to other methods available.

### Author's Closure

Professor Klotter has given an admirable summation of the principal goals of the paper. With regard to the relative advantages of this method over others, the author feels that there probably are none when the method is considered to be a one-term analytical approximation. It may, however, have advantages when used as a purely numerical method, similar to Brock's original treatment. The most promising facet of the method is relative to higher approximations. However, as stated in the paper, the general questions of convergence and relation to classical existence theorems have not been examined thoroughly.

## Stress Singularities Resulting From Various Boundary Conditions in Angular Corners of Plates in Extension[1]

Prof. A. Erdélyi has called to the author's attention a paper by Lelia Ricci[2] which tabulates the minimum roots of the complex equation

$$\sin z = \pm kz$$

which equation is of the type occurring for several of the boundary-condition combinations given in the author's paper.

By using Ricci's values to check Fig. 1, a slight error was found in Case 2 between 180 and 360 deg. The following values should be used:

| Degrees | | | | |
|---|---|---|---|---|
| 180 | 225 | 270 | 300 | 360 |
| 1.000 | 0.736 | 0.604 | 0.555 | 0.500 |

The author wishes to thank Professor Erdélyi for this reference as the solution of this eigen equation is quite time-consuming.

[1] By R. E. Roberson, published in the June, 1953, issue of the Journal of Applied Mechanics, Trans. ASME, vol. 75, pp. 237–240.

[2] Professor of Engineering Mechanics, Stanford University, Stanford, Calif.

[1] By M. L. Williams, published in the December, 1952, issue of the Journal of Applied Mechanics, Trans. ASME, vol. 74, pp. 526–528.

[2] "Tavola di radici di basso modulo di un'equazione interessante in Scienza delle Costruzioni," by L. Ricci, Pubblicazioni N. 296, Istituto per le Applicazioni del Calcolo, Rome, Italy, 1951.

# Stability of Thin Elastic Plates[1]

M. Z. v. Krzywoblocki.[2] The author has referred to a paper by the writer on the theory of plates.[3] In order to clarify some of the points which may not be obvious to the reader, let us consider Bergman's method. Bergman's method has two important features, highly valuable from the application standpoint: (*a*) In the solution of the differential equation in question there are two arbitrary analytic functions of the argument $\frac{1}{2} z (1 - t^2)$. Besides the condition of analyticity (in a complex variable) and regularity for sufficiently small values of the argument no other conditions are superimposed upon these functions. As a matter of fact, they may be given or chosen. In the first part of his work, Bergman proved that the theorem which concerns the solution yields a local result; i.e., it states that the solution is valid only in a sufficiently small neighborhood of the origin. (*b*) By proving a theorem concerning analytical continuation in the complex domain of solutions of the differential equation with analytic coefficients, Bergman has shown that his representation is valid in the large, i.e., in a finite domain.

In the writer's application of Bergman's method the property (*a*) was not fully utilized. As a matter of fact, it was assumed that these functions $f$ and $g$ are expressible in terms of a power series with all of the coefficients equal identically to 1. Certainly one cannot choose a simpler representation. The reason for this was that no one had any experience in dealing with this new method. But it must be emphasized that owing to the existence of these functions there are great possibilities from the application standpoint, greater perhaps than we may expect today. These possibilities are fully utilized in Bergman's method applied to second-order equations (hodograph method) but not as yet as applied to fourth-order equations. The point (*b*) of course, was fully utilized.

The author assumed a priori a solution in the form of a power series in the complex plane. From the form of the differential equations in question he obtains conditions on the coefficients, but in his approach, he does not possess arbitrary functions $f$ and $g$. Thus he does not utilize fully all the advantages of Bergman's method but only a part of them, namely, the use of the complex plane and the solution of the boundary-value problem. Although his approach is Bergman's proposition, it is—strictly speaking—not Bergman's method in the full meaning of this word. It is a "degenerated" Bergman's method. Dr. Zizicas reproduces Bergman's proposition of solving the boundary-value problem but does not use his powerful method of solving the fourth-order partial differential equation (which the writer used).

Moreover, his solution is valid only in the neighborhood of the origin. Nothing is said about the domain of convergence and no analytic continuation considerations are given. Since his conditions on the coefficients are essentially equivalent to those proposed by Bergman which is quite understandable from the forms of these series, and since he utilizes the writer's solutions of those coefficients, one cannot wonder that his final form of the solution of the equation is similar to the writer's. But his statement that the writer's results "become a special case and are reached directly in a simple way" seems to prove a misunderstanding of the entire method.

Bergman's method and the writer's results are proved to be valid in "the large" and they involve arbitrary functions $f$ and $g$ which are "being carried" throughout the entire solution and domain. On the other hand, the author's method is valid in the neighborhood of the origin, and it does not possess arbitrary functions, except two arbitrary conditions for defining the first functions in the recursion formulas, which subsequently serve to determine higher-order coefficients. The full discrepancy between these two approaches will come to light in numerical approaches and in the rate of convergence of both propositions.

When reading the paper, one may get the impression that the author proposed a simplified method and that (using his words) Bergman's method and the writer's results "become a special case." Whereas the fact is that Bergman's method is today one of the most general methods of solution of the discussed type of differential equations because of its validity in the large and its content of arbitrary functions. The author's "simplifications" are valid locally in the neighborhood of the origin; they do not possess arbitrary functions, and thus they are only a special case of the writer's solutions. The latter are valid in the large and may be referred in an elucidative way to the entire class of functions $f$ and $g$. Instead of generalizing the writer's results by using different possibilities of those functions, the author simply got rid of them, thus restricting his approach to a little significant case, ignoring completely the crucial and the most valuable and general point in Bergman's method.

Truly speaking, one may wonder what is the purpose of the author's approach. There is no contribution to the theory of plates, since by simple assumptions in the first steps of Bergman's method one can always express Bergman's solution in terms of a simple power series (as the author did), thus restricting and not generalizing the solution. Why use a solution in "the small" if one has a solution in the large? There is no contribution to the theory of differential equations. The most recent tendency in that theory is to use not power series of a medieval flavor but much stronger methods, and Bergman's integral-operator method is one of the most significant developments in recent years in that respect. Instead of twisting this method, one should follow it. It is of a secondary importance that in subsequent steps of the approach one can develop these integral operators into some special forms of power expansions due to the "analyticity" of the functions. Any other representations may be used, as well. Anyhow, the power-series representation is not an ordinary one. The coefficients of this expansion contain the notion of arbitrary functions and validity in the large.

There are numerous well-known disadvantages of ordinary power series, their restrictions being one reason why we do not want to use them. Thus it is not understandable, why, after Bergman proposed a strong method of integral operators, the author attempts to reduce the problem back to the worst possible power series, from which Bergman separated by taking a great step forward toward something better. Perhaps the author will contribute something more in subsequent papers, since the present paper is only a reproduction of the solution of a boundary-value problem which was proposed by Bergman 20 years ago and subsequently elaborated by the writer, plus changes which, in effect, reduced Bergman's powerful method of solving the fourth-order partial differential equation to the less powerful method previously existing (ordinary power series), the result being simply meaningless.

[1] "Stability of Thin Elastic Plates Covering an Arbitrary Simply Connected Region and Subject to Any Admissible Boundary Conditions," by G. A. Zizicas, published in the March, 1953, issue of the Journal of Applied Mechanics, Trans. ASME, vol. 75, pp. 23–29.

[2] Professor of Gasdynamics, Department of Aeronautical Engineering, University of Illinois, Urbana, Ill.

[3] "A General Approximation Method in the Theory of Plates of Small Reflection," by M. Z. v. Krzywoblocki, *Quarterly of Applied Mathematics*, vol. 6, 1948, pp. 31–52; also vol. 7, 1949, p. 236.

H. F. Weinberger[4] and A. Weinstein.[5] This paper is of great interest and deserves closer scrutiny. The author expects to find an approximation to the critical buckling load from values of $k$ for which the Equations [18] of the paper $\sum_{j=1}^{n} a_{ij}c_j = 0$ have a nonzero solution. If these equations are multiplied by $c_i$ and summed, one finds that $\Sigma\Sigma a_{ij}c_ic_j = 0$ or, in other words, that the linear combination [10] $\Sigma c_jf_j(kx, ky)$ satisfies exactly the boundary conditions of the buckling problem. That such an occurrence is extremely unlikely can be seen by putting $n = 1$. Then the determinant which has to vanish is just

$$\oint_c \{[G_1(f_1)]^2 + \Lambda[G_2(f_1)]^2\}ds$$

If this is zero for some $k$, $f_1(kx, ky)$ must satisfy the boundary conditions as well as the differential equation of buckling. Thus either $f(kx, ky)$ is the correct buckling mode, in which case $k^2$ is the critical value, or $f_1(kx, ky)$ is one of the higher buckling modes. It is unlikely that a random choice of the function $f_1$ will result in such a mode. Thus the determinant usually will not vanish and will yield not only no approximation but no value of $k$ at all. The method gives a result only if the solution is already guessed.

### Author's Closure

The author wishes to express his appreciation to Profs. M. Z. v. Krzywoblocki, and A. Weinstein and Dr. H. F. Weinberger for their interest in the paper and their critical comments. Several of the points they raised make mandatory an amplification on the paper.

Professor Krzywoblocki appears to have overlooked the main contribution of the paper which consists in presenting a method for the solution of elastic stability problems of thin *anisotropic* plates. Bergman's theory of integral operators for fourth-order linear partial differential equations[6] and Krzywoblocki's application of the method[7] are restricted to equations with biharmonic fourth-order terms, i.e., to isotropic plates. Therefore any comparison between Krzywoblocki's and the author's approach can be made only for isotropic plates, and such plates constitute a special case of anisotropic plates. Hence the statement that "there is no contribution to the theory of plates" seems to prove a misunderstanding of the paper.

In comparing his approach to Bergman's, for *isotropic* plates, the author nowhere in the paper tried to underestimate, as Professor Krzywoblocki's discussion seems to imply, the theoretical contributions of Professor Bergman. It may be pointed out, however, that in both Bergman's[6] and Krzywoblocki's[7] papers after the formulation in terms of integral operators is given, recourse is made to a representation of particular solutions by means of expansions in series. The author then felt that if the final result is going to be a series expansion anyway, why not proceed in a simpler way with a series expansion to begin with, especially when such a method is not restricted to isotropic plates only but is applicable to anisotropic plates as well, and conceivably also could be extended to any linear partial differential equation. Moreover, both Bergman[8] and Krzywoblocki[7] have shown that the series expansion is very satisfactory for practical purposes if punch-card machines are used. Krzywoblocki[7] found explicit solutions for the recursion formulas of Bergman associated with power-series expansions and applied them to the solution of a specific problem. Essentially the same recursion formulas were derived by the author by specializing his direct-series approach from anisotropic to isotropic plates.

An argument against the use of power series can only be based on the existence of procedures for the solution of the problem at hand which have practical advantages in comparison to the power-series expansion. Such a proof is not given in the discussion. On the contrary, it is inconceivable that Professor Krzywoblocki can argue against the power-series expansion which he himself followed and at the same time defend his paper in which this approach was applied.

The author did not assume a priori a solution in the form of power series as Professor Krzywoblocki claims. This is proved by the statement in the paragraph preceding Equation [20] of the paper, "This equation is of the elliptic type and, at least when the coefficients are polynomials in $x$ and $y$, it has analytic solutions in the finite $xy$-plane." Any criticism therefore should have been concerned with this statement. If anything, Bergman's theorem of analytic continuation of particular solutions in the large[6] presents corroborating evidence for the author's point. Once such an analyticity of solutions is established the expressions of Equations [26] and [34] of the paper follow rigorously on the basis of the elementary theory of complex variables and are valid for the entire finite complex plane. Hence the argument that the author's expressions are not valid in the large is not tenable either.

A point also is claimed in favor of the presence of arbitrary analytic functions $f$ and $g$ in the integral-operator approach as contrasted to the author's use of two arbitrary analytic functions in his recursion formulas. Any analytic particular solution obtained by a certain choice of the functions $f$ and $g$ can be expanded in power series within its domain of convergence, and since it satisfies the differential equation it also must satisfy the author's recursion formulas and thus give certain values for the arbitrary analytic functions appearing in the formulas. If these functions are inserted in the author's recursion formulas the result clearly will be the same particular solution which was obtained through the chosen functions $f$ and $g$. Likewise one may argue in the converse direction, but this is hardly necessary since it has been established that any particular solution resulting from an arbitrary choice of the analytic functions $f$ and $g$ can be obtained also by a suitable choice of the arbitrary analytic functions of the author's recursion formulas. Furthermore, the only proposed evaluation of the integral operators is by means of power series and recursion formulas, as seen from Equations [7] and [8] of reference (35) of the paper. In view of this correspondence, Professor Krzywoblocki's statement that "the full discrepancy between these two approaches will come to light in numerical approaches and in the rate of convergence of both propositions," becomes meaningless.

The author did not have in mind a contribution to the theory of partial differential equations when preparing his paper. But since such a question was raised in the discussion he wishes to point out that his method is applicable to a much wider class of equations (the anisotropic-plate equation being only one such case) than Bergman's. Moreover, he is not aware of any case in which his approach has been followed and would welcome any such references if they exist.

The criticism of Dr. H. F. Weinberger and Prof. A. Weinstein is very pertinent. Their scrutiny proves that the author's hopes, stated in the last paragraph of the paper, for substantially diminishing the computational work by omitting an additional constraint (which incidentally Professor Krzywoblocki used correctly in his paper) cannot be realized. As a result a modification of the procedure for the computation of critical loads is necessary which can be best established by means of the energy

[4] Research Associate, Institute for Fluid Dynamics and Applied Mathematics, University of Maryland, College Park, Md.

[5] Research Professor, Institute for Fluid Dynamics and Applied Mathematics, University of Maryland.

[6] Reference (33) of paper.

[7] Reference (35) of paper, or Footnote 3 of discussion.

[8] Reference (34) of paper.

criterion of elastic stability of plates. It can be seen readily that the critical value of the parameter $\lambda$ can be obtained as the minimum of the expression $\lambda = V_b$, where $V_b$ is the bending strain energy of the plate associated with the deflection $w(x, y)$ of the middle plane, subject to the constraining condition $A = 1$, where $A$ is the work done by the forces acting within the middle plane of the plate.[9] Admissible functions $w(x, y)$ are any functions of sufficient continuity satisfying the prescribed boundary conditions. On the basis of the Lagrangian multiplier theory these conditions lead to Equation [1] subject to the boundary conditions, Equations [11], of the paper. Now in the approximate formulation of the boundary conditions by means of Equations [16] the associated requirements are

$$\left.\begin{aligned} &\lambda = \text{minimum } V_b \\ &A = 1 \\ &\rho = \left(\oint_c \{[G_1(w)]^2 + \Lambda[G_2(w)]^2\} ds\right) = \min \end{aligned}\right\} \quad \ldots [1]$$

where $\rho$ is the value of the integral expression for the boundary conditions. The first two of Equations [1], herewith, lead again to the differential equations of the paper on the basis of which the particular solutions were constructed. However, the third equation cannot any more be taken separately, as it is permissible for an exact formulation of the boundary conditions, but must be taken in conjunction with the constraining condition $A = 1$, which must be thought of as imposed on both the first and the third of Equations [1].

As stated in Equation [18] of the paper, the performance of integration for an expression of the type of Equation [10] reduces the boundary condition to an expression

$$\rho = \sum_{i=1}^{n} \sum_{j=1}^{n} a_{ij} c_i c_j = \min \quad \ldots [2]$$

while a similar integration would reduce the constraining condition $A = 1$ to a form

$$1 = \sum_{i=1}^{n} \sum_{j=1}^{n} b_{ij} c_i c_j \quad \ldots [3]$$

By the Lagrangian multiplier theory again, a necessary condition for the minimal problem of Equations [2] and [3], herewith, is that the determinant of the equations $(i, j = 1, 2, 3, \ldots n)$

$$\sum_{j=1}^{n} (a_{ij} - \rho b_{ij}) c_j = 0 \quad \ldots [4]$$

vanishes, i.e.

$$|a_{ij} - \rho b_{ij}| = 0 \quad \ldots [5]$$

The quadratic forms entering Equations [2] and [3] of this discussion are positive definite and hence Equation [5] has $n$ real roots, which are in particular positive because of Equation [2]. Each root gives an approximation for the boundary value expression $\rho$ of Equations [1]. For elastic-stability problems one seeks the closest possible approximation of the boundary conditions so that only the smallest root $\rho = \rho_1$ is needed. The value of $\lambda$ (or $k^2$) for which $\rho_1$ obtains its minimum is the critical one. In other words, the conditions of Equation [19] of the paper must be substituted by the foregoing Equation [5]. The remaining roots $\rho_2 \ldots \rho_n$ correspond to higher modes of vibration.

[9] See, for instance, author's dissertation, reference (36) of the paper, pp. 85–89.

# Damping Constants and Stress Distribution in Resonance Response[1]

A. P. Boresi.[2] The paper is a clear, concise exposition upon an increasingly important aspect of engineering design. Undoubtedly, with the increasing emphasis on welding of structural joints and the resulting decrease of damping due to slippage and other joint factors,[3] inherent damping of materials will play a more important role in limiting resonance amplitudes in structures.

In applying the author's theory to a particular case, since the resonance-amplification factor is highly sensitive to changes in stress amplitude, it may be well to point out that in practice, if the damping capacity of a material is to be determined for design purposes, the setting up of testing conditions equivalent to the service conditions and the determining of a stable value of the specific damping are necessary requirements.[4] If, for example, damping is observed as an indication of progressive damage by repeated stress cycles, the specimens in the damping and the fatigue tests must be subjected to identical stress amplitudes. Furthermore, if under these conditions the damping properties tend to arrive at stable values, the damping values are characteristic of the material only in the condition of the material as changed by the test. If different testing procedures are used in the damping and fatigue test, usually the equivalence of these tests may be assumed only for very small stress amplitude.

In the author's tests the foregoing conditions are fulfilled and the correlation between experiment and theory is satisfactory. However, when these conditions are not satisfied, no correlation between experiment and theory should be expected.

Another observation may be made in the case of vibrations of beams of constant cross section. The natural frequencies of lateral vibration of a simply supported beam may be written as[5]

$$\omega_n = \frac{n^2 \pi^2}{l^2} \sqrt{\frac{EI}{\mu}}, \quad n = 1, 2, 3$$

For a continuous beam the fundamental frequency is

$$\omega_1 = \frac{(3.416)^2}{l^2} \sqrt{\frac{EI}{\mu}}$$

and similar expressions give the higher frequencies. Hence, for beams of constant cross section, reducing the resonance-amplification factor by exposing as much volume as possible to near peak stresses, as suggested by the author, is equivalent to increasing the moment of inertia $I$ and hence changing (increasing) the natural frequency of vibration from the resonant condition.

Alexander Yorgiadis.[6] This paper is a substantial contri-

[1] By B. J. Lazan, published in the June, 1953, issue of the Journal of Applied Mechanics, Trans. ASME, vol. 75, pp. 201–209.

[2] Assistant Professor of Theoretical and Applied Mechanics, Department of Theoretical and Applied Mechanics, College of Engineering, University of Illinois, Urbana, Ill.

[3] Preliminary tests, conducted at the University of Illinois, of a tubular steel model bridge with weld rather than rivet joints indicate that damping in the weld-jointed structure is decreased greatly. In practical cases it may be necessary to incorporate additional damping in the design of weld-jointed structures, dashpots, and so on, to limit resonant amplitudes to safe magnitudes.

[4] "The Inelastic Behavior of Engineering Materials and Structures," by A. M. Freudenthal, John Wiley & Sons, Inc., New York, N. Y., 1950, chapter 10.

[5] "Mechanical Vibrations," by J. P. Den Hartog, McGraw-Hill Book Company, Inc., New York, N. Y., 1947, p. 188.

[6] Chief Engineer, Sonntag Scientific Corporation, Greenwich, Conn. Mem. ASME.

bution to the field of resonance vibrations. Analyses and data for predicting performance of uniformly stressed members have been available, but little has been done to analyze the behavior of nonuniformly stressed structures, made of material of known damping constants. Hence it is believed that this paper will be of great use to those who are confronted with problems of structural resonance.

The writer has the following critical comments on certain specific parts of this paper:

1 The maximum fatigue stress in a member subjected to direct stress loading cannot be assumed to be $P/A$ at a section of sharp discontinuity because of stress concentrations. Formulas for cases IC and ID therefore would have to consider this in order to make them valuable in practice.

2 Table 3 of the paper gives amplification factors of three beams of the same material but of different cross-sectional shape and shows a theoretical variation of 3.75 to 1 in the two extreme cases. All these beams are assumed to have a maximum stress of 80,000 psi induced at resonance, by proper excitation. It is interesting to see what happens if the beams are compared on the basis of stress $S_0$, the maximum stress in the beam if the exciting force or moment were applied statically. From the definition of $A_r$

$$A_r = \frac{S_m}{S_0} \quad \ldots\ldots [1]$$

From Equations [8] and [16] of the paper

$$A_r = \frac{\pi K_s K_c}{E_d J S_m^{n-2}} \quad \ldots\ldots [2]$$

Eliminating $S_m$ from Equations [2] and [1] and solving for $A_r$

$$A_r = \sqrt[n-1]{\frac{\pi K_s K_c}{E_d J S_0^{n-2}}} \quad \ldots\ldots [3]$$

Now, comparing a diamond and square-shaped beam subjected to the same $S_0$, we see that the relative values of $A_r$ are proportional to the $(n-1)$th root of $K_c$. The author selected a material for which $n$ is 13, so that $(n-1)$ is 12. While $K_c$ in the diamond-shaped beam is 3.75 times larger than that in the square beam, $A_r$ is only 1.116 times larger. Similarly, the circular beam has a $K_c$ which is 1.875 times as large as that of the square beam, but its $A_r$ is only 1.054 times larger if calculated by means of Equation [3] of this discussion.

Rearranging Equations [1] and [2] and solving for $S_m$

$$S_m = \sqrt[n-1]{\frac{\pi S_0 K_s K_c}{E_d J}} \quad \ldots\ldots [4]$$

If we now compare the same three beams on the basis of the same cross-sectional area and same exciting bending moment, we find that the diamond-shaped beam with a section modulus 1.414 times that of the square beam has a smaller $S_0$, and therefore, while its resonance $S_m$ is higher than that in the square beam, their difference is only 8.5 per cent. The round beam with a section modulus 0.845 that of the square beam has an $S_m$ which is 6.9 per cent higher.

All these values are meant to show that while shape is a factor in these calculations, the magnitude of this factor depends on the basis of comparison.

3 The denominator of Equation [15] of the paper for $K_c$ has the following integral

$$\int_{t'}^{t} y^n Z dy \quad \ldots\ldots [5]$$

Under certain conditions, this integral will equal zero. This will occur, for example, when $Z$ is constant, $n$ is an odd integer, and $t$ is equal to $t'$. The author may have accounted for this by changing the sign of $t'$, although this is not clear. To avoid any possible error it is suggested that this integral be expressed as the sum of the following two integrals

$$\int_0^t |y^n| Z dy + \int_0^{t'} |y^n| Z dy \quad \ldots\ldots [6]$$

The first of these is proportional to the energy lost in the region above the neutral axis, while the second is proportional to the energy lost in the region below the neutral axis. These two are always added, and never subtracted, as might be the case if the author's expression were used.

## Author's Closure

Mr. Boresi emphasizes the importance of considering the effect of stress history on damping in relating laboratory tests to service behavior. Considering the magnitude of the stress-history effects illustrated in the paper this certainly is a major factor in some cases. Unfortunately, a theory for predicting the effects of a variable-magnitude stress history, such as might be encountered in service and duplicated in the laboratory, from constant-magnitude stress-history data, such as procured in most laboratory tests, is not available at this time.

There are many different bases for comparing the resonance behavior of beam and other types of members, since there are many different conditions and design requirements encountered in service. Mr. Boresi, in his discussion of laterally vibrating beams, compares beams of constant cross-sectional area. Mr. Yorgiadis, in his second comment, also does this and analyzes the author's experimental data on the basis of the same *exciting* moment (rather than same *excited* moment, as used by the author). As would be expected, the basis for comparison may pronouncedly affect the relative rating of cross-sectional shapes, material (with regard to damping capacity), and other design factors. In justification of the author's method of comparison on the basis of the same *excited* stress, this approach is probably best when concerned with the fatigue-failure problem during resonance. In such cases one is usually more concerned with the relative ability of parts to receive *exciting* force without exceeding the fatigue stress rather than the relative stresses caused by constant excitation. The Yorgiadis' basis of comparison would probably be best if the problem were one of noise generation under constant exciting force.

Needless to say, many refinements in the equations presented can be made to cover actual stress distributions rather than assumed ones. This is covered in Mr. Yorgiadis' first point. However, the main purpose of this paper was to reveal and discuss general trends rather than specific cases. Thus several simplifying assumptions were made, as discussed in the paper. The approach presented can now be used to cover specific cases involving complicated stress distribution.

Regarding Mr. Yorgiadis' third point, it was intended that using the appropriate sign for $t'$ would avoid a zero integral. However, Yorgiadis' equation [6] would avoid any possible confusion on this point and is therefore probably preferable.

The author thanks the discussers for their aid in clarifying a neglected subject.

# Book Reviews

## Elasticity and Plasticity

THEORY OF ELASTICITY AND PLASTICITY. By H. L. Westergaard. Harvard Monographs in Applied Science Number 3. Harvard University Press, Harvard University, Cambridge, Mass., and John Wiley & Sons, Inc., New York, N. Y., 1952. Cloth, 6 × 8¼ in., xiii and 176 pp., 19 figs., tables, bibliography, author and subject indexes, $5.

REVIEWED BY J. N. GOODIER[1]

IT is evident in this book that its author did not rest in the orthodoxies of his subject without searching for fresh points of view. Almost everything is done otherwise than the reader is likely to expect unless he has had the privilege of hearing the late Professor Westergaard's lectures recently. These had undergone development from their beginning in 1925 at the University of Illinois and since 1936 at Harvard University. In 1949 the author was able to begin forming them into a book in the conviction that they had reached a justifying maturity. At his death in 1950, enough had been done to form the present volume.

The plan was to proceed as quickly as possible to the treatment of problems in three dimensions. The problems included are those of Lamé on the cylinder and sphere under pressure; the rotating disk; thermal stresses, briefly; the problems of Kelvin, Boussinesq, Cerruti, and Mindlin as to concentrated forces within the infinite solid, on the surface of the semi-infinite solid, and in its interior; concentration of stress at a spherical hole; and the Hertz theory of contact stress. The preparation for this, the general theory forms the first half of the book, after two introductory chapters. One—"Scope"—skillfully distills the simple precise elements of the idealized theory from the complexities of the real, delineates the roles of theory and experiment in this particular subject, and sets it in relation to mechanics of materials, structural mechanics, and soil mechanics. The second—"Historical Notes"—is intended to be read at the beginning, not to be treated as though it were a conventional preface—"Historical notes can be a natural and most suitable means of presenting ideas, provided that the ideas can be explained in terms that are understood." The beginner will, I think, find here much that must remain strange until he has studied the subject itself, yet helpful if taken as an aerial view, preceding the intimate familiarity with the countryside which can come only with pedestrian effort. These historical notes can be read again with new satisfaction after the whole book has been traversed.

The systematic development of the general theory is in terms of vectors and dyadics. The distinctiveness of the treatment appears at once in the "dyadic circle" (due to Mohr and Land) used instead of the more familiar Mohr circle for stress in a plane. Mohr's three circles for three-dimensional stress are derived by a method of the author's. This originality of method is also characteristic of the book, making it one whose contents include much that is not to be found in the same form elsewhere. The general analysis of stress and strain terminates with octahedral strain, plastic strain deviations, and plastic detrusions (a term preferred to "shearing strain"), a discussion of the simplest conceivable laws of plasticity, and comments on departures from them. This is the extent of the excursion into plasticity. It is of course most probable in view of the title given to the work that something further was intended.

The solutions of specific problems are in terms of "strain potentials" (the displacement, the gradient of a harmonic function), which are adequate for the Lamé problems and some others, and in terms of the "Galerkin Vector" as well as for the concentrated force problems. This is a general form of elastic (Hooke's law) displacement in terms of three biharmonic scalar functions, which in turn are easily expressible in terms of harmonic functions. Simple choices of these functions furnish the specific solutions. An interesting item of originality here is the author's method of "twinned gradient," devised to convert solutions for mathematically advantageous special values of Poisson's ratio—for instance the value ½ for the incompressible solid—to solutions for the general value. It is neatly effective in several instances. The derivation of Mindlin's problem—the solving of which was inspired by Westergaard's appreciation of Galerkin's papers—is recast by resort to "strain potentials."

This small book is written in an elegant, lucid, and compact style, inviting the reader to regard pencil and paper as essential equipment. If he fills in conscientiously from one signpost to the next from a knowledge of the usual engineering-degree subjects, he will come to see the book as bigger than it looks, although still, as was the author's evident intention, one to accompany and not to supersede the older treatises. He is thought of as a first-year graduate student. The question "At what level was the book to be?" brought from the author the pregnant reply, "The trail begins at the foot of the mountain." The pace is brisk, the mountain always interesting, the view rewarding. The subject would have been further permanently enriched if it had been possible also to have the distinguished author's report of the trail all the way to the top.

[1] Professor of Mechanical Engineering, Stanford University, Stanford, Calif. Mem. ASME.

## Mechanics

MECHANICS. Lectures on Theoretical Physics, Vol. 1. By Arnold Sommerfeld. Translated from the fourth German edition by Martin O. Stern. Academic Press Inc., New York, N. Y., 1952. Cloth, xiv and 289 pp., figures, index, $6.50.

REVIEWED BY GERALD PICKETT[2]

A TEXTBOOK in mechanics for students of physics. This is the first of a series of six textbooks based, respectively, upon six general courses in classical physics that Dr. Sommerfeld taught at Munich. The courses were:

1 Mechanics
2 Mechanics of Deformable Bodies
3 Electrodynamics
4 Optics
5 Thermodynamics and Statistical Mechanics
6 Partial Differential Equations in Physics

The first chapter applies Newton's laws of motion to the movement of a particle. Planetary motion is included as well as discussions on variable masses and space-time reference systems.

The second chapter takes up the principles of virtual work and d'Alembert's principle. These are applied to various problems of rigid-body motion such as a rolling sphere, the maneuvering of a

[2] Professor of Mechanics, University of Wisconsin, Madison, Wis. Mem. ASME.

falling cat so as to land on its feet, and the balancing of marine engines.

Chapter 3 is a fairly brief treatment of vibration problems including the simple, compound, spherical, and double pendulums.

Spinning tops, gyroscopes, and planets are discussed in Chapter 4. The chapter is closed with supplementary material on the game of billiards.

Chapter 5 is a brief treatment of relative motion. Foucaults' pendulum, and Lagrange's case of the three-body problem are among the applications.

Chapter 6 treats the integral and Chapter 7 the differential variational principles of mechanics. Applications are made to problems previously treated such as pendulums and tops. Other topics are the principles of "Least Action," "Least Constraint," and "Least Curvature." The eighth and final chapter is on the "Theory of Hamilton."

Problems for each chapter and hints on their solutions are given at the end of the book. These problems make a fine source of material for student participation in the class period. They supplement rather than repeat the text material.

The book is more than a text on mechanics. It is also a message from a great science teacher to students who will never have the privilege of sitting in his classes. An engineer with some interest in physics should find this book interesting and valuable.

# Physics

INTRODUCTION TO SOLID STATE PHYSICS. By Charles Kittel. John Wiley & Sons, Inc., New York, N. Y., 1953. Cloth, 6 × 9 in., 174 figs., 56 tables, xii and 396 pp., $7.

REVIEWED BY FRANCIS BITTER[3]

THIS should be a most useful addition to the relatively limited literature on the physics of solids not only for the college senior or beginning graduate student in physics, chemistry, or engineering for whom it is written, but for many physicists, chemists, and engineers who wish to review recent advances in this field. During the past decade or so, many new concepts have been developed and accepted. These have been, and to a certain extent still are, hidden from many readers in original papers where the main interest lies in describing tests for checking their validity rather than in simple descriptions of the concepts themselves. We have here an excellent example of the presentation of new ideas integrated with older inherited knowledge in such a way as to present to the student in readily understandable terms what the crux of the matter in this or that field is today.

The general plan of the book is to emphasize descriptive material first and then to turn to explanations. For example, the electron band theory is introduced after the main discussion of the electric and magnetic properties. This arrangement is particularly suited to the reader who may expect to encounter difficulty in connection with the theoretical parts. The writing is clear and the illustrations are good. The modern tendency to compress the text by leaving only very little space between captions and text is perhaps carried a bit far. There are numerous problems at the end of each chapter and of course a complete index.

As to content, the first five chapters deal with crystal structure and lattice energies, leading to a review of elastic and thermal properties. This part includes a discussion of symmetry properties, of Miller indexes, of x rays, an analysis of stresses, strains, and elastic constants, of lattice vibrations in one, two, and three dimensions, and of various thermal properties, including a brief discussion of the phonon concept. This is followed by six chapters on electric and magnetic properties, including dielectric properties, ferroelectric crystals, dia-, para-, ferro-, and antiferromagnetism, and a most welcome chapter reviewing facts and theories about superconductivity. Then finally we come to two chapters devoted to a theoretical discussion of electrons in a box and in a periodic potential. The last three chapters deal with impurity phenomena, i.e., semiconductors, rectifying barriers, transistors, order-disorder in alloys, various kinds of lattice defects, and their effect on the optical, mechanical, and thermal properties of solids.

[3] Professor of Physics, Massachusetts Institute of Technology, Cambridge, Mass.

# Superconductivity

SUPERCONDUCTIVITY. By D. Shoenberg. Cambridge Monographs on Physics, Cambridge University Press, New York, N. Y., second edition, 1952. Cloth, 5½ × 8½ in., x and 256 pp., figs. tables, appendixes, bibliography, author and subject indexes. $6.

REVIEWED BY AARON WEXLER[4]

THIS excellent monograph is written by one who has himself not only watched with great interest the exciting developments in a field of physics at its very frontier but has also contributed importantly to its development by a voluminous amount of original research. Since the appearance of the first edition of this book in 1938, there has been added to this intensely active field a body of knowledge which has resulted in a new volume about twice the size of the original one.

The chapter headings serve as an excellent guide to the material covered: 1 Introduction, 2 Magnetic Properties of Macroscopic Superconductors, 3 Thermodynamic and Other Thermal Properties, 4 Structure of the Intermediate State, 5 The Depth of Penetration of a Magnetic Field into a Superconductor, and 6 Theoretical Aspects.

The author has written a thorough, yet selective book, which should be valuable to students as well as research workers. Each topic is set in proper historical perspective and is subjected to critical discussion by the author. In keeping with the practice adopted in the first edition, which incorporated an appendix on recent work, he has made this book as up-to-date as is possible in a field in which new findings appear almost daily. One is struck by numerous references to personal conversations with the authors of work on which crucial arguments turn.

Adding to the merit of the book is a series of well-organized tables and graphs of critically evaluated data. The author's familiarity with the Russian literature has insured firsthand consideration of an important segment of the literature on superconductivity.

This book merits a distinguished place in every scientific library. Students and low-temperature specialists can, with profit, read the entire book. Those who are content with a more cursory consideration of the subject will profit from reading the introduction and the small, descriptive section on fundamental theories.

[4] Manager, Magnetics and Solid State Physics Department, Westinghouse Research Laboratories, East Pittsburgh, Pa.

# AN ASME PAPER

## *Its Preparation, Submission and Publication, and Presentation*

**To a large degree the papers prepared and presented under the ASME sponsorship are evidence by which its professional standing and leadership are judged. It follows, therefore, that to qualify for ASME sponsorship, a paper must not only present suitable subject matter, but it must be well written and conform to recognized standards of good English and literary style.**

**The pamphlet on "AN ASME PAPER" is designed to aid authors in meeting these requirements and to acquaint them with rules of the Society relating to the preparation and submission of manuscripts and accompanying illustrations. It also includes suggestions for the presentation of papers before Society meetings.**

**CONTENTS**


***PREPARATION OF A PAPER—***

**General Information—Style, Preferred Spelling, Length Limitation, Approvals and Clearances.**

**Contents of the Paper—Title, Author's Name, Abstract, Body of Paper, Appendixes, Acknowledgments, Bibliographies, Tables, Captions, Photographs, Other Illustrations.**

**Writing the Paper—Outline Tabulations, Tables, Graphs, Charts for Computation, Drawings, Mathematics, Accuracy, Headings and Numbering, Lantern Slides, Motion Pictures, Typing, Number of Copies.**

***SUBMISSION AND PUBLICATION OF A PAPER—***

**Intention to Submit Paper Required in Advance, Meeting Dates, Due Dates for Manuscript, Discussers, Review and Acceptance, Proofs, Advance Copies and Reprints, Discussion and Closure, Publication by Others.**

***PRESENTATION OF A PAPER—***

**Time Limit, Addressing Your Audience, Public Address Systems, Use of Slides.**

***REFERENCES—***

**References on Writing and Speaking, Engineering Standards.**


**Price 40¢. No discount allowed.** ***A remittance must accompany all orders for $5.00 or less. U. S. Postage Stamps are acceptable.***


**THE AMERICAN SOCIETY OF MECHANICAL ENGINEERS**

**29 West 39th Street, New York 18, N. Y.**

## DESIGN DATA AND METHODS

Here under one cover are all of the design data which were published in the Journal of Applied Mechanics from 1945 to March 1953 along with all of the material in the first (1944) edition of Design Data. The compilation—200 pages in length—includes formulas and methods of calculating stresses in beams, bars, columns, plates, shafts, and crane hooks; stress component formulas; procedures for computing stresses and deformation in pressure vessels; design data on press- and shrink-fitted assemblies and also for piping; factors of working stresses; numerical values of tangential stress in thick-walled cylinders; numerical solution of problems of gas flow when properties change continuously; and graphical and numerical procedures for method of characteristics for two dimensional supersonic flow; chart for oblique shock waves under water; accurate bearing calculations; and methods of treating and solving problems of vibration and of balancing rotating apparatus.

SECOND EDITION 1953 $4.00

## GLOSSARY OF TERMS IN NUCLEAR SCIENCE AND TECHNOLOGY

Now, under one cover, precise definitions for about 2000 terms used in the fields of reactor theory, reactor engineering, chemistry, chemical engineering, biophysics and radiobiology, instrumentation, isotopes separation, metallurgy, and physics. The Glossary is divided into nine sections to enable the user to readily locate the terms peculiar to each of the afore-mentioned fields. An alphabetical arrangement of the terms has also been included to indicate the section or sections in which the definitions and the terms will be found.

Seventeen scientific and technical societies, ten governmental agencies, and four divisions of the National Research Council have co-operated in the preparation of this Glossary.

$7.00

## DIGITAL AND ANALOG COMPUTERS AND COMPUTING METHODS

This book summarizes the present state of high speed computation in the field of applied mechanics. It discusses the use of analog computers and their application to aircraft design problems and to mechanical problems. It also shows how digital analog computers are being used to solve linear algebraic equations and to find eigenvalues and eigenvectors.

1953 $3.00

## PROCEEDINGS OF THE FIRST (1951) U. S. NATIONAL CONGRESS OF APPLIED MECHANICS

One hundred and fifty nationally recognized authorities have pooled their knowledge and experience to make possible this record of advances in modern applied mechanics. The 130 papers in its thousand pages were presented at the first technical conference to be held in the United States in 1951; the objective of which was to survey the problems confronting the field and to find out what engineers were doing to solve them. The coverage includes researches and investigations in dynamics, vibration, impact, elasticity, photoelasticity, plate theory, elastic instability, plasticity, behavior of materials, fluid flow, aerodynamics, and heat.

Supplementing the text are comprehensive bibliographies keyed to many of the articles, numerous charts, illustrations, and graphs.

$20.00

## DRAMATIC LIFE STORIES OF DISTINGUISHED ENGINEERS

*TO READ—TO OWN—FOR CHRISTMAS GIVING*

**DEXTER S. KIMBALL**—A vital story of a dynamic era and an equally engrossing story of the apprentice machinist who became Dean of Cornell's Engineering School.

$4.00

**W. F. DURAND**—Creation of the National Advisory Committee for Aeronautics, invention of the radial planimeter, activities as consultant on the Hoover Dam and other similar projects are among the hundreds of stories reported in this varied career.

$4.00

**FRANK and LILLIAN GILBRETH**—Here is the full impressive story of Frank Gilbreth's early work in motion study and of Lillian Gilbreth's insistence upon sound psychological approach as a tool of management.

$5.50

**MORTIMER E. COOLEY**—Dean of the College of Engineering, University of Michigan, active in consulting engineering, in public service, and as a leader in the work of engineering societies his autobiography reflects a breadth of experience achieved by few engineers.

$3.75

**WILLIAM LEROY EMMET**—Best known for his invention, design, and development of the mercury-vapor power system, Mr. Emmet was also prominently identified with other important phases of electrical development. Interesting accounts of these and his many other tasks are interwoven into this self-told story.

$3.50

**THE AMERICAN SOCIETY OF MECHANICAL ENGINEERS**

29 W. 39th St., New York 18, N. Y.

20% DISCOUNT TO ASME MEMBERS

# RESOLUTION CHART

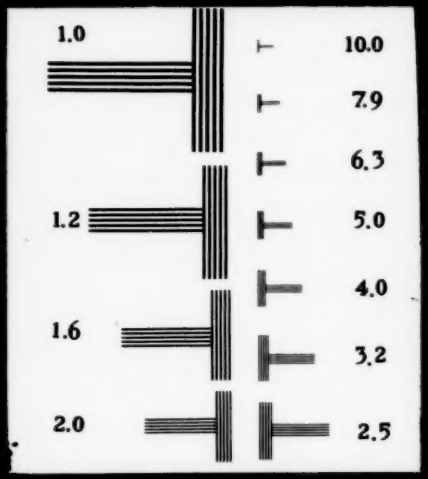


100 MILLIMETERS

**INSTRUCTIONS** Resolution is expressed in terms of the lines per millimeter recorded by a particular film under specified conditions. Numerals in chart indicate the number of lines per millimeter in adjacent "T-shaped" groupings.

In microfilming, it is necessary to determine the reduction ratio and multiply the number of lines in the chart by this value to find the number of lines recorded by the film. As an aid in determining the reduction ratio, the line above is 100 millimeters in length. Measuring this line in the film image and dividing the length into 100 gives the reduction ratio. Example: the line is 20 mm. long in the film image, and $100/20 = 5$.

Examine "T-shaped" line groupings in the film with microscope, and note the number adjacent to finest lines recorded sharply and distinctly. Multiply this number by the reduction factor to obtain resolving power in lines per millimeter. Example: 7.9 group of lines is clearly recorded while lines in the 10.0 group are not distinctly separated. Reduction ratio is 5, and $7.9 \times 5 = 39.5$ lines per millimeter recorded satisfactorily. $10.0 \times 5 = 50$ lines per millimeter which are not recorded satisfactorily. Under the particular conditions, maximum resolution is between 39.5 and 50 lines per millimeter.

Resolution, as measured on the film, is a test of the entire photographic system, including lens, exposure, processing, and other factors. These rarely utilize maximum resolution of the film. Vibrations during exposure, lack of critical focus, and exposures yielding very dense negatives are to be avoided.

THIS PUBLICATION
IS REPRODUCED BY AGREEMENT
WITH THE PUBLISHER. EXTENSIVE
DUPLICATION OR RESALE WITHOUT
PERMISSION IS PROHIBITED.